Proceedings of the International Symposium on Vegetation Monitoring

August 29 - 31, 1995
Chiba, Japan

CEReS
Center for Environmental Remote Sensing, Chiba University, Japan.

Proceedings of the International Symposium on Vegetation Monitoring

August 29 - 31, 1995
Chiba, Japan

CEReS
Center for Environmental Remote Sensing.
Chiba University, Japan.

Edited by Shizuo Shindo and Ryutaro Tateishi

Published by
Center for Environmental Remote Sensing (CEReS), Chiba University
1-33 Yayoi-cho, Inage-ku, Chiba, 263 Japan
Fax: +81-43-290-3857

International Symposium on Vegetation Monitoring

August 29 - 31, 1995
at the University Convention Hall, "Keyaki-Kaikan", Chiba University

Organized by the Center for Environmental Remote Sensing (CEReS) , Chiba University

Program

August 29, Tuesday

9:00 - 9:30 Registration

9:30 - 10:00 **Opening Ceremony**

Welcome Speech *Dr. Koscak Maruyama, President, Chiba University*

Welcome Address *Mr.Masayuki Inoue, Director, International Science Division, Science and International Affairs Bureau, Ministry of Education, Science, Sports and Culture*

Opening Address *Prof. Shizuo Shindo, Director, Center for Environmental Remote Sensing*

10:00 - 11:00 **Keynote Speech**

African Famine Early Warning from Satellite Data 1
Compton J. Tucker (USA)

11:00 - 11:20 **Report**

Introduction of ADEOS- II /Global Imager 10
Hiroyuki Oguma (Japan)

11:20 - 12:00 Session 1a **Land Cover Mapping Projects**

1-1 Land Cover Database of Asia 13
Ryutaro Tateishi and Wen Cheng Gang (Japan)

1-2 Remote Sensing Monitoring on Land Use Change in China 20
Wang Changyao (China)

12:00 - 13:00 lunch

13:00 - 14:45 Session 1b Land Cover Mapping Projects

1-3 Use of Satellite Imagery to Map and Monitor Vegetation in New Zealand 27
P. R. Stephens, J.R. Dymond and L. J. Brown (New Zealand)

1-4 Using the Remote Sensing Technique to Establish a Land Use Map in Vietnam on Scale 1:1,000,000 35
Nguyen Thuong Hung (Vietnam)

1-5 Land Cover Assessment and Monitoring at UNEP/EAP-AP: A Remote Sensing and GIS Approach 40
Chandra P. Giri and Surendra Shrestha (Thailand)

1-6 Vegetation Mapping of Iran through Using NOAA AVHRR Data 50
Ahmad Mohammadpour and M.Forouhar (Iran)

1-7 Vegetation Cover Mapping of Kadmous Area Using TM Data 58
Abdul Rahim Loulou (Syria)

14:45 - 15:15 coffee break

15:15 - 17:45 Session 2 **Vegetation Parameters / Physical Quantities**

2-1 Spruce Stand Parameter Estimation Using Airbone Sensor Imagery 64
Yoshio Awaya (Japan)

2-2 Ground Based Observation of Vegetation Coverage, LAI and APAR to Develop New Vegetation Indices Algorithm for ASTER 72
Yoich Numata, Kazuya Saito, Yoshiaki Yamano, Yoshifumi Yasuoka and Manabu Kaku (Japan)

2-3 Monitoring Global Energy Flow to Primary Production 79
Dennis Dye (Japan)

2-4 Vegetation/Land Cover Changes in Monsoon Asia and Its Influence on Areal Evapotranspiration 87
Akihiko Kondoh (Japan)

2-5 Estimation of Methane Emission from Western Siberian Wetlands by Using of Satellite Remote Sensing Techniques 95
M. Tamura, Y. Yasuoka and Y. Yamagata (Japan)

2-6 Surface Temperature Decrease, NDVI and Humidity Deficit, and Latent Heat Flux in Forested Region from TM and Routine Meteorological Data – A Summary – 99
Daijiro Kaneko and Mikio Hino (Japan)

2-7 Monitoring of Radiant Temperature Distribution of Urban Vegetation Using High Resolution Multi-temporal Remote Sensing Data 107
Akinaru Iino and Akira Hoyano (Japan)

18:00 - 20:00 Welcome party

August 30, Wednesday

9:30 - 11:30 Session 3 **Correction / Classification**

3-1 Effects of Sensor Degradation and Solar-Sensor Geometry on Land Cover Monitoring Using NOAA/AVHRR Data 115
Shoji Takeuchi and Yasushi Mitomi (Japan)

3-2 Atmospheric Effect and Its Correction of the Remotely Sensed VNIR Data for the Vegetation Monitoring 123
Masao Moriyama (Japan)

3-3 Scaling between NOAA AVHRR Data and LANDSAT TM Data for Monitoring and Mapping of Wetland 131
Yoshifumi Yasuoka, Mikio Sugita, Yoshiki Yamagata, Masayuki Tamura and Tomoyuki Suhama (Japan)

3-4 Selecting a Suitable Model for Vegetation Monitoring Using Satellite Data 137
Sumith Pathirana and B. Boyd (Australia)

3-5 A Study on Construction of Enhanced Vegetation Cover Map Considering Vegetation Cover Ratio in a Pixel by Remote Sensing Data 146
Donkyu Yun and Akira Hoyano (Japan)

3-6 Spectral Delineation of Large-area Tropical Forest Lands and Timberlands Using a Combination of Visible, Near-infrared and 3.7 μm Thermal-infrared AVHRR Data from the NOAA-12 (Morning Pass) Satellite 154
Bobby A. Crisostomo (Philippine)

11:30 - 13:00 lunch

13:00 - 15:00 Session 4 **Reflectance / Ground Truth / SAR**

4-1 Indicatrices of the Leaves of Various Woody Plant Species 162
Hiroshi Okayama (Japan)

4-2 A Monte Carlo Reflectance Simulation of Rice Canopy Based on Digital 3-D Structure 170
Keiji Kushida, Kunihiko Yoshino and Eiji Yamaji (Japan)

4-3 Ground Truth Database for Global Scale Research 178
– Grassland Bio-mass Monitoring using NOAA AVHRR and Ground Truth –
Yoshiaki Honda (Japan)

4-4 Ground Truth Database for Vegetation Remote Sensing 182
Koji Kajiwara (Japan)

4-5 Contribution of Enhanced SAR Imagery for Agricultural Land Use Classification 186
Harahsheh Hussein (Jordan)

4-6 Phenological Characteristics of Cultivated Vegetation Covers in JERS-1 and ERS-1 Synthetic Aperture Radar Data – Preliminary Results – 194
Ake Rosenqvist and Hiroyuki Oguma (Japan)

15:00 - 15:30 coffee break

15:30 - 17:10 Session 5 **Environmental Analysis**

5-1 Land Use Change Study for South East Asia (LUCS-ASIA) 199
Ryosuke Shibasaki, Masao Takagi and Koki Iwao (Japan)

5-2 Analysis of Environmental Profile of Walawe River Basin, Sri Lanka, by Remote Sensing and GIS 206
L.. Kithsiri Perera, Satoru Ueno, Koji Shigehara and Ryutaro Tateishi (Japan)

5-3 Life Cycle Assessment for Hydroelectric Power Plant Construction Considering Vegetation Change Effect Using Vegetation Map 214
Shintaro Goto and Toshikazu Sakai (Japan)

5-4 A Case Study on Changes in Vegetation Cover and Settlements in Bangladesh Using Remote Sensing Techniques 215
Md. Abul Kalam (Bangladesh)

5-5 A Comparative Study of Urbanization and Impact on the Natural Environment in Colombo City in Sri Lanka and Nagoya City in Japan Using Remote Sensing Data 224
Makoto Kawamura, Sanath Jayamanna and Yuji Tsujiko (Japan)

August 31, Thursday

9:30 - 11:50 Session 6 **Vegetation Change**

6-1 Monitoring Global Vegetation Degradation Using GVI Data 231
Shiro Ochi (Japan) and Shunji Murai (Thailand)

6-2 Monthly Vegetation Changes in the Arabian Peninsula: Observations from AVHRR Global Vegetation Index Composite Data 233
Andy Yaw Kwarteng and Dhari Al-Ajmi (Kuwait)

6-3 Monitoring of Climax Forest Area for Global Environment Study 242
Haruo Sawada and Hideki Saito (Japan)

6-4 Forest Restoration Monitoring and Erosion Control Work Planning 247
Kiyoshi Honda, Ryousuke Shibasaki and Shunji Murai (Japan)

6-5 Monitoring Changes of Lake Water and Vegetation Area in Central Asia 253
Y. Nakayama, S. Tanaka, K.Endo and Y. Suga (Japan)

6-6 Monitoring Deforestation in Luzon, The Philippines Using Remote Sensing Data 259
Akira Hirano, Genya Saito and Nobuyuki Mino (Japan)

6-7 Use of Vegetation Index of Satellite Data for Updating Land Use Data in Japan 267
Kohei Cho, Haruhisa Shimoda, Toshibumi Sakata and Mitsunori Yoshimura (Japan)

11:50 - 13:00 lunch

13:00 - 14:40 Session 7 **Agriculture / Grassland**

7-1 Crop Maps and Yield Maps of Sugar Beets in the Tokachi Plains, Japan, Developed from Multitemporal Landsat TM Data 275
Chiharu Okano, Katsuo Okamoto, Michikazu Fukuhara and Akira Nishimune (Japan)

7-2 Agriculture Monitoring in Japan Using NOAA/AVHRR Data 282
Genya Saito, Nobuyuki Mino and Yoshizumi Yasuda (Japan)

7-3 The State of Land Cover and Pasture Condition on Territory of Mongolia 288
Gombosurengiin Tsolmon (Mongolia)

7-4 Monitoring of Grassland Annual Change Using Multi-Temporal Satellite Data 292
Nobuyuki Mino, Genya Saito and Akira Hirano (Japan)

7-5 Generation of the Landcover Map of the State of Kedah, Malaysia Using Satellite Data
Loh Kok Fook (Malaysia)

14:40 - 15:00 coffee break

15:00 - 16:40 Session 8 **Mangrove / Desert**

8-1 Similarities between Manda, Sumatera and Iriomote, Okinawa on the Distribution of TM Data of Landsat 5 in a Multidimensional Space for Mangrove and the Surroundings 298
Dwi Setyono and Kazuhiro Sato (Japan)

8-2 Identification and Mapping of Mangrove Forest along the Coast of Pakistan 304
Jawed Ali and Amina Rangoonwala (Pakistan)

8-3 Ground Surface Features of Taklimakan Desert
—Features of Spectral Reflectance of Soils,Vegetation etc.— 307
Takashi Ishiyama, Shigehiko Sugihara and Kiyoshi Tsuchiya (Japan)

8-4 Monitoring of Anthropogenic Changes in Desert Vegetation 315
Nikolai Kharin (Turkmenistan)

8-5 Monitoring of Desertification and Possibility for Agro-Farming-Forestry Development 322
Ken Nishida, Keni-chi Shibata and Fumiko Makita (Japan)

16:40 - 17:00 **Closing Ceremony**

African Famine Early Warning from Satellite Data

Compton J. Tucker
Laboratory for Terrestrial Physics, Code 923
NASA/Goddard Space Flight Center
Greenbelt, Maryland 20771 USA

Satellite data obtained from the NOAA series of meteorological satellites and the METEOSAT geostationary satellite are operationally used in near-real time to provide objective assessment of famine early warning for Africa. Advantages of the use of time-series satellite data are timeliness and consistency. When combined with ground-collected socioeconomic information, an integrated assessment of distributed agricultural potential is possible at a fraction of the cost of traditional inventories. This is the approach taken by the U. S. Agency for International Development's Famine Early Warning System (FEWS) and by the United Nation's Food and Agriculture Organization's Food Security program. In addition to providing spatially continuous and objective information in a timely fashion for a complete continent, these satellite-based early warning systems enable famine relief resources to be directed to those areas most affected at a fraction of the cost of previous methods of relief allocation for Africa. In addition, recent work relating El Nino Southern Oscillation events to African vegetation dynamics suggests that famine early warning in selected areas of Africa may be directly related to sea surface temperature anomalies in the tropical Pacific.

Background

Large areas of Africa have experienced serious droughts resulting in agricultural shortfalls in recent years. This has been most evident in Sahelian and Sudanian Africa, where a run of deficient precipitation years beginning about 1970 has occurred with 1984 being the driest year this century (fig. 1). The reasons for this curious and persistent run of year after year of below average rainfall are not understood. Suggested climate system forcings or explanations include large-scale land surface modification from overgrazing and tree cutting, increases in atmospheric dust from anthropogenic causes, and unusual Atlantic and Indian Ocean sea surface temperature conditions. Whether this is natural or/and anthropogenic in nature, the Sahelian rainfall situation since the late 1960's is rather unusual and warrants detailed study. However, it is

important to note that a high degree of within-year variability also exists, as will be shown later.

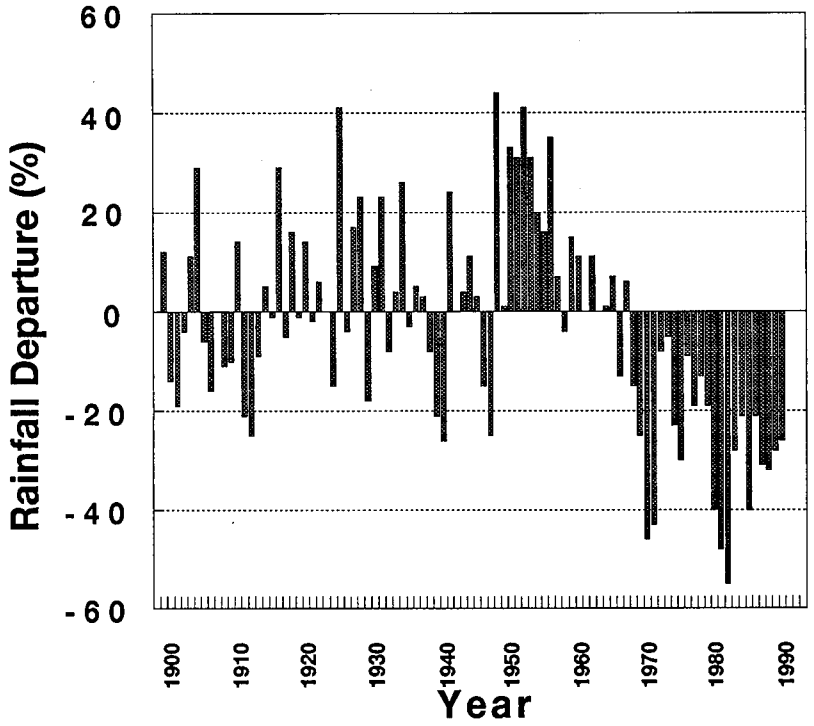

Figure 1. Sharon Nicholson's rainfall departure for Sahelian Africa from 1900 to 1992. Note the unusual run of drier years from the late 1960's to the present.

Serious droughts in Africa were not limited to Sahelian and Sudanian Africa during the 1980's and 1990's. In 1982-1983 Southern and Eastern Africa experienced significant precipitation shortfalls; similar droughts also occurred in the late 1980's and in 1991-1992. It unfortunately seems to be the case that serious drought is frequently present somewhere in Africa, with the attendant consequences of famine if external food relief is not supplied.

As much of Africa is based on subsistence agriculture, serious droughts often result in widespread famine, sometimes exacerbated by political instability and even civil war. Donor-country relief activities to prevent famines from developing have been complicated by lack of quantitative information describing actual conditions and that famine could not be anticipated. Frequently, traditional information describing famine magnitude and spatial extent is incorrect or highly contradictory.

Furthermore, in times of serious drought it is not uncommon for many areas to overstate the magnitude of their food requirements to maximize donor relief for their specific areas, in the process perhaps denying donor relief for truly deserving areas. These factors led the Food and Agricultural Organization of the United Nations (FAO) and the U. S. Agency for International Development (USAID) to begin famine early warning programs based, to a large extent, upon NOAA advanced very high resolution radiometer (AVHRR) and METEOSAT satellite data in 1983. This topic has previously been reviewed by Hutchinson (1991).

Two satellite techniques are used in famine early warning for Africa: Normalized difference vegetation index (NDVI) measurements derived from daily advanced very high resolution radiometer (AVHRR) data from the National Oceanic and Atmospheric Administration (NOAA) series of polar-orbiting meteorological satellites (NOAA-7, NOAA-9, NOAA-11, NOAA-9, and now NOAA-14); and cold cloud duration rainfall estimates derived from METEOSAT geostationary satellite data. While both satellite data types are used in famine early warning, I will focus largely on the NOAA AVHRR normalized difference vegetation index measurements.

NOAA AVHRR Satellite Data

The NOAA-series of sun-synchronous polar-orbiting meteorological satellites orbit at an altitude of ~850 km and have a daytime overpass time of ~ 1430 hours local solar time. The AVHRR sensor scans ~55^{o} from nadir and complete coverage of the earth is available twice daily at a spatial resolution of ~5.5 x 3.3 km at the satellite subpoint. Daily data from channels 1 (0.55-0.70 μm), 2 (0.72-1.1 μm), and 5 (11.5-12.5 μm) were used with a scan angle of 40^{o} or less, processed to produce a vegetation index of (2-1)/(2+1), and formed into 10-day maximum value composites after Holben (1986). Channel 5 was used as a cloud filter where every pixel cooler than 12^{o}C was labeled as a cloud. Holben (1986) and Holben and Fraser (1985) have shown that maximum value vegetation index composites simultaneously minimize scan angle, atmospheric effects, clouds, and all other degrading effects upon the vegetation index. Every 7.6 km grid-cell has ~ 6-7 potential data values to choose from every 10-day period. The NOAA AVHRR data are processed into three "10-day" composite images every month: from day 1 to day 10; from day 11 to day 20; and from day 21 to the end of the month. A monthly composite is also produced.

The normalized difference vegetation index is a non-destructive estimate of the photosynthetic potential or capacity of the area measured after Sellers (1985, 1987). Consequently, when normalized difference vegetation index measurements are made over time they provide information on the time history of the photosynthetic potential or capacity which has been shown to be highly related to total biomass production. This assumption has been tested in the Sahelian zone of West Africa where Tucker et al. (1985) and Prince (1991) have shown multi-temporal NOAA AVHRR normalized difference vegetation index data to be directly related to herbaceous above-ground biomass production.

Biomass production and green vegetation density are usually closely related to precipitation in grasslands and savannas. Precipitation ceases to be the primary factor in primary production when the rainfall is greater than ~700-800 mm/yr (Lamotte and Bourliere, 1983; Le Houreou and Hoste, 1977; Nicholson et al., 1990). The relationship of precipitation to green vegetation density and biomass or primary production depends upon the amount and timing of the rainfall, evapotranspiration and runoff, soil infiltration, and the ability of vegetation to respond to rainfall.

There is usually a strong and direct relationship between precipitation and the normalized difference vegetation index (figure 2). Similar, but slightly different, relationships have been reported from other arid and semi-arid grassland settings in Africa and elsewhere, although factors such as temperature, type of precipitation, timing, intensity, etc. are also important (Lauenroth, 1979; Nicholson et al., 1990; Rutherford, 1979; Seely, 1978). Figures 2 and 3 show the reasons why NOAA AVHRR normalized difference vegetation index data are so useful in famine early warning detection--they are directly linked to precipitation and hence primary production.

The data set presently in use from July 1981 to the present is a 7.6 km grid cell size equal-area projection NDVI product for Africa. In early 1996, this data set will be replaced by a 6-km grid cell size data product comprised of the NDVI, associated channel values, pixel angular information and day of acquisition, and cloud mask overlays. As soon as each "10-day" composite image is produced, it is transmitted to U.S. AID's Famine Early Warning Office for analysis.

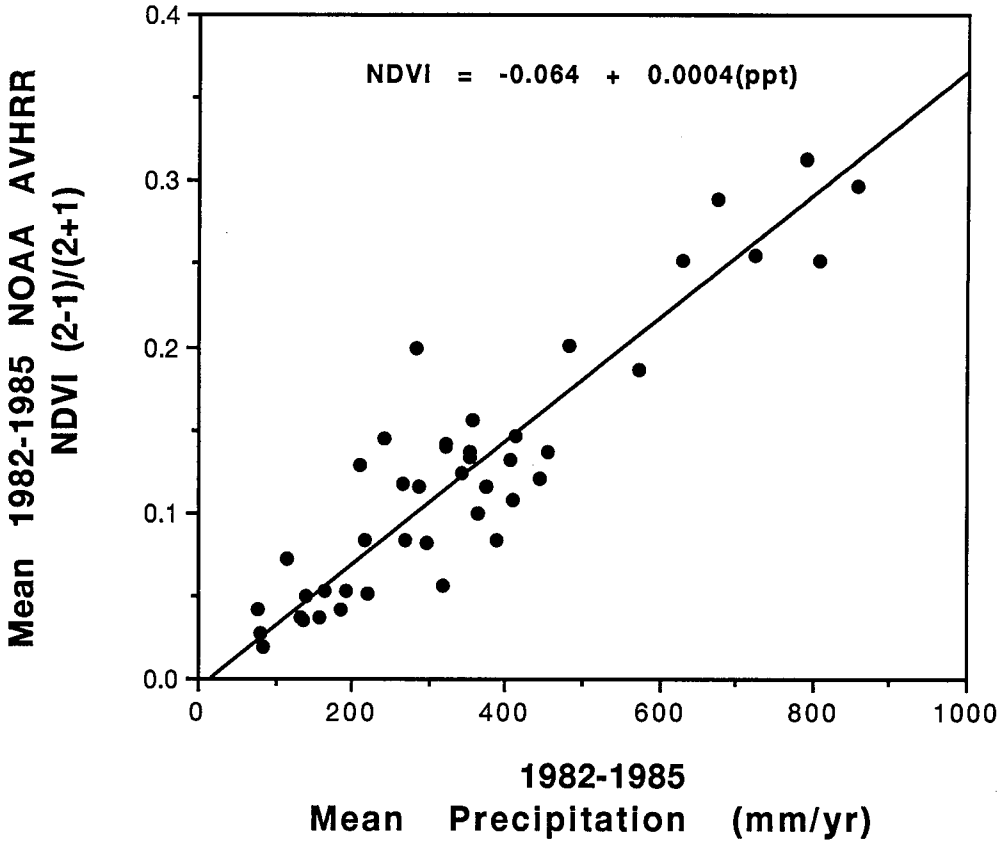

Figure 2. Correlation between the average 1982-1985 normalized difference vegetation index and the 1982-1985 station precipitation at specific reporting meteorological stations. Note the high degree of correlation between these two variables (from Tucker et al., 1991).

Famine Early Warning Analysis

When the time series of AVHRR normalized difference vegetation index data are available, simple comparisons among years serve to identify areas within Africa experiencing drought and hence the potential for subsequent famine. For example, within the Sahelian zone (broadly defined as the long-term 200 to 400 mm/yr precipitation zone immediately south of the Sahara), AVHRR normalized difference vegetation index data from 1980 to 1994 identify marked differences among three geographic subdivisions of this ecological or climatic zone (fig. 3).

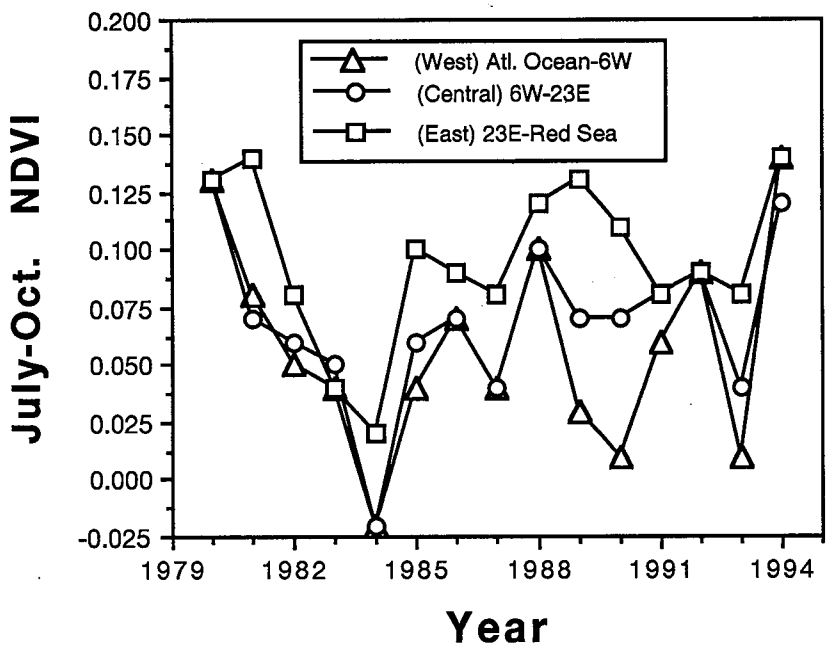

Figure 3. The average growing season normalized difference vegetation index for the Sahel Zone is disaggregated in a western component (the Atlantic Ocean to 6° W), a central component (6° W to 23° E), and an eastern component (23° E to the Red Sea). The Sahel Zone is defined as the long-term 200-400 mm/yr precipitation zone (see also Tucker et al. 1991).

For example, very similar normalized difference vegetation index values were found for the Western, Central, and Eastern portions of the Sahelian Zone from 1980 to 1983 and in 1992 to 1994. In contrast, from 1989 to 1990 and again in 1993, the Eastern Sahel exhibited higher normalized difference vegetation index values than the Central Sahel, which in turn was higher than the Western Sahel (fig. 4). NOAA AVHRR normalized difference vegetation index data from 1981 to 1995 (and continuing) enable comparisons to be made pixel by pixel, district by district, country by country, and region by region which readily identifies changes in surface conditions directly related to primary production. When combined with historical socioeconomic information, a much better understanding will emerge regarding the agricultural potential for the area(s) in question.

ENSO Cycle Anomalies and Famine Early Warning

Recently Cane et al. (1994) and Myneni et al. (1995) have reported that El Nino Southern Oscillation (ENSO) cycle sea surface temperature anomalies can highly influence African primary production and agricultural yield in specific areas. Cane et al (1994) have shown that ENSO cycle sea surface

temperature anomalies are related to maize yield in Zimbabwe (figure 4). Mymeni et al (1995) have shown that ENSO cycle sea surface temperature anomalies seem to be related to precipitation patterns in other areas of Africa. Both of these types of ENSO cycle sea surface temperature anomalies as they affect African agriculture and natural vegetation are presently under detailed study to determine to what extent they exist and where within African they can be generalized.

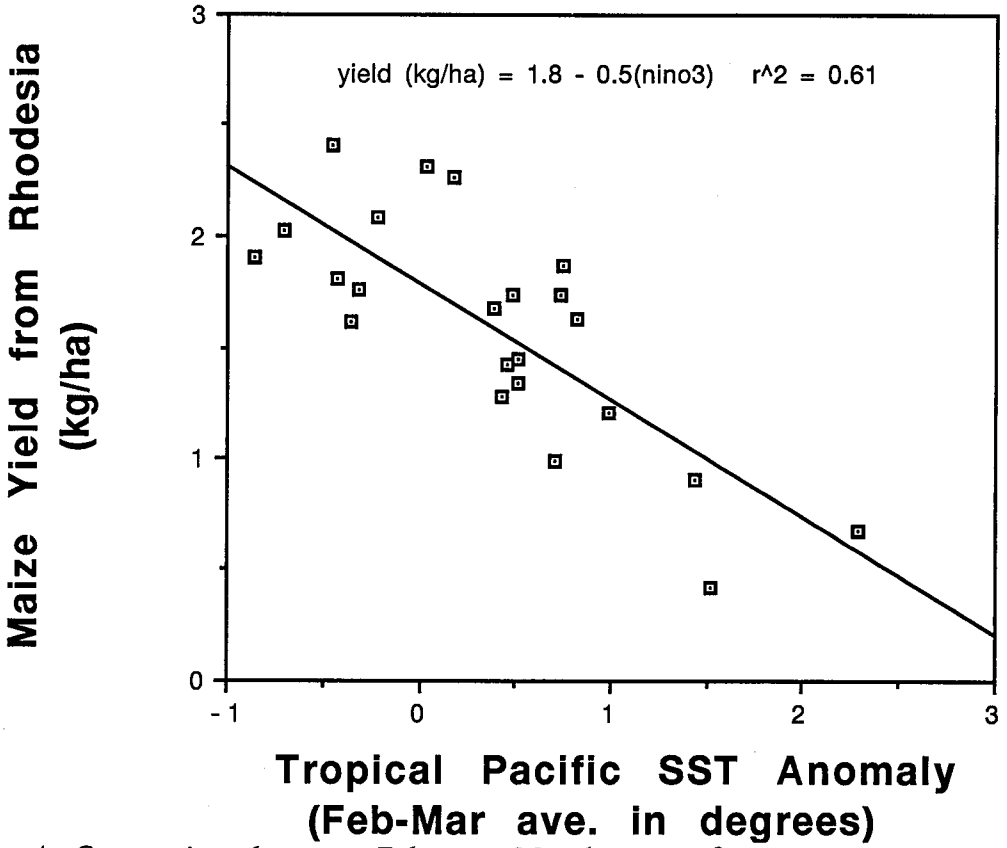

Figure 4. Comparison between February-March sea surface temperature and maize yield from Zimbabwe (Cane et al., 1994).

In summary, NOAA AVHRR data and other types of famine early warning satellite-derived information (sea surface temperature in the tropical Pacific and METEOSAT data) provide invaluable, very timely, cost-effective, and objective information which is be used to minimize the adverse effects of famine within Africa. This has resulted in tremendously reducing human suffering in a much more economical manner than is commonly realized. Without satellite data, this type of humanitarian work would not be possible.

References

M. A. Cane, G. Eshel, R. W. Buckland,1994. Forecasting Zimbabwean maize yield using eastern equatorial Pacific sea surface temperature. Nature, 370, 204-205.

Holben, B.N., 1986, Characteristics of maximum-value composite images from temporal AVHRR data. *International Journal of Remote Sensing,* **7**, 1417-1434.

Holben, B.N. and Fraser, R.S., 1984, Red and near-infrared sensor response to off-nadir viewing. *International Journal of Remote Sensing,* **5**, 145-160.

Hutchinson, C. F., 1991. Use of satellite data for famine early warning in sub-Saharan Africa. *International Journal of Remote Sensing,* **12**, 1405-1421.

Lamotte, M. and Bourliere, F., 1983, Energy flow and nutrient cycling in tropical savannas. In *Tropical Savannas, Ecosystems of the World,* **13**, F. Bourliere, editor (Elsevier, New York), pp. 583-612.

Lauenroth, W.K., 1979, Grassland primary production: North American grasslands in perspective. In *Perspectives in Grassland Ecology*, edited by N. French, Springer-Verlag, New York, pp. 3-24.

Le Houerou, H.N. and Hoste, C.H., 1977, Rangeland production and annual relations in the Mediterranean Basin and in the African Sahelo-Sudanian Zone. *J. Range Manage.,* **30**, 181-189.

Mynemi, R. B. , Los, S. O., and Tucker, C. J., 1995. Satellite-based identification of linked vegetation index and sea surface temperature anomaly areas from 1981-1990. Submitted to the journal of climate.

Nicholson, S.E., Davenport, M.L., and Malo, A.R., 1990, A comparison of the vegetation response to rainfall in the Sahel and East Africa, using normalized difference vegetation index from NOAA AVHRR. Climate Change 17:209-242.

Prince, S.D. 1991, Satellite remote sensing of primary production: comparison of results for Sahelian grasslands 1981-1988. *Int. J. Remote Sens.* 12:1301-1312.

Rutherford, M.C., 1980, Annual plant production-precipitation relations in arid and semi-arid regions. *So. African J. Science,* **76,** 53-56.

Sellers, P.J., 1985, Canopy reflectance, photosynthesis, and transpiration. *Int. J. Remote Sens.,* **6,** 1335-1372.

Sellers, P.J., 1987, Canopy reflectance, photosynthesis, and transpiration. II. The role of biophysics in the linearity of their interdependence *Remote Sens. Environ.,* **21,** 143-183.

Seely, M.K., 1978, Grassland productivity: The desert end of the curve. *So. Afr. J. Sci.,* **74,** 295-297.

Tucker, C.J., C.L. Vanpraet, M.J. Sharman, and G. Van Ittersum, 1985, Satellite remote sensing of total herbaceous biomass production in the Senegalese Sahel: 1980-1984. *Remote Sens. Environ.,* **17,** 233-249.

Tucker, C. J., Dregne, H. E., and Newcomb, W. W., 1991. Expansion and contraction of the Sahara Desert from 1980 to 1990. Science 253, 299-301.

Tucker, C. J., Newcomb, W. W., and Dregne, H. E.,1994. AVHRR data sets for determination of desert spatial extent. *International Journal of Remote Sensing* ,**15,** 3547-3565.

Introduction of ADEOS-II/GLI

Hiroyuki Oguma, Masakatsu Nakajima

National Space Development Agency of Japan
2-4-1,Hamamatsu-cyo,Minato-ku,Tokyo,105 Japan

1.INTRODUCTION

In 1999, ADEOS-II is planned to launch. This satellite is a polar orbiting earth observation satellite, and aims to observe the global changes of environment based on the carbon, water and energy cycle.
For this purpose, ADEOS-II will carry two core instruments developed by NASDA and three,ILAS-II, SeaWinds and POLDER,developed and delivered by other Agencies. Now two core instruments are under development.
One is microwave imaging radiometer named AMSR and the other is optical imaging radiometer named GLI. The primary objectives of the AMSR are to obtain the physical quantities related to the water, for example atmospheric water vapor, cloud and precipitating liquid water, sea ice concentration and terrain snow coverage and sea surface temperature. AMSR observes with 8 frequency, dual polarization, wide swath width, high radiometric sensitivity and high spatial resolution.
The primary objectives of the GLI are to obtain the ocean color and ocean temperature, cloud distribution , land coverage , vegetation index and so on. GLI observes the reflectance and radiation from the earth with 36 observation channels from visible to thermal infrared, 375nm to 12.5μm, 1600km of swath width, over 800 of signal to noise ratio and 1km and 250m spatial resolution.
The satellite bus design is to succeed the basics of 3.5 ton class ADEOS satellite.

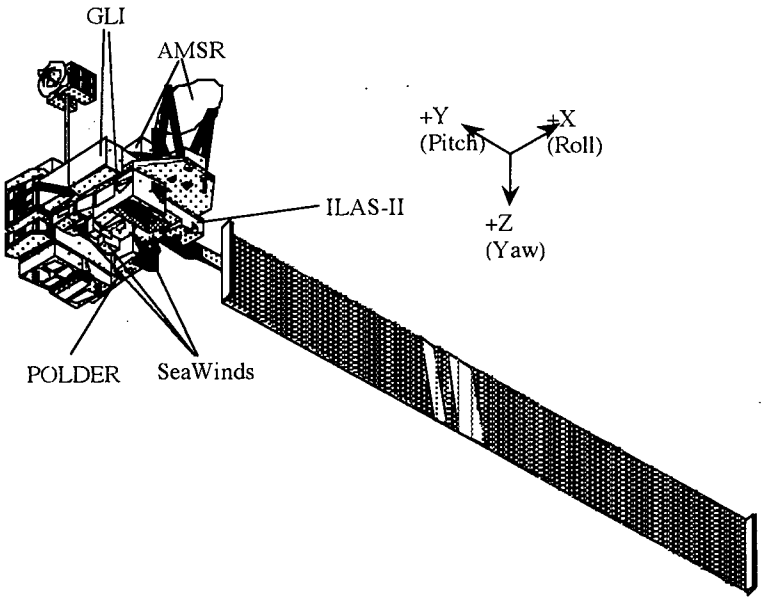

Figure.1. Conceptual view of ADEOS-II

Table.1. The specification of ADEOS-II

orbit	sun synchronous sub-recurrent orbit
local time	10:30am±15 min.
revolution	14+1/4 rev./day
recurrent	4 days
altitude	802.9 km
inclination	98.62 deg.
period	101min.
revolution per one recurrent	57 rev.
minimum interval between the orbits (on the equator)	728.62 deg
accuracy of recurrent position	±5 km
attitude control accuracy	±0.3 deg
attitude stability	±0.008 deg/sec
attitude determine accuracy	±0.05 deg*

* by combination navigation (when normal navigation is applied these are ±0.155 deg.)

2. GLI:GLobal Imager

2.1. Mission of GLI

The mission of GLI is to know the global cycle of carbon which is included in CO_2,CH_4 and so on being major cause of global warming. through the land and ocean biological activities.

2.2. Spectral resolution

For ocean color analysis Spectral resolution is required under 10 nm so that it may not includes two spectral characteristics of ocean and it is required from 8nm to 220 nm for each spectral bands for cloud and vegetation.

2.3. Spatial resolution

The characteristic length of phytoplankton biomass distributions are generally in the range of 1 to 10 km (MODIS instrument panel report;EARTH OBSERVING SYSTEM REPORTS, Volume IIb,1986). Because the spatial resolution of GLI should be on the order of 1 km in the coastal region and 4 km in the open ocean.

For the analysis of vegetation index it will be needed 250 m spatial resolution at least. And to compare with Landsat data, it is necessary that spatial resolution is 250 m.

Table.2. Requirement to the GLI(wavelength, bandwidth, IFOV and S/N or NEDT)

No.	λ (nm)	Δλ (nm)	IFOV (mrad/m(at nadir))	S/N , NEDT (K)	No.	λ (nm)	Δλ (nm)	IFOV (mrad/m(at nadir))	S/N , NEDT (K)
1	380	10	1.25/1000	>600	20	460	70	0.3125/250	>184
2	400	10	1.25/1000	>800	21	545	50	0.3125/250	>143
3	412	10	1.25/1000	>800	22	670	60	0.3125/250	>136
4	443	10	1.25/1000	>800	23	825	110	0.3125/250	>247
5	460	10	1.25/1000	>800					
6	490	10	1.25/1000	>800	24	1050	20	1.25/1000	>TBD
7	520	10	1.25/1000	>600	25	1100	20	1.25/1000	>TBD
8	545	10	1.25/1000	>600	26	1240	20	1.25/1000	>70
9	565	10	1.25/1000	>800	27	1380	40	1.25/1000	>TBD
10	625	10	1.25/1000	>800	28	1640	200	0.3125/250	>100
11	667	10	1.25/1000	>800	29	2210	220	0.3125/250	>TBD
12	678	10	1.25/1000	>800		(μm)	(μm)		(K)
13	678	10	1.25/1000	>TBD	30	3.715	0.33	1.25/1000	<0.15
14	710	10	1.25/1000	>700	31	6.7	0.5	1.25/1000	<0.1
15	710	10	1.25/1000	>TBD	32	7.0	0.5	1.25/1000	<0.1
16	748	10(TBD)	1.25/1000	>550(TBD)	33	7.3	0.5	1.25/1000	<0.1
17	763	8	1.25/1000	>TBD	34	8.3	0.5	1.25/1000	<0.1
18	865	20	1.25/1000	>TBD	35	10.8	1.0	1.25/1000	<0.1
19	865	10	1.25/1000	>TBD	36	12.0	1.0	1.25/1000	<0.1

* the channel which number are expressed in italic bold letter are required to be applied piecewise linear method

Table.3. Characteristics of GLI system

spectral bands	visible and near infrared:23 short wavelength infrared:6 middle and thermal infrared:7
IFOV	1.25mrad(1000 m at nadir) :30 bands 0.3125mrad(250 m at nadir) :6 bands
FOV	about ±43 degree (swath=1600 km)
quantization	12bits
polarization sensitivity	under 2%
registration among total bands	under 0.2 pixels (1 km resolution)
data rate	about 4 Mbps (1 km resolution) about 60 Mbps (250 m resolution)with dummy data
tilt angle	+20 degrees, 0 degree, -20 degrees

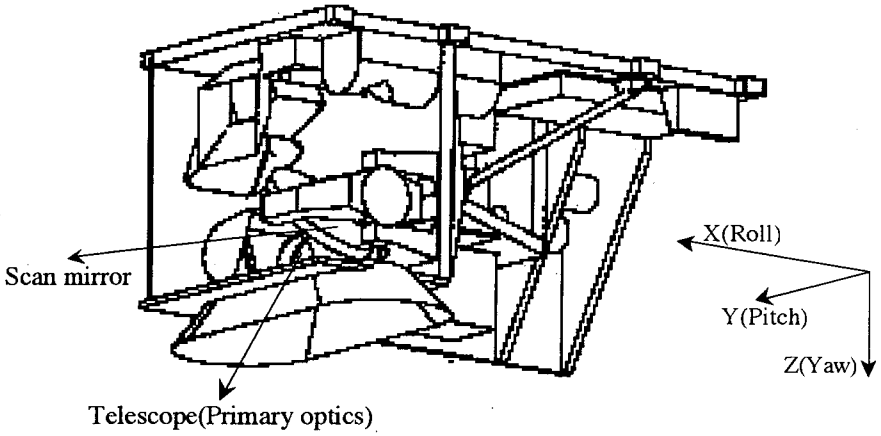

Figure.2.perspective view of GLI

3. SCHEDULE OF THE DEVELOPMENT OF GLI

Figure 3 illustrates the development schedule of ADEOS-II and core instruments which include GLI.

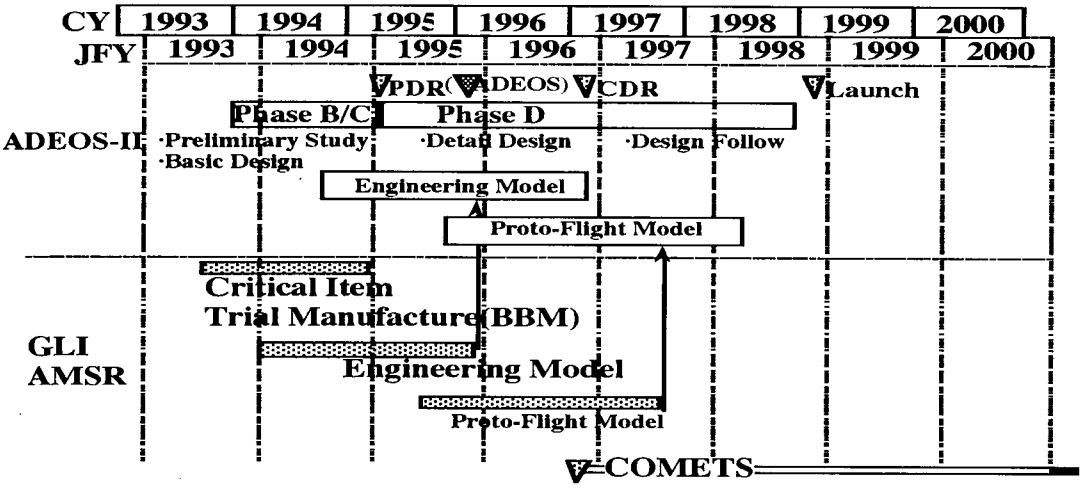

Figure.3. Schedule of the development of ADEOS-II and GLI ,AMSR

4.SUMMARY

The development of GLI is in progress. In April trial manufacture of critical items had been finished.

At present the basic design is being carried forward. The result of the trial manufacture are reflected in the decision of this design.

The manufacture of the engineering model(EM) will be started before long. GLI function and performance described above will be confirmed by the result of the test of EM. Moreover observation wavelength may be changed by the start of the manufacture of proto-flight model.

Land Cover Database of Asia

Ryutaro Tateishi and Wen Cheng Gang

Center for Environmental Remote Sensing, Chiba University
1-33 Yayoi-cho Inage-ku Chiba 263 Japan
Fax: +81-43-290-3857
Email: tateishi@rsirc.cr.chiba-u.ac.jp

Abstract

The Working Group on "1-km Land Cover Database of Asia" (LCWG) of the Asian Association on Remote Sensing (AARS) was established in October 1993. The WG consists of 49 members from 28 Asian and Oceanian countries. The present activity of the WG is to develop 8-km land cover dataset using NOAA/NASA Pathfinder AVHRR Land Data Set. The dataset will be completed early 1996. Land cover dataset with better resolution will be developed subsequently. This paper describes requirements of land cover data, land cover classification system, and classification methodology in the LCWG activity. Emphasis is placed on the development of land cover classification system.

1. Requirements of land cover data

The awareness of global environmental problems enforced us to prepare datasets of key environmental variables. Land cover data is one of them. As shown in Figure 1, there are two needs for land cover data: scientific needs and social needs.

As the scientific needs, main global change studies include (1) climate studies, (2)hydrological cycle, and (3)biochemical cycles and atmospheric chemistry. For climate studies, albedo and surface roughness (or canopy height) is important for the estimate of sensible heat flux. Information about vegetation (LAI) is one of the inputs for the estimate of latent heat flux. For the study of hydrological cycle, simple land cover classification of trees, shrubs, grassland, and bare soil is required. Information about vegetation such as LAI, percent cover, canopy height, and evergreen/deciduous is also one of the main inputs. For the study of biochemical cycles and atmospheric chemistry, land cover conversion such as biomass burning and functional land cover classification such as net primary product and nitrogen mineralization rate. In other words, land surface properties for global change studies, which can be derived from land cover, are albedo, surface roughness, physical quantities about vegetation, and part of soil type.

As the social needs, necessary land use information includes Built-up area, Agricultural land of various crops, Forest, and others. Different countries have different necessary land use information such as Production forestry, Horticulture (New Zealand), Coconut, Palm (Philippine), Wheat, Orchard (Jordan), Pasture (Mongolia), Rubber, Oil palm (Malaysia), Paddy (Sri Lanka).

Some land surface properties and some land use information can be derived directly from remote sensing data as shown in Figure 1. As required information are diverse due to various purposes, land cover data can act a common environmental variable from which further land information can be derived.

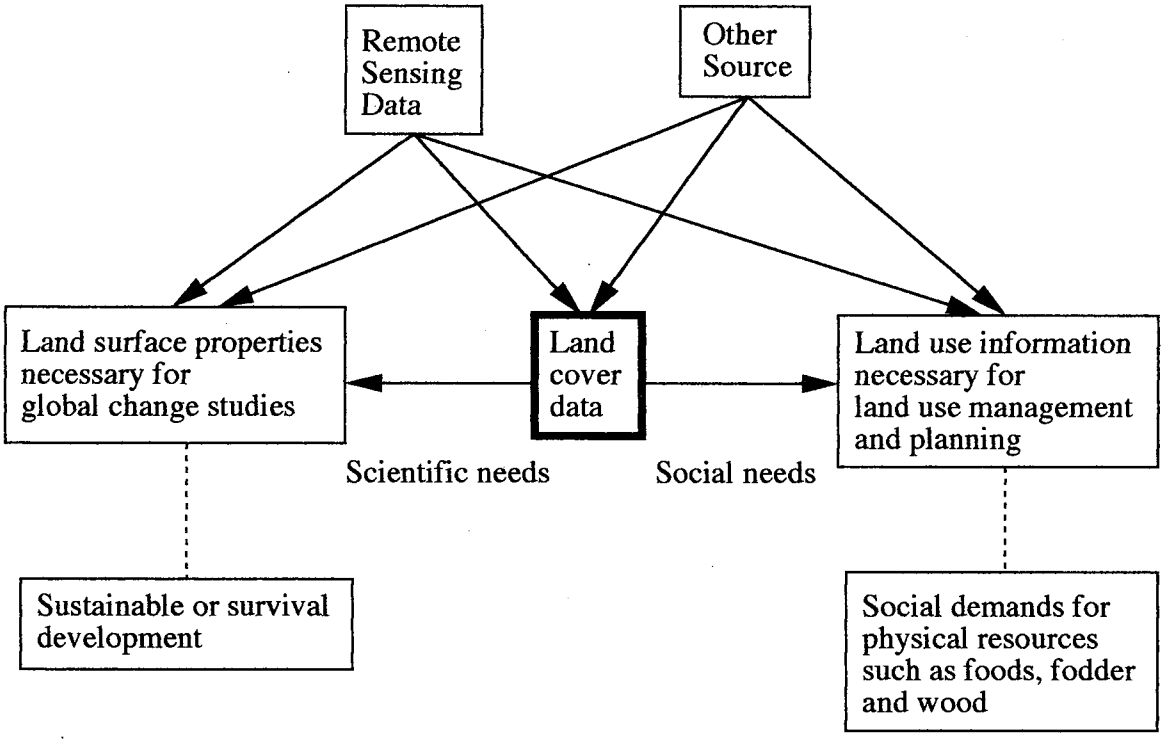

Figure 1 Requirements of land cover data

2. Land cover classification system

2.1 Background

One general problem of land cover classification system is that there are many kinds of legends in different countries and different projects. This fact prevents data exchange and integration. This is why UNEP/FAO has a project on harmonization of land cover and land use classifications. The goal of this project is to make clear the relationships among different land cover/use classification systems both within and between countries, both within and between applications, from national to regional to global scales (UNEP/FAO 1993). In the International Workshop on Global Databases, this problem was discussed (Tateishi 1995). One question in the discussion was "Is the standard land cover legend possible?" The answer was No because users community is diverse and there are a variety of needs for land cover. However it was suggested to get several standards for each of the users community. The important thing here is that a legend must reflect needs of users. It must be also noted that needs are not static. They will evolve over time.

2.2 Development of land cover classification system

The objectives of the production of land cover database of Asia by the LCWG, AARS are:

- First, global change studies (from scientific needs) and
- Secondly, land use management and planning (from social needs)

The Land Cover Working Group is developing new land cover classification system. Table 1((a) and (b)) is tentatively proposed land cover classification system. This system will be amended and finalized within a couple of months by considering comments from WG members. The basic concept of the proposed land cover classification system is described below.

Table 1(a) Proposed land cover classification system (LCWG, AARS) July 1995

Land cover class	Class code
Vegetation	10
Forest or shrubs	12
Evergreen	14
Forest	16
Broadleaf	18
Natural	20
Tree crops	22
Oil palm	23
Coconut	24
Others	25
Needleleaf	36
Shrubs	42
Natural	44
Shrub crops	46
Tea	47
Others	48
Forest and shrubs	60
Deciduous	70
Forest	72
Broadleaf	74
Natural	76
Tree crops	78
Rubber	79
Others	80
Needleleaf	90
Shrubs	92
Natural	94
Shrub crops	96
Cotton	97
Others	98
Forest and shrubs	110
Mixed forest or shrubs	120
Grassland	130
Natural grassland	132
Pasture	136
Agricultural land --- Grass crops	140
Paddy	141
Wheat	142
Sugarcane	143
Corn	144
Others	145
Mixed vegetation	160
Grassland and forest	162
Grassland and shrubs	164
Wetland	170
Mangrove	172
Swamp	174
Tundra	180
Non vegetation	190
Bare soil and rocks	192
Desert	194
Semi-desert	196
Rocks	198
Perennial snow or ice	210
Built-up area	212
Water	220
Inland water	222
Water with seasonal change	224
Tidal flat	226

Table 1(b) Explanation of land cover classes

Class code: Class name and Explanation

10: Vegetation
Vegetation but cannot be interpreted into any class from 12 to 180
12: Forest or shrubs
Forest or shrubs canopy cover is > 60%
14: Evergreen forest or shrubs
Canopy is never without green foliage. Evergreen canopy cover > 60%
16: Evergreen forest
Forest canopy cover is > 60%. Tree height is exceeding 2 meters.
18: Evergreen broadleaf forest
20: Natural evergreen broadleaf forest
22: Evergreen broadleaf tree crops
23: Oil palm
24: Coconut
25: Others
36: Evergreen needleleaf forest
42: Evergreen shrubs
shrubs canopy cover is > 60%. Tree height is less than 2 meters.
44: Natural evergreen needleleaf shrubs
46: Evergreen shrub crops
47: Tea
48: Other evergreen shrub crops
60: Evergreen forest and shrubs
10% < forest canopy cover < 60%
10% < shrub canopy cover < 60%
70: Deciduous forest or shrubs
With an annual cycle of leaf-on and leaf-off periods. Deciduous canopy cover > 60%.
72: Deciduous forest
Forest canopy cover is > 60%. Tree height exceeding 2 meters.
74: Deciduous broadleaf forest
76: Natural deciduous broadleaf forest
78: Deciduous broadleaf tree crops
79: Rubber
80: Other deciduous broadleaf tree crops
90: Deciduous needleleaf forest
92: Deciduous shrubs
Shrub canopy cover is > 60%. Tree height is less than 2 meters.
94: Natural deciduous shrubs
96: Deciduous shrub crops
97: Cotton
98: Other deciduous shrub crops
110: Deciduous forest and shrubs
10% < forest canopy cover < 60%
10% < shrub canopy cover < 60%
120: Mixed forest or shrubs
Neither evergreen nor deciduous forest or shrubs exceeds 60% of coverage.
130: Grassland
Tree and shrub cover is less than 10%.
132: Natural grassland
132: Pasture
Grassland for grazing
140: Grass crops
141: Paddy
142: Wheat
143: Sugarcane
144: Corn
145: Other grass crops
160: Mixed vegetation
Either 162 or 164
162: Grassland and forest
10% < forest canopy < 60%
10% < grass cover < 60%
shrub canopy < 10%
164: Grassland and shrubs
10% < shrub canopy < 60%
10% < grass cover < 60%
forest canopy < 10%
170: Wetland
172: Mangrove
174: Swamp
190: Tundra
192: Bare soil and rocks
194: Desert
196: Semi-desert
Desert with little vegetation
198: Rocks
210: Perennial snow or ice
212: Built-up area
220: Water
Either of 222, 224 or 226
222: Inland water
Lake, pond, river, reservoir
224: Water with seasonal change
Inland water with dry period
226: Tidal flat

The structure of land cover classification system

- Hierarchical
- Maximum number of possible land cover classes : 255

There are three policies to establish the land cover classification system.

(a) Harmonization with internationally accepted land cover class system
(b) Inclusion of Asian main land cover types
(c) Possibility to extend globally applicable classification system

For (a):
The objective of IGBP-DIS LCWG is to produce land cover data of the global land area for global change studies. This is the first attempt to produce global land cover data by remote sensing technique. The IGBP-DIS Land Cover Working Group has established land cover classification system based on Running's methodology (Running 1994). In this classification system, forest are divided into four main classes such as Evergreen Broadleaf, Evergreen Needleleaf, Deciduous Broadleaf, and Deciduous Needleleaf. These four classes are introduced to the proposed classification system.

For (b):
One of the main concern in land use management and planning in Asian countries is agricultural land. Therefore main crop types are included in the classification system.

For (c):
Since our classification system has hierarchical structure, new classes can be easily added up to 255 classes.

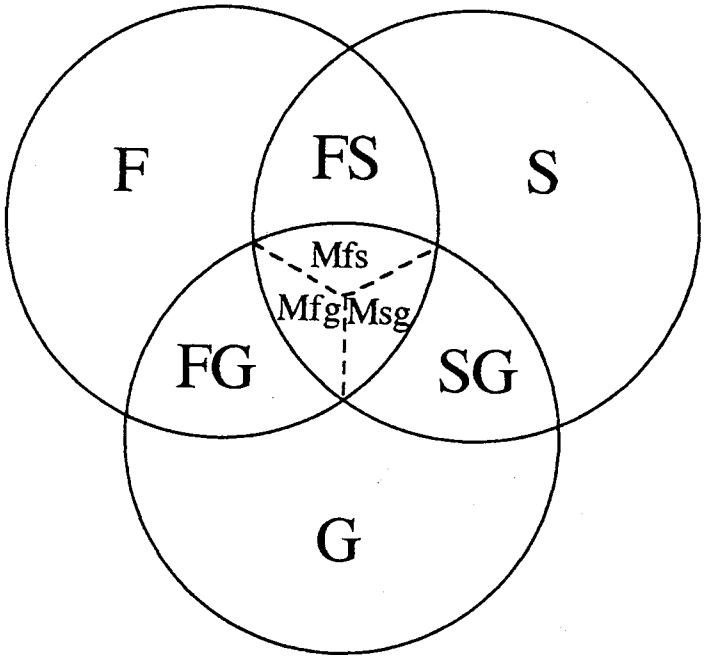

F: Forest
S: Shrubs
G: Grassland

FS: Forest and shrubs
FG: Forest and grassland
SG: Shrubs and grassland

FSG: Mfs + Mfg + Msg
Mfs: Forest, shrubs and grassland; with the least coverage of grassland
Mfg: Forest, shrubs and grassland; with the least coverage of shrubs
Msg: Forest, shrubs and grassland; with the least coverage of forest

"Forest or shrubs" (class code 12): **F + S + FS + Mfs**
"Grassland" (class code 130): **G**
"Mixed vegetation" (class code 160): **FG + SG + Mfg + Msg**

Figure 2 Forest, Shrubs and Grassland

Classification of Forest, Shrubs, and Grassland:
For the purpose of global change studies, the discrimination of vegetation into forest, shrubs, and grassland is important. Shrubs is small woody plants that are branched from the base. The IGBP-DIS LCWG uses the threshold value of 2 meter height to discriminate trees and shrubs. As shown in Figure 2, there are logically seven categories in the combination of forest, shrubs and grassland such as F, S, G, FS, SG, FG, FSG in the figure. Since the category of FSG is too detail, FSG is divided into Mfs, Msg, and Mfg and these three are combined to FS, SG, and FG, respectively. By this alternation, seven categories are reduced to six categories. Moreover, since the discrimination between forest and shrubs by AVHRR data is difficult, three categories, F, S, and FS are combined into a larger category, "Forest or shrubs". Similarly, FG and SG are combined into a larger category,"Mixed vegetation". Finally, seven categories in the figure are merged into three categories such as "Forest or shrubs (F, S, FS, and Mfs)", "Grassland (G)", and "Mixed vegetation (FG, SG, Mfg, and Msg)".

Agricultural land (Tree crops, shrub crops, and grass crops) is divided into "Forest or shrubs" class and "Grassland" class because the discrimination between agricultural land and natural vegetation by AVHRR data is more difficult than the discrimination between "Forest or shrubs" and "Grassland".

3. Classification methodology

The Pathfinder AVHRR Land Data Set with 8-km resolution was used for land cover classification. However source information for classification is not restricted to only AVHRR data. Any reliable information may be used for classification It includes national land cover maps and ground surveys.

The used Pathfinder AVHRR Land Data Set is 10 days composite data in 1990 (Agbu 1994). The Data Set has twelve bands consisting of NDVI, Cloud flag, Quality control flag, Scan angle, Solar zenith angle, Relative azimuth angle, Ch.1, Ch.2, Ch.3, Ch.4, Ch.5, Day of year.

10 days composite data of NDVI and Ch.4 (or Ch.5) were integrated to monthly data using cloud flag. The following features were derived from monthly NDVI and Ch.4 (or Ch.5) data. The second to fifth features are based on Loveland's (1994) method.

- Result of cluster analysis from NDVI
- Onset of greenness from NDVI
- Duration of greenness from NDVI
- Peak greenness from NDVI
- Total NDVI from NDVI
- Two phenological cycles from NDVI
- Seasonal temperature from Ch.4 (or Ch.5)

Ground truth data based on the land cover classification system is collected by WG members using their national land cover maps, the above seven feature images and other geographical data such as DEM. Key features to identify a specific land cover type is selected with the reference of ground truth data.

4. Concluding Remarks

Land cover classification system of Table 1 is not finalized. Any opinions about the proposed land cover classification system are welcome.

Acknowledgement

The authors would like to thank members of Land Cover Working Group of the Asian Association on Remote Sensing. The proposed land cover classification was developed by the cooperation of the members and it is being modified by considering their inputs.

References

Agbu,P.A. and M.E. James, " The NOAA/NASA Pathfinder AVHRR Land Data Set User's Manual", Goddard Distributed Active Archive Center, NASA, Goddard Space Flight Center, Greenbelt, September 1994

Loveland,T.R., J.W. Merchant, D.O. Ohlen, and J.F. Brown, "Development of a Land-Cover Characteristics Database for the Conterminous U.S., Photogrammetric Engineering and Remote Sensing, Vol.57, No.11, pp.1453-1463, 1994

Running,S.W., T.R. Loveland, and L.L. Pierce,"A Vegetation Classification Logic Based on Remote Sensing for Use in Global Biochemical Models", Ambio, Vol.23, No.1, 1994

Tateishi, R., C.Wen, and K. Perera,"Working Group Report and Land Cover Database of Asia", Proc. 15th ACRS, 17-23 Nov., 1994, pp.M-3

Tateishi,R.(Ed.), "Report of the International Workshop on Global Databases", International Archives of Photogrammetry and Remote Sensing, Vol.XXX, Part 4W1, Boulder, 30-31 May, 1995

UNEP/FAO, "Report of the UNEP/FAO Expert Meeting on Harmonizing Land Cover and Land Use Classifications", Geneva, 23-25 November, 1993

Remote Sensing Monitoring On Land Use Change In China

Wang Changyao

Institute of Remote Sensing Application,CAS
P.O.Box 9718,Beijing 100101,China

Abstract

Since 1978,China land use mapping has been started ,the scale of the map is 1 : 1000000. The work lasted more than 10 years. From 1980, a national project of land use survey in China has been implemented by using aerial photography at large scale in the county and province level. So far this project has not been completedyet. In order to study the land use change in period of 2–3 years,a project concerning the land use study has been conducted since 1992 by using Landsat TM acquired around 1990 and the mapping scale in east China and in west China are 1 : 250,000 and 1 : 500,000 separatly. After digitizing the land use maps, a land use data base for the whole territory will be established in 1995. For the typical area with great land use change, remote sensing montoring with large mapping scale in the period 1–3 year has been included. Meanwhile,the land use frequently monitoring has been taken using NOAA AVHRR data at resolution of 16 km,4 km and 1 km in the whole country.

1. Introduction

In today's world, rapid population growth, accompanied by food and resource shortages,as well as environmental degradation is threatening social and economic development. China's population is over one–forth of the total world population but its arable land per capital is much lower even than most developing countries. The population of China was 1.05 billon and its total cultivated area was only 98 million ha in 1983. That is to say ,the land per capital is 0.09ha. When 2000 comes ,the population will reach 1.3 billion, meanwhile,with the development of national economy,urban and industrial land expanding,the arable land has reduced year by year . The area of nonagricultural land will reach 10 million ha,and the area of badly degraded land will take 10% in whole territory of the conditions , such as the desertiffication land caused by unreasonable use, has increased by more than 1000km^2 each year . It is clear

that changes in land conditions and food supply have a significant influence on sustainable development .Recently, as the progress of China's opening and reforming, the structure and area of cropping has greatly affect the national ecorcomic development of our country.So the land use moitoring is very important in China.and the ability to obtain the information about the land dynamic timely and provide scientific decision–making.

1. Study on land use / land cover

The first national project on land use mapping was carried out in 1978 in China. The scale of the map is 1 : 1000,000.

The preparatory work started since 1978,and by 1981 sampling studies in all provines were launched,the compliling and mapping completed in 1988,the whole process lasted nearly 10 years.

The compiling of 1 : 1000,000 land use map of China was based on multiple informations,including sampling studies and route survey in each provine, interpretation of landsat images and air–photos,and facts gathered from large scale thematic maps.

From 1980, a national project of land use survey in China has been implemented by using aerial photography at large scale (1 : 100,000 in agriculture area) in the county and provine level. so for this project has not been completed yet.

In order to study the land use change in the period of 2–3 years, a project concerning the land use has been conducted since 1992.Main remote sensing data source is Landsat TM acquired around 1990. The interpretation mapping scale in east China and in west China are 1 : 250,000 and 1 : 500,000 separatly.After digitizing the land use maps ,a land use data base for the whole territory will be established in 1995.

To counter the demands of macro–investigation for results data and remote sensing characteristics, landuse and cover types was classified two classes including 6 first class types and 22 second types . In order to create environment classification system and further understand the relationship between land resource and geographical environment background,type boundary of basic geographical units will be drawn while remote sensing image is interpreted for land resource.Multi–attribute judgments of one unit are realized through matching remote sensing date with non–remote sensing data.The classification system is consisted of 43 types and two classes.(Tab.1and Tab.2)

Table.1 Macro–classofication system of land use / land cover

1. Farmland
   - 1.1 irrigated field
   - 1.2 non–irrigated field
2. Forest
   - 2.1 forest coverland
   - 2.2 shrub land
   - 2.3 other
3. Grassland
   - 3.1 high coverage grassland
   - 3.2 middle coverage grassland
   - 3.3 low coverage grassland
4. Water body
   - 4.1 river channel
   - 4.2 lake
   - 4.3 reservoir
   - 4.4 glacier and firn
   - 4.5 beach
5. Resident and Industrial Site land
   - 5.1 township
   - 5.2 industrial Land
   - 5.3 other
6. Others
   - 6.1 sandy land
   - 6.2 desert
   - 6.3 salinized alkaline
   - 6.4 marshland
   - 6.5 bareland
   - 6.6 bare rock gravel land

Table 2.China geographical environment basic unit classification system

A. Temperature

Classified 9 classes according to accumulated temperature index(> ° C)

B. Moisture Coefficient

Classified 5 classes based aridity

C. Geomorphological features

Four type is differentiated from geomorpholoical forms

1.Mountainous land

Four sub–types area divided according to relative elevation differcnces

2. Hilly land

Four sub–types according to elevation

3. Plat form

Four sub–types according to plat form altitudc

4. Plain

Seven sub–types according to relative elevation differcnces

D. Soil texturc

Sandy,loam,and fine soil are divided

The project was based on fully studying practicable technique routines. Landsat TM will be used as main information sources. Image interpreting work will be carried out according to the divided map sheets of international standard. Area measurement,graphic data input and creating information system will be finished at same time under the support of computer software and hardware environment.The main procedures is shown as Fig.1.

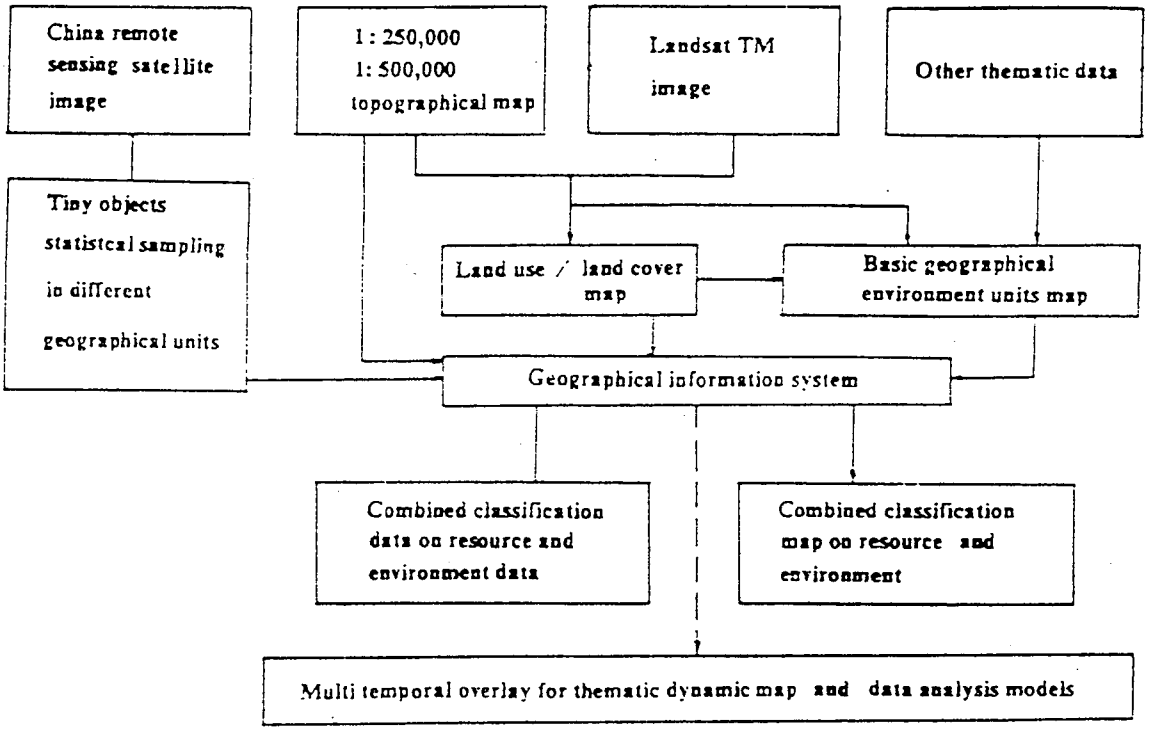

Fig. 1 The procedure of land use data base establishment

So far there are three levels of this data base in China. The first level of data base was established based on a series map at scale of 1 : 4,000,000.The layers included in data base are soil,vegetation,desert,desertification,drainage system,lake,railway,road,political boundary,etc., The development of second layer data base is on the way which is made based on a series map at scale of 1 : 1,000,000.The layer of the data base include landuse, land evaluation,drainage system,communication etc.The DEM data base is generated by the topographic map at scale of 1 : 1,000,000.

2. Study on land use change

The"Three Norths"protective forest system covers 13 privinces with a total area of 4.067 millon square kilometers. In order to evaluate the practical economic and ecologic benefits resulted from the huge investment in afforestation,the

prject of "Comprehensive Inventory and Moniroring of "Three Norths "Shelter Forest Region by Remote Sening Data" was put on the list of national key scientific and technical projects since 1986.

All the resource data needed were obtained and 1747 sheets of serial thematic maps were compiled on the scale of 1 : 100000, 1 : 2000000 and 1 : 5000000, including forest maps, forest site maps, grassland resource maps, land use maps, and land resource evaluation maps. Data analysis shows that forest coverage in the invesigated region raised significantly from 6.3% in 1977 to 8.43% in 1988, and the ecological environment in priority afforestation region has obviously improved. The construction of the "Three Norths" protective forest system really made tremendous achievements. At the same time, some problems were discovered, such as mono-speies afforestation, low survival rate of arbor forest in some of arid and semi-arid regions, insect and disease development in some regions. Especially, desertification is very seriously in the fragile zone. For instance, the desertification area increased by 9.36% from 1960 to 1987 in Yulin county.

The North China Plain along the Bohao Bay was selected as the study area on coastal changes and the project was performed by the Chinese Academy of Sciences. Nine Paleo-coastal lines since the Holocene Epoch have been determined throug processing and analyses of multi-temporal Landsat MSS, TM image data, and integrated analysis of remote sensing data, archaeological data, and lithosphere data.

Study shows that coastal change is a reflection of change in sea-level and global climate. The rate of shore line forward movement is uneven, for example, during the sea invasion of the Holocene Epoch(700 yrs. B.P.) the horizontal speed of sea water invasion was about 70-75km / 100yrs, the extent of invasion towards west was up to 150-160km. During the dry-cool time of paleo-climate(e.g.7800yrs. B.P., 5300yrs. B.P.,3800yrs. B.P.,200yrs. B.P.), sea levels dropped down, river brought a great amount of silt and sand which deposited in the plain and river mouth area and coastal lines moved towards the sea. In the map made in this study, it can be seen that the delta of the Huanghe River has moved 412km^{2}seaward from 1975-1985. The sea level change is very sensitive to climate change and will influence greatly human activities, especially in distribution of industry and agriculture in the coastal region.

As for land cover change we have used the IDRISI GIS software system(Eastman, 1992b) to run a series of 36 monthly AVHRR-derived NDVI images for China for the time period of January, 1986 to December, 1988. The data was extracted from the NOAA-EPA Monthly Generalized Global Vegetation Index data set which is part of the NOAA-EPA Global Ecosystem Data

Set (NOAA–EPA,1992).The images were in raster format and had a 10–minute resolution.

Using the standardized PCA, the first component created represented the mean annual vegetation pattern for China regardless of temporal change. Component 1 shows the characteristic vegetation cover found in China. Vegetation is most sparse in the west ,especially in the Tarim Basin, and then the Gobi Desert and Ordos Plateau to the north. Vegetation as depicted by NDVI is more dense in East China, though areas of low NDVI in the East are areas of population centers as well as open water. Of interest in the low NDVI over the Sichuan basin, and area of intensive agriculture. Although this area has a high population density, the low NDVI may be from the high humidity and frequent fog–cover over the region , lowering the NDVI recorded by the NOAA satellite. The greatest NDVI comes from the tropical regions of southern Yunnan and Hainan island. Because component 1 explains the greatest variation in the temporal data set, and the resulting component depicts the typical vegetation pattern for China, this indicates that the major element of element of variability in NDVI is that which occurs spatially.

Concerning the component loadings, figure graphs the component loadins for component 1 and shows that the original 36 images all correlate very highly with Component 1. Briefly, the loading chart illustrates the correlation betweeneach of the 36 monthly images and the cmmponent being diagramed. For example, the pixels of the component image with a positive correlation

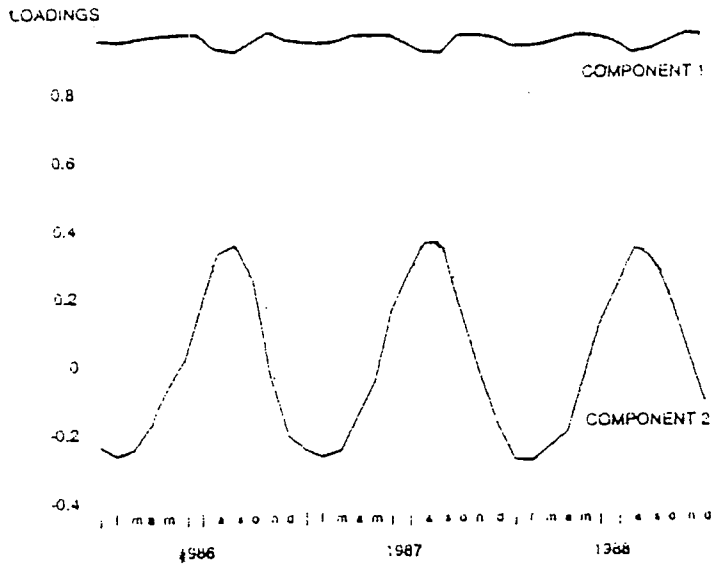

Fig 2. Loading cart of component 1 and 2

have a similar monthly variation (more overt in earlier components than in later ones) as indicated by the component loadings. Pixels which are negatively correlated tend to have anopposite motly variation as indicated by the component's loadings. Another way of explaining the loading is ,according to Eastman and Fulk(1993), if a month shows a strong positive correlation with a specific component, it indicates that that month contains a latent (to some extent a hidden or unapparent)spatial pattern that has a strong similarity to the one depicted in the component image. Similarly, a strong negative correlation indicates that the monthly image has a latent pattern that is the inverse of that shown.

To demonstrate this concept component 2 shows a strong positive correlation in the northeast of China, and a strong negative correlation in the Southwest, with much of the country in between the positive and negative correlations, though statistically most of the country is more positively correlated. The loadings for component 2 show a high correlation in the summer months and a low correlation in the winter months. What this indicates is that the next greatest change after component 1 is the temporal change caused by the changes in seasons from summer to winter.

3. Conclusion

As part of the world ,China also confronts with the seriousness of resources and environment problems caused by human activities and the change of natural conditions. It is important for China, to pay more attention to the study of global change and to enhance international cooperation in the field, so as to adjust the policy of economic development in the process of modernization in the country.

4. Reference

〔1〕 Eastman , J.R., and Fulk ,M.1993. Long time series evaluation using standardized principal components. Photogrammetric engineering and Remote Sensing. 59(6):991–996.

〔2〕 Liu Jiyuan (1993)″ Remote Sensing Invstigation and Dynamic Study on Resources and Environment in China .″, Presented at the 25th International Symposium, Remote Sensing and Global Cange, Graz, Austria, 4–8 April 1993.

〔3〕 Xu Guanhua(1990), The comprehensive inventory and montioring of forest and other renwable natural resources by means of remote sensing data in the ″Three Norths ″ Shelter Forest Region, space and Forest Management, Special Current Event Session, 41st IAF Congress, PP.11–22.

Use of satellite imagery to map and monitor vegetation in New Zealand

P. R. Stephens, J. R. Dymond and L. J. Brown
Landcare Research
Private Bag 11052
Palmerston North
NEW ZEALAND
Fax: +64 6 355-9230
E-mail: stephensp@landcare.cri.nz

Abstract

Land resource and environmental decision makers require quantitative information on the spatial distribution of vegetation types and their condition, and changes in these over time. Such vegetation mapping and monitoring is often required to be undertaken quickly. Remotely-sensed satellite imagery, in conjunction with other data sources, have been used to satisfy this need.

This paper describes the uses of satellite imagery by reference to three regional mapping projects in New Zealand. The first project describes the use of Landsat TM imagery to map forest, scrub, pastural and cropping vegetation types. The second project concerns the innovative use of SPOT imagery, colour infrared aerial photography and ground observations to map percent vegetation cover for a degraded rangeland. The remaining project combines NOAA AVHRR imagery with daily dairy farm production data, as a means of monitoring sustainability and productivity of pastoral land use.

1.0 Introduction

In New Zealand the concept of environmental monitoring and land-use sustainability feature prominently in legislation, namely the 1991 Resource Management Act (RMA), and policy (Ministry for Environment 1995). The RMA requires local government natural resource management agencies to ensure that land use is sustainable, and that any effects of land use practices are environmentally acceptable. To aid RMA compliance with respect to sustainable land management, land resource and environmental decision makers require quantitative information on vegetation types and condition, and changes in these over time.

Satellite imagery is ideally suited to the task of quickly providing vegetation information over large areas (Congalton *et al.* 1993, Townshend 1992, Ehrlich *et al.* 1994). Since 1982, imagery has been available in which a substantial proportion of the main vegetation types can be mapped and monitored, especially in rural areas. Principal sources of data include the high spatial resolution imagery from Landsat's Thematic Mapper (TM) and SPOT's High Resolution Visible (HRV) sensor. Numerous examples of applications of these data can be found in the literature: tropical forest classification in Mexico (Garcia and Alvarez 1994); monitoring forest defoliation by insects in the USA (Muchoney and Haack 1994); agricultural land use classification in France (Hill and Megier 1988); mapping vegetation changes on a coastal environment in New Zealand (Wilde 1992); and monitoring and modelling semi-arid landscape responses to climate

change in the USA (Yuhus and Goetz 1994). For these applications the detailed view provided by the TM and SPOT HRV sensors has been essential. In parallel with the expanding range of land resource applications of these data, there has, in recent years, been interest in the use of coarse spatial resolution data from sensors such as the National Oceanographic and Atmospheric Administration (NOAA) Advanced Very High Resolution Radiometer (AVHRR). Due to their daily coverage, synoptic overview and (low) data volumes AVHRR data are used increasingly for global and regional land-cover studies principally(Ehrlich *et al.* 1994).

This paper describes the uses of satellite imagery in New Zealand for environmental and land sustainability purposes, by reference to three regional projects (see Fig 1). The first project describes the use of Landsat TM imagery and ancillary data from a geographic information system (GIS) to map forest, scrub, pastural and cropping vegetation types (see Section 2.0). The second project concerns the innovative use of SPOT imagery, colour infrared aerial photography and ground observations to map percent vegetation cover for a degraded rangeland (see Section 3.0). The remaining project (Section 4.0) combines NOAA AVHRR imagery with daily dairy farm production data, as a means of monitoring sustainability and productivity of pastoral land use.

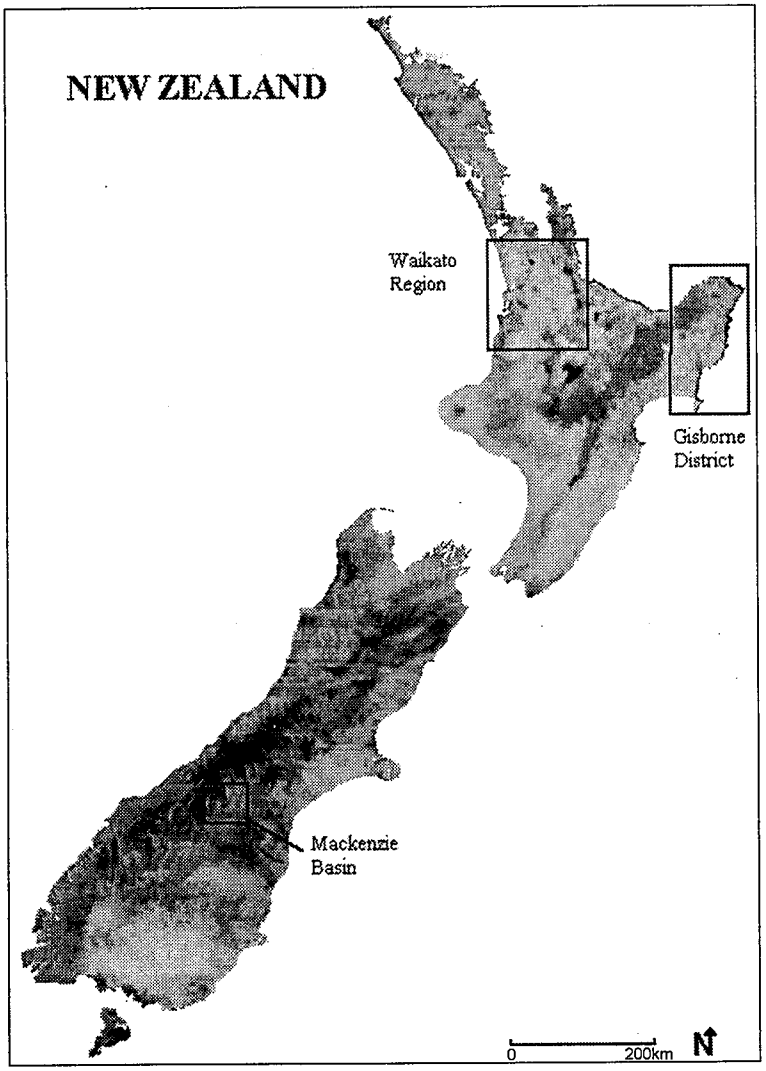

Figure 1. NOAA-11 monthly composite vegetation index image of New Zealand showing location of the three regional project sites.

2.0 Large area vegetation mapping using Landsat TM imagery

National and local debate over a Government-sponsored forestry scheme, designed to prevent erosion in the 830 000 hectare Gisborne district (see Fig 1), highlighted the need for up-to-date information on vegetation cover. Some of the debate concerned a major landowner wanting to take advantage of monetary incentives to convert erosion-prone land to production forestry. Much of the land was in various stages of reversion to original indigenous forest, and environmental groups argued that the incentive scheme should not be applied in this case as the reverting vegetation cover already prevented erosion. To help resolve this issue, land management policy makers wanted up-to-date, quantitative information on vegetation cover in the district, with a special focus on areas of reversion characterised by kanuka (*Kunzea ericoides*) and manuka (*Leptospermum scoparium*).

Four maps of vegetation, at a scale of 1:100 000, were produced by automatically classifying January 1993 Landsat TM imagery. By reference to information from earlier vegetation surveys, 100 training polygons were used to characterise spectral signatures. A maximum likelihood classifier was used on all seven TM bands to map eleven vegetation types. To identify gross classification errors, the classified imagery was compared with a rasterised version of existing vegetation information from a geographic information system (GIS) database. The existing vegetation information was 20 years old. Through field checking the discrepancies were confirmed as either real (changes) or errors in classification. Correction of the errors increased the overall classification accuracy from 84 per cent to 90 per cent (Dymond *et al.* in press).

In addition to the vegetation maps, land planners also required information on the distribution of vegetation according to land use suitability. The vegetation maps were intersected with land suitability data from a national land resource inventory GIS database (Eyles and Newsome 1990), and the areas of each vegetation class on three critical types of land suitability were calculated (see Table 1). Although 90 per cent accuracy is high enough to permit the calculation of vegetation areas and to achieve an adequate representation of regional vegetation patterns, it is not considered high enough to permit the digital vegetation map to be used as a vegetation database where point queries are important, as approximately 10 per cent of the point queries would be totally wrong. Errors associated with point queries should be less than 5 per cent, ideally less than 2 per cent. In such cases, detailed field surveys of vegetation would be required.

3.0 Mapping changes in percent vegetative cover using SPOT imagery

The semi-arid Mackenzie Basin in the central South Island (see Figure 1) has significant land degradation attributed to drought, an explosion in rabbit numbers, and overgrazing by sheep (Cuff and Dymond 1994). A Rabbit and Land Management Programme was introduced by Government as the institutional response to these environmental problems. Monitoring systems were required to determine the effectiveness of this programme. Indicators of change have been rabbit numbers and traditional vegetation surveys undertaken annually at a large number of sites (c. 300). Remotely-sensed satellite data have also been used as a means to monitor regional vegetation changes.

Vegetation class	Land suitable for pastoral farming	Land suitable for conservation farming or production forest	Land suitable for protection forest
Fernland	170	1160	150
Kanuka/manuka	18700	38900	2140
Secondary forest	10500	16500	2460
Podocarp forest	120	120	0
Primary forest	20000	36700	35800
Beech forest	2900	7300	9900
Subalpine vegetation	90	150	870
Exotic forest	28500	76800	3100
Pasture	239600	227800	6100
Bareground	14900	7900	1340
Water	50	0	6
Undefined	2310	14700	110

Table 1. Areas in hectares of vegetation classes on land suited for three critical land uses in the Gisborne district.

Dymond *et al.* (1992) developed a technique, using SPOT multispectral imagery, to map percent vegetative cover in the Mackenzie Basin. This technique relied on the establishment of a relationship between normalised difference vegetation index (NDVI) and percent vegetative cover. This relationship was derived from ground cover measurements from 20 60m x 60m quadrats which represented the soil and vegetation patterns in the basin. Specially flown colour infrared aerial photographs, which covered the quadrats, were used to locate the quadrats in the SPOT images. The relationship between NDVI and percent vegetative cover was expressed as a simple non-linear calibration curve (see Fig 2)

$$C=50\tanh(6.1(NDVI-0.22))+50$$

where C is percent vegetative cover and tanh (x)=(expx-exp(-x))/(expx+exp(-x)). The spread of the quadrat points about the calibration curve gives the accuracy of a percentage vegetative cover predicted from the NDVI. In the linear part of the calibration curve, the upper and lower prediction limits (80 per cent confidence interval) are ±15 per cent cover.

Using this technique, Cuff and Dymond (1994) mapped percent vegetative cover in the basin, for 1987 and 1990. The February 1987 imagery was SPOT multispectral, and the January 1990 imagery was Landsat TM. Comparison of the 1987 and the 1990 percent vegetative cover images was used to produce a 1:50 000 scale land cover change map. Analyses of the satellite images provided overall trends in vegetative ground cover as well as the ability to determine the change at the pixel level. An assessment of the change indicated a four per cent decrease in overall vegetative cover, which was consistent with the perceived decline in land condition during this period. This confirmed the usefulness of this satellite technique to provide an overview of vegetative cover changes.

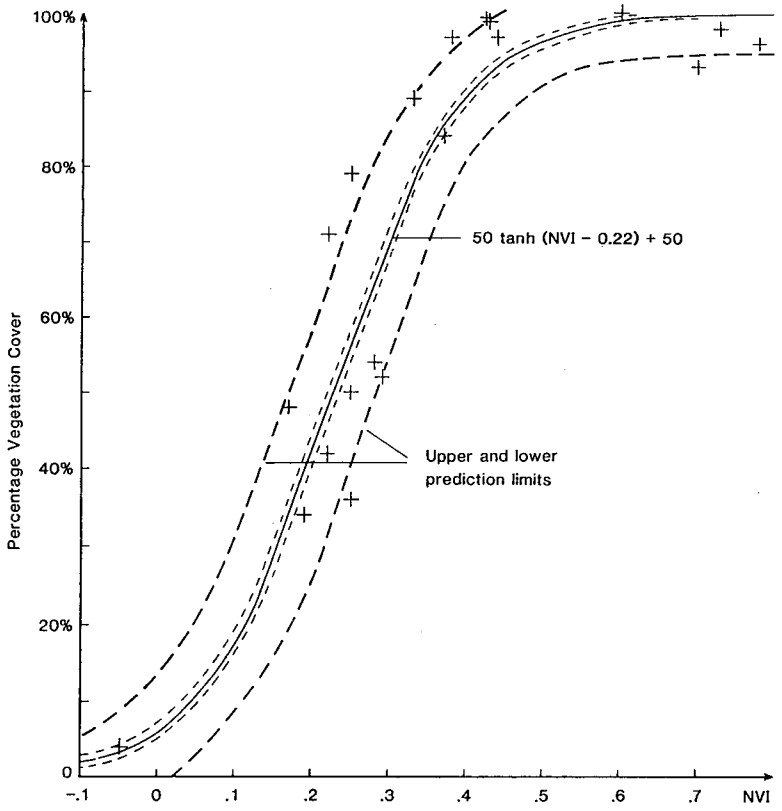

Figure 2. Calibration plot of per cent vegetation cover versus NDVI. Crosses indicate quadrat plotting positions.

4.0 AVHRR imagery to monitor sustainability and productivity of pastoral land use

A number of land management and environmental agencies in New Zealand are concerned about land-use sustainability. The productive capacity of the land is inescapably linked to its biophysical condition. The condition of vegetation - its biomass and photosynthetic activity - provides a direct measure of biophysical sustainability in managed environments. NOAA AVHRR data have been used to improve the monitoring of vegetation condition and productivity (Brown and Stephens 1995). Containing a large number of dairy farms, the Waikato region (see Fig. 1) was used for the project.

The use of NOAA AVHRR data in agricultural studies gives rise to two problems: the large ground area covered by each pixel relative to field size, and the collection of adequate ground data. In this study, actual pasture productivity was not measured directly. Instead, daily milkfat production from dairy farms was used as a productivity surrogate. The use of milkfat production data provides a temporal and spatial resolution that cannot be logistically obtained by pasture-cut samples. As dairy farming operations in New Zealand are usually located in extensive areas of contiguous pastoralism, the pixel size versus size of land unit problem is overcome.

The AVHRR imagery was transformed to radiance, corrected for atmospheric effects using the 5S code (Tanré *et al.* 1987), and resampled to 1km spatial resolution. An NDVI image was then calculated. Images of AVHRR channels 1 and 4 were also produced for a cloud identification procedure. In this procedure, images having a thick cloud layer are visually identified and discarded. For the remaining imagery, study sites (within the Waikato region) were rated for

the effects of scattered cloud using the range in channel 1 pixel values as the criterion. A mean NDVI was then determined for each site, for each cloud-free day, and plotted against milkfat production (see Fig 3). For the 1992/1993 lactation, milkfat production and NDVI exhibited a similar pattern in the study sites - both peaking in Spring and declining over Summer, with two other smaller plateaus and rises (attributable to rainfall events). These results show a probable causal relation between the AVHRR-derived NDVI and milkfat production. Farm production models will be needed to quantify the relationship further. We are presently using successive years NOAA AVHRR data to improve the relationship between pasture and milk production, in order to monitor land productivity. This work also involves partitioning the AVHRR imagery with ancillary GIS data, with which homogeneous land cover types are identified.

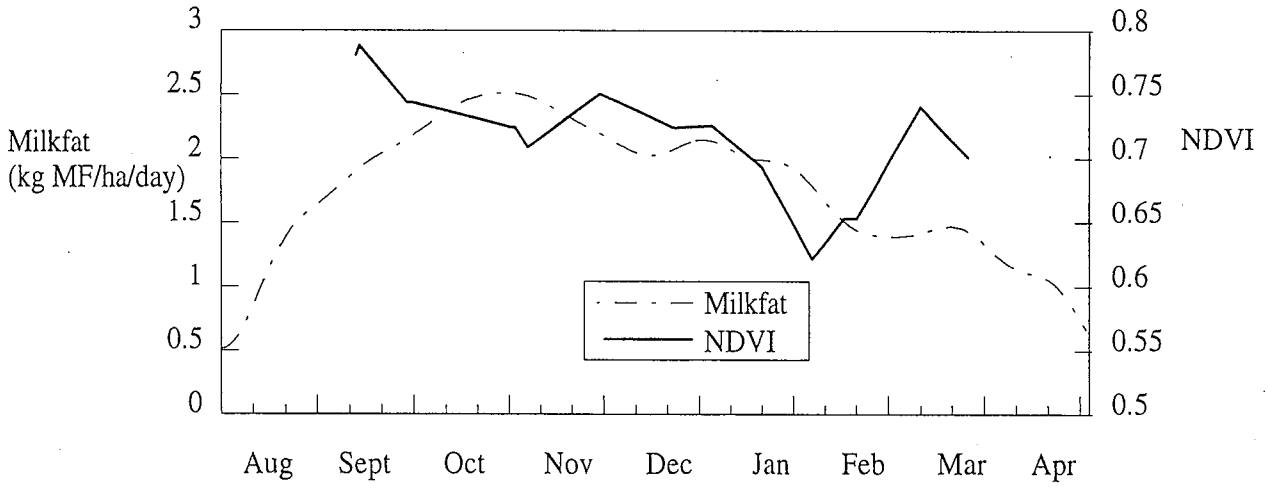

Figure 3. Milkfat production and NOAA NDVI for the 1992-93 lactation for one of the sites in the Waikato region.

5.0 Summary

In these three vegetation mapping projects, remotely-sensed satellite imagery, in conjunction with other data sources, has been used to help land resource and environmental decision makers in New Zealand who have required quantitative information on vegetation types and condition, and changes in these over time.

A range of ancillary data sources was used to help classify and calibrate satellite imagery. The data used varied according to the nature of environmental issue; the availability and form of existing data; the time frame for the project; the availability and spatial and temporal resolution of remotely-sensed imagery; and the type of information required for land resource and environmental planning.

SPOT and Landsat TM images are suitable for providing vegetation baseline and vegetation change information in a quantitative manner. Mapping scales range from 1:50 000 to 1:100 000. However, the timeliness of information delivery depends on availability of suitable imagery: New Zealand does not have an earth resource satellite receiving station, so is presently dependent on the SPOT tape recorder to obtain high spatial resolution data. TM data has not been available since 1994.

Errors associated with such vegetation mapping are acceptable for calculating vegetation areas and achieving an adequate representation of regional vegetation patterns and changes, but are too high to produce databases where point queries are important. NOAA imagery requires additional pre-processing (atmospheric correction, cloud-removal and compositing (over durations of 10-30 days)) before it can be considered useful for regional and national monitoring of the sustainability and productivity of pastoral land use.

Despite the issues of mapping accuracy and imagery availability in New Zealand, the use of remotely-sensed satellite imagery provides the only cost-effective means to obtain useful land cover data for large areas. The promise of soon-to-be-launched satellite systems with sensors recording in the visible, near infrared and mid-infrared, and with on-board tape recorders augurs well for the future operational use of remotely-sensed data for vegetation mapping and monitoring.

6.0 Acknowledgments

Much of the research reported here was funded through the New Zealand Foundation for Research, Science and Technology contracts CO9222 and CO9419. We gratefully acknowledge the assistance of the following agencies: AnchorProducts NZ Ltd, Livestock Improvement, Ministry of Forestry, Department of Conservation, Canterbury Regional Council, Gisborne District Council, and Hikurangi Forest Farms.

7.0 References

Brown, L.J., P.R. Stephens, "Monitoring pasture productivity in New Zealand - an investigation using NOAA-11 AVHRR data and dairy farm milk fat production", *International Journal of Remote Sensing*, Vol 16(5), pp.967-972, 1995

Congalton, R.G., K. Green, and J. Tepley, " Mapping old growth forests on national forest and park lands in the Pacific Northwest from remotely sensed data", *Photogrammetric Engineering and Remote Sensing,* Vol 59, pp.529-535, 1993

Cuff, J.R.I., J. Dymond, "Satellite data to map changes in vegetative cover in the Mackenzie Basin", Proceedings 4th National Remote Sensing and GIS Workshop, April 7-8 1994, Landcare Research, Palmerston North, pp.55-64, 1994

Dymond, J., P.R. Stephens, P.F. Newsome, and R.H. Wilde, "Percentage vegetation cover of a degrading rangeland from SPOT", *International Journal of Remote Sensing*, Vol 13 (11), pp.1999-2007, 1992

Dymond, J.R., M.J. Page, and L.J. Brown, "Large area vegetation mapping in the Gisborne district, New Zealand, from Landsat TM", *International Journal of Remote Sensing*, in press

Ehrlich, D., E. Estes, and A. Singh, "Applications of NOAA-AVHRR 1 km data for environmental monitoring", *International Journal of Remote Sensing*, Vol 15(1), pp. 145-161, 1994

Eyles, G.O., P.F. Newsome, "A decade of experience of using a New Zealand GIS", *New Zealand Geographer,* Vol 46, pp.43-47, 1990

Garcia, M.C., R. Alvarez, "TM digital processing of a tropical forest region in southeastern Mexico", *International Journal of Remote Sensing*, Vol 15(8), pp.1611-1632, 1994

Hill, J., J. Megier, "Regional land cover and agricultural area statistics in the Department Ardeche, France, by use of Thematic Mapper data", *International Journal of Remote Sensing*, Vol 9, pp.1573-1596, 1988

Ministry for Environment, "A sustainable land management strategy for New Zealand. A discussion paper", New Zealand Ministry for the Environment, Wellington, 21p., 1995

Muchoney, D.M., B.N. Haack, "Change detection for monitoring forest defoliation", *Photogrammetric Engineering and Remote Sensing*, Vol 60 (10), pp.1253-1251, 1994

Tanré, D., C. Deroo, P. Duhaut, M. Herman, J.J. Morcrette, J. Perbos, and P.Y. Deschamps, "Simulation of the satellite signal in the solar spectrum (5S)", Laboratoire d'Optique Atmosphérique, Université des Science et Techniques de Lille, Cedex, France, 1987

Townshend, J.R.G., "Land cover", *International Journal of Remote Sensing*, Vol 13 (6 & 7), pp.1319-1328, 1992

Wilde, R.H., "Mapping changes in vegetation and bare ground from historical aerial photographs and satellite imagery", Proceedings of 6th Australian Remote Sensing Conference, Wellington, New Zealand, Vol 2, pp.108-119, 1992

Yuhus R.H., A.F.H. Goetz, "Monitoring and modelling semi-arid landscape response to climate change", Proceedings 1994 International Geoscience and Remote Sensing Symposium, California, USA, August 8-12, Vol 2, pp.1036-1038, 1994

USING THE REMOTE SENSING TECHNIQUE TO ESTABLISH A LANDUSE MAP IN VIETNAM ON SCALE 1:1.000.000.

Prof. Nguyen Thuong Hung.
NATIONAL CENTRE FOR NATURAL SCIENCES AND TECHNOLOGY OF VIETNAM (NCSTV).

Remote sensing technique have been using for establishing of landuse map on differece areas of Vietnam. This report will discuss about the result of this work which had been carried out for mapping on scale 1:1,000,000 for all territory of Vietnam after each 5 years.

I. SOURCES OF DATA:

* LANDSAT TM imageries FCC, scale 1:100,000, 1:250,000, (all territory), 1:100,000 for several parts.
* SPOT imageries of some key areas: Red river delta, Mekong river delta, middle part area of Vietnam. (date 1990)
* Landsat tape of landsat V on Red river delta, Mekong river delta (date 1989).
* Documents of the institute for forestry planning and investigation.
* Documents of the institute for agriculture planning and management.
* Imageries of NOAA and MOS I satellites (date 1993).

II. METHODOLOGY:

* Visual interpretation by specialists of institutes as: geography agricuture, forestry, cartography.
* Digital processing for some trainning areas (with software such as: PERICOLOUR, ERDAS, ACR/VIEW, ILLWISS...)
* Grouth truth collection on training areas and fastly checking.
* Comparing with documents of departments for land management.
* Cartographical methods: correction, location, coordinate transformation
* Classify ofjects base on categories of different map scale.

III. PRINCIPLES FOR ESTABLISHMENT OF LAND USE MAP:

`III.1 Establishe legend of the map:

* Principle for: establish legend which corresponding to map scale and suitable with study method.
* Requirement:
  - Fully reflect landuse units of the territory correspording to map scale and suitable to the National landuse clasification legend.
  - Express capacities for recognization, clasification difference objects on remote sensed data.

III.2 Map drawing:

- Reflect high- detailly with map contours and correct to the coordinate UTM map- net.
- Colour system is suitable to the traditional principles of the land use map.

III.3 Establish the commentary of the map:

- Adequate statistic the area and distributted characteristic of land use unit for each part of the territory administrative zone or district.
- Interpretation and comparate to the previously data for changing assesement of essentical landuse units.
- To point out corcerned problems of land using and propose resolutions to the management offices for the purpose that land will be suitable investigated and stability development.

IV. RESULT OF STUDYING:

IV.1 Map content:

Land units on the map have been distinguished to 4 groups and 25 units as follow:

100. Agriculture land
   - *110. annual cultivated land*
     - 111. crop land
     - 112. pasture and interative agriculture land
   - *120. Longtime plantation land*
     - 121. pasture and industrial plant
     - 122. shifting cultivated land
     - 123. orchard land
     - 124. other long-time plant

130. Other land

131. grass- brush land

132. water surface (lake and pond)

200. Forestry land

210. Evergreen forest

211. dence evergreen forest

212. average evergreen forest

213. sparse evergreen forest

220. Decidous forest

230. Mixed forest

240. Pointed leaves forest

250. Growth forest

260. Mangro forest

300. Special use land

310. constructed land and human settlement area

320. salt field

330. seage field

340. other specially land

400. Barren land

410. exposed rock

420. sand and gravel other than beaches

430. beaches

440. natural surface water

450. other non vegetated wetlands

Remark: By principle, detail level of the map: Contours with area of 5mm^2 are separated (corresponding to the area of 2,5 ha on ground). But, due to mixed condition between cultivated land and settlement areas on delta region, and on other, in mountain region, due to complicated condition of forest land, detail of contour will not be followed the principle carefully. That means, contour of land use units in these regions had been generalized, but still present correctly for natural condition.

IV.2 Characteristic of distribution and changing of land use

* Distributed characteristic of land use units:
  Calculation on the land use map of scale 1:1,000,000 land use distribution can be show on the below table (on next page).
* Changing of the landusing during recent 5 years:
  Comparize with documents of several years since 1985, 1989 and existing condition, landuse changing in Vietnam as follow:

- Forest land and humansettlement areas have been changed in all of regions of Vietnam, especially in the central plateau, East South region, middle part coastal zone.
- In forest land, growth forest area have been enlarged fastly, especially in low land and hilly land of the North and middle part.
- In present, bare land have been restricted but it is still rather large (41,24%) of the total territory.

It is the area for alot of problems of land used plant in Vietnam such as: reforestation, management and improving improverished soil, investigation wetland areas, catchment management...

Land use condition up to the year 1994

(unit :1,000 ha)

region	natural area	land is being used				barren land
		agriculture land	forest land	special use land	settlement area	
- Mountain and hill on North part	10297	1326	2175	245	220	6331
- North part delta (Red river delta)	1251	695	59	225	115	157
- North middle part	5118	701	1570	162	97	2588
- Coastal zone of middle part	4578	521	1620	152	105	2180
- Central plateau	5557	725	3450	115	82	1385
- East part of the South	2345	1036	562	197	168	382
- Mekong river delta	3956	2790	170	192	175	629
Total	33102	7594	9606	1288	962	13652

CONCLUSION:

- Using aerial photography, checking in training areas, interpretation with difference remoted sensed data: KOSMOS, LANDSAT, SPOT, NOAA, MOS I, IRS... give capacity of having hightly correction on the landuse mapping.
- Using difference remote sensing data give a facility method to fastly management landuse process. This work is very useful and have been publicized for land use mapping in difference scale: it will be more useful if we have multitemporal data, multidata... but, it is the most difficult for us in present.

LAND COVER ASSESSMENT AND MONITORING AT UNEP/EAP-AP: A RS AND GIS APPROACH[1]

Chandra P. Giri
Surendra Shrestha
UNEP Environment Assessment Programme-Asia and Pacific
P.O. Box 2754, Bangkok 10501, Thailand
Tel: (66-2) 524-5365
Fax: (66-2) 516-2125
Email: GRID@cs.ait.ac.th

Abstract

The paper presents a synopsis of Land Cover Assessment and Monitoring Project of UNEP Environment Assessment Programme for the Asia and Pacific. The project, covers eleven countries in the region and is expanding every year, utilizes remote sensing and GIS techniques to assess and monitor land cover status of each country on a regular basis.

The broad goal of the project is to assess the present status of major land cover types of target countries using NOAA AVHRR 1 Km resolution satellite data incorporating secondary information within GIS environment. The principal purpose is to assess and monitor the land cover status of these countries in a near real time basis. It also aims to develop a methodology, strengthen the capacity of the government, train the personnel and ultimately hand over the technique to the respective countries. In the long run, it is expected that the target countries will do the similar exercise as a part of their regular land cover assessment and monitoring exercise. The role of UNEP/EAP-AP will then be to compile the data for macro analysis and reporting at the regional scale, provide technical and financial assistance and information transmission from national to regional to global and vice versa.

Another aspect of the study is to identify "hot spot" (i.e. areas undergoing major land cover transformations) areas and investigate in detail, using high resolution satellite data supplemented by field data collection.

[1] Paper presented at the " International Symposium on Vegetation Monitoring" 29-31 August, 1995, Tokyo, Japan.

Introduction

In reflection of change in kind, quantity and quality of information needed for decision makers and policy planners, UNEP through its new Environment Assessment Programme which includes GEMS (Global Environment Monitoring System), GRID (Global Resources Information Database), SoE (the State of the Environment unit) and UN system-wide Earth-Watch Coordination, focuses more on the need and capabilities of its users. As envisaged in Agenda 21 of UNCED for the need of enhanced accessibility of integrated environment and development information and enhanced national capacity to deal with such information in decision making and policy setting, UNEP has focused its attention to provide the world community with improved access to meaningful environmental data and information, and to help increase the capacity of governments to use environmental information for decision making and action planning for sustainable human development. The programme has four programme components namely assessment an reporting, data and information management, capacity building and servicing and UN system-wide Earthwatch coordination.

In line with above goals, UNEP Environment Assessment Programme for Asia and Pacific (UNEP EAP-AP), has been involving in various undertakings including the Land Cover Assessment and Monitoring of selected countries in the region.

The Project and its Rationale

Human induced land cover change occurring at an unprecedented rate and scale particularly that of forest cover change is one of the major environmental concern in the region. Such changes contribute towards the change in climate and conversely the ecosystem is subjected to the changing environmental conditions. An accurate and up-to-date information base on the status and change pattern of land cover dynamics at multi-level (national, regional and global) is pre-requisite for the sustainable management of natural resources as policy decisions are made at different levels and issues and priorities vary accordingly (Fig. 1).

Fig.1 Multi-scale information need for priority setting at different levels

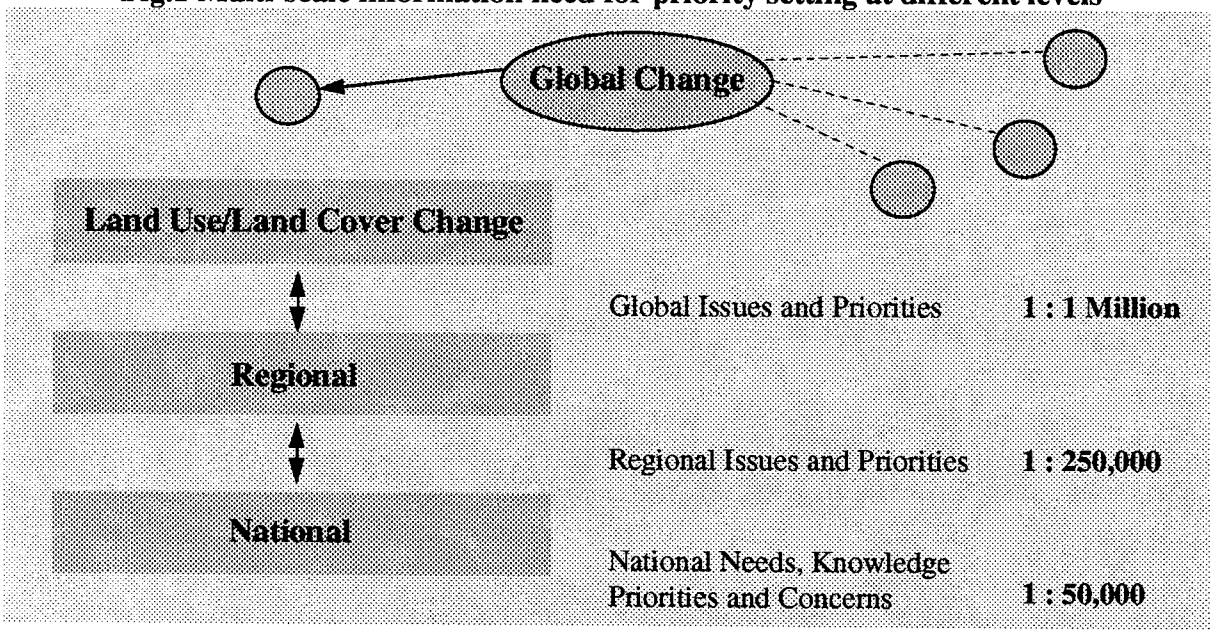

Information pertaining to the present status of land cover, their change patterns and identification of driving forces for the change are lacking in many Asian and Pacific countries. The underlying reasons are multifarious and are country specific. Existing land cover data, if any, tend to be sectorial in nature and vary in primary data sources, their classification systems and data formats and are often static and non-spatial. A consolidated and harmonized effort to come up with the information utilizing the latest techniques of RS and GIS was lacking. Additionally, an interest and need for the better and timely information as an input to the decision making processes is ever increasing.

Objectives/Scope

The objectives of the project includes:

1. Regular assessment and monitoring of major land cover types in the region using Remote Sensing and GIS technology.

2. Through regular monitoring, identify "hot spot" areas (areas undergoing major land cover transformations) for detailed investigation using high resolution satellite data supplemented by field verification. The information can act as an "early warning system" to prioritize and direct the scarce resources for action plan.

3. Develop methodological guidelines and the capacity of participating countries with tools such as image processing and GIS transfer technology to the countries to make them self reliant on their regular assessment and monitoring exercise.

4. Ultimate roles of the EAP-AP are to compile and analyze time series land cover data at the regional scale.

The project currently covers eleven countries viz. Pakistan, India, Iran, Sri Lanka, Nepal, China, Bangladesh, Burma, Laos, Cambodia and Vietnam. The following map shows the coverage of present project areas (Fig. 1).

The analysis of the data for Pakistan and Sri Lanka is on-going. In case of China, India and Iran, experts' from these countries will be invited to the EAP-AP and all the procedures will be discussed and exercised. On their return, they are expected to do the same exercises targeted for 1996. The present paper summarizes the experience gained from work in the six countries viz. Bangladesh, Burma, Cambodia, Lao P.D.R., Nepal and Vietnam.

Why NOAA AVHRR ?

Among several types of satellite data available, NOAA AVHRR data has been selected primarily because of its high temporal resolution, low data volume and low cost compared to high resolution satellite data such as Landsat and SPOT.

Fig. 2 Location Map Showing Coverage of the Project
(shaded countries corresponds to Project Area)

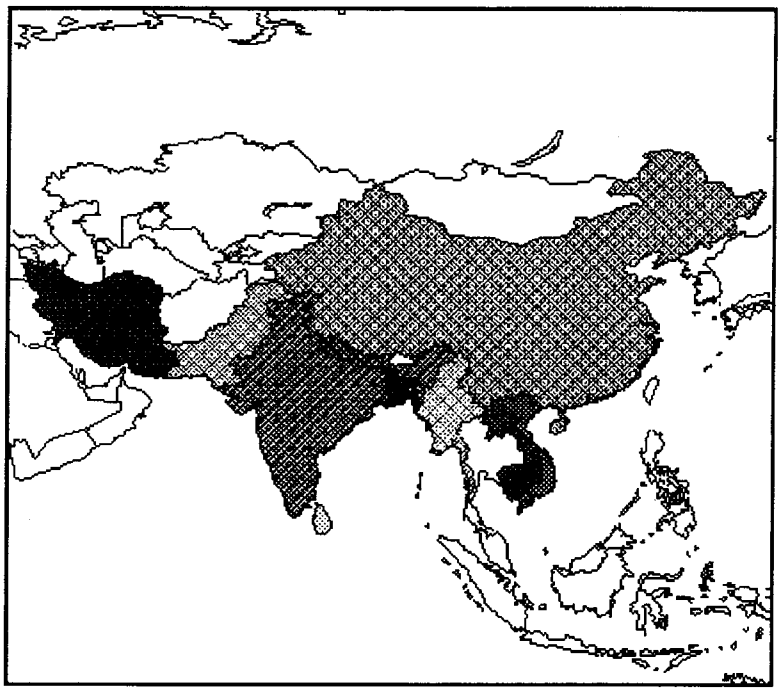

Persistent cloud cover throughout the year is a major hindrance for operational land cover monitoring over the tropics. Due to the high temporal resolution of AVHRR data, the probability of acquiring cloud free image increases. The advent of RADAR technology in remote sensing has put forward some high expectations due to their own source of energy for sensing and all weather capability, however, such technology needs further improvement for operational use. Considering these facts, it seems that AVHRR will remain the only viable source of information for land cover monitoring over a large area, at least for the next few years. The following table highlights the advantages and disadvantages of NOAA AVHRR data.

Table 1.0 Advantages and Disadvantages of NOAA AVHRR HRPT Data

Advantages	Disadvantages
1. Synoptic coverage and hence low data volume	1. Coarse resolution (1.1 km at the Nadir)
2. High radiometric resolution (10 bit)	2. Pre-processing is time consuming
3. Relatively low cost (Free!, only handling cost)	3. The methodology is not well developed
4. Twice daily coverage and hence high possibilities of having cloud free data.	4. LAC data has limited capability to record on-board

Methodology

Data Acquisition

A number of AVHRR HRPT and LAC data were acquired from different sources including NOAA NESDIS (USA), EROS Data Center (USA), NRCT (Thailand) and SMA/SMC (China). In general at least four scenes for the harvest season and four for the summer season were acquired for each country covering two time frames 1985-1986 and 1992-1993. Afternoon pass of NOAA-9 for 1985-1986 and NOAA-11 for 1992-1993 were selected for the study.

Phenological characteristics of the vegetation and hence the seasonality were given due consideration in procuring the AVHRR data. Basically data representing two seasons viz. harvest season and summer season were selected for each country. Acquiring summer season data has its clear advantage that it facilitates discriminating deciduous and evergreen forests. The selection of these data sets that exhibit complementary information was found to be informative in distinguishing different forest types and also in distinguishing forest from agricultural lands.

Fig. 2 An Overview of Methodology Used

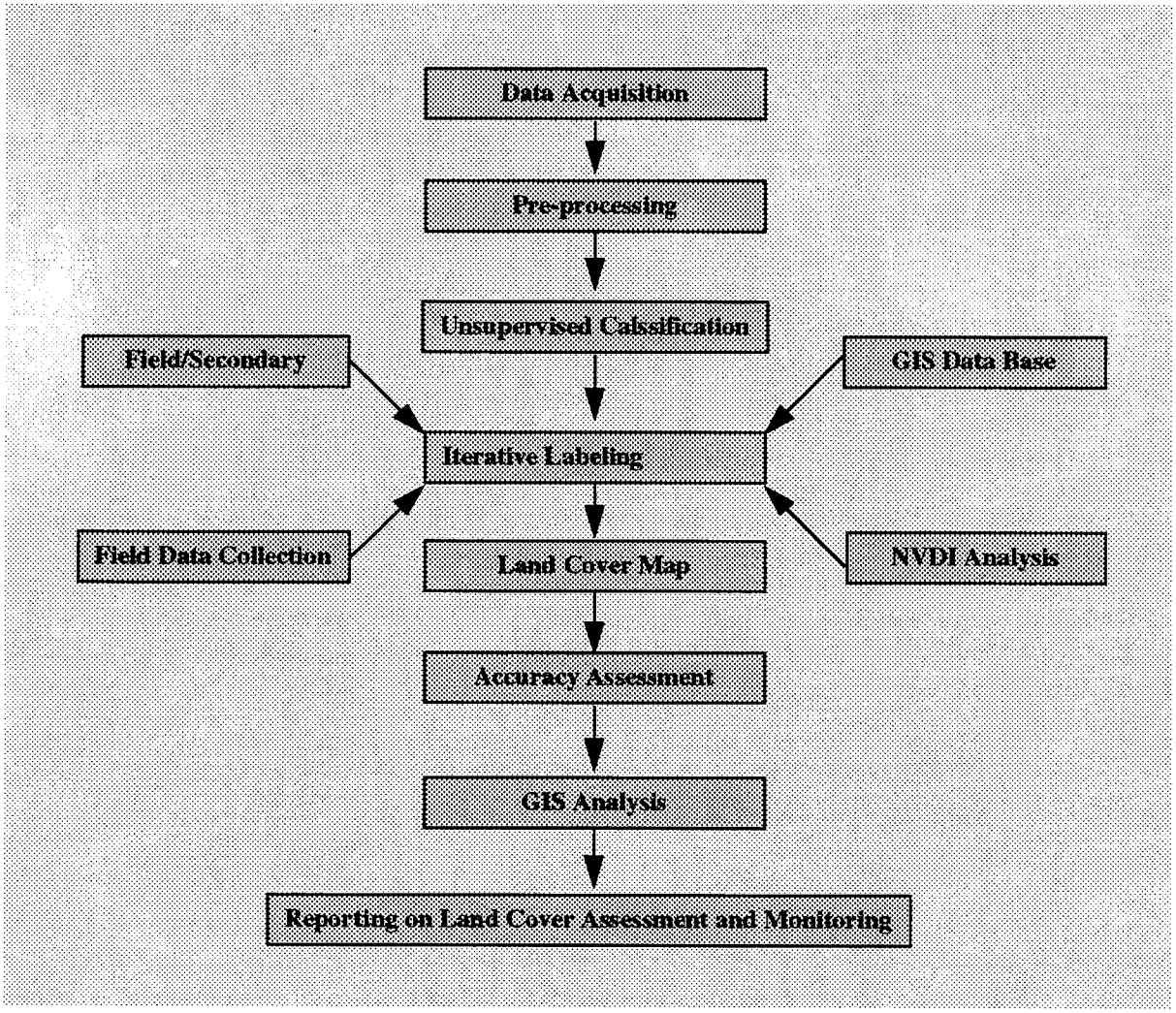

NOAA AVHRR HRPT data were analyzed using PC ERDAS and IDRISI image processing softwares. Further analysis were performed in GIS (ARC/INFO software) environs. In-house software has been written for the down loading, band selection, calibration, geometric correction and cloud masking of AVHRR data as pre-processing steps. Fig. 2 shows the flowchart of the methodology adopted.

Pre-processing

AVHRR data pre-processing mainly consisted of: data extraction and noise removal, radiometric calibration, geometric correction, and cloud masking procedures.

The HRPT Level-1B received in packed format were converted from BIL to BSQ format using appropriate programs. The original radiometric resolution of 10 bit pixel values was maintained by using two bytes for each pixel for all 5 channels. The bad/noisy lines were than identified by visual inspection of each channel of an image. All such bad/noisy lines were marked as being areas of "no data" by assigning zero values.

Radiometric calibration were performed based on the procedures outlined by European Space Agency (ESA) Handbook on "SHARP LEVEL-2 : Development Procedures and Format Specifications" and by NOAA Technical Memorandum NESS 107 on "Data Extraction and Calibration of TIROS-N/NOAA Radiometers".

Due to the lack of readily available atmospheric data in South and South East Asia atmospheric correction was not performed. Besides, although several possible approaches for the correction of water vapor absorption and aerosol scattering exist, there is presently no agreement on an acceptable method for atmospheric corrections. Some methods need further validation and are far from straight forward (IGBP, 1992).

The bi-directional reflectance effect caused by the viewing geometry and surface angular anisotropy also affects the AVHRR channels 1 and 2 (Gutman 1990). The bi-directional effect depends upon the vegetation type and could differ from one type to another. In order to correct the effect of viewing direction, angular corrections should be developed for different vegetation types and different seasons. However, images taken at large view angles (off-nadir views) which fall at the extreme of the scan line was excluded and thus, such effects, due to atmospheric scattering and absorption, and viewing geometry, are partly reduced.

A two step procedure has been used for the geometric correction of AVHRR images. The images were first resampled to a reference map projection based on location data generated by orbital model navigation and then further corrected by a linear first order rectification based on ground control points.

Interactive visual cloud masking procedure was used to identify the threshold value for clouds. Use of such an interactive cloud screening procedure proved to be highly effective in removing the clouds without losing useful data.

Finally, country masks was generated by rasterizing the vector boundaries of the study area obtained form the World Data Bank II.

Classification

Unsupervised classification was performed followed by interacting labeling. Secondary information were fully utilized during the analysis. Field trips were organized to collect secondary data and for results validation.

Results and Discussions

Land Cover Assessment

The utility of AVHRR HRPT data for discriminating and delineating of major land cover types proved to be promising. Land cover maps of 1992/93 and 1985/86 were produced for each countries accompanied with country report, the later is in the process of publication. Major land cover types discerned were forest, crop land, grass land, marshes, barren land, shrub land, savannas, rock, snow and waterbodies. Forest have been further subdivided into evergreen, deciduous and mangrove forest. Country specific variations in selecting the classes and details were noted to be of practical use. For example, Boro rice in Bangladesh has been classified as a separate class.

The following observations were noted regarding the Land Cover classification systems.

1. The contrast between forest and non-forest areas was distinct in the images acquired during the harvest season. In this season much of the agricultural crops, predominantly rice in this region, is being harvested. However, there is problem of discriminating evergreen and deciduous forest at this time. To avoid this problem, images taken during the summer season were utilized to discriminate evergreen and deciduous forest. By combining these results, improvements in the results were accomplished. This clearly demonstrates the usefulness of multi-temporal satellite data.

   It is to be noted here that the harvest season and summer season varies slightly among these countries. For example, harvest season for rice extends up to December in the case of Vietnam and up to March in the case of Bangladesh. Therefore, season selection should be considered carefully. This variation in season causes variation in the Phenological characteristics of the vegetation and in the cropping system.

2. Mangrove forest in the Sundar Ban possesses a very distinct signature to be classified as a separate class. Smaller patches of mangrove forests in Burma and Vietnam were also detected. Swamp forest on the other hand possesses a unique identity and has been classified as separate class. Due to the difference in Phenological characteristics of the vegetation and their corresponding unique signature, several forest types were discriminated with a reasonable accuracy.

3. It is very difficult to distinguish forest and some other vegetation types such as tea gardens in Bangladesh spectrally without the help of secondary information. With the help of ancillary information and GIS as a tool, it is possible to classify it as a separate class. Plantations areas less than the resolution of AVHRR data were not able to discriminated in the present study neither the Beach forests occurring in a narrow strips along the coastlines.

4. Shifting cultivation, conversion of forest to agricultural land, forest fire and indiscriminate felling are found to be the main reasons for the deforestation in these countries. Population pressures and the change in consumption patterns were identified as two detrimental factors contributing to deforestation. Shifting cultivation is no longer sustainable practice. Examples of unsustainable types of shifting cultivation can be found in northern Laos and in the Chittagong hill tracts of Bangladesh.

5. A clear demarcation of national boundary between Bangladesh and India and Thailand and Laos/Cambodia was visualized due to the devoid of vegetation in Bangladesh and Thailand side.

6. Mosaic of forest and shifting cultivated areas in Northern Laos were invisible in the AVHRR data because of its low resolution. Similar problem was encountered in discriminating small patches of forest areas in Vietnam.

Change Detection

Change in land cover has been attributed by various reasons and those reasons are site specific. Shifting cultivation has been identified as a major cause of forest destruction which is prominent in case of Laos and in the Chittagong hill tracts of Bangladesh. Conversion of forest to agricultural land was noticed in many countries including the Terai region of Nepal and southern part of Burma. Conversion of swamp forest to other land use were noticed in the Mekong Delta in Vietnam.

The pattern of conversion varies from place to place. The following diagram shows the conversion pattern and its strong linkages between forestry and agricultural land. Although there is a reciprocal relationship of change between closed forest and open forest, the change from closed forest to open forest is much, much higher than the change from open forest to closed forest. Similar explanations hold true for other classes.

Fig. 3. Change pattern showing strong link between forestry and agricultural land

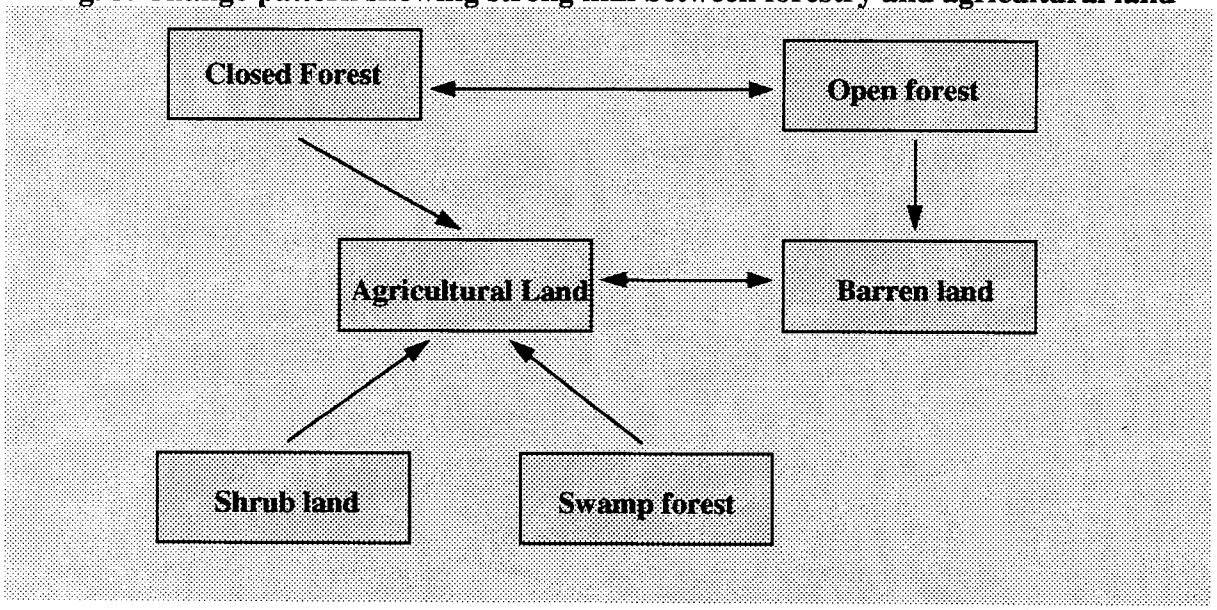

Hot Spot Areas Investigation

Once the areas where there is major land cover transformation occurring called "hot spots" are identified, the next step is to investigate the area in detail using high resolution satellite data. The primary data source for hot spot area detection is the high resolution satellite data such as SPOT, Landsat and ERS-1. Three "hot spot" areas has been identified and is being analyzed in Northern Laos, Mekong Delta and in Chittagong Hill Tract of Bangladesh.

Conclusions and Recommendations

The experience gained so far illustrates both the potential and limitations of AVHRR HRPT data for national/regional tropical forest assessment and monitoring endeavors within the framework of land cover assessment and monitoring project of UNEP environment assessment programme for the Asia and Pacific. From the study following conclusions and recommendations could me made.

1. This exercise demonstrated that the NOAA AVHRR is a major source of information for land cover assessment and monitoring at the macro scale. "Hot Spot" areas could be identified for further investigation with high resolution data and field verification;

2. The availability and reliability of ancillary data for the analysis of AVHRR data are of utmost importance in order to come up with better classification results. Analysis of the data by the local experts definitely improves the precision and quality;

3. A number of data sources for acquiring and distributing AVHRR data both within and outside the region were identified but a systematic data archiving is lacking;

4. The acquisition of data should be done carefully considering the phonology and structure of the forest vegetation, seasonality and agricultural practices in particular;

5. Various land cover classification systems exists, a consolidated and harmonized land cover classification system for the purpose of NOAA AVHRR classification needs to be developed with the coordination of concerning agencies;

6. Pre-processing of NOAA AVHRR data is time consuming and tedious. Appropriate standardized means and techniques needs to developed.

Acknowledgments

A number of individuals in various organizations including Mekong Secretariat, ICIMOD, GTZ and IUCN contributed towards the realization of the project. A number of government agencies in various countries including, the Land Use Mapping Office in Cambodia, Forest Inventory and Planning office in Laos, Survey Department and Forest Department in Nepal, Institute of Forest Inventory and Planning in Vietnam, Forest Department in Burma and Local Government Engineering Department, SPARSSO, and Forest Department in Bangladesh extended their profound cooperation and help to the project. **Our sincere thanks to all.**

References

Gutman, G., "Vegetation Indices from AVHRR : An Update and Future Prospects", Remote Sensing of the Environment, Vol. 35, pp. 121-136, 1991.

IGBP, "Improved Global Data for Land Applications", The International Geosphere-Biosphere Programme (IGBP), Global Change Report No. 20. IGBP, Stockholm, 1992.

Vegetation Mapping of Iran by using NOAA AVHRR Data

A. Mohammadpour

M. Forouhar

Iranian Remote Sensing Center

P.O.Box 11365/6713

Tehran-IRAN

Abstract

This report describes and demonstrates techniques for vegetation and land cover mapping by the use of NOAA AVHRR DATA.

The NDVI combined with maximum Liklihood (MLC) Method were found to give good results for such studies. NOAA-9 AdVanced Very High Resolution Radiometer(AVHRR) were examined to determine their utility for vegetation and land cover of whole country.

Introduction

Iran with an area of about 165 m.ha. bounded by Latitude 25° 40′ N and 39° 45′ (N) and a Longitude of 44° to 63° (E), situated in the south west of Asia in the Dry Lands Belt of the world.

About 60% of the country is mountainous and the remaining is desert.

Iran central Plateau is Located between two major mountain ranges of Alborz and Zagross.

Average annual Precipitation throughout the country is approximately 230 mm. which is unevenly distributed . From the climatological point of view Iran is considered as an arid to semi arid zone

Regarding biodiversity, Iran is divided into three main regions as Caspian, Balouch and Omanian, and Irano Touranian regions.

Because of the bioclimatical conditions and water resources scarcity in this country, the vegetation has very little chance to grow,therefore protection of vegetation cover, is of vital importance.

Objectives:

The main Purposes of this study are as follow :

1- Vegetation mapping of the country by utilizing of the NOAA Data (LAC).

2- Land cover mapping of the country by using of the AVHRR Data.

3- Evaluation of the AVHRR Data, regarding to their application in vegetation mapping.

Materials

Iranian satellite Receiving station is now acquiring the Data from NOAA 11 and 12, 4 times a day. Due to instrumental limitations the acquired Data are not geometricaly corrected,so it is impossible to provide computer compatible data of AVHRR.

The data used for this study acquired by NOAA 9 which is directly received by IRSC Receiving station in 1986.

Methodology

The spectral reflectance of chlorophyl pigment in both the visible and infrared Portions of electromagnetic spectrum, provides a means to evaluate and monitor green vegetation vigour and density in the band widths of Channels 1 (.58 to- .68m) and band 2 (.72 to 1.1m) of the AVHRR.

" Mathematical Combinations of channels 1 and 2 were in some cases, found to be good indicators of the Presence of green vegetation "(Gray and mccrary 1981).

The Gray and Mccrary lndex (GMI) is defined as GMI= CH2- CH1,but in this paper we applied NDVI (Normalized Difference vegetation lndex) method. This method uses the red and near infrared bands (i-e. Band 2 and band 1) of the NOAA AVHRR Data which is calculated using the following equation:

$$NDVI = \frac{CH2 - CH1}{CH2 + CH1}$$

The NDVI is basically a measure of the amount and vigour of vegetation within a scene. the values ranges from -1 to +1 with +1 representing very high vegetation cover and viguor while -1 represents non vegetation areas.

Before to do any digital processing of data it is necessary to correct and register the data, and resample them to a map grid, so that the resampled data could be integrated into a National Geographic Information system if needed

In order to do Geometric correction the control points have been extracted from 1:2,500,000 scale national topographic map.

Resampling was considered most acceptable.

Application of NDVI to the project Area

An unsupervised clustering routine was applied to the composite NDVI data set resulting in 16 clusters after 2 iterations.

A maximum likLihood classification procedure , was applied to the data. Maximum Likilihood classification revealed 8 different classes which are composed of 7 different vegetation types,the latest class represents water bodies.

The various class means are shown in figure 1, plotted on a bi-Spectral plat of NDVI.

The various numbered class are as follows:

class no	class name
Class 1	Mixed Dense Forest with Agriculture
Class 2	Grass and shrub Land
Class 3	Mixed Shrub with Deciduous Vegetation
Class 4	Sparse Range Land
Class 5	Mixed Psammophile with Halophite Veg.
Class 6	Semi Desert Steppique
Class 7	Mixed Bare Soil with Steppique Vegetation
Class 8	Water Bodies (Seasonal and Perrenial)

Land Cover Mapping

The same procedure has been applied for land cover mapping of the country. An unsupervised clustering on data set, disclosed 14 different clusters.

14 different clusters are obtained by an unsupervised clustering techniques.

The various class means are shown in figure 2 as follows:

Class	Definition of class
Class 1	Water bodies(Seasonal and Perrenial)
Class 2	Dense vegetation (mostly Forests)
Class 3	Mixed
Class 4	Rangeland,(Hilly-mountainous)
Class 5	Desert Area
Class 6	Bare,Saline Soils (salt plats)
Class 7	Sandly Area (Sand Dunes)
Class 8	Unclassified

From the 14 clusters, only 9 classes are identified, the other clusters are remained Unknown due to the small amount of Pixel association and interfering the Pixels.

Conclusion

The Remotely Sensed Data acquired by NOAA Meteorological satellite can provide very useful and important information in meteorology, oceanography, as well as vegetation and land cover mapping.

This kind of satellite can observe a wide range scene within a simultaneous view.

By comparing the NDVI (derived from AVHRR) for every data set on a Pixel by pixel it should be possible to determine whether vegetation has changed from time to time and where such a changes have been occured.

Vegetation mapping requires temporal data on growth and autumn time according to crop calendar.therefore a better results

could be accomplished if all required temporal data were available

Due to lack of efficient data, change detection of V.C.were not possible .

Generally ;

1- Despite of its resolution,NOAA Data can be used for evaluation purposes in earth resourses progect.

2- Change detection of dynamic features through continious monitoring in a regional scale is feasible if the required data were available .

3- vegetation mapping on a regional base requires multitemporal data according to crop calendar of the study area.

References:

I.Application of Normalised Vegetation Index Differencing for Urban Change Monitoring, B.Forster,Center for Remote Sensing Univ.of New South Wales.

II.Global Land Cover Classification by NOAA GVI Data. R.Tateishi.& Koji Kajiwara.Remote Sensing & Image Research Center, Chiba Univ.JAPAN.

III.Research & Training Programs Implemented for Sand Dune Fixation & Computing Desertification in the Islamic Republic of IRAN.

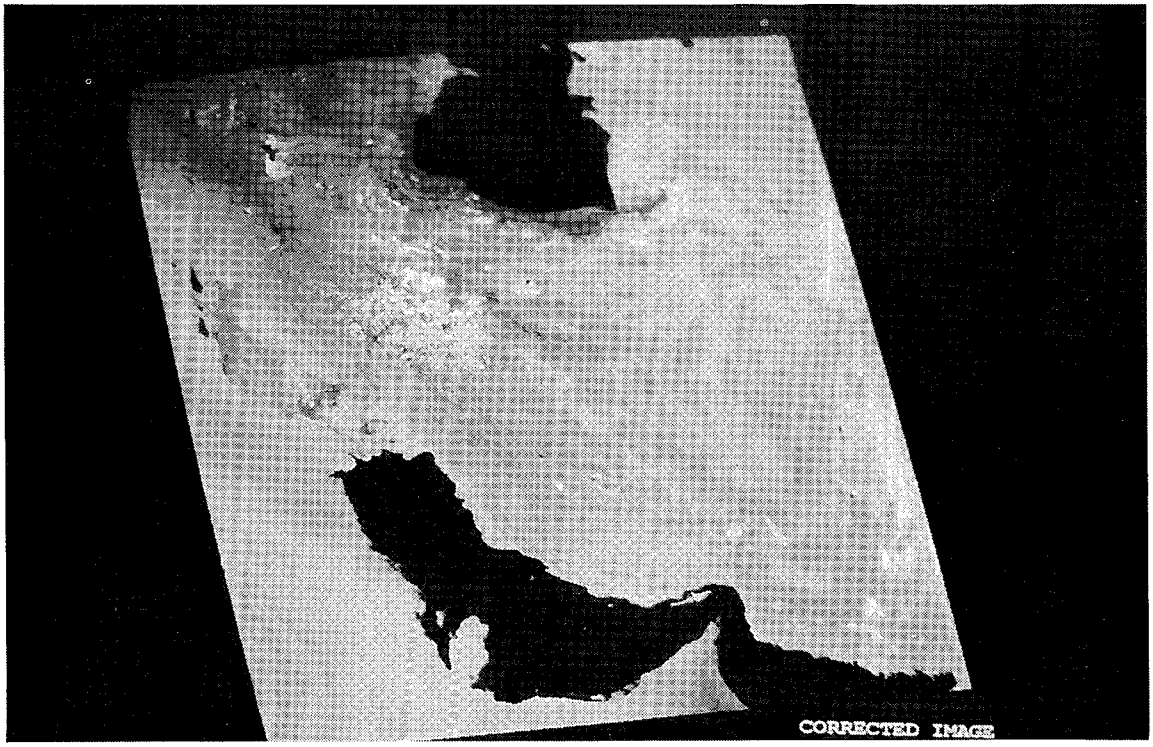
CORRECTED IMAGE

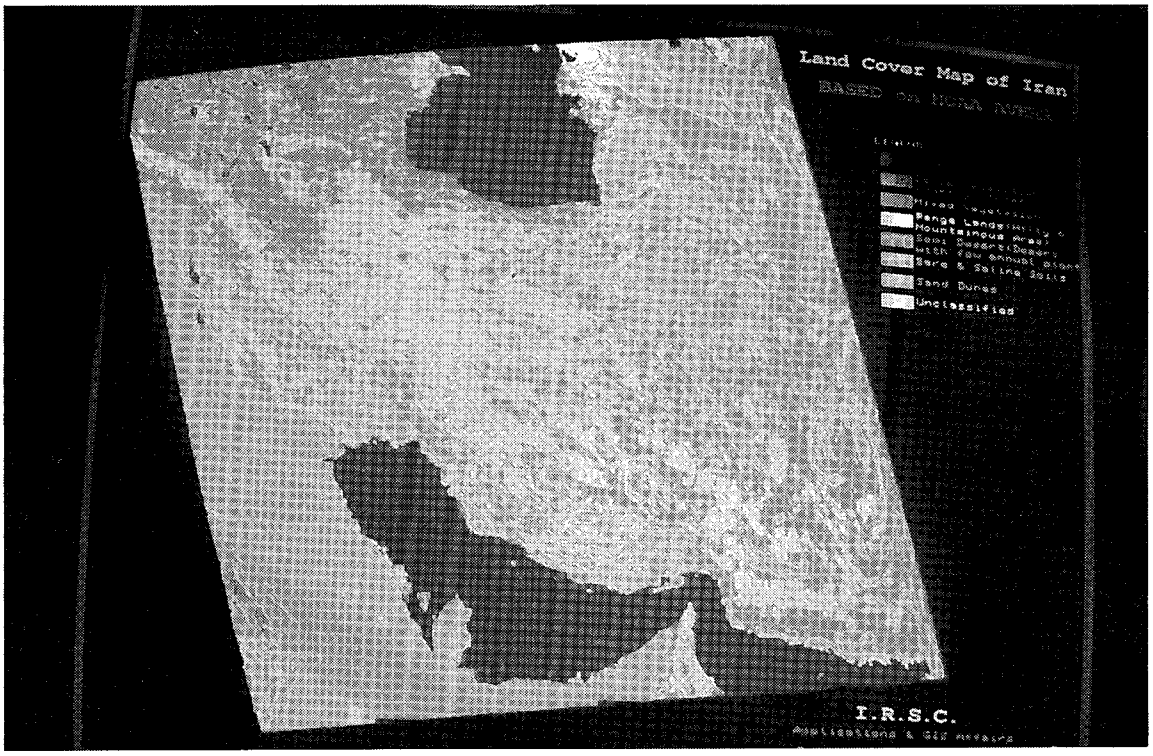
Land Cover Map of Iran
Sand Dunes
Unclassified
I.R.S.C.

VEGETATION COVER MAPPING

OF KADMOUS AREA USING

T. M DATA

PREPARED BY : ABDUL RAHIM LOULOU
REMOTE SENSING ADVISOR
GORS _ SYRIA

INTRODUCTION

Thematic mapping is essential for natural resources monitoring , inventory and survey , one of the importing thematic maps are vegetation cover maps which show vegetation types and reflect the general situation of the plants , also help in vegetation cover monitoring and land cover changes .

Remotely sensed data can be used to map and monitor vegetation cover , because such data are multitemporal and multispectral data . This was applied in vegetation cover mapping of Kadmous area using TM data .

LOCATION :

The studied area occupies the southern part of Kadmous region in west Syria , it lays between latitudes 35° 2′ and 35° 6′ north and longtudes 36° 5′ and 36° 14′ east .

Geology and Geomorphology

The geological features of the area consists of :

- Limestone , dolomitic limestone , dolomite and marl with flint nodules of lower to middle jurassic .
- Bedded dolomitic limestone , dolomitic marl , limestone of upper jurassic .
- Limestone and dolomitic limestones alternation of thin to thick - bedded dolomite of cretaceous .

Within Kadmous territory and according to the general geomorphological map of the region , geomorphological structure of the area can be classified into hills , pediments and wadies .

Soils :

Information about the soils of the area were extracted from the soil map of west Syria which was prepared from Landsat5 TM images , the soils of the area were classified according to USDA soil taxonomy as follow :

- Lithic xerorthents ,medium and fine , steep .

- Calcixerollic xerochrepts , medium and fine , level and sloping.

- Lithic haploxerolls , medium , steep .

- Rock outcrops , lithic xerorthents , medium and fine sloping .

Climate :

Climate of Kadmous region is a mediterranean mountainous climate which is cold in winter and fair in summer , the monthly average of minimum tempreture ranges between 1.4 in February and 23.1 in Augest .

The monthly maximum temperature ranges between 11.3 in February and 30.8 in Augest . The mean annual precipitation is 620 mm most of it falls in the rainy season between October and April , monthly average of relative humidity range between 45 - 78% .

Remote Sensing Application

Unsupervised classified image of the study area was prepared from Landsat5 TM data , it was processed using ERDAS software , the classification was made according to the brightness values of the pixels and accompanied by a colour scale showing the following :

- Unplanted areas (bare soil and rocks) seven diffirent colours from B1 to B7 .
- Shadows : one colour T1
- Vegetation cover : five diffirent colours from V1 to V5 .
- Agricultural fields : five deffirent colours from F1 to F5 .

In order to prepare a vegetation cover map from this image , the following steps were taken :

1 - Specifying the study area on topographic map , scale 1:50.000 and preparing a base map from it on transparent paper .
2 - The base map was compared with the unsupervised classified image scale 1:50.000 and test areas represent the spectral signitures were chosen.
3 - The test areas were varified and analized and provisional map was prepared .
4 - Related documents were prepared to do the field verification in the test areas .

FIELD CHECK

Field check has been done in three diffirent test areas representing spectral signiture on the image . The results of the field check reveals that the colours of the colour scale have the following meaning :

- T1 : represents forests of coniferous trees (cedars , pines , cypresses)
- V1 : represents dense bush land of mainly dwarf - oaks .
- V2 : represents broad - leaved forest trees .
- V3 : represents woold lots of pine trees .
- V4 : represents woold lots of cypresses .
- V5 : represents orchads and vinyards .
- F1 : represents wet grass land on slops .
- F2 : represents terraces covered with tobacco .
- F3 : represents orchards (mainly apple)
- F4 : represents winter and summur crops on rainfed fields , which have been recently plowed and prepared for winter crops .
- F5 : represents very dense and healthy bush land .
- B1 : represents stony land with moderately deep to deep soils .
- B3 and B4 : represents rocky land with rock out crops and very shallow soils .

VEGETATION COVER

The type of vegetation cover coincides with geomorphology , physiography and soil , the variation in such feature was reflected on the plant life and vegetation cover , so diffirent vegetation cover types occur in the area which are the following :

1 - Coniferous forests : The dominant types are pinus brutia , cupressus sempervirens and cedrus libani.
2 - Broad leave forests the dominant types are Pistacia Palestina , Arbustus andrachne , cerasus mahaleb , and pirus syriaca mixed with orchards and vinyards .
3 - Bush land : indicates areas where plant conopy covers ground surface but trees are small ; like crataegus sp. and fraxinus sp.
4 - Grass land : indicates areas where the natural vegetation is predominantly grass like plant , forbs or shrubs .
5 - Rock outcrops : indicates areas covered with bare rocks and less than one - third of the area covered with vegetation .

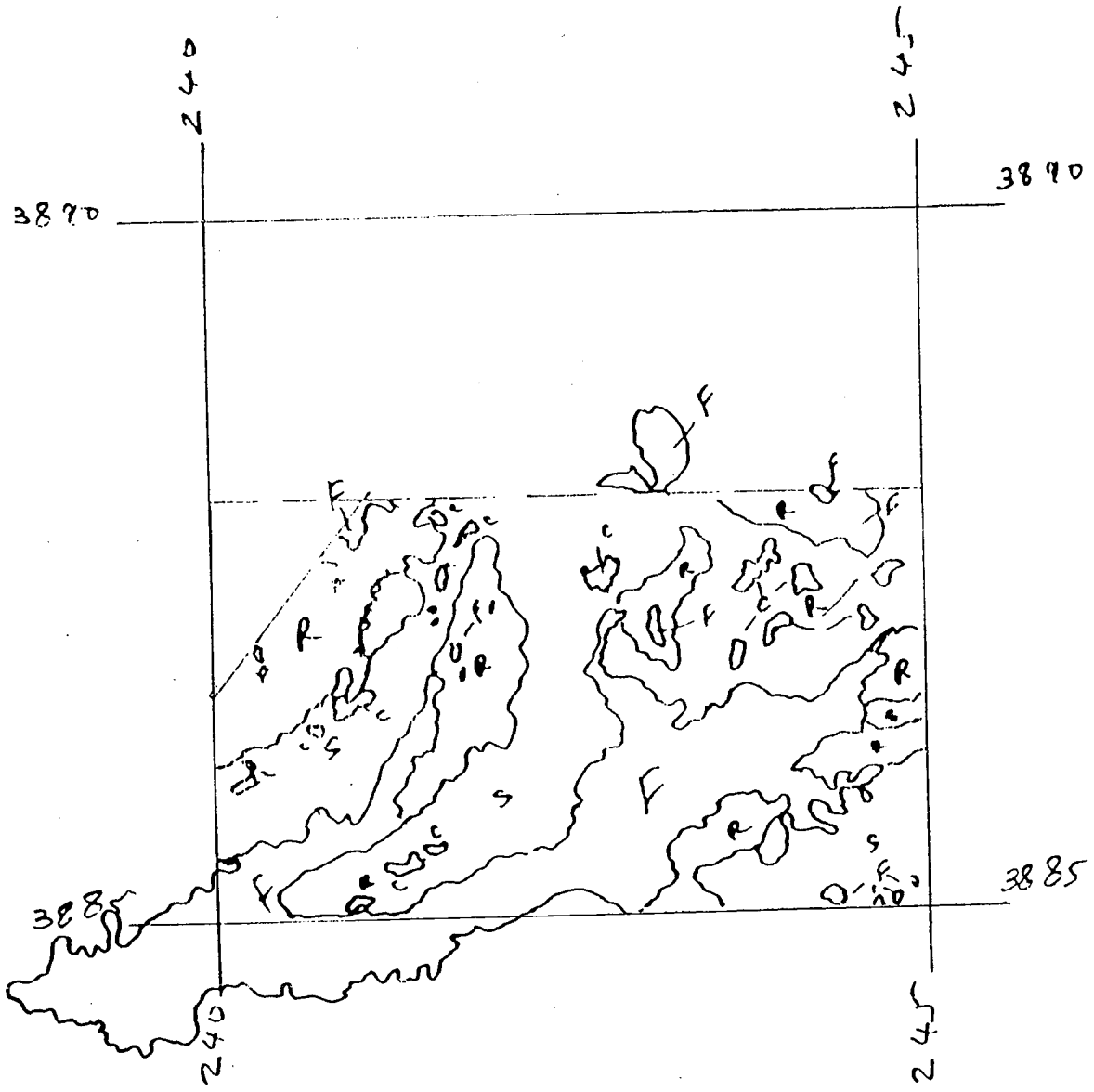

Test area interpretation

F: Forests
b: Bushland
R: Rangeland and crops
C: Rock outcrops.

CONCLUSION

Vegetation cover changes with time due to various reasons , which make it necessary to map and update vegetation cover maps using suitable techniques , like remote sensing techniques which are an effective tool in natural resources thematic mapping , because satellite remote sensing has been improved considerably over the last years in both the spatial domain as well as the spectral domain . For this reason remote sensing was used in this study .

****

Spruce Stand Parameter Estimation Using Airborne Sensor Imagery

Yoshio Awaya

Forestry and Forest Products Research Institute
P.O. Box 16, Tsukuba Norin Kenkyudanchi-nai, Ibaraki 305 Japan

Abstract

Ability of visible infrared radiometer for stand parameter estimation was evaluated. The diameter at breast height, tree height, timber volume and so on were selected as the stand parameters. High correlation coefficients between those stand parameters and remote sensing data were observed in some channels. Though channels with stronger absorption by chlorophyll in the visible channels showed lower correlation, other channels like at the green peak and the red edge showed higher correlation with the stand parameters. The tendency was observed for the imagery observed in early August and early September, then those wavelength were seemed useful to estimate woody biomass

Though high correlation between leaf biomass and the normalized difference vegetation index (NDVI) was reported, no clear relationship was observed between the NDVI and stand parameters. However, high correlation coefficients exceeding 0.8 were observed between stand parameters and a normalized ratio between the 730nm and the 2200nm channels (ND730&2200), and little observation angle effect was identified on the ND730&2200. Thus the index was probably useful for biomass estimation of evergreen coniferous forests using wide view angle sensor imagery.

1. Introduction

There were many studies about relationships between biomass and data which were obtained by visible infrared optical sensors such as Landsat Thematic Mapper. Though the relationships between crop leaf biomass and radiation or vegetation are numerically well understood (Asrar et.al. 1989), there only some detail works about tree leaf biomass (Franklin 1986, Peterson et.al. 1987, Spanner et.al. 1990, Herwitz et.al. 1990) and woody biomass (Ahern et.al. 1991). In many studies, available number of channels and their spectral ranges were limited and wide. Current technological improvement makes it possible to observe radiation from the ground in narrower spectral channels with finer gain like Compact Airborne Spectrographic Imager (CASI, Babey et.al. 1993).

The Advanced Very High Resolution Radiometer (AVHRR) made it possible to analyze global vegetation distribution, however, its limitation is already recognized because it has only two optical channels. On the other hand, it has been requested to reveal useful wavelength for vegetation analysis for the next generation satellite sensors. The Global Vegetation Science Team of the Earth Environmental Observation Committee organized by the National Space Development Agency of Japan (NASDA) has been studied useful wavelengths for woody biomass estimation using airborne imagery aiming at certifying the usefulness of the Global Imager (GLI) channels, which will be the core sensor of ADEOS II satellite. Results of the analysis are described in this paper.

2. Study Area and Data

A test site was selected in the national forest in the north west of Tomakomai city (141°30'E, 42°40'N) in southern Hokkaido island (Fig. 1). The topography was very flat and the elevation was between 100 m and 250 m in the test site. Two spruce species (*Picea yezoensis* GORD. (yedo spruce), *Picea glehnii* MAST. (akaezo spruce) were major planted species for these 80 years. Though yedo spruce was planted in a large area before 1940's, akaezo spruce were planted in rows after late 1950's. Because of it, well growing old stands were almost monoculture stands, but young stands were almost mixed stands with broad-leaved trees for airborne data processing.

One Airborne Multispectral Scanner (MSS) image and two CASI images were obtained in 1993 (Fig. 2), and they were used in this study. Specifications of those image are shown in the table 1. Forest planning maps in the scale of 1 to 20,000 and two kinds of aerial photos were used as the ground

truth. One of them was black and white photo of 1 to 20,000 in scale taken in 1990, and the other was natural color photo of 1 to 30,000 in scale, which was obtained at the same time of the MSS observation.

Field surveys were conducted in July, 1993 and in September, 1994 in advance of the airborne data acquisitions. Thirty one plots in 1993 and ten plots in 1994 were selected along the flight line in relatively dense spruce stands in each age class. The diameter at breast height (D.B.H.) of all trees and height of 5 upper story trees were measured. The plots were 30 m circles in diameter for mature stands (top tree height exceeds about 12 m) and quadrates about 0.04 hector for younger stands.

3. Analysis

A height-diameter curve, for which the Näslund curve was applied, was estimated using the plot data in 1993. Height of all trees were computed from the D.B.H. using the height-diameter curve, and timber volume was estimated for each tree using 3 volume tables for spruce, fir and broad-leaved species each. Average, median, top three trees and upper story's values of D.B.H., height and volume were computed for each plot. The upper story was defined as trees between 12.5 % and 25 % in the order from the tallest tree. Stand age, basal area and stand density, which was number of trees per hector, were also calculated. Those parameters were called stand parameters hereafter.

Some normalized difference indices using the MSS data were computed as follows according to results of a preliminary multiple regression analysis using the original channels.

NDVI = (860nm-660nm) / (860nm+660nm)
ND860&1600 = (860nm-1600nm) / (860nm+1600nm)
ND1600&660 = (1600nm-660nm) / (1600nm+660nm)
ND730&545 = (730nm-545nm) / (730nm+545nm)
ND730&1050 = (730nm-1050nm) / (730nm+1050nm)
ND730&2200 = (2200nm-730nm) / (2200nm+730nm)

Training areas at the plots were selected from the airborne sensor imagery and the indices. Since the location of plots were not satisfactory clear in the imagery, larger training areas than plot sizes were selected to include the observed plots. Clouds in the two CASI images prevented from selecting the same training areas among all images, but about 30 plots were used for each image analysis. Averages of channels and indices (hereafter; average airborne data) were computed from the training areas. The CASI data were supplied as digital numbers, which showed radiance.

Correlation coefficients between the average airborne data and the stand parameters were computed. Then the correlation coefficients were evaluated to know effective channels and indices for stand parameter estimation. Scattergrams between the average airborne data and stand parameters were examined to make clear their relationships.

A stepwise multiple regression analysis, selecting each parameter as the dependent variable and the average airborne data as the independent variables, was employed to know ability of optical sensor data or indices for stand parameter estimations. Then the upper story height was estimated using the MSS imagery and three regression models, and tendencies of the estimation were visually examined to know view angle effects.

4. Results and Discussion

Since both sensor had wide viewing angles (Table 1), the observation angles were different among plots, and it would cause different bi-directional reflectance effects on reflectance of the forests. However, this effect was almost neglected in the following discussion due to difficulty of numerical evaluation of it. Though MSS had wider view angle than CASI, the plots spread almost within the view of CASI. Then wider view angle of MSS won't be a serious problem in the following discussion. On the other hand, different observation date and time caused different sun-sensor locations, and severe bi-directional reflectance effects was recognized at the opposite side of the sun in the MSS imagery (Fig. 2).

4.1 Correlation Coefficients

Correlation coefficients between stand parameters and digital numbers were shown in Figure 3.

Higher correlation coefficients appeared in channels other than shorter visible channels (<500nm), the chlorophyll-a absorption channel (with its peak around 660nm, Wessman 1989) and short wave infrared channels. The reason for the case of short wave visible may be as follows. Since the correlation coefficients became worse in shorter wavelength, atmospheric scattering probably made reduce spectral information badly. Though it is quite hard to tell the reason for the 660nm channel, strong absorption by chlorophyll might make radiation, which would be different by each stand due to crown size and stand density, unclear.

On the other hand, higher correlation around green peak and red edge channels suggest that rather neutral spectral properties, which are balanced absorption, transmission and reflection, of green leaves may keep much canopy shape information within the radiation than chlorophyll absorption channels. Though the reason was unclear, the results suggested that green peak and red edge regions were important for woody biomass estimation.

By the way, there was a tendency that average digital numbers showed higher correlation with the median D.B.H. and height other than any other forms including averages especially in the visible channels (Fig. 3). Ahern et.al. (1991) reported that multiple regression models using median values for all variables showed higher determinant coefficients than using average values to estimate spruce-fir volume. It seems similar with our results.

It was recognized in the preliminary multiple regression analysis that 730nm had the highest correlation with many stand parameters, and 2200nm or 1050nm was selected as the second independent variables in most cases. It was clear that the longer short wave infrared (2200nm) was more useful for stand parameter estimation than shorter one (1600nm) in multiple regression models. Ahern et.al. (1991) reported a similar result about indices using those infrared channels.

The ND730&2200 had the highest correlation coefficients with all stand parameters except the basal area (best case, r=0.86 with D.B.H. top 3). The correlation coefficients were significantly higher than those derived using original channels. The index had higher correlation with parameters of upper story than those by average and median. Similar tendency was found in the ND860&1600, which showed the second best index showing high correlation with many stand parameters (ex. r=0.82 with D.B.H. top story).

4.2 Scattergram

The scattergrams (Fig. 4) between digital number and stand parameters showed a linear relationship between digital number and stand parameters. High correlation coefficients exceeding 0.8 (or -0.8) encourage to estimate stand parameters with usable accuracy by optical remote sensing. One reason of such a high correlation may be that the mix rate of deciduous trees have clear relationships with stand age until spruce stand closed in the test site (Awaya et.al. 1995).

The plots were widely spread in the small tree group in the scattergrams of MSS data (Fig. 4a,b), and the correlation coefficients were worse than those of CASI data (Fig. 3). This may be caused by the bi-directional reflectance feature of spruce due to view angle differences.

As described before, the ND730&2200 had significantly bigger correlation coefficients with most stand parameters. Above all, the ND730&2200 improved the correlation coefficients significantly comparing with those in original channels (Fig. 4b and 5b). The main reason is probably that taking ratio reduced the view angle effect significantly. However, since the other indices could be caught the same benefit, there would be any other reason of the excellence. Unfortunately, any other reason was unknown. If it become clear, the usefulness and limitation of the ND730&2200 will be recognized.

There was a curve-linear relationship between the ND730&2200 and a few stand parameters (Fig. 5d). For example, the top 3 tree volume showed more clear curve-linear feature than the volume per hector. This may be related with forest structures, which would have a great influence on radiation from the stands.

Other indices including the NDVI showed much poor results than those of the ND730&2200 (Fig. 5). Though it was reported that the NDVI had curve-linear relationships with leaf biomass for crops (Asrar et.al. 1989) and evergreen conifer forests (Peterson et.al. 1987, Spanner et.al. 1990), it was

not useful to estimate stand parameters used in this study.

4.3 Multiple Regression Analysis

The ND730&2200 was chosen as the first variable in the stepwise regression analysis except age, tree density and volume per hector. Even if the second and the third independent variables were put, correlation coefficients didn't improve well. It and the high correlation with the stand parameters might suggest that the ND730&2200 contained most spectral information relating with forest stand parameters , which were related with the size.

Since clear view angle effects were observed in the original channels, it was one of interest that each index reduced the effect how well. Though I did not show indices photos, the view angle effect was hard to recognize visually in the ND730&2200 and the NDVI. However, it was numerically evaluated that there was a clear view angle effect on the NDVI of spruce stands (Awaya et.al. 1994), a numerical evaluation is also necessary for the ND730&2200. The visual inspection also showed that channels with higher correlation with stand parameters didn't show forest types clear.

The estimated upper story height using the ND730&2200 alone showed little view angle effect. However, if models with other indices or channels were used, tree height was estimated lower in the middle than in the case of the ND730&2200 alone model (Fig. 6). Though further evaluation is necessary, the ND730&2200 seemed very useful for spruce stand parameter estimation.

5. Conclusion

The following items became clear in this study.

1. The chlorophyll absorption channel around 660-670nm didn't have high correlation with forest stand parameters such as the stand density, D.B.H. and tree height. On the other hand, channels about 700 to 715nm had the greatest correlation coefficients with most of stand parameters. However, the reason is not revealed.
2. Median values of D.B.H., height and volume had greater correlation coefficients with original channels, especially with the visible channels than average values or upper story values.
3. The ND730&2200 had greatest correlation with many stand parameters. It was selected as the first variable in the stepwise regression analysis, and because of the greater correlation, other channels didn't improve correlation coefficients when they were combined with the index.
4. The ND730&2200 seemed to make reduce viewing angle effects significantly and showed a reasonable estimation of upper story height.
5. The NDVI, which is the most common vegetation index, didn't have any clear relationships with stand parameters used in this study. The ND860&1600 would be most useful index for spruce stand parameter estimation among indices, which can be derived using TM data.

Thus usefulness of red edge channels and indices using the channel became clear. However, since the red edge inflection position moves seasonally, usefulness of the spectral region must be carefully evaluated.

6. Acknowledgment

This study was executed by the support for the MSS data acquisition and field surveys of NASDA. The author expresses deep gratitude to NASDA staff, Dr. Moriyama for his coordination and Mr. Maesato for his support on the field study with Dr. Tsukada, Mr. Nakajima and Mr. Ikeda. The author also expresses deep appreciation to Dr. Inose, Mr. Sano, Mr. Ishibashi and Mr. Amano of FFPRI, Hokkaido office, Dr. Tsuyuki and his students of the University of Tokyo, and Mr. Kato and Mr. Watanabe of the Hokkaido Prefecture Forestry Institute for their supports on the field measurements.

7. References

Ahern,F.J., T.Erdle, D.A.Maclean, and I.D.Kneppeck, , "A quantitative relationship between forest growth rates and Thematic Mapper reflectance measurements", INT.J.Remote Sensing, Vol.12, pp.387-400, 1991

Asrar,G. R.B.Myneni, and E.T.Kanemasu, "Estimation of plant-canopy attributes from spectral reflectance measurements (in Theory and applications of optical remote sensing)", John Wiley and

Sons, New York, pp.252-296,1989

Awaya,Y., G.Saito, T.Moriyama, S.Maesato, and M.Tsukada, "Forest Analysis Using Multi-sensor Data (I) - Analysis of Bi-directional Reflectance Factor Using Airborne MSS data", Proceedings of the Japan Society of Photogrammetry and Remote Sensing Annual Meeting, Chiba, pp.237-242, 1994, in Japanese

Awaya,Y., N.Tanaka, T.Häme, and A.Lohi, "Vegetation Change Monitoring in the Boreal Area Using Remote Sensing - Changes in the Northern Finland and Spectral Characteristics of Spruce-", Proceedings of The International Arctic Science Symposium, STA Japan, Tsukuba, pp.D30-61, 1995

Babey,S.K. and C.D.,Anger, "Compact Airborne Spectrographic Imager (CASI): A progress review", Presented at the SPIE Conference, Orlando, Florida, 12pp. , 1993

Franklin, J., "Thematic Mapper Analysis of Coniferous Forest Structure and Composition", INT.J.Remote Sensing, Vol.7, pp.1287-1301, 1986

Herwitz, S.R., D.L.Peterson, and J.R.Eastman, "Thematic Mapper Detection of Changes in the Leaf Area of Closed Canopy Pine Plantations in Central Massachusetts", Remote Sens. Environ., Vol.29, pp.129-140, 1990

Peterson, D.,L., M.A.Spanner, S.W.Running, and K.B.Teuber, "Relationship of Thematic Mapper Simulator Data to Leaf Area Index of Temperate Coniferous Forests", Remote Sens. Environ., Vol.22, pp.323-341, 1987

Spanner,M.A., L.L.Pierce, D.L.Peterson, and S.W.Running, "Remote sensing of temperate coniferous forest leaf area index: The influence of canopy closure, understory vegetation and background reflectance", INT.J.Remote Sensing, Vol.11, pp.95-111, 1990

Wessman, C.L., "Evaluation of Canopy Biochemistry (in Remote Sensing of Biosphere Functioning)", Springer-Verlag, pp.135-156, 1989

Table 1. Specification of images

Sensor Name	MSS (J-SCAN-AT18M)	CASI (vegetation mode)	CASI (red edge mode)
Observation date	1993/8/2	1993/9/2	1993/9/2
Observation Time	14:57	11:08	
Flight altitude	4,000 m	3,000 m	3,000 m
FOV	80°	35°	35°
IFOV	about 10m	about 3.7 m	about 3.7 m

channel	range (μm)	channel	range (μm)	channel	center (μm)*
1	0.340-0.430	1	0.431-0.459	1	0.6817
3	0.462-0.481	2	0.461-0.489	2	0.68705
5	0.535-0.557	3	0.491-0.519	3	0.6924
8	0.654-0.669	4	0.521-0.550	4	0.6978
9	0.688-0.708	5	0.551-0.580	5	0.7032
10	0.723-0.740	6	0.582-0.608	6	0.7086
11	0.762-0.782	7	0.610-0.639	7	0.714
12	0.820-0.900	8	0.640-0.669	8	0.7194
14	1.000-1.100	9	0.671-0.700	9	0.7248
15	1.520-1.720	10	0.701-0.728	10	0.7302
16	2.060-2.450	11	0.730-0.759	11	0.7356
17	8.000-12.00	12	0.761-0.788	12	0.741
		13	0.790-0.819	13	0.7464
		14	0.821-0.849	14	0.7519
		15	0.851-0.878		

*:Spectral resolution was approximately 3.6nm.

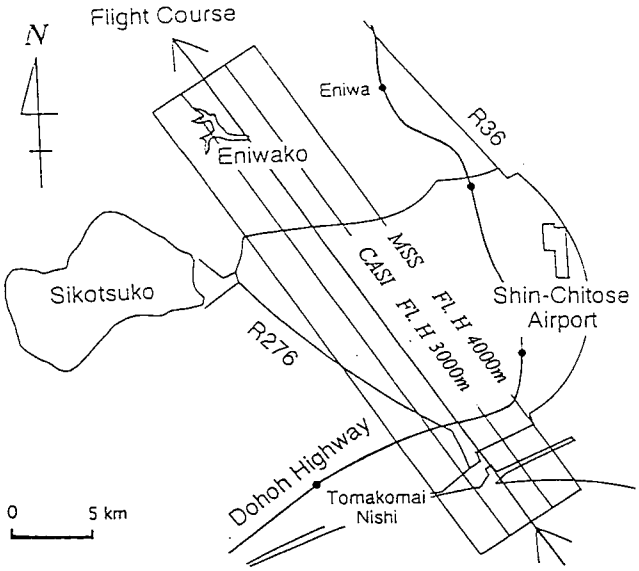

Fig. 1. Test site and flight course location map.

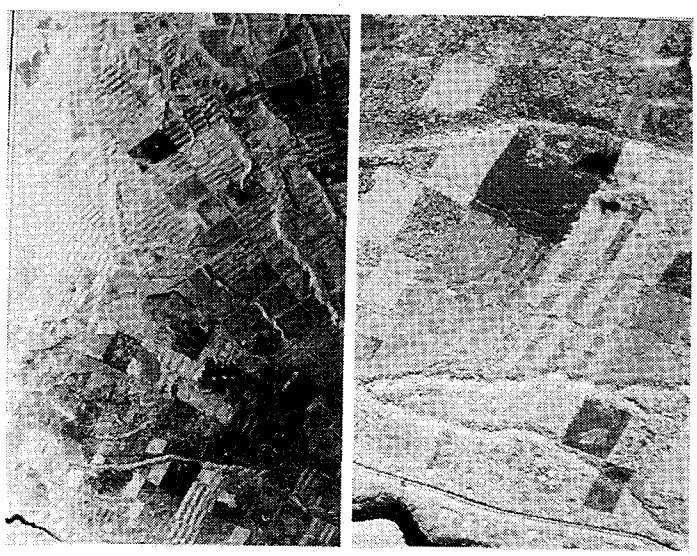

Fig. 2. MSS and CASI (vegetation mode) images. left: MSS channel 10 (723-740nm), right: CASI channel 11 (730.2-759.1nm). A part of the images are shown. A river in the left bottom in each image is the same one. The longer side of the largest rectangular forest compartment is 1 km, and the shorter side is 550m. Dark forests are spruce stands.

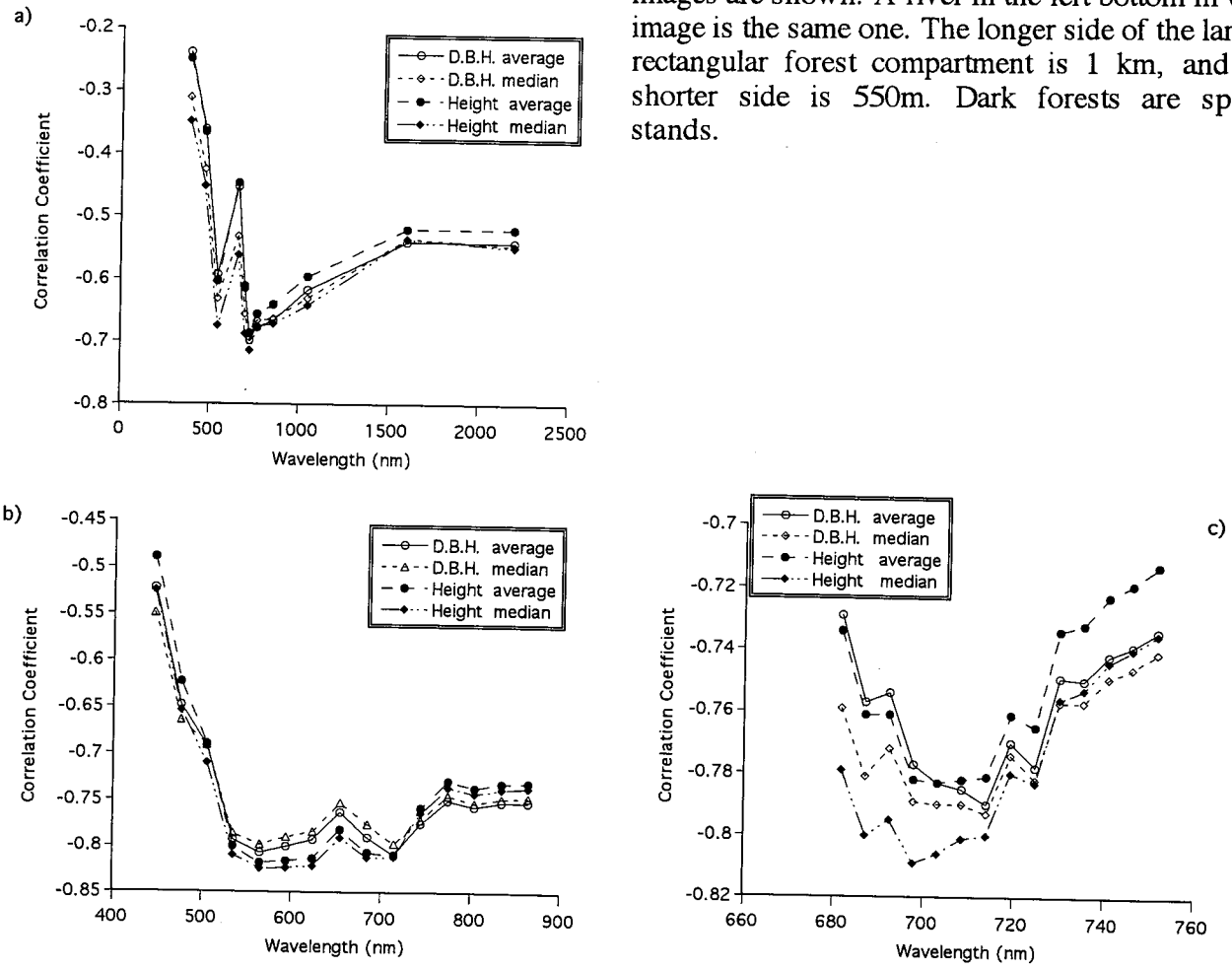

Fig. 3. Correlation coefficients between D.B.H., height and digital number.
D.B.H. and Height of a) MSS data, b) CASI vegetation mode data, and c) CASI red edge mode data.

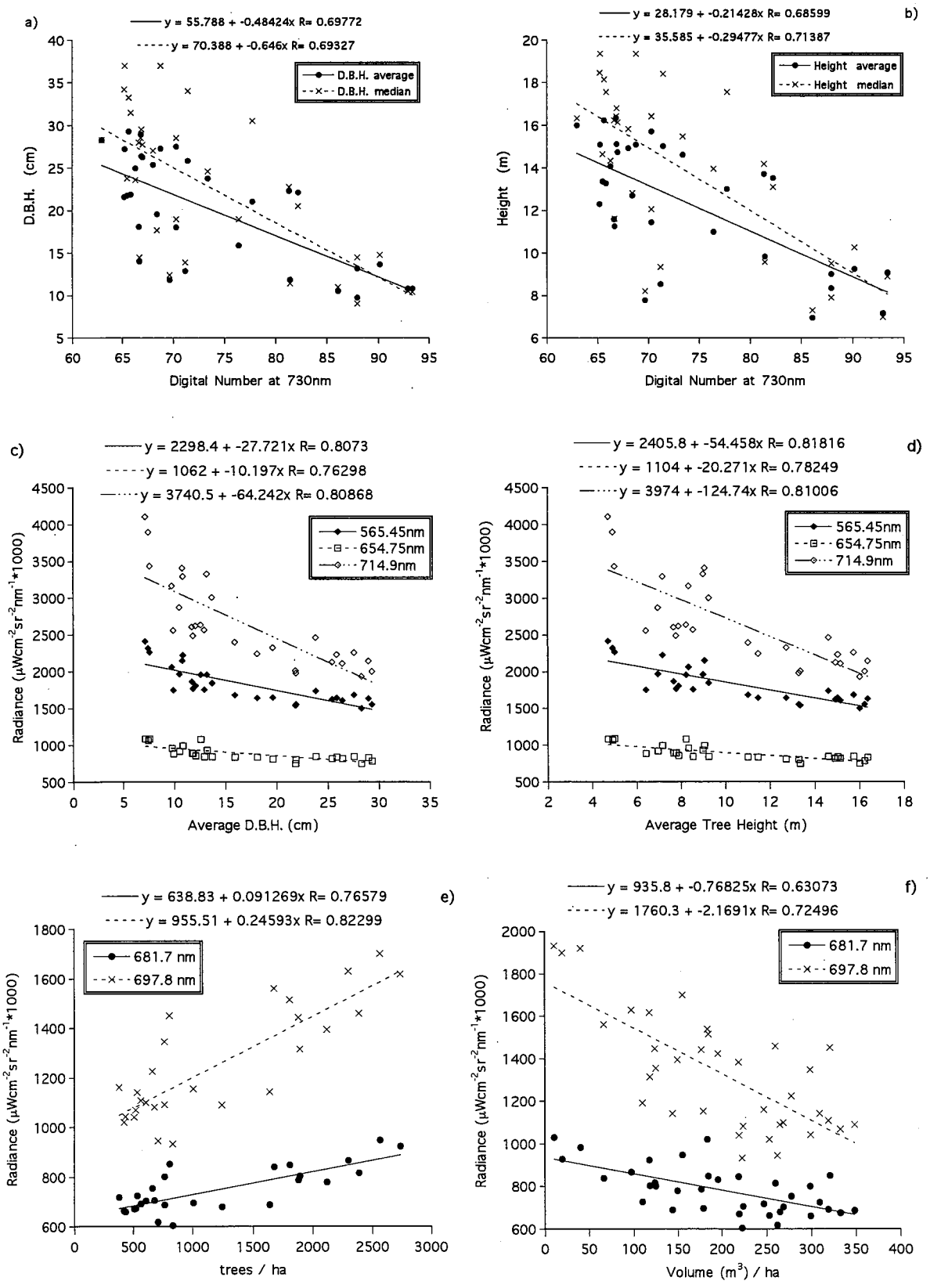

Fig. 4. Scattergrams between stand parameters and digital number.
a) D.B.H. and b) Height in the case of MSS, and c) D.B.H., d) Height. e) tree density and f) Volume in the case of CASI images.

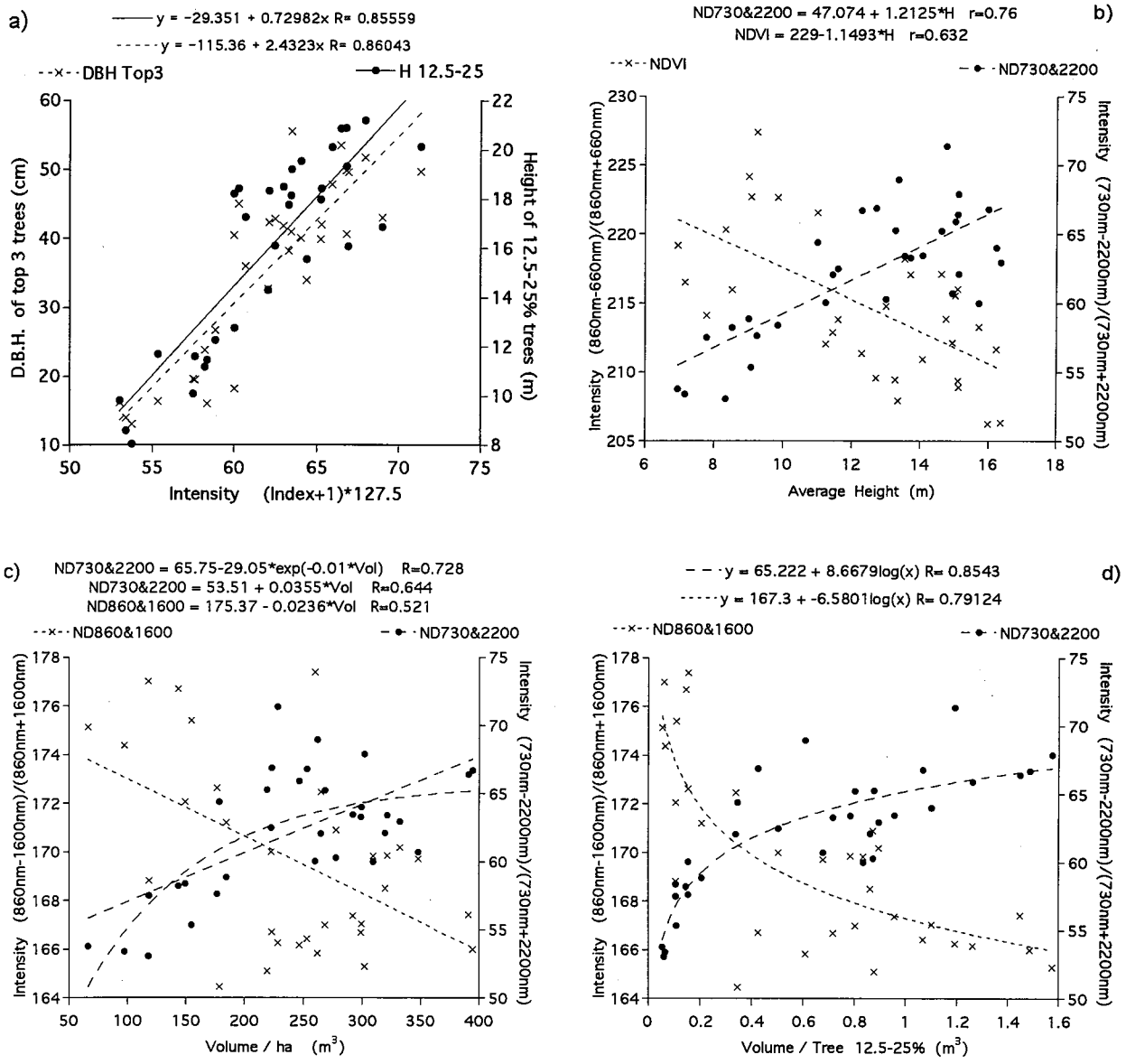

Fig. 5. Scattergrams between stand parameters and indices of MSS image.
a) D.B.H. of top 3 trees and upper story height against ND730&2200, b) Height against NDVI and ND730&2200, c) Volume per hector against ND860&1600 and ND730&2200, d) Volume per upper story tree against ND860&1600 and ND730&2200.

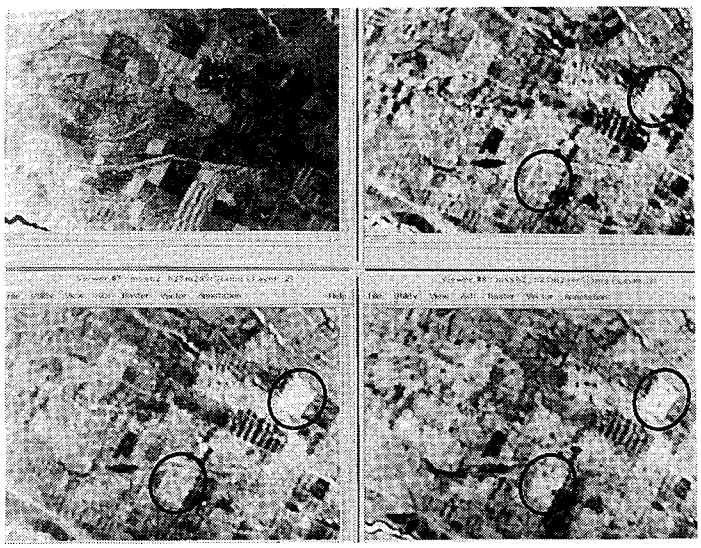

Fig. 6. Results of upper story height estimation using 3 models.

upper left: ch-10 (723-740nm)
Results are
upper right: using ND730&2200 r=0.856, lower left: using ND730&2200, ND730&545 r=0.865, lower right: using ND730&2200, ND730&545, 2200nm r=0.865
Though the left and the right circles show stands with similar tree height, results show significant difference in the lower two cases.

Ground Based Observation of Vegetation Coverage, LAI and APAR to Develop New Vegetation Indices Algorithm for ASTER

Y. Numata(*), K.Saito(*), Y. Yamano(*),Y. Yasuoka(**) and M. Kaku(***)

* Asia Air Survey Co.,Ltd.
13-16, Tamura-cho, Atsugi-shi, Kanagawa-ken, Japan 243
Fax +81-462-22-1281
E-mail : KFH02140@niftyserve.or.jp

** National Institute For Environmental Studies
16-2, Onogawa, Tsukuba-shi, Ibaragi-ken, Japan 305
Fax +81-298-51-4732

***Earth Remote Sensing Data Analysis Center
3-12-1, Kachidoki, chuo-ku, Tokyo, Japan 104
Fax +81-3-3533-9383

Abstract

To develop new vegetation indices algorithm, some vegetation parameters which are Vegetation Coverage(VC), Leaf Area Index(LAI) and Absorbed Photosynthetically Active Radiation(APAR) were obtained by ground based observation with spectral reflectance for cypress, willow, konara oak and grasses.

VC data was obtained through interpretation of photograph which had taken from cherry picker sited above the vegetation canopy. LAI was directly measured through the number of leaves and their area. APAR data was acquired by using Line quantum sensor. Wide spectral range data was used to relate these vegetation parameters to spectrum.

As a result of statistical analysis using these data, significant correlation was found between spectral data and these vegetation parameters. It suggests the possibility of new vegetation indices algorithm.

1. Introduction

In recent years attention has been focused on environmental problem such as global deforestation and desertification that causes soil erosion, climatic change and so on [ex) Univ. Tokyo,1993 ; Zorpette. G,1993]. Vegetation monitoring from space helps us to solve these environmental problems.

NDVI has been used for vegetation monitoring in various environmental study. But it is difficult to get biological information of vegetation by using NDVI, because the index is affected by a lot of different vegetation factors such as species, biomass, photosynthetic activity and coverage.

EOS-AM which will be launched in 1998 has five optical sensors. ASTER is one of the

characteristic sensor which has many spectral bands in short wave infrared region. Most important role of these bands is the application for geological studies. In addition it is also expected to be applicable for ecological survey.

The objective of this study is to develop new vegetation indices algorithm for ASTER data. The indices are expected to be evidently correspondent with biological parameters of vegetation not but vegetation species.

LAI, APAR and VC were observed for grass, deciduous tree and coniferous tree. Each parameter corresponds to vegetation volume, quality and distribution respectively. Spectral data was acquired together with these vegetation parameters observation. Statistical analysis was applied for the investigation of the relationship between these vegetation parameters and spectral data. Then we discussed the optimum vegetation indices for ASTER.

We mainly described observation methodologies of vegetation parameters and field spectrum measurement in this paper.

2. Observation Methodologies

2.1 Observation site

Observation was carried out at Tsukuba which locates southern part of Ibaragi pref. (Figure 1). Because a lot of agricultural laboratories with various vegetation field exist in this region, it is easy to get data for many kinds of vegetation under various conditions.

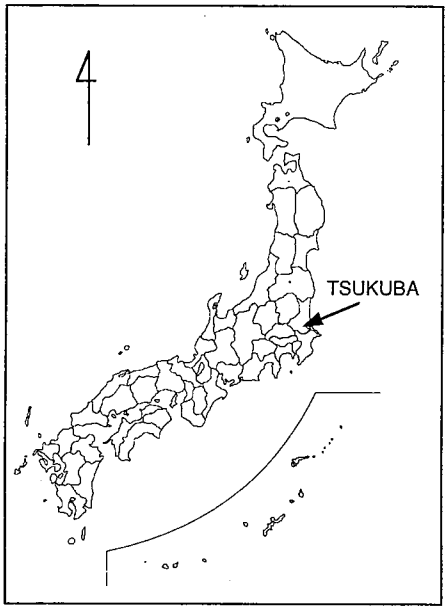

Figure 1. Observation site in this study

2.2 Observation targets

Observation targets were cypress, willow, konara oak and grasses. Their colony can be seen everywhere in Japan. Because each field has more than about 10m x 10m area, it is possible to regard them horizontally uniform for radiation.

2.3 Observation platform

As our concern is oriented toward satellite based indices, VC, APAR and spectrum must be perpendicularly observed by instruments just above the vegetation canopy. Because each target is more than about 5m tall, cherry picker was used as a observation platform (Figure 2). Figure 3 shows the workable area of basket loaded on the cherry picker which was used in this study. It is possible to observe perpendicularly around the center of a colony far enough from the top of vegetation canopy.

Figure 2. The cherry picker (the right side)

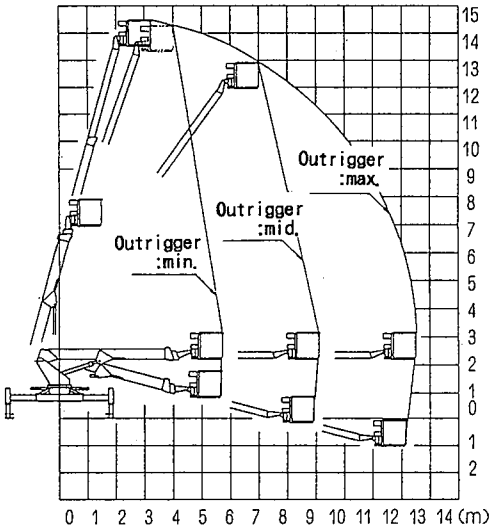

Figure 3. Workable Area of the cherry picker

2.4 Spectrum observation

MSR-7000 spectrometer loaded on the cherry picker basket was used for the vegetation spectrum observation. Main specifications of MSR-7000 is given in table 1.

Table 1. Specifications of MSR-7000

Spectral range	80 - 2500 nm
Spectral interval	1nm
Focal length	350 mm
IFOV	22°
Scan time	about 3 min.

MSR-7000 with wide spectral range is very easy to set on a small basket of the cherry picker, because light-gathering instrument is made by fine optical fiber. On the other hand it is difficult to grasp precise position of targets, because MSR-7000 has no view-finder. Therefore we attached optical fiber to CCD camera with two dimensional level and true up each optical axis as shown in Figure 4. Operator can easily decide position of the optical sensor by monitoring a video CRT.

Figure 5 shows a typical example of spectral radiance of vegetation. As S/N value is extremely low in short wave infrared region, it was necessary to use moving average with wide window. A discontinuity which is appeared near 1500 nm was corrected by manual interpolation.

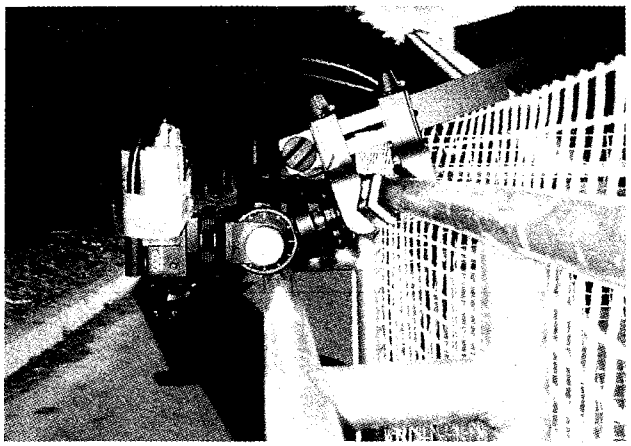

Figure 4. Optical fiber of MSR-7000 on CCD camera

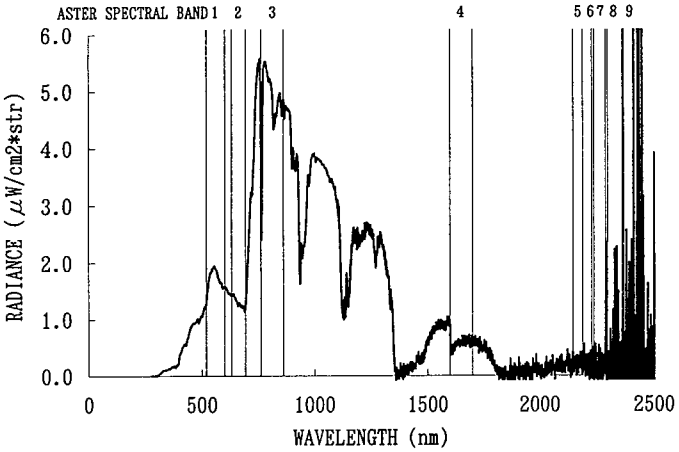

Figure 5. Radiance of vegetation acquired by MSR-7000

2.5 VC observation

At the same time of spectrum observation, several photographs of the same point were taken under different exposure so as to take all canopy layer.

Photographs were digitized by image scanner in 24-bit data with masking sheet which corresponds to IFOV of spectrometer. To extract canopy part on the image, [green] / [red] ratio was calculated, and binary image was made from the ratio image. Then VC can be got by summing up both canopy area and no-canopy area. Figure 6 gives photograph of grass and its binary image. In this case VC is 63%.

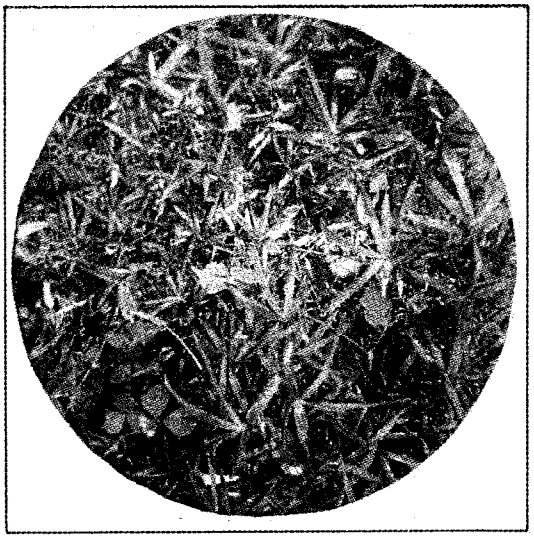

Figure 6-a. Original image

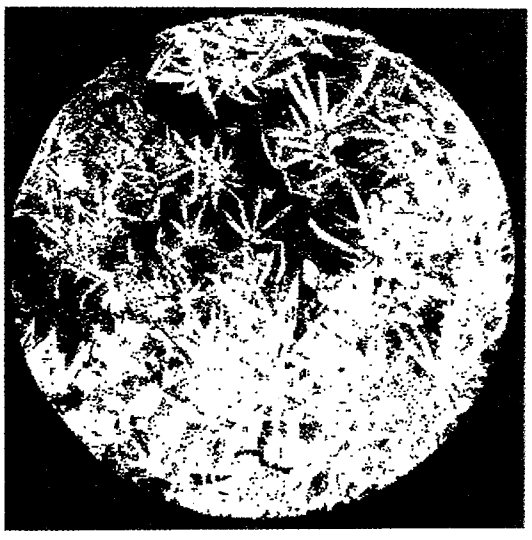

Figure 6-b. Binary image

2.6 LAI observation

LAI is a botanically important parameter. However LAI is difficult to measure accurately, because it is almost impossible to count directly leaf number per unit area.

In this study leaf area was measured by planimeter for some sample leaves. We count leaf number directly both from ground and cherry picker using frame of 50cm x 50cm area as a reference.

2.7 APAR observation

LI-191S line quantum sensor was used to get APAR data. Table 2 gives specifications of LI-191S.

Table 2. Specifications of LI-191S

Spectral range	400 - 700 nm
Response time	10 μ sec
Cosine correction	Corrected up to 80° of incidence
Azimuth	1% error over 360° at 45° elevation

We quickly measured the following PAR elements by using two line quantum sensors.

At↓ : Downward PAR above the vegetation canopy
At↑ : Upward PAR above the vegetation canopy
Ab↓ : Downward PAR below the vegetation canopy
Ab↑ : Upward PAR below the vegetation canopy

APAR and FAPAR are defined as follows. Each parameter gives absorbed PAR amount and rate respectively.

$$APAR = (At\downarrow + Ab\uparrow) - (At\uparrow + Ab\downarrow) \quad (1)$$

$$FAPAR = APAR / At\downarrow \quad (2)$$

3. Results and Discussion

We used the data which was obtained by observation mentioned above for preliminary analysis. Figure 7 shows the relationship between ASTER spectral bands operation and VC with regression curve. Figure 8 shows LAI versus ASTER spectral bands operation with regression curve. Significant correlation can be seen in each figure.

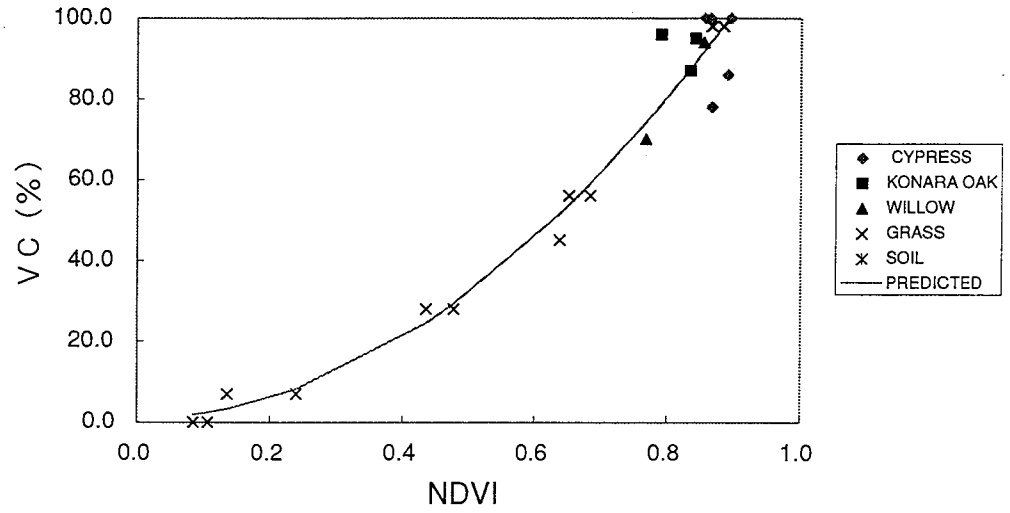

Figure 7. Relationship between ASTER spectral bands operation and VC

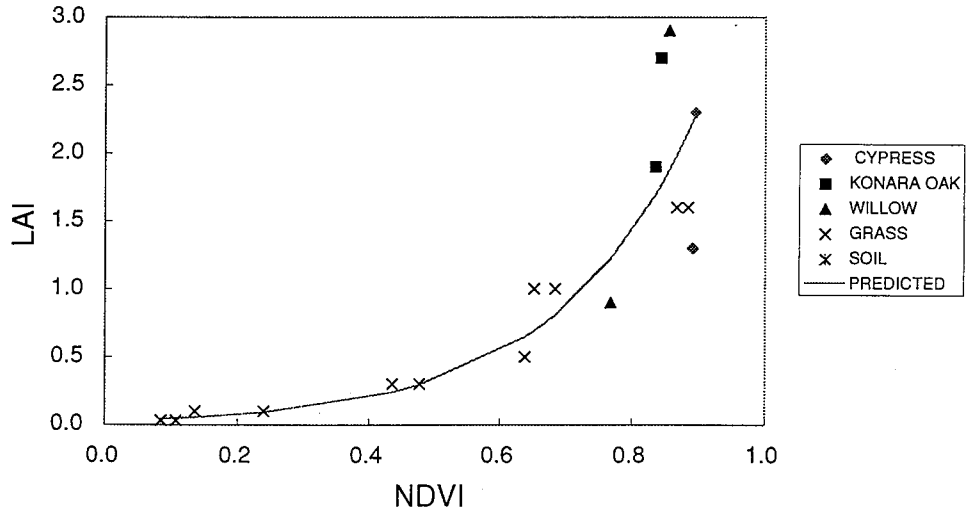

Figure 8. Relationship between ASTER spectral bands operation and LAI

There is remarkable noise in spectral data especially in short wave infrared region. Because the noise is not excludable using any type of digital filter, we cannot use band 8 and 9 which are the longest bands of ASTER VNIR. Although main target of these bands is geological use, they are expected to include much information of vegetation. Because leaf moisture affects the reflectance in these spectral range. If these spectral bands are available, higher correlation will be appeared between ASTER spectral bands operation and these two vegetation parameters. Consequently it is necessary to improve spectrometer for data acquisition in near future.

4. Conclusion

VC, LAI, APAR and spectrum was observed to develop algorithm of new vegetation indices for ASTER data. Methodologies of observation are very simple, practical and applicable to satellite data. As a result of this observation, accurate data was acquired for each vegetation parameter. Clear correspondence was found between ASTER spectral bands operation and each vegetation parameters. In near future improvement of spectrometer will make it possible to relate spectrum

to vegetation parameters with higher correlation.

5. Acknowledgment

This study was implemented by financial support of ERSDAC "Research and Development of remote sensing technology for non-renewable resources - Development of technology for ASTER data application" project.

6. References

Univ. Tokyo, "Global Environment Monitoring from Space. Proceedings of SEIKEN SYMPOSIUM, Vol. 12. ", Glob Environ Monit Space. Proc Seiken Symp, Vol.12, 340p, 1993

Zorpette. G, "Special report : Environment. Part 1. Sensing climate change. ", IEEE Spectrum, Vol.30. No.7, pp.20-27, 1993

Monitoring Global Energy Flow to Primary Production

Dennis G. Dye

Institute of Industrial Science
University of Tokyo
7-22-1 Roppongi, Minato-ku
Tokyo 106, Japan
Fax: +81-3-5411-0441
E-mail: dye@shunji.iis.u-tokyo.ac.jp

Abstract

Global satellite estimates of annual incident and terrestrial vegetation-absorbed photosynthetically active radiation (PAR, 400-700 nm) are evaluated for the 11 years from 1979 to 1989. The data sets were derived from Nimbus-7 Total Ozone Mapping Spectrometer (TOMS) and NOAA Advanced Very High Resolution Radiometer (AVHRR) observations. The mean annual total PAR incident at the Earth's surface between 60°N and 60°S latitudes is estimated to be 1.26 x 10^6 EJ, of which 9.17 x 10^5 EJ (73%) is incident on ocean surfaces and 3.42x 10^5 EJ (27%) is incident on terrestrial surfaces. A 1.7% reduction in northern hemisphere (60°N-0°) incident PAR in 1982 is attributed to changes in cloud amount and distribution associated with El Niño-Southern Oscillation conditions and possibly aerosols from the 1982 El Chichón volcanic eruption. The estimated annual total PAR absorbed by terrestrial vegetation (APAR) between 60°N and 60°S is 1.10 x 10^5 EJ, or 8.8% of total incident PAR (11-year means). The observed patterns of distribution and variability account for the primary flow of energy to global primary production.

1. Introduction

Life processes on Earth, with limited exceptions, are supported by the solar energy that is initially captured through photoautotrophic primary production. This captured energy becomes stored in the chemical bonds of plant biomass and comprises the basic energy reservoir for the planetary food web. Primary production also influences the state and functioning of the biosphere through linkages to physical processes of the Earth system, including the global biogeochemical, hydrological and nutrient cycles.

The amount of PAR energy absorbed by terrestrial vegetation over a particular time interval (APAR, MJ m^{-2}) may be computed as

$$APAR = FAPAR \cdot S, \quad (1)$$

where FAPAR is the fraction of incident PAR absorbed by the photosynthetic elements of the vegetation cover, and S is the total incident PAR (MJ m^{-2}). The term FAPAR is a measure of the capacity of the vegetation in the observed landscape to intercept and absorb incident PAR, and is closely related to green-leaf biomass and leaf area index (LAI). The S term defines the amount of PAR energy that is available for interception and absorption. The product of FAPAR and PAR determines the amount of energy diverted to the primary production process, and reflects the combined influence of vegetation cover and solar climate.

Global patterns of incident and absorbed PAR can be effectively estimated and monitored on a global basis using satellite remote sensing techniques [Dye and Goward, 1993]. This paper reports on an initial examination of the global space-time patterns in global incident PAR and terrestrial APAR.

2. Data and Methods

2.1 Incident PAR

A data set consisting of monthly total of incident PAR was produced in earlier work [Dye, 1992, Dye and Shibasaki, 1995] using 370 nm reflectivity measurements from the Nimbus-7 Total Ozone Mapping Spectrometer (TOMS) [Eck and Dye, 1991]. The data set's original spatial resolution of 1° x 1.25° (latitude x longitude) was changed to 1° x 1° for consistency with the FAPAR data set. The resolution change was made by computing the spatially weighted average of each original-resolution grid cell overlapping each 1° x 1° grid cell. This study considers only latitudes between 60°N and 60°S to avoid inconsistencies among months caused by missing or possible ice or snow-contaminated observations at higher latitudes. The surface area in this latitudinal region is 4.47 x 10^8 km^2, or approximately 86% of the total global surface area of 5.20 x 10^8 km^2. The time coverage available from Nimbus-7 TOMS covers more than 14-years from November 1978 until March 1993. The performance of the TOMS instrument, however, declined after 1989. This study examines data from the period 1979 to 1989.

2.2 PAR-Absorption Capacity of Vegetation Cover

Field and modeling studies have demonstrated that a strong, near-linear relationship exists between remote sensing-derived measurements the normalized difference vegetation index (NDVI) and FAPAR. The time-series, global-coverage NDVI estimates available from the NOAA AVHRR sensor provide an effective means for estimating FAPAR on a global basis [Dye and Goward, 1993]. An existing global data set of monthly FAPAR values was adopted for this study. The FAPAR data set was produced by Mr. Sietse Los and others at NASA Goddard Space Flight Center as part of the International Satellite Land Surface Climatology Project (ISLSCP) Initiative I data collection effort [Sellers et al., 1994]. Global FAPAR data from this source are currently available for two years, 1987 and 1988. Monthly averages for these years were averaged for this analysis. Because FAPAR patterns are assumed invariant, any observed variations in APAR are attributable to variations in incident PAR..

Although a decadal scale global archive of calibrated NDVI measurements from the AVHRR is available, application of the data to monitoring interannual variations in FAPAR is hindered by difficulties in separating the residual effects of clouds and other atmospheric sources of contamination (aerosols, water vapor) from real changes in vegetation properties. The problem is particularly acute in seasonally or perennially moist subtropical and tropical regions, where persistent cloudcover reduces the effectiveness time-composite methods for reducing cloud contamination. It is noteworthy that whereas atmospheric effects constitute noise for the NDVI, they constitute the target signal in the TOMS UV reflectivity data since they account for variation in atmospheric transmission of PAR. Until the problem of atmospheric effects on global, time-series NDVI observations can be further resolved, it is likely that subtle variations in incident PAR may be detected with greater certainty than subtle variations in FAPAR, at least for snow and ice-free surface conditions.

3. Results and Discussion

3.1 Incident PAR

The potential (clear-sky) distribution of annual total PAR at the Earth's surface is determined by seasonal variations in Earth-sun distance and latitudinal and seasonal variations in sun-earth geometry. In the absence of variable clouds and aerosols, incident PAR would decrease as even gradient from the tropics to the poles. Seasonal and geographic variations in clouds and aerosols, however, interact with the potential pattern, resulting in the observed distribution of annual total PAR (Fig. 1) and space-time dynamics (Fig. 2a). In the equatorial regions, perennially abundant cloud cover substantially reduces PAR at the surface relative to the global maximum potential amount. The greatest annual amounts of PAR are received at

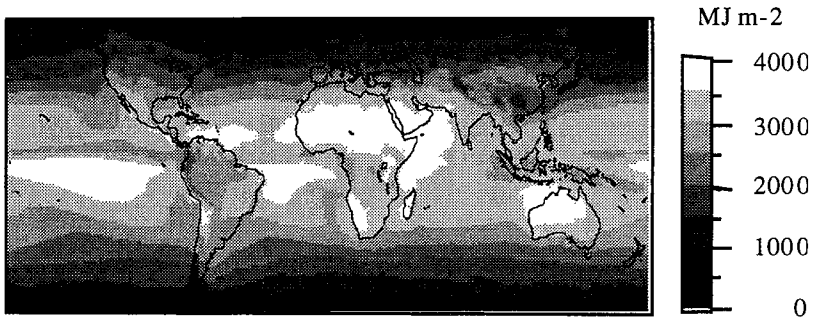

Figure 1. Mean of annual total PAR for years 1979 to 1989, excluding 1982 and 1983. Estimates are based on 370 nm reflectivity data from Nimbus-7 TOMS.

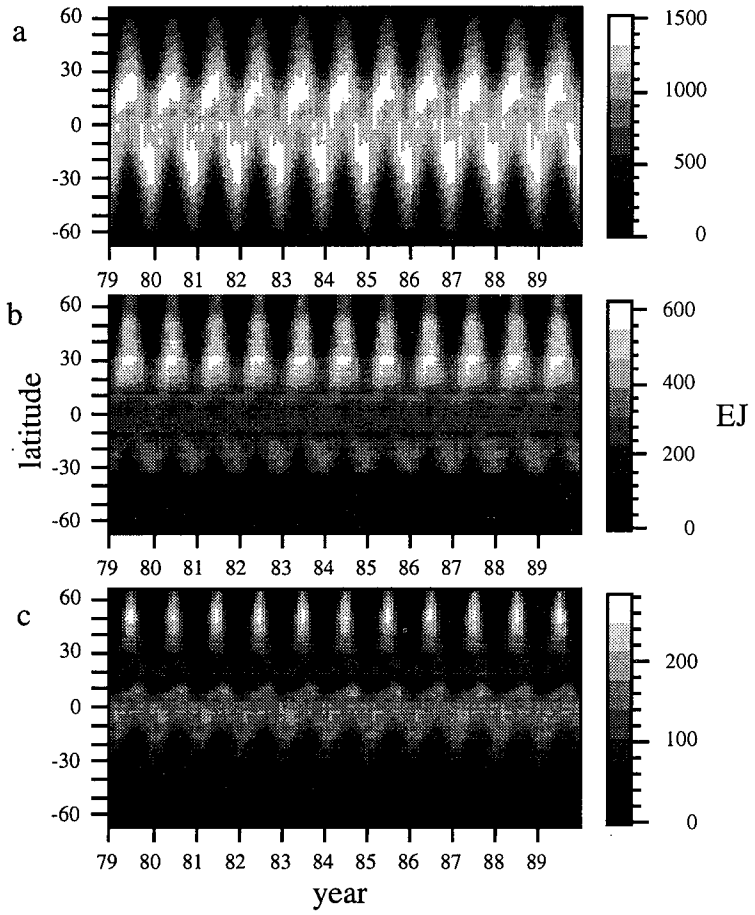

Figure 2. Temporal and latitudinal variation in monthly 1° zonal totals of (a) incident PAR, (b) terrestrial incident PAR, and (c) terrestrial absorbed PAR (APAR).

subtropical latitudes in zones characterized by atmospheric subsidence. These areas are associated with major arid regions of the globe.

For the 11-year observation period, the mean of the total annual PAR received at the Earth's surface (60°N-60°S) is 1.259 x 10^6 EJ (1 EJ = 10^{18} J). The minimum value of 1.250 x 10^6 EJ occurred in 1982, and the maximum value of 1.263 x 10^6 EJ occurred in 1986. These values represent the maximum energy available annually for use in photosynthesis and primary production. The effective incident PAR, however, would be less than the total incident PAR

when taking into account PAR received when photosynthesis is restricted by freezing temperatures.

The time series of annual total global PAR shows no strong decadal trend (Fig. 3a). The year 1982, however, is marked by an anomalous reduction in PAR, which is particularly pronounced in the northern hemisphere (Fig. 3a,b). At least two events of global significance occurred in 1982 that may account for this anomalous reduction. One is the onset of a major El Niño/Southern Oscillation event that carried over into 1983. ENSO conditions are characterized in part by regional changes in cloudiness, notably a shift in cloud cover (and sea surface temperature) from the western to the eastern tropical Pacific Ocean. Another notable event in 1982 was the eruption of Mexico's El Chichón volcano, which released a large volume of aerosol material into the atmosphere and reduced the transmissivity of the atmosphere.
From an analysis of the geographic distribution of yearly anomalies in annual total PAR relative to a 1979-1989 base period (excluding 1982 and 1983), the maximum observed deviations occur in 1982 and 1983 in the tropical Pacific Ocean (Fig. 4). The large negative anomaly in the tropical Pacific Ocean in 1983 is evidently counterbalanced by positive anomalies in other regions, such that the effect on the global total PAR is less than in 1982. The observed PAR anomalies in the tropical Pacific Ocean are generally consistent with the cloudcover shifts associated with ENSO conditions. Possible teleconnections of anomalies in other regions to ENSO conditions requires additional investigation. Atmospheric mixing may cause the potential effects of El Chichón aerosols to be more spatially homogeneous than ENSO effects, particularly over the annual periods represented here, and thus less readily detectable in the anomaly maps.

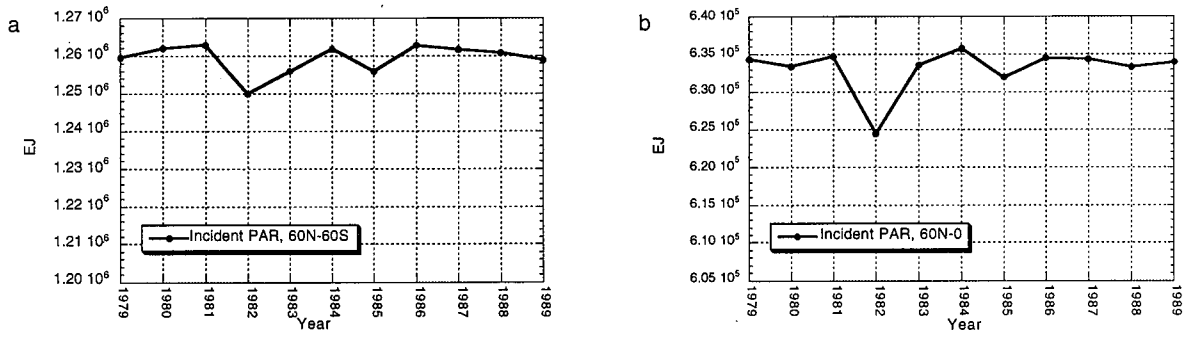

Figure 3. Time series (1979-1989) of annual total surface-incident PAR for (a) 60°N to 60°S and (b) 60°N to 0° (northern hemisphere).

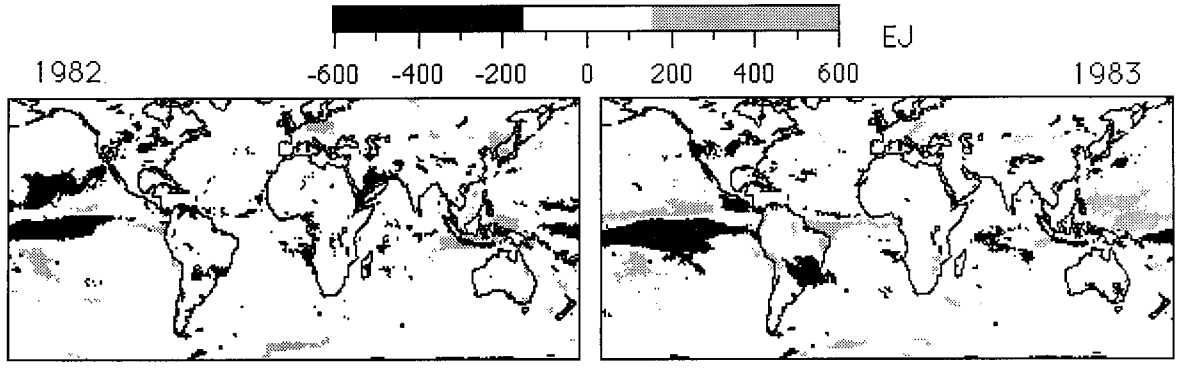

Figure 4. Anomalies in 1982 (left) and 1983 (right) in the annual total PAR per 1° grid cell, relative to base period for 1979-1989, excluding 1982-83.

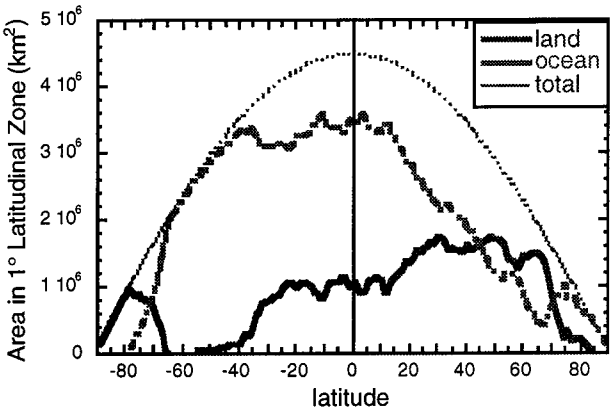

Figure 5. Variation in the total surface area within 1° latidudinal zones for land, ocean and combined (land + ocean) surfaces.

3.2 Ocean and Terrestrial-incident PAR

The calculated 11-year (1979-1989) means of annual total PAR incident for the terrestrial and ocean surfaces (60°N-60°S) are 3.42 x 10^5 EJ (27% of total) and 9.17 x 10^5 EJ (73% of total), respectively. These calculations involved reference to Matthews' [1983] global 1° vegetation map for discriminating land and ocean areas. The key factors that influence this distribution between land and ocean are the proportion and latitudinal distribution of land and ocean surface areas (Fig. 5), and land-ocean differences in cloud cover distribution and seasonality.

The geographical configuration of the land masses and associated seasonal cloud patterns causes the space-time pattern of terrestrial incident PAR (Fig. 2b) to diverge markedly from the global (land + ocean) pattern (Fig. 2a). The proportion of land in southern hemisphere latitudes declines rapidly from about 23% in the tropic zone to 0% near 55°S latitude, which marks the southernmost extent of the South American continent. No significant land area occurs between 55°S and the beginning of the Antarctic continent at approximately 64°S. South of the southern extent of Australia at about 40°S latitude, terrestrial incident PAR is limited primarily to that intercepted by southern Argentina and Tierra del Fuego in South America, and is absent altogether below 55°S latitude in the 60°N-60°S study area (Fig. 2b). In both proportional and absolute terms, the greatest land surface areas occur at middle latitudes in the northern hemisphere, between about 15°N and 50°N (Fig. 5). In this region of the northern hemisphere, land comprises between about 40% to 60% of the total zonal surface area. The highest annual amounts of terrestrial incident PAR occur in this region. A distinct global peak of between 500 and 600 EJ per 1° latitude occurs in the summer months near 30°N. This peak is attributable to the combination of extensive land area coincident with the occurrence of zones of atmospheric subsidence associated with major desert or arid regions. The strong latitudinal contrast in the seasonality of terrestrial incident PAR is also apparent. Tropical latitudes are characterized by a steady monthly rate of energy receipt, with seasonality increasing steadily with increasing latitude.

Separation of the global total annual PAR figures into ocean and terrestrial components permits their interannual dynamics to be evaluated independently. The time patterns of incident PAR for land and ocean areas (Fig. 6) suggest that the 1982-83 ENSO event (and possibly El Chichón) had a pronounced effect on the PAR regime in both ocean and terrestrial environments. The likely source for the anomalous reduction in terrestrial PAR is observed in 1985 (Fig. 6b,d) cause remains to be identified.

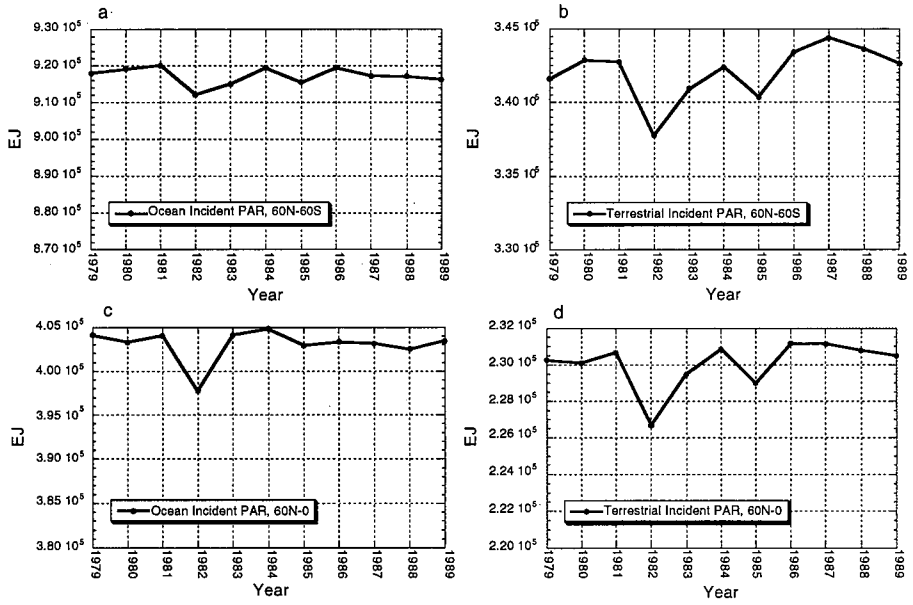

Figure 6. Time series for 1979-1989 of annual total incident PAR for (a) ocean surfaces (60N-60S), (b) terrestrial surfaces (60N-60S), (c) northern hemisphere oceans (0°-60°S), and (d) northern hemisphere terrestrial surfaces (0°-60°N).

3.3 Terrestrial Absorbed PAR

The analysis indicates that terrestrial vegetation between 60°N and 60°S latitudes intercepts and absorbs an average of 1.10 x 10^5 EJ PAR annually (mean for 1979-1989). This amount corresponds to 8.8% of the global total incident PAR and 32.3% of the total terrestrial incident PAR in this latitude zone. During the 11-year study period, annual terrestrial APAR varied from a minimum of 1.09 x 10^5 EJ in 1982 to a maximum of 1.12 x 10^5 EJ in 1987, corresponding to a dynamic range of 0.03 x 10^5 EJ or 2.7% of the 11-year mean. These figures assume the no interannual variation in monthly FAPAR patterns, as discussed earlier.

By definition, APAR at a given location and time is dependent on the simultaneous magnitude of FAPAR and PAR (Fig. 7). In effect, each variable scales the other. High incident PAR coincident with low FAPAR (e.g. a low or mid-latitude desert) produces low APAR. Conversely, high incident PAR coincident with high FAPAR produces high APAR (e.g, lush, irrigated croplands in an arid region). Global patterns in APAR thus cannot be reliably predicted from knowledge of either FAPAR or PAR alone.

The combination of discrete FAPAR and incident PAR patterns results in a space-time pattern for APAR (Fig. 2c) that is distinct from the component FAPAR and PAR patterns (Fig. 2a,b) [Dye and Goward, 1993]. The equatorial belt between approximately 10°N and 10°S latitude is characterized by perennially consistent, moderate zonal average rates of terrestrial APAR (150-200 MJ m^{-2} mo^{-1}). The global maximum rates occur in the middle latitudes the northern hemisphere summer months (200-280 MJ m^{-2} mo^{-1}). The relative paucity of vegetation cover relative to available PAR and land surface area in the subtropical belt between about 10°N and 30° N latitudes results in a relatively low zonal average APAR (50-100 MJ m^{-2} mo^{-1}). These latitudes of low photosynthetic activity form in effect a geographical buffer zone between the seasonally intensive productivity in the northern temperate latitudes and the perennially productive tropics.

The time series of annual total terrestrial APAR (60°N-60°S) exhibits notable interannual variation (Fig. 8). The influence of the ENSO and possibly El Chichón-related reduction in incident PAR on terrestrial APAR in 1982 is evident. The time series pattern of terrestrial incident PAR and terrestrial APAR, however, are distinct from one another. Although the monthly FAPAR patterns are fixed in this analysis, it is reasonable for the incident PAR and APAR time patterns to be unique. The differences may arise from interannual variations in spatial distribution of incident PAR over the fixed monthly FAPAR fields. A common time pattern would be expected only in the unlikely scenario that variations in incident PAR are perfectly and positively correlated in location and time with the fixed monthly variations in FAPAR.

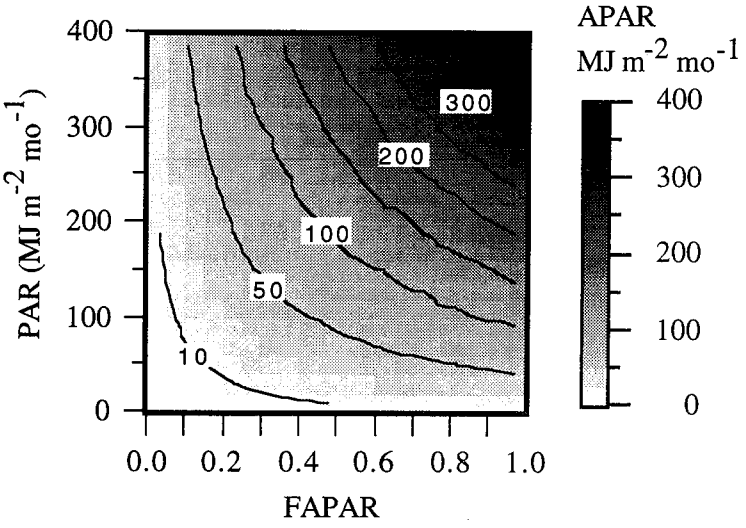

Figure 7. Variation in APAR (contours and gray levels) as a function of monthly incident PAR and FAPAR.

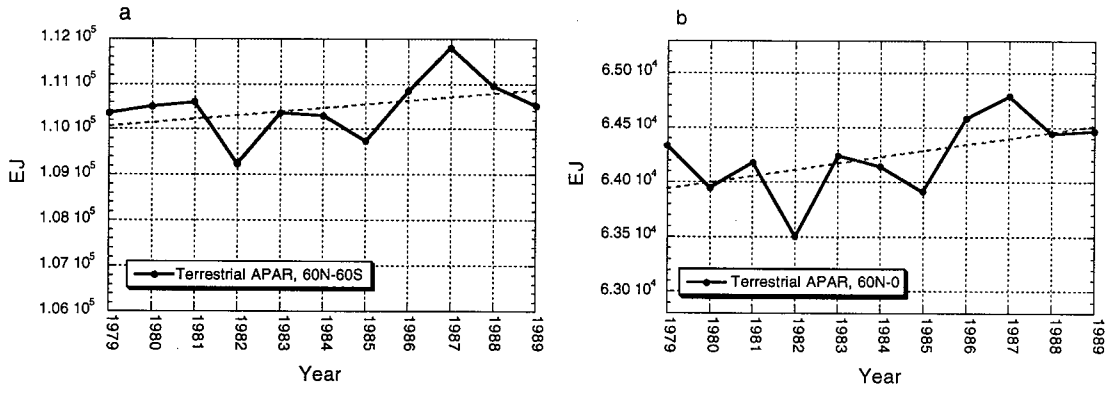

Figure 8. Annual variability in terrestrial APAR for (a) global land areas (60°N-60°S), and (b) the northern hemisphere land areas (60°N-0°). The dashed lines indicate the line of least-squares from linear regression.

A decadal-scale trend toward increasing terrestrial APAR is evident over a dominant portion of the 11-year observation period. Based on line of least squares from linear regression, terrestrial APAR increased at an average rate of 79.7 EJ y^{-1}, corresponding to a proportional increase of approximately 0.07% per year. A slightly stronger trend is evident when considering only the northern hemisphere, where the rate is 57.56 EJ y^{-1}, or approximately 0.9% of the 11-year mean northern hemisphere terrestrial APAR value of 6.42 x 10^4 EJ y^{-1}. The significance and reliability these statistical trends, their relation to other climate indices and biospheric functioning are currently under investigation.

4. Discussion and Conclusions

The results reported in this paper constitute a first satellite-based examination of the global receipt and biological diversion of photosynthetically active radiation. The observed patterns define the energy basis for global primary production and biospheric functioning. The observed interannual variations and trends, if confirmed, may have significant influence on global patterns of primary production. This influence may occur directly through fluctuations in the energy flow to photosynthesis, and indirectly through relations to other climatic variables, such as temperature and precipitation, that influence growth and production.

A limitation of the present analysis is the lack of accounting for possible interannual variations in FAPAR. Removal of cloud contamination from time-series NDVI observations while maintaining sensitivity to real variations in vegetation conditions is a vexing problem in remote sensing, particularly in seasonally or perennially cloud-prone regions. Time-series global NDVI data that are sufficiently free of cloud or other atmospheric contamination are critical to enable reliable detection of interannual variability in FAPAR.

Incident PAR and APAR data are typically required for application to physically based, mechanistic models of primary production. Incident or absorbed PAR may be used to predict rates of canopy photosynthesis based on a specified photosynthetic light-response curve [e.g., Goward and Dye, 1987] or by accounting for the overall "efficiency" with which time-integrated APAR is converted to dry matter [e.g., Prince et al., 1991]. Reliable parameterization of such models over the global range of vegetation physiognomic types and climatic conditions, however, remains a major research challenge. Given presently large uncertainties in such parameterizations, the satellite estimates of the global energy flow into primary production described here may be among the variables in which the most confidence may currently be placed. Additional research is in progress to provide additional validation and refinement of the satellite PAR and FAPAR measurements, and to achieve an improved quantitative assessment of the distribution and dynamics of global ocean and terrestrial productivity.

5. References

Dye, D.G., 1992. Satellite estimation of the global distribution and interannual variability of photosynthetically active radiation. Ph.D. dissertation, University of Maryland, College Park.

Dye, D.G., and Goward, S.N., 1993, Absorption of photosynthetically active radiation by global land vegetation in August 1984. *International Journal of Remote Sensing*, 14(18):3361-3364.

Dye, D. G., and Shibasaki, R., 1995, Intercomparison of global PAR data sets. *Geophysical Research Letters*, 22(15):2013-2016.

Eck, T.F., and Dye, D.G., 1991. Satellite estimation of incident photosynthetically active radiation using ultraviolet reflectance. Remote Sensing of Environment, 38:135-146.

Goward, S.N., and Dye, D.G., 1987, Evaluating North American primary productivity with satellite observations. *Advances in Space Research*, 7:165-174.

Prince, S.D., 1991, A model of regional primary production for use with coarse resolution satellite data. *International Journal of Remote Sensing*, 12:1313-1330.

Sellers, P.J., S.O. Los, C.J. Tucker, C.O. Justice, D.A. Dazlich, G.J. Collatz, and D.A. Randall, 1994. A global 1 by 1 degree NDVI data set for climate studies. Part 2: The generation of global fields of terrestrial biophysical parameters from the NDVI. *International Journal of Remote Sensing*, 15(17):3519-3545.

Vegetation/Land Cover Changes in Monsoon Asia and its influence on Areal Evaporation

Akihiko KONDOH (*)

* Center for Environmental Remote Sensing(*CEReS*),
Chiba University
1-33, Yayoi-cho, Inage-ku, Chiba 263, JAPAN
Fax. +81-43-290-3857
E-mail : kondoh@rsirc.cr.chiba-u.ac.jp

Abstract

The existing vegetation/land cover map is created by using NOAA's vegetation index product based on the seasonality of the vegetation formations. Hydrological parameters are assigned to each class by using available global datasets, and potential evaporation is calculated. Natural vegetation is restored based on the relationship between climate and vegetation(of cause it is a challenge to be solved), and it enables to assess the change in potential evaporation due to anthropogenic vegetation/land cover changes.

The datasets currently available are limited, and we cannot say that the hydrological processes in global or continental scales are sufficiently understood. The author regards this research as a trial study on the methodology. It is necessary to improve the accuracy of datasets and models with the use of new datasets, including satellite data, that are available in near future.

I. Introduction

Most important influence of anthropogenic vegetation/land cover alterations on regional environment is the changes in water balance at the ground surface. Human history can be regarded as the history of vegetation/land cover alteration. Through the man's activity during the historic era, the water balance in a region should be changed considerably and current environment has thus been established. To get the perspective for future global environment, it is necessary to recognize properly the result of land cover alteration during past several thousand years. For the purpose of it, the precise recognition of existing land cover is necessary, and then potential vegetation must be restored to estimate the changes in land cover. Hydrological function of each vegetation class is another important issue to be searched to estimate the changes in water balance due to land cover alterations.

2. Datasets

Seven datasets, listed below, are employed from the *Global Ecosystem Data Base(GEDB) CD-ROM* compiled by NOAA/NGDC(National Oceanic and Atmospheric Administration / National Geophysical Data Center).

(i) EDC-NESDIS Monthly Experimental Calibrated Global Vegetation Index
(ii) Legates and Willmott Annual Temperature
(iii) Legates and Willmott Annual Corrected Precipitation
(iv) Leemans and Cramer IIASA Mean Monthly Cloudiness
(v) Matthews Seasonal Albedo
(vi) Leeman's Holdridge Life Zone
(vii) Global Elevation and Bathmetry(ETOPO5)

It is easy to point out defects or problems of the datasets, however, the datasets are treated here as given data because they are currently the best datasets.

3. Existing Vegetation/Land Cover

Satellite remote sensing is the most suitable means to provide a existing land cover map in continental or global scales(Townshend *et al.*,1991). Vegetation/ land cover classification is made using seasonal trend of NDVI(Normalized Difference Vegetation Index).

EDC-NESDIS Monthly Experimental Calibrated Global Vegetation Index is used to classify land cover in Asia. The value of NDVI is sometimes smaller than zero. It means that red band reflectance is higher than that of near infrared band, and the signals on vegetation hardly contain in the index. The minus NDVI is replaced by zero, and produce new NDVI dataset.

Investigated area(60° N-20° S, 60° E-160° E) includes Monsoon Asia. Cluster analysis is applied to twelve monthly NDVIs, and forty-eight classes are obtained of which three are meaning-less classes due to the effect of mixels.

Each class is expected to represent characteristic hydrological parameters. They are the parameters, such as albedo, air temperature, precipitation, etc., necessary for the calculation of hydrological model, and small variance in each class is expected. Several global datasets are superimposed on the classification map, and the average hydrological parameters for each class are extracted.

Table 1 Forest types by Kira's warmth index. Tropical forest is divided into tropical seasonal forest and tropical rain forest based on the number of months which exceed 50mm in monthly precipitation.

Forest Type	Code	Warmth Index	Pm>50mm
Tropical Rain Forest	FTR	240 <	12
Tropical Seasonal Forest	FTS	240 <	< 12
Subtropical Forest	FST	180 - 240	----
Evergreen Broad Leaf Forest	FEB	85 - 180	----
Deciduous Broad Leaf Forest	FDB	45 - 85	----
Coniferous Forest	FND	< 45	----
	(℃·month)	(Num. of month)	

Kira(1945a,b) and Kira *et al.*(1976) revealed that the distribution of the warmth index is well

correspond to the distribution of vegetation formation in Asia. The index is defined as:

$$WI = \Sigma (T_i - 5) \quad i=1 \text{ to } 12,\ T_i > 5,$$

where T_i is monthly mean air temperatures(℃).

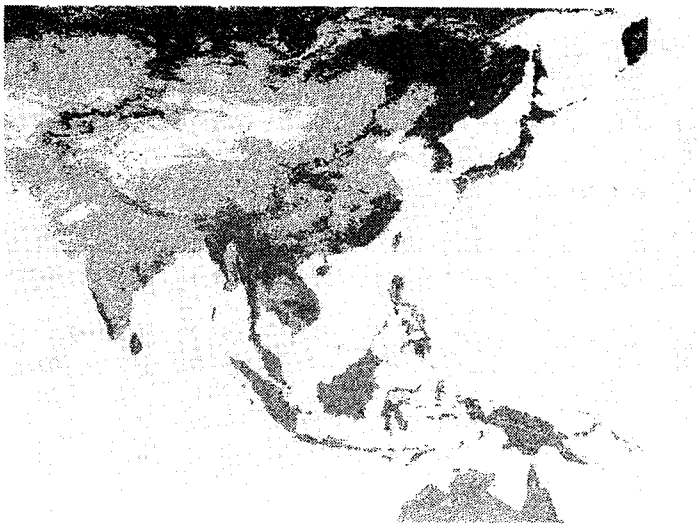

Figure 1 Current land cover. Grey level(0-255) denotes the vegetation/land cover classes. FND(32), FDB(64), FEB(96), FST(128), FTS(160), FTR(192), FBS(208), AGR/GRS(224), SEA(240) and DES(255).

The average indices of each class are calculated from the *Legates and Willmott Annual Temperature* dataset. Based on the criterion shown in Table 1, current forest type is assigned to each class. Other class is interpreted by referring geographic locations, ΣNDVI, and so on.

Table 2 shows the characteristic values of hydrological parameters for each vegetation/land cover class. Fig.1 shows current vegetation/land cover map over Monsoon Asia. Forest is drawn by darker tones, and grass and agriculture land looks bright. Ocean and deserts are white.

4. Restoration of Natural Vegetation

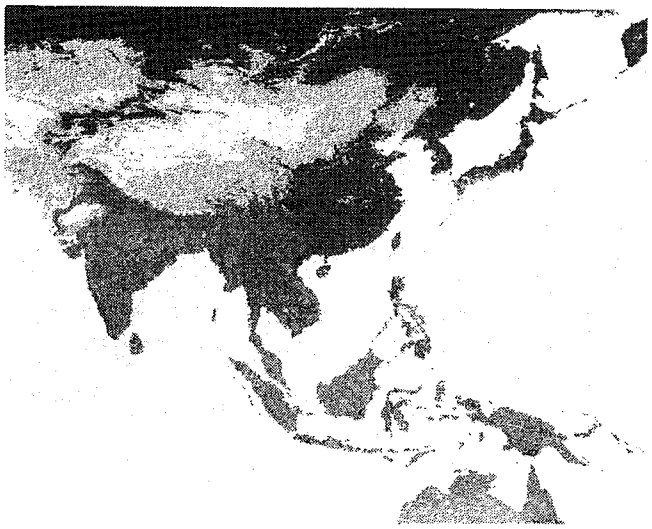

Figure 2 Natural land cover. Grey level(0-255) denotes the vegetation/land cover classes. FND(32), FDB(64), FEB(96), FST(128), FTS(160), FTR(192), FBS(208), AGR/GRS(224), SEA(240) and DES(255).

Table 2 contains the classes of *Leeman's Holdridge Life Zone(LHLZ)* dataset, which means possible vegetation formations under given climatic conditions. It is obtained as the most frequent *LHLZ* class within a vegetation/land cover class. The classes with aster(*) mean that current vegetation/land cover is grassland or cropland, but climatic condition allows the existence of the forest. Namely, the areas of these classes are subject to change in land cover by humans' activity in the historic era.

These classes account for about 24 per cent of the land area within the calculated region. Most of which occupies India and

Table 2 Results of vegetation/land cover classification by cluster analysis based on seasonal trend of NDVI. Characteristic values of ΣNDVI, warmth index(WI), annual precipitation(Pa) and the number of months which exceed 50mm in monthly precipitation(Pm>50mm), and they are used to determine the vegetation/land cover classes.

						ΣNDVI		WI		Pa		Pm>50mm		
	No.	Current Class	Restored Class	Leeman's Holdridge	Number of Pixels	(%)	mean	std.	mean	std.	mean	std	mean	std.	mode
	1	FND	FND	Bor Mois	6124	2.1	2.2	0.1	35.5	12.0	517.5	152.8	4.0	1.8	3
	2	DES	DES	ClTmp D/B	1767	0.6	0.2	0.1	114.9	69.9	390.0	733.5	0.0	0.0	0
	3	GRS	GRS	Po Des	2250	0.8	1.0	0.2	83.4	64.4	612.4	705.0	2.8	3.0	0
	4	GRS	GRS	ClTmp Ste	3928	1.4	1.4	0.2	51.4	25.6	411.8	224.6	2.5	2.0	3
*	5	AGR	FEB	WmTmp DryF	936	0.3	2.6	0.3	126.5	28.7	806.0	437.9	5.1	2.4	3
*	6	GRS/AGR	FND	Bor Mois	4303	1.5	1.9	0.2	38.8	20.7	483.1	185.4	3.5	1.8	3
	7	GRS	GRS	ClTmp Ste	3663	1.3	0.9	0.2	70.5	32.7	417.9	331.2	1.6	2.1	0
	8	FND	FND	Bor Mois	3050	1.1	2.4	0.2	38.1	15.5	594.4	206.3	5.2	2.4	4
*	9	AGR	FST	SbTrp MsF	2358	0.8	3.7	0.3	205.5	59.0	1573.1	582.1	6.9	1.7	6
	10	GRS	GRS	Po Des	5290	1.8	0.7	0.2	91.6	61.2	522.0	594.2	2.7	2.5	0
	11	GRS	GRS	SbTrp ThnS	3176	1.1	1.1	0.2	222.8	61.8	650.3	632.9	3.5	2.0	4
	12	FDB	FDB	ClTmp MsF	2819	1.0	3.2	0.3	58.4	15.0	711.7	220.0	5.8	2.2	5
	13	FEB	FEB	ClTmp MsF	1900	0.7	3.7	0.3	90.6	28.1	1076.7	454.9	7.9	2.7	7
*	14	AGR	FEB	WmTmp MsF	1462	0.5	2.6	0.3	137.8	44.1	1260.9	489.3	8.4	2.7	11
	15	FND	FND	Bor Mois	4734	1.6	2.5	0.2	37.6	12.9	454.3	158.3	3.2	1.7	2
	16	FDB	FDB	Bor Mois	3659	1.3	2.7	0.2	52.4	22.7	598.1	233.1	4.6	2.0	5
	17	FBS	FBS	Trp VDryF	1888	0.7	2.0	0.3	245.2	48.3	1008.7	710.1	4.9	2.0	5
*	18	GRS	FDB	Bor Mois	2246	0.8	2.0	0.2	54.2	29.9	516.9	259.9	3.7	2.5	3
	19	GRS	GRS	ClTmp Ste	3070	1.1	1.5	0.3	70.4	40.8	475.0	426.2	3.1	2.2	2
	20	FND	FND	Bor Mois	5304	1.8	2.7	0.2	41.3	8.7	511.3	155.8	4.1	1.7	4
	21	GRS	GRS	ClTmp Ste	4436	1.5	2.0	0.2	56.8	27.1	467.1	239.6	3.7	1.7	3
	22	FST	FST	SbTrp MsF	1467	0.5	4.3	0.3	212.9	42.4	1795.4	532.9	8.4	1.7	7
	23	GRS	GRS	Po Des	8402	2.9	0.4	0.1	104.6	61.9	369.0	510.0	1.4	2.1	0
	24	GRS	GRS	Po Rain T	1465	0.5	3.0	0.3	60.6	31.9	663.7	313.9	5.3	1.7	5
	25	FTR	FTR	SbTrp WetF	2403	0.8	6.0	0.4	248.6	28.9	2827.6	694.0	11.2	1.6	12
*	26	AGR	FEB	WmTmp DryF	1485	0.5	2.6	0.3	110.7	55.2	937.2	539.0	6.4	2.9	7
*	27	AGR	FTR	Trp DryF	1448	0.5	2.3	0.3	243.4	16.1	920.7	595.0	4.1	2.0	4
*	28	GRS/AGR	FTR	Trp VDryF	1862	0.6	1.5	0.4	246.6	34.9	1108.5	748.5	5.7	1.9	5
*	29	AGR	FEB	WmTmp DryF	979	0.3	3.3	0.3	135.3	30.0	928.8	465.2	6.4	2.1	6
	31	FTR	FTR	Trp MsF	1547	0.5	4.3	0.3	242.4	36.0	2343.7	691.3	10.6	2.3	12
	32	FTR	FTR	Trp MsF	2289	0.8	5.2	0.3	250.1	23.3	2736.2	653.7	11.2	1.5	12
	33	GRS/AGR	GRS/AGR	ClTmp Ste	900	0.3	1.7	0.3	100.1	52.2	616.5	590.8	3.2	3.0	2
	34	FEB	FEB	SbTrp MsF	1144	0.4	3.7	0.3	173.3	38.6	1620.1	310.8	9.7	1.5	10
*	35	AGR	FEB	WmTmp MsF	1921	0.7	3.3	0.2	147.0	35.0	1362.0	360.6	9.1	2.1	9
*	36	AGR	FST	SbTrp DryF	663	0.2	3.3	0.4	226.4	22.8	1012.5	646.8	4.7	2.3	4
*	37	GRS/AGR	FTR	SbTrp DryF	1639	0.6	1.9	0.3	246.7	23.2	1103.8	537.5	4.6	1.5	4
*	38	AGR	FTR	SbTrp MsF	1101	0.4	2.9	0.4	246.7	33.6	1678.9	803.4	6.7	1.5	7
*	39	GRS/AGR	FTR	Trp DryF	1440	0.5	3.2	0.3	247.3	34.6	1512.2	729.1	7.0	2.5	6
	40	FTR	FTR	SbTrp WetF	2023	0.7	5.2	0.3	250.5	35.5	2740.2	633.2	11.7	1.1	12
*	41	GRS/AGR	FTR	Trp DryF	1654	0.6	2.6	0.3	248.0	22.9	1375.2	466.3	5.5	1.3	5
	42	FST	FST	SbTrp MsF	963	0.3	4.3	0.4	238.6	34.9	2323.0	890.9	8.0	1.9	7
	43	FST	FST	SbTrp MsF	2237	0.8	4.9	0.3	216.3	40.4	1861.9	635.0	7.9	1.7	8
*	44	AGR	FST	SbTrp MsF	1587	0.6	2.8	0.3	217.3	62.3	1539.0	638.0	7.2	1.7	7
	46	FEB	FEB	WmTmp MsF	1193	0.4	4.2	0.3	150.2	56.7	1738.9	582.3	10.4	2.1	12
	47	FST	FST	SbTrp MsF	1265	0.4	5.5	0.3	220.0	29.9	2299.6	784.0	8.0	1.4	7

China. Central plains of Myanmar and Thailand are also experienced large land cover changes.

Natural vegetation is restored based mainly on the warmth index. Fig.2 shows the natural vegetation in Monsoon Asia. Darker impression compared with Fig.1 indicates the restoration of forest. Forest class, FTS(Tropical Seasonal Forest), appears in the restored classes based on the number of months with monthly precipitation over 50mm.

5. Areal Evaporation and its changes due to vegetation/land cover changes

Ahn and Tateishi(1994) developed a method to calculate the global potential evaporation(*Ep*) by using datasets contained in *GEDB*. Their method is based on the Priestley and Taylor method(Priestley and Taylor,1972). It is possible to incorporate the variation of land cover through albedo.

Table 3 shows the class means of seasonal albedos from *Matthews Seasonal Albedo* dataset in the *GEDB*. Meteorological parameters are extracted from *GEDB*. With these values, monthly potential evaporations(*Ep*) are calculated. As for the details of the method, refer to Ahn and Tateishi(1994).

Fig.3 shows annual *Ep* in Monsoon Asia for current vegetation cover. The magnitude of the evaporation seems appropriate in the mid latitudes and in the humid tropics, however, it is obvious that *Ep* overestimates actual evaporation in the semi-arid and arid areas.

Table 4 shows the average seasonal albedo for forest classes. It is determined as an average of the same class in Table 2. Albedo distribution for natural vegetation is restored by converting natural vegetation map to albedo map using Table 4, and *Ep* is recalculated with the same method as Fig.3.

	Current	Winter		Spring		Summer		Fall	
No.	Class	mean	std.	mean	std.	mean	std.	mean	std.
1	FND	12.5	1.7	14.7	2.0	17.6	1.5	13.6	1.8
2	DES	24.8	6.3	26.8	6.4	26.4	4.6	25.5	5.5
3	GRS	17.5	5.5	19.9	5.5	21.4	4.5	19.2	5.0
4	GRS	15.9	4.0	18.5	4.3	20.3	3.2	17.8	3.8
5	AGR	14.9	1.1	14.9	3.0	19.3	1.4	16.6	1.3
6	GRS/AGR	13.2	2.2	15.3	2.7	17.9	1.9	14.6	2.5
7	GRS	17.9	5.0	20.4	5.2	22.6	3.9	20.0	4.3
8	FND	13.1	2.1	14.9	2.7	17.4	1.9	14.2	2.1
9	AGR	14.7	3.1	14.9	3.0	15.5	3.2	14.6	2.9
10	GRS	20.0	6.5	22.0	6.0	23.8	4.8	21.7	5.5
11	GRS	20.3	5.9	19.6	6.3	19.5	6.1	19.8	5.9
12	FDB	12.9	2.1	15.0	2.6	17.7	2.2	14.1	2.4
13	FEB	13.2	1.8	15.2	2.2	17.7	2.1	14.5	2.2
14	AGR	14.4	2.7	16.0	3.0	17.4	3.1	15.6	2.9
15	FND	11.5	1.1	13.1	1.8	16.0	1.6	12.6	1.2
16	FDB	13.0	2.0	15.2	2.5	17.8	2.0	14.3	2.4
17	FBS	14.4	4.1	14.6	3.6	15.9	3.6	14.7	3.5
18	GRS	14.9	4.1	17.2	4.4	19.2	3.3	16.4	4.1
19	GRS	17.4	5.1	19.6	4.9	22.1	4.3	19.5	4.6
20	FND	12.2	1.3	14.1	1.6	17.0	1.5	13.2	1.3
21	GRS	16.1	3.9	18.2	3.7	21.2	3.9	18.2	3.8
22	FST	14.0	2.9	14.3	2.7	15.0	3.0	14.2	2.7
23	GRS	22.7	6.7	24.7	6.8	25.1	4.8	23.7	5.8
24	GRS	15.6	3.9	17.9	4.0	19.2	3.5	16.9	4.0
25	FTR	11.7	1.9	11.6	1.6	11.7	1.7	11.6	1.5
26	AGR	13.8	2.9	15.5	3.1	17.4	3.1	15.0	3.0
27	AGR	17.2	2.4	18.1	2.7	19.0	2.7	17.9	2.5
28	GRS/AGR	16.7	2.9	18.2	3.4	19.1	3.3	17.7	3.1
29	AGR	14.8	1.4	17.0	1.4	19.1	1.6	16.4	1.6
31	FTR	12.5	2.8	12.5	2.4	12.6	2.5	12.4	2.4
32	FTR	12.2	2.4	12.1	2.1	12.3	2.4	12.1	2.1
33	GRS/AGR	20.7	6.6	22.8	6.7	23.0	5.1	21.7	5.9
34	FEB	13.5	2.1	14.5	2.3	15.6	2.6	14.4	2.2
35	AGR	13.6	1.8	15.0	2.3	16.5	2.8	14.7	2.3
36	AGR	16.6	2.1	18.1	2.6	19.0	2.9	17.5	2.4
37	GRS/AGR	16.8	1.9	17.4	2.1	18.2	2.5	17.3	1.9
38	AGR	16.3	3.2	17.1	3.9	17.7	3.8	16.8	3.3
39	GRS/AGR	13.7	3.2	13.9	2.6	14.7	2.8	13.9	2.6
40	FTR	11.6	1.5	11.7	1.6	11.8	2.0	11.6	1.5
41	GRS/AGR	16.7	2.0	16.7	2.0	17.1	2.7	16.7	1.9
42	FST	13.3	2.9	13.3	2.8	13.6	3.1	13.2	2.7
43	FST	13.2	2.9	13.2	2.5	13.5	2.9	13.1	2.5
44	AGR	15.2	2.9	16.1	3.0	17.1	3.3	15.9	3.0
46	FEB	13.0	2.1	14.2	2.5	15.5	3.1	13.7	2.4
47	FST	13.0	2.9	12.7	2.4	12.6	2.4	12.7	2.4

Table 3 Average albedos for current vegetation/land cover classes and standard deviations.

Table 4 Average albedos(%) for each forest type. Tropical seasonal forest does not appear in the current vegetation cover map(Figure 1).

Class	N	SPRING	SUMMER	FALL	WINTER
FND	9	14.6	17.2	13.8	12.7
FDB	5	15.5	17.7	14.7	13.4
FEB	1	14.2	15.7	13.8	12.8
FST	3	13.0	13.6	12.9	12.8
FTR	2	10.6	10.7	10.6	10.6

Fig.4 shows *Ep* for natural vegetation over Monsoon Asia, and Fig.5 shows the amount of changes in *Ep* between natural and current vegetation. The region which subject to large areal change in *Ep* is India and eastern and southern China. Central plain of Myanmar and Thailand is the largest affected area next to India and China. The amount of change is large in India, Myanmar and Thailand.

6. Concluding Remarks

This paper describes a result of tentative work concerning the global hydrological changes due to fundamental transformations of Earth's surface by human's activity. We still have to consider more about several issues to approach the conclusion. They are, (1) to improve the accuracy of the global datasets, (2) to get precise recognition on the hydrological phenomena and vegetation dynamics, and (3) to enhance the skills of the model.

Among the global datasets, land cover map is crucial for distributed hydrological modeling. Several international projects are progressing to make high resolution global land cover map with the use of satellite data. The GLI(*GLobal Imager*) is one of the most promising sensor, which is planning to board ADEOS-II satellite.

In the hydrological viewpoints, it is important to search proper definition of existing land cover that minimizes the variance of hydrological parameters within a class. In other words, it is desirable that a number of hydrological parameters can be derived from the land cover definition for use in the flux calculations. It is the significant subject that must be resolved at an early date.

Regarding the third problem, many sophisticated models are appeared in recent days(for example, Shukla *et al.*, 1990). The accuracy of the results, however, depends on that of input data and its spatial distributions. After solving the problem, these complicated models will be useful to understand the dynamic behavior of the vegetation and the climate.

The most important problem is concerning the appropriate recognition of the natural phenomena concerned. Many field investigations, that appear in the journals, reveal that there are many factors that must be considered in the model. For example, energy advection, plant growth stage, degree of soil conservation, etc., can influence the water balance at the ground surface. Nonequilibrium phenomena between vegetation and climate is the most important issue but difficult to solve.

It is possible to state further difficulties concerning the method adopted in this paper. Such an empirical method is one possible way to assess the anthropogenic change in global water balance, and it is an urgent theme in the context of Earth environmental changes. There must be a simple

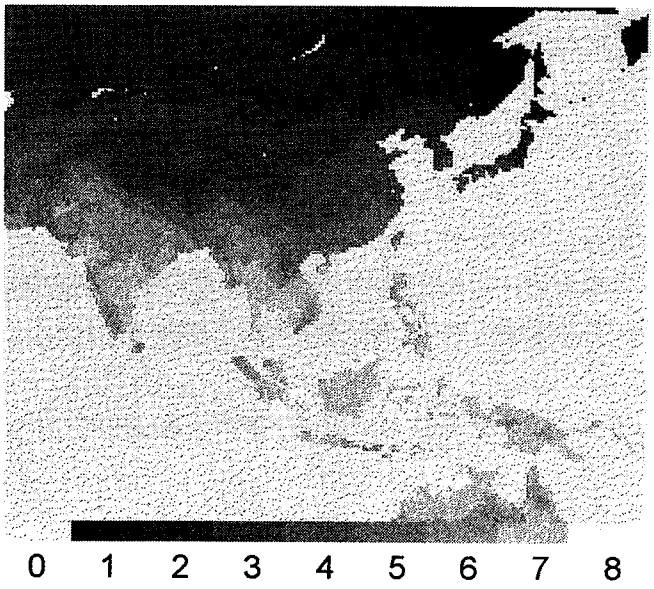

Figure 3 Potential evaporation for current land cover. 0: Ocean, 1: 0-400, 2: 400-600, 3: 600-800, 4: 800-1000, 5: 1000-1200, 6: 1200-1400, 7: 1400-1600, 8: 1600- (mm/year)

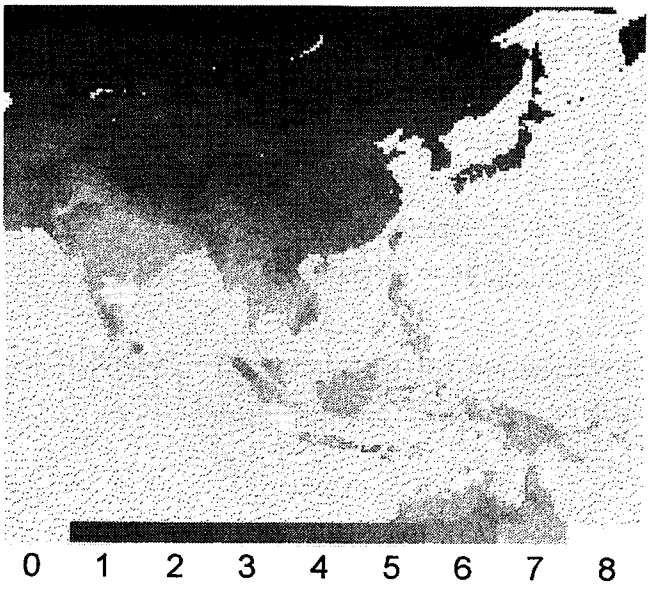

Figure 4 Potential evaporation for natural vegetation. 0: Ocean, 1: 0-400, 2: 400-600, 3: 600-800, 4: 800-1000, 5: 1000-1200, 6: 1200-1400, 7: 1400-1600, 8: 1600- (mm/year)

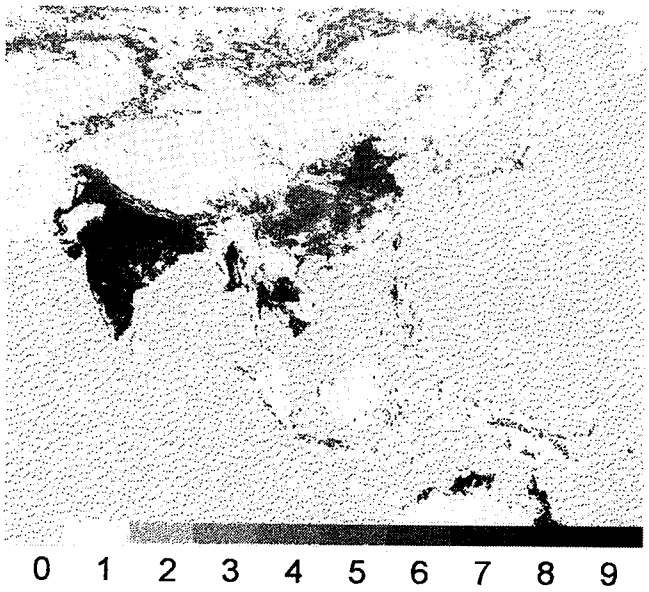

Figure 5 Changes in annual potential evaporation due to land cover changes. 0: Ocean, 1: no change, 2: 0-2, 3: 2-4, 4: 4-8, 5: 8-16, 6: 16-32, 7: 32-64, 8: 64-128, 9: 128- (mm/year)

relationship or rule between hydrological phenomena and surface parameters that could be detectable by satellite remote sensing(for example, Kondoh,1995), and it is a clue to understand global environmental change during the historic era.

References

Ahn,C-H. and Tateishi,R., "Development of Global 30-minute grid Potential Evapotranspiration Date Set", *Journal of the Japan Society of Photogrammetry and Remote Sensing*, **33**, 2, 12-21, 1994.

Kira,T.," New climatic zonation in eastern Asia as a basis of agricultural geography." Kyoto Imperial University, 24p, 1945a. (*in Japanese*)

Kira,T., "New Climatic zonation in southeastern Asia." Kyoto Imperial University, 24p, 1945b. (*in Japanese*)

Kira,T., Shidei,T., Numata,M. and Yoda,K., "Vegetation in Japan -Situation in a global vegetation-." *Iwanami Kagaku*, **46**, 235-247, 1976. (*in Japanese*)

Kondoh,A., "Relationship between the Global Vegetation Index and the Evapotranspirations derived from Climatological Estimation Methods. *Journal of the Japan Society of Photogrammetry and Remote Sensing*, **34**, 2, 6-14.", 1995.

Priestley,C.H.B. and Taylor,R.J., "On the assessment of surface heat flux and evaporation using large-scale parameters." *Monthly Weather Review*, **100**, 81-92, 1972.

Shukla,J., Nobre,C. and Sellers,P., "Amazon deforestation and climate change." *Science*, **247**, 1322-1325.

Townshend,J., Justice,C., Li.W., Gurney,C. and McManus,J., "Global land cover classification by remote sensing: Present capabilities and future possibilities." *Remote Sensing of Environment*, **35**, 243-255, 1991.

Estimation of methane emission from western Siberian wetlands by using satellite remote sensing techniques

M. Tamura, Y. Yasuoka and Y. Yamagata
National Institute for Environmental Studies
16-2 Onogawa, Tsukuba, Ibaraki 305, Japan
Phone: +81-298-50-2479, Fax: +81-298-51-4732
E-mail: m-tamura@nies.go.jp

1. Introduction

Western Siberian wetlands are presumed to be large sources of atmospheric methane. Recent Japan-Russia airborne measurements conducted by the National Institute for Environmental Studies of Japan and the Central Aerological Observatory of Russia have yielded the results supporting this presumption. To evaluate the role of the western Siberian wetlands as sources of atmospheric methane, it is necessary to classify wetland ecosystems and to measure the mean methane flux for each ecosystem type. In this study we use a SPOT/HRV image to classify wetland ecosystems in a test area. As to the mean methane flux, there are not many data in western Siberian wetlands, but it is possible to obtain rough estimates from the results of the ground measurements performed in the Japan-Russia Siberian project. The methane emission from a test area is estimated by combining the result of ecosystem classification and the values of mean methane flux for different ecosystem types.

2. SPOT/HRV image at Plotnikovo in western Siberian wetlands

A SPOT/HRV image was obtained at Plotnikovo on 9 August 1994, three days after the intensive airborne measurements (which took place on 3, 5, and 6 August 1994) of greenhouse gases over the same area. Plotnikovo is located at the longitude 85°05'E and the latitude 56°51'N and in the wetland region along the Ob' river (see Fig. 1). Figure 2 shows the area covered by the SPOT/HRV image, whose size is approximately 60 × 60 km.

The SPOT/HRV is a high resolution imaging system with a ground resolution of 20 m and has three spectral bands of green, red and near infrared wavelengths (0.50-0.59,

0.61-0.68 and 0.79-0.89 μm). Figure 3 shows the image taken by SPOT/HRV sensor in a black and white picture, though it has originally three color components. By using an unsupervised classification technique (Interactive self-organizing data analysis technique) we classified the image pixels into fifteen clusters in three-dimensional spectral space. We then merged them into seven categories (wetland 1, wetland 2, forest, water, grass, cloud and cloud shadow) using spectral feature and spatial distribution of each cluster. Figure 4 shows the result of land cover classification. From aerial photographs, wetland 1 is identified as bog area with dwarf trees and shrubs and wetland 2 as bog area with peat moss and grasses.

3. Estimation of methane emission from a test site

In the Japan-Russia joint experiments Panikov measured methane fluxes in wetland areas near Plotnikovo and reported that mean methane fluxes in summer time were 233.9 mg CH_4 m^{-2} d^{-1} for open bogs and 21.1 mg CH_4 m^{-2} d^{-1} for forested bogs [Panikov, 1994]. We used his flux data to calculate methane emission from the SPOT image area and obtained the result that the total amount of methane emission was 470×10^6 g CH_4 d^{-1} and the average methane flux was 170 mg CH_4 m^{-2} d^{-1}. In this calculation, we eliminated cloud and cloud shadow areas and assumed that the mean methane fluxes of wetland 1 and 2 are equal and that methane fluxes from grass and water areas were negligible because these areas have small ratio (6.9 %) to the total area and no methane flux data were available in these land cover types.

4. Summary

A SPOT/HRV image was obtained at Plotnikovo shortly after the flight measurements of greenhouse gases in August 1994. The image area was classified into seven categories using spectral features and aerial photographs. Mean methane fluxes for different kind of ecosystems have been obtained from the ground measurements. Methane emission from the SPOT image area was estimated by combining the result of ecosystem classification and the values of mean methane fluxes.

References

N.S. Panikov, CH_4 and CO_2 emission from northern wetlands of Russia: Source strength and controlling mechanisms, Proceedings of the International Symposium on Global Cycles of Atmospheric Greenhouse Gases, 100-112, 1994.

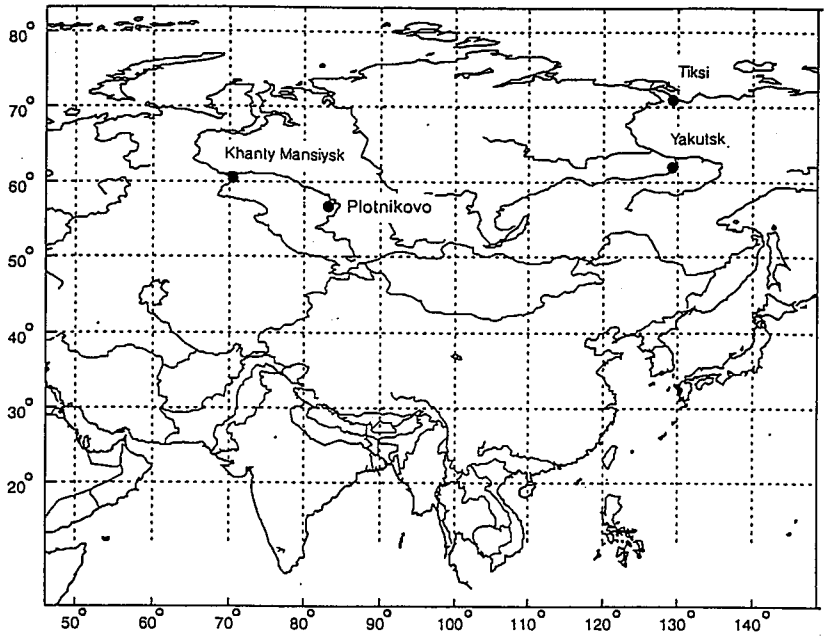

Fig. 1 Location of Plotnikovo.

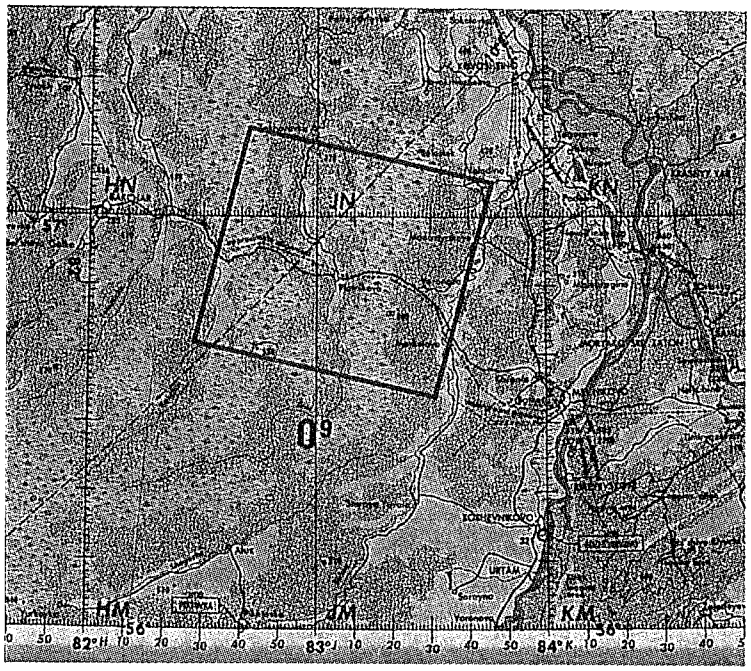

Fig. 2 Area covered by the SPOT/HRV image.

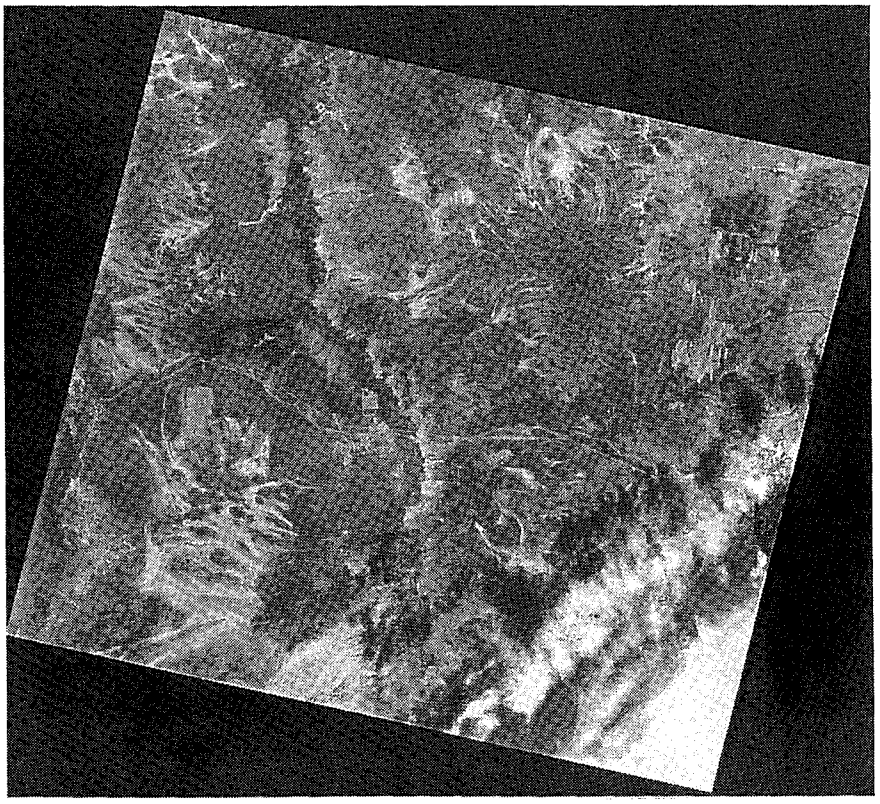

Fig. 3 SPOT/HRV image at Plotnikovo.

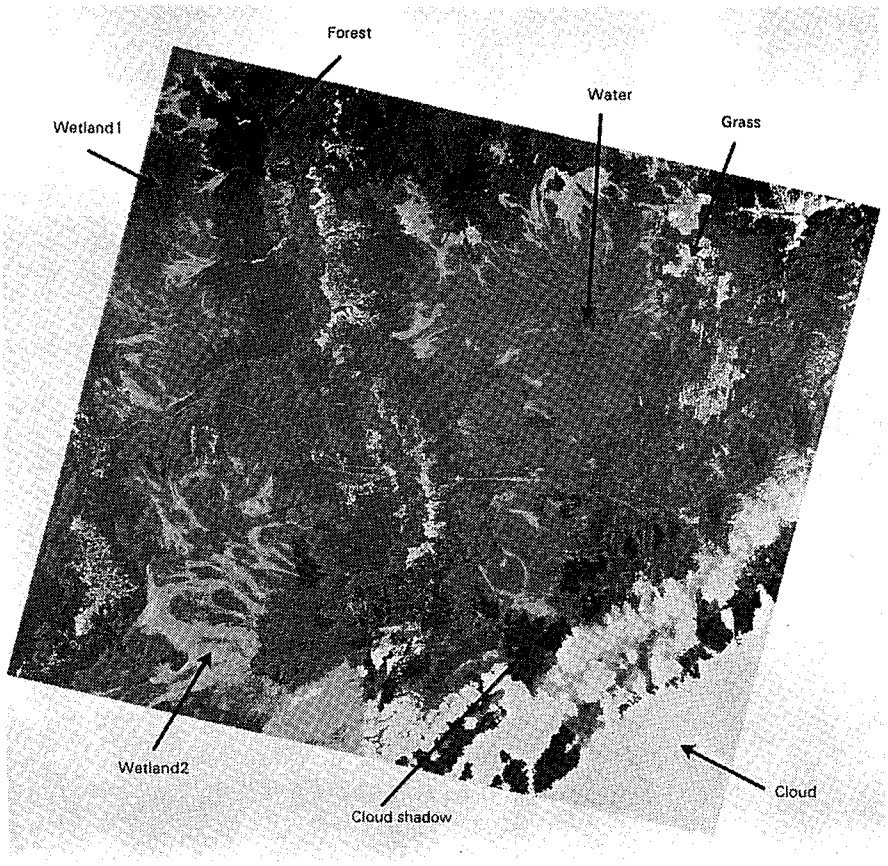

Fig. 4 Result of land cover classification.

Surface Temperature Decrease, NDVI and Humidity Deficit, and Latent Heat Flux in Forested Region from TM and Routine Meteorological Data - a Summary -

Daijiro Kaneko(*) and Mikio Hino(**)

*Department of Civil Engineering
Matsue National College of Technology
14-4, Nishiikuma-cho, Matsue, Shimane, 690 Japan

**Faculty of Policy Studuies
Chuo University
742-1, Higashinakano, Hachioji, Tokyo, 192-03 Japan

Abstract

A new method for estimating directly the latent heat flux in regional forested area from remotely sensed data and routine data measured at a meteorological observatory is proposed by applyng the similarity theory of Monin-Obukhov. The key idea (Eq.19) of the estimation method is to express the specific humidity deficit at forest canopies by an analogy with the relation derived above between the temperature decrease, NDVI and the specific humidity deficit in terms of the newly defined evapotranspiration indices.

1. INTRODUCTION

This paper attempts to derive a prediction relationship of the surface temperature decrease in forested area,and then to develop a method to estimate the latent heat flux directly from remotely sensed satellite data, applying the Monin-Obukhov theory on the atmospheric boundary layer flow. The present paper developes the augmented summary of our method presented in the previous preliminary papers (Kaneko and Hino (1994)).

As the evapotranspiration increases, the surface temperature falls by the effect of latent heat flux. Hall et al. (1991) showed that the canopy temperatures estimated from remote sensing correlated well with the measured canopy temperature. Nemani and Running (1989a) related the surface temperature to NDVI and several researchers has discussed this T_s/NDVI relationship so far (Goward and Hope (1989), Larsson (1993)).

It is shown in this paper that the surface temperature decrease over the forested area is represented as a function of the surface (leaf) temperature, NDVI and the specific humidity deficit at the leaf temperature, these factors being estimated by TM data.

In the second part of this paper, a method of remote sensing direct estimation of latent heat flux in regional area of forests is proposed applying the Monin-Obukhov similarity theory along with the three factors; leaf temperature fall due to transpiration estimated from TM, the value of NDVI derived also from TM and routine meteorological data obtained at an observatory.

Most methods of remote-sensing estimation of the latent heat flux reported so far are, to the authors' knowledge, the indirect method which estimates the latent heat flux by subtracting from the net radiation the sensible heat flux evaluated by remote sensing (for instance, Carlsonet al.(1981), Seguin and Itier (1983), Pierce and Congalton (1988), Moran et al.(1989)). Sugita and Brutsaert (1992) recently calculated the latent heat fluxes by indirect estimation, showing that the estimated values were generally in good agreement with the mean fluxes obtained by field measurement. Taconet, Bernard and Vidal-Madjar (1986) developed a methodology to

predict surface fluxes by a one-dimensional boundary layer/vegetation/soil model over dense vegetation, applying surface temperature obtained by remotely sensed data.

Generally speaking, the method of direct estimation of latent heat flux is essentially superior to the indirect one because the latter method calculates the latent heat flux as residual and is apt to include undesirable errors.

Since the values of forest biomass are not uniform seasonally and spatially, its effect must be considered in the regional estimation of latent heat flux. The authors' method takes the forest biomass into account by defining an effective leaf area index (LAI).

The authors' present method combines the technique of remote sensing to estimate the forest evapotranspiration with the well-known similarity theory of Monin-Obukhov.

2. SURFACE TEMPERATURE FALL BY FOREST EVAPOTRANSPIRATION

2.1 Land Use in the Test Area

Fig.1 shows the horizontal distribution of land uses in the test region, Shimane Prefecture which is situated in the western part of Japan. The land-use data are derived from Digital Land Information supplied from the Geographical Survey Institute, Ministry of Construction.

Matsue City, at about the center of the area is the administrative center of the Prefecture, with population of 142,000, and is surrounded by dense forests as shown in Fig.1 by symbol of tree.

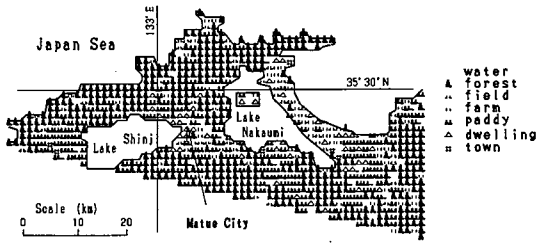

Figure 1. Land use of the test region in Shimane Prefecture.

2.2 Relation between Surface Temperature and NDVI

The surface temperature of forested regional area decreases almost linealy with the increase of NDVI by the effect of latent heat flux caused by evapotranspiration of forest. Fig.2 shows the relation between the surface temperature and NDVI for the whole areas of Shimane Prefecture with a variety of land-uses.

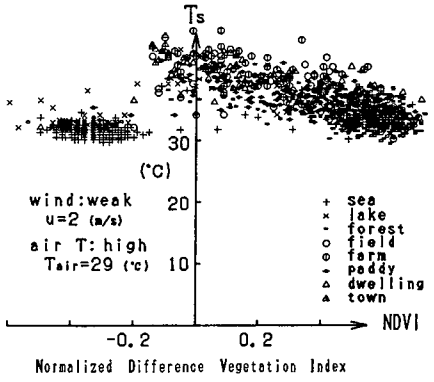

Figure 2. Relation between the surface temperature derived from Landsat TM and NDVI for all kinds of land-use.

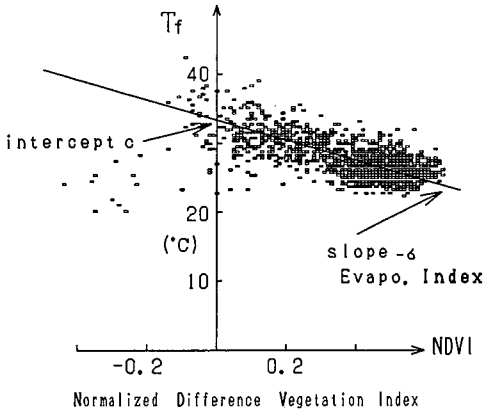

Figure 3. Definition of the normalized evapotranspiration index on the scene of 9 May 1990.

As Nemani and Running (1989a) reported firstly, the surface temperature is related to NDVI by Eq.(1),

$$T_f = \sigma \cdot NDVI + c \qquad (1)$$

where T_f is the surface temperature at forest sites, σ a proportionality constant, and c a constant.

2.3 Evapotranspiration Index ($-\sigma$)

The intercept c on the ordinate (temperature axis) in Fig.3 represents the surface temperature at the sites where vegetation is scarce. The temperature decrease ($c-T_f$) is due to evapotranspiration.
The rate of temperature decrease

$$-\sigma = \frac{c-T_f}{NDVI} \qquad (1a)$$

can be defined as the normalized evapotranspiration index to indicate the degree of the evapotranspiration effect of vegetation (Kaneko and Hino (1993)). The gradient of the relation changes seasonally, showing that the evapotranspiration is affected by the variation of meteorological as well as plantphysiological conditions.

It is soon conceivable that the evapotranspiration is effected not only by the vegetation biomass(NDVI) but also by such factors especially as the leaf temperature and specific humidity deficit. We have examined a variety of combinations of these factors with the mean values of $-\sigma$ for each scene. A candidate for the most appropriate factor explaining $-\sigma$ was (q_c-q_a);i.e. the specific humidity deficit between the saturation specific humidity $q_c(T_f)$ at the leaf temperature T_f, and the humidity of air flow q_a. The value q_c means the humidity inside the stomata.

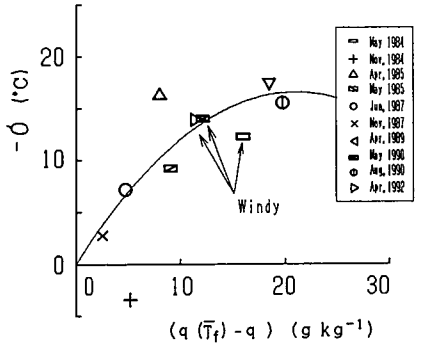

Figure 4. Relation between the normalized evapotranspiration index $-\sigma$ and the specific humidity deficit $(q_c(\overline{T_f})-q_a)$ between the saturation specific humidity q_c at average leaf temperature $\overline{T_f}$ and the value q of air flow.

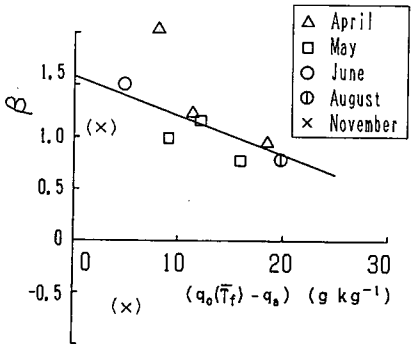

Figure 5. Relation between the stomatal opening index β and the specific humidity deficit $(q_c(\overline{T_f})-q_a)$.

The index $-\sigma$ increases initially with the increase in the humidity deficit (Fig.4). While as the value of $(q_c(T_f)-q_a)$ approaches near 20(g kg^{-1}), the index $-\sigma$ saturates and

begins to decline with the increase of the deficit $(q_c(T_f)-q_a)$. As a first approximation, the relationship is described by Eq.(2).

$$-\sigma = \beta \cdot [q_c(T_f) - q_a] \tag{2}$$

2.4 Stomatal Opening Index (β_s)

As the forest transpiration may be proportional to the specific humidity deficit (q_c-q_a) as well as the stomatal opening, the proportionality constant β in Eq.(2) may define a stomatal opening index. In other words, if the surrounding air becomes excessively dry, the plants would close the stomatal opening.

Data of the index β in Eq.(2) obtained from ten TM scenes at different seasons show that the index β decreases, as shown in Fig.5, linealy with the increase of the specific humidity deficit (q_c-q_a) except for the winter season of November when the evapotranspiration of leaves ceases completely. The tendency may be explained by the fact that the large values of the deficit (q_c-q_a) cause the stomatal closure to restrain the transpiration against excessive loss of water from plant. From the regression analysis, the index β is expressed by Eq.(3).

$$\beta = -0.0378 \cdot (q_c - q_a) + 1.58 \tag{3}$$

The correlation coefficient for the present analysis for a wider area is r=0.731. In narrower area already reported (Kaneko and Hino (1994)), the value 0.71 of correlation coefficient increases to 0.91. The two constants of the regression formula (3) depended slightly on the places where vegetation and geology are different.

The index of stomatal opening β_s is defined so that its value is limited within a range of $(0 \leqq \beta_s \leqq 1)$, as

$$\beta_s = \frac{\beta}{1.58} = 1 - \frac{0.0378}{1.58}(q_c(T_f)-q_a) \tag{4}$$

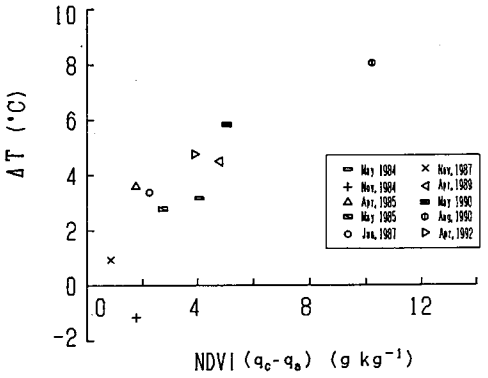

(a) Relation between the temperature decrease ΔT $(=c-\overline{T_f})$ and the average values of $NDVI\cdot(q_c(\overline{T_f})-q_a)$. The ten data especially the case on 18 June 1987 of the low leaf temperature approach on a single curved line.

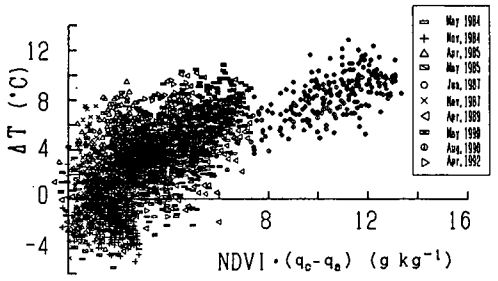

(b) Relation between the temperature decrease ΔT and the values of $NDVI\cdot(q_c(\overline{T_f})-q_a)$ at all pixels of 10 TM scenes.

Figure 6. Relation between the temperature decrease ΔT and the values of $NDVI\cdot(q_c(\overline{T_f})-q_a)$.

2.5 Formulas on $-\sigma$ and T_f

To summarize, the evapotranspiration index $(-\sigma)$ and the surface temperature T_f are

expressed, respectively, by

$$-\sigma = [1.58-0.0378(q_c(T_f)-q_a)](q_c(T_f)-q_a) \tag{5}$$

$$T_f = c-[1.58-0.0378(q_c-q_a)](q_c-q_a)\cdot NDVI \tag{6}$$

$$\Delta T = \beta (q_c-q_a)\cdot NDVI \tag{7}$$

where $\Delta T(=c-T_f)$ is the temperature decrease.

3. ESTIMATION OF LATENT HEAT FLUX

3.1 Basic Equation

In this section, a new method for the estimation of latent heat flux in forested areas is developed based on the the above discussions and the Monin-Obukhov similarity theory. The idea has been presented in Kaneko and Hino (1994).

According to the Monin-Obukhov theory (originally Monin and Obukhov (1954), for reference at hand see for instance, Lumley and Panofsky (1964), Raupach and Thom (1981)), the latent heat flux is expressed as

$$E = -\rho l U_* q_* \tag{8}$$

where ρ is the density of air, U_* means the friction velocity, l is the latent heat of evaporation, q_* is the friction specific humidity, defined by Eq.(9) as

$$q_* = -\overline{wq}/U_* \tag{9}$$

where $\overline{wq}$ is the specific humidity flux.

Integral of the universal function ϕ_h in the Monin-Obukhov theory yields the following equation between q_*, q_a and q_f as

$$q_a - q_f = \frac{q_*}{\kappa}\,[\Psi_h(\zeta)-\Psi_h(\zeta_0)] \tag{10}$$

where

$$\Psi_h = \int_{\zeta_0}^{\zeta} \frac{\phi_h(\zeta)}{\zeta}\,d\zeta, \quad \zeta = (z-d_0)/L, \quad \zeta_0 = z_0/L \tag{10a}$$

where z is the height at which the values of wind speed U_a, atmospheric temperature T_a, and specific humidity q_a are measured; z_0 the roughness length, d_0 the zero-plane displacement, ζ the dimensionless height, and κ the von Karman constant, q_f the specific humidity on ground surface and/or over forestcanopy. As far as the ground surface is not wet, $q_f < q_c$.

The wind speed and the temperature are written in terms of the integral universal functions Ψ as

$$U_a = \frac{U_*}{\kappa}\,[\Psi_m(\zeta)-\Psi_m(\zeta_0)], \tag{11}$$

$$T_a - T_f = \frac{\theta_*}{\kappa}\,[\Psi_h(\zeta)-\Psi_h(\zeta_0)]. \tag{12}$$

In Eq.(10a), L is the Monin-Obukhov length defined by the following form,

$$L = \frac{\overline{\theta} U_*^2}{\kappa g \theta_*} \tag{13}$$

where the friction temperature θ_* is defined by

$$\theta_* = -H/U_* \tag{14}$$

where H is the sensible heat flux = $\overline{w\theta}$, and g the acceleration of gravity. The value of $\overline{\theta}$, the representative potential temperature, is defined by the following expression so as to include the convection effect of the average surface temperature $\overline{T_s}$ in surroundings into the leaf temperature T_f of the forest site concerned,

$$\overline{\theta} = (\overline{T_s} + T_f)/2 \ . \tag{15}$$

The surface temperature T_f is derived from Landsat TM. The temperature $\overline{T_s}$ is determined either also from Landsat TM or an iterative computation to be explained subsequently.

The functional form of ϕ proposed by Businger (1988) and Dyer (1974) was applied.

3.2 Estimation of atmospheric stability ζ by TM and routine meteorological data

Equations (10a),(11), and (13) lead to the following well known relationship,

$$\zeta = R_i \phi_m^2(\zeta)/\phi_h(\zeta) \tag{16}$$

where R_i means the Richardson number which is approximated by the bulk Richardson number B,

$$B = \frac{g(T_a - T_f)}{\overline{\theta}\ U_a^2}(z-d_0) \ . \tag{17}$$

3.2 Meteorological Data Available

The routine meteorological data are measured at the Matsue meteorological observatory; i.e. the air temperature and the humidity at the height of 1.5m, and the wind speed U_a at z = 26.7m from the ground.

Since the area concerned is relatively flat, the atmospheric stability condition is unstable and the air masses are well mixed by forced thermal convection. The same meteorological conditions are expected to prevail at the higher level in the mixing (surface boundary) layer over the study area. Moreover, nearly homogeneoues land use spreads widely as shown in Fig.1. Consequently, the similarity theory of Monin-Obukhov in the surface boundary layer can be applied with the common use of U_a, T_a, and q_a, over the test area. The value of B which stands for R_i is calculated from TM and routine meteorological data. Consequently the value of ζ can be deduced from Eqs.(16) and (17).

3.4 Definition of Effective Leaf Area Index (α_{NDVI})

The values of NDVI have already recognized by Nemani and Running (1989b) that those have a logarithmic relationship with leaf area index (LAI).

In urban areas where no vegetation exists, the value of NDVI approaches a limit of -0.1. On the other hand, in densely forested areas, the surface temperature scarcely falls with the increase of NDVI, after the value of NDVI reaches a value of 0.5 and NDVI becomes nearly constant in dense forests. Consequently, an effective leaf area index is defined as follows,

$$\alpha_{NDVI} = \begin{cases} 0 & (NDVI < NDVI_0) \\ \dfrac{NDVI - NDVI_0}{NDVI_{100} - NDVI_0} & (NDVI_0 \leqq NDVI \leqq NDVI_{100}) \\ 1 & (NDVI > NDVI_{100}) \end{cases} \tag{18}$$

where $NDVI_0$ takes a value of -0.1 for no vegetation areas, and $NDVI_{100}$ is given a value of 0.5

in dense forests.

From the definition of NDVI, the meaning of the word 'effective' reflects not only the leaf area density in a unit pixel but also the richness of chlorophyll in forest leaves which are actively transpirating.

3.5 Expression of Specific Humidity Deficit on Ground Surface

Considering the facts that the profile of q(specific humidity) over the bare soil surface is approximately constant because both of nearly zero vapour flux from the ground and of violent turbulent mixing, and that the value of q over the upper part ($z=z_a$) of the mixing layer is nearly constant (i.e. $q_{0,bare} = q_{a,bare} = q_{a,forest}$), and that the humidity deficit at the forest canopy ($q_f - q_a$) is proportional to the evaporation flux from it derived in the preceding section, the authors propose the relationship of Eq.(19) from the analogy with Eq.(7).

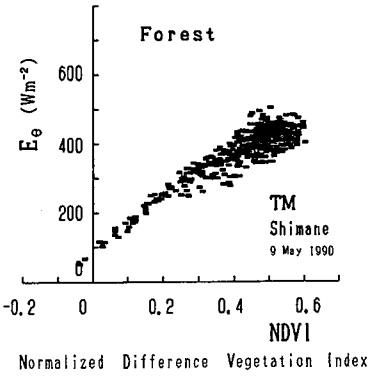

Figure 7. Relation between NDVI and latent heat flux E_e, estimated by means of Eq.(20) together with Eqs.(4),(10), (16) and (18).

$$q_f - q_a = a_c \cdot \alpha_{NDVI} \cdot \beta_s (q_c(T_f) - q_a) \tag{19}$$

where α_{NDVI} is the index of effective leaf area, β_s means the index of stomatal opening (Eq. (4)), and a_c is the conversion coefficient which is selected so that the coefficient makes the latent heat flux E at dense forests (NDVI>0.5) equal to the net radiation.

3.6 Estimation Formula of the Latent Heat Flux

Insertion of Eqs. (10),(11) and (19) into Eq.(8) yields the final expression for the latent heat flux as Eq.(20)

$$E_e = -\frac{\rho l \kappa^2}{[\Psi_m(\zeta)-\Psi_m(\zeta_0)]\cdot[\Psi_h(\zeta)-\Psi_h(\zeta_0)]} \cdot U(z)\cdot(a_c \alpha_{NDVI} \beta_s)\cdot(q_c - q_a). \tag{20}$$

In other words, E_e is a function of the atmospheric stability L or ζ, the wind speed U_a, the effective leaf area index α_{NDVI}, the humidity deficit ($q_c - q_a$), and the stomatal opening β_s,

$$E_e = \mathrm{fun}\{U_a, L(\zeta), \alpha_{NDVI}, \beta_s, (q_c - q_a)\} \tag{21}$$

where α_{NDVI} is a function of NDVI and β_s which is given by Eq.(4) depends on ($q_c - q_a$) as well as T_f (leaf temperature) through $q_c(T_f)$.

4. CONCLUSION

The surface temperature falls with the increase of NDVI and it is also affected by the humidity deficit between the saturation humidity at leaf temperature and that of air flow. The relation is derived as Eq.(6) from the analysis of TM data. Since q_c is a function of T_f, and $\Delta T = \beta (q_c - q_a)\cdot NDVI$, solution of Eq.(6) will give explicitly the value of T_f with parameters q_a and NDVI. The decrease in the surface temperature in forested areas reflects the effects of evapotranspiration.

Based on the above result, a new method for estimating the latent heat flux over forested

Based on the above result, a new method for estimating the latent heat flux over forested areas from the surface temperature data derived by the remote sensing technique as well as routine data observed at a meteorological observatory has been proposed by applying the Monin-Obukhov similarity theory. The latent heat flux is shown to depend on such factors as the value of NDVI, the specific humidity deficit, the leaf temperature which effects the stomatal opening for forest to control transpiration.

REFERENCES

Carlson,T.N., Dodd,J.K., Benjamin,S.G. and Cooper,J.N. (1981), Satellite estimation of the surface energy balance, moisture availability and thermal inertia, J. of Applied Meteorology, 20: 67-87.

Friedl, M.A., and Davis, F.S. (1994), Sources of variation in radiometric surface temperature over a tall gras prairie, Remote Sensing of Environment, 48: 1-17.

Goward, S.N., and Hope, A.S. (1989), Evapotranspiration from combined reflected solar and emitted terrestrial radiaiton: preliminary FIFE results from AVHRR data, Advances in Space Research, 9(7); 239-249.

Kanda,M., and Hino,M. (1990a), Numerical simulation of soil-plant-air system (1) Modeling of plant system, J. of Japan Society of Hydrology and Water Resources, 3: 37-46. (in Japanese with English abstract).

Kaneko,D., and Hino,M. (1993), Analysis of forest temperature descent due to evapotranspiration using Landsat TM, J.of the Remote Sensing Society of Japan, 13,(1);1-13. (in Japanese with English abstract).

Kaneko,D., and Hino,M. (1994), A method for evaluation of surface energy balance in regional forest using normalized difference vegetation index derived from Landsat TM and routine meteorological data, J.of Japan Society of Hydrology and Water Resources,7,(1): 10-21. (in Japanese with English abstract).

Lumley,J.L., and Panofsky,H.A. (1964), The structure of atmospheric turbulence, Interscience Publishers, 239pp.

Monin,A.S., and Obukhov,A.M. (1954), Basic turbulent mixing laws in the atmospheric surface layer. Trudy Geofiz. Inst, AN SSSR, 24(151):163-187.

Moran,M.S., Jackson,R.D., Raymond,L.H., Gay,L.W., and Slater,P.N. (1989), Mapping surface energy balance components by combining Landsat Thematic Mapper and ground-based meteorologicl data, Remote Sensing of Environment, 30: 77-87.

Nemani,R.R. and Running,S.W. (1989a), Estimation of regional surface resistance to evapotran-sp iration from NDVI and thermal-IR AVHRR data, J. of Applied Meteorology, 28,(4): 276-284.

Nemani,R.R. and Running,S.W. (1989b), Testing a theoretical climate-soil-leaf area hydrologic equilibrium of forests using satellite data and ecosystem simulation, Agricultural and Forest Meteorology, 44: 245-260.

Pierce,L.L., and Congalton,R.G. (1988), A Methodology for mapping forest latent heat flux densities using remote sensing, Remote Sensing of Environment, 20: 405-518.

Raupach,M.R., and Thom,A.S.(1981), Turbulence in and above plant canopies, Ann. Rev. Fluid Mech., 13: 97-129.

Seguin,B., and Itier,B. (1983), Using midday surface temperature to estimate daily evaporation from satellite IR data, I. J. of Remote Sensing,4,(2): 371-383.

Sugita,M., and Brutsaert,W. (1992), Landsat surface temperatures and radio soundings to obtain regional surface fluxes, Water Resources Research, 28,(6): 1675-1679.

Taconet,O., R.Bernard, and D.Vidal-Madjar (1986), Evapotranspiration over an agricultural region using a sufrace flux/temperature model based on NOAA-AVHRR data, J. of Climate and Applied Meteorology, 25,(3):284-307.

Monitoring of Radiant Temperature Distribution of Urban Vegetation Using High Resolution Multi-temporal Remote Sensing Data

Akinaru IINO and Akira HOYANO

Department of Environmental Physics and Engineering
Tokyo Institute of Technology
4259 Nagatsuta-cho, Midori-ku, Yokohama 226 JAPAN
TEL : +81-45-924-5501 Fax : +81-45-924-5519
Email : aiino@nc.titech.ac.jp

Abstract

In most studies concerning the basic analysis of spectral reflectance of vegetation surface, only visible, near infrared, and middle infrared images from satellite views, i.e., LANDSAT, SPOT, etc., are analyzed. Thermal infrared images, though, should also be used to indicate the characteristics of its radiant temperature distribution of urban vegetation, from the point of the deterioration of the urban thermal environment. This paper describes the results of the analysis using high resolution images of multi-temporal airborne multi-spectral scanner (MSS) data. The relationship between the radiant temperature distribution of urban vegetation and the area of each group of vegetation is investigated, considering weather parameters, i.e., incident solar radiation and air temperature. Furthermore, the relationship between the normalized vegetation index (NVI) and the temperature of urban vegetation is indicated.

1. INTRODUCTION

In recent years, the importance of urban vegetation have been re-recognized from the point of preventing to deteriorate the urban climate. The effect of declining the air temperature by a large land cover with vegetation is being proved by lots of investigations or measurements. However, there are a lot of small groups of trees in urban areas, i.e., the roadside trees or shrubbery, so the condition of vegetation distribution is different from that of either forest area or a green tract of land. It is very important to prove the effect of preventing the deterioration of the heat island phenomenon by the small groups of trees.

Satellite remote sensing is often informed for the investigation of surface temperature distribution of the vegetation or the activated degree of the vegetation. In the past, the basic

studies of characteristics of spectral reflectance were mainly carried out with the range of visible or near infrared using satellite remote sensing data, i.e., LANDSAT or SPOT. Only the large-scale green tract of land can be handled because the spatial resolution is low. The characteristic of the radiant temperature distribution of a group of trees hasn't made clear.

A group of trees which exists in urban areas is focused on in this paper. The characteristic of the radiant temperature distribution of a group of trees which is projected on the multi-temporal airborne MSS data with 1.9 m of spatial resolution is clarified. And it is also made clear by image processing that the radiant temperature distribution of the tree crown surface is distinguished by the area, the shape, normalized vegetation index and the weather parameters.

2. OBSERVATION OUTLINE OF AIRBORNE MULTI-SPECTRAL SCANNER DATA AND AN ANALYSIS OF ACTUAL DISTRIBUTION OF VEGETATION

To analyze the diurnal or the annual change of the spectral characteristic of urban vegetation, we use airborne MSS data observed at noon and at the sunset on a clear sky day in summer and in winter. The specification and the observation outline of the airborne MSS sensor are shown in table 1. The characteristics of observation data are as follows.

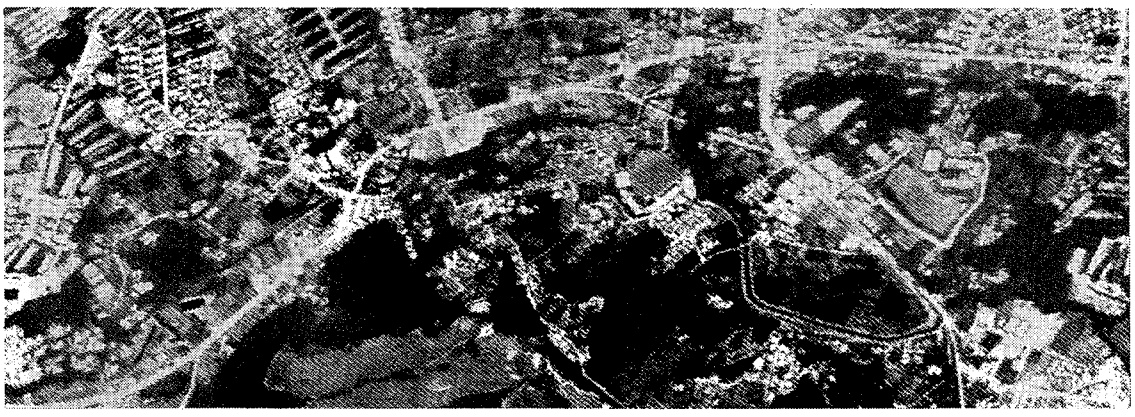

Fig. 1 An example of a thermal image obtained by airborne MSS (August 9, 1987, 13:47–13:54)

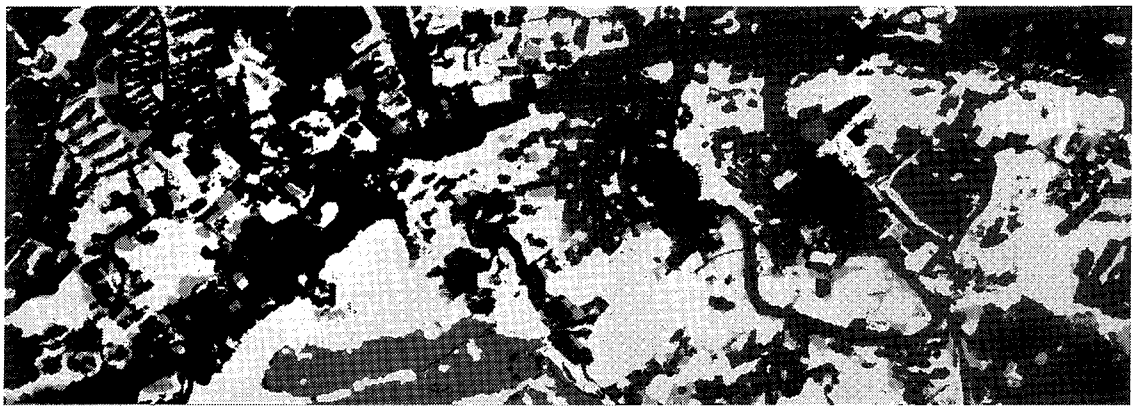

(white: trees, gray: grass, black: other land cover)

Fig. 2 Training image of vegetation distribution

1) The small-scale vegetation, i.e., the roadside trees and the shrubbery could be observed, because of 1.9 m of spatial resolution.

2) The dynamic range of the radiant temperature of urban vegetation could be obtained dealing with daytime and nighttime of the summer and of the winter season.

In the analysis of the airborne MSS thermal images, the training image of the vegetation distribution was made on the MSS image to grasp the shape of a group of trees, based on the aerial color photograph and the ground research. An example of infrared thermal images observed by the airborne MSS is shown in the figure 1, and the training image is shown in figure 2. Three categories, i.e., trees, lawn and grass were deciphered by watching for making-up training image. In this paper, only trees are analyzed. Although mixels which contains both vegetation and other materials exist in the airborne MSS image, mixels are not described on this paper. The minimum unit of vegetation which was dealt with on the analysis is the 1 central pixel of the 3×3 pixels of vegetation.

Table 1 Outline of airborne MSS observation and weather data

Date: August 9, 1987	
13:47 – 13:54	S: 711W/m², A: 31.4℃ H: 58%, W: 3.0~4.0m/s(SSW)
18:42 – 18:49	S: 0 W/m², A: 29.7℃ H: 71%, W: 3.0~4.0m/s(SSW)
January 13, 1988	
12:57 – 13:04	S: 396 W/m², A: 12.4℃ H: 25%, W: 1.5m/s(ENE)
16:15 – 16:21	S: 0 W/m², A: 11.5℃ H: 30%, W: 1.6m/s(SE)
S: solar radiation incident upon a horizontal surface, A: air temperature, H: relative humidity, W: wind velocity	
Place: Miyamae, Kawasaki, Japan	
Resolution: 1.9 m	
Band : Visible	0.60–0.65 μm
Near Infrared	0.92–1.00 μm
Thermal Infrared	8.00–12.0 μm

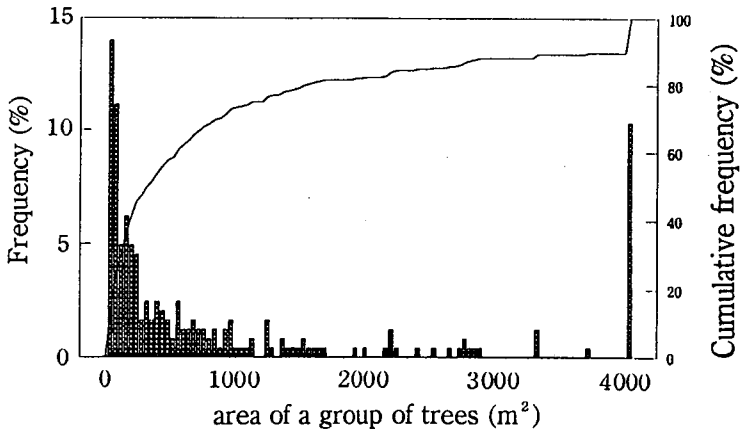

Fig. 3 Histogam of groups of trees from a point of the area

Figure 3 shows the actual distribution of each group of trees in the target field. A cumulative histogram is also indicated. The frequency of the groups of trees with more than $80m^2$ is very high. That means we cannot recognize urban vegetation distribution even if we use SPOT data.

3. RELATIONSHIP BETWEEN NORMALIZED VEGETATION INDEX AND RADIANT TEMPERATURE OF A GROUP OF TREES

The activated degree and the leaf density of the tree crown have mainly influence on the normalized vegetation index (NVI) which is calculated from visible and the near infrared data, and it is expected that there is good correlation between NVI and the radiant temperature of the tree crowns. Figure 4 shows the relationship between the average of NVI and the average of radiant temperature of every group of trees.

Though the correlation coefficient with 0.7 is comparatively high of the daytime in summer, small groups of trees vary widely. At night, the radiant temperature of most groups of trees are

about 1 degree lower than the air temperature for the reason of the sky radiation, so the radiant temperature is hardly related with NVI and the area of a group of trees. Also NVI in winter season is lower than that in summer season, and no relationship exists between NVI and the radiant temperature. NVI value and the area of a group of trees can be the parameters which distinguishes the radiant temperature of a group of trees.

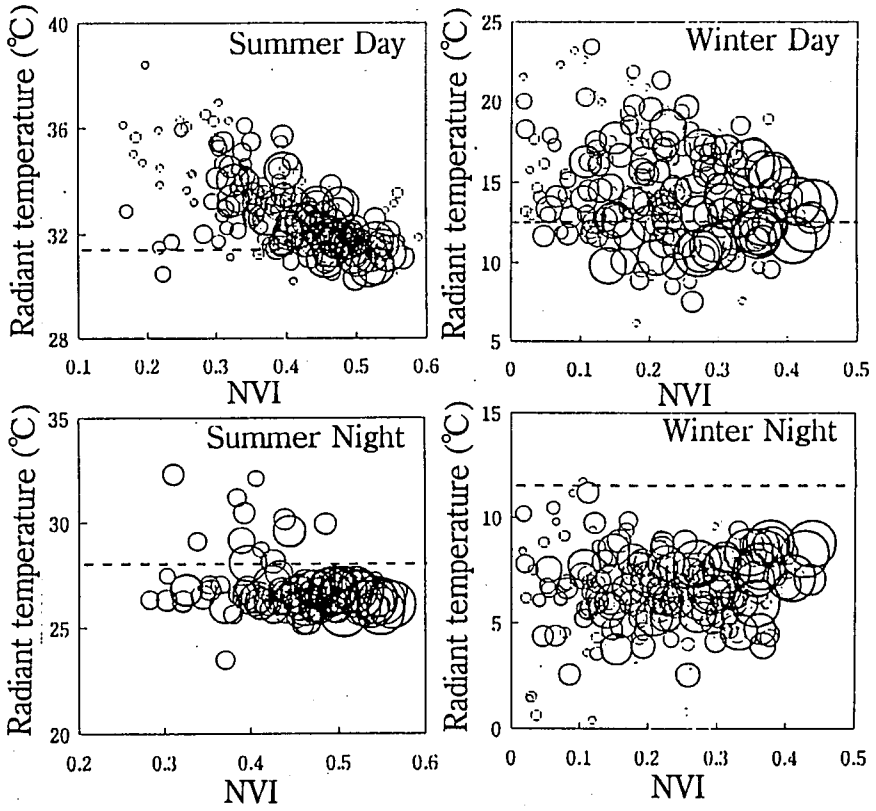

Fig. 4 Relationship between averaged NVI and averaged radiant temperature of a group of trees

4. CHARACTERISTICS OF RADIANT TEMPERATURE DISTRIBUTION IN A GROUP OF TREES

It is estimated that the distributions of NVI and the radiant temperature exist in one group of trees from the following points.

a) The surface of a group of trees is uneven, so both the shaded part and the sunlit part are shown in MSS thermal images.

b) The center part of a group of trees show lower temperature in MSS thermal images, because the larger the scale of a group of trees is, the lower the air temperature near the center of the trees is.

We verify a) and b) using the thermal infrared images observed by airborne MSS.

1) Relationship between the sun beam vector and the radiant temperature of the edge parts of trees

The relationship between the averaged NVI and the averaged radiant temperature at the edge of a group of trees using airborne MSS data observed at daytime in summer, is shown in

figure 5, dividing into the sunlit side and the opposite side. The negative correlation exists, and the sunlit side is about 2°C higher than the shaded side even though NVI is same.

2) Radiant temperature distribution of a group of trees consisted of the shaded and sunlit pixels

Figure 6 shows a histogram of radiant temperature of a group of trees. Comparing the mode value, the radiant temperature of the first pixels facing to the sun at the edge of a group of trees shows 2°C higher than the air temperature. The difference is within 1℃ at two or three pixels inside, so the far from the edge of a group is, the smaller the temperature difference between the radiant temperature and the air temperature is.

Figure 7 shows the histogram of averaged radiant temperature difference between that of sunlit side and that of shaded side of a group of trees. The radiant temperature is higher than the air temperature at the pixels which are closer to the edge of a group of trees and the incident solar radiation is large.

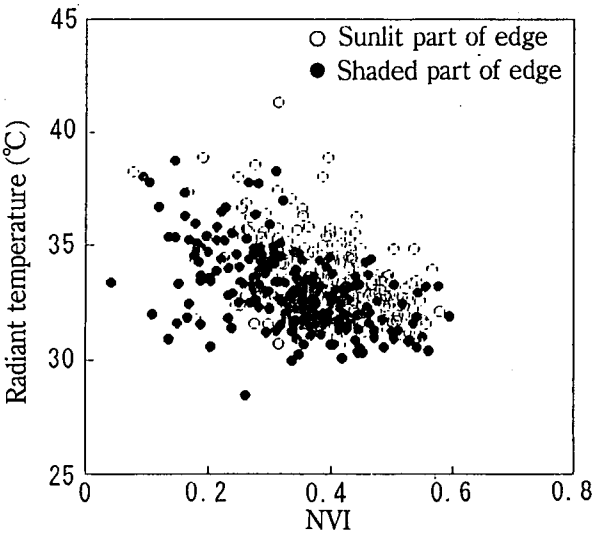

Fig. 5 Relationship between NVI and radiant temperature at the first pixel from the edge part of a group of trees

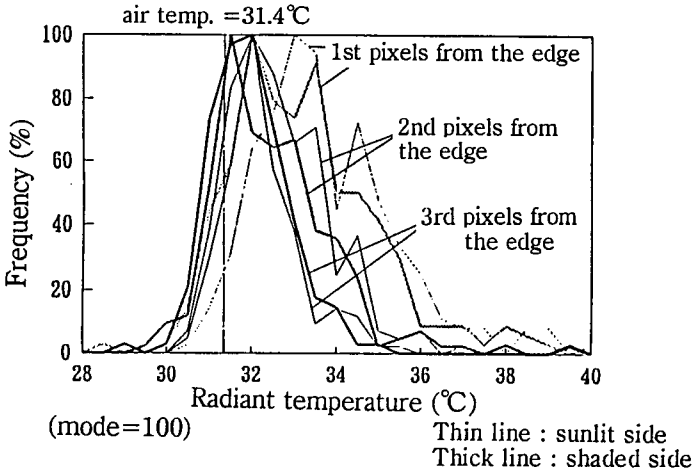

Fig. 6 Histogram of the radiant temperature at each pixels inside from the edge of a group of trees

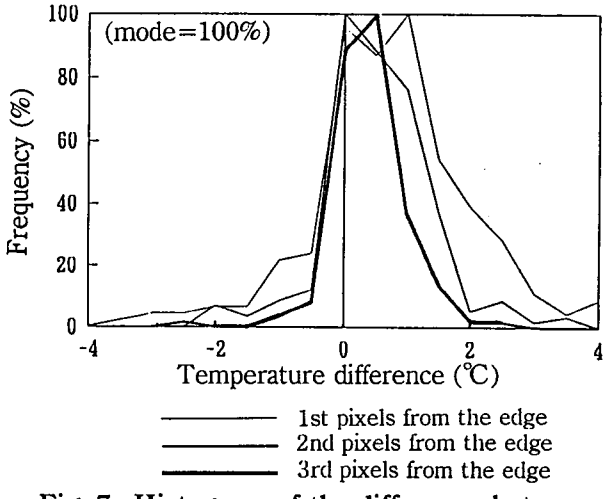

Fig. 7 Histogram of the difference between the radiant temperature of sunlit part and that of shaded part in a group of trees

5. CHARACTERISTICS OF RADIANT TEMPERATURE DISTRIBUTIONS OF URBAN VEGETATION AND ITS RELATIONSHIP TO WEATHER PARAMETERS

The sensible heat flux from a group of trees is investigated in this chapter. Figure 8 shows the relationship between the difference of the radiant temperature and the air temperature of a

group of trees, and the solar radiation incident upon a horizontal surface. Weather data was measured at the rooftop of the building in the center of Yurigaoka, Kawasaki City, Japan.

At noon, the difference between averaged radiant temperature at the sunlit edge of a group of trees and the air temperature is the largest value, i.e., the central value of about 3°C and maximum about 6°C. The average and the dispersion shows smaller at the shaded edge, and at the one pixel inside from the sunlit edge of group of trees. The averaged radiant temperature of pixels located at more than 4 pixels inside from the edge of a group of trees is equal to the air temperature. At night, the averaged radiant temperature of a group of trees is 2°C lower than the air temperature, because of the sky radiative cooling effect.

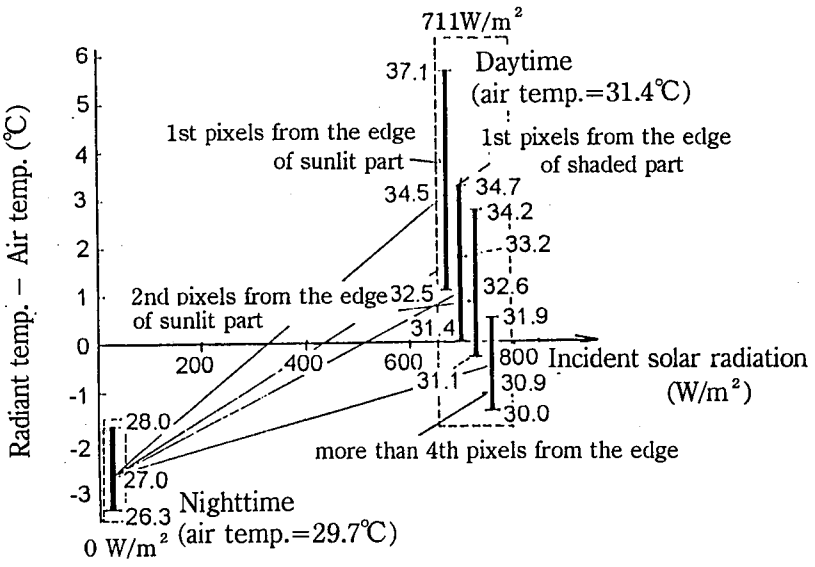

Fig. 8 Relationship between the radiant temperature of groups of trees and weather parameters

Time series observation using airborne MSS has limitation, therefore the method to presume the temperature difference between daytime and nighttime observation data is required. Penman-Monteith formula ([8], [9]) is proposed, as the method of formulating the trees heat and moisture budget using the weather parameters. This formula includes two resistance values, i.e. aerodynamic resistance *ra* at the crown surface and canopy resistance *rc*. The difference between the surface temperature of a group of trees and the air temperature is shown as below.

$$Ts - Ta = \frac{ra\ \gamma\ (\ 1 + rc/ra\ )\ (Rn-G)}{\rho\ Cp\ \ (\Delta + \gamma\ (1+rc/ra)\ )} + \frac{es(Ta) - ea}{\Delta + \gamma\ (1+rc/ra)} \qquad (1)$$

Ts: surface temperature of a group of tree (K), Ta: air temperature (K), ra: aerodynamic resistance (s/m), rc: canopy resistance (s/m), Rn: net sky radiation (W/m^2), G: heat conduction to the ground, ρ : density (kg/m^3), Cp: specific heat (J/kgK), Δ: the slope of the tangent of saturated vapor pressure curve, γ : constant of wet and dry bulb thermometer (Pa/K), es(Ta): saturated vapor pressure at Ta (Pa), ea: vapor pressure of the air (Pa)

Using weather data when the airborne MSS observation was performed in summer, the relationship between the incident solar radiation and the difference between the radiant temperature and the air temperature was calculated by the equation (1) (Figure 9). As the *rc* value, the measured data of keyaki [10] was used. Though both the air temperature term and relative humidity term are contained in the right side of the equation, the curve shown in figure 9

is assumed to be a straight line. We have already examined the heat and moisture budgets of lawn-planting are examined and showed that the difference between the surface temperature of lawn and the air temperature is linear to incident solar radiation [11]. The same results are shown in the case of tree crowns.

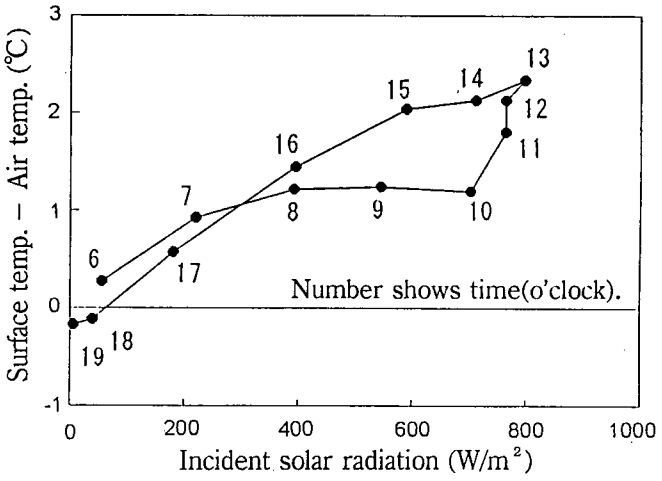

Fig. 9 Calculated results of the difference between the surface tempeature of a group of trees and the air temperature

Comparing the difference between the radiant temperature and the air temperature of a group of the trees of figure 8 to the computational result of figure 9, the observed radiant temperature is about 2°C lower than the calculated temperature. In the measurement of the radiant temperature of the ground surface, an infrared spot thermometer was used, so the calibration error of the infrared thermometer can not be ignored in the measurement result. Moreover, the air temperature in the daytime and nighttime is considered to be higher than the air temperature near the center of a group of trees, because the air temperature at the weather observatory was measured at the rooftop of a building in the city place. That is, the result of figure 9 shows a decline effect of the air temperature by a large group of trees, which has been pointed out as usual.

6. CONCLUSIONS

Using the airborne MSS data observed in the daytime and nighttime both in summer and the winter, the actual spatial distribution of the radiant temperature of every group of trees was investigated from the point of the relation with the weather condition. NVI value and the area of a group of trees could be the parameters which distinguishes the radiant temperature of a group of trees. Furthermore, a decline effect of the air temperature was clarified by a large group of trees.

7. REFERENCES

[1] Akira Hoyano, Sumio Yagi and Takehisa Kimura : Features of Thermal Environment Made by Plants in Outdoor Space, J. of Archit. Plann. Environ. Eng., AIJ, No.433, pp.1-10 (1992) (in Japanese).

[2] Mitsuo Kondo, Kazuyuki Manita, Yozo Yokoyama and Tomoo Ozawa : A Quantitative Study on the Effect of Micro-climate Control by an Existence of the Tree and the Lawn Area, J. of JILA, No46(3), pp. 161-175 (1983) (in Japanese).

[3] Tadahisa Katayama et al. : Cooling Effects on Thermal Environment in a Built-up Area

-Survey on Amount of Green and Air Temperature -, Engineering Science Reports. Kyushu University, Vol.12, No.2, pp. 215-220 (1990) (in Japanese).
[4] Akira Hoyano and Masunori Kato : Extraction of Urban Vegetation by Airborne Multi-spectral Scanner Data with High Spatial Resolution, J. of Archit. Plann. Environ. Eng., AIJ, No.407, pp. 37-45 (1990) (in Japanese).
[5] Kirk C. McDaniel : Assessing Mesquite-Grass Vegetation Condition from Landsat, Photogrammetric Engineering and Remote Sensing, Vol.48, No.3, pp. 441-450 (1982).
[6] John C. Price : Estimating Vegetation Amount from Visible and Near Infrared Reflectances, Remote Sensing Environ. 41, pp. 29-34 (1992).
[7] J.R. Dymond, P.R. Stephens, P.F. Newsome and R.H. Wilde : Percentage Vegetation Cover of a Degrading Rangeland from SPOT, INT. J. Remote Sensing, Vol.13, No.11, pp.1999-2007 (1992).
[8] Penman, H.L. : Natural Evaporation from Open Water, Bare Soil and Grass, Proc. Roy. Soc. London, A 193 (1948).
[9] Monteith, J.L. : Evapotranspiration and Environment. In 'The state and movement of water in living organs' (Fogg, G.E.,ed.), Soc. Exp. Biol. Symp., 19, Cambridge University Press (1965).
[10] Y. Tsukamoto : Forest Hydrology, Bun'eido (1992) (in Japanese).
[11] A. Hoyano, J. He, T. Horiguchi and G. Wang : Experimental Study on Heat Budget for Foliage Layer of Lawn-planting, J. of Archit. Plann. Environ. Eng., AIJ, No.462, pp.31-39 (1994) (in Japanese).

Effects of Sensor Degradation and Solar-Sensor Geometry on Land Cover Monitoring Using NOAA/AVHRR Data

Shoji Takeuchi* and Yasushi Mitomi**

*Remote Sensing Technology Center of Japan
1-9-9,Roppongi,Minato-ku,Tokyo 106 JAPAN

**National Space Development Agency of Japan
1-9-9,Roppongi,Minato-ku,Tokyo 106 JAPAN

Abstract: The authors studied the effects of the degradation of NOAA/AVHRR sensor sensitivity and the geometry concerning to the zenith and azimuth angles of the sun and a sensor on the monitoring of land cover conditions using multi-temporal AVHRR data. The effect of sensor degradation on calibration of AVHRR visible and near-infrared channels was tested using the data taken in a desert area where the surface albedo was considered to be stable. The effect of solar-sensor geometry was tested using the three temporal data which were observed within a week and in different geometrical conditions and regression analysis was performed to study the effect of geometrical parameters on the correlation of surface albedos and NVI among the three different data.

1.Introduction

As optical sensor data like NOAA/AVHRR contain data variations due to sensor degradation and geometric conditions of ground observation, it is quite important to consider these variations for the creation of wide-range mosaicked images and the monitoring of the ground surface by multi-temporal data.

Two kind of approaches can be considered for the correction of the variations. One is the statistical approach in which the brightnesses of the images are adjusted by a statistical method. But the statistical adjustment causes the loss of the original radiance information. The other approach is to convert the brightnesses of the images to the physical amount like radiance or reflectance. The first step of the latter approach is to establish the accurate calibration method to acquire accurate radiance or reflectance at the sensor observation. The second step is to correct the variations caused by the geometric observation condition based on the model for the atmospheric effect on various geometric conditions.

In this study, first, the radiometric correction of AVHRR visible and near IR data which considers the sensor degradation and solar-zenith angle was tested as the calibration procedure and the effect of this correction was evaluated using the data taken in a desert area where the surface albedo was considered to be stable. Next, the effects of the geometric conditions related to solar zenith and sensor zenith angles were investigated using the three temporal data which were observed within a week and in different geometrical conditions. The latter investigation is expected to make clear the actual variation due to the difference of the geometry and to offer the evidence for the necessity of the appropriate atmospheric correction for the monitoring by multi-temporal satellite images.

2. Effect of Sensor Degradation on AVHRR Radiance

In order to evaluate the effect of the sensor degradation of AVHRR, two AVHRR LAC images observed on 27/Jan.,1986 (NOAA-9) and 30/Jan.,1993 (NOAA-11) were used for the analysis. For each image, total 192 pixel samples were selected within Thar Desert of India under the geometrical conditions in which the solar zenith angle was restricted from 55° to 65° and the sensor scan angle from 0° to 20° . This restriction was applied to confirm the stability of the reflectance of the desert areas.

2.1 Calibration and correction of AVHRR data

(a) Preflight calibration

The calibration for AVHRR visible (CH.1) and near IR (CH.2) data generally uses the coefficient calculated from the preflight test data. In this calibration, the observed radiance in units of $\mu W/cm^2/nm/sr$ is obtained as follows;

$$R_{pre} = \alpha (C\text{-}C_0) \qquad (1)$$

where R_{pre} is the observed radiance, α is the preflight radiometric coefficient as follows;

NOAA-9 : CH.1;0.055 , CH.2;0.036 NOAA-11: CH.1;0.047, CH.2;0.028

C is the AVHRR output digital count level, and C_0 is the count level measured when the instrument is observing deep space.

(b) Calibration considering the sensor degradation

As AVHRR visible and near IR data are affected by the sensor degradation at a launching time or during in orbit (Kaufman and Holben (1992)), the calibration considering the sensor degradation is necessary to acquire an accurate radiance at the sensor observation. So, the coefficient by Kaufman and Holben (1992) was applied as the calibration coefficient as follows;

$$R_{deg} = (\alpha / \gamma)(C\text{-}C_0) \qquad (2)$$

where R_{deg} is the observed radiance considering the sensor degradation , α / γ is the radiometric coefficient for the test data considering the sensor degradation as follows;

NOAA-9: CH.1 ;0.06320, CH.2;0.04397 NOAA-11: CH.1;0.05927, CH.2;0.04086

(c) Solar zenith angle correction

The radiance values of AVHRR CH.1 and CH.2 change according to the variation of the solar zenith angle by the reason that the reflected radiance from the target pixel is affected by the incident energy of solar illumination. Therefore the observed radiance was normalized by the cosine of solar zenith angle to correct the change of incident solar radiance as follows;

$$R_{sol} = R/\cos\theta_0 \qquad (3)$$

where R_{sol} is the observed radiance considering the solar zenith angle, R is the radiance calculated by Eq. (1) or (2), and θ_0 is the solar zenith angle.

2.2 Result of calibration and correction

Fig.1(a) and 1(b) shows the radiance distribution of AVHRR data (27/Jan. 1986 and 30/Jan. 1993) corrected with preflight calibration coefficients for visible (CH.1) and near IR (CH.2) respectively. Fig. 2(a) and 2(b) shows the radiance after the calibration considering the sensor degradation. These results indicate that the difference of the mean radiance between the two data in Fig.2 is smaller than that in Fig.1. This fact suggests that the calibration considering the sensor degradation is useful for the comparison of multi-year AVHRR data taken by different satellites.

Fig.3(a) and 3(b) show the radiance distribution of AVHRR data (27 Jan. 1986 and 30 Jan. 1993) after the calibration considering the sensor degradation and after the solar zenith angle correction. In these figures, the difference of mean radiance between the two data becomes smaller after the solar zenith angle correction. In addition, the mean radiance values of the two data are nearly same in the range where the sensor scan angle is small. This fact suggests that the consideration of the sensor degradation can result in more appropriate correction by the combination of the solar zenith angle correction.

2.3 Discussion

From above experimental results, it is obvious that the calibration considering the sensor degradation is necessary to derive an accurate radiance at the satellite observation. If the geometric condition is in a very good condition that the sensor scan angle is very small, the derived radiance by the above calibration and correction will be able to be used directly for the comparison of the ground surface between the plural data taken at different times.

Actually, it is impossible to acquire all necessary data in a good geometric condition. Therefore the archived data like a mosaicked product at least should include the geometric information (solar and satellite zenith angles and solar-satellite relative azimuth angle) for every pixels, which might be used for a later atmospheric correction procedure if possible.

3. Effect of Solar-Sensor Geometry on Surface Albedo and NVI

When the multi-temporal AVHRR data are used for the monitoring of land cover conditions, the effects of the geometric conditions among the sun, a sensor and a ground should be considered, because these conditions bring the change of the surface albedo and NVI derived from AVHRR data. In order to investigate these effects, three AVHRR data which were observed within a week and have different geometric conditions were used. The data were acquired on 6/Feb. (9303708), 7/Feb. (9303808) and 13/Feb. (9304409) in 1993 respectively.

Under the assumption that the ground surface conditions are same among the three, total 16 sample area triplets corresponding to the same location were selected. Each sample area was composed by 5 by 5 windows and the average value in the window was used as the representative data of the sample area. The land cover classes of the samples were forest, agricultural land and bare soil.

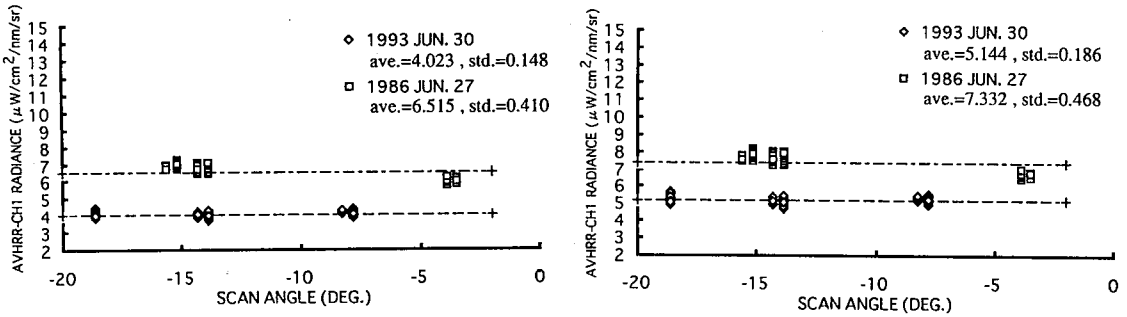

(a) Channel-1 data (b) Channel-2 data

Fig.1 Result of preflight calibration.

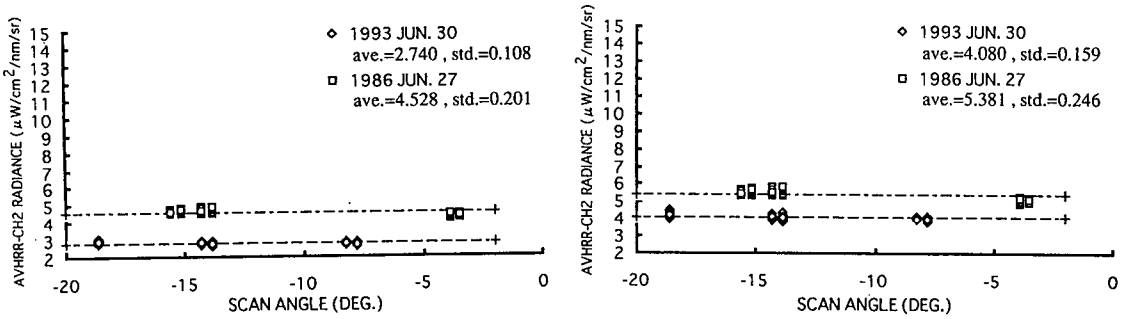

(a) Channel-1 data (b) Channel-2 data

Fig.2 Result of the calibration considering sensor degradation.

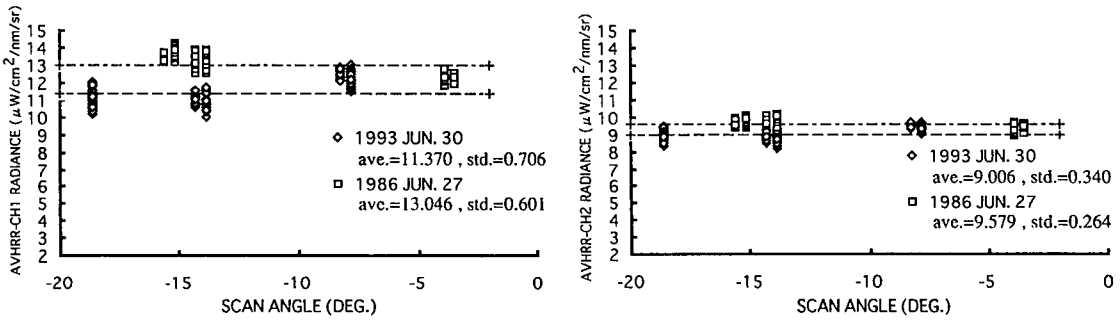

(a) Channel-1 data (b) Channel-2 data

Fig.3 Result of solar zenith angle correction after the calibration of Fig.2.

3.1 Relation between surface albedo and geometric condition

Fig.4(a - e) shows the values of the samples for solar zenith angle, satellite zenith angle, albedo in CH.1 and CH.2, and the normalized vegetation index (NVI) derived as follows;

$$NVI = (A2-A1)/(A2+A1) \quad (4)$$

where A1 and A2 are the albedos in CH.1 and CH.2 respectively. The sign of the satellite zenith angle was inverted when the solar azimuth and satellite azimuth is in a reverse direction, namely if the relative azimuth of the two is larger than 90 deg..

It is obvious that the variations of the albedos in CH.1 and 2 are clearly related to the two geometric parameters, the solar zenith and satellite zenith angles. Because the albedo is derived after the solar zenith angle correction described in 2, The main parameter affecting the albedo is considered to be the satellite zenith angle. Generally, the albedo becomes larger in the case of positive large satellite zenith angle, namely in the case of large satellite zenith angle in the same direction of the sun and a satellite. It is obvious that this variation is caused by the larger effect of the path radiance. On the contrary, in the case of small positive values and negative values of the satellite zenith angle the variation of the albedo is smaller.

On the other hand, the variation of NVI is rather reverse of that of the albedo, namely NVI decreases in the case of positive large satellite zenith angle. For the data 9303708 and 9303808, the NVI values are almost similar except the sample 6, which is the bare soil surface and has the positive large satellite zenith angle.

3.2 Regression analysis of albedo and NVI between two different data

Fig.5 shows the results of regressions of the albedos and NVI between two different data. The results show that the correlation coefficient for the pair of 9303708 and 9303808 is always larger than that for the pair of 9304409 and 9303808 for both of albedo and NVI. Therefore it is obvious that the data in the geometric condition of positive greater satellite zenith angle degrade the linearity of the correspondences of albedo and NVI with other data.

As to NVI, in the pair of 9303708 and 9303808 almost of the samples are in a region of acceptable variations of NVI for the comparison even if there remains relatively large variation in albedo. This result suggests some effect of NVI for the compensation of the variation due to the geometric conditions. However, for the pair of 9304409 and 9303808, almost of the samples result in under estimation of NVI for one of the pair, 9304409. In this sense, the samples from 9304409 have quite poor quality for the comparison with others, even if the NVI is used for the comparison.

3.3 Discussion

From the above results, it is obvious that the geometric condition, especially the satellite zenith angle brings the large effect on surface albedo and NVI, not only to the absolute values but also the linearity of data correspondences even after a linear data conversion. The NVI is less affected by the geometry compared with the albedos in CH.1 and 2, which has proved some

(a)

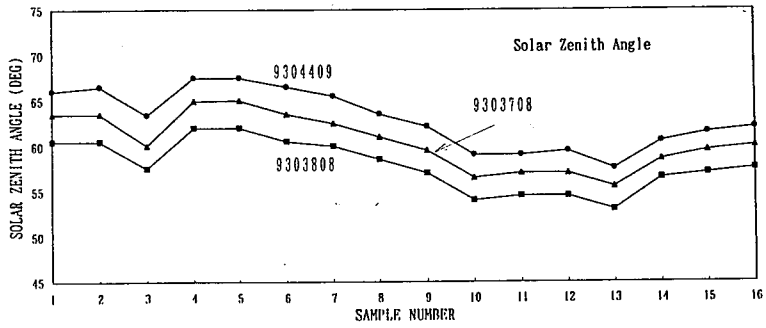

(b)

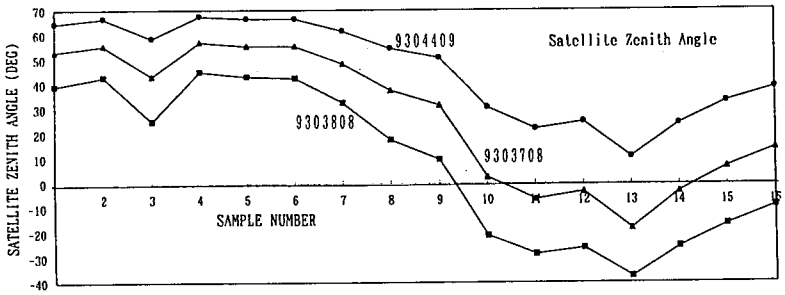

(c)

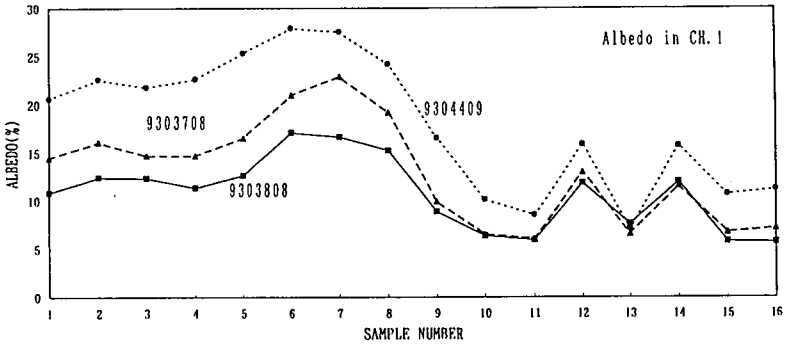

(d)

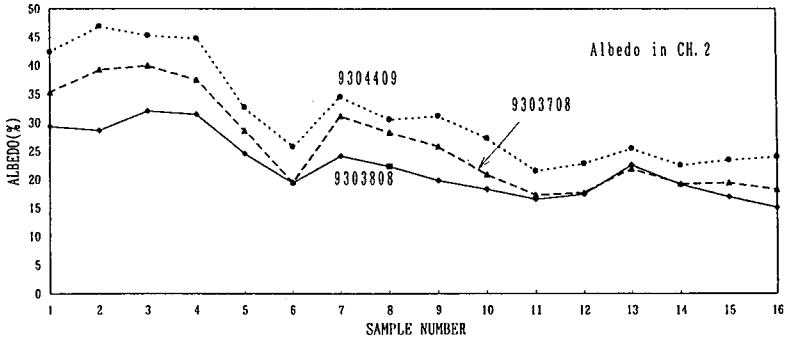

(e)

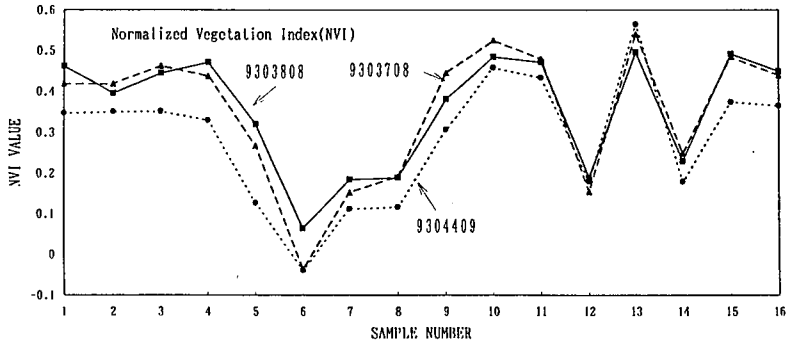

Fig.4 The values of solar zenith angle(a), satellite zenith angle(b), albedo in CH.1(c) and CH.2(d) and NVI(e) of all the samples of the three different AVHRR data.

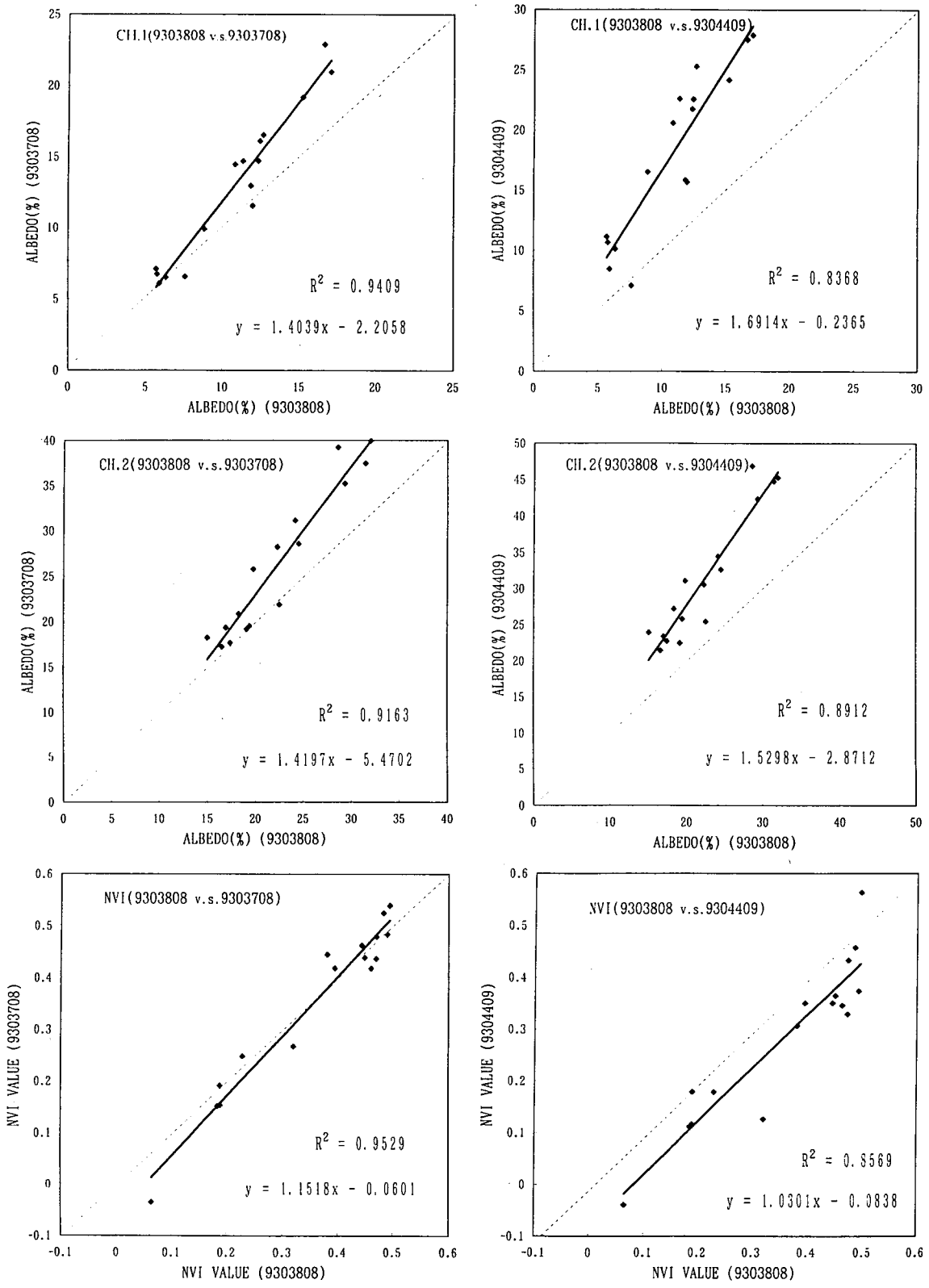

Fig.5 Results of the regression of the albedo in CH.1 and 2 and NVI between two different data (9303808 v.s. 9303708 and 9303808 v.s. 9304409).

effect of the NVI for compensation of unexpected variation of surface albedos. However, if the satellite zenith angle is much larger than an acceptable value, may be 50 degree from Fig.4, it is recommended not to use that sample for the comparison with other data. If only the data sample in such a bad condition is available, it should be recognized that the NVI values are always under estimated compared with the real values.

4. Conclusion

The effects of the sensor degradation and the geometric conditions related to the sun, a satellite and a ground were studied in the situation of the comparison of multi-temporal AVHRR data. The calibration considering the sensor degradation was proved to result in more appropriate correction for the comparison of the AVHRR radiance derived from different satellites. The geometric parameter, especially the satellite zenith angle was proved to have the large effect on albedo and NVI derived from the calibrated AVHRR visible and near IR data.

The ideal case seems to be that an appropriate atmospheric correction is applied to the calibrated data based on the geometric parameters computed in the calibration procedure. However, even if the atmospheric correction is difficult to be applied, at least these geometric parameters should be always taken into consideration for the comparison among the multi-temporal AVHRR data. This consideration may be useful to avoid misunderstanding about the temporal change of ground surface conditions.

References

1) NOAA/NESDIS/SDSD, Noaa Polar Orbitor Data Users Guide, July,1991
2) B.N.Holben,Y.K.Kaufman and J.D.Kendall(1992),NOAA-11 AVHRR visible and near-IR inflight calibration, INT.J.REMOTE SENSING, Vol.11,No.8, 1511- 1519.

Atmospheric effect and its correction of the remotely sensed VNIR data for the vegetation monitoring

Masao Moriyama (*)

* Dept. Mechanical Systems Eng., Faculty of Eng., Nagasaki Univ..
1 – 14 Bunkyo-machi Nagasaki 852 Japan.
Email: matsu@study-rs.mech.nagasaki-u.ac.jp

Abstract

To make the brief correction of the remotely sensed VNIR data, the atmospheric correction method which uses only the optical thickness is proposed. In this method, the satellite detected radiance is assumed to be separate into three terms, path radiance, directly reflected radiance and the diffusely reflected radiance. All of the three terms are approximated by the geometry and optical thickness based function. The coefficients in the functions are defined from from the multiple regression analysis between the optical thickness and the computed values from the radiative transfer code LOWTRAN 7. From the comparison between the model surface albedo and the estimated albedo from the proposed method, this method has the potential to use and the possibility to improve from the ground based surface/atmosphere observation.

1 Introduction

The vegetation monitoring from the satellite is the one of the key factors for the earth environmental science. The NDVI (Normalized Differential Vegetation Index) derived from the NOAA/AVHRR data show us the dynamic change of the global vegetation change [Justice 85]. But some researchers pointed out the atmospheric effect over the NDVI data [Fraser 85] [Singh 88]. On the other hands, the radiative transfer process in the VNIR spectrum are well studied [Chandrasekher 60], [Meador 80] and atmospheric correction methods are proposed [Kaufman 88], [Richter 90]. These researches show us the difficulty of the simplified expression of the radiative transfer process and the difficulty of the atmospheric data gathering for the atmospheric correction.

In this study, to make the brief expression of the surface albedo from the remotely sensed VNIR data, the simple atmospheric correction method which use the optical thickness and the solar–surface–satellite geometry is proposed. All of the coefficients in the proposed method are defined from the multiple regression analysis between the values computed from the radiative transfer code LOWTRAN 7 [Kneizeys 88] and the variables derived from the optical thickness and the geometry. Also to verify the correction performance, the comparison between the model and the estimated surface albedo are made.

2 Radiative Transfer Process

The exact formula of the radiative transfer process in VNIR spectrum is expressed as follows [Chandrasekher 60].

$$\begin{aligned}\cos\Theta\frac{dI(\xi,\Theta,\Phi)}{d\xi} &= I(\xi,\Theta,\Phi) - \frac{\varpi_0}{4\pi}p(\Theta,\Phi;\theta_0,\phi_0)I_0\exp[-\frac{\xi}{\cos\theta_0}] \\ &- \frac{\varpi_0}{4\pi}\int_{-\pi/2}^{\pi/2}\int_0^{2\pi}p(\Theta,\Phi;\theta',\phi')I(\xi,\theta',\phi')d\theta'd\phi', \qquad (1)\end{aligned}$$

where

ξ: Optical thickness from the top of the atmosphere,

$I(\xi,\Theta,\Phi)$: Radiance at ξ toward the direction of zenith angle of Θ and the azimuth angle of Φ,

ϖ_0: Albedo for single scattering of the atmosphere,

θ_0: Solar zenith angle,

ϕ_0: Solar azimuth angle,

$p(\Theta,\Phi;\theta_0,\phi_0)$: Scattering phase function of the atmosphere from (θ_0,ϕ_0) to(Θ,Φ),

I_0: Extraterrestrial solar radiance.

To evaluate the radiance reaching the satellite, it is necessary to know the optical thickness, albedo for single scattering and the phase function, however, the last two parameters are difficult to know, only the optical thickness from the top of the atmosphere to the surface is relatively easy to know by using the sun photometer [Shaw 83].

3 Simplified Radiative Transfer Equation

3.1 Overview

To estimate the surface albedo from the remotely sensed data, this means the atmospheric correction, the atmospheric parameters such as optical thickness, scattering phase function and so on are had to be known. But only the optical thickness is relatively easy to observe. So in this study, the radiative transfer equation which uses only the optical thickness and the solar–surface–satellite geometry is defined and the atmospheric correction method which uses this equation are made.

The radiance reaching a satellite:I is assumed to be the sum of the next three component, 1) path radiance: P_r, 2) direct reflection radiance: R_d and 3) diffused reflection radiance: R_f. And all of the three terms are the function of the optical thickness from the top of the atmosphere to the surface: ξ_s, solar zenith angle: θ_0 and the observation zenith angle (scan angle): θ. The approximated radiative transfer equation is formulated as follows.

$$I = P_r + R_d + R_f \qquad (2)$$

The solar and observation azimuth angle effects are neglected and all term are normalized by the extraterrestrial solar radiance so that all term are shown in the albedo unit. The

functions and the coefficients are defined from the multiple regression analysis between the values and the optical thickness and the geometry.

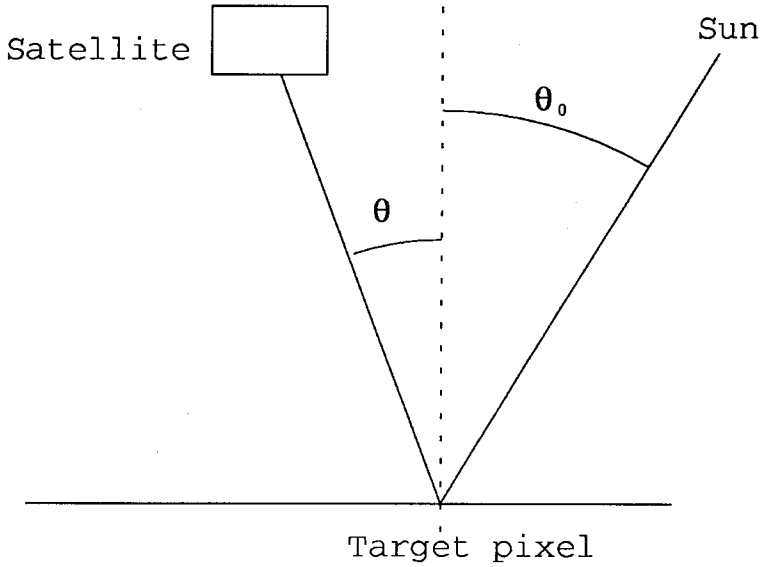

Figure 1: The geometry of the observation.

3.2 Path radiance formulation

The path radiance reaching a satellite :I_a in the case of single scattering approximation is expressed into the next expression [Tsuchiya 90].

$$I_a = \frac{\varpi_0}{4\pi} I_0 p(\theta, \phi; \theta_0, \phi_0) \frac{m}{m + m_0} \{1 - \exp[-(m + m_0)\xi_s]\} \tag{3}$$

where m and m_0 are observation and solar air mass respectively.

From this fact and the consideration of the multiple scattering, path radiance P_r is assumed to be the next formula.

$$P_r \simeq C_1 m \xi_s + C_2 \frac{1 - \exp(-m_0 \xi_s)}{m_0} + C_3 \frac{m}{m + m_0} \{1 - \exp[-(m + m_0)\xi_s]\} + C_0 \tag{4}$$

where C's are the coefficients.

3.3 Direct reflection radiance formulation

The direct reflection radiance is exactly expressed as follows.

$$R_d = A_s \frac{\exp[-(m + m_0)\xi_s]}{m_0} \tag{5}$$

where A_s is the surface albedo. And in this case the surface is assumed to be the Lambertian.

3.4 Diffuse reflection radiance formulation

The diffuse radiation can be proportional with the rest of the direct transmitted radiation, so in this case the diffuse reflect radiance is approximated as follows.

$$D_f = A_s[c_1\xi_s \exp(-m_0\xi_s) + c_0]\{1 - \exp[-(m + m_0)\xi_s]\} \tag{6}$$

where c's are the coefficients.

3.5 Atmospheric correction formula

From the above consideration, the atmospheric correction formula is expressed as follows.

$$A_s = \frac{I - P_r}{\frac{\exp[-(m+m_0)\xi_s]}{m_0} + [c_1\xi_s \exp(-m_0\xi_s) + c_0]\{1 - \exp[-(m + m_0)\xi_s]\}} \tag{7}$$

4 Verification

To define the coefficients and the verification, the numerical simulation based on the radiative transfer code LOWTRAN 7 are made. In this simulation, the radiance reaching a satellite, path radiance, direct reflection radiance and diffuse reflection radiance are computed, and from the these values, the coefficients are defined from the multiple regression analysis. In this simulation, channel 1 and 2 of NOAA/AVHRR is supposed to be a the target sensor, and the regression formula in each channel and the forward/backward scattering direction is established.

4.1 Simulation conditions

Atmospheric models: Tropic, Midlatitude summer/winter, Subarctic summer/winter.

Wavelength: 0.635 (ch. 1), 0.833 (ch. 2) [μm]

Surface visibility: 5, 23 [km]

Aerosol: Rural model

Surface albedo: 0.01, 0.05, 0.1, 0.15, 0.2, 0.25, 0.3, 0.4

Solar zenith angle: 30, 50, 60, 70, 80 [deg.]

Observation zenith angle: -60, -30, 0, 30, 60 [deg.] (- means the backward scattering direction)

4.2 Result (Path Radiance)

The coefficients and the RMS error of the path radiance estimation are tabled as follows, and the comparison between the model and the estimated path radiance are shown.

Table 1: Coefficients and RMS error of the path radiance estimation

	C1	C2	C3	C0	RMS
Ch. 1 Forward	.1196E-01	.9957E-01	.1209E-02	.7911E-03	.6904E-02
Ch. 1 Backward	.1129E-01	.1191E+00	-.5729E-01	.8509E-02	.6113E-02
Ch. 2 Forward	.1227E-01	.8015E-01	-.2016E-01	.3108E-03	.6717E-02
Ch. 2 Backward	.1215E-01	.8441E-01	-.4985E-01	.5655E-02	.6480E-02

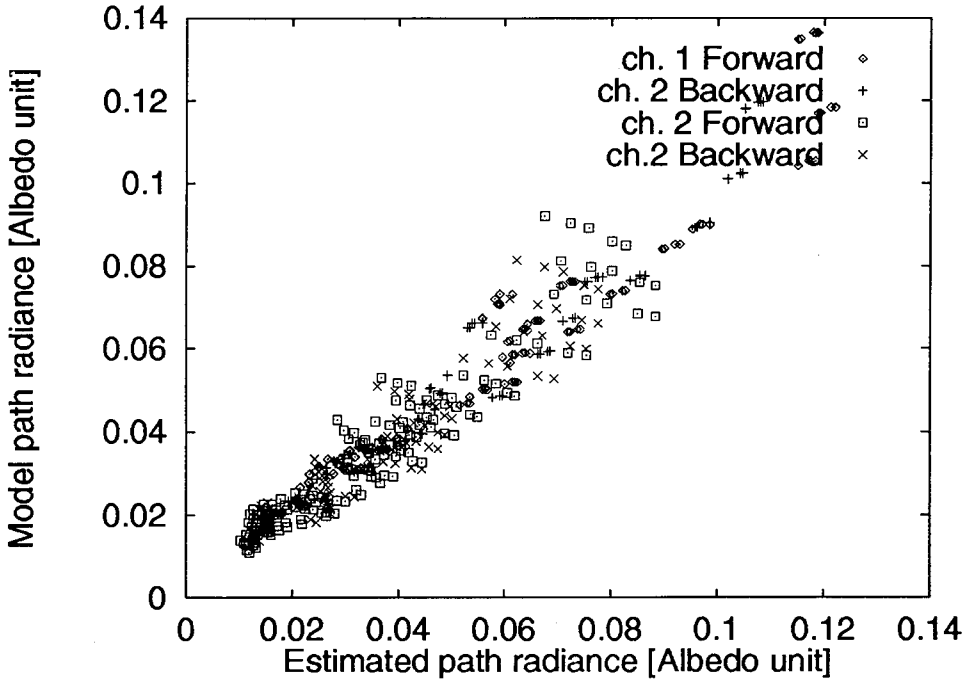

Figure 2: Comparison between the model and the estimated path radiance

The result shows the good correspondence, but some dispersion are shown in large path radiance. This is because the neglect of the scattering phase function.

4.3 Result (Diffuse reflection radiance)

The coefficients and the RMS error of the diffuse reflection radiance estimation are tabled as follows, and the comparison between the model and the estimated diffuse reflection radiance are shown.

Table 2: Coefficients and RMS error of diffuse reflection radiance estimation

	c1	c0	RMS
Ch. 1 Forward	.1601E+01	.3035E-01	.9923E-02
Ch. 1 Backward	.1607E+01	.4217E-01	.9591E-02
Ch. 2 Forward	.1507E+01	.2022E-01	.1084E-01
Ch. 2 Backward	.1542E+01	.2670E-01	.1074E-01

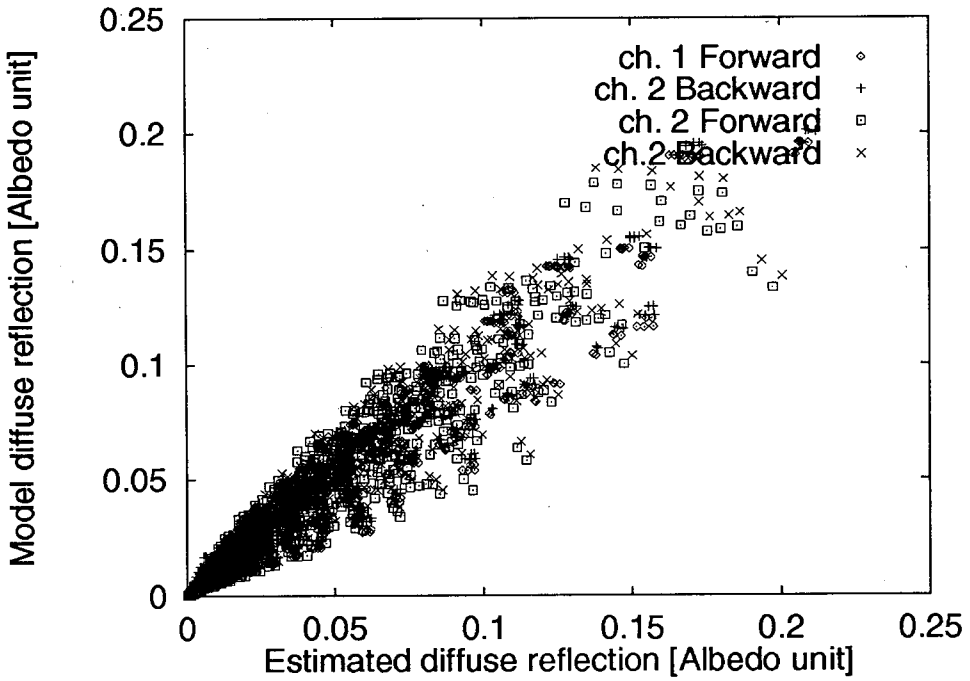

Figure 3: Comparison between the model and the estimated diffuse reflection radiance

The result shows the relatively large dispersion. The main cause of the dispersion is the lack of the downward irradiance characterization, in this case it is necessary to use the scattering parameters.

4.4 Result (Surface albedo estimation)

From the above consideration, the surface albedo can be estimated from the proposed simplified radiative transfer equation. The surface albedo is estimated from the computed radiance from LOWTRAN 7, optical thickness and the geometry, and is compared with the model values. The RMS error of the surface albedo estimation are tables as follows and the comparison between the model and the estimated surface albedo are shown.

Table 3: RMS error of the surface albedo estimation

	RMS
Ch. 1 Forward	.3580E-01
Ch. 1 Backward	.3774E-01
Ch. 2 Forward	.4162E-01
Ch. 2 Backward	.4151E-01

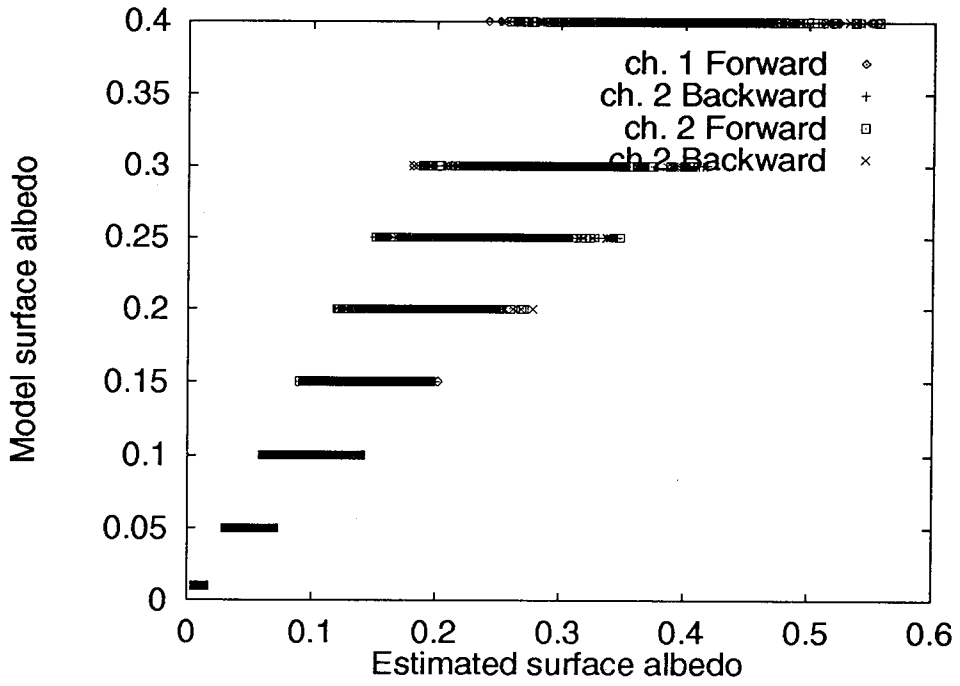

Figure 4: Comparison between the model and the estimated surface albedo

The result shows the large dispersion in large surface albedo case. This main cause is the uncertainty of the diffuse reflection characterization. This will be the limitation of the atmospheric correction which uses only the optical thickness and the geometry.

5 Conclusion

The results lead the following conclusion. The atmospheric correction method based on the simplified radiative transfer equation which uses only the optical thickness and the geometry has the potential to make the brief estimation of the surface albedo and has the convenience to define the parameters from the ground based atmosphere/surface observation. To improve this method, it is necessary to consider the following items.'

- mode detailed characterization of the diffuse reflection radiance,
- consideration of the inter-channel dependence of the radiation parameters,
- robustness of the observation error.

References

[Chandrasekher 60] Chandrasekher, S., Radiative transfer, 393pp., Dover Pub. Co., 1960.

[Fraser 85] Fraser, R. S. and Y. J. Kaufman, The relative importance of aerosol scattering and absorption in remote sensing, Trans. Geosci. and Remote Sensing, Vol. GE23, No. 5, 625–633, 1985.

[Kaufman 88] Kaufman, Y. J. and C. Sendra, Algorithm for automatic corrections to visible and near-IR satellite imagery, Int. J. Remote Sensing, Vol. 9, No. 8, 1357–1381, 1988.

[Kneizeys 88] Kneizeys, F. X., *et. al.* Users' guide to LOWTRAN 7, AFGL-TR-88-0177, 137pp., 1988.

[Justice 85] Justice, C. O. *et. al.*, Analysis of the phenology of global vegetation using meteorological satellite data, int. J. Remote Sensing, Vol. 6, No. 8, 1271–1318, 1985.

[Meador 80] Meador, W. E. and W. R. Weaver, Two-stream approximation to radiative transfer in planetary atmosphere, J. Atom. Sci., Vol. 37, No. 3, 630–643, 1980.

[Richter 90] Richter, R., A fast correction algorithm applied to LANDSAT TM images, Int. J. Remote Sensing, Vol. 11, No. 1, 159–166, 1990.

[Shaw 83] Shaw, G. E., Sun photometry, Bull. Amer. Meteoro. Soc., Vol. 64, No. 1, 4–10, 1983.

[Singh 88] Singh, S. M., Simulation of solar zenith angle effect on global vegetation indev (GVI), int. J. Remote Sensing, Vol. 9, No. 2, 237–248, 1988.

[Tsuchiya 90] Tsuchiya, K., *et. al*, Remote sensing, 327pp, Asakura Pub. Co., 1990.

Scaling between NOAA AVHRR Data and LANDSAT TM Data for Monitoring and Mapping of Wetland

Yoshifumi Yasuoka, Mikio Sugita, Yoshiki Yamagata, Masayuki Tamura, Tomoyuki Suhama

National Institute for Environmental Studies
Onogawa 16-2, Tsukuba, Ibaraki 305, Japan
Phone +81-298-51-2543, Fax +81-298-51-4732
E-mail yyasuoka@nies.go.jp

Abstract

A scaling technique was investigated to extrapolate the local information on landcover type mixtures derived from high spatial resolution data (TM) to more extensive area through low spatial resolution but wide coverage data (AVHRR). Over a combined set of TM and AVHRR, first, landcover types of the area was classified into three categories including vegetation, water and others (non-vegetation) with TM data, and next AVHRR image density was statistically regressed with category mixture conditions derived from TM pixels in each AVHRR pixel. Based on the regression model (scaling model) local information on the category mixture was estimated only from AVHRR data over more extensive area. The method is applied to the wetland type categorization and mapping with AVHRR where landcover is required to be characterized by the complex mixtures of vegetation, water and soil..

1. Introduction

Wetland is one the most valuable ecosystems on the earth. It abounds biological diversity and are treasure houses of living things. Also today the importance of wetland is pointed out as a major emission source of methane which is one of the green house gases. As changes in wetlands are now serious due to various human activities, it is urgent to monitor wetlands and their surrounding environment from physical, biological or social viewpoints. Ground survey of wetland is, however, difficult and time-consuming, and because of its difficulty there have been very few information on wetland in both of the local and the global scale. Remote sensing may provide an effective tool for monitoring a wide range of wetland parameters.

There are two approaches to apply remote sensing to wetland monitoring (Yasuoka et al. 1994). The first approach is local, and in this approach various kinds of thematic maps including a vegetation map or a landcover map are produced with high spatial resolution data over individual wetlands. The other approach is continental/global, and in this approach wetland type maps are produced on a continental or a global scale by classifying wetlands into several categories such as bog, fen or marsh in terms of mixture conditions between vegetation, water and soil. This approach would require to use wide coverage (but low spatial resolution) data.

There have been several studies to produce landcover maps of individual wetlands by using high spatial resolution data from LANDSAT MSS, TM , SPOT HRV or JERS-1 SAR (e.g., Federal Geographic Data Committee 1992; Yamagata et al. 1992). High spatial resolution data is effective to

monitor wetland environment on a local or a regional scale, however, it can not cover an extensive area because their coverage is not so wide. Extending the area would require to use wide coverage data from NOAA AVHRR. Normalized Difference Vegetation Index (NDVI) from AVHRR, for example, has been successfully utilized to monitor vegetation conditions on a global scale (e.g., Tucker et al. 1995; Defries et al. 1995). However, on the other hand, AVHRR data can not detect fine spatial structures in mixtures of vegetation, water and soil in wetland because its resolution is too coarse (1.1km).

In this study a scaling technique between TM and AVHRR is investigated to unmix each AVHRR pixel and to estimate the landcover mixture conditions in vegetation, water and soil from AVHRR data. Scaling model relates high spatial resolution data to low spatial resolution data, and to extrapolate the local knowledge derived from high spatial resolution data to global scale (Hlavka et al. 1995; Iverson et al. 1989). In this paper, first, vegetation index and other parameters are compared between TM and AVHRR, and next the relation between the AVHRR image density and the landcover mixture condition based on TM classification is investigated.

2. Comparison of Vegetation Index between TM and AVHRR

LANDSAT TM data of February 9, 1990 and NOAA AVHRR data of February 1, 1990 over Kohn Kaen area in Thailand were geometrically corrected and overlayed so that one pixel of AVHRR covers a set of TM pixels in a rectangular block of 36 x 36 (Fig. 1). Spatial resolution of one pixel of AVHRR is around 1.1 kilometers and that of TM is around 30 meters. Then the relations between each pixel of AVHRR and corresponding block of 36 x 36 pixels of TM were statistically investigated in several parameters including image densities (CCT counts), vegetation index values, landcover categories.

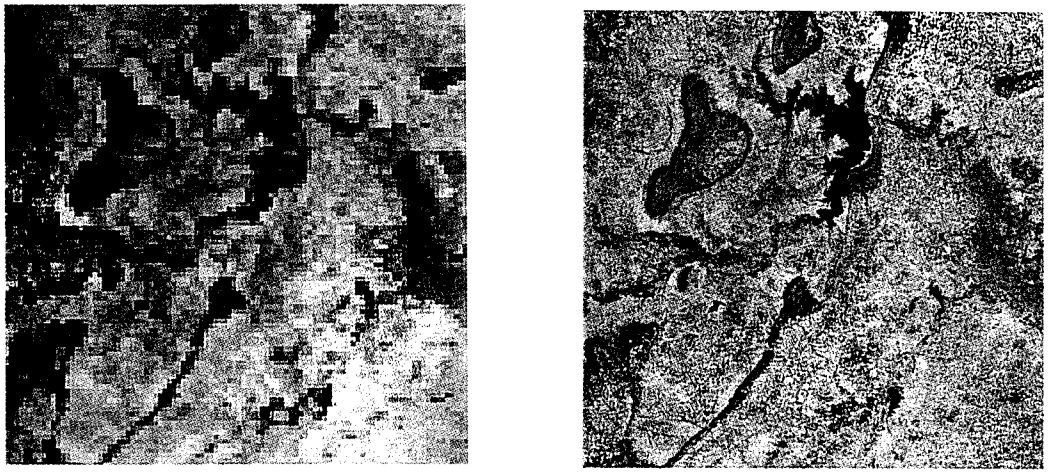

(a) NOAA AVHRR: Feb.1, 1990

(b) Landsat-5/TM: Feb.9, 1990

Fig.1 Image overlay between NOAA AVHRR and LANDSAT TM over Kohn Kaen in Thailand (AVHRR: 1990/2/1, TM: 1990/2/9).

(1) AVHRR NDVI and TM NDVI
Normalized Difference Vegetation Index (NDVI) for AVHRR and TM are defined by

$$NDVI_{AVHRR} = (AV_2 - AV_1) / (AV_2 + AV_1) \quad (1)$$
$$NDVI_{TM} = (TM_4 - TM_3) / (TM_4 + TM_3)$$

where AV_1, AV_2, TM_3 and TM_4 are the CCT counts for NOAA AVHRR band 1 and 2, and LANDSAT TM band 3 and 4 respectively. The relation between NDVI value for each AVHRR pixel and an average NDVI value for a corresponding TM block of 36 x 36 pixels is examined (Fig.2). Regression analysis between $NDVI_{AVHRR}$ and $NDVI_{TM}$ shows high correlation between the vegetation index of LANDSAT TM and NOAA AVHRR (r=0.88);

$$NDVI_{AVHRR} = 0.52\ NDVI_{TM} + 0.14. \quad (2)$$

(2) AVHRR NDVI and TM Tasseled Cap Greenness Index
Greenness Index (GI) was calculated from TM data by

$$GI = -0.27TM_1 - 0.22TM_2 - 0.55\ TM_3 + 0.72\ TM_4 + 0.07\ TM_5 - 0.16\ TM_7 - 0.73. \quad (3)$$

The relation between AVHRR NDVI and TM GI is shown in Fig.3.

$$NDVI_{AVHRR} = 0.28 + 0.0070\ GI \quad (4)$$

It indicated lower correlation than the case for AVHRR NDVI and TM NDVI and this may be the effect of water area in TM data which shows relatively lower GI values than NDVI.

3. Estimation of category mixing ratio from NOAA AVHRR data

Scaling model between LANDSAT TM and NOAA AVHRR was investigated to estimate the mixing ratio of landcover categories in each pixel of AVHRR data. Based on the derived model, the local information around Kohn Kaen derived from TM data was extrapolated to the whole South-East Asia region through AVHRR data.

(1) AVHRR NDVI and TM landcover category (vegetation, non-vegetation, water)
Each pixel of LANDSAT TM was, first, classified into three categories including vegetation, non-vegetation and water area by using unsupervised classification, and in each block of 36 x 36 pixels, ratio in area of each category , V, N, W for vegetation, non-vegetation and water respectively, was calculated (V+N+W=1). Then AVHRR NDVI was correlated with V, N, W using multiple regression analysis. The regression model

$$NDVI_{AVHRR} = 0.24\ V + 0.10\ N - 0.04\ W \quad (5)$$

was obtained in high correlation (Fig.4). Three parameters V, N, W are mixing ratio of vegetation, non-vegetation and water in one AVHRR pixel, therefore, Eq.(5) shows that AVHRR NDVI can be

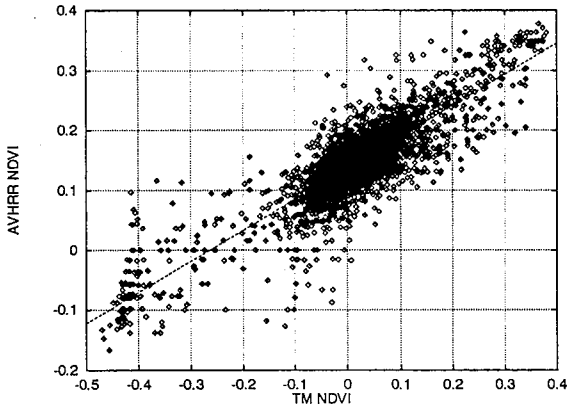

Fig. 2 Relation between AVHRR NDVI and TM NDVI

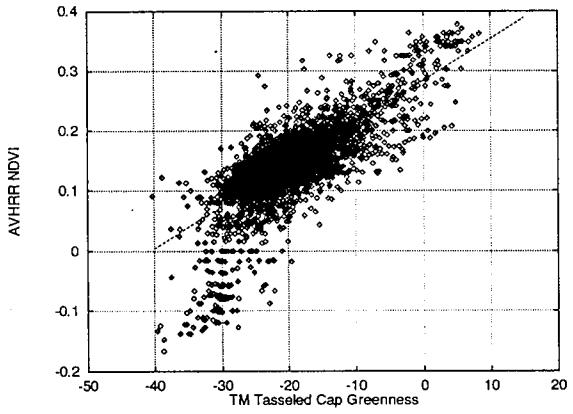

Fig. 3 Relation between AVHRR NDVI and TM Greenness Index

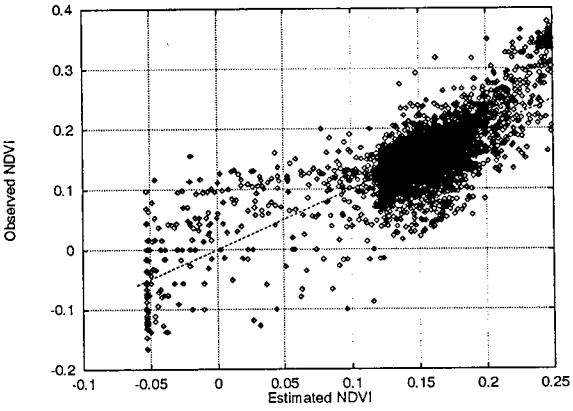

Fig. 4 Relation between AVHRR NDVI and landcover category mixing ratio from TM classification.

estimated from the category mixing ratio based on the landcover classification using TM data.

(2) AVHRR CCT count and TM landcover category (vegetation, non-vegetation, water)

The relation between AVHRR image densities (CCT counts) and the category mixing ratio (V,N,W) was examined, and the multiple regression equations

$$AV_1 = 31.1\ V + 52.6\ N + 33.4\ W \qquad (6)$$
$$AV_2 = 52.6\ V + 67.5\ N + 30.0\ W$$

were derived for AVHRR image density in band 1 (AV_1) and band 2 (AV_2). This relation shows that the category mixing ratio (V, N, W) can be inversely solved from Eq.(6) and the relation V+N+W=1, and that the category mixing ratio can be estimated from NOAA AVHRR image density (AV_1 and AV_2). Figure 5 shows the category mixing ratio image of South-East Asia from NOAA AVHRR image based on Eq.(6) . This scaling model indicates that the local information (category mixing ratio) derived from LANDSAT TM data is extrapolated to more extensive area by using NOAA AVHRR data.

4. Conclusions

This study demonstrated that scaling techniques would provide a tool to extrapolate local information from high spatial resolution data to larger scale by using low spatial resolution data. As most of the global issues including deforestation or desertification originate from local events such as shifting cultivation or extensive logging, monitoring earth surface changes requires that observation of landcover should embrace the terrain from local to global. Linking local with global is one of the key aspects in tackling with global environmental issues and a method proposed in this study is expected to play a role in realizing the bridge between the local and the global in remote sensing.

Acknowledgement

The study is carried out as a part of the research project "Global Monitoring and Mapping of Wetlands by Remote Sensing" supported by the Japan Environment Agency (Global Environment Research Fund).

References

Defries,R.S., et al.," NDVI-derived landcover classification at a global scale. International Journal of Remote Sensing", vol.15, pp.3567-3586(1995).

Federal Geographic Data Committee," Application of satellite data for mapping and monitoring wetlands", Wetland Subcommittee. US.Fish and Wild Service (1992).

Hlavka,C.A., et al., " Unmixing AVHRR imagery to assess clearcuts and forest regrowth in Oregon", IEEE Trans. GRS. vol.33, pp788-795(1995).

Iverson, L.R., et al.," A technique for extrapolating and validating forest cover across large regions", International Journal of Remote Sensing, vol.10, pp.1805-1812 (1989).

Tucker, C.J., et al.," AVHRR data sets for determination of desert spatial extent", International Journal of Remote Sensing, vol.15, pp.3547-3565 (1995).

Yasuoka, Y., et al, " Application of Remote Sensing to Environmental Monitoring - Wetland Monitoring", Optical Methods in Biomedical and Environmental Sciences (H. Ohzu and S. Komatsu eds.), Elsevier, pp269-272 (1994).

Yamagata, Y., et al., " Classification of Wetland Vegetation by Texture Analysis Methods Using ERS-1 and JERS-1 Images", Proceedings of IGARSS'93, pp1614-1616 (1992).

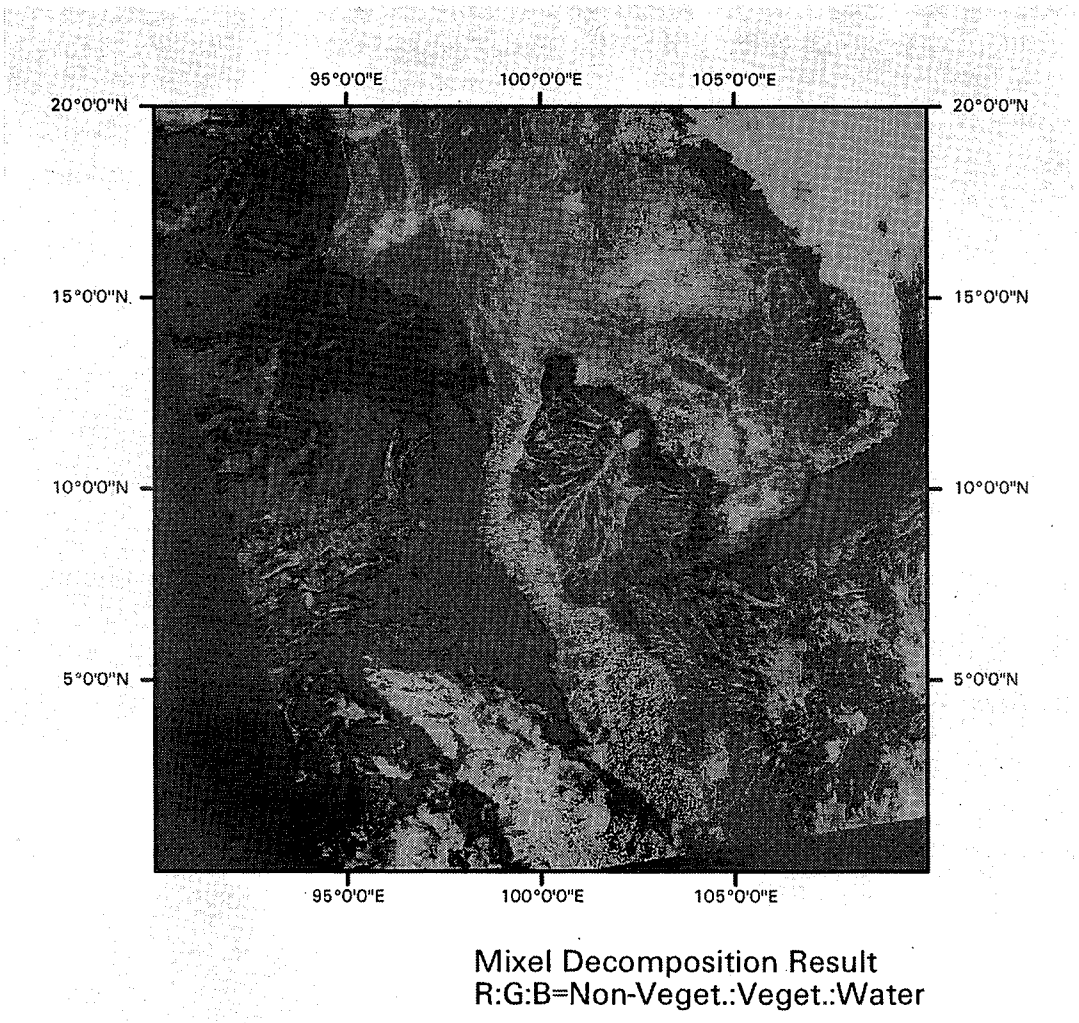

Fig.5 Category mixing ratio map derived from NOAA AVHRR based on the scaling model.

SELECTING A SUITABLE MODEL FOR VEGETATION MONITORING USING SATELLITE DATA

Sumith Pathirana[1] and W.E. Boyd
Centre for Coastal Management
Southern Cross University
PO Box 157 Lismore 2480
NSW. AUSTRALIA
SPATHIRA@SCU.EDU.AU

ABSTRACT

During the last 20 years remotely sensed satellite data have been widely used for vegetation studies. In this period, spatial and spectral resolutions of satellite sensors have been improving, allowing wider applications in resource studies. However, as with many other cover types, increased resolution has produced an added diversity in vegetation interpretation. Objects such as vegetation stands become fuzzy at higher resolutions, indicating that conventional per-pixel-based discrete models may produce difficulties in interpretation. At high resolution levels, objects become a set of interactions between various cover types which are measured according to their relative proportions within the pixel. This problem highlights the issue of identifying a suitable form of remotely-sensed data analysis in studies such as the monitoring of vegetation. Traditionally, the degree of resolution in such work has been determined by the resolution available within the remote sensing methodology. This paper discusses the need to invert this relationship, using the required or identified monitoring resolution to assess the appropriateness of the analysis of remotely-sensed data. The paper discusses a methodological decision-making model for assessing the appropriateness of resolution levels within remotely-sensed data for the application in vegetation monitoring studies. Several outcomes are possible from this decision-making approach, one of which is that a technical response to adjusting resolution levels of remotely-sensed data images may be required. A case study from northeast New South Wales, Australia is used to illustrate such a potential increase in image interpretation resolution, in which the fuzzy membership approach is adopted to examine intra-pixel characteristics proportionately resulting from various cover types in a pixel. This approach allows the user to examine and compare the measured interactions according to their relative proportions, rather than as discrete pixels for environmental monitoring purposes.

INTRODUCTION

For many years visible light aerial photographs have been used by ecologists to study and map plant communities and to monitor the growth and distribution. Later development of infrared film helped identify spectral changes that occur because of the changing condition of vegetation (Hoffer and Johannsen, 1969). Since early 1970s, digital satellite data have been available in multispectral bands allowing to record reflected and emitted energy in visible and infrared wavelengths. These developments helped to study the plant characteristics and conditions that vary due to many factors.

The ability of a satellite system to obtain earth resource information on a regular basis has made a significant impact on monitoring studies. Development of satellite remote sensing technology during the last two decades, specifically improvements in spatial and spectral resolution have contributed to the increasing use of satellite data in vegetation monitoring studies. Spatial resolution, generally defined as the size of the area on the ground from which the measurements that comprise the image are derived (Townshend, 1980), has been considered to be the fundamental characteristic of remotely sensed images. For any type of land cover and land use analysis, the investigator has traditionally selected an appropriate resolution level for a study based on the image resolution level. However, whereas the increasingly higher levels of image resolution have allowed greater detail of the scene structure to be identified than for lower resolutions, added diversity of the scene structure caused by the high resolution has created confusion in identifying, for example, forest cover types for monitoring purposes. A simple

---

[1] Currently Australian Academy of Science Research Fellow, Geographical Survey Institute, Japan.

scene which characterises some elements within one group and its background at one resolution may have elements belonging to more than one group elements at another resolution (Woodcock and Strahler, 1987:312). Further, Woodcock and Strahler (1987) indicate that the choice of an appropriate resolution level for a particular application depends on the kind of information desired and the type of environment used. Selecting an appropriate resolution for vegetation monitoring may become difficult since the analyst should evaluate both the expectations of the ecologist and the remote sensing technical constraints. Ecological conditions of forests often change rapidly. While digital remote sensing offers an excellent opportunity to collect information over large areas in short time periods, massive data volume and the cost have been important issues in vegetation studies (Hoffer and Johannsen, 1969). Here we argue that image analysis resolution has been a hidden issue influencing the application of remote sensing to vegetation monitoring.

This paper discusses two related themes. The first is the issue of resolution levels of remotely-sensed data and the assessment of appropriate level to truly serve the needs of the monitoring programme. This assessment provides three outcomes, that monitoring resolution needs to be revised, that the remote sensing analysis needs to be further developed, and that the remote sensing analysis matched the monitoring needs. This paper then discusses one example of a remote sensing analytical response to better match image and monitoring resolutions.

ASSESSMENT OF APPROPRIATE IMAGE RESOLUTION FOR VEGETATION MONITORING

Most standard texts of both remote sensing and field survey techniques deal with the issue of image resolution in absolute terms -- the pixel size, the waveband width, etc. Harrison and Jupp (1989) and Ritchie *et al.* (1988), for example, discuss image resolution in terms of the following measurable characteristics: (i) spatial, the pixel size or the "physical size of the smallest feature or closest separation of two features distinguished by the imaging system" (Ritchie *et al.*, 1988: 111); (ii) spectral, the number and width of wavebands; (iii) radiometric, the number of levels of brightness detectable; and (iv) temporal, the time between overpasses. Whereas this approach is useful in defining quantifiable characteristics of, and thus limitations to, the remote sensing system, the natural conclusion to such an approach is the system-limiting definition of ground level resolution. This results in, for example, statements of minimum objects size detectable by the sensing system, or the calculation of values such as the "ground resolution distance" discussed by Lillesand and Kiefer (1987: 100) for photographic sensing. More importantly, limits and determination of resolution in land classification and mapping systems become dependent upon the remote sensing resolution rather than reflecting the intrinsic characteristics of the data being classified or mapped (e.g. Lounsbury and Aldrich, 1986: 199; Avery and Berlin, 1992: 216).

From the point of view of environmental monitoring, such a methodological approach appears contrary to logic. The monitoring programme should define the spatial resolution required to meet the, for example, ecological needs of that programme, and then assess the appropriateness of the data collection methodology against its own scientific criteria. For this reason, a model of image resolution outlined by Strahler *et al.* (1986) provides a relevant starting point from which to develop an assessment methodology with which to resolve the resolution requirements of the monitoring programme against the resolution limitations of the remotely-sensed data. The key elements in Strahler *et al.*'s model are the "scene", the "spatial and temporal distribution of matter and energy fluxes from which the sensor draws measurements", that is the earth surface sensed, and the "image", the "collection of measurements from a sensor that are arrayed in a systematic fashion" (1986: 122), that is the remote sensing digital data base or image. The average area within the scene associated with each measurement defines the image resolution. The scene resolution is represented by the size of scene elements and reflects the amount of detail available on the ground. The important aspect of such an expression of remotely-sensed data is that the image resolution is then defined by the relationship between scene and image resolution, that is, it is expressed as a relative rather than an absolute value. Where the scene elements are larger than the resolution cells, the image is described as being an "H-resolution model", and conversely where the scene elements are smaller than the resolution cells, an "L-resolution model" is present.

Strahler *et al.*'s model can readily be extended and adapted to the application of remotely-sensed data in environmental monitoring (Figure 1). In this case, the scene resolution (scene element size) is equated with some measure of monitoring resolution as defined by, for example, the project ecologist, and the image resolution is extended to be defined by not just the pixel size,

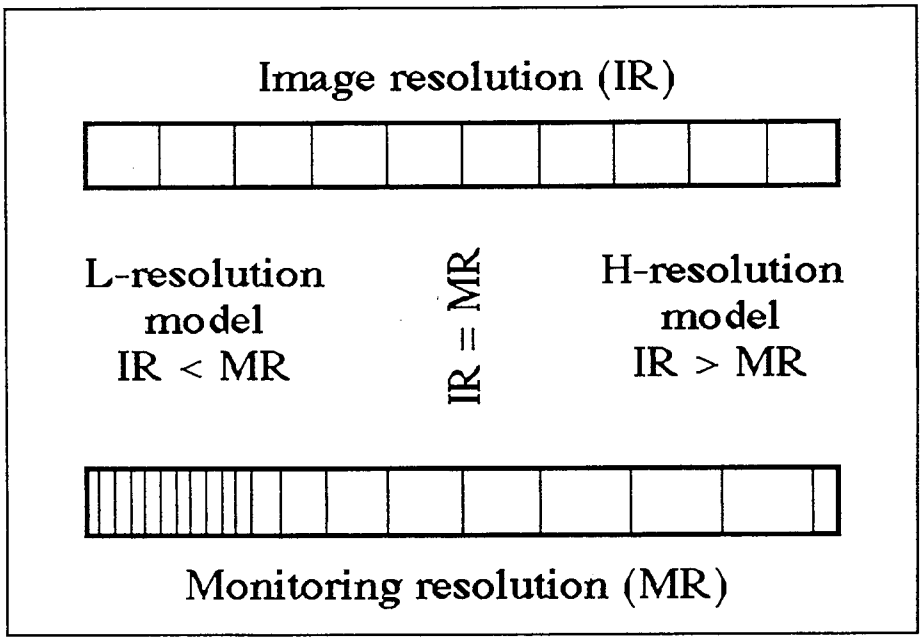

Figure 1: Adaption of Strahler *et al.*'s (1986) model of remotely-sensed image resolution to assess the resolution limitations of remotely-sensed data against the resolution requirements of a monitoring programme.

to include variables such as spectral diversity. The appropriateness of the remotely-sensed data to the specific needs of the monitoring programme can now be assessed in terms of both systems (Figure 2). Defining the available remotely-sensed data or image as either an L- or an H-resolution model in the context of the monitoring programme thus yields three possible outcomes. Two of the outcomes require adaptive responses by either the monitoring ecologist and the remote sensing specialist. For an H-resolution model outcome, the remote sensing system is deemed adequate for the monitoring programme, and will yield data of greater resolution than is required by the monitoring programme; no response other than to continue the analysis is required. However, for an L-resolution model outcome, the sensing resolution is identified as being inadequate to meet the needs of the monitoring programme. Either the acceptable levels of monitoring resolution need to be adjusted (that is action is required by the ecologist in redefining the required level of monitoring resolution) or the remote sensing analysis requires to be further developed to yield greater levels of interpretative resolution. This latter action by the remote sensing specialist is discussed in the second part of this paper.

A TECHNOLOGICAL RESPONSE TO RESOLUTION INCOMPATIBILITY: SPATIAL STRUCTURE OF THE IMAGE SCENE AND THE FUZZY MEMBERSHIP FUNCTION

The approach used in this paper is based on the evaluation of the complexity of the image scene in a multispectral environment. A new method of evaluating the complexity of an image scene is presented. In a conventional image classification system, multispectral data are used to allocate a pixel to a class whether the cover type present in a pixel is highly dominant or less dominant depending on the cover types present (Fisher and Pathirana, 1989, Pathirana, 1990, Gong and Howarth, 1990). Therefore, conventional multispectral classifiers do not show actual spatial elements found within the spatial structure of an image scene. The fuzzy membership approach used in this study allows to evaluate whether any dominant groups exist in an image. Before identifying cover types suitable for monitoring studies, sample data obtained in different resolutions for the study area can be evaluated using fuzzy membership approach to examine the dominant classes and can be used as the criteria in selecting appropriate scale for vegetation monitoring purposes. A fuzzy membership function for each pixel is produced for the pixels in three data sub-sets (Landsat MSS, TM, SPOT MSS) for a study area selected from the northeast New South Wales, closed to Ballina urban centre (Figure 3).

Spatial structure is an indication of the relationship between environment and spatial resolution (Woodcock and Strahler, 1987). Therefore it is important to understand the spatial structure to

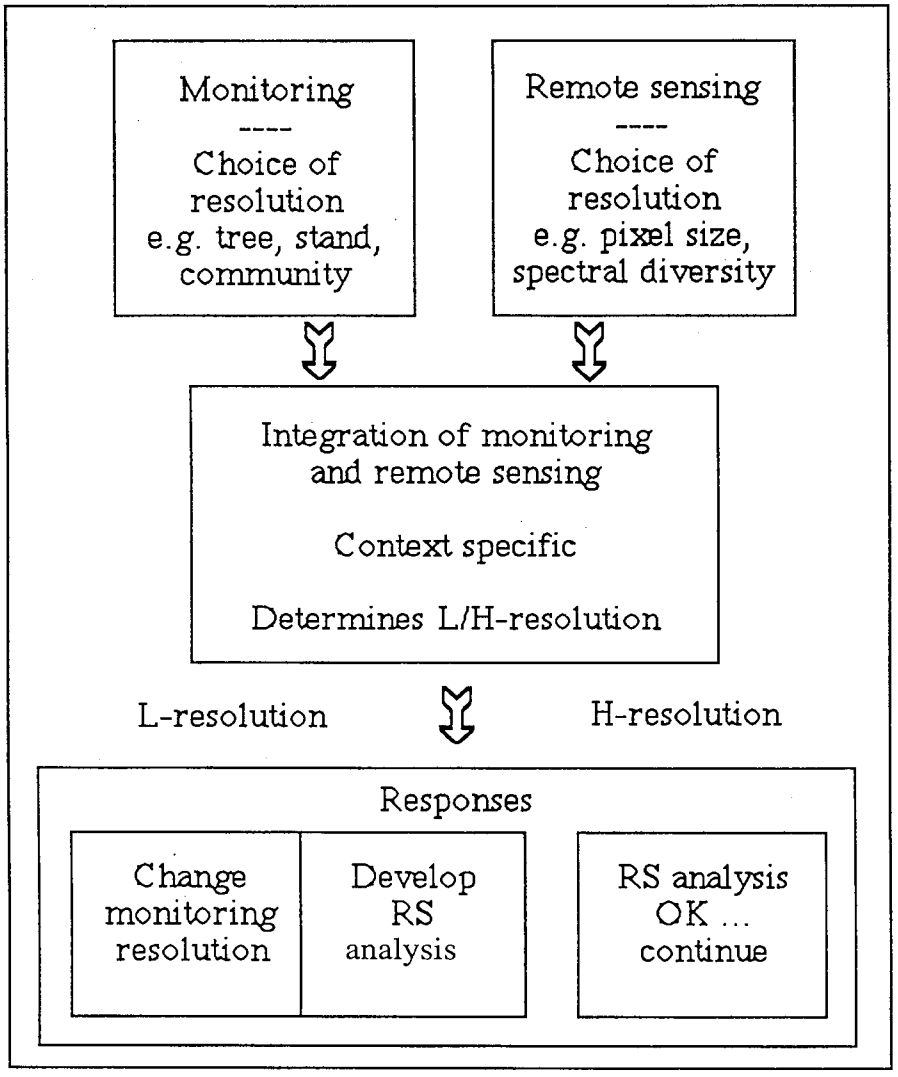

Figure 2: Assessment process of the resolution levels of remotely sensed data against the required resolution levels of a monitoring programme.

examine the manner in which images change as a result of resolution. Spatial structure of an image is simple if the local variance is low in a multispectral environment. In this situation, local variance is low and the pixels belong to more or less one group or two including the background. If the local variance is high, spatial structure of an image consists with more than one group. A group is a collection of pixels where pixels have closer association with other pixels. There have been a number of approaches used in studying spatial structure of an image. Labovitz *et al.* (1982) found autocorrelation to be higher in images with high resolution, whereas Simonett and Coiner (1971), using different grid cell sizes to examine the effect of spatial resolution on image structure, found that the number of pixels containing more than one cover type was a function of both the complexity of the scene and the spatial resolution. Woodcock and Strahler (1987) used the local variance measured as the mean value of the standard deviation of a moving 3 x 3 window.

As an alternative, fuzzy membership approach is adopted in this paper to examine the effect of spatial resolution on the spatial structure. The fuzzy membership approach has been previously applied to study the measurements of pixel composition (Robinson and Thongs, 1985), mixed pixels of land cover land use classes (Fisher and Pathirana, 1990; Pathirana, 1990), Soil survey and land evaluation studies (Burrough, 1989), segmentation of Landsat images to identify homogeneity of cover types (Trivedi and Bezdek, 1986) and for the detection of linear and sub-pixel phenomena (Pathirana, 1992). In this study, the fuzzy membership function for each pixel was developed using Fuzzy c-Means classifier (FCM) of Bezdek *et al.* (1984). For each class identified by the user, the FCM produces a membership value (u) such that:

$$u_{ijk)} > 0 \qquad \text{and} \qquad \sum_{z=1}^{k} u_{ijz} = 1.$$

A membership function of a pixel that has memberships to all identified clusters at varying degree of likelihoods. A membership value approaching 1 indicates that the pixel is very likely to belong to that cluster, while 0 indicates that the pixel is unlikely belong to that cover type or a mixed pixel. If a particular cluster shows the dominance of high membership values (e.g. $u_{ijk)}$ >.5), it indicates a presence of a distinct cluster within the scene.

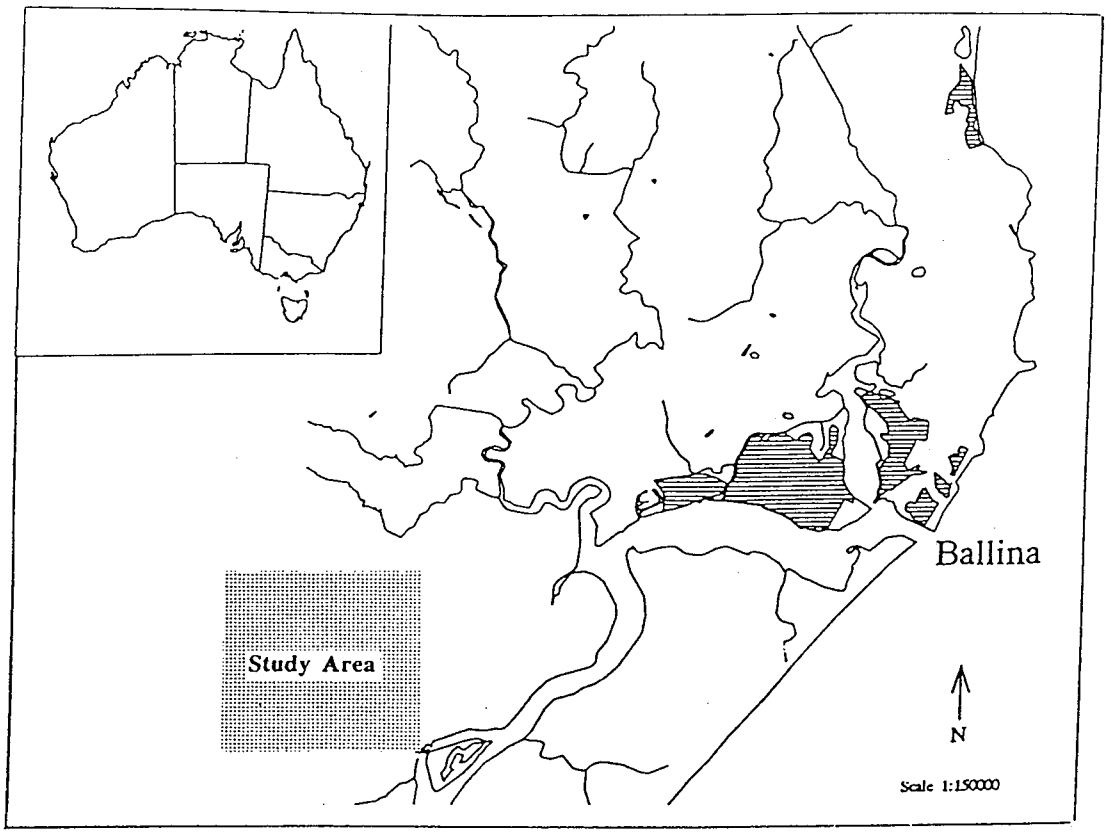

Figure 3: Study area location.

METHODS

Three subsets from Landsat MSS, Thematic Mapper, and SPOT MSS images were extracted for the study area located in the northeast New South Wales near Ballina. The dominant cover types in the study area are forest, agricultural land and grassland (Figure 4). For this study, forest areas were spectrally separated from the other cover types. The FCM was run for 3 clusters to find out whether any dominant clusters exist within the forest area using all three image sets.

RESULTS

Figure 5 shows the coefficient of variation (CV) of the image data sets obtained for three resolutions. The coefficient of variation was calculated for each band. Among the three image sets, the highest CV were found in TM band 7 data (0.28), indicating high variance of the spatial structure of images (Table 1).

Overall, all MSS bands show high variance while in TM and SPOT image scenes, the variance is high for infrared bands. A low CV indicates that the spatial structure is simple and the pixels are more or less related to the dominant group. However, a major limitation of CV method or local variance method (Woodcock and Strahler, 1987) is that the variance value is not a representation of the combined effect of multispectral bands.

Table 2 and Figures 6, 7 and 8 show the distribution of fuzzy membership values for all three

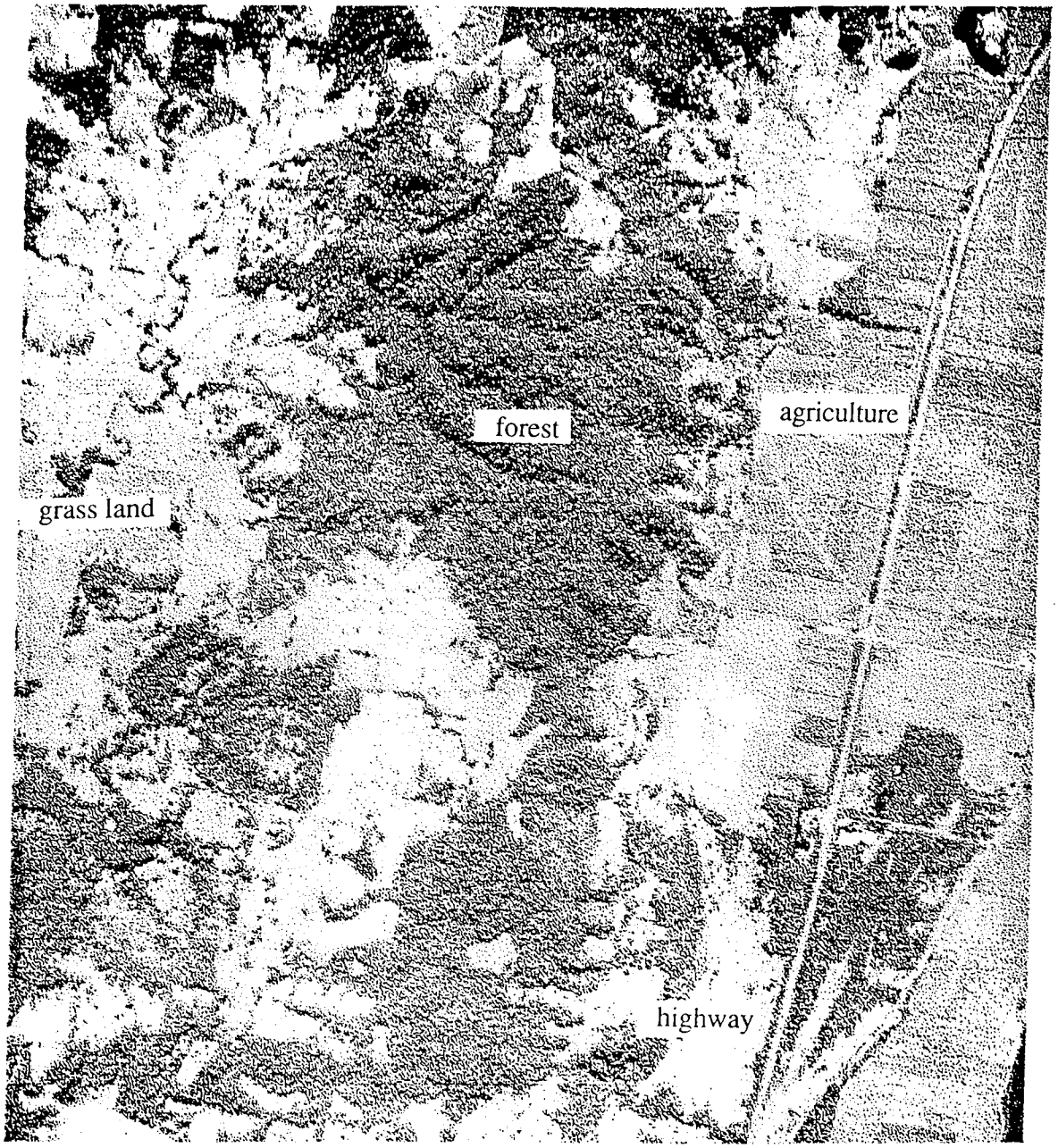

Figure 4: General land cover and land use types in the study area.

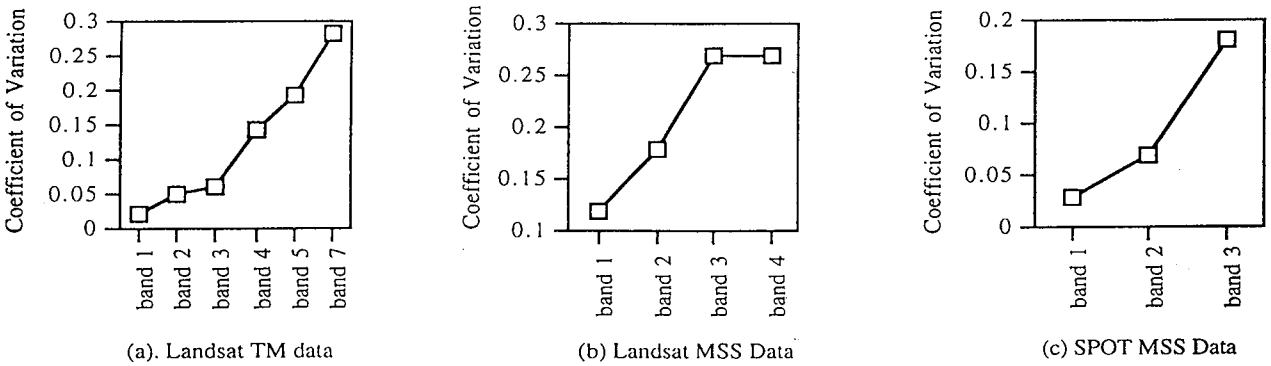

Figure 5: Local coefficient of variation of the image scene.

Thematic Mapper		Landsat MSS		SPOT MSS	
Bands (mm)	*C.V.*	Bands (mm)	*C.V.*	Bands (mm)	*C.V.*
0.45-0.52	*0.02*	0.50-0.60	*0.12*	0.50-0.59	*0.03*
0.52-0.60	*0.05*	0.60-0.70	*0.18*	0.61-0.68	*0.07*
0.63-0.69	*0.06*	0.70-0.80	*0.27*	0.79-0.89	*0.18*
0.76-0.90	*0.14*	0.80-1.10	*0.27*		
1.55-1.75	*0.19*				
2.08-2.35	*0.28*				

Table 1. Distribution of coefficient of variation (CV) values in three image data sets

image data sets. According to Figure 6, there is only one dominant cluster present in Landsat MSS image (Figure 6c). About 56% of all pixels in the vegetation area has a greater than 0.5 membership value indicating a dominant cluster while the other two clusters have only 0.0% (Figure 6a) and 42.7% (Figure 6b) pixels, respectively, with more than 0.5 membership value. Similarly, Thematic Mapper image scene has 2 clusters, one with the highest percentage of pixels, 58.6% (Figure 7b), and the other with 41% (Figure 7a), greater than 0.5 membership value. On the other hand, SPOT image shows a presence of two dominant clusters having with 50% (Figure 8b) and 49.8% (Figure 8c) pixels with more than 0.5 membership values. As mentioned above, bi-normal distribution of clusters with a large number of pixels approaching 1 indicate dominant clusters in an image scene. This will reflect the nature of spatial structure under investigation and may also provide an alternative method in selecting appropriate resolution levels for vegetation monitoring purposes.

fuzzy values	landsat clus 1	landsat clus 2	landsat clus 3	TM clus 1	TM clus 2	TM clus 3	SPOT clus 1	SPOT clus 2	SPOT clus 3
0	94.4	30.6	20	21.5	9.3	100	99.1	26.8	27.8
1	2.9	14.2	9.4	18.8	15.9	0	0.4	10.4	9.9
2	1.5	4.5	5.9	8.3	7.5	0	0.3	6.5	6
3	0.9	4.2	4.1	5.6	4.3	0	0.1	3.1	3.4
4	0.2	3.7	4.6	4.8	4.5	0	0.1	3.2	3.2
5	0	4.2	4.6	4.3	4.8	0	0	3.5	3.1
6	0	4.1	6.1	4.4	5.7	0	0	4	3.4
7	0	6.5	7.5	8.1	9.5	0	0	6.3	6.7
8	0	9.1	12.5	15.3	18.3	0	0	9.7	10.6
9	0	18.8	25.3	9	20.3	0	0	26.5	26

Table 2. Distribution of fuzzy membership values

The general characteristic of the data sets is that there are two clusters exist in all three scenes. The SPOT scene clearly demonstrates a presence of two clusters while the TM scene shows the lowest number of pixels (41%) and the highest number of pixels (58%) above 0.5 membership value indicating only one dominant cluster. It appears, therefore, that the TM image is best suitable for monitoring the vegetation change in this study area as the diversity of the image scene is low in this resolution.

CONCLUSION

In this paper, the issue of the use of resolution levels of remotely-sensed data in determining the acceptable resolution of monitoring studies is inverted by providing a methodology for assessing the appropriateness of remotely-sensed data resolution. Three possible outcomes are available: (i) image resolution is adequate for monitoring; (ii) monitoring resolution requires to be reassessed; and (iii) the interpretative resolution requires to be improved. The latter requires a remote sensing technological response to improve the resolution level. An example of such an approach is illustrated, in which the fuzzy membership approach is used to examine whether any distinct clusters exist in a vegetation scene using multi-resolution, multi-spectral data sets. Membership values produced by the Fuzzy c-Means Classifier identifies several dominant clusters in all three image sets used in this case study. Among the clusters produced for this image sets, Thematic Mapper image scenes shows the highest number of pixels in the dominant

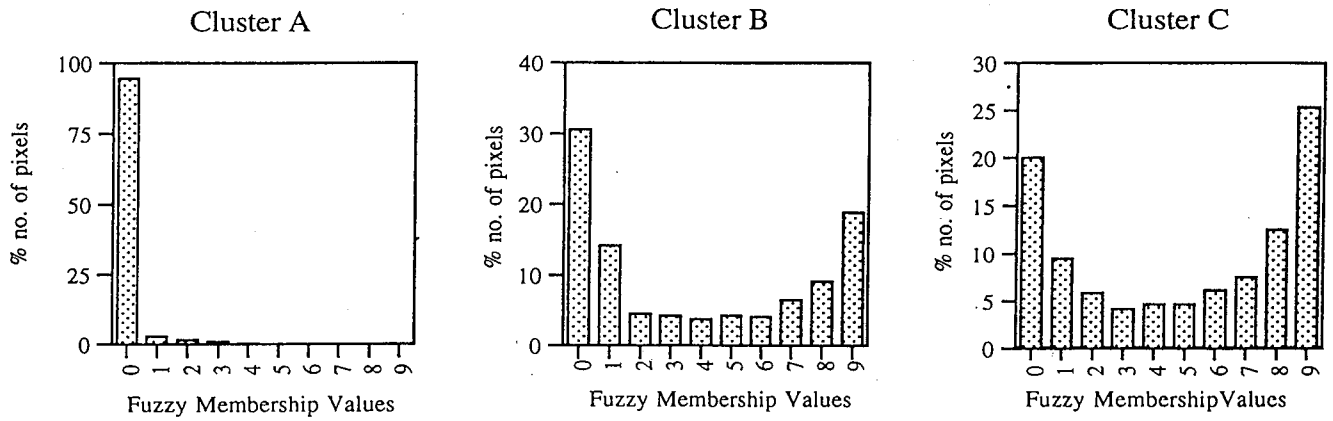

Figure 6: Clustering of Landsat MSS Data

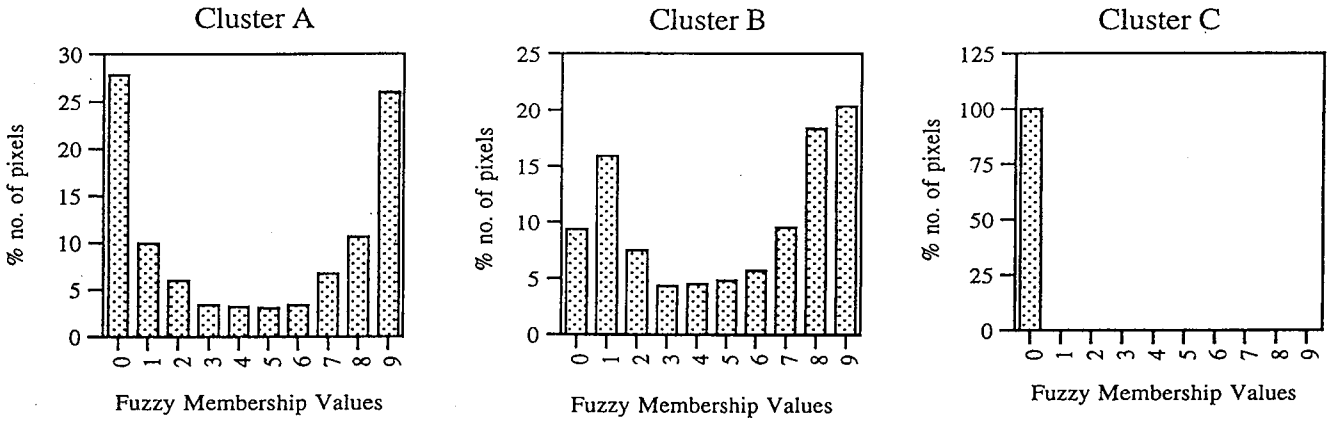

Figure 7: Clustering of Landsat TM Data

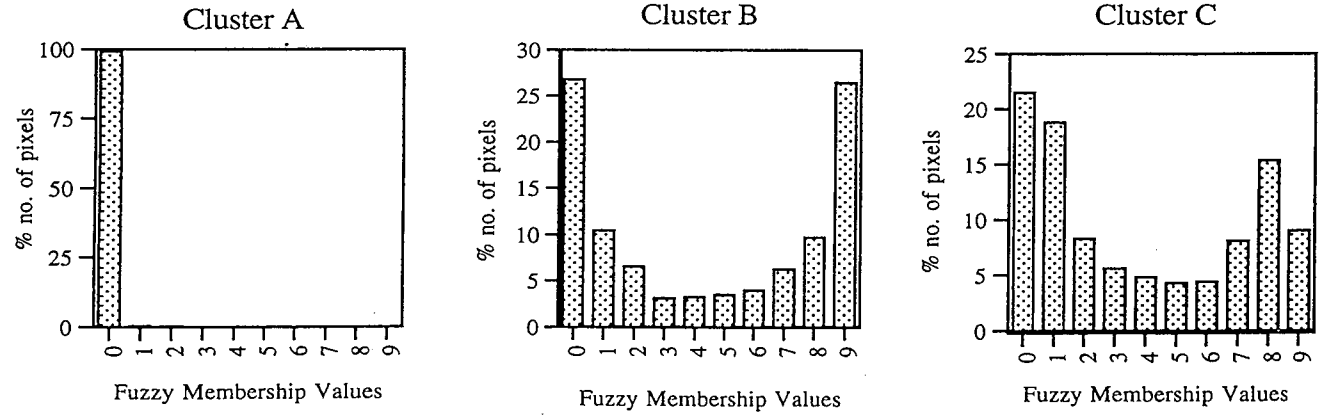

Figure 8: Clustering of SPOT MSS Data

catagory indicating the presence of low variance in the data set, and illustrates how optimal interpretative resolution may be achieved.

REFERENCES

Avery, T.E., and G.L. Berlin, Fundamentals of Remote Sensing and Airphoto Interpretation (5th edition), Macmillan, New York, 1992.

Bezdek, J.C., R. Ehrlich, and W. Full, "FCM: The fuzzy c-means clustering algorithm", Computers and Geoscience, Vol.10, pp. 191-203, 1984.

Burrough, P.A., "Fuzzy mathematical methods for soil survey and land evaluation", Journal of Soil Science, Vol.40, pp. 477-492, 1986.

Fisher, P.F. and S. Pathirana, "The evaluation of fuzzy membership of land cover classes in the suburban zone", Remote Sensing of Environment, Vol.34, pp.121-132, 1990.

Gong, P., and P. J. Howarth, "The use of structural information for improving land-cover classification accuracies at the rural-urban fringe", Photogrammetric Engineering and Remote Sensing, Vol.56, pp.67-73, 1990.

Harrison, B.A., and D.L.B. Jupp, Introduction to Remotely Sensed Data, CSIRO, Canberra, 1989.

Hoffer, R. M., and C. J. Johannsen, "Ecological potentials in spectral signature analysis", Remote Sensing in Ecology, pp. 1-16, 1969.

Labovitz, M. L., D.L. Toll and R.E. Kennard, "Preliminary evidence for the influence of physiography and scale upon the autocorrelation function of remotely sensed data", International Journal of Remote Sensing, Vol. 3, pp. 13-30, 1982.

Lillesand, T.M., and R.W. Kiefer, Remote Sensing and Image Interpretation (2nd edition), Wiley, New York, 1986.

Lounsbury, J.F., and F.T. Aldrich, Introduction to Geographic Field Methods and Techniques, Merrill, Columbus, 1986.

Pathirana, S., "Fuzzy membership approach to the mixed pixel problem of remotely sensed data: An application in the suburban fringe zone of Northeast Ohio", Ph.D. Dissertation submitted to the Kent State University, unpublished, 1990.

Pathirana, S., "Detection of linear and sub-pixel phenomena using the fuzzy membership approach", Proceedings, 6th Australasian Remote Sensing Conference, Wellington, New Zealand, Vol.2, pp.424-433, 1992.

Ritchie, W., M. Wood, R. Wright, and D. Tait, Surveying and Mapping for Field Scientists, Longman, Harlow, 1988.

Robinson, V. B., and D. Thongs, "Fuzzy set theory applied to the mixed pixel problem of multispectral land cover databases", in Geographic Information Systems in Government, (B. Opitz, Ed)., pp.871-886, 1986.

Simonett, D. S., and J. C. Coiner, "Susceptibility of environments to low resolution imaging for land-use mapping", Proceedings of the 7th International Symposium on Remote Sensing of Environment, Michigan, Ann Arbor, pp. 373-394, 1971.

Strahler, A.H., C.E. Woodcock, and J.A. Smith, "On the nature of models in remote sensing", Remote Sensing of Environment, Vol. 20, pp. 121-139, 1986.

Townshend, J. R.G, "The spatial resolving power of earth resources satellites", A Review, NASA Goddard Space Flight Centre, Greenbelt, MD, 1980.

Trivedi, M. M., and J. C. Bezdek, "Low level segmentation of aerial images with fuzzy clustering", IEEE Transactions on Systems, Man, and Cybernetics, Vol. SMC-16, No.4, July-Aug., 1986.

Woodcock, C., and A. Strahler, "The factor of scale in remote sensing", Remote Sensing of Environment, Vol.21, pp. 311-332, 1987.

A Study on Construction of Enhanced Vegetation Cover Map considering Vegetation Cover Ratio in a Pixel by Remote Sensing Data

Donkyu YUN and Akira HOYANO

Dept. of Environmental Physics and Engineering, Tokyo Institute of Technology
4259 Nagatsuta-cho, Midori-ku, Yokohama, 226, JAPAN
TEL : +81-45-924-5510 FAX : +81-45-924-5519
Email: dyun@ncio.nc.titech.ac.jp

ABSTRACT

In order to evaluate the urban environment, the vegetation information is very important. This information should be constructed as the expression of real vegetation, not as that of scale or usage, and also updated to accommodate the change of vegetation. The vegetation cover ratio in a pixel using the remote sensing data simulated by airborne MSS data with high resolution was examined. In this examination a correct vegetation coverage is needed to establish assumption algorithm of vegetation cover ratio in a pixel. This map was constructed by airborne MSS data of high resolution and airborne photograph, which is verified by field investigation. The remote sensing data of low resolution was simulated by high resolution airborne data. The vegetation cover ratio in a pixel is defined as the ratio of correct vegetation in one pixel of simulated data. On the view point of mixel, the relationship between the vegetation cover ratio in a pixel and the mean NVI (normalized vegetation index) was investigated. This investigation was seen that the relationship between the vegetation cover ratio in a pixel and the mean NVI was linear. On the basis of this relationship, the vegetation cover ratio in a pixel can be assumed by NVI of remote sensing data.

1. INTRODUCTION

The vegetation coverage information is essential to evaluate the urban environment. The traditional stocks of vegetation coverage information is subjected to the scale of vegetation or the use of that. There is few result expressed the real vegetation distribution. So, it is necessary to establish the construction method of real vegetation cover map and to update method of the vegetation change. On the basis of the above request, the construction of vegetation cover map using remote sensing data is expected because the satellite remote sensing data is usually obtained large area and periodically.

When urban vegetation is subjected it is difficult to extract the urban vegetation, because the scale of some vegetation is smaller than the resolution of remote sensing data. The vegetation cover ratio in a pixel is introduced as an index for extraction and expression the urban vegetation. Vegetation cover ratio in a pixel is defined as a ratio of vegetation quantity of one pixel. Then the relationship between the vegetation cover ratio in a pixel and its mean NVI (normalized vegetation index) is examined.

The purpose of this study is to show the relationship between the vegetation cover ratio in a pixel and its mean NVI and to suggest the estimation method of vegetation cover ratio in a pixel using NVI.

2. ANALYSIS METHOD

NVI expressed the activity of vegetation is introduced for an estimation of vegetation cover ratio in a pixel. First, correct vegetation coverage defined as training data is constructed by using high resolution airborne MSS data, air photograph and field investigation. Since the satellite remote sensing data is useful to vegetation cover map, the remote sensing data with low resolution was simulated by using the airborne MSS data with high resolution. Vegetation cover ratio in a pixel is defined the quantity of vegetation in simulated data. Thus it is investigated the relationship between NVI of simulated data and vegetation cover ratio in a pixel.

2.1 STUDY SITE AND DATA USED

Some areas in Kawasaki were selected as the study site. The characteristics of this site are

(1) The scale of a group of vegetation is various.
(2) There are complex distribution types such as point, line, area and so on.
(3) The vegetation categories are various such as tree, grass, lawn or mixture of those.

It is selected for data observed in summer to extract the vegetation because the activity of vegetation in summer is higher than that of any other season. (Table 1). The center 512 columns were selected in all 802 columns observed. This means that the selected pixels have almost homogeneous resolution and have no low quality pixels due to the side looking effect.

2.2 TRAINING DATA BUILT-UP

To build up training data, pure vegetation pixels have been extracted using airborne MSS data as shown in Fig.1, This means that the training data exclude the boundary pixels between vegetation and non-vegetation. The extracted vegetation is classified into three subcategories such as tree, grass, lawn. However there are many mixels of vegetation and non-vegetation in the boundary of those in the training data constructed. These mixels are discussed in the following part of this paper.

2.3 SIMULATED REMOTE SENSING DATA

It is necessary for OTF (optical transfer function) of the remote sensor to construct the remote sensing data with different resolution . Current technique is, however, not established the OTF extraction from remote sensing data. So the OTF effect is ignored in this paper.

The simulated data with n times resolution of original data were constructed by the mean of n×n pixels on original data. The image of vegetation cover ratio in a pixel (Plate 4) is calculated by above definition.

2.4 STUDY OF USED NVI

3 NVIs given below are investigated to select the best NVI for assumption of the vegetation cover ratio in a pixel.

Table 1 Summery of Airborne MSS Data

Observation Date	1987.8.9
Study Site	Kawasaki,Japan
Channel No	Wave Length (μm)
ch03	0.45 - 0.49
ch05	0.49 -0.53
ch07	0.60 - 0.65
ch13	0.92 - 1.00
ch16	2.06 - 2.45
ch17	8.00 - 12.0

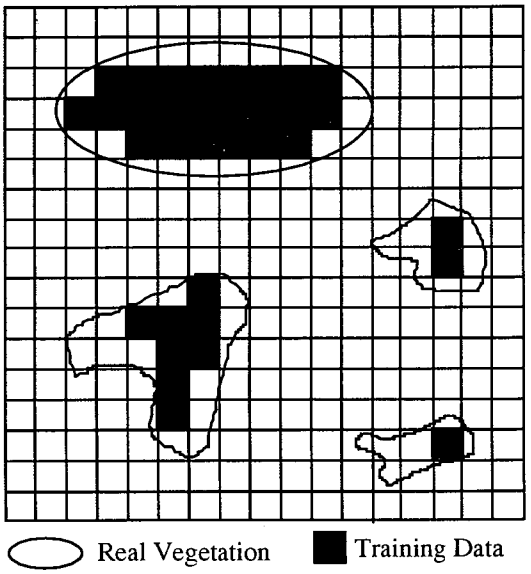

Fig.1 Construction Method of Training Data

ch13/ch07 (1)

(ch13 - ch07) / (ch13 + ch07) (2)

ch13 / ∑chi (i=03,05,07,13,16) (3)

To give a coherence each NVI "mean ± standard deviation" of either NVI is transformed from 0 to 255, the relative value. Fig.2 is an example distribution of NVI(3) with land cover and statistical values of all NVIs were shown in Table 2.

Because it is desirable for the variation of non-vegetation to be small and for the difference of vegetation and non-vegetation to be large, NVI(3) was selected. What is evident from Fig.2 is that lawn among the vegetation and water among the non-vegetation are different distribution from the other vegetation or non-vegetation. So Lawn and water are dealt with particular categories and excluded from following discussion.

3. NVI AND VEGETATION COVER RATIO IN A PIXEL DERIVED FROM TRAINING DATA

Figure 3 shows an example of the relation between vegetation cover ratio in a pixel and its mean NVI in simulated data. The relation between the mean NVI of mixels and the vegetation cover ratio in a pixel of those is almost linear. But the relation in perfect vegetation, perfect non-vegetation or their vicinity is nonlinear.

In order to measure the nonlinear with various resolution, accumulated Beta distribution is introduced as Eq.(4). The relationship between the vegetation cover ratio in a pixel and its mean NVI is regressed using Eq.(4) and the regression curves are shown solid line in Fig.3. Coefficients q and r of Eq.(4) with resolution variation are shown in Fig.4. The coefficient q and r at low resolution gradually approaches to 1. This means that very low resolution data may be linear. Coefficients, q and r, however, are not equal to 1 in this examination. The cause of nonlinear may be mixel effect, leave density effect, and so on.

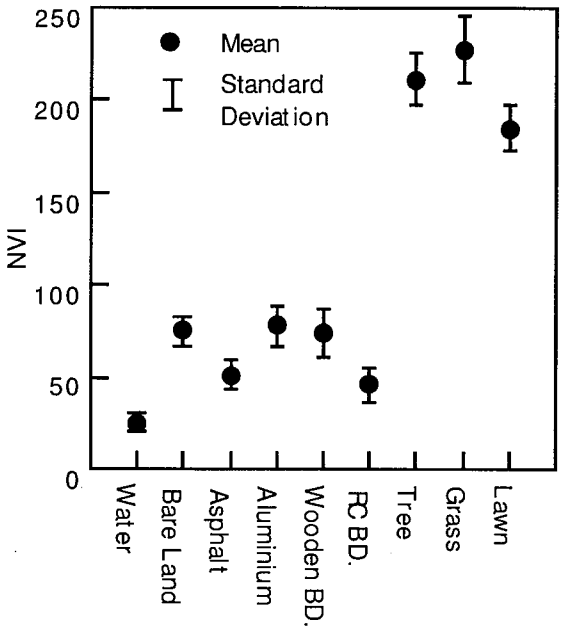

Fig.2 Distribution of NVI(3) in Land Covers

Table 2 Statistic Values of Vegetation and Non-Vegetation

NVI	(1)	(2)	(3)
Standard Deviation of Vegetation	19	10	14
Standard Deviation of Non-Vegetation	10	16	6
Defference between Vegetation and Non-Vegetation	110	139	143

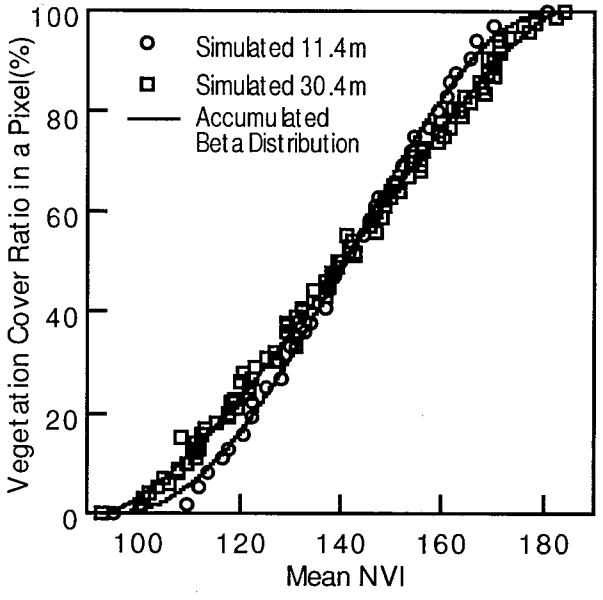

Fig.3 Vegetation Cover Ratio in a Pixel and its Mean NVI in Simulated data

$$Y = B(q, r)^{-1} \int_0^X X^{q-1} (1-X)^{r-1} dX \quad (4)$$

Y : vegetation cover ratio in a pixel

$X = (x-x_0) / (x_{100}-x_0)$

x : mean NVI

x_0 : mean NVI for vegetation cover ratio in a pixel equal to 0%

x_{100} : mean NVI for vegetation cover ratio in a pixel equal to 100%

$$B(q , r) = \int_0^1 X^{q-1} (1-X)^{r-1} dX$$

4. NVI AND VEGETATION COVER RATIO IN A PIXEL CONSIDERING MIXELS

A section A-A on the part of the study site (Plate 5~8) is chosen in order to examine the nonlinear in perfect vegetation and perfect non-vegetation or their vicinity. NVI and training data are discussed on the view point of location. NVI on the center of vegetation is grater than NVI on the side of it. Boundary pixels which is located in the interval of vegetation and non-vegetation have in-between value of NVI in vegetation and in non-vegetation. It is showed that boundary pixels should be mixels.

The normalized histogram of the boundary pixels are shown in Fig.6. It shows that Non1, Non2, Veg1 and Veg2 have very high possibility of becoming mixel. But Non3 and Veg3 are almost same distribution of either of vegetation or non-vegetation. It is assumed that the vegetation cover ratio in a pixel is linearly proportional to NVI from discussion of Fig.4. The vegetation cover ratio in a pixel of mixel on the training data can also be assumed linear as shown in Fig.7. Using the assumption of Fig.7, the relationship between the vegetation cover ratio in a pixel and its mean NVI in simulated data is reconstructed considering the following 3 cases (Fig.8).

(1) Consider inside and outside pixels as mixels
(2) Consider only outside pixels as mixels

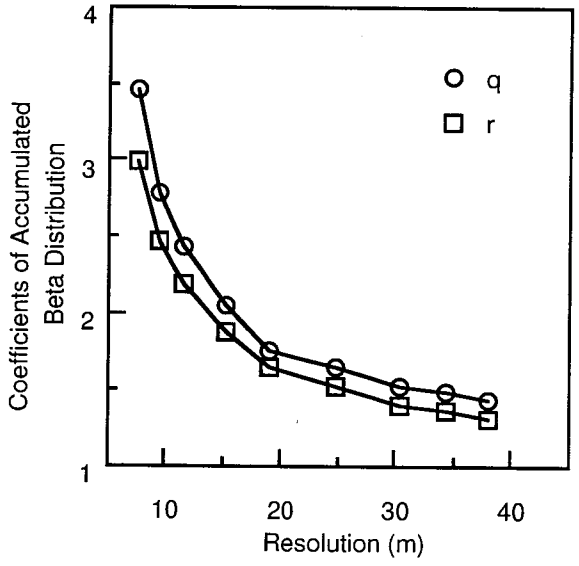

Fig.4 Coefficients of Accumulated Beta Distribution in simulated Image

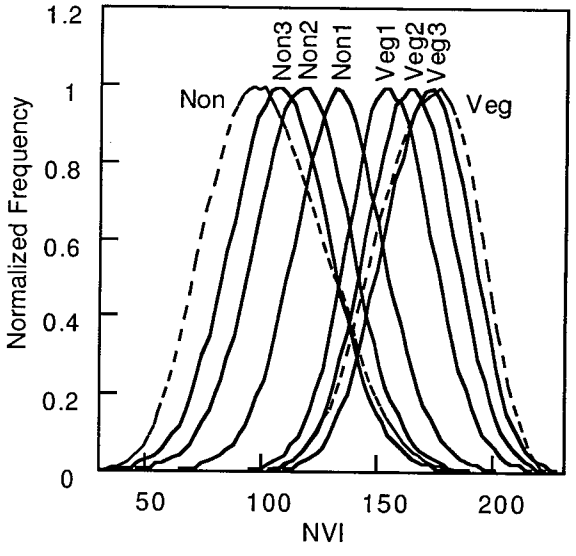

Fig.6 Histogram of Boundary Pixels in Training Data

This is normalized by maximun frequency. Non:Non-vegetation, Non1: 1st Pixels in non-vegetation from boundary, Non2: 2nd Pixels non-vegetation from boundary, Non3: 3rd Pixels in non-vegetation from boundary, Veg:Vegetation, Veg1: 1st Pixels in vegetation from boundary , Veg2: 2nd Pixels in vegetation from boundary, Veg3: 3rd Pixels in vegetation from boundary

(3) Consider only inside pixels as mixels (outside : side of vegetation from boundary, inside : side of non-vegetation from boundary, boundary : boundary of vegetation and non-vegetation)

In the case(1), the relation between the vegetation cover ratio in a pixel and mean NVI is almost linear in spite of different resolution. In the case(2), the relation of those is nonlinear in the vicinity of 100%. In the case(3), the relation of those is nonlinear in the vicinity of 0%.

This showed that the vegetation cover ratio in a pixel is linearly proportional to the mean NVI, and the cause of nonlinear of the vicinity of 0% is outside mixels and also the cause of nonlinear of the vicinity of 100% is inside mixels. The case(1), however, is not perfectly linear. The causes of nonlinear in case(1) are discussed as follow.

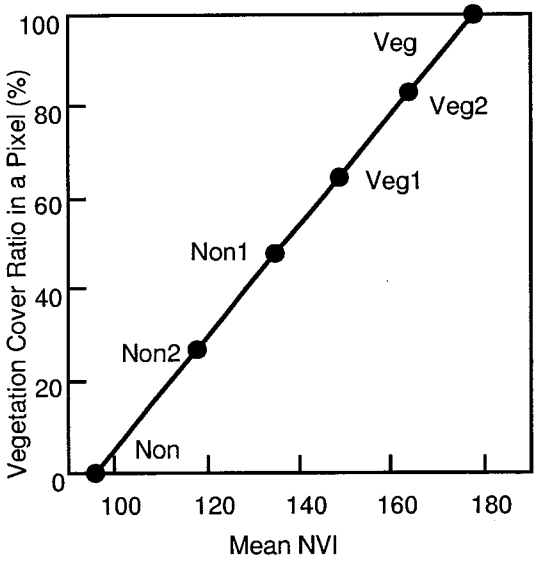

Fig.7 Assumtion of Vegetation Cover Ratio in a Pixel on Mixels of Training Data

Cause of nonlinear in the vicinity of 0%

Some of mixels exist in the boundary of vegetation and non-vegetation and others exist in independent place as the very small scale, which can't be caught as the pure pixel by the remote sensing data. Those are also mixels. In above discussion, those mixels did not consider in the training data. So the cause of nonlinear in the vicinity of 0% is mixels which is not considered, and is independently located.

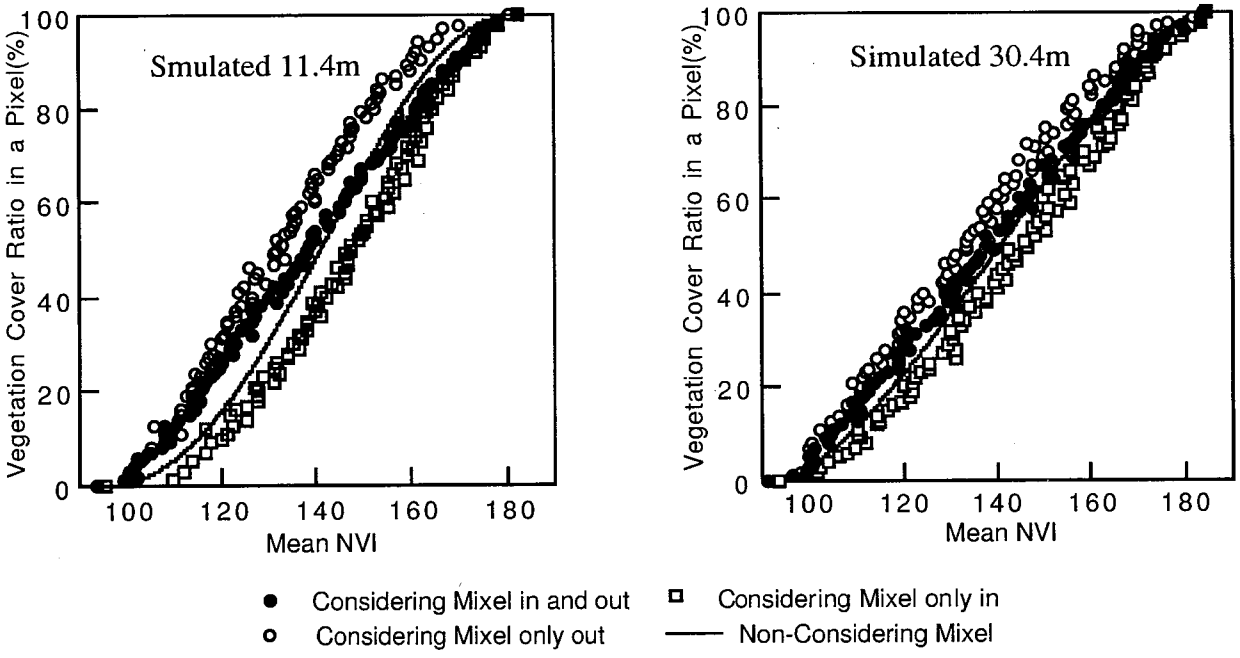

Fig.8 Relationship between Vegetation Cover Ratio in a Pixel and Mean of NVI in Simulated Data
in : side of vegetation fron boundary, out : side of non-vegetation from boundary, boundary : boundary of vegetation and non-vegetation

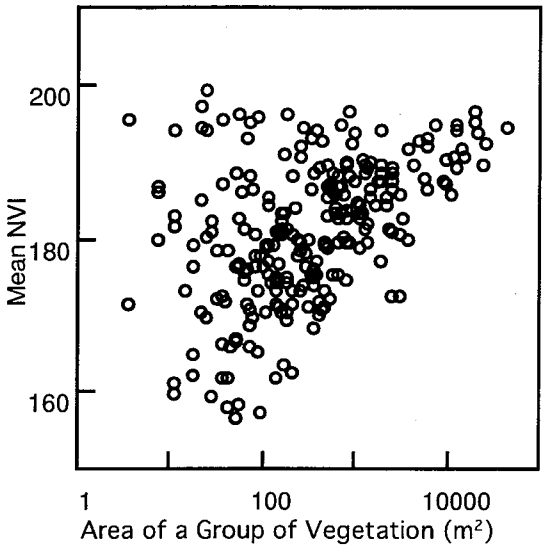

Fig.10 Vegetation Area and mean NVI

Cause of nonlinear in the vicinity of 100%

In order to verify the cause in the vicinity of 100%, first, location type of the vicinity of 100% pixels is discussed as shown in Fig.9. 100% pixels is located in the middle of large scale vegetation. 95~99% pixels is located in the boundary of large scale vegetation, but 95% or less independently is located as the small scale. Secondly, the relation between an area of a group of vegetation and its mean NVI is shown in Fig.10. It can be seen that the distribution of small area is scattered. This observation shows that the area of vegetation is influenced in NVI. So, the cause of nonlinear at the vicinity of 100% can be the NVI variation on the vegetation quality.

Consequently, the relationship between vegetation cover ratio in a pixel and mean NVI is linear. This line is located to 100%, 0% and connection of those. Using this relationship, the vegetation cover ratio in a pixel can be assumed by NVI of remote sensing data. And the small scale vegetation can be expressed by the vegetation cover ratio in a pixel.

5. CONCLUSION

The vegetation cover ratio in a pixel is used in order to express the small vegetation in urban area which is not caught as the pure pixel in remote sensing data. Then the extraction of relationship between the vegetation cover ratio in a pixel and mean NVI was proposed and discussed. Main results obtained are as follows.

(1) When vegetation and non-vegetation are set up as the land cover categories, mixels of two categories exist in boundary of two.
(2) Some of pixels not caught as pure pixel of the vegetation in remote sensing data was also mixel.
(3) The relationship between the vegetation cover ratio in a pixel and mean NVI is linear if mixels which is located on boundary was considered.
(4) The vegetation cover ratio can be assumed with NVI calculated by remote sensing data.

6. REFERENCE

1) A.Hoyano, H.Haga and Y.Komatsu, "A study of vegetation cover ratio in a pixel in urban areas using remote sensing data", J.Archit. Plann. Environ.Eng., AIJ, No.459,1-8, May, 1999 (in Japanese)
2) A.Hoyano and Y.Komatsu, "Optimum spatial resolution of MSS data for land cover classification in residential area", J.Archit. Plann. Environ.Eng., AIJ, No.426, 57-65, Jan, 1991 (in Japanese)
3) A. Hoyano and M. Kato, "Extraction of urban vegetations by airborne multi-spectral scanner data with high spatial resolution", J.Archit. Plann. Environ.Eng.,AIJ, No.407, 37-46, Jan, 1990 (in Japanese)
4) S.Oinuma, A.Hoyano, A.Iino and D.Yun, "Research on estimating vegetation cover ratio in a pixel using MSS data", Proc. of 17th conference on remote sensing, 11-14, Dec. 1994 (in Japanese)
5) D.Yun,A.Hoyano and A.Iino "Vegetation cover map in consideration of vegetation cover ratio in a pixel",Proc.of 18th conference on remote sensing, 165-166, May. 1995 (in Japanese)

Plate 1 False color Image of Airborne MSS (Resolution:1.9m, ch13)

Plate 2 Training Data of Study Site ■ Non-vegetation ■ Lawn ■ Grass □ Tree

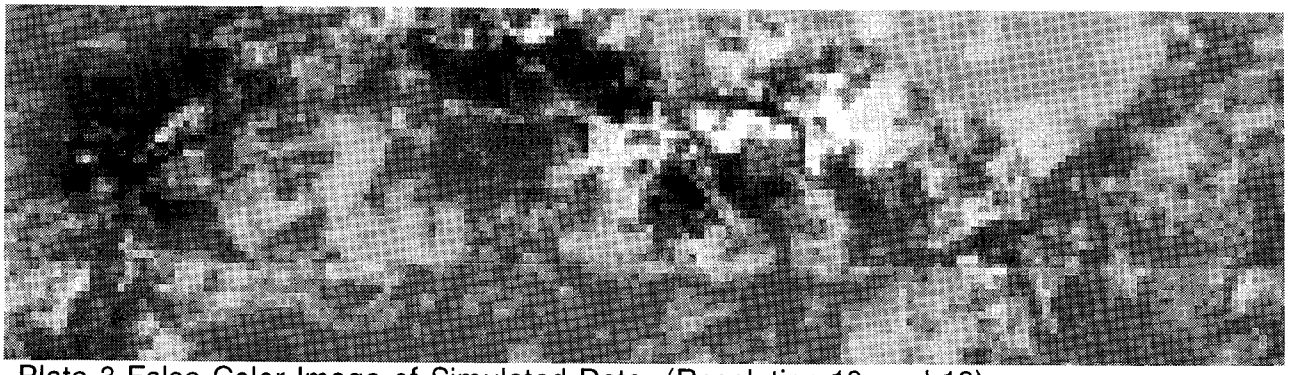

Plate 3 False Color Image of Simulated Data (Resolution:19m, ch13)

Plate 4 Vegetation Cover Ratio in a Pixel of Simulated Data (Resolution:19m)

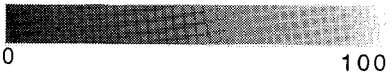

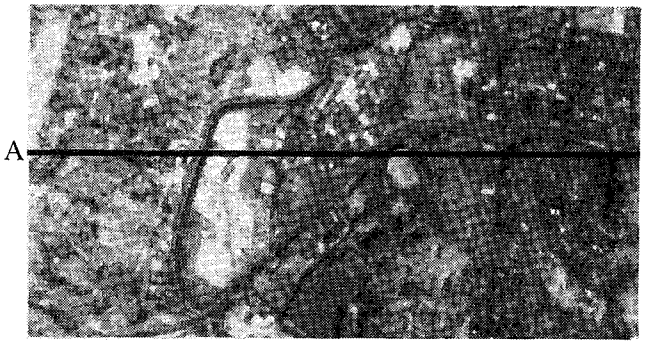

Plate 5 False ColorImage of Section A-A
(Resolution:1.7 , ch 17)

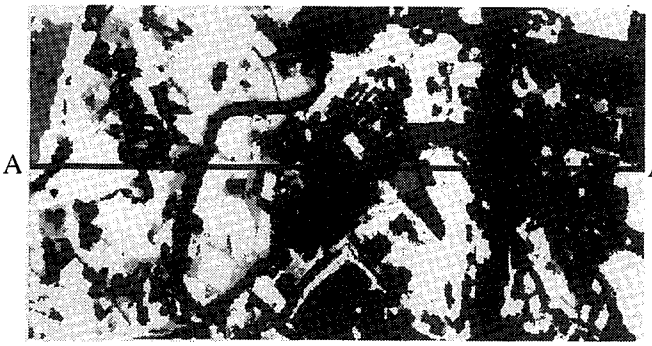

Plate 6 Training Data of Section A-A

Non-vegetation Lawn Grass Tree

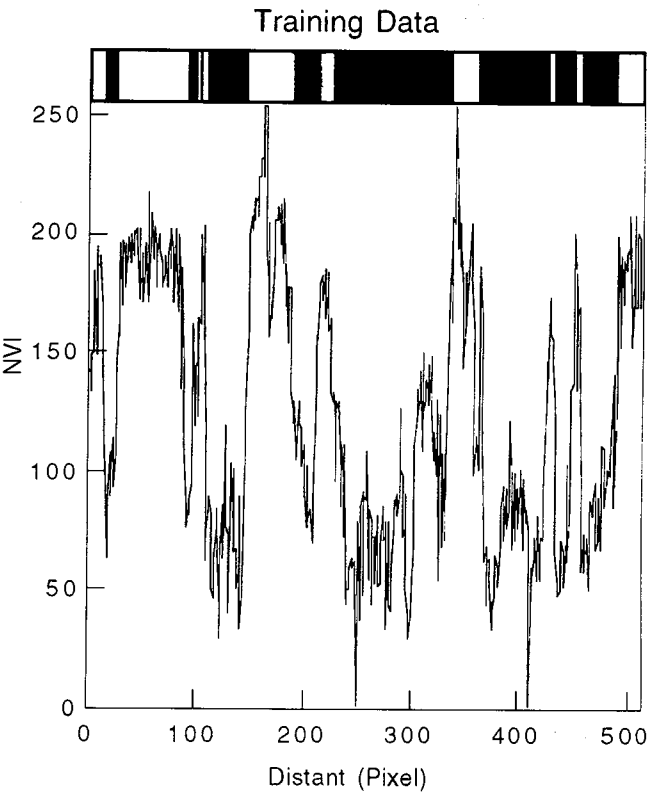

Fig.5 NVI Distribution of Section A-A

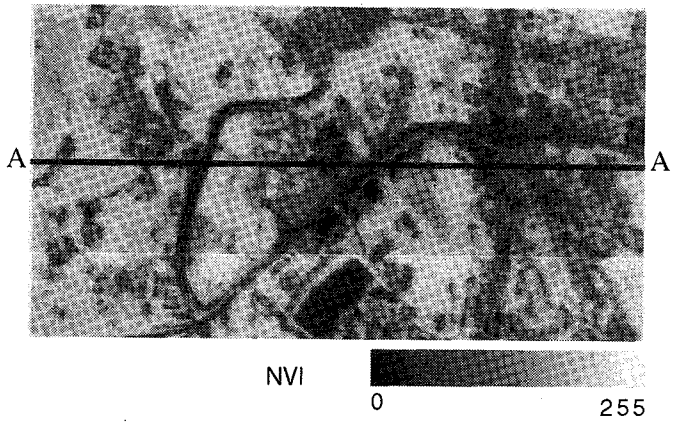

Plate 7 NVI Image of Section A-A
(Resolution:1.9m)

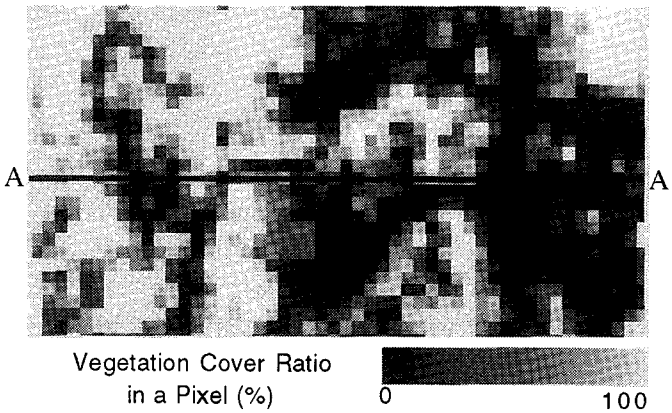

Plate 8 Vegetation Cover Ratio in a Pixel of Section A-A (Resolution: 19m)

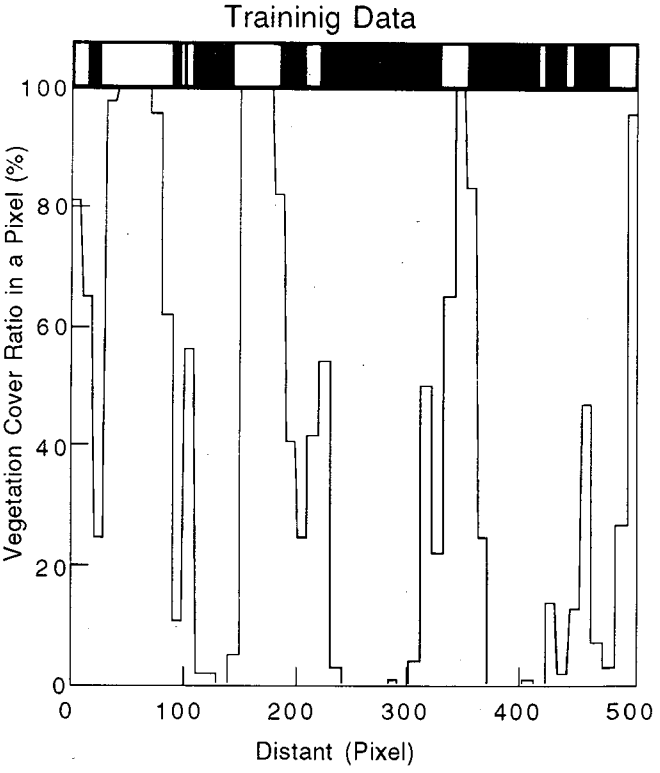

Fig.9 Vegetation Cover Ratio in a Pixel of Section A-A(Simulated Data,Resolution:19m)

SPECTRAL DELINEATION OF LARGE-AREA TROPICAL FOREST LANDS AND TIMBERLANDS USING A COMBINATION OF VISIBLE, NEAR-INFRARED AND 3.7 μm THERMAL-INFRARED AVHRR DATA FROM THE NOAA-12 MORNING PASS SATELLITE

BOBBY A. CRISOSTOMO

Remote Sensing Center
National Mapping & Resource Information Authority
Fort Bonifacio, Makati 1200, Metro Manila, Philippines

ABSTRACT

Satellite mapping of large-area forest lands and timberlands is also accomplished in the Philippines with the use of a combination of visible, near-infrared and 3.7 μm. thermal-infrared AVHRR data of NOAA-12 morning pass (0730 - LST) satellite. This technique was performed on a series of NOAA-12 morning pass images acquired from 1992 to 1994. The linear contrast stretch of the 95 % (2 standard deviations from the mean) of the data of the 3 AVHRR channels combined with the use of the 1988 Land Use Map of the Philippines, the 1989 Land Classification Map of the Philippines and the 1:250,000 topographic maps as reference data enabled the detection of a spectral pattern for forest and timberlands and checking of its suitability for delineation. The ranges of the digital values defining this spectral pattern were determined and used in the classification. The separability of the data values of forest/timberlands from those of the surrounding cover types was evaluated using means, standard deviations and data values profiles. A normalized difference vegetation index image was generated and compared with the classification output. Accuracy assessment performed by pixel-to-pixel comparison with the digital 1988 Land Use Map yielded 85 % classification accuracy.

1. INTRODUCTION

Satellite mapping of large-area vegetation cover is commonly accomplished using the vegetation index (VI) technique on NOAA-AVHRR data. The VI technique employs the visible and near-infrared channels of NOAA-AVHRR data to derive values which will indicate the greenness and density of plant canopies. The vegetated areas generally yield higher VI values than clouds, water, rocks and soil because of relatively high near-infrared reflectance and low visible reflectance (Lillesand and Kiefer,1987). The nature of this VI technique, however, shows

limitations in spectral separation of some contiguously growing distinct vegetation cover types such as forest lands and coconut plantations which abound in tropical countries like the Philippines. One simple technique which can be of great help in mapping out large tropical timberlands and forest lands and which had been used in the Philippines in the past 3 years is using a combination of the visible, near-infrared and 3.7 μm. thermal-infrared AVHRR morning pass (0730 - LST) data of NOAA-12 satellite. The linear contrast stretch of the 95 % (2 standard deviations from the mean) of the data of these NOAA-12 channels coupled with apriori knowledge or use of the land use/classification maps of the area under investigation enables detection of spectral pattern for forest/timberlands and examination of its suitability for delineation. The NOAA-12 images which are determined to be suitable for delineation will then be classified using the ranges of the digital values which define the spectral pattern for forest and timberlands. The characteristics of the forest lands and timberlands delineated by this technique are as follows: (1) at least approximately 2 to 25 sq. km. in extent depending on the position of the pixel in the image from the nadir; (2) have more than 50 % timber, scrubs or broad-leaved trees whose densities range from medium to high; (3) mixed with grassland and other low-density vegetation such as shrubs and coconut trees; and (4) include pine forest but not mangrove forest. One striking feature of this technique is the separation of forest and timberlands from areas dominantly covered with coconut trees. Combining factors that led to the development of this technique are (1) familiarity on the existing land cover types, (2) repeated display of the first 3 bands of morning pass NOAA-12 AVHRR data, (3) habitual linear contrast enhancement of 95 % of the histograms of any image data to be displayed, (4) the failure of the VI technique applied on NOAA data to separate forest from coconut plantations, and (5) the urgency of the need to re-inventory the forest cover in the Philippines using satellite data.

The objectives of this paper are to discuss the procedures and observations in applying the forest/timberland mapping technique, and to evaluate the separability of the data values of forest/timberlands from those of the surrounding cover types using means, standard deviations and data values profile.

2. DATA ACQUISITION AND PROCESSING

The satellite data used in mapping the timberlands and forest cover in the Philippines were the visible, near-infrared and the 3.7 μm thermal-infrared AVHRR data from the NOAA-12 morning pass satellite acquired from 1992 to 1994. The selection of only NOAA-12 morning pass data instead of in combination with those from the other NOAA satellites and passes was historical and was attributed to the first NOAA data used on which the spectral pattern for forest and timberlands had been detected. The softwares used to download and process NOAA-12 data were the Device-Independent Software for Image Processing (DISIMP) and ERMapper.

Conversion of the visible and near-infrared channels into albedo values, and the 3.7 μm thermal-infrared channel, as well as the 11 μm and 12 μm channels, into brightness temperatures using Planck's radiation equation was performed for the separation of land, clouds, glint and sea, and to derive additional data and information for the investigation of the spectral pattern for the delineation of forest and timberlands.

Land, clouds, glint and sea on the raw image were first classified using the algorithms suggested by K. Muirhead (1989) for the automatic classification of AVHRR images. Its output was then used to mask out clouds, glint and sea on the raw data to enable the independent processing and further classification on the land area. The raw image was displayed on the screen by assigning the visible, near-infrared and 3.7 μm thermal-infrared bands to blue, green and red components, respectively. Linear contrast stretch was, then, applied to the 95 % of the histograms. The 1988 Land Use Map of the Philippines (Figure 3), the 1989 Land Classification Map of the Philippines (Figure 4) and topographic maps on scales of 1:2,000,000, 1:1,600,000 and 1:250,000, respectively, were then used to check if a spectral pattern for forest and timberlands was provided, and was suitable for delineation. Contrast enhancement of the 99 % and 68 % of the data were also performed and compared with that of the 95 % of the data in terms of suitability for the delineation. Only the NOAA-12 images determined to be suitable for the delineation of forest and timberlands were further processed and evaluated. The spectral radiances interpreted as belonging to forest and timberlands, as well as to other land cover types, were analyzed using data values profiles, means and standard deviations. Ranges of digital values defining the spectral patterns for forest and timberlands were then determined. Using ERMapper, these ranges were utilized as decision regions for classification of forest and timberlands. The accuracy assessment was performed by first registering the classification output to the digital 1988 Land Use Map (Figure 3) to enable their overlay and, then, doing a pixel-to-pixel comparison to determine the percentage of pixels correctly classified. A normalized difference vegetation index (NDVI) image (Figure 7) was also generated from the same NOAA-12 data for comparison with the classification output, the 1988 Land Use Map, the 1989 Land Classification Map and topographic maps.

3. RESULTS AND DISCUSSIONS

The application of linear contrast enhancement to the 95 % of the data provided better distinction of forest/timberland versus surrounding areas regardless of the illumination conditions of the NOAA-12 image than the enhancement on the 99 % and 68 % of the data. With the 95 % data enhancement and an assignment of visible, near-infrared and 3.7 μm thermal bands to blue, green and red components, respectively, on the display of the image, the lighter red-toned pattern of forest/timberland as compared to the green tone of the land, blue to white tone of the clouds, and a darker red tone of the sea made the forest/timberland readily observable as shown in Figure 1. The observations of the delineation in one image over another showed the changes in the geographic area and the spatial extent of the pixels defining the spectral pattern for forest and timberland. These changes ranged from minimal to non-existence of the spectral pattern for forest/timberland, and were influenced by factors such as satellite zenith angle, geometric distortion, solar elevation angles, and atmospheric conditions (e.g., presence of clouds and haze). Apriori knowledge or use of the land use/classification maps of the area under investigation was essential for the detection of all these changes.

With the use of the Land Use Map and the Land Classification Map as reference data, the coconut plantations area on the enhanced composite NOAA-12 image was observed to exhibit tone and color different from those of the forest and timberland (Figure 1) These differences permitted

the separation of coconut plantations from forest lands and timberlands. The Normalized Difference Vegetation Index (NDVI) image generated (Figure 7), on the other hand, failed to delineate these coconut plantations area versus forest and timberlands.

The spectral pattern for forest lands and timberlands is not dependent on the elevation of the area under investigation. Figure 8 shows the barren lands on the mountainous island of Mindoro, Philippines having elevations which range from 1,000 to 1,500 m. above sea level. These barren lands give tone and color very much different from those of the contiguously lying forest lands and timberlands.

The masking of clouds, sea and glint on the raw data before the classification of forest and timberlands was critical. Classification of forest lands and timberlands without first masking them out had also resulted in the classification of pixels on the sea because of similar spectral radiances in the selected AVHRR channels of some forest/timberlands and sea pixels.

The Timberland/Brushland category in Figure 3 is categorized in the original Land Use Map as "cultivated area mixed with brushland and grassland". Examining the Land Use Map (1988) against other reference data, this category is correctly and normally classified as "medium to high density timberlands/brushland mixed with grassland and cultivated area" in the Land Classification Map (1989), in 1:250,000 topographic maps and even in the 1:50,000 topographic maps and other data produced by the National Mapping & Resource Information Authority (NAMRIA), Philippines. With this rectified category definition, the accuracy assessment resulted in an 85 % classification accuracy. The Land Classification Map and topographic maps were not used directly for accuracy assessment on account of restraining factors but only as reference data during classification and to countercheck the categories of the Land Use Map.

Figure 5 compares the typical data values profiles of forest/timberland with those of clouds, sea and land/mixed land cover types. In both the visible and near-infrared bands, forest and timberland have generally lower average data values than those of clouds and land/mixed land cover types but have almost the same average data values as those of the sea. In the 3.7 μm thermal-infrared band, forest and timberland have slightly higher average data values than those of the sea and land/mixed land cover types but have generally lower data values than those of the clouds. The configurations of these profiles are indicative of the reflectances of the land cover types in the visible and near-infrared bands, and temperatures in the 3.7 μm thermal-infrared bands at the time of satellite pass. The configurations, moreover, show the possibility of separating forest and timberland from other land cover types or features by using either a single band or a combination of bands. Aside from the typical data values profiles, the separability of the data values of forest/timberlands from those of the surrounding cover types can be further investigated by using the means and standard deviations (Table 1) derived from training areas. The behavior of the means for each cover type in the 3 bands as shown in Table 1 resembles the configuration of the data values profiles. The analysis of albedo and brightness temperature values, likewise, gave the same results as that of the raw data values, i.e., having the same behavior of means, standard deviations and data values profiles.

Table 1. Means and Standard Deviation Summary Report for n12_10606

	Means			Standard Deviations		
Class/	Band1	Band2	Band3	Band1	Band2	Band3
clouds1	176.106	149.565	580.094	26.718	17.789	30.128
clouds2	372.667	319.926	939.207	58.608	50.321	17.058
forest1	59.409	66.227	700.727	1.368	4.264	12.279
forest2	59.750	67.800	723.000	1.682	7.431	25.510
forest3	75.364	87.500	715.864	3.048	5.878	15.839
forest4	58.786	87.857	672.357	2.914	4.802	9.410
forest5	54.667	72.333	658.667	0.577	2.082	6.658
land1	74.500	101.607	579.464	2.317	2.685	20.306
land2	94.852	98.481	461.074	3.666	3.130	20.608
sea1	73.964	61.391	629.600	3.020	3.095	15.003

4. CONCLUSIONS

The satellite mapping of large-area tropical forest lands and timberlands of the Philippines was accomplished with success using a combination of visible, near-infrared and 3.7 μm thermal-infrared AVHRR channels from the NOAA-12 morning pass satellite. The linear contrast enhancement of the 95 % (2 standard deviations from the mean) of the data of these channels coupled with the use of the 1988 Land Use Map of the Philippines, the 1989 Land Classification Map of the Philippines and 1:250,000 topographic maps as reference data enabled the detection of a spectral pattern for forest and timberlands and checking of its suitability for delineation. Ranges of digital values defining this spectral pattern were used for classification. The classification output yielded an accuracy of 85 %. This mapping technique was performed on a series of NOAA-12 morning pass images acquired from 1992 to 1994.

5. REFERENCES

Lillesand, T.M., R.W. Kiefer, ***Remote Sensing and Image Interpretation***, 2nd ed., Wiley, New York, 1987.

Muirhead, K., "Automatic Classification of AVHRR Images", ***4th AVHRR Data User Meeting***, 1989.

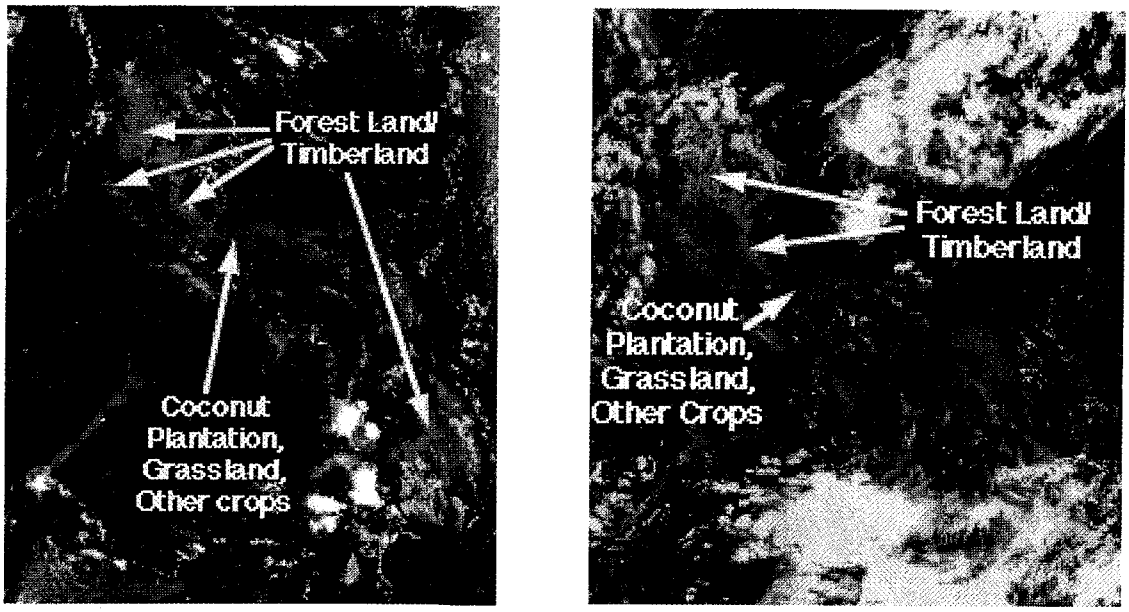

Figure 1: A combination of visible, near-infrared and 3.7 μm thermal-infrared AVHRR data acquired on April 11, 1994 (left image) and May 30, 1993 (right image), respectively, from the NOAA-12 morning pass satellite. The contrast linear enhancement of the 95% of the histograms of these channels provides a spectral pattern that enables the delineation of large-area forest lands and timberlands.

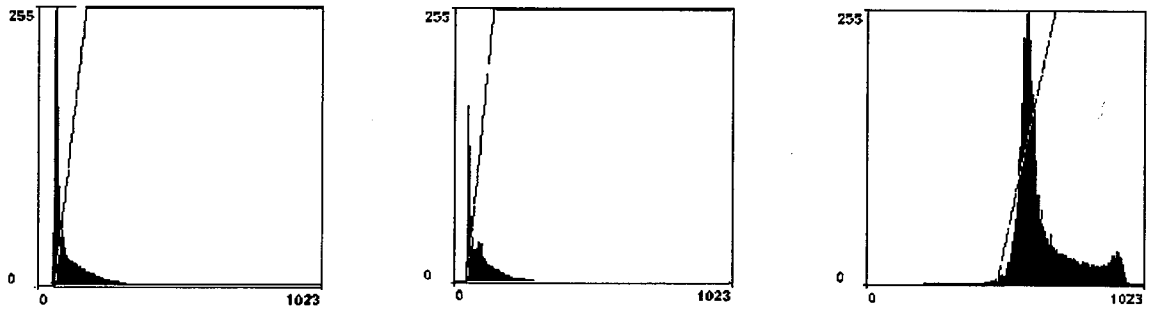

BAND 1 **BAND 2** **BAND 3**

Figure 2: Typical histograms of visible (band 1), near-infrared (band 2) and 3.7 μm thermal-infrared (band 3) AVHRR data.

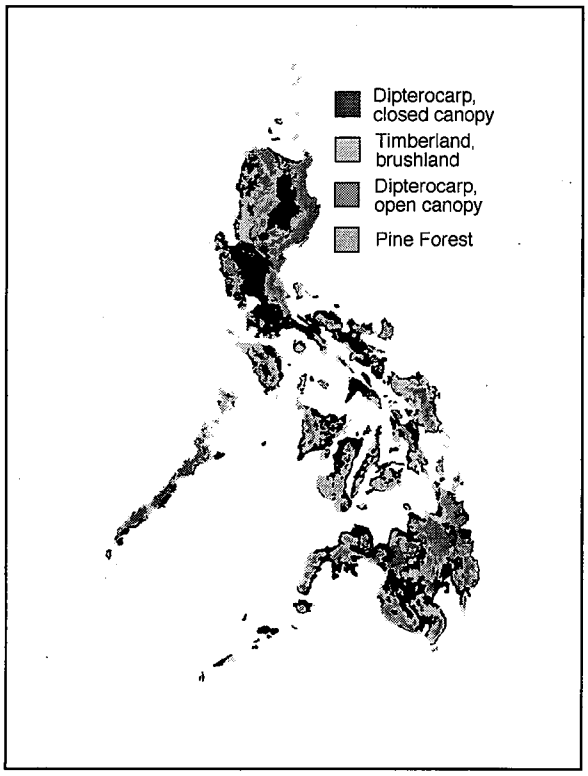

Figure 3: Classification made by Swedish Space Corporation in cooperation with the Department of Environment and Natural Resources using SPOT XS 1987-1988 images.

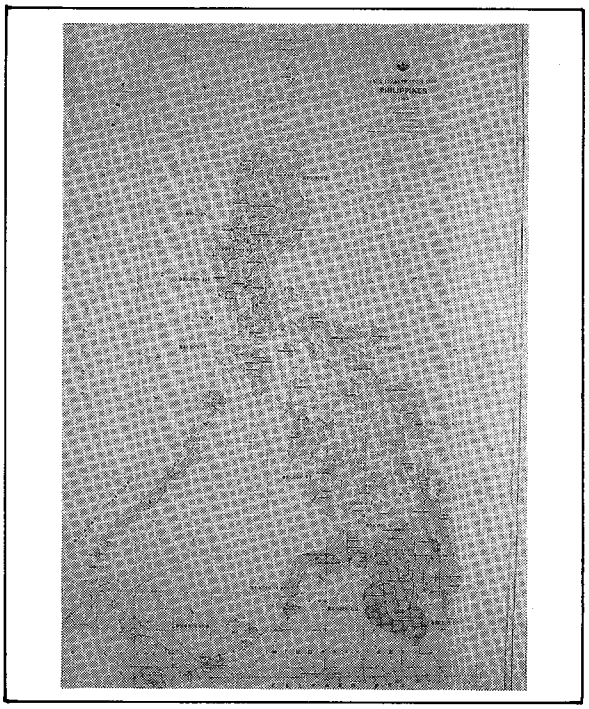

Figure 4: 1989 Land Classification Map produced by the National Mapping and Information Authority (NAMRIA) on a scale of 1:1,600,000 showing in dark shade the classified and unclassified forest lands and timberlands.

FIGURE 5: TYPICAL DATA VALUES PROFILES

CLOUDS

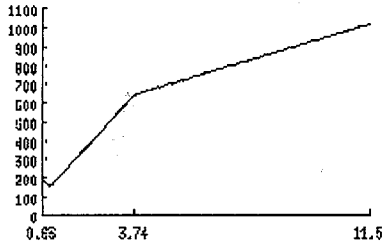

SEA

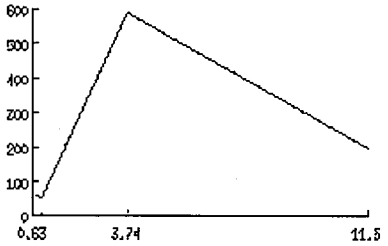

FOREST

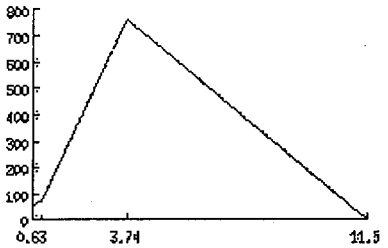

LAND/MIXED LAND COVER TYPES

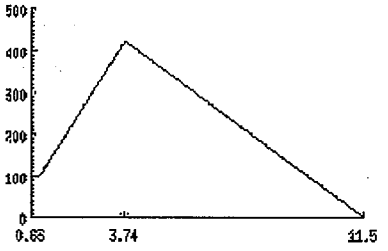

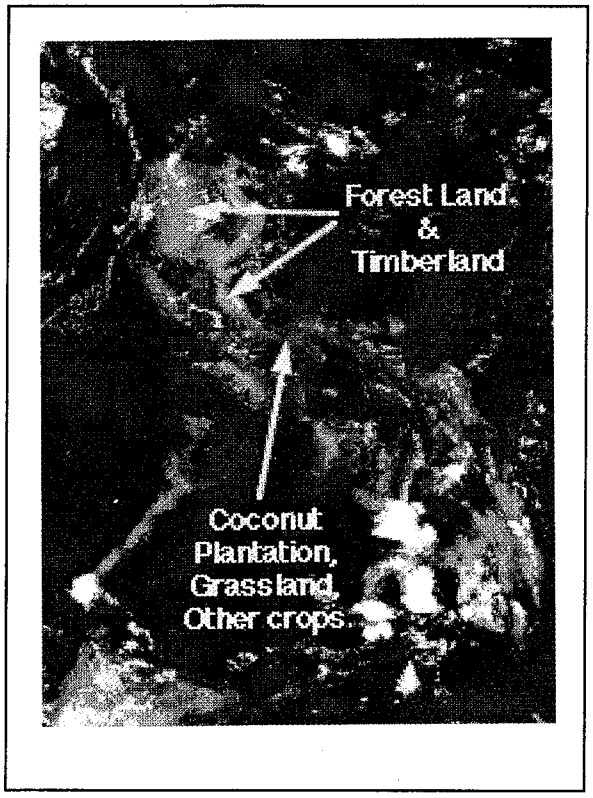

Figure 6: Classification of large-area forest lands and timberlands generated using the combination of visible, near-infrared and 3.7 μm thermal-infrared AVHRR bands.

Figure 7: A Normalized Difference Vegetation Index (NDVI) image derived from the visible and near-infrared bands of NOAA-12 data.

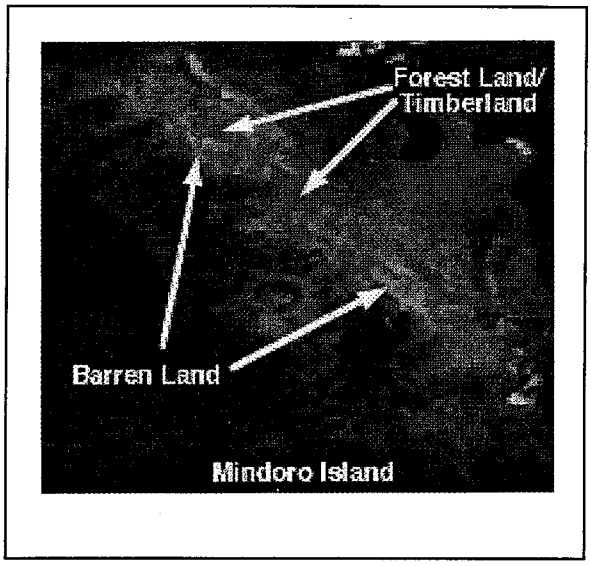

Figure 8: The linear contrast stretch of 95 % of the histograms of visible, near-infrared and 3.7 μm thermal-infrared AVHRR data from NOAA-12 morning pass satellite provides a distinction between barren land and forest.

Indicatrices of the leaves of various woody plant species

Hiroshi Okayama

Center for Environmental Remote Sensing , Chiba University,
1-33 Yayoi-cho Inage-ku, Chiba 263 Japan

Abstract

The indicatrices of the leaves of various woody plant species are measured by use of a goniophotometer. Minnaert constants calculated from these indicatrices are used for their quantitative evaluation. From the results of the measurement, we have found that the characteristics of light scattering from some of the leaves follow Lambertian law and that those of the others don't. It is discussed why the light scattering from leaves does not obey Lambertian law.

Key words ; Leaf, Indicatrix, Minnaert constant

1. Introduction

To estimate the environment of the earth's surface, multispectral remote sensing technology has been largely developed in recent years. There have been many reports on the identification and the detection of stress of vegetative canopies. In the multispectral remote sensing for the vegetated area, the fundamental and important data on the correlation between the incident light and the leaf canopies are acquired. Suits (1972) calculated the directional reflectance of a vegetative canopy. His model is an extension of the canopy model of Allen, Gayle and Richardson (1970) which, in turn, is an extension of Duntley (1942) equations that are, in turn, extension of the Kubelka-Munk equations(1948, 1954).

In a study on light scattering from leaf layers, the individual leaves are treated as perfect Lambertian diffuser. But there are various species of leaves in nature. Though Verhoef (1984) has discussed that the leaf on which the light scatters is a perfect Lambertian diffuser, does the light scattering from all of the leaves follow Lambertian law ? To solve this question we studied the indicatrices of leaves in various species. Table 1 is a list of the studied woody plants in scientific names and in local names as well as in Japanese names because they were collected in Japan. In the text they are referred to by local names which are more commonly used. Breece, H. T. III and Holmes, R. A. (1971) has reported the bidirectional scattering characteristics of healthy green soybean and corn leaves and Thomas W. Brakke (1989, 1993) has reported the non-Lambertian characteristics as to the reflection on the leaves according to seasons and bidirectional reflection characteristics. But we report non-Lambertian characteristics of various leaves by using Minnaert constants (M. Minnaert, 1941).

2. Indicatrix

We used a goniophotometer shown in Fig. 1 to measure the indicatrices. The halogen lamp is used as an optical source of the goniophotometer. The light from the optical source is collimated by a collimator lens, and enters on the leaf sample. The light from the sample is collected by a lens, and it reaches a photomultiplier through a filter. The signals from the photomultiplier are converted in an A/D convertor, and are processed by a personal computer. The optical flux 1.5 cm in diameter enters the leaf sample. The measurement was taken at each 5° of the scattering angle.

The indicatrix is a graph of the angular distribution representing the intensity of the scattered light from the surface of an object on the polar coordinate. Then an indicatrix shows in which angular direction and in what quantity the light from the surface is scattered. Minnaert constants are used for quantitative estimation of the indicatrices. Let the detecting angle and the incident angle be e and i, respectively. Detected radiance L is

$$L(\lambda, e) = L_n(\lambda) \cdot \cos^{k(\lambda)} i \cdot \cos^{k(\lambda)-1} e , \tag{1}$$

where k is Minnaert constant [10]. When $i = e = 0^\circ$, $L_n(l)$ is an effective vertical response.

In equation (1), when $e = 0^\circ$,

$$L(\lambda) = L_n(\lambda) \cdot \cos^{k(\lambda)} i . \tag{2}$$

The value of k is estimated by regression analysis from (2). Equation (2) is written as follows ;

$$Log\, L(\lambda) = Log\, L_n(\lambda) + k(\lambda) Log \cos i . \tag{3}$$

Here by letting

$$Y = Log\, L(\lambda), \tag{4}$$

$$X = Log \cos i, \tag{5}$$

and

$$b = Log\, L_n(\lambda), \tag{6}$$

we obtain

$$Y = k(\lambda) \cdot X + b . \tag{7}$$

If k = 1.0 , (2) becomes a Lambertian equation. The indicatrices obtained when k = 0.7 , 1.0 and 2.0 are shown in Fig. 2. If k = 1. 0 the indicatrix becomes spheric, and when it is smaller than 1.0, the indicatrix swells outward, while when it is larger than 1.0, the indicatrix becomes slender.

The equation (2) is obtained when e is assumed to be 0° in equation (1), but in the experiment, the light vertically enters on the sample and the data are obtained not when $e = 0^\circ$, but by varying the detecting angle. However if we assume the reciprocity law [11] of the

scattering, the detecting angle is considered to be 0° when the incident angle is 0° . In this measurements, the illumination spot size is about 4 cm, and the aperture of a detector is 2 cm. A parallel beam is incident on the sample. The detector is set to detect the light from an infinite distance. Therefore it would be reasonable to represent indicatrices using Minnaert constants.

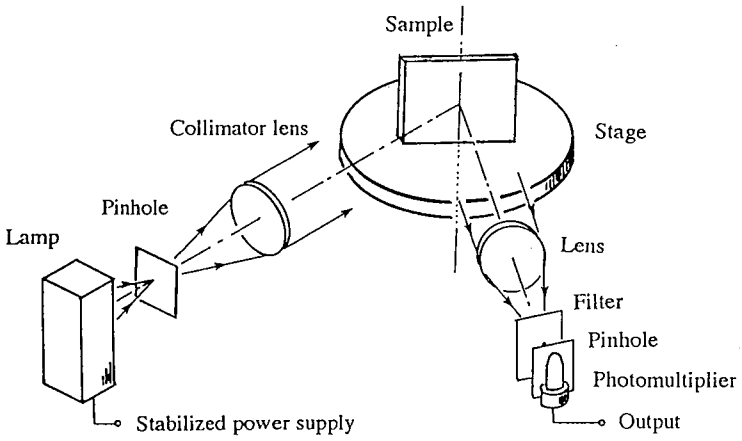

Fig. 1. Schematic diagram of the experimental equipment.

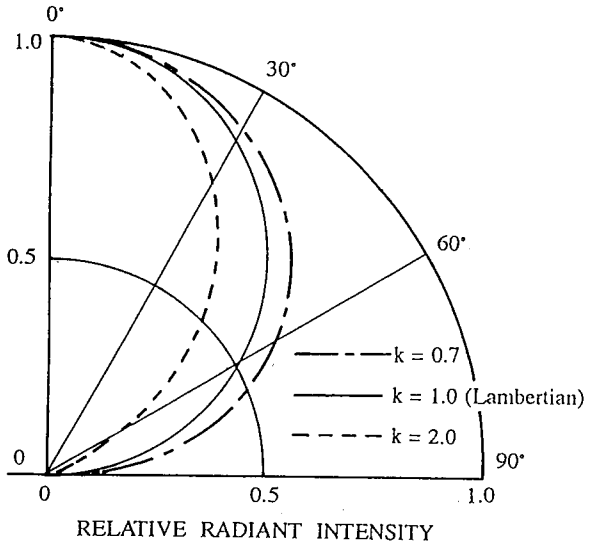

Fig. 2. Indicatrices obtained by calculation when the Minnaert constant k are 0.7, 1.0, and 2.0.

3. Experiments

Several experiments have been done by use of a goniophotometer shown in Fig. 1. The scientific names and local names as well as Japanese names of the leaves used in the experiment are shown in Table 1. First the indicatrices were measured in the case the detecting angle is zero degree. The incident angles into the sample are from 15° to 90° . The measurement points with Camellia and Cherry fit a $\cos^k\theta$ curve when Minnaert constant k=1.12. When k=1.42, they do

Table 1. Scientific names, local names, and Japanese names of woody plants used in the experiment.

Scientific name	Species (Local name)	Japanese name
Acer palmatum	Japanese maple	Momiji
Camellia japonica	Camellia	Tsubaki
Carpinus laxiflora	Hornbeam	Akashide
Carpinus japonica	Japanese hornbeam	Kumashide
Cedrus deodara	Himalaya cedar (deodar)	Himarayasugi
Cinnamomum camphora	Camphor	Kusunoki
Citrus tachibana	Mandarin orange (tangerine)	Mikan
Clethra barbinervis	Clethra	Ryoubu
Cornus florida	Flowering Dogwood	Hanamizuki
Diospyros kaki	Japanese persimmon	Kaki
Euonymus japonicus	Spindle	Masaki
Ginkgo biloba	Ginkgo (maidenhair)	Icho
Juniperus chinensis	Sabina endlicher	Kaizukaibuki
Nerium indicum	Oleander	Kyouchikutou
Pinus thunbergii	Pine	Matsu
Photinia glabra	Chinese hawthorn	Kanamemochi
Platanus orientalis	Platan (sycamore)	Puratanasu
Prunus × yedoensis	Cherry	Sakura
Sorbus commixta	Mountain ash (rowan)	Nanakamado
Stewartia pseudo-camellia	Deciduous camellia	Natsutsubaki
Styrax japonica	Snowbell	Egonoki
Viburnum odoratissimum	Coral	Sangoju
Zelkova serrata	Zelkova	Keyaki

not fit as is shown in Fig. 3. However, they fit well when the scattering angle is larger than 50° . The correlation coefficients and the experimental results are shown in Table 2. The number of times of measurements is 16. The measurement points fit the $\cos^k\theta$ curve when the correlation coefficient R^2 is near 0.98, but not when it is near 0.89. An indicatrix is obtained by connecting measurement points. Minnaert constants are obtained from these indicatrices. In Figs. 4 and 5, the curves called indicatrices are drawn by connecting the measurement points. We obtained Minnaert constant k from these curves. Nine samples of them with appropriate dispersion were selected and plotted on Figs. 4 and 5. The indicatrix shows the diffuse components of reflectance. Minnaert constant does not represent the total reflectance of a leaf, but represents the degree of the reflectance intensity in angular directions. Fig. 4 shows the indicatrices of **Pine, Himalaya ceder,** and **Sabina Endlicher** giving Minnaert constants smaller than unity, which are more swelling than the Lambertian curve. The characteristics of the first group including **Pine, Himalaya cedar** and **Sabina Endlicher** are that they have a mass of needle leaves. Thus the light is scattered in various directions and probably by that reason Minnaert constants are smaller than 1.0. Fig. 5 shows the indicatrices giving Minnaert constants larger than unity. The

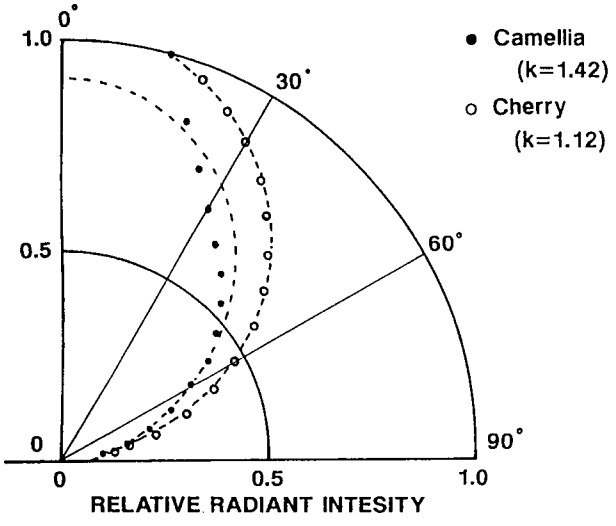

Fig. 3. Minnaert function $\cos^k\theta$ curves for Camellis and Cherry.

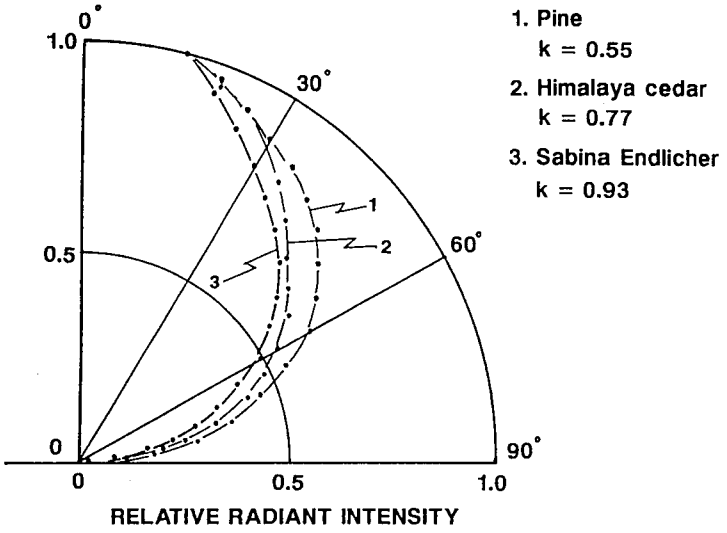

Fig. 4. Indicatrices of needle leaves of Woody plants.

photograph of a leaf of this classification is shown in Fig. 6 (a), which is **Himalaya cedar** (k = 0.77) and consists of small construction units. In the second group the leaves of Minnaert constants 1.05 to 1.09 shown in Fig. 6 (b) have a surface covered with downy hair, and for that reason, the light may be scattered uniformly. This photograph was magnified twenty times. Different from the others **Ginkgo (maidenhair)** leaves have no downy hair but fine tucks over the surface and therefore their Minnaert constant is as small as 1.07. The third group with Minnaert constants of 1.10 - 1.28 as is shown in Fig. 6 (c) include the leaves with a rough surface without downy hair and not very glassy. The leaves in the fourth group (Fig. 6 (d)) carry the specular nature and Minnaert constants are larger than those in the other groups.

Next we measured the indicatrices when the incident angle is 45 degrees to the surface of the leaf. Experimental results are shown in Figs. 7. Fig. 7 was replaced by a new one which shows Minnaert constants of Platan (k=1.05), Cherry (k=1.12), Hornbeam (k=1.27) and Coral (k=1.57) as representative leaves in classification of Table 2. In the leaves with Minnaert constants of 1.05,

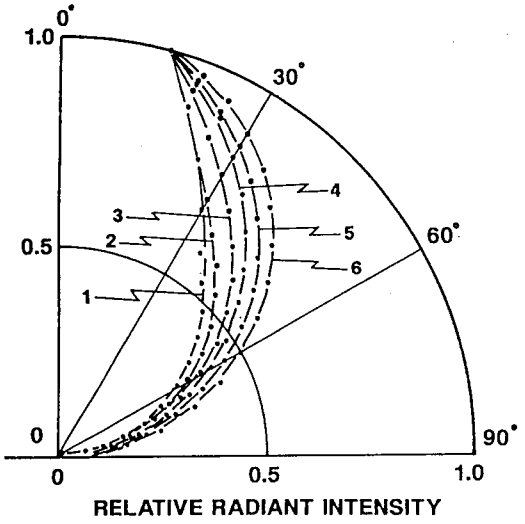

1. Coral
   k = 1.57
2. Camellia
   k = 1.42
3. Japanese pernimmon
   k = 1.37
4. Mandarin Orange
   k = 1.25
5. Mountain ash
   k = 1.15
6. Clethra
   k = 1.05

Fig. 5. Indicatrices of leaves of woody plants.

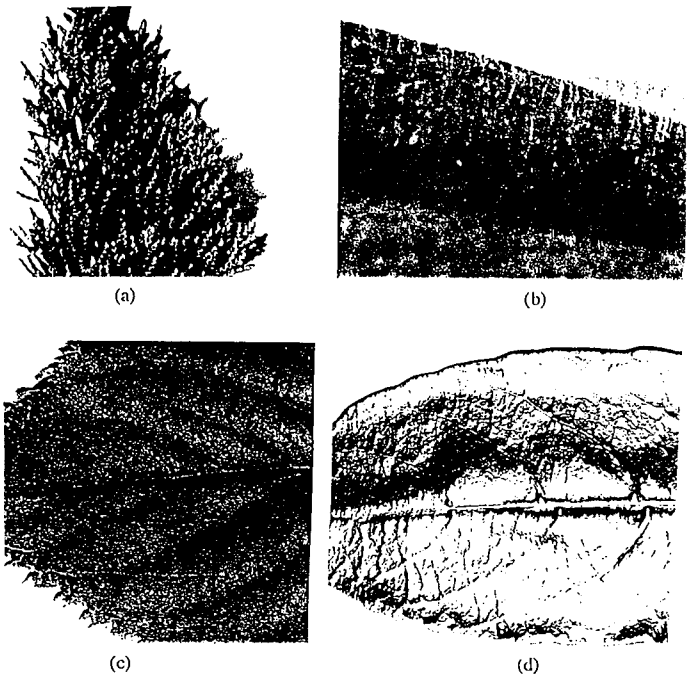

Fig. 6. Photographs showing the characteristics of leaves. (a) : **Himalaya Cedar** (k = 0.77), a needle leaf, (b) : **Snowbell** (k = 1.10), a leaf surface covered with downy hair, (c) : **Cherry** (k = 1.12), a non-specular broad leaf, (d) : **Coral** (k = 1.57), a specular leaf.

Table 2. Minnaert constants obtained from indicatrices of leaves and correlation coefficients. Leaves are classified coefficients. Leaves are classified in four groups by their Minnaert constants.

Species (Local name)	Minnaert constant k	Correlation coefficient R^2	Characteristics of leaves
Pine	0.55	0.99	
Himalaya cedar (deodar)	0.77	0.98	Needle leaves .
Sabina Endlicher	0.93	0.90	
Platan (sycamore)	1.05	0.98	
Clethra	1.05	0.99	The surface of a leaf is
Ginkgo (maidenhair)	1.07	0.96	usually covered with
Deciduous Camellia	1.07	0.89	downy hair.
Japanese maple	1.09	0.99	
Flowering Dogwood	1.09	0.98	
Snowbell	1.10	0.99	
Cherry	1.12	0.98	
Zelkova	1.12	0.99	The leaf has a
Japanese hornbeam	1.13	0.98	non-specular broad
Mountain ash (rowan)	1.15	0.98	leaves.
Mandarin Orange (tangerine)	1.25	0.95	
Hornbeam	1.27	0.97	
Chinese hawthorn	1.28	0.97	
Oleander	1.28	0.96	
Camphor	1.35	0.90	
Japanese persimmon	1.37	0.89	The surface of a leaf
Camellia	1.42	0.89	shows specular
Spindle	1.46	0.88	reflection.
Coral	1.57	0.87	

for example **Platan (sycamore)**, the indicatrices present near-spherical shapes, not depending on the incident angle. The indicatrices of **Coral** with Minnaert constants of over 1.57 shown in Table 2 have the maximum in the 90° direction because the incident angle is 45° as is shown in Fig. 7.

The experimental results immediately after collection of the leaves are shown in Table 2, but the

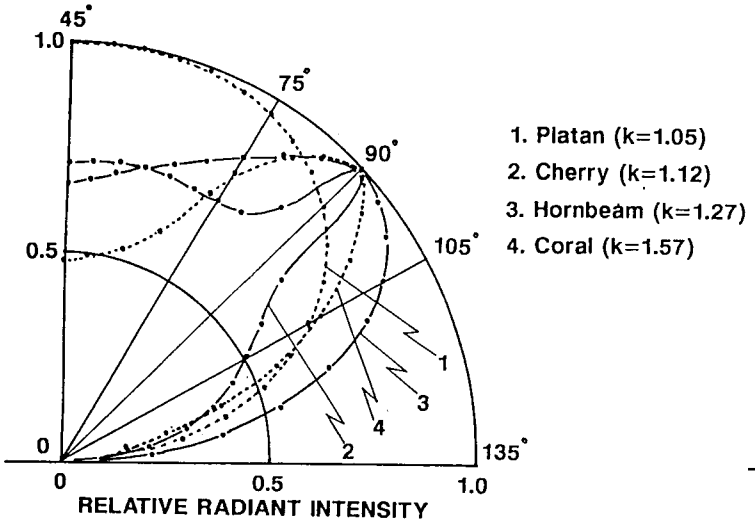

Fig. 7. Indicatrices of leaves, when the incident angle is 45 degrees to the surface of the leaf.

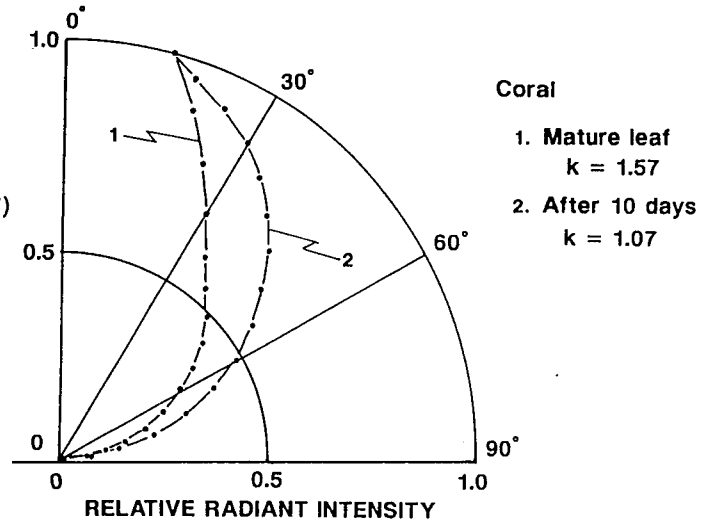

Fig. 8. Indicatrices of leaves obtained by measuring again after 10 days in the laboratory.

results which are shown in Table 3 were obtained by measuring the indicatrices again after 10 days in the laboratory. The indicatrices of the mature leaves are measured on the day of collection and 10 days after collection and the comparison is shown in Fig. 8. The leaf of **Coral** which had shown the specular reflection (1.57) in Fig. 7 did not show the specular reflection in after -10-days experiments (1.07). As shown in Table 3, Minnaert constants became smaller after ten days. This is because the leaf surfaces got rougher by evaporation of the moisture during the 10 days. Namely Minnaert constant of the leaf showing Lambertian reflection is near 1.0 and does not change even when the incident angle changes from 0° to 45° .

Table 3. Minnaert constants of leaves obtained by measuring the indicatrices again after 10 day in the laboratory.

Species (Local name)	Minnaert constant	Minnaert constant after 10 days
Ginkgo (maindenhair)	1.07	1.01
Platan (sycamore)	1.05	1.01
Cherry	1.12	0.93
Zelkova	1.12	0.68
Chinese hawthorn	1.28	1.10
Oleander	1.28	1.09
Camphor	1.35	0.86
Spindle	1.46	1.19
Coral	1.57	1.07

4. Conclusion

In general, when the reflection characteristics from the leaves of woody plants are discussed, it is assumed from the simplicity of calculation that the reflection from leaves obeys Lambertian law. However we made an experiment to obtain the indicatrices of light scattering from leaves of real woody plants. As the results from various kinds of leaves, we have found that the scattering characteristics of some of them do not obey Lambertian law. The indicatrix shows the diffuse components of reflectance. Minnaert constant does not represent the total reflectance of a leaf, but represents the degree of the reflectance intensity in angular directions. We made estimation of leaves by using Minnaert constants calculated from the indicatrices of leaves, and found that differences in the construction of the leaves gave different indicatrices.

Here we have made measurements on each piece of leaf in order to know the characteristics of respective species, but many leaves construct a layer and many layers, in turn, compose a canopy, and different results may be obtained when measured on such a scale outdoors.

References

Allen, A. William, T. Vincent Gayle, and Arthur J. Richardson, "Plant-Canopy Irradiance Specified by the Duntley Equations", J. Opt. Soc. Am., **60**, 372-376 (1970).

Brakke, T. W. , J. A. Smith and J. M. Harnden, "Bidirectional Scattering of Light from Tree Leaves", Remote Sensing Environ., **29**, 175 - 183 (1989).

Brakke, T. W. , W. P. Wergin E. F. Erbe and J. M. Harnden, "Seasonal Variation in the Structure and Red Reflectance of Leaves from Yellow Poplar, Red Oak, and Red Maple", Remote Sensing Environ., **43**, 115 - 130 (1993).

Breece H. T. III and R. A. Hollmes , "Bidirectional Scattering Characteristics of Healthy Green Soybean and Corn Leaves in Vivo", Appl. Opt., **10**, 119 - 127 (1971).

De Hoop, A. T. , "A Reciprocity Theorem for the Electromagnetic Field Scattered by an Obstacle", Appl. Sci. Res., Section B, **8**, 135-140 (1960).

Duntley, Q. Seibert , "The Optical Properties of Diffusing Materials", J. Opt. Soc. Am., **32**, 61-70 (1942).

Kubelka, Paul , "New Contributions to the Optics of Intensely Light - Scattering Materials. Part I", J. Opt. Soc. Am., **38**, 448-457 (1948).

Kubelka, Paul , "New contributions to the Optics of Intensely Light - Scattering Materials, Part II : Nonhomogeneous Layers", J. Opt. Soc. Am., **44**, 330-335 (1954).

Minnaert, M. , "The Reciprocity Principle in Lunar Photometry", Astrophys. J., **93**, 403-410 (1941).

Suits, Gwynn H. , "The Calculation of the Directional Reflectance of a Vegetative Canopy", Remote Sensing of Environment, **2**, 117-125 (1972).

Verhoef, W. , "Light Scattering by Leaf Layers with Application to Canopy Reflectance Modeling : The SAIL Model", Remote Sensing of Environment, **16**, 125-141 (1984).

A Monte Carlo reflectance simulation of rice canopy based on digital 3-D structure

Keiji KUSHIDA(*), Kunihiko YOSHINO(*), Eiji YAMAJI(*)

* Department of agricultural Engineering
Faculty of agriculture, University of Tokyo
1-1-1 Yayoi, Bunkyo-ku, Tokyo 113, JAPAN
Tel: +81-3-3812-2111 (ex.5345), Fax: +81-3-5684-3632
E-mail: kusy@tansei.cc.u-tokyo.ac.jp

Abstract

NIR bidirectional reflectance distribution of thirteen kinds of rice canopy is simulated using the 3-D Monte Carlo method and measured in an experimental field. The simulation is carried out under two different field conditions. One is similar to the condition of the experimental field (condition A) and the other is the wide spread field condition under the parallel solar beam (condition B).

The framework of the simulation model is 1cm x 1cm x 1cm sized rectangular solid cell. Each cell has an information of leaf area, inclination, and direction which is calculated using a 3-D digital stereo measurement method. Other than the structural information, the sensitivity of individual leaf reflectance is accounted.

The sensitivity is decided by measuring some kinds of individual leaf reflectance. From the measurement, NIR reflectance and transmittance of rice leaves has low coefficient of variation.

The simulated bidirectional reflectance under condition A fitted the measured one relatively well. As the result of the simulation, the ratio of the reflectance factors from wide spread field to different view zenith angles is suggested to give average inclination of rice canopy.

1. Introduction

Radiative transfer simulation of plant canopy is basic to remote sensing of plant canopy state. A complex scene is hard to model with analytical models. With the simulation models such as Monte Carlo method, one can consider canopy structure which is hard to model with analytical models. Therefore, the simulation has been carried out using the Monte Carlo method.

Ross et al. (1988) modeled plant elements (leaf, stem) as simple geometrical shapes. Round or elliptic leaves are assumed and the difference of bidirectional reflectance factor

is estimated under the conditions of different variance of leaf inclination, different degrees of ellipticity, the row effect, and the influence of stems.

Kimes et al. (1982) represented information of plant canopy physical state as 3-D cell matrix and developed a simulation model. A size of one cell is about 10cm. Each cell which corresponds to leaf has information of leaf inclination distribution function and leaf area index. Each cell has the same theoretical or empirical leaf inclination distribution. Simulation is carried out with homogeneous dense canopy (Kimes, 1984), homogeneous sparse canopy (Kimes et al., 1985), and inhomogeneous canopy (Kimes et al., 1986). The results of the simulation is compared with measured value, and bidirectional reflectance characteristics of various vegetation canopy are explained.

However, simulations and validation of their result has hardly carried out from the viewpoint of estimation of canopy physical state of a fixed crop canopy. One of the reason is thought to be that the structural measurement of canopy has been hardly carried out so that the cells are small enough to correspond to a minute region of an individual leaf. G.V.Menzhulin et al. (1991) also pointed out this as a shortcoming of the simulation model.

Therefore, NIR bidirectional reflectance distribution of thirteen kinds of rice canopy is simulated using the 3-D Monte Carlo method based on cell information given from 3-D structure obtained by the leaf edge matching method (Kushida et al., 1994a; Kushida et al., 1994b) and stereo photogrammetry in this paper. And the simulated reflectance factor is compared with measured. Using this model, rice canopy bidirectional reflectance characteristics is analyzed.

2. Simulation model

2.1 Field and light condition

Basically straight forward method, which traces photon time sequentially is used. A photon comes out of a light, travelling in a canopy, and then absorbed in the canopy or get out of the canopy. Radiative transfer in canopy and bidirectional reflectance from canopy can be simulated by increasing the number of photon. The fate of a photon is decided by condition of both incident light and canopy physical state. The former is presented using light's incident direction - intensity characteristics as probability density function. The latter is mentioned in **2.2** and **2.3** in detail.

Simulation of wide spread canopy is restricted by capacity of computer memories. But, when a canopy can be presented by repeat of a basic unit, the simulation can be carried out with as much memories as necessary for basic unit simulation. Namely, a photon which gets out of a basic unit is equivalent to the one which entered from the opposite surface of the basic unit (Kimes et al., 1982). The conception of the model is

shown in Fig. 1.

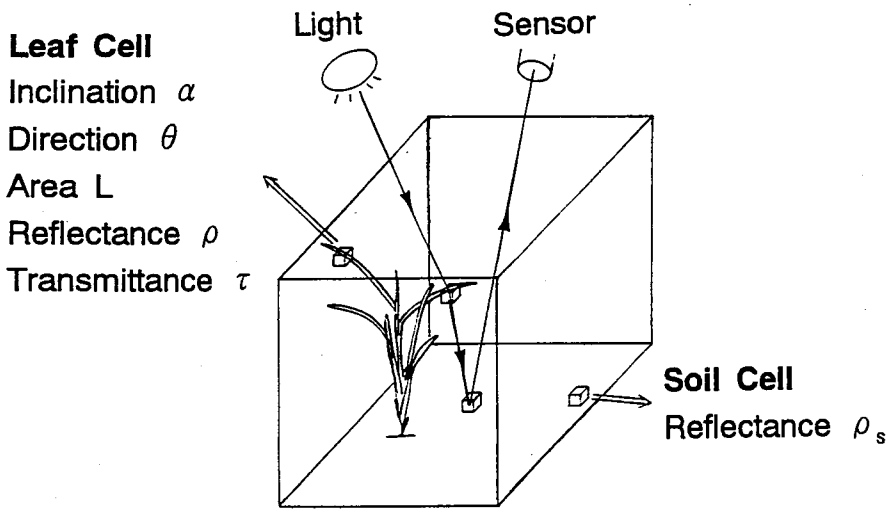

Fig. 1. The conception of the model

2.2 cell information

When radiative transfer in canopy is tried to simulate more realistically, more canopy information is necessary. The framework of the simulation model is 1cm x 1cm x 1cm sized rectangular solid cell.

There supposed to be not more than two individual leaves in the space of each cell. Each cell has an attribute of air or leaf or soil. A cell which has attribute of leaf is given information of leaf area, direction, and inclination. These information is obtained as follows. At first, leaf direction and inclination on each leaf edge lines are calculated using a 3-D measurement method, the leaf edge matching method and stereo photogrammetry. The lines are divided into shorter unit lines. A cell which includes each point of a unit line is given information of inclination and direction of the unit line. Vertical resolution of this method is about 1.7 mm, and the perpendicular resolution is about 6.8 mm. Then, the projected leaf area of each cell is calculated from the rectified disparity image obtained by the method. Cells which have only leaf area information are given information of leaf direction and inclination by supplementation. Attribute of soil is given to all the cell that is situated at 0 cm height.

2.3 Cell-photon interactions

1) air cell : A photon is not forced by this cell. Namely, a photon go straight forward in this cell.
2) leaf cell : Let ρ be leaf reflectance factor, τ leaf transmittance factor. S_c and S_L are projected area of a cell and leaf in the cell respectively to a plane which is perpendicular to incident vector. When a photon enters into the cell, the probability

of the photon distributing is $(S_L/S_c)(\rho+\tau)$, and that of being absorbed is $(S_L/S_c)(1-\rho-\tau)$, and that of transmitting is $1-S_L/S_c$. Distribution phase function of the cell obeys Lambertian.

3) soil cell : When a photon entered this cell, the photon is distributed at the incident point. Distribution phase function obeys Lambertian without the specular reflectance. The specular reflectance factor caused by the ponding water is 2.1% here.

3. Refrectance measurement

3.1 Measurement condition of canopy bidirectional reflectance factor

Rice crop (*Oliza Sativa*, variety: *koshihikari*) is cultivated at an experimental field of University of Tokyo in 1992. Thick plot (15 cm X 15 cm) and thin plot (30 cm X 30 cm). Reflectance measurement is carried out a week interval under artificial light (450W lump) just after sun set. Reflectance factor is measured with 10 degrees FOV. Data is obtained three times per one object and averaged. Fig. 2 shows the device for reflectance measurement. Incident angle to the canopy is 15 degrees. View azimuth angle is 0 degree (the opposite of the light) and view zenith is 0, 45, 60 degrees. Soil reflectance (8 cm water ponding) is also measured.

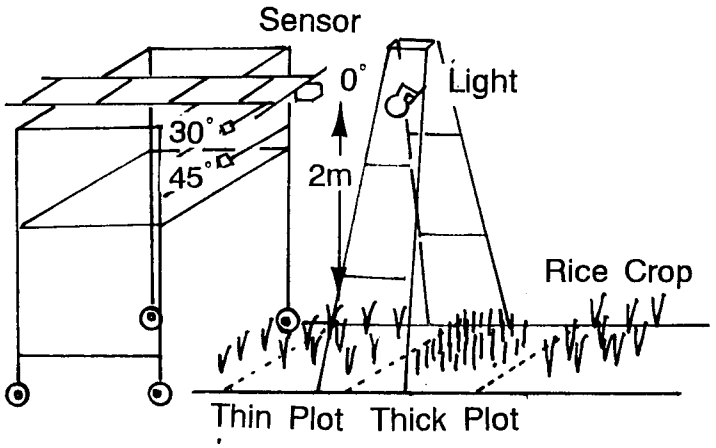

Fig. 2. Canopy reflectance measurement in an experimental field

3.2 Measurement of individual leaf reflectance factor

Reflectance factor ρ and transmittance factor τ of ten samples of rice individual leaves are measured nondestructively in 1994. Incident angle is 0 degree and reflection angle is 45 degrees.

For the result, in the NIR region (850nm - 950nm), the average of ρ is 0.50 and that of τ is 0.45. These values and measured soil reflectance ρ_s=0.055 are used for the simulation. Coefficient of variation of ρ is about 5%. In the other regions, coefficient of variation is higher than 15%. This shows that NIR region is the most optimal to use as the indicator of the 3-D structure of rice canopy which is not withered.

4. Simulation of canopy bidirectional reflectance

4.1 Condition of the simulation

Simulation is carried out under the following two conditions.

A. Experimental field : This is the condition that is similar to the experimental field measurement condition. In the other words, direction – intensity characteristics of the incident light is approximated by a function of $y=I(0)\cos^{7.16}\theta$. Where $I(\theta)$ shows the intensity to the direction θ. Basic unit is situated based on the measurement situation.

B. Wide spread field : This is the condition that specular light enters homogeneously to a scene which is composed of repeat of basic unit which spread enough widely to the vertical direction. IFOV of the sensor can be any combinations of basic unit. In order to account for the air effect, It is necessary to combine air reflectance models with this model. The probability concerning to photon fate remarked in **2.3** is given by causing a suspected random number. Individual leaf reflectance and soil reflectance are given by in situ and field measurement respectively.

B–1. Leaf reflectance ρ, absorbance α and transmittance τ are constants.

B–2. ρ, α and τ are given as follows.

$$\begin{aligned} \rho &= \rho_c + \rho_v \\ \alpha &= \alpha_c + \alpha_v \\ \tau &= 1 - \rho - \alpha \end{aligned} \qquad (1)$$

Where ρ_c and α_c are constants. ρ_v and α_v are $\pm 0.05\rho_c$ and $\pm 0.05\alpha_c$ respectively.

4.2 Comparison between simulated and measured

NIR bidirectional reflectance distribution of thirteen kinds of rice canopy is simulated under condition A. Fig. 3. shows the comparison of the calculated reflectance factor to the view azimuth 180 degrees, view zenith 0, 45, 60 degrees with the measured one in an experimental field. Root mean square error is respectively. This shows the simulation is effective for valuating the rice canopy bidirectional reflectance.

4.3 Simulation of rice canopy reflectance in wide spread fields

Fig. 4. shows simulated NIR bidirectional reflectance distribution of thirteen kinds of rice canopy under condition B–1. Incident zenith angle is 15 degrees. 1.15 X 10^6 photons are traced. Following results are obtained by the simulation.

Basically, reflectance factor inclined to be higher to each direction as rice grows up. This shows that the effect of the total leaf area increasing on bidirectional reflectance is

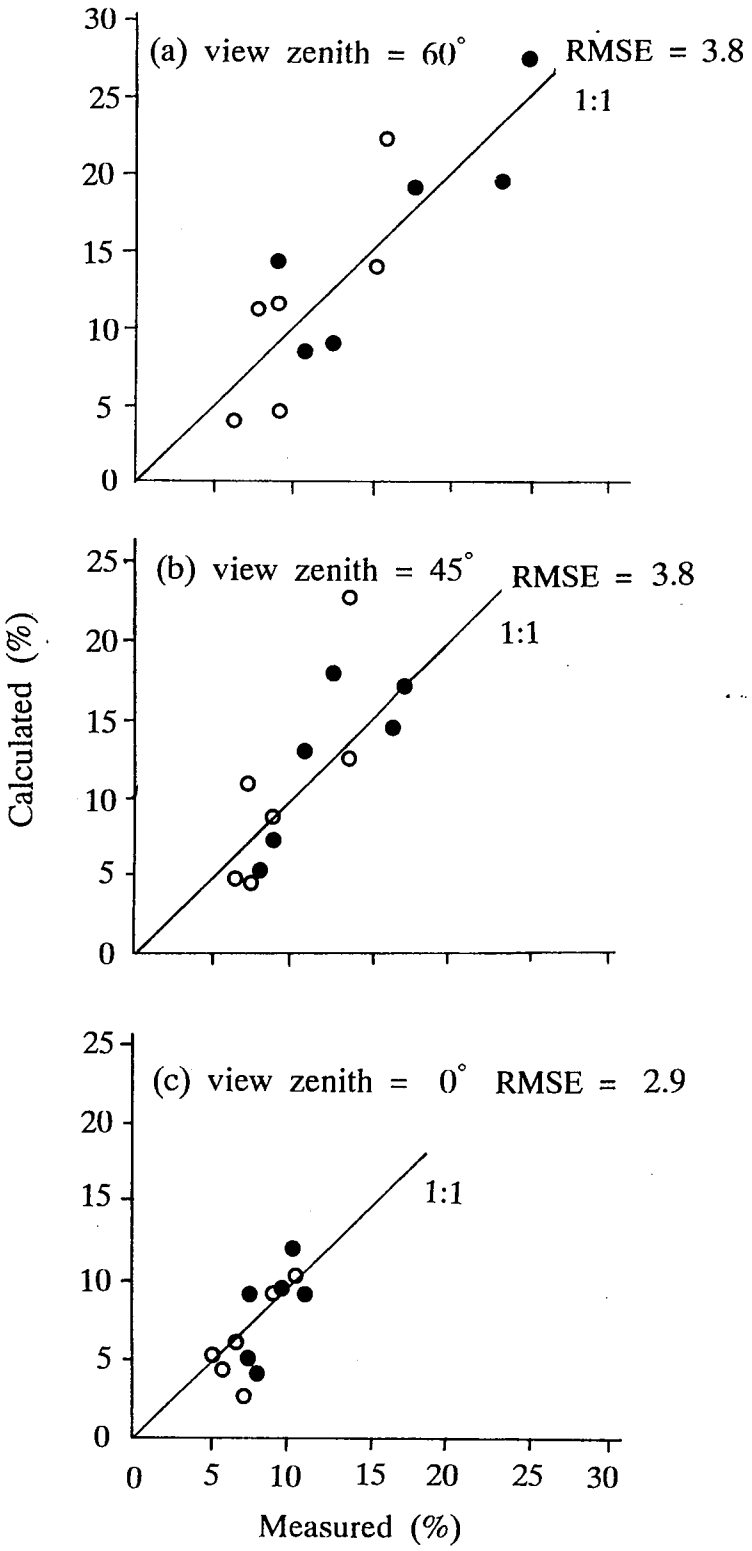

Fig. 3. Relation between calculated and measured reflectance factor (condition A, view azimuth = 0°)
Thick Plot : ● , Thin Plot : o

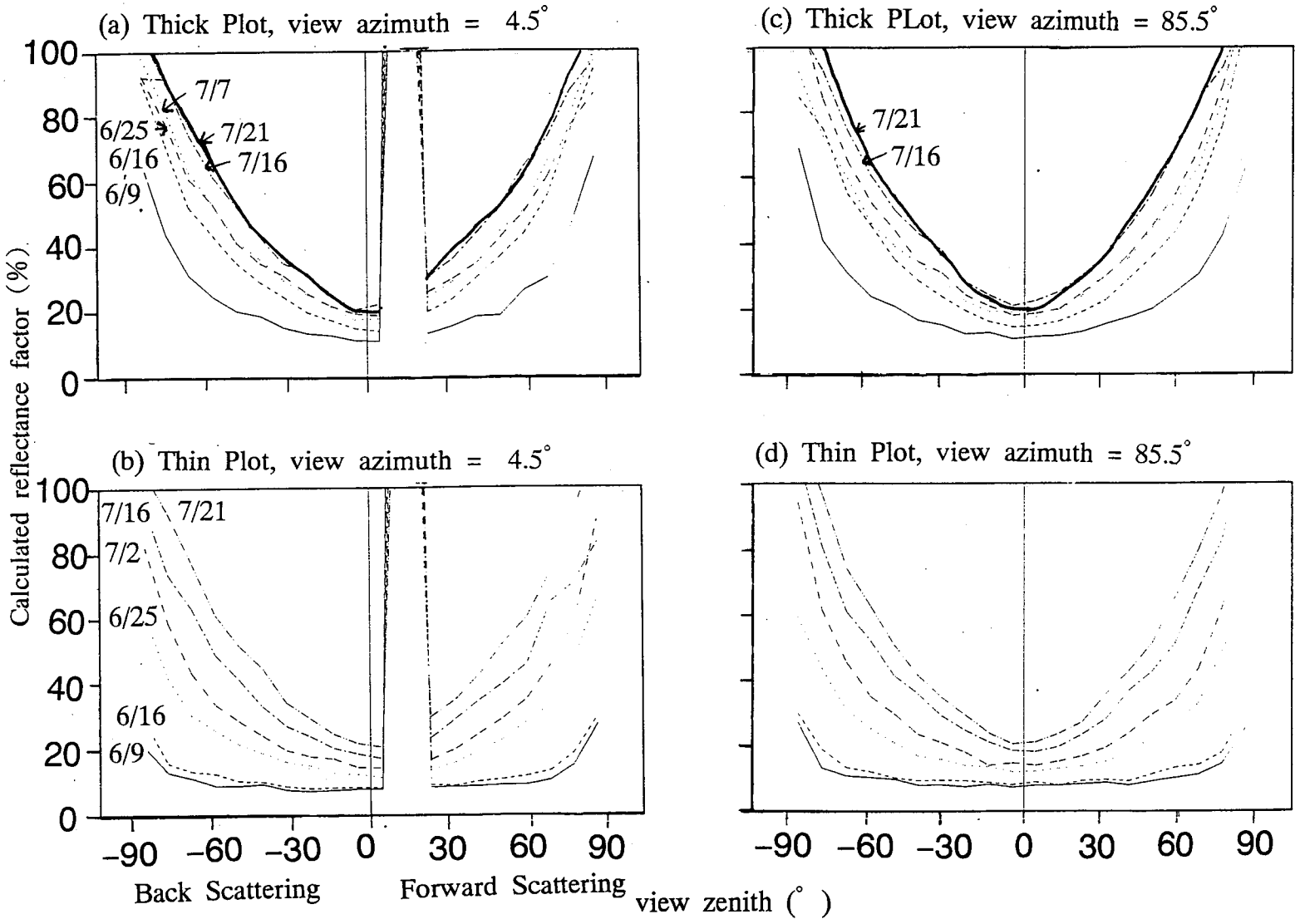

Fig. 4. Bidirectional reflectance characteristics of rice canopies obtained by simulation (condition B-1)

more dominant than that of leaf inclination in each direction.

However, comparing the dense plot in July 16th with that of July 21th, the former has higher reflectance to the nadir direction, and has lower reflectance to greater than 30 degrees zenith angle. This is the case of either 0, 45, 90 degrees azimuth angle. This seemed to be caused by the difference of leaf inclination.

Therefore, relation between leaf average inclination and R(45°)/R(0°) is analyzed. Where R(ϕ) is the reflectance factor to view zenith angle ϕ, azimuth angle 180° . Without earlier growth stages (without data of thin plot in June 9th and June 16th), the two parameters are adequately correlated. The correlation coefficient is 0.84.

5. Conclusion

In this paper, NIR bidirectional reflectance distribution of thirteen kinds of rice canopy is simulated using the 3-D Monte Carlo method and measured in an experimental field. The simulation is carried out under two different field conditions. One is similar to the condition of the experimental field and the other is the wide spread field condition under the sun shine. The simulated reflectance factor under the former condition fitted the measured one relatively well. As the result of the simulation, the ratio of the reflectance factors from wide spread field to different view zenith angles is suggested to give average inclination of rice canopy.

In consequence of this research, bidirectional reflectance characteristics of rice canopy should be analyzed using this model under some kinds of physical conditions.

References

Kimes,D.S., J.A.Kirchner (1982) : Radiative transfer model for heterogeneous 3-D scenes. Applied Optics 21(22), 4119-4129

Kimes,D.S. (1984) : Modeling the directional reflectance from complete homogeneous vegetation canopies with various leaf-orientation distributions. J. Opt. Soc. Amer. A 1, 725-737

Kimes,D.S., J.M.Norman, C.L.Walthall (1985) : Modeling the radiant transfers of sparse vegetation canopies. IEEE Trans. Geosci. Remote Sens. GE-23(5), 695-704

Kimes,D.S., W.W.Newcomb, R.F.Nelson, J.B.Schutt (1986) : Directional reflectance distributions of a hardwood and pine forest canopy. IEEE Trans. Geosci. Remote Sens. GE-24(2), 281-293

Kushida,K., K.Yoshino, E.Yamaji (1994a) : A matching algorithm for rice plant images. J. Japan Soc. Photogrammetry and Remote Sens. 33(3), 33-40 (In Japanese with English abstract)

Kushida,K., K.Yoshino, E.Yamaji (1994b) : Analysis of rice 3-D structure with digital stereo photographs. J. Japan Soc. Photogrammetry and Remote Sens. 33(3), 41-47 (In Japanese with English abstract)

Menzhulin,G.V., O.A.Anisimov (1991) : Principles of statistical phytoactinometry. In *"Photon-vegetation interactions. "* (R.B.Myneni, J.Ross Eds.) Springer-Verlag, pp.121

Ross,J.K., A.L.Marshak (1988) : Calculation of canopy bidirectional reflectance using the Monte Carlo method. Remote Sens. Environ. 24, 213-225

Ground Truth Database for Global Scale Research
- Grassland Bio-mass monitoring using NOAA AVHRR and Ground Truth -

Yoshiaki Honda
Center for Environmental Remote Sensing (CEReS)
Chiba University

1. Introduction

In Semi-arid and arid area, vegetation conditions are quite changed by even small climate changes. Therefore, many people die due to natural disaster, for example, drought. The desertification is enhanced by a human activity (over grazing, over cultivation and deforestation). It is very important to apply a management of ecosystem using satellite information. In this study, a joint research between Japan and Mongolia is reported.

2. Joint Research

This joint research is supported by Konica co., and Mongolia Nature and Environment Agency. The purpose is development of management system for Mongolian grassland. This joint research is under processing like Table 1.

Table 1 Joint Research

Stage	Year	Action
1st step	1993～1995	Bio-mass monitoring by integration obf remote sensing and ground truth data
2nd step	1996～1999	modelling of climate and bio-mass
3rd step	2000～2003	development of grassland ecosystem management

3. 1st. step process

Semi-arid area is the most sensitive area against environmental change or human activity. It is very difficult to measure slight bio-mass using satellite. Therefore, ground measurement is very important. 37 ground monitoring stations were set up from grassland to desert in Mongolia. Each station was working for 16 weeks, from June to September in 1993. Each station took 3 photographs like Fig. 2 - 4 and measure dry grass a weight etc. like table 2. Dry grass weight and green coverage are known from these measurement.

NOAA AVHRR data are received by National Remote Sensing Center in Ulan bator, Mongolia. That receiving station's antenna has a mechanical problem. There are a few HRPT data in 1993. Final result is measurement of dry grass weight from NOAA AVHRR and ground measurement (see Fig. 5).

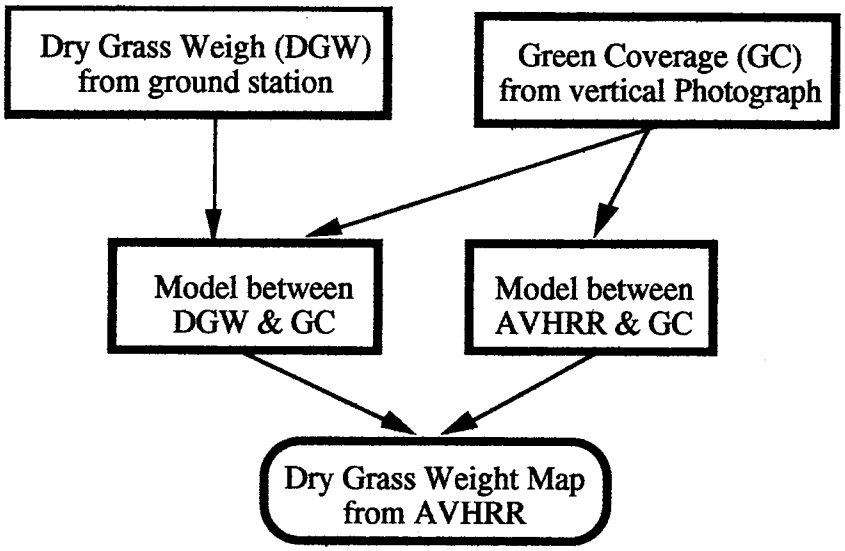

Fig. 5 Flow

4. Result in 1993

26 ground stations had submitted ground measurements until January 1994. Only 19 ground stations data are available data. Fig.6 shows a ground measurement in Man lai. Man lai is a very dry area. Fig.7 shows a ground measurement in Dash balbar. Dash balbar is a dense grassland. It is impossible to estimate dry grass weights from only grass height. Green coverage is very useful for dry grass weight estimation. Therefore, Green coverage ratios were computed from vertical photograph (Fig.8).

Fig.9 shows relationship between dry grass weight and green coverage ratio. There are 4 groups in Fig.9. There are a linear equation between GDW & GC in each group. There are weak correlations over 200g/m^2 dry weight areas.

5. Conclusions

In 1995, 15 ground stations were selected by our joint research group. In 1994, NASA group will fix an antenna system in Ulan Bator. From 1995 Mongolian side can keep every NOAA data.

Reference

1) Y.Honda, K.Fujiwara, S.Murai, S.Goto (1993) Global Change Monitoring of Vegetation using NOAA & Geo-information. International Botanical Conference:63

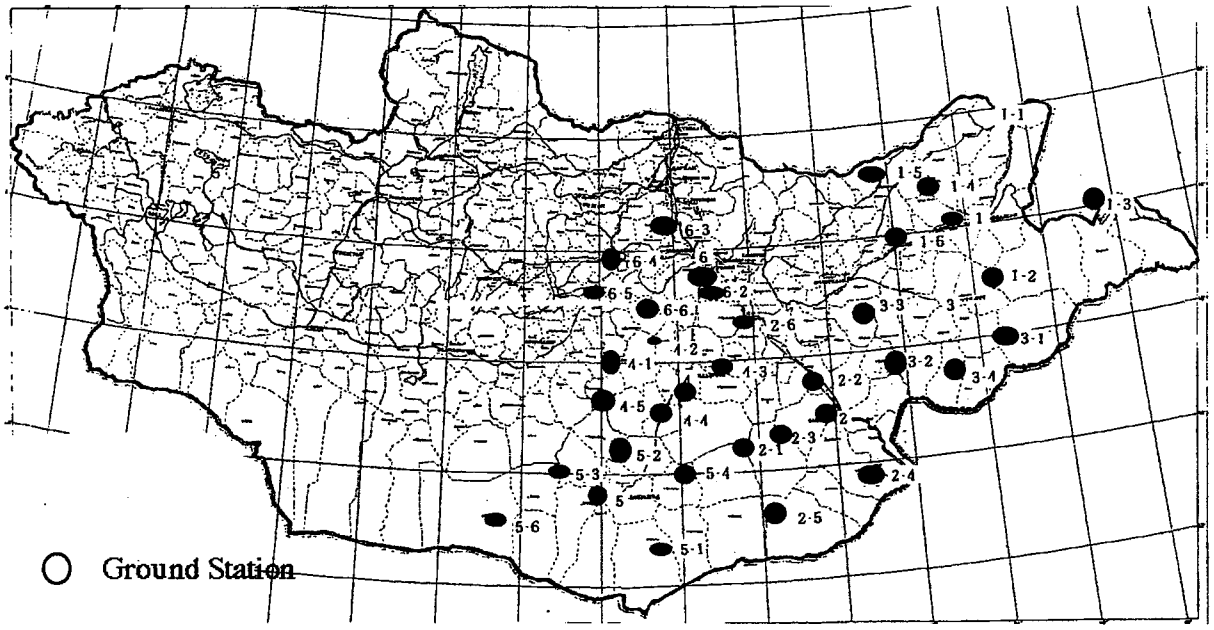

Fig.1 Distribution Map of observing station in Mongolia

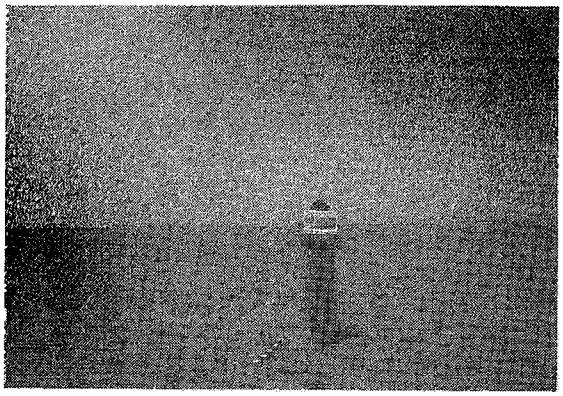

Fig.2 Horizontal photogrph

Fig.3 Horizontal photograph

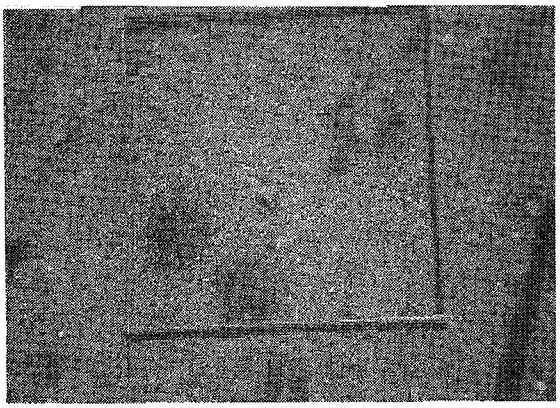

Fig.4 Vertical photograph

Table 2 Ground measurment

Measurement	Unit
Grass height	cm
Fresh grass weight	g/m^2
Dry grass weight	g/m^2

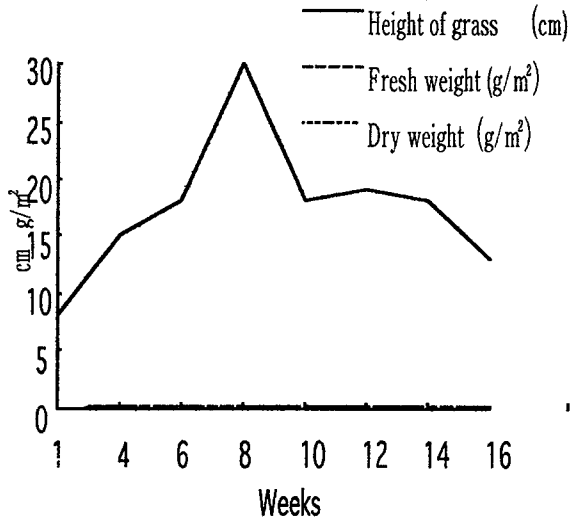

Fig.6 Man lai

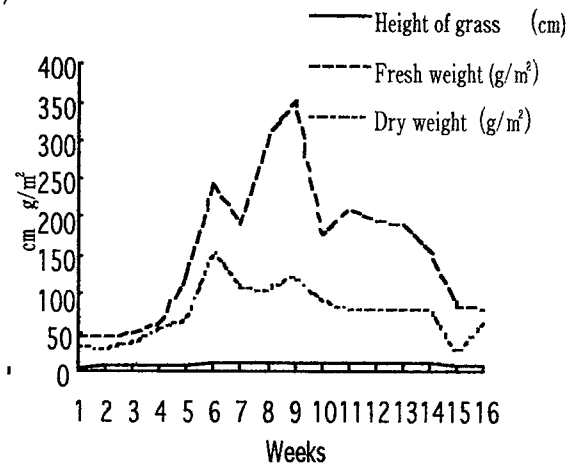

Fig.7 Dash balbar

Vegetation/Non-vegetation data as binary

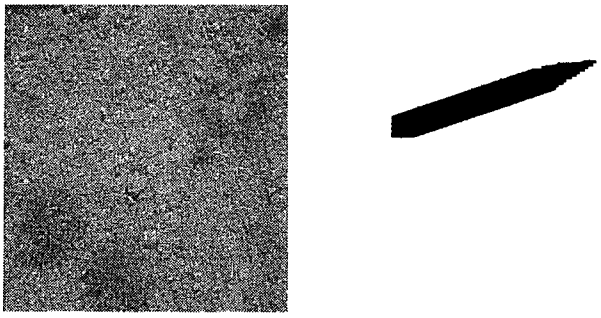

Green Coverage 9.34%

Fig.8 Green Coverage ratio

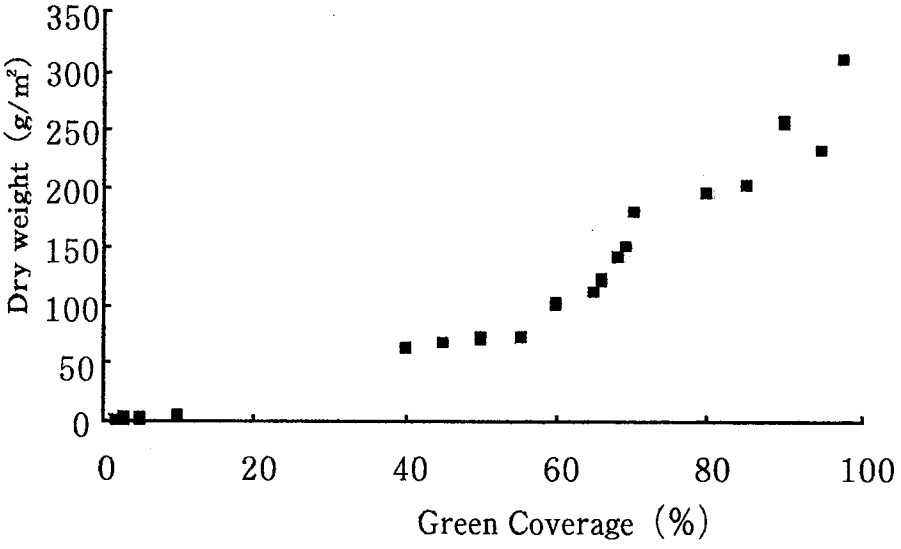

Fig.9 Dry grass weight & Green coverage ratio

Ground Truth Database for Vegetation Remote Sensing

Koji Kajiwara

Center for Environmental Remote Sensing (CEReS), Chiba University, JAPAN

1.Introduction

In the vegetation remote sensing application, especially on quantitative estimation of vegetation parameter such as standing biomass, we must built some indirect estimation models connecting the physical parameter value and the spectral information obtained from remote sensing data. Therefore, we should correct the ground truth spectral reflectance data and physical parameter applicable for modeling. Actually, so many ground measurement were carried out by many researchers and we can find measured reflectance data in many literature. In most cases, however, since ground measurement was made for a specific purpose focused on author's interest, these data are difficult to use for the other applications. In addition, after making the tables or plots of spectral data, we can not know the detail condition of the target.

Considering the continental scale or global scale vegetation monitoring, we need ground truth data and the models designed from them for each typical vegetation type. Currently, it is very difficult to make a standard style for common-usable ground truth database because required parameters for the modeling depend upon what kind of information we want to estimate. But , at least, it is able to select the common information to be measured and/or recorded for each vegetation type.

In following section, which kind of information should be contained in the ground truth database and required specification for spectral measurement system are proposed.

2. General information to be contained in the database

For most vegetation remote sensing application, target of reflectance measurement is vegetation 'colony', not a single leaf. Thus, we should consider the change of reflectance in various observing and light incident geometry, coverage ratio of vegetation, background effect, structure of vegetation colony, etc. The most important information to be cleared is which factor affects apparent spectral reflectance in how much magnitude. In order to create the ground truth database applicable for remote sensed data analysis, we need some models describe the effect of sun-target-sensor geometry and the

vegetation colonies structure.

In table 1, general information to be contained in the spectrum database for grassland measurement are listed. For other vegetation type, items listed in 2nd line of the table will be changed. But observing condition should be always recorded. And the measurement always should be made in various different observing geometry.

Table 1. The information to be contained in the database. (for grassland measurement)

Observing condition	Location & time of Observation, Solar zenith & azimuth angle, Sensor viewing zenith & azimuth angle, observing height, Sensor's field of view spectral resolution
Target condition	average grass height, coverage ratio, background spectral reflectance

In addition, recording the image of the target is important information for the spectrum database. If the database has image information of the target, user can see the condition of the target such as vegetation coverage condition, shadowing condition, etc.

3. Required specification of spectrum measurement instrument

In order to built the models describe the spectral reflection in various conditions, we should make many measurement for same target. For this purpose, spectrum measurement instrument which has capability of quickly measurement is required. This is very important point to design the measurement instrument system. Because, if it takes long time for changing the sensor geometry, we cannot make measurement for various sensor geometry in the same solar geometry.

CEReS has developed the prototype system for grassland spectral measurement instrument. This system can change the sensor geometry by remote control.

In July 1995, we made field measurement for grassland in Mongolia and checked the efficiency of the system. Figure 1 and 2 shows a part of the measurement result. We successes to obtain the spectral reflectance data in various sensor's geometry in short time.

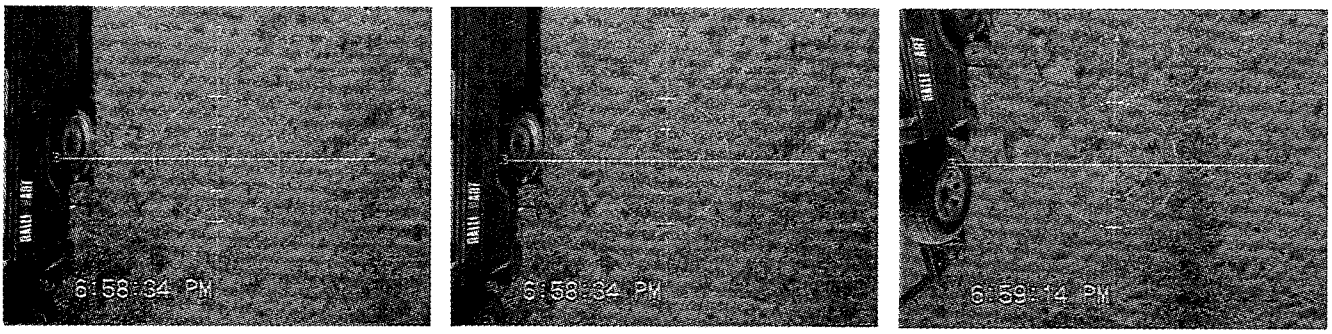

0° 20° 30°

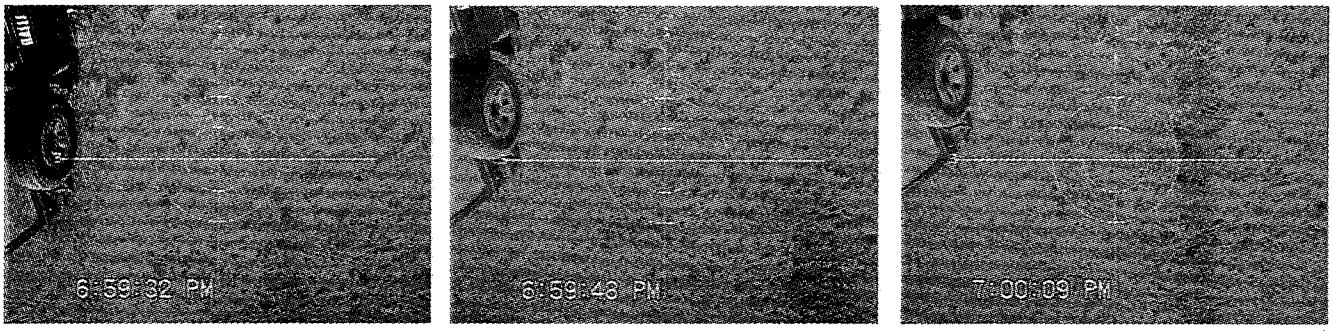

40° 50° 60°

SZ : 63°
SA : 275°
Scan Direction :
275°(Forward scan)

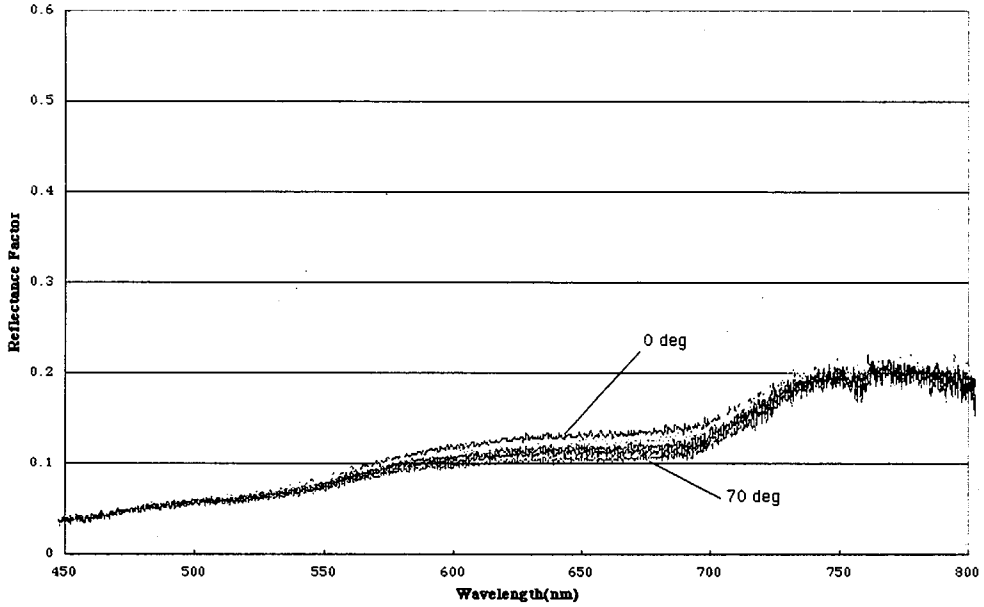

Figure 1. Spectral reflectance of grassland. (Forward scan)

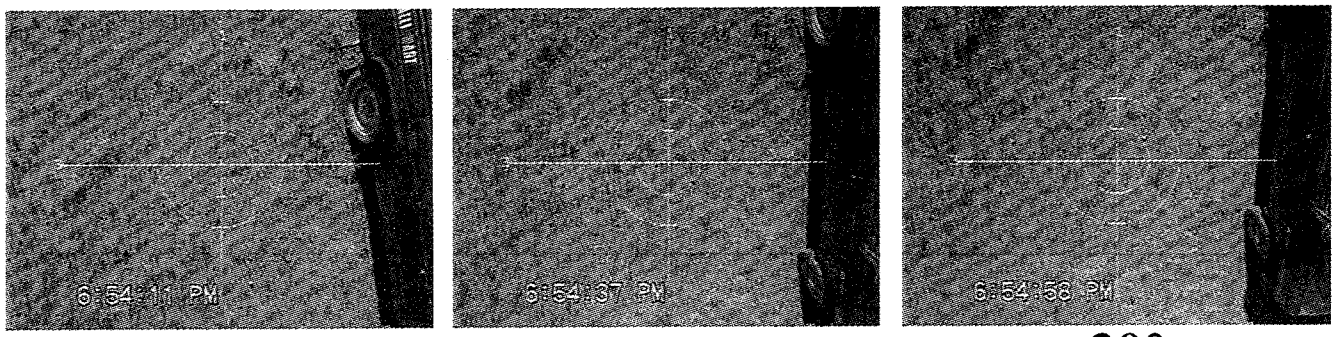

SZ : 63°
SA : 275°
Scan Direction :
95°(backword scan)

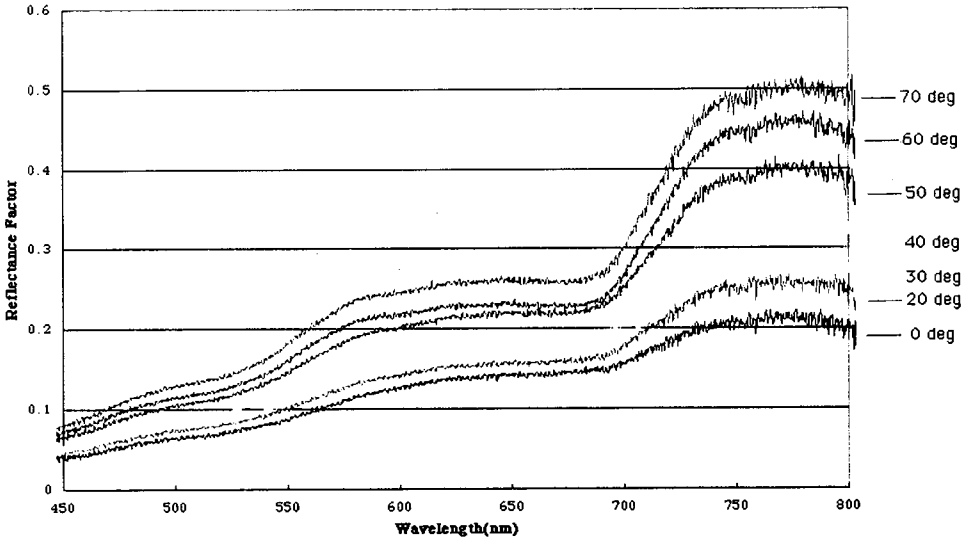

Figure 2. Spectral reflectance of grassland. (Backword scan)

Contribution of Enhanced SAR Imagery for Agricultural Land Use Classification*

Eng. Hussein Harahsheh
Royal Jordanian Geographic Center
Amman / Jordan
1995

Abstract

This study demonstrated how interpretation of SAR images improved our understanding of surface and signal/terrain interaction which result in terms of textures and other's characters of SAR imagery.
Focusing was placed on visual interpretation of SAR images in order to make a good distinguishes between different tones, textures shapes, patterns and signatures. The next step was the establishment of charts for tones and textures, which were employed together with the signature characteristics of SAR images to develop an "interpretation key" for agricultural land use purposes. We applied supervised classifications on Landsat TM images and on Landsat TM images integrated with SAR images. Then comparisons of tones ,textures and patterns were done between the two kinds of images.
We found that characteristics of SAR images such as tone ,texture signature and pattern are very important elements for visual interpretation of land use types , where the importance to establish an "interpretation key" of SAR images , which is already done . A significant difference in terms of texture and pattern was approved. Also SAR imagery was improved our supervised classification using Landsat TM integrated with SAR images .

1.0 Introduction

On December 8 , 1993 Synthetic Aperture Radar (SAR) imagery band C-HH(5.6cm) was acquired over four sites in Jordan , included by the Globesar project. These data were acquired in order to develop some researches and analysis of SAR imageries .This paper will demonstrate how SAR imageries improved our understanding of surface and signal/terrain interactions which result in the tonal , textural and pattern characters of SAR imageries. The specific objectives of this study are to develop interpretation keys for agricultural land-use from SAR integrated techniques, to interpret management practices from enhanced SAR images, to demonstrate what SAR imagery could add for land use classification and to compare SAR images with Landsat images especially in terms of tone and texture.

---

*Presented at the International Symposium " Vegetation Monitoring" ,29-31 August, 1995, Chiba University,**Chiba-JAPAN.**

2.0 Methodology

Emphasis was placed on visual interpretation of SAR imagery in order to make a good distinguishes between difference tones , textures ,shapes and others characters of SAR imagery. The next step was the establishment of charts for tones and textures which are employed to develop an interpretation key for agricultural land-use. We applied supervised classifications on SAR and Landsat imagery, and made a comparison between the two classifications .And a comparison of tones, texture and pattern were done between the two kinds of images.

3.0 Elements of Image Interpretation

Due to the longer of wavelength used for sensing , radar is more sensitive to difference terrain elements than visible , near infrared and thermal infrared imagery (i e Landsat, Spot). Radar back scatter is basically a function of surface geometry(topography) , surface roughness defined by bare ground or vegetation canopy and surface dielectric properties (influence of humidity). These elements of the terrain can be highlighted depending how the radar system is configured . Changes in radar look direction , incidence angle , frequency and polarization can have considerable effect on the enhancement or suppression of certain terrain features.
Element of interpretation of radar imagery for land use and agricultural studies are presented in applications of aerial photography's and other remote sensing imageries. These elements of radar imagery interpretation are ; pattern , shape , size , association , tone , textures. Some rules of photo interpretation can be used for radar image interpretation , which can be divided into three basic procedures:
- Photo reading , this involves recognition of boundaries on the basic of considering all the elements listed above.
- Photo analysis , this involves the recognition of what is within the boundary previously identified.
- Deductive interpretation of image , in this part the interpreter uses all his thematic knowledge and experience and to interpret the data.

4.0 Results

4.1- Interpretation key

Each kinds of land-use was examined and interpreted in terms of tones, textures and signatures. A chart of tones was created in which we distinguished five degrees of tones from dark to light, then a chart of textures was created where five classes of textures were presented from fine to mottled texture ,and we added a class where is no texture appears on the images. Depending on these charts and the signature characteristics of each class of land-use, an interpretation Key for agricultural purposes was established, **Figure 1**shows this result.

4.2- Management practices

Radar imagery show the reclamation and management made by farmers , we can identify exactly the number , shape and pattern of these management practices. Also the boundaries of agricultural fields unless their is no plantation inside were very well recognized.

4.3-Comparison between TM and Radar imageries

We chose two study areas to compare Radar imagery and Landsat TM imagery(acquisition date April 1994) , first area located in north of Madaba and the second located in Azraq area. In this paper we analyzed the first study area.

4.3.1- Study Area

The study area approximately 60 km2 in extent , on the northern plateau of Jordan and situated just south of Amman . Geological formation occurring within the area consist of limestone and alluvial of Cretaceous , and the dominant soils are Chromoxererts and Haploxeraifs. Morphologically the study area is nearly level to gently sloping . In altitude it range from 700m to 1000m. The climate is classified as semi-arid Mediterranean climate , which it is recognized by four seasons with warm summer and cold winter , and average annual rainfall is about 350 mm.

4.3.2- Spectral characteristics

To achieve this , statistical analysis (**table 1**) for six bands of Landsat TM imagery and the band of Radar imagery was carried out . For selection of three suitable bands for FCC generation , the index factor indicated that band 4 , band7 and the radar band form the best combination. The study of individual bands show that the radar band occupies a greater dynamic range (2-255) , and has high variance when compared to others. Near infrared band 4 is having least covariance with radar band. The scattegram combined band 4 and radar data demonstrates the uncorrelation between them which was explained by the small value of covariance.

4.3.3- Radar Characteristics and IHS Transformation

We remarked that texture in radar imagery has great help for identification and delineation of units contained within boundaries of homogeneity. High intensity returns representing a large interception of back scatter appear as light tones in radar image whereas low signal returns appear as dark tones. Also the spatial arrangement of features in radar imagery was distinguished very well.

Landsat TM data (bands 2 , 3 and 4) was transformed in the IHS space , radar was contrast stretched to replace the intensity component , then the image was brought back to original space (RGB). . This transformation was contributed to the visual and automated interpretation interms of texture, structure, shape, topography, and linear features as benefits of Radar band, especially to extract the isolated settlements and houses, and to delineate the boundaries of forests. On the anther hand Landsat TM bands contributed to the interpretation in terms of tone, shape and multispectral characteristics of features. See **Figure 2.**

4.3.4 Classification

A maximum likelihood classification was used with Landsat TM imagery and with Landsat TM integrated with radar imagery. Over 30 training sets were generated using 1:30 000 aerial photography supplemented by field inventory then digitized , and there were at least two training sets for each class, we could separate twelve land cover classes. Statistical analysis reveal a considerable difference in standard deviations between Landsat TM bands and radar band, this is explained by the existing of speckles in radar imagery which should be removed by multiple filtering.

The accuracy and specificity of classifications were assessed and "pixel by pixel" comparison was made between a reference data set and the automated classification . The training sets were used as reference data set . A total number of 21000 pixels (representing about 8% of total number of pixels) were used for comparison purpose, confusion matrices for both classification were generated , the results for which are given in **table 2** The errors of omission and commission derived from the confusion matrix are considerably reduced.
Classification accuracy performance for the specific classes and overall accuracy performance are given in **table 3**. These statistics indicate that inclusion of radar imagery as an additional band in the classification significantly increased the overall accuracy of the classification (from 77.2% to 81.3%) , for agricultural classes the improvement of accuracy was about 11% in average.
The specificity of any given classification was determined by the number of landuse classes that could be identified without significant confusion with other classes, this was essentially a judgment as to whether the classes were sufficiently separable, the errors of omission and commission assisted this determination by showing what proportion of classes were misclassified into which other classes. To study the inter classes separability, inter-distance signature calculation was generated, the average separability improved from 10.9 to 11.9, the maximum change was observed for the barely and plowed area pair (from 19.5 to 27.3) . **Figure 3** shows the result of classification.

5.0-Conclusion

An interpretation key for agricultural land use was performed from radar imagery, this key will allow users to interpret visually radar imagery. It is found that radar imagery provided interesting information about management practices and other linear features.
Radar imagery and Landsat TM imagery have been combined to produce hybrid image data having the spectral resolution of TM and the spatial resolution of radar , we found that an intensity hue saturation (IHS) transformation based on the combination of radar and TM data did improve the delineation of topographic features, urban area and agricultural fields.
Radar imagery and Landsat TM imagery of the study area have been used to separate twelve classes, statistics indicated that inclusion of radar imagery as an additional band in the classification significantly increased the overall accuracy of the classification , approximately 4% of improvement was achieved.
The radar was shown to be critical in providing explanation of surface cover variability.

6.0- Knowlodgement

The author is highly thankful to Prof. Fred Campbell GlobeSAR project manager, Canada Center for Remote Sensing and Dr. Vern Singhroy. P. Eng. Senior Research Scientist, Canada Center for Remote Sensing , for their encouragement to write this paper and their various help.

7.0-Bibliography

-Allan T.D Satellite Microwave Remote Sensing ,1983 New York,USA.
-Lichtenegger J(ESA-Earthnet) and Dallemamnt, Principles of Radar Imagery FAO,Remote sensing center,Rome,Italy 1989.
-Globesar group,Radar Basics,Introduction to synthetic aperture radar remote sensing,1993.
-Singhroy V.H,Radar geology:Techniques and results.
-Singhroy V.H,Radarsat and Radar in Canada.
-Zuidam R.A,ITC Textbook of photo-interpretation Volume VII ch 6:Terrain analysis and photographs,1979,The Netherlands.
-Graham D.F and Harris J:Shuttel imaging Radar-A scenes from Iran and China 1986.Ottawa,Ontarrio,Canada.
-Harris J.R et al :IHS transform for the integration of Radar imagery with other remotely sensed data.Intera Technologies,Canada center for remote sensing.Ottawa,Canada.

"This work is carried out with the aid of a great from International Development Research Center - IDRC, Ottawa, Canada."

Table 1

1-Statistical characteristics of study area(Madaba).

	Band 1	Band 2	Band 3	Band 4	Band 5	Band 7	Radar
Mean	78.8	42.4	55.2	77.5	89.3	47.2	46.8
ST. DV	17.6	11.9	18.9	15.2	24.9	16.4	23.6
Min	51	21	19	31	29	12	2
Max	198	108	146	125	221	126	255

2-Variance-covariance matrix

	Band 1	Band 2	Band 3	Band 4	Band 5	Band 7	Radar
Band 1	305.9						
Band 2	200.7	138					
Band 3	301.5	208.4	329.6				
Band 4	122.2	91.1	113.4	227.3			
Band 5	353.6	245.2	388.1	197.4	607.8		
Band 7	246.2	170.1	274.7	92.9	384.6	266.6	
Radar	84.3	48.9	71.4	-1.2	64.4	55.9	609

3-Correlation matrix

	Band 1	Band 2	Band 3	Band 4	Band 5	Band 7	Radar
Band 1	1						
Band 2	0.977	1					
Band 3	0.949	0.977	1				
Band 4	0.463	0.514	0.414	1			
Band 5	0.820	0.846	0.867	0.531	1		
Band 7	0.862	0.887	0.927	0.377	0.955	1	
Radar	0.195	0.169	0.159	-0.003	0.106	0.139	1

Table2
Confusion matrix comparison

a) Landsat TM

	Wht	Brl	Lnt	Hms	Olv	Frut	Pl A	Rg1	Rg2	Rck	Urb	Fort	Tot	Om	Cm
Wheat	436	7	132	0	3	1	0	33	2	0	0	0	614	178	291
Barely	4	358	5	0	5	0	0	0	13	1	0	0	386	28	271
Lentil	263	24	1326	0	7	0	0	120	67	5	0	0	1812	480	246
Hums	0	0	0	277	14	4	0	0	0	0	0	0	295	18	200
Olives	18	243	35	160	1376	180	100	3	252	1	25	0	2513	1137	486
Fruits	0	0	0	25	160	274	74	0	23	13	0	90	569	295	416
PlowedA	1	5	4	5	107	116	1358	0	1	0	0	0	1692	239	174
RangeL1	2	0	11	0	0	0	0	300	19	0	0	0	332	32	301
RangeL2	0	0	56	0	93	115	0	145	3177	8	14	0	3608	431	430
Rocks	0	0	0	0	0	0	0	0	0	1901	5	0	1906	5	99
Urban A	0	0	0	0	0	0	0	0	16	71	3347	2	3436	89	65
Forests	3	2	3	10	47	0	0	0	7	0	21	3841	3940	99	92

b) Landsat TM and Radar

	Wht	Brl	Lnt	Hms	Olv	Frut	Pl A	Rg1	Rg2	Rck	Urb	Fort	Tot	Om	Cm
Wheat	476	3	182	0	7	0	0	38	8	0	0	0	614	156	148
Barely	2	365	5	0	1	0	0	0	11	2	0	0	386	21	159
Lentil	115	35	1077	0	5	0	0	112	62	6	0	0	1812	335	167
Hums	0	0	1	283	9	2	0	0	0	0	0	0	295	12	125
Olives	30	121	22	111	1599	242	49	1	256	0	28	84	2513	944	271
Fruits	0	0	0	13	110	356	55	0	14	11	0	0	569	213	445
PlowedA	1	0	1	1	125	128	1340	0	1	0	0	0	1597	257	104
RangeL1	0	0	12	0	0	1	0	300	19	6	0	0	332	28	300
RangeL2	0	0	40	0	88	66	0	149	3246	8	11	0	3608	362	371
Rocks	0	0	0	0	0	0	0	0	0	1889	17	0	1906	77	92
Urban A	0	0	0	0	0	0	0	0	14	65	3355	2	3436	81	56
Forests	0	0	4	0	41	6	0	0	9	0	0	3860	3940	66	86

Table 3
Classification accuracy comparison

	TM	TM & Radar	Difference
Wheat	**48.12**	**62.1**	**13.9**
Barely	**54.5**	**66.7**	**12.2**
Lentil	**64.4**	**75**	**10.6**
Hums	**65.6**	**68.8**	**12.8**
Olives	**46.7**	**55.6**	**8.9**
Fruits	**27.8**	**40**	**8.1**
PlowedA	**77.7**	**78.8**	**2.1**
RangeL1	**47.4**	**50**	**2.6**
RangeL2	**78.**	**81.2**	**2.5**
Rocks	**94.5**	**96.1**	**1.1**
Urban A	**95.6**	**95.6**	**0**
Forests	**95.3**	**96.1**	**0.8**
Total	**77.2**	**81.3**	**4.1**

FIG. 1

LAND USE INTERPRETATION KEY

LAND USE TYPE	TEXTURE	TONE	SIGNATURE MEAN	SIGNATURE ST.DV	EXAMPLE
FORESTS	COARSE	GREY	62	26	
ORCHARDS 'OLIVES'	FINE	GREY	51	14	
VEGETA-BLES	FINE	LIGHT	218	37	
ANNUAL-CROPS	FINE	MIXED TONE	35	11	
GREEN-HOUSES	MEDIUM-FINE	LIGHT-GREY	82	22	
GRASS-LAND	MEDIUM-FINE	GREY	45	15	
LOW DENSE FOREST	MEDIUM-COURSE	GREY	51	16	
URBAN AREA	MOTTLED	LIGHT-GREY	91	59	
SALT-PANS	MEDIUM-FINE	LIGHT	156	47	
BASALT AREA	COARSE	LIGHT	136	39	
QUARRIES	MOTTLED	DARK TO LIGHT	71	61	

GLOBESAR PROJECT 1994 RJGC/JORDAN

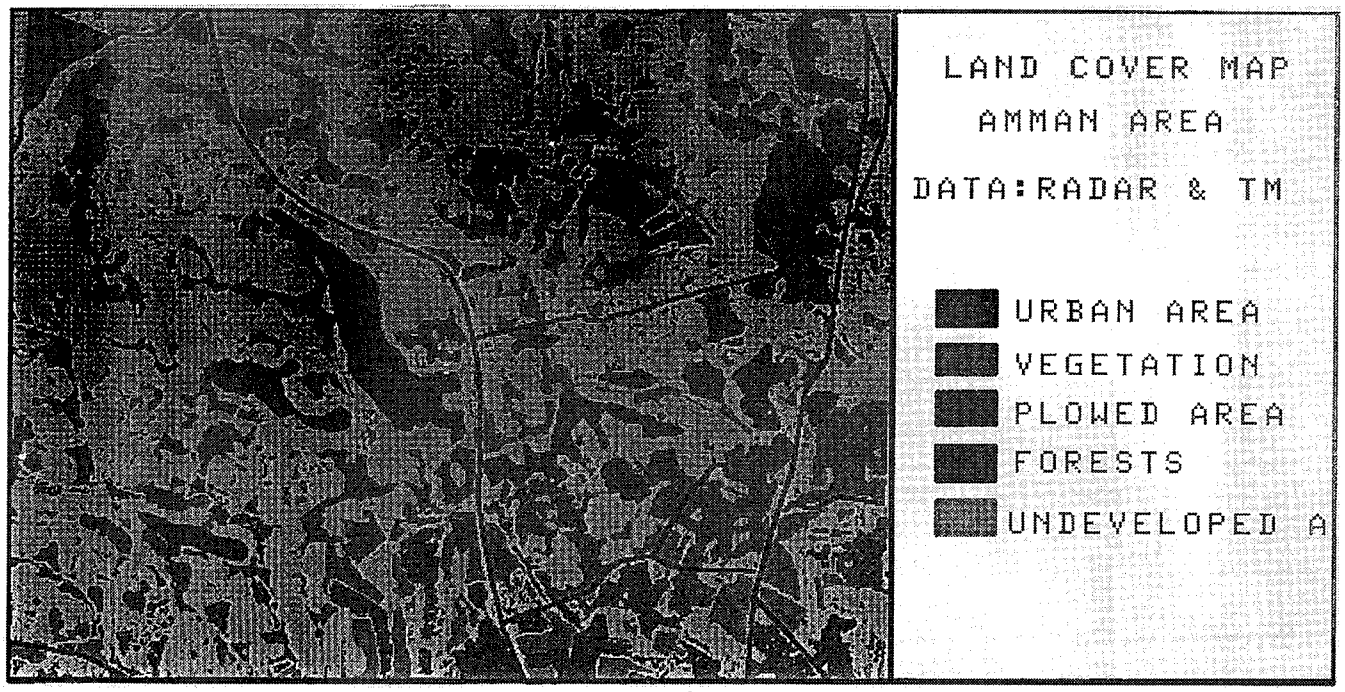

FIG. 2

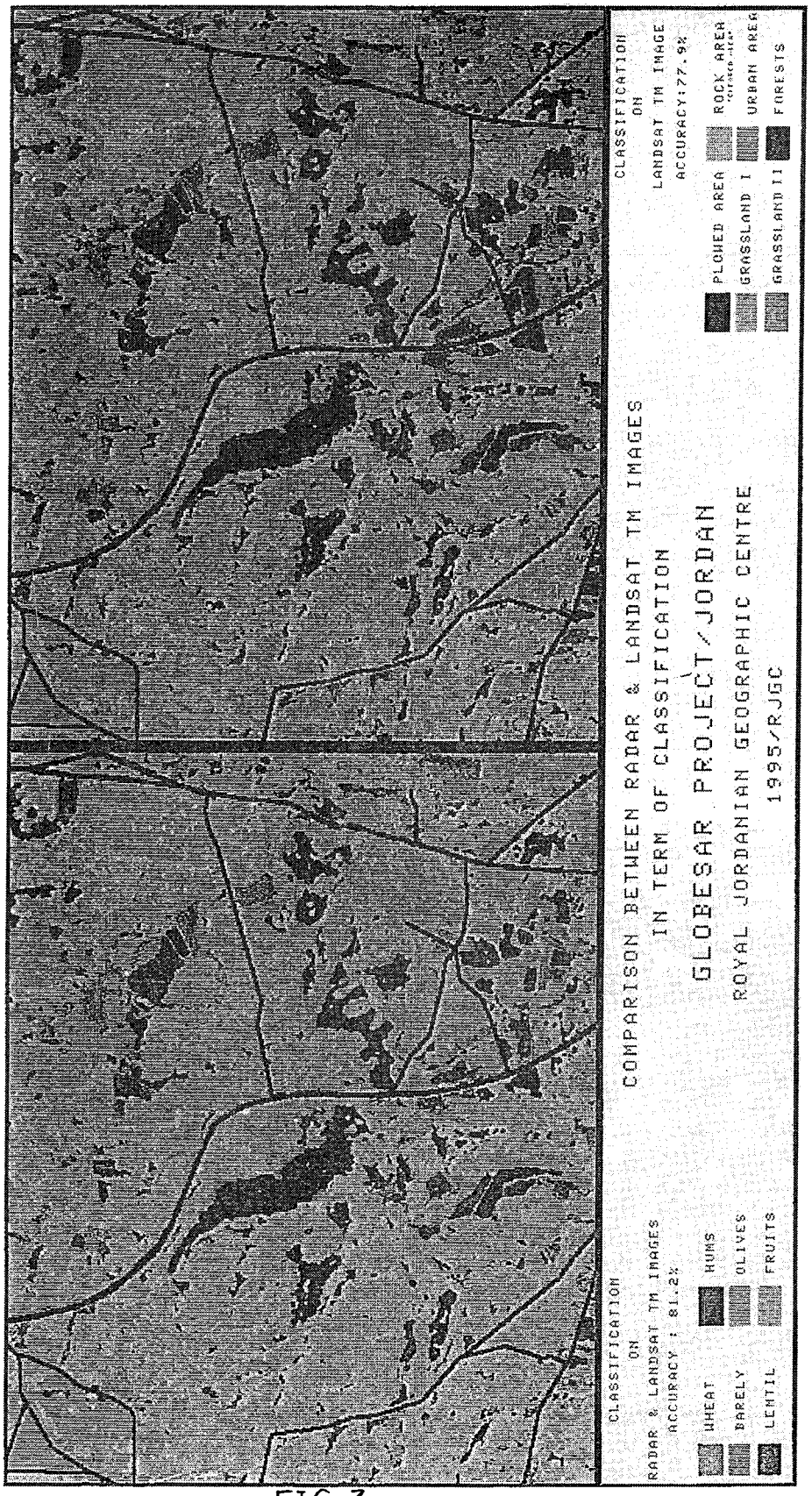
COMPARISON BETWEEN RADAR & LANDSAT TM IMAGES
IN TERM OF CLASSIFICATION
GLOBESAR PROJECT/JORDAN
ROYAL JORDANIAN GEOGRAPHIC CENTRE
1995/RJGC
CLASSIFICATION ON RADAR & LANDSAT TM IMAGES ACCURACY : 81.2%
WHEAT
BARELY
LENTIL
HUMS
OLIVES
FRUITS
CLASSIFICATION ON LANDSAT TM IMAGE ACCURACY:77.9%
PLOWED AREA
GRASSLAND I
GRASSLAND II
ROCK AREA
URBAN AREA
FORESTS

FIG. 3

Phenological Characteristics of Cultivated Vegetation Covers in JERS-1 and ERS-1 Synthetic Aperture Radar Data - Preliminary Results -

Åke Rosenqvist
National Space Development Agency of Japan - Earth Observation Center
1401 Numanoue, Ohashi, Hatoyama-machi, Hiki-gun, Saitama 350-03, Japan

Hiroyuki Oguma
National Space Development Agency of Japan - Earth Observation Research Center
Roppongi First Bldg. 13F, Roppongi 1-9-9, Minato-ku, Tokyo 106, Japan

ABSTRACT

JERS-1 and ERS-1 SAR data have been used to investigate the usefulness of space borne synthetic aperture radar for monitoring of three different vegetation types and their subsequent growing stages. One study area is located on Peninsular Malaysia, where rice paddy, rubber and oil palm are the dominating crop types, and the other in Niigata, Japan, where rice paddy is being studied.

Results show a clear (positive) correlation between the L-band backscatter and the different growing stages for all three vegetation types. For rubber and oil palm the correlation is most pronounced during their early growing stages after which the signals become saturated before the plants reach their fully grown stages. For paddy, the backscattered signal appears to be sensitive even for fully grown plants. The behavior of paddy in SAR data is however different when comparing the paddy sites in Malaysia and in Japan. This is a result of different geometrical properties of the paddy fields, which, in turn, are due to special growing practices in the both countries. For rice fields in Japan, preliminary results show a significant difference in backscatter response dependent on the planting direction of the rice. This feature is not apparent for rice paddy in Malaysia.

C-band backscatter proved virtually insensitive for detecting different growing stages for rubber trees, but, surprisingly enough, showed a clear correlation for oil palms. This effect is due to the different architecture of the two tree types. Due to lack of multi-temporal ERS-1 data, rice paddy has not been investigated for C-band.

Keywords: SAR, rice paddy, rubber, oil palm.

INTRODUCTION

Space borne SAR is a very interesting complement to traditional optical sensors for vegetation monitoring, in particular for monitoring of agricultural crops where its all-weather capability enables regular data takes during the growing season.

Preliminary results from two efforts to monitor the growth of irrigated rice with JERS-1 L-band SAR, one in Malaysia and one in Japan are being presented in this paper. Although the projects are on-going, results obtained up to date are being discussed. The paper also briefly presents results obtained from studies of C- and L-band backscatter for rubber trees and oil palms in Malaysia.

WORKING APPROACH

Fieldwork in Malaysia were conducted in April '94, one week prior to the JERS-1 pass, and in August '94, during acquisition. In total, some 150 test fields were selected for ground truth. For rubber and oil palm the following parameters were measured or estimated: tree/plant height, stem dbh, planting density, canopy closure, planting direction, ground vegetation and slope. For rice paddy, information about growing stage, plant height, soil condition and soil texture were collected.

Fieldwork in Niigata, Japan, is currently being conducted every 44 days, i.e. at every JERS-1 pass, for detailed study of the relationships between radar response and relevant parameters for rice growth, such as plant height, planting density, planting direction, plant moisture content and leaf area index.

The JERS-1 and ERS-1 data was processed to level 2.1 and "PRI", respectively (3 looks intensity image; range and azimuth correlated; ground range). Sub-images covering the test fields were co-registered with an overall RMS accuracy of 0.5 - 0.7 pixels. The pixels covering the selected test fields were extracted and the normalized radar cross section, σ^o, was computed for each field as follows:

$$\sigma^o = 10 * \log_{10}[(DN^2)_{mean}] + CF$$

where,
DN is the digital number of a pixel in the SAR image and CF is an offset calibration factor.

The fields were then divided into groups corresponding to vegetation type and growing stage, after which group means and std.dev. were computed.

RESULTS

Irrigated rice in Malaysia

Rice paddy in Kedah and Perlis states in the northern part of West Malaysia is planted in April and May and harvested about 120 days later, in August and September. A second season stretches from October-November to February-March. One full growing season typically comprises the following stages: plowing, soil preparation/inundation, planting, plant growth, budding, ripening and harvest. In order to preserve the water for the following season, the fields are normally not drained before harvest.

Planting is performed either by manual planting in inundated fields or by so called broadcasting, where seeds are spread on wet bare soil fields. In the former case, the inundated fields appear black in the SAR image as the backscattered signal from the water surface is very low, between -17 and -15 dB. Ripples or waves on the water caused by wind or rain have no effect on the L-band backscatter. As for broadcasted fields, the soil surface is typically wet and very smooth, giving rise to about the same low backscatter as for inundated fields.

The target response increases only slowly during the first 1.5 month after planting, with about 1 dB in average, as the tender plants barely affect the signal. Throughout the following 1.5 months however, as the plants grow to their full length of about 100 cm, a significant change can be seen in the backscatter which apparently follows the plant growth. It reaches its maximum value about 3 months after planting.

During the last month before harvest, a decrease of about 1.5 dB can be observed in the SAR data. This event coincides with the final growing stage of the rice plants when the moisture contents in stalks and leaves decrease and the rice begins to ripen.

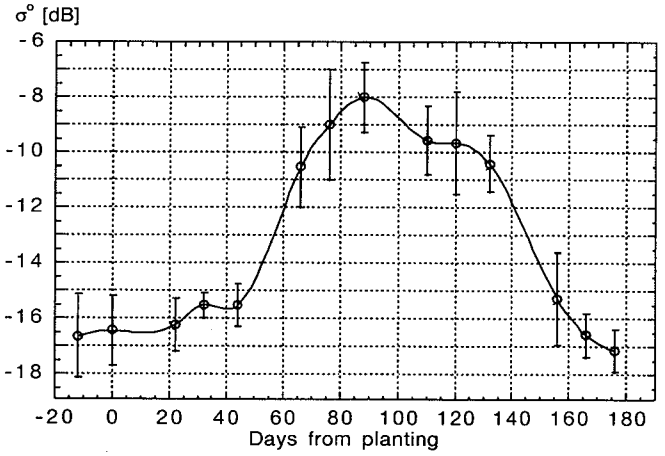

Figure 1. Temporal behavior of JERS-1 L-band backscatter observed for irrigated rice in Malaysia. Day 0 corresponds to the day of planting, day 120 to the day for harvest. Errorbars show +/- 1 standard deviation.

As the plants finally are removed during harvest, a significant decrease in the backscatter would be expected. The large harvesting machines however, leave deep wheel tracks in the soft smooth soil and the increased surface roughness partly compensates for the above loss. The net effect is a mere decrease of about 1 dB.

After harvest however, σ^o again undergoes a drastic change, falling some 6-7 dB in 1.5 months. Although it has not been verified more than once during field work, it is believed that weathering and additional water supply contribute to breaking down the rough soil surface.

Fig.1 shows the temporal change of the radar backscatter during the full growing season April-October 1994. The error bars show ±1 standard deviation for σ^o for each respective growing stage. Day 0 indicates (estimated) day for planting; day 110 ripe fields; day 120 a mix of ripe and harvested fields; and day 132 harvested fields.

Irrigated rice in Japan

Rice cultivation in Japan is in many respects different from that in Malaysia, both physically and with regard to growing practices. In the Niigata area, the paddy fields are very small, typically only some 60 by 70 meters in size and neighboring fields are separated by low mud barriers, some 10 cm high. Roads large enough to carry a car run parallel with the fields at a distance of no more than 200 meters from each other.

Planting is performed by mechanical planting devices mounted on the back of small tractors. This results in near-perfect straight lines of rice plants, which as we shall see later, has a most significant effect on the radar backscatter. The fields are always irrigated at the time of planting, which in this area of Japan occurs during the first week of May every year. Depending on the species, the growing period varies between 120 and 135 days. As a part of the normal practices, fields may be irrigated and drained several times during the growing period, depending on weather conditions, need for additional nutritions etc.

Due to the above circumstances, monitoring of rice growth in Japan is not as straight forward as e.g. in Malaysia. The fact that different species well may be planted at fields next to each other, or that one field may be irrigated while the next one is drained further complicates the picture. On the other hand, as almost all fields are planted within a period of a week or 10 days, they are all at approximately the same growing stage, independent of the species. The fact that the soil surface of drained fields normally is moist and very smooth, also decreases the difference in backscatter between drained and irrigated fields.

Dependent on the geometric properties of the fields, the radar backscatter varies significantly. Fields with rows oriented in range direction have a

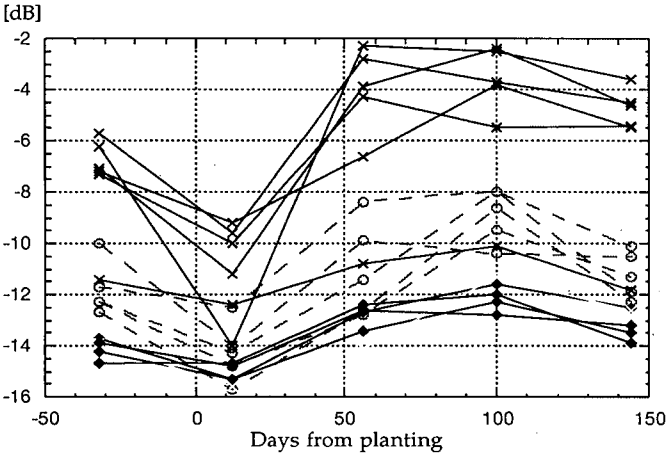

Figure 2. Temporal behavior of JERS-1 L-band backscatter for irrigated rice fields in Niigata, Japan. "x" corresponds to fields planted in range direction, "o" to fields planted in azimuth and "♦" to fields planted in other directions.

very different appearance compared to fields with other planting directions, both in terms of total temporal radiometric dynamic, as well as in terms of the initial intensity for bare soil fields. A dynamic range of about 7 dB for fields planted in range direction has been observed, compared to only some 3 dB for fields planted in other directions. A second peak of has been observed for fields planted perpendicular to range, i.e. in azimuth direction, showing a total radiometric range of approximately 5 dB (Fig. 2). An important observation, however, is that the overall shape of the temporal curve, resembling the temporal curve for fields in Malaysia (Fig. 1), appears to be the same for any planting direction.

Analysis of the variations in the total temporal radiometric ranges between fields with different planting directions is apparently not trivial. At first thought, one could expect that fields planted in range direction would give rise to a lower backscatter, opposite to what has been observed, since the open spaces of water or bare soil between the plant rows are most visible then and a large part of the transmitted signal therefore would not be scattered back. In any other direction, the ratio of rice plants vs. open space would be much larger and thus result in a stronger backscattered signal. But as we have seen, this is not the case. A possible explanation to the strong backscatter is that the strict geometry of the planting rows and columns result in that all plants within one resolution cell (18*18 meters) interact to give rise to a uniform strong backscatter response. For fields oriented in other directions than range direction, the strict geometry will instead cause the backscatter to decrease. The fact that the planting geometry is strict in row direction, i.e. the direction which the tractor has been moving, but less strict in the direction perpendicular to this, may explain the second peak that occurs for fields planted in azimuth direction. Here, the lines of plants are not as straight as the rows in the planting direction. Nevertheless, it appears to be sufficient to enhance the backscattered signal above the level of fields oriented in other directions.

The initial offset variation in the backscatter for fields with different planting direction can be explained as resulting from backscatter caused by the roads and mud barriers which contaminate pixels near the edges of the fields. Roads oriented perpendicular to the range direction give rise to a strong backscatter caused by a dihedral type of double bounce of the radar signal on the smooth soil and the road sides. Due to the very small sizes of the fields however, it is difficult to exclude such pixels.

It is obvious that the above discussion about the backscatter mechanisms are mere speculations and that a more thorough study is required. Such a study is currently under way, aiming at providing a more solid theoretical background to the directional behavior of paddy fields in Japan.

Rubber

Next, let us return to Malaysia, to have a look at the backscatter behavior at L- and C-band for two common tree crops; rubber trees and oil palms.

Rubber trees in Malaysia normally grow to a total height of 12 - 20 meters, depending on the soil and terrain conditions. The trunk diameter seldom exceeds 30 cm. After 20 - 25 years, the productivity decreases and the fields are normally cleared for a new generation of trees to be planted.

Results from the current study show a clear correlation between JERS-1 L_{HH} band backscatter and tree height (Fig. 3). The dynamic range is about 5 dB, with the signal saturating at a tree height of about 12 meters. Tree height is closely correlated to growing stage for individual stands but depending on

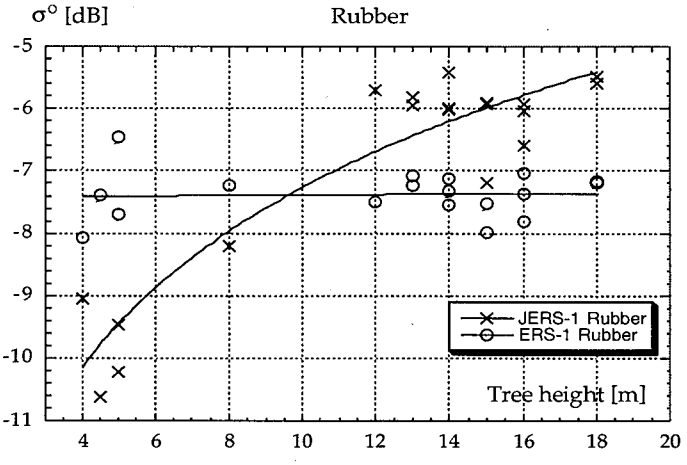

Figure 3. L- and C-band backscatter vs. rubber tree height.

soil and terrain conditions, growing speed and height at full growth vary between stands. In general however, 12 meters will correspond to an intermediate growing stage, implying that saturation occurs before the stands reach their full growths. The major scattering mechanism for rubber trees is ground /trunk interaction and scattering on twigs and branches. The leaves have little effect on the total backscatter.

ERS-1 C_{VV} band data shows no correlation between backscatter and tree height for rubber, σ^o varying between -7 and -8 dB even for newly planted fields. The major scattering mechanism at C-band is scattering on the leaves and twigs. This insensitivity even for the young stages when the canopy is not yet fully developed may be due to that the ground is covered by grass and/or so called legumes with leaves of about the same size as rubber leaves.

Oil palm

Oil palms normally grow to a total height of about 12-16 meters, including the large fern-like branches which extend from the top of the trunk like an umbrella. The trunk is very rough, with scales like a large spruce cone. As with rubber, the oil palms are productive for about 20 - 25 years, after which they also will start to fall over if they are not cleared.

For L-band, the dynamic range between newly planted and old oil palm plantations is about 4 dB. The signal saturates at a level of around -7 dB, which is about 1 dB lower than for rubber. This difference can be attributed to the difference in structure between oil palms and rubber trees. Due to the very rough surface of the trunks of the palm trees, the ground/trunk interaction is likely contribute less to the total backscatter, while, on the other hand, the contribution from the canopy with its large branches can be expected to contribute more. Attenuation by the canopy layer in both directions can be assumed to further weaken the double-bounce effect from the trunks and the ground.

For C-band, there is a clear correlation between radar backscatter and growth of the palm trees, in strong contrast to the situation for rubber. The dynamic range is about 3 dB with saturation around -6 dB, about 1.5 dB higher than the saturation level for rubber. With the large leaves and branches of the palm trees, the canopy layer is expected to be the by far most dominating scatterer for C-band.

Fig. 4 and 5 show the L- and C-band backscatter as functions of the height of the trunks and the length of the branches, respectively. Notable is that the radar responses are very similar for L- and C-band, for both trunks and branches, indicating that the major scatterers for both frequencies may be the same. Given the better separability by branch length than trunk height for young palms further leads to the conclusion that the large branches are the most significant scatterers also at L-band.

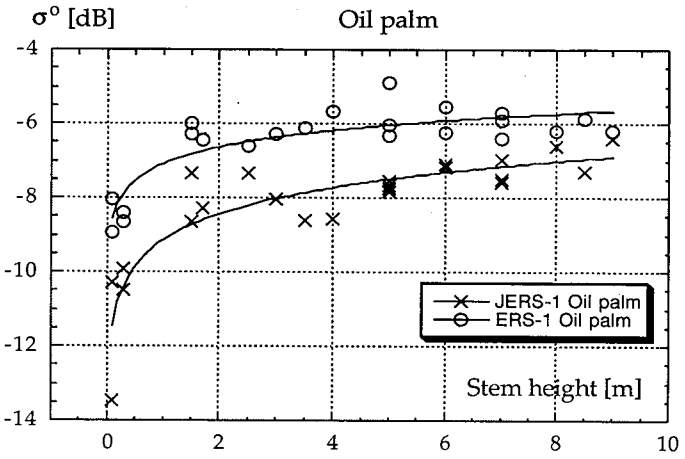

Figure 4. L- and C-band backscatter vs. oil palm stem height.

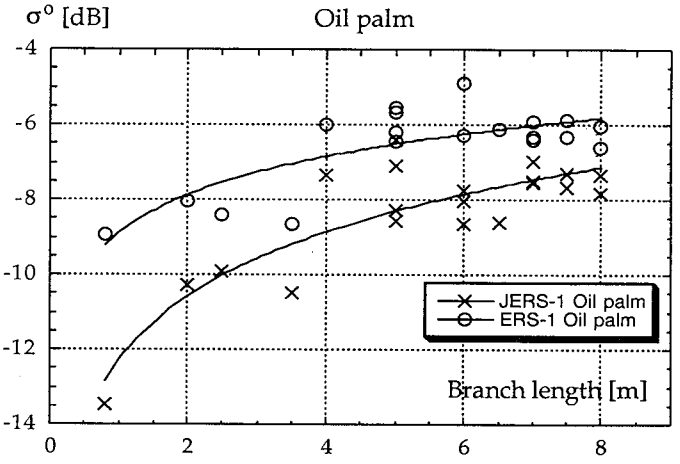

Figure 5. L- and C-band backscatter vs. oil palm branch length.

SUMMARY

Results presented in this paper show that L_{HH}-band SAR is sensitive for different growing stages of irrigated rice. The backscatter reaches it peak value about one month before harvest, after which it drops about 1.5 dB. The total radiometric ranges for paddy fields in Malaysia and paddy fields in Japan were however found to be different. The backscattered intensity for paddy fields in Japan were found to be strongly dependent on the planting direction of the fields, while in Malaysia, the backscattered signal was very homogeneous. The difference between the backscatter behavior can be explained by that in Malaysia, where manual planting broadcasting is practiced, the rice plants can be considered spread randomly over the fields, while in Japan, mechanical planting result in fields with strict geometrical patterns. The difference in size of the fields was found to be another factor which had significant effect on the radar backscatter.

The results from the study of rubber and oil palm show that L_{HH}-band SAR is sensitive for monitoring the growth of the two tree crops to a certain level. C_{VV} band in turn, proved to be virtually insensitive to the growth of rubber in the test area, while being correlated with the growth of young oil palm up to a (trunk) height of 2 meters after which the signal saturated. The saturation levels for rubber and oil palm were found to be different. In conclusion, L- and C-band SAR appear to complement each other quite well for monitoring of the two tree crops. C-band seems suitable for distinguishing the two species as it saturates at different levels already for young growth. L-band appears more useful for monitoring growth, as well as for distinction between the species for fully grown plantations.

ACKNOWLEDGEMENTS

The study of the Malaysian crops was performed as a part of a joint research cooperation between the National Space Development Agency of Japan (NASDA), the Malaysian Centre for Remote Sensing (MACRES) and the Malaysian Department of Agriculture (DoA). Field work was performed jointly by the agencies, while the data analysis presented in this paper was performed at NASDA by Å. Rosenqvist.

The study of irrigated rice in Japan was performed by NASDA in cooperation with local farmers in the Niigata area. Field work was performed by Å. Rosenqvist and H. Oguma, analysis work performed by Å. Rosenqvist.

REFERENCES

Dobson M.C., Ulaby F.T., Le Toan T., Beaudoin A., Kasischke E.S. and Christensen N. (1992). Dependence of Radar Backscatter on Coniferous Forest Biomass. *IEEE Transactions on Geoscience and Remote Sensing,* 1992, Vol. 30, No. 2, pp 412-415.

Hsu C.C., Shin R.T., Kong J.A., Le Toan T. and Beaudoin A., (1993). Application of Theoretical Model for Microwave Remote Sensing of Forest. *International Geoscience and Remote Sensing Symposium (IGARSS'93).* Tokyo, Japan, August 18-21, 1993. Digest, pp 595-597.

Karam M.A., LeVine D.M., Amar F., Fung A.K., Mougin E. and Lopes A. (1993). Understanding the Relation between Forest Biomass and the Radar Backscatter Signals. *International Geoscience and Remote Sensing Symposium (IGARSS'93).* Tokyo, Japan, August 18-21, 1993. Digest, pp 573-575.

Kurosu T., Fujita M. and Chiba K. (1994). Rice Crop Monitoring with ERS-1 C-band SAR. *Final Report of JERS-1/ERS-1 System Verifivation Program, Vol 2, pp 120-126.*

Miranda F.P. and Carr J.R. (1994). Application of the Semivariogram Textural Classifier (STC) for Vegetation Discrimination Using SIR-B Data of the Guiana Shield, Northwestern Brazil. *Remote Sensing Reviews*, 1994, Vol 10, pp 155-168.

Ramberg E. (1984). Zeroes in the Gauss-Doolittle Scheme. *Lantmätar Digest 1984.* Royal Inst. of Technology, Stockholm. KTH-fmi/Lmk-84.

Rosenqvist Å. (1995). Evaluation of L-, C- and S-band SAR for Characterization of Tropical Tree Crops. *Remote Sensing in Action '95; 21st Annual Conference and Exhibition of the Remote Sensing Society.* Southampton, UK, Sept. 10-14, 1995.

Le Toan T., Laur H., Mougin E. and Lopes A. (1989). Multitemporal and Dual-Polarization Observations of Agricultural Vegetation Covers by X-Band SAR Images. *IEEE Transactions on Geoscience and Remote Sensing,* 1989, Vol. 27, No. 6, pp 709-718.

Yamagata Y., Shibayama M., and Akiyama T., (1987). Measuring equipment for all weather monitoring of agricultural fields - estimation of LAI and dry weight. (Japanese). *56th Japan Symposium on Agricultural Crops, 1987.*

Land Use Change Study of South East Asia (LUCS-ASIA)

Ryosuke SHIBASAKI, Masataka TAKAGI and Koki IWAO
Institute of Industrial Science
The University of Tokyo
7-22-1,Minato-ku,Tokyo 106 JAPAN
fax:+81-3-5411-0441
e-mail:shiba@shunji.iis.u-tokyo.ac.jp

ABSTRACT: In Asia, especially South East Asia, which is growing most rapidly in the world, land use is changing very drastically. Rapid land usechanges cause a variety of serious environmental issues. However, we are stillsuffering from serious lack of information and tools to handle and analyze it forformulating better land use management schemes. To learn lessons in the past,and to support decision for the future, LUCS-ASIA Project set up severaltargets such as geographic data development which allow us to trace the pastchanges and their consequences, development and coupling of environmentalsystem models and development of GIS-based computer technologies forhandling a mass of geographic data. To pursue these targets, key technologiesare identified and development projects are now promoted. Present status ofthese key technologies and future prospects for the development are discussed.

1.Land Use Changes and Environment in Asia ----Background of LUCS-ASIA Project----

Asian region is growing region most rapidly in the world. Land use is also changing very drastically. Expansion of agricultural land results in rapid deforestation and soil degradation, while many cities are growing as "mega cities", attracting larger population and emitting carbon dioxide and other pollutants.

Land use changes cause a variety of serious environmental issues. Followings are examples of such impacts to human environment.

1) Damages to human health;
   - -water pollution due to fertilization and urbanization.
   - -air pollution due to traffic and industrialization.
   - -toxic chemicals due to pesticide application.

2) Threats to sustainable agricultural food production and risks of famine
   - -soil degradation (salinization, erosion)
   - -population explosion
   - -increase of livestock
   - -climatic impacts on water resource availability

3) Threats to sustainable biomass energy production
   - -degradation of forest biomass

4) Acceleration of global climate changes
   - -emission of carbon dioxide due to decrease in energy consumption efficiency, and deforestation (Houghton et.al.1983)

-emission of methane due to waste processing, paddy field development and livestock increase

These are examples of environmental impacts from land use changes. On the other hand, impacts and damages may be enhanced under some specific land use patterns. Concentration of population and economic activities in low flat lands in coastal regions may increase vulnerability to sea level rise.

Land use is one of major interfaces between socio-economic systems and local/global environmental systems. In order to control and mitigate environmental impacts from land use activities, more advanced land use management schemes have to be formulated and implemented urgently. Better management of land use is very important due to the following reasons.

1) Impacts due to failure of land use management likely threaten the basis of continuous human habitation such as stable food production and drinking water supply.

2) Land use can be a dimension which allow us to harmonize environmental policies at local/national level and global level, because land use at national/regional level is large enough to affect global environmental systems and at the same time small enough to be directed by national development planning and land policies.

2. Objectives----Approach of LUCS-ASIA

However, we are still suffering from serious lack of information and tools to handle and analyze it for formulating better land use management schemes. To learn lessons in the past, and to support decision for the future, following objectives are set up for this LUCS-ASIA Project.

The project will be driven by a core group of universities in Japan under the cooperation with research institutes/universities and governmental organizations in SE Asian countries.

1) GIS database development:

It has passed more than 20 years since Landsat satellite was launched for land observation. Using remote sensing data, especially high resolution remote sensing data, time-series of land use/land cover data in the past 20 years are developed. The land use/land cover dataset will be developed with close coordination with Landsat Pathfinder Project and Asia 1km Land Cover Data Project chaired by Prof.TATEISHI, CEReS, Chiba University. In LUCS-ASIA, in addition to land cover/land use database, more comprehensive GIS databases will be developed including environmental resource data, basic geographic data such as digital elevation data, and socio-economic data such as population and agricultural production data. These will be integrated to describe the dynamics of land use/environment/resource changes in Asian region.

2) Model development and coupling

To understand and simulate dynamics of land use changes and their consequences, we have to develop models of land use changes, water cycles (to be a part of climate system),

biogeochemical cycles. Land use change models is a major driving force of land use/ environment dynamics. There have been several national-level studies on land use changes. However many of existing models such as (Matsuoka et.al. 1994, Iverson,L.R. et.al. (1993) etc. are not very successful in representing mechanisms of land use changes, because those models are based on empirical relations of macroscopic national statistics such as national population density and forest area percentage. More mechanistic models making full use of geographic information are keenly needed for more realistic simulations and supporting policy-formulation.

For more detailed and mechanistic description of major actors in water and biogeochemical cycles, we may need to develop vegetation model and soil model separately. Vegetation and soil models will link water cycle and biogeochemical cycles. Soil model is also important in describing possible soil degradation and their impacts on agricultural productivity.

Development, coupling and visualization of the dynamic models will be supported by GIS with enhanced capabilities for temporal data management and integration.

3)Development of a computer environment ---Distributed very large GIS databases---

Huge amount of data have to be stored and processed to handle and analyze remote sensing images such as Landsat images. For example, approximately 600 Landsat scenes will have to be processed, mosaiced and classified to generate 20-year time-series land use/land cover data for SE Asia. Very large GIS databases will be developed and distributed among research member organizations as a information infrastructure. At the same time, development of national databases in each SE Asian country members can also be encouraged by sharing experiences and knowledge for developing very large GIS.

4) Exchanges and sharing knowledge and databases for promoting better management of environmental resources

The GIS databases and knowledge will be exchanged and shared among project members during the project for better management schemes of land use and environmental resource. In addition, information on the present and future (possible) status of environment and resources in SE Asia will be distributed and visualized for supporting policy formulation, calling public attentions to environmental issues and even for environmental education through network.

Figure.1 schematically shows the targets of LUCS-ASIA project. Figure.2 summarizes examples of research subjects of the project.

3. Key Technologies ---Prospects of development and present status

Key technologies in the first stage of the project are identified, and present status/future prospects of the development are summarized.

3.1 Development of time-series land use and land cover datasets

To develop time-series land use and land cover datasets, a large numbers of high resolution data have to be geo-coded (mosaiced) and land use/land cover changes have to be extracted

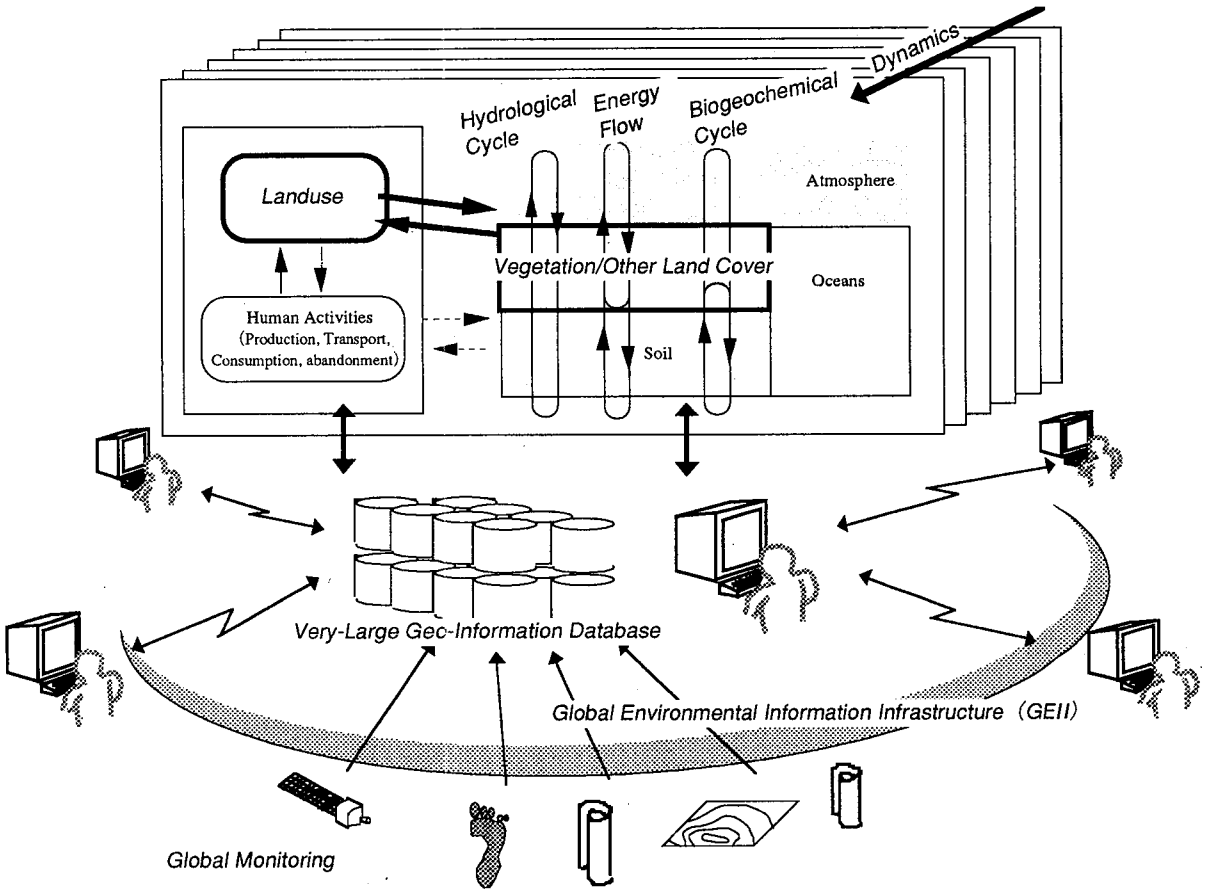

Fig.1 Ecosystem, Climate and Landuse Models, and Global Environmental Information Infrastructure of SE Asia

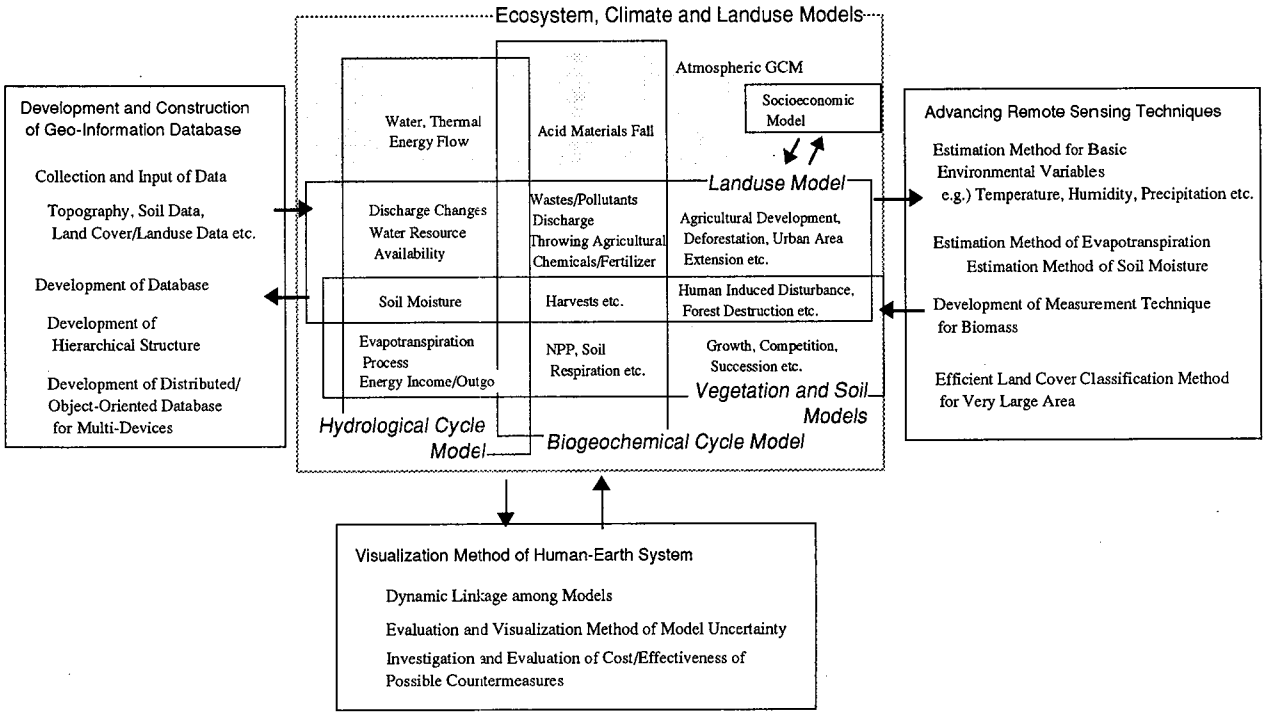

Fig. 2 Examples of researh subjects and their relaitons

stably and reliably.

To automate geo-coding process, techniques of extraction and matching of conjugate points and ground control points have to be developed. For conjugate points, common feature points have to be extracted and matched between neighboring images, while for ground control points common feature points are to be identified between digital map data such as Digital Chart of the World (DCW) and remote sensing images. Selection of interest operator for extracting feature points and development of a reliable matching procedure and robust error adjustment method over entire conjugated scenes are major research topics.

For reliable detection of land use/land cover changes through classification of time-series Landsat images, fluctuation in detecting changes due to independent classification errors in each time-slice image have to be eliminated. To decrease the fluctuations and even to improve classification efficiency, supervised classification with common training data and corrected image data will be tested. And to complement cloud cover and insufficient frequency of observation, remote sensing images such as NOAA AVHRR images with coarser resolution and higher observation frequency will be overlaid with a hierarchical structure.

For training/reference data and validation data, existing paper maps such as topo-maps and land use maps are now being collected and digitized. In parallel, database of ground photos is being developed by using GPS camera. With GPS camera, ground coordinate values and a viewing angle can be recorded together with pictures, which can be scanned to develop a ground picture database.

3.2 Very large GIS database development

Since the total size of remote sensing images and other geographic data will exceed several ten terra byte, Juke box of 8mm tapes and D1 tapes is used. To improve the performance of database drastically, database architecture is under development based on parallel processing. Juke boxes, though the capacity is very large, are not very quick in recording and reading data compared with hard disks. Hierarchical structure where very large raw data is stored with Juke boxes while aggregated data such as quick-look images which may be used more often are stored in disk-array system. Images and digital maps are divided into small tiles and stored tile by tile (partial migration) because user usually do not need to use a whole scene. And as soon as a user make an access to a quick-look image, the system starts transferring original image data from the Juke box to the disk array, because the user will likely make an access to the original image in the next step. To efficiently distribute data, the database is now connected with a very high capacity network (max.152Mbs) connecting university researchers(Fig.3).

3.3 Development and coupling of dynamic models

Major models describing basic cycles in terrestrial ecosystem are water(hydrological) cycle models and biogeochemical cycle models. To describe coupling effect of water and biogeochemical cycles, we will develop vegetation models and soil models. In this stage, we

apply existing regional scale models of those cycles, such as MIKE SHE to check the behavior and test the whole structure of the system. Development of both models and databases especially of hydrological data will be conducted under close coordination with GAME (Gewex Asia Monsoon Experiment) project.

Especially to support the coupling of dynamic models with different temporal steps(resolution) and spatial resolutions, spatio-temporal interpolations and aggregation/disaggregation techniques have to be implemented as a one of very basic functions of GIS. In simulation of models, parallel processing can also be very effective, because grids so far apart from each others may have only negligible interactions.

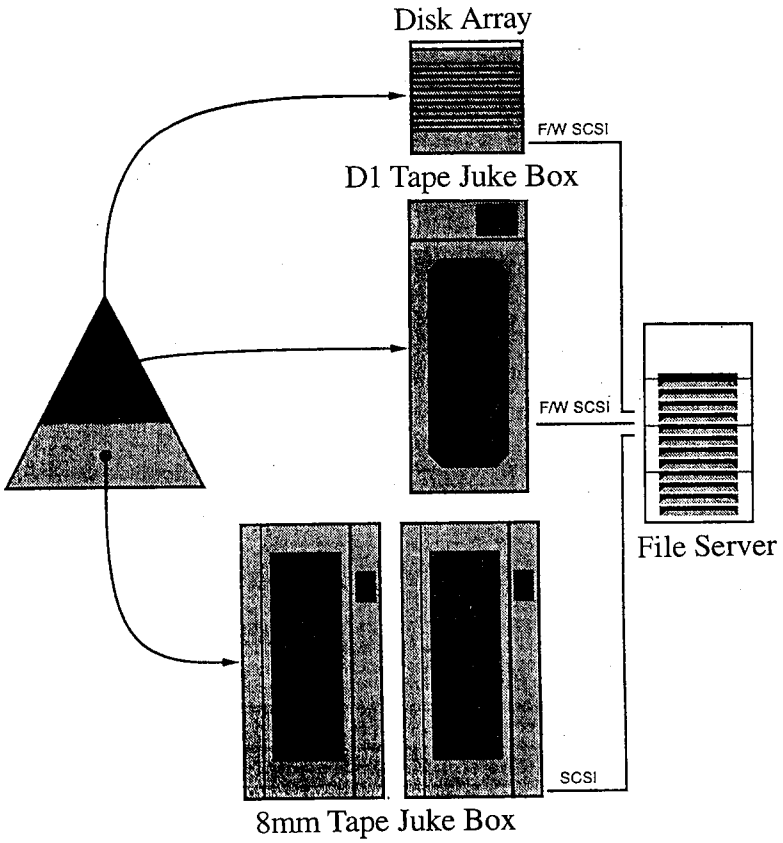

Fig.3 Configuration of Experimental System for Very Large GIS Database (Nemoto et.al, 1995)

4. Future Prospects

LUCS-ASIA project has just started developing GIS databases to cover SE Asia with a 5 year scope. Recognizing very pressing need to better management schemes of environmental resources in the regions surrounding SE Asia, we will also encourage and support developing GIS databases in other countries. These GIS database development at the national level will make tremendous contributions in the long term to formulate better national development/ environmental policies for continuous human habitation.

By linking these national databases, regional environmental issues can be addressed, which will have increasing importance in the next decade due to rapidly growing economy beyond national borders and it's impact to human environment. Regional-scale mitigation of environmental impacts and development on the sustainable basis will also make significant contribution to global environmental issues because more than one thirds of global population are now concentrated and still rapidly increasing in this region.

We believe LUCS-ASIA project will make significant contribution to harmonization of

local solution with global solution to environmental/development issues.

5. References

Houghton,R.A.(1983): **Changes in the carbon content of terrestrial biota and soils between 1860 and 1980: Net release of CO2 to the atmosphere**, Ecological Monographs 53:pp.235-262.

Iverson,L.R. et.al. (1993): **Use of GIS for estimating potential and actual forest biomass for continental South and Southeast Asia, Effects of Land Use Changes on Atmospheric CO2 Concentrations,** Springer Verlag, pp.67-116.

Dale,V.H. et.al.(1993): **Causes and effects of land-use change in central Rondonia, Brazil,** Photogrammtric Engineering and Remote Sensing, vol.59. No.6, June 1993, pp.997-1005.

Y.Matsuoka et al (1994): **Estimation of Carbon Dioxide Flux from Tropical Deforestation**, Center for Global Environmental Research.

T. Nemote et.al (1995): **Design of Hierarchical File System for Fast Access to Satellite Data,** Proceedings of Seiken Forum on Global Monitoring from Space. pp.104-109.

Parks,P.J. (1993): **Economic reasons for forest land-use change: relevance to tropical deforestation and the carbon cycle, Effects of Land Use Changes on Atmospheric CO2 Concentrations,** Springer Verlag, pp.329-364.

R.Shibasaki., S.Murai.and X.Bai.(1993): **Global Planning of Sustainable Use of the Earth -- Potential Applications of Global GIS ---,** Proceedings of ISPRS Workshop on Global GIS, 1993. pp.322-329.

UNESCO and FAO(1986): **Carrying capacity assessment with a pilot study of Kenya.**

Analysis of Environmental profile of Walawe River Basin, Sri Lanka, by Remote Sensing and GIS

L. Kithsiri Perera*, Satoru Ueno*, Koji Shigehara*, and Ryutaro Tateishi**

***WEATHERNEWS Inc.**, D21, 1-3, Nakase, Mihama-ku, Chiba-shi, 261-01, JAPAN, Fax: +81-43-274-5012

****CEReS**, Chiba University, 1-33, Yayoi-cho, Inage-ku, Chiba-shi, 263, JAPAN, Fax: +81-43-290-3857

ABSTRACT

Environment of a river basin in Sri Lanka was analyzed by digital mapping, GIS, and remote sensing data. The "Walawe" river in selected basin is one of the major rivers in Sri Lanka. It brings water for one of the most active agricultural settlement area and also for number of other smaller reservoirs. The river basin covers over 2400 sq. km. area of land from central mountains to south coast. Vegetation distribution of this area was classified using digital data of Landsat MSS, and produced the other related Geographical data files into a GIS data base with 5x5 sec ground resolution. Significant features in; land cover, elevation, slope, soil, climate, and other social phenomena were observed and inter-relations of these elements were analyzed by GIS. Thematic maps such as; soil + paddy, slope + forest, were produced using data file of the GIS data base. The results indicated the; environmentally poor present vegetation structure, neediness for forest conservation and reforestation, and better management of soil and water resources of the area. The extensive use of water and soil of the area for agriculture also discussed.

1. Introduction

Digital mapping and Geographical Information System(GIS) are well recognized research tools in natural environmental studies. This field was started with the SYMAP mapping program and developed to a new research field which uses grid-sell or raster mapping systems(Burrough, 1989). Here, we emphasize the importance of these technologies for a river basin study. A river basin from Sri Lanka was selected as the study area, with the consideration of its rainy mountains and dry low land physical structure. Its river system, "Walawe" which consists with an area of about 2450 sq.km, is one of the major rivers in Sri Lanka. Landsat MSS data of the river basin were digitally classified to produce the land cover map. The use of satellite data gives the easiness of inserting future and historical information to the land cover data set. The study mainly uses personal computer based data processing methods. Some of the data files and basic information were extracted from previously conducted research works(Perera, et .al, 1994, 1995). Throughout the study, number of geographical data files have been produced and these data were used to evaluate the environmental status of the river basin.

2. Research objectives

There are two main objectives of the study as follows;

1. Production of a digital geographical data set for the river basin.
2. Evaluate the present level of natural and agricultural environment of the river basin.

Under the first objective, digital data files have been designed with a ground resolution of 5x5 seconds, or 153x153 m. This gives the possibility to merge with; other existing or future geographical data sets or link with larger area data sets. Evaluation of the present environmental conditions of the Walawe river basin mainly deals with the information such as; forest cover, paddy cultivation, river basin data, and land cover data of Sri Lanka.

3. Study area

Walawe river is the 7th longest river in Sri Lanka, which starts from the central high mountains and runs to down south coast passing 137 km. Its river basin covers an area of 2450 sq. km. of land and provides home for over 375,000 of mainly rural population(Survey dept. 1988). Much of the precipitation of the area comes from south west monsoon and inter monsoon rains, and further modifications of rain fall distribution are caused by relief(Goetz 1987). Mean annual rain fall ranges from about 4000 mm in mountains to less than 1000 mm in south

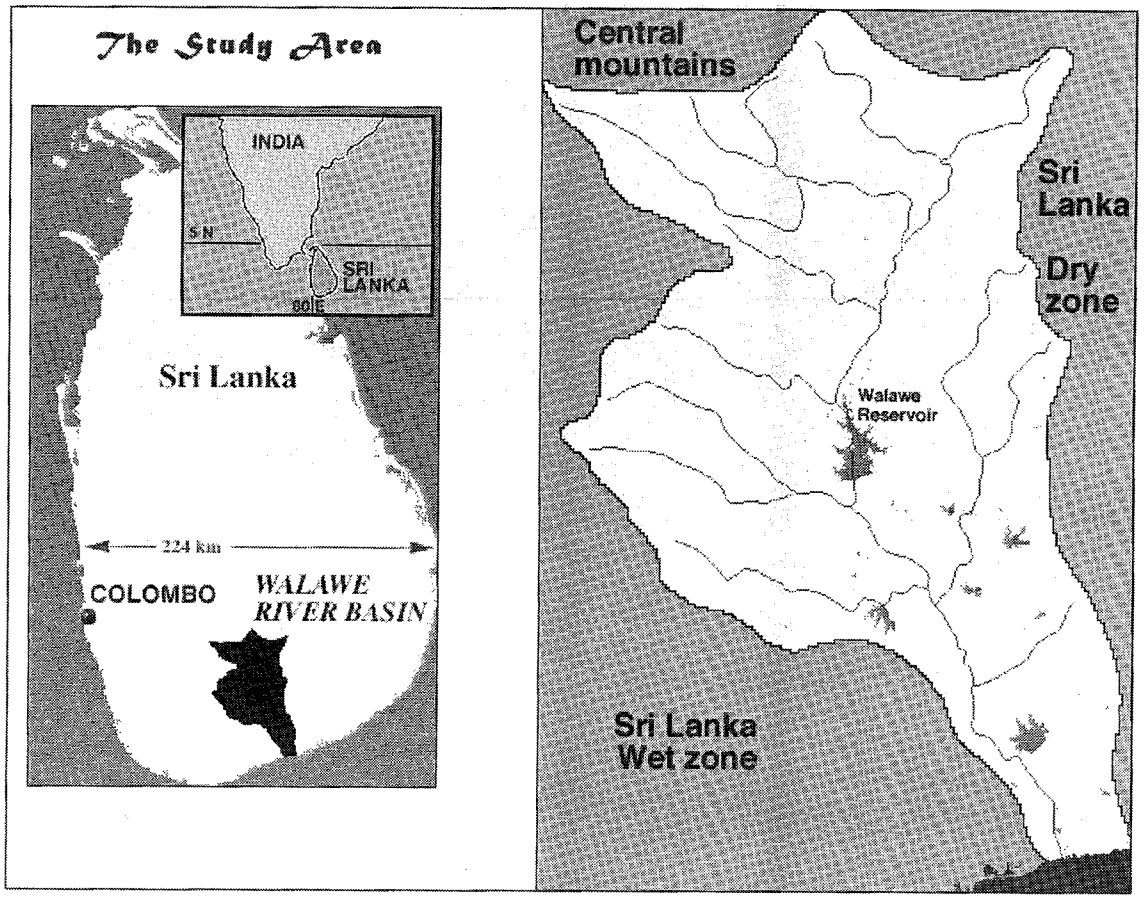

Figure 1. Location and the river system of the Walawe river basin.

coast. Temperature of the area differs from about 15 C in mountains to about 27 C in low lands that are relatively dry. The river basin contains only one medium level urban center, "Balangoda", and one important transportation junction,"Beragala". Both locations are in mountain area of the basin. Physical structure of the basin will be presented as maps in following sections. The main feature of the Walawe river basin is its large river development project, centered on 'Walawe reservoir'. It irrigates one of the major agricultural areas of Sri Lanka, while protecting down river area by occasional floods. Location and the river system is presented in figure 1.

4. Digital geographical data structure

A study based on GIS, needs a verity of data, which can be widely categorized into two sectors. 'Physical data' stands for geographical, climatological, vegetation, soil, elevation, slope, and such other data. 'Socio-economical data' represents; demographic, economic, transportation, and similar data. In present study, these data were collected from maps by re-drawing, scanning and filling polygons in the computer; except application of Landsat MSS data for the land cover map. All data files have been resample to a basic resolution of 5x5 seconds or 153x153 m. The data set consists following data files in raster form.

a. River basin and the river system, including inland water resources, b. Land cover map with 7 land cover categories, c. Soil map, d. Digital Elevation Model(DEM), e. Slope map, f. Population distribution and major roads, g. Mean annual rainfall

4.1 Land cover map

Land cover map was based on Landsat MSS images, obtained in 1987 and 1988. To match with the existing data, 1 pixel skipped image was used to produced the land cover map. The mosaic was geometrically rectified using 1: 250,000 map of Sri Lanka. The river basin was apart from the mosaic and it contained 371 pixels and 575 lines. Observing the band characteristics, color composites and principal component images; training sites were selected. Some aerial photographs, 1:63,360 maps, field work information, and other published data sources were used to select training sites. Through the Maximum Likelihood classification method, image band 1, 2, 3, and 4 were digitally classified into 7 land cover categories(see figure 2).

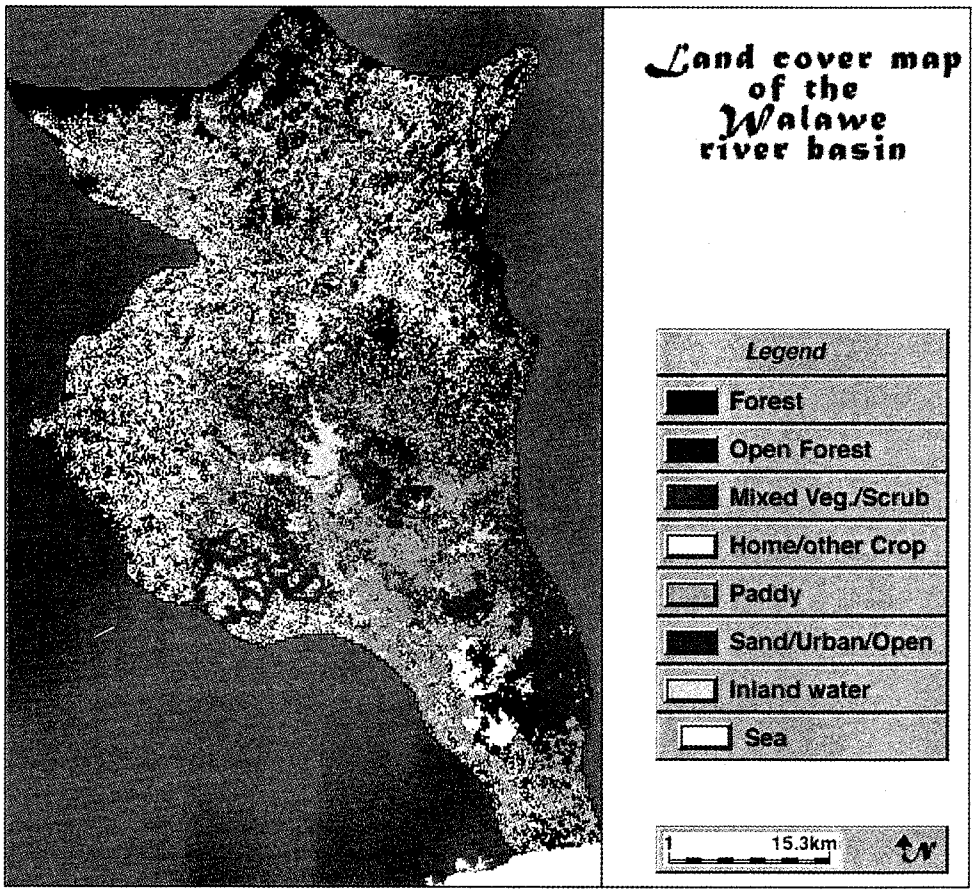

Figure 2. The land cover map of Walawe river basin, based on Landsat MSS data.

4.2 Soil map

Analog soil distribution map of the area converted into a digital map, and contains 12 major soil types(see figure 3). In Walawe river basin, soil types can be used in the connection of Paddy cultivation.

4.3 Digital Elevation Model(DEM) and slope map

In this study, the DEM is stands for its warble meaning and shows value of the highest ground place in each pixel. The DEM data were generated by reading highest values from 1:63,360 maps. The resolution has a relatively low level, and 1 pixel represents by 30 x 30 seconds or by 918.72 x 918.72 m(see figure 4 a.). Slope data file was constructed using DEM. Slope map was reclassed into 4 levels as in figure 4 b.

4.4 Climatological data set

For the production of climatological data set, it is reasonable to pay more attention on the rainfall, since it is the governing force of the local environment. The figure 5 shows the distribution of mean annual rainfall. Mean monthly temperature data gives much higher reliability than rainfall data since the diurnal and annual fluctuation of the temperature is rather low in the area. Mean annual rainfall and paddy cultivated areas have been compare in later section of the paper.

4.5 Other geographical data files

The rest of the digital data base mainly consists with following digital maps; Population density map, River basin map, River network and reservoirs, and Transport network. Some of these data were extracted from a previous study(Perera et . al., 1995). All relevant information from each analog map were carefully delineated and scanned into the computer. Then each polygon was filled with different colors, and finally produced the digital data files. Distribution of the population and major roads are shown in figure 6.

With production of the digital data set, one of the basic objectives of the study is completed. Different usages and developments of the data set can be expected in future studies. As the second part of the study, the environmental condition of the river basin is evaluated using the produced data set.

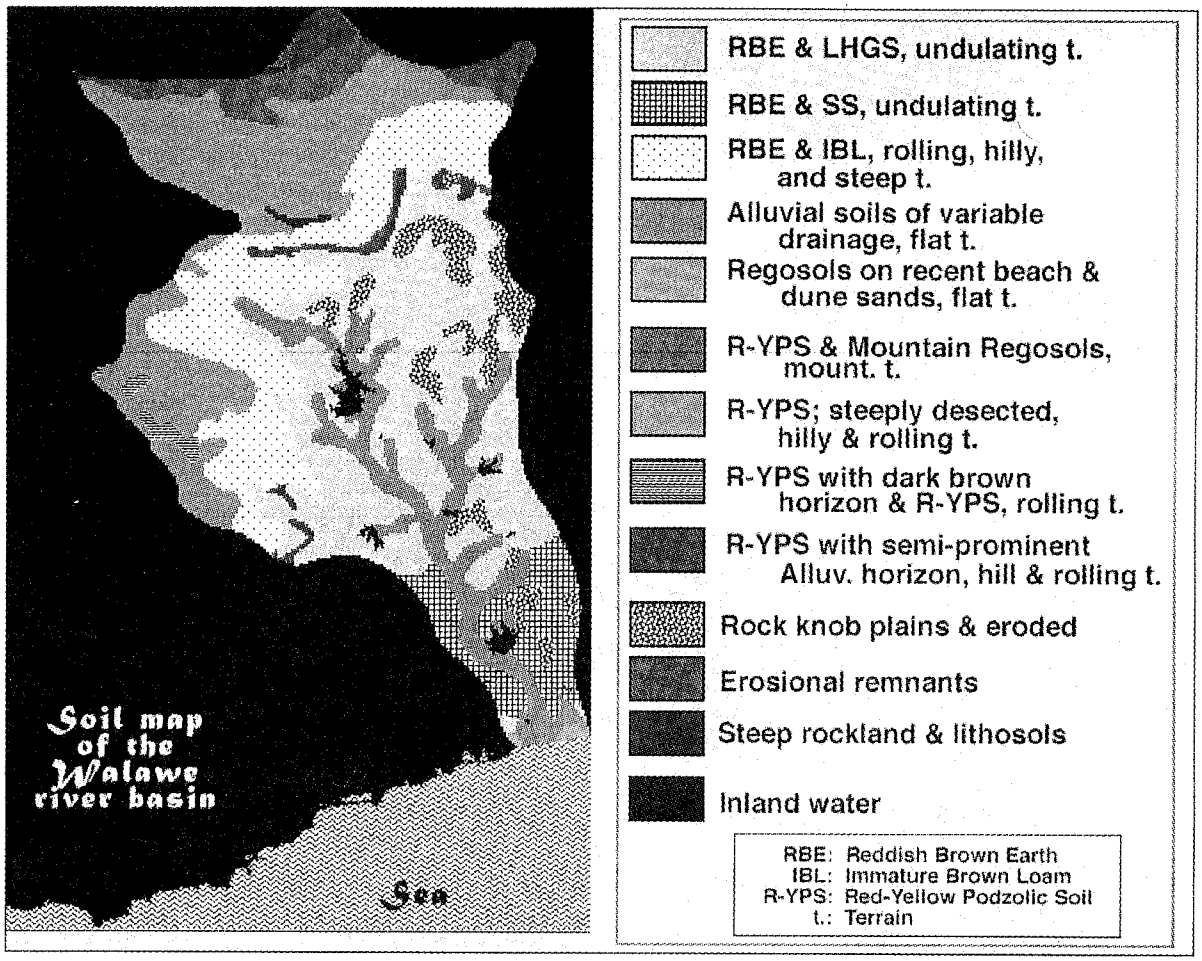

Figure 3. Soil type distribution of the area.

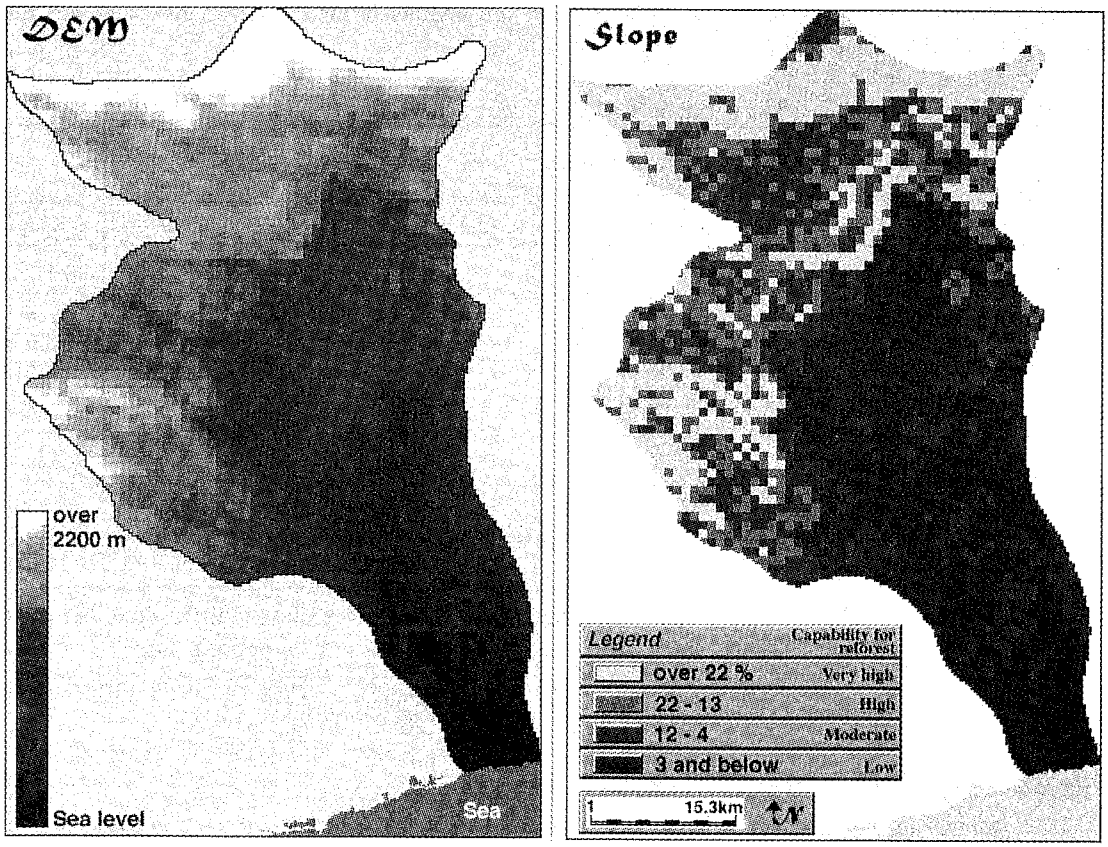

Figure 4 a and 4b. Digital Elevation Model(DEM) and reclassified slope map produced from the DEM.

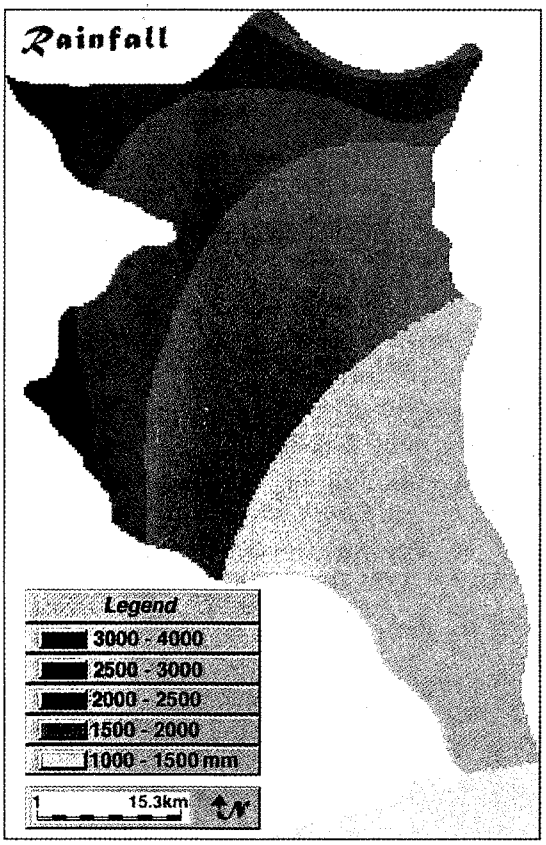

Figure 5. The distribution of mean annual rainfall.

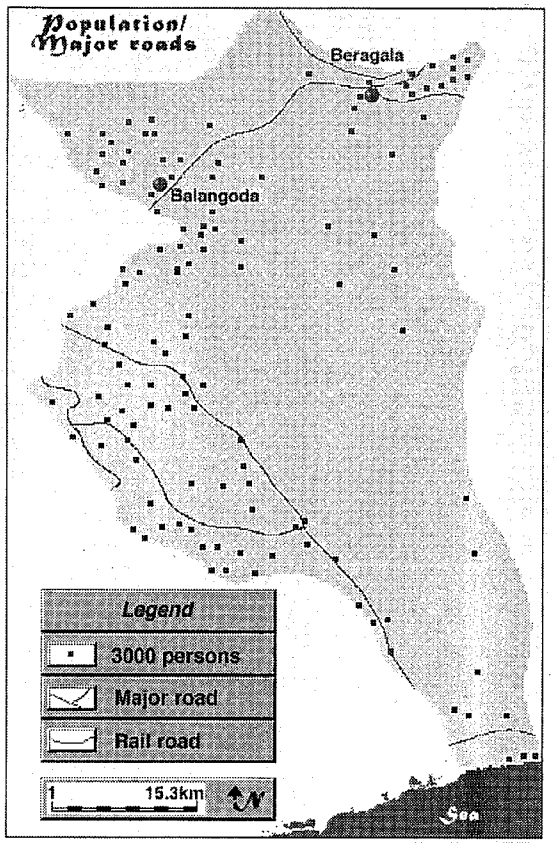

Figure 6. Distribution of the population and major roads.

5. Environment profile

Walawe river basin is an area that should be undergo with intensive observations, in the field of environmental management. According to the table 1, there are number of facts that can be presented to show the importance of the Walawe river basin.

Table 1. Land cover data of Sri Lanka and Walawe river basin.

Land cover type	Sri Lanka in sq.km	%	Walawe river basin in sq.km.	%
1. Forest	20032	**30**	503	**21**
2. Open forest	4587	**7**	80	**3**
3. Mixed vegetation	14801	**23**	681	**27.8**
4. Home/other crop	16093	**25**	694	**28.2**
5. Paddy	8549	**13**	448	**18.2**
6. Open land/sand/urban	958	**1**	11	**0.4**
7. Open water	622	**1**	33	**1.4**
TOTAL	65642	**100**	2450	**100**

Here, specially the forest cover and the paddy area data are showing significant differences between country scale and river basin scale data. Walawe river basin is producing more rice, proportionately to its size, when compare with the total country. Mean time it is having less % of forest area. Using these two basic facts, we have analyzed few elements of the river basin, to evaluate its environmental conditions.

5.1 Utilization of water and soil in the river basin

By the figure 7, a comparison of relatively similar(in size) river basins of Sri Lanka is forwarded. The Walawe river basing has the lowest water discharging percentage. Apart from the possible other reasons such as climatological elements for this situation, the intensive use of the river water is keeping the figure at 22%.

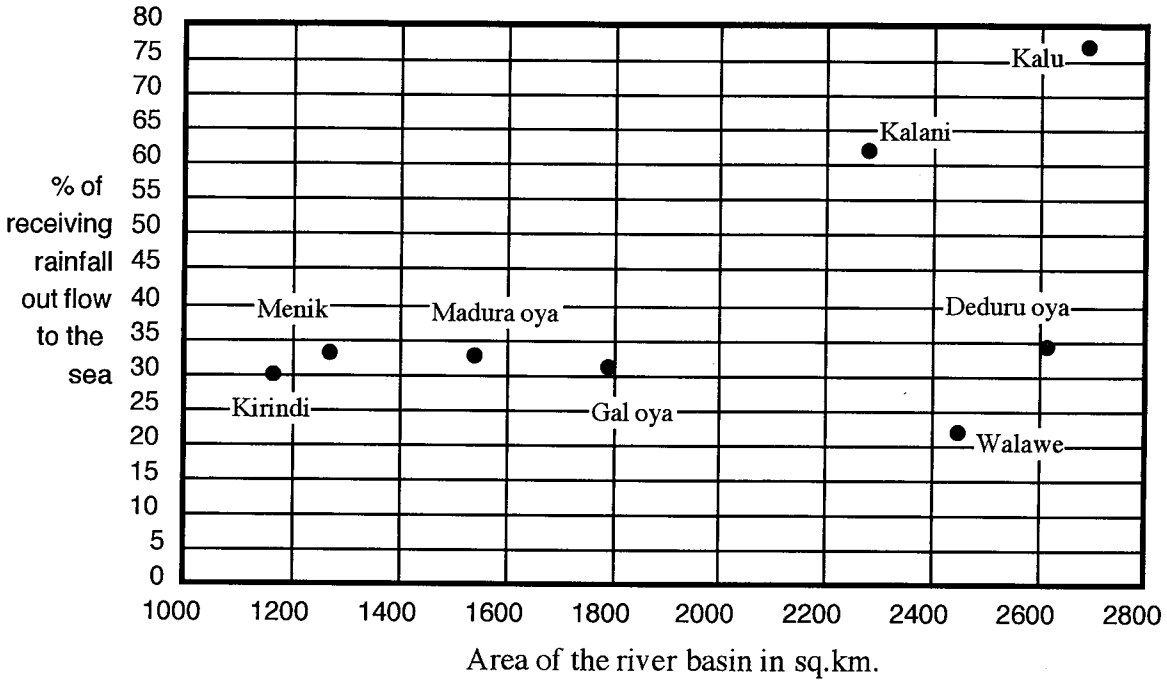

Figure 7. Percentage of receiving rainfall out flow to the sea and river basin size in similar river basins of Sri Lanka.

Mean annual rainfall map(see figure 5) and the distribution of the paddy cultivation area(see figure 2) are also providing evidence for the high use of river water. Almost all paddy areas are located in low rainfall receiving area and depends on irrigated water from the river.

Soil requirement for paddy cultivation were gathered(Dept. of Agricultural 1990), and soils were reclassed into 4 major groups, and then into 2 types. This reclassification was based on the capability to conduct paddy cultivation in respective soil type as is shown in figure 8. This map, and the related table 2 show that most of the areas with high capable soils are used for paddy cultivation(about 87%). According to these two factors, the Walawe river basin can be counted as a highly active agricultural area.

Table 2. Paddy area under high and low capability soil for cultivation.

Paddy in different soils	area in sq. km.	%
In Very high & high capable soils	387.5	87
In moderate & low capable soils	60.5	13
TOTAL	448	100

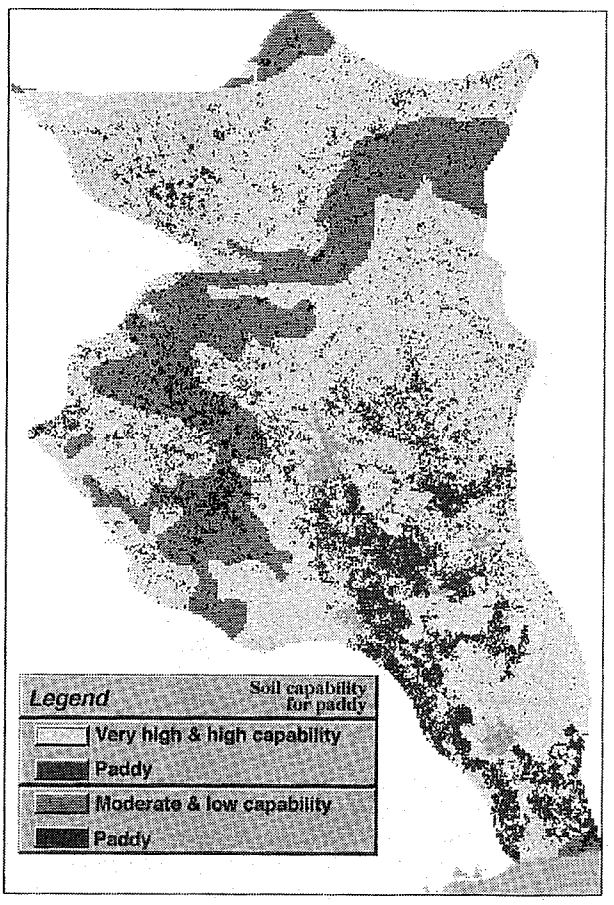

Figure 8. Paddy area and soil capability for paddy cultivation.

5.2 Land cover profile and vegetation structure

Vegetation structure has many influences on rivers and other water sources. It protects the soil layers, and supports to the efficient circulation of the hydrological cycle. As noted in the table 1, the river basin has a poor forest cover. In figure 9, a land cover profile of the river is presented. The profile shows vegetation types along about 92 km of the central river and only first 23 km has a forest cover. Even around the Walawe reservoir, no forest cover can be seen. Existence of Open forest also around 3% of the area and hardy visible along the profile. Most of the river system is running through mixed vegetation, and paddy cultivated area. By the figure 10, forest cover and river system is presented. This shows the scattered forest patches and the lack of gallery forest very clearly.

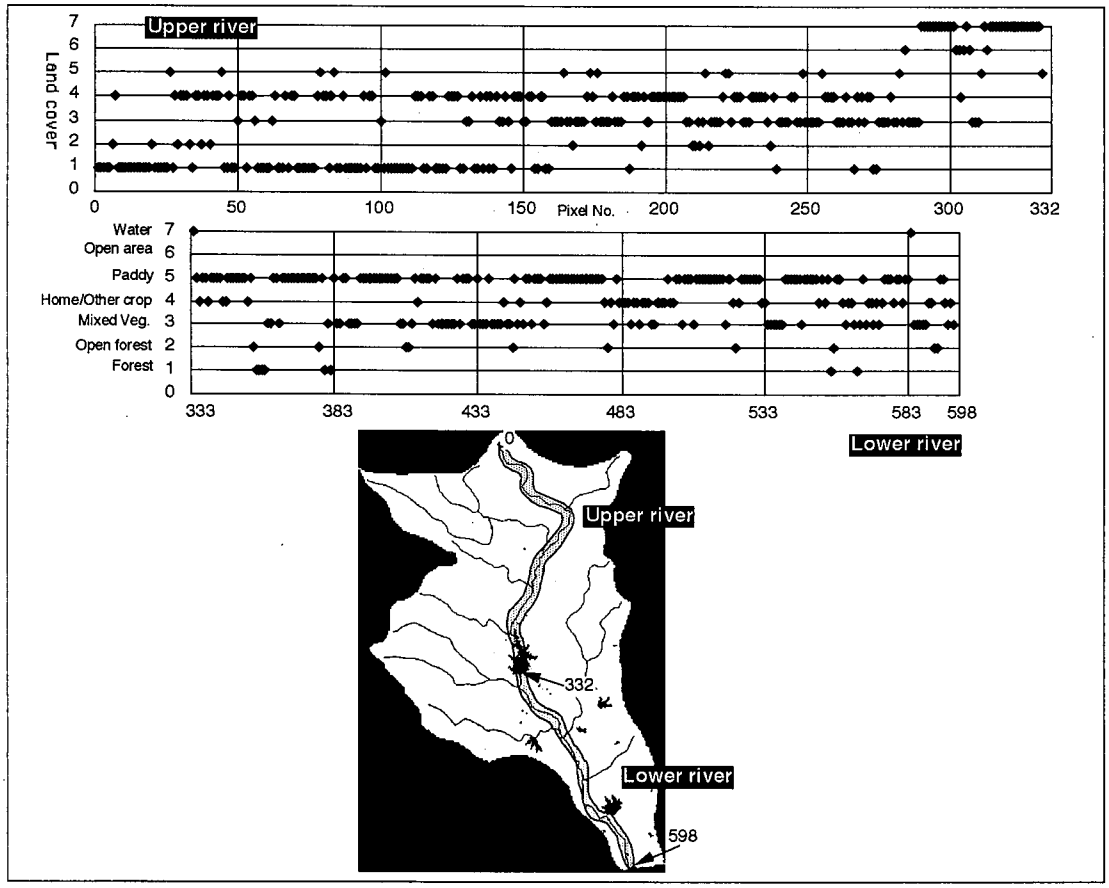

Figure 9. Land cover profile along the central river of Walawe river system. The forest cover only exists in about first 25% of the upper river area.

Slope data of the area were used to make further analysis. With the use of published information(MacRae and Burnham 1981), slope have been reclassified into 4 and then into 2 classes according to the suitability to conduct reforestation. Then these data were merged with the forest cover(see figure 11). Calculated results of the map in table 3 explains, forest cover is not available in most of the areas that are suitable for reforestation.

Table 3. Forest area under high and low capability slope for reforestation.

Forest and slope data	area in sq. km.	%
Very high & high capable slopes for reforestation **with** forest	310	12.7
Very high & high capable slopes for reforestation **without** forest	555	22.7
Moderate & low capable slopes for reforestation **with** forest	192	7.8
Moderate & low capable slopes for reforestation **without** forest	1393	56.8
TOTAL	2450	100

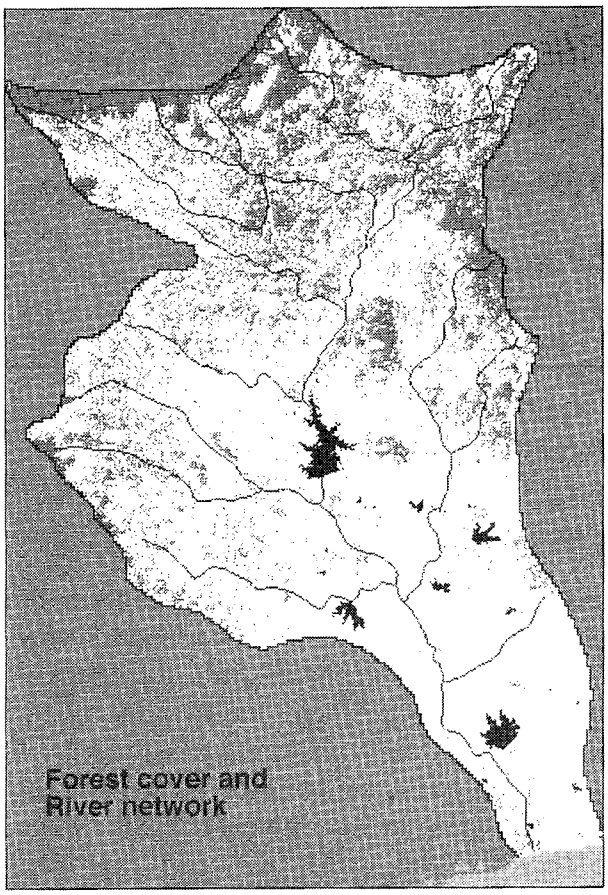

Figure 10. The poor forest cover of the river basin, mainly with scattered small forest patches.

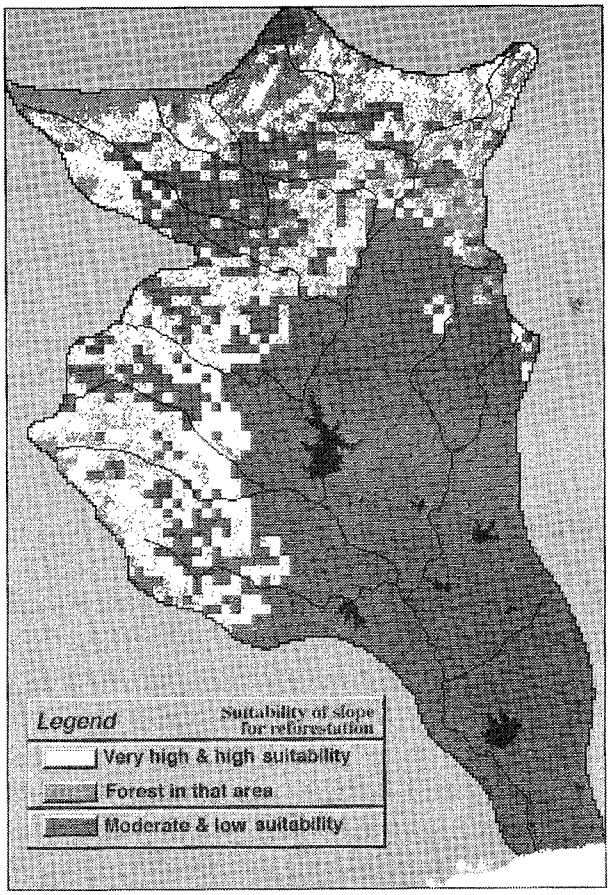

Figure 11. Distribution of present forest in slopes where highly suitable for reforestation.

This situation makes adverse effects on the soil structure, water resources, and to the total environmental balance. The study explains the efficient use of river basin for agriculture. Furthermore the results show the poor existence and distribution of its forest cover. This will consequently effect to the presently highly active agricultural structure of the river basin.

6. Conclusions

Digital geographic data and GIS technology were applied to analyzed an environmental profile of a river basin. The production of the digital data set of Walawe river basin(in Sri Lanka) accounts for a large potion of the study, which will able to use in many applications in future. The present situation of the river basin was analyzed using two main factors, its paddy cultivation and forest cover. Results of the study explains the efficient use of water and soil resources of the basin for paddy cultivation. But, in contrast to that situation, its forest cover and distribution of the forest cover shows a poor environmental condition of the river basin. The total forest area(21%) in this remote river basin is lower than the national figure. A higher priority should be give to conduct conservation of available forest and water resources and reforestation in mountain slopes.

References

Burrough, P. A., 1989, Principles of Geographical Information Systems for Land Resources Assessment (Oxford University Press)

Department of Agriculture , 1990, Crop recommendations technoguide, Dept. of Agriculture, Sri Lanka.

Department of Survey , 1988, National Atlas of Sri Lanka, Dept. of Survey, Sri Lanka.

Goetz,.P . W. (Editor in Chief), 1987, The New Encyclopedia Britannica, London, UK.

Mcrae, S. G., and Burnham, C.P., 1981, Land evaluation, Oxford University Press, Oxford, UK.

Perera L.K. and Tateishi R.(1995): Do remote sensing and GIS have a practical applicability in developing countries ? (including some Sri Lankan experiences). Int. Journal of Remote Sensing. Taylor & Francis, Vol. 16, 1, 18-35

Perera, L. K., Tateishi, R., Furuya, T., 1995, Land suitability for highland crops., Proceedings of annual symposium of the Japan Society of Photogrammerty and Remote Sensing, May, 1995, Tokyo Univ.

Life Cycle Assessment for Hydroelectric Power Plant Construction Considering Vegetation Change Effect Using Vegetation Map

Shintaro.Goto, and Toshikazu Sakai
Environmental Information Research Laboratory
Kanazawa Institute of Technology
7-1 Ohgigaoka Nonoichi Ishikawa 921, Japan.
Tel: +81-762-9210 Fax: +81-762-9211
E-mail: got@Gaia.env.kanazawa-it.ac.jp

Abstruct

The concept of LCA (Life Cycle Assessment) is necessary for protection of the earth from the greenhouse effect caused by CO2 release. Many commercial products are going to be assessed using LCA concept. But in the big project such as Hydroelectric Power Station construction, the effect of CO2 release is considered only on the practical using and managing stage (Stage2), but is not considered on the construction stage (Stage1) when the effect of CO2 release is larger than Stage2.

In this study, we developed the assessment flow for the life cycle of hydroelectric power plant using vegetation map from the view point of CO2 cycle. And the model was applied to the water resource development in the Nam Pong Basin of Northeastern Thailand.

A CASE STUDY ON CHANGES IN VEGETATION COVER AND SETTLEMENTS IN BANGLADESH USING REMOTE SENSING TECHNIQUE

Md. Abul Kalam*

* Bangladesh Space Research and Remote Sensing Organization
(SPARRSO)
Agargaon, Sher-E- Banglanagar, Dhaka, Bangladesh

Abstract

This paper presents a case study on changes in vegetation cover & settlements and a brief description on the findings of four other vegetation monitoring projects in the study areas of Bangladesh. Case study shows that vegetation cover decreased from 2.5% in 1975 to 1.71% in 1983 and increased to 2.9% in 1990 and the growth of settlements was turned negative.It was also found from other monitoring projects/studies that the areas of the vegetation cover in Madhupur, Chittagong, and Chokoria Sunderban decreased by 46%, 3.58% and 100% respectively; on the other hand 87% and 56% areas of the total project areas were planted under coastal afforestation projects during the study period.

1. Introduction

A healthy vegetation cover plays a very important role in keeping the environment in balance.Bangladesh with an estimated population of 120 million has a total area of 14.3 million hectares.Due to high population density(8.4 persons/hectare), tremendous pressure is being exerted on the natural vegetation cover.The land area and surface water bodies of Bangladesh are 13.36 and 0.94 million hectares respectively. Out of the 13.36 million hectares land area, the forest land, agricultural land and the urban areas are 18%, 64% and 8% respectively. The present forest cover, is however, around 9%. The remaining forest land are the denuded state owned forest, vested forest and enchroached forest land. Natural vegetation cover of these forest lands has almost been cleared up for shifting cultivation, agriculture and other uses.

1.1 Objective

For an efficient management of vegetation cover and to prepare an effective plan for the afforestation programme in

---

Paper to be presented at the International Symposium on "Vegetationtation Monitoring" Aug., 29-31,1995, Chiba University, Chiba, Japan.

raising the vegetation cover to an optimum level, it is necessary to monitor the vegetation/forest cover at regular intervals. The vegetation cover monitoring work through conventional field work survey techniques is time consuming involving high cost. Here the satellite remote sensing as well as aerial photography techniques play an important role. Data available from satellite remote sensing cover relatively large area in a single pass of the satellite and are easily accessible due to their relatively lower cost. The sensors on board of the resource satellites like Landsat and SPOT provide multispectral digital data with high ground resolution, which can effectively be used for identifying various features of earth surface including vegetation covers of different types.

The main objectives of this study are :

i) to prepare a set of vegetation cover,settlements and surface water bodies map for different years using remote sensing data to monitor the vegetation cover and settlement status of the area.

11) to give an idea about the status of vegetation cover in some other important areas of the country by giving brief descriptions of the recently completed monitoring projects/studies.

2. Case Study

2.1. Study Area

The study area chosen for the case study is the Nachole area shown in the Fig.-1. Its total area is 28,490 hectares. It lies between the latitudes $24^0 35'$ N and $240^0 55'$ N and longitude 88^0 E and $88^0 30'$ E.

2.2. Vegetation Cover

Dry deciduous forest or scrub appear to have covered the relatively higher altitude of the well drained soils of the study area and its surroundings which is generally known as Barind Tract. Most of the original vegetation cover has been cleared for cultivation. There is no evidence of any natural vegetation that may formerly have existed on the intermittently flooded, relatively lower altitude of the poor drained soils,but it seems most probably that these supported grasslands.

2.3. Land Forms

The landform of the study area falls under two major physiographic units. These are (i) Mixed Ganges and Mahananda river floodplain and (ii) The Barind Tract. The first unit consists of nearly level to very gentle undulating ridges, broad

basins and small beels. The proportions of calcareous Gangetic and noncalcareous Mohananda sediments have apparently varied from time to time in the past. The Mahananda river flows directly from the Himalayan foot hills, but it is also connected with the Teesta river and with a distributory of the Ganges. The parent material of the higher ridges and basins appear to have been derived mainly from the Ganges river; the ridges sediments are predominantly silty and calcareous throughout; the basin alluvium is clayey and non calcarious to about 1-3 feet from the surface. The parent materials of the lower ridges are rather acidic,predominantly silty and clayey and are believed to have been laid down by the Mahananda river. The second unit appears as a terrace landscape, but in fact represents a series of fault blocks.In the west, the Tract is hilly and dissected by narrow, usually streamless, valleys (locally known as bydes), there it is up-warped and slopes downwards both to the west and east. In the east, the Tract is nearly level, undissected, slightly tilted to the southeast and passes under the adjoining floodplain sediments. Elevations above mean sea level range from a maximum of more than 130 feet in the west to a minimum of 40-50 feet in the east.

2.4. Climatic Condition

Extreme climate prevails in this area.Very hot and cold climatic conditions are experienced due to the very high and low temperatures ie, 42.2^0 C and 5^0 C in the summer and winter seasons respectively. Rainfall(1282 mm everage) is also lower in comparison with average rainfall of the country (3600 mm). Distribution of rainfall is also not even. 2% occurs during November-February, 15% occurs during March-May and 83% occurs during June-October .

2.5. Settlements

Due to the adverse climatic conditions and geomorphological position, the density of population as well as settlements are quite low in the higher altitude of the central Barind Tract.

2.6. Preparation of the Maps

Two vegetation covers, settlements and surface water bodies map of 1975 and 1983 were produced using black & white and colour infrared aerial photographs of 1975 and 1983 respectively. Similar type of another (3rd) map was prepared using panchromatic SPOT imagery of 1990. Homestead forest and settlements are considered as same feature in the map for the convenience of interpretation.

2.7. Calculation of the Areas

The areas of all features were measured from the maps using digital planimeter and are shown in Table-1.

Table-1

Aerial distribution of the vegetation cover/settlements and surface water bodies(Areas are in ha).

Items/Year	1975	1983	1990
1)Area of the vegetation cover and settlements	1705	1678	1937
2) Area of the surface water bodies:-			
- Standing water bodies	648	1030	1000
- River	54	45	45

2.8. Statistical Analysis

It is found from another study(Jabbar-90) that vegetation covers were 2% and 1.71% i.e.712 and 487 hectares(approx.) in 1975 & 1983 respectively.Subtracting these areas of vegetation covers from the area of vegetation covers & settlements(Table-1), the areas of settlements were obtained as 993 and 1195 hectares in 1975 and 1983 respectively.

According to statistical data (source BBS-1974,1983 and 1990), the number of households increased from 10910 in 1975 to 12303 in 1983 and then decreased to 12274 in 1990.Considering the rate of increment(199) and decrement(4) of the number of households,the actual number of households have been found as 11,109,12,895 and 12,871 in the years of 1975, 1983 and 1990 respectively.The area covered by single households has been found as 0.09/hectare.Multiplying the area covered by single households with the number of households available in 1990, the total area covered by the households in 1990 have been found as 1104 hectares(Table-2).

Table-2

Aerial distribution of the vegetation cover and settlements
Areas in hectares/percentage

Item/Year	1975	1983	1990
1) Areas of the vegetation cover	712 2.5%	483 1.71%	833 2.9%
ii) Areas of the settlements	993 3.45%	1195 4.19%	1104 3.84%

3.Other Vegetation Cover Monitoring Projects/Studies

3.1. Studies/Project Areas

All the studies/project areas are shown in the location map

3.2. Forest Cover-Madhupur.

The forest under Madhupur area are " Moist Deciduous Forest" The forest comprises sal coppice in patches, occasionally with other tree species, intersected by low lying areas.

A study has been completed on the " Monitoring of Madhupur Tract Forest Cover using Remote Sensing techniques"(Kalam et al -91). Changes of forest cover in 1977, 1983 and 1989 are shown in above mentioned study.

3.3. Forest cover- Chittagong Forest Division

The forest under Chittagong forest division is mainly evergreen and semievergreen forest. Ecologically the forest is in the state of transition. It possesses many of the characteristics of Burmese forest and also of the eastern Himalayan forest, with the exception of the indigenous trees, occuring in association with bamboo as undergrowth. There are more than a hundred tree species. Though no single tree type is uniform or clearly defined over a large tract, Garjan (Dipterocarpus spp.) is predominant in that area.

The forest types often intermingle and merge with one another. The majority of the species in the understorey are evergreen, while the bulk of the dominant and emergent trees are deciduous, some shade leaves in winter, while others just before monsoon, resulting in apparent evergreen appearance of the forest. The forests are generally uneven aged and multistoried and pure stands of a single species are limited. Even aged stands occur only in areas subjected to jhum cultivation in the past.

Recently(1993) a study has been conducted on the " Monitoring of Forest Cover in Chittagong Forest Division using Remote Sensing Technique" by SPARRSO .Landsat MSS data of March 1984 and TM data of March 1990 and October 1991 were used. GIS based statistical analysis was made and area statements were produced separately for 1984 and 1991 along with a comparative statement between 1984 and 1991.

3.4. Forest Cover-Chokoria

The Chokoria Sunderbans in the deltaic region of the Matamuhuri river extending over 4,540 hectare,is situated in greater Chittagong districts. This is one of the oldest notified reserved forests of the subcontinent. But most of it has disappeared due to heavy human interference.

A study has been completed on the " Deforestation of Chokoria sunderbans" (Kalam & Jabbar -90). A statistical description was given on the deforestation activities of Chokoria Sunderbans.

3.5. Coastal Afforestation- Bangladesh Coast

The coastal afforestation programme in Bangladesh has been very successful and the local available technology was applied to implement the programme.It comes from the deep concern to protect loss of human lives caused by cyclones and storm surge over centuries. It was taken up after the cyclone of 1970's. Over one million people of greater districts of Barisal, Noakhali and Chittagong lost their lives. Khulna city and Mongla port were least damaged due to protection accorded by natural mangrove forests of the Sunderbans.From this experience, the ideas of creating a green shelter belt by planting trees along the coastal belt was conceived.

Practically, since 1967 onward, the Bangladesh Forest Department started planting Babul (Acacia nilotica) along the embankment. Since 1970, plantation of Keora was initiated in the newly accreted coastal lands. This helps to stabilize the incoming silt load from upper catchments, reclaiming the land stabilizing the coastal ecosystem.

So far, about 120,000 ha. of plantations were raised successfully in the districts of Chittagong, Cox's Bazar, Noakhali, Bhola and Patuakhali along the coastal belt, to protect human lives and properties during cyclones and storm surge and also to produce timber and fuelwood.

Bangladesh Space Research and Remote Sensing Organization(SPARRSO) was entrusted with responsibility of monitoring the above mentioned afforestation programme of the Department of Forests.

The monitoring project activity included the study of satellite and aerial photographic data along with ground information collected from the field to produce maps in the scale of 1:10,000 showing the plantation areas as well as the morphological changes in the coast.

Satellite imagery were analysed both visually and digitally to identify plantation areas, damages, newly accreted lands, and other geomorphological changes in the coastal area. The detailed plantation maps were prepared from the stereoscopic study of 1:30,000 scale aerial photographs. The area of different features were measured from maps.

3.6. Statistical Analysis:

Statistical analysys of the other 4 vegetation monitoring projects/studies are also given in (Table-3).

Table-3

Aerial distribution of the vegetation cover in other monitoring projects.Areas are in hectares/percentage

Title of the Project/Study	Study period	Study area	Forest area (before study)	Deforested area	Forested/ afforested area(after study)
Madhupur Thana Forest Inventory	1977-1989	1,18,046	18530 15.69%	8691 7.36% (46.9 of forest area)	9839 8.33% (53.09 of forest area)
Chokoria Sunderbans	1967-1988	8500	7500 88.25%	7500 88.25%	00 00%
Chittagong forest division	1984-91	445056	163,370 37.01%	5856 1.33%	157514 35.69%
Coastal Afforestation	1980-85	41,000		35,722 87.12%	35,722 87.12%
	1985-90 1991	76,568		44,470 56.60%	44,470 56.60%

4. Results & Discussion

According to Table-2, the vegetation cover decreased from 2.5% in 1975 to 1.71% in 1983 and again increased to 2.9% in 1990. On the other hand, the settlements increased from 3.45% in 1975 to 4.19% in 1983 and again decreased to 3.84% in 1990. The rate of loss and growth of vegetation cover were found to be 32.16% and 72.46%, while the rate of growth and loss of settlements were 20.34 and 7.4% during the periods of 1975-1983 and 1983-1990 respectively. The increase of vegetation from 1983 to 1990 occured due to the plantation activities under Barendra Development Project. An abnormal situation is observed in this study that the area of the settlements decreased which was contrast to the expectation.Because population is increasing, so, the settlement area should also be increased.Very low vegetation cover which leads to adverse climatic condition might be one of the main factors for the above mentioned abnormal phenomenon. According to Table -3, the forest cover of Madhupur reduced from 15.69% in 1977 to 7.36% in 1989, the forest cover of Chittagong reduced from 37.01% in 1984 to 35.69% in 1991, the forest cover of Chokoria reduced from 88.23% in 1967 to 00% in 1988 and the coastal afforestation project achieved 87% and 56% of its target of plantation in 1980-85 and 1985 to 1990 respectively.

Conclusion:

It is found from the case study that the settlement growth has turned negative due to the very low vegetation cover. It is seen from this study that the optimum level of vegetation cover is an essential factor for the existence of human beings. It is also observed from other monitoring projects/studies that the areas of the natural vegetation cover has been reduced alarmingly. If the unplanned deforestation activities is not stopped, we have to face very adverse climatic condition as evidenced in the case study area.It is our solemn duty to increase vegetation cover to an optimum level for the safe living of our future generation. Regular monitoring of vegetation cover using latest remote sensing technique will surely help us to achieve the desired goal.

References

1. Jabbar M.A., The causes and effects of drought/ aridity in Bangladesh, Dhaka, Bangladesh, 1990.

2. J.Islam, Chokoria Sunderban, the depleted forest of Bangladesh, Dhaka, Bangladesh, Sept.1989.

3. Kalam Md. Abul and Jabbar M.A., Application of remote sensing technique in the study of environmental degradation of land and water covering north-western part of Bangladesh, Graz, Austria, April,1993.

4. Kalam Md. Abul, Pramanik M.A.H. and Jabbar M.A., Monitoring of Madhupur Forest Tract forest cover using Remote Sensing Techniques, Dhaka, Bangladesh, July 1991.

5. Kalam Md.Abul and Jabbar M.A., Deforestation study of the Chokoria Sunderbans using Remote Sensig Rechnique forvthe period 1972-87, Mymensingh,Bangladesh, March, 1988.

6. Rahman Shamsur, Forests of Bangladesh, Dhaka, Bangladesh,1995

7. SPARRSO, UNDP,BGD/85/031, Monitoring of forest cover in Chittagong Forest cover, Sectoral study K, Dhaka, Bangladesh, Dec,1993

8. SPARRSO, Report on Remote Sensing and Monitoring Component for Mangrove Afforestation Programme of Ist and 2nd forestry priject, Dhaka, Bangladesh, Oct.1993.

9. Salamat Ali Syed, Biological Diversity-Bangladesh persepective, Dhaka, Bangladesh, 1995

10. Bangladesh Bureau of Statistics(BBS), Small Area Atlas of Bangladesh, 1974, 1983 and 1989.

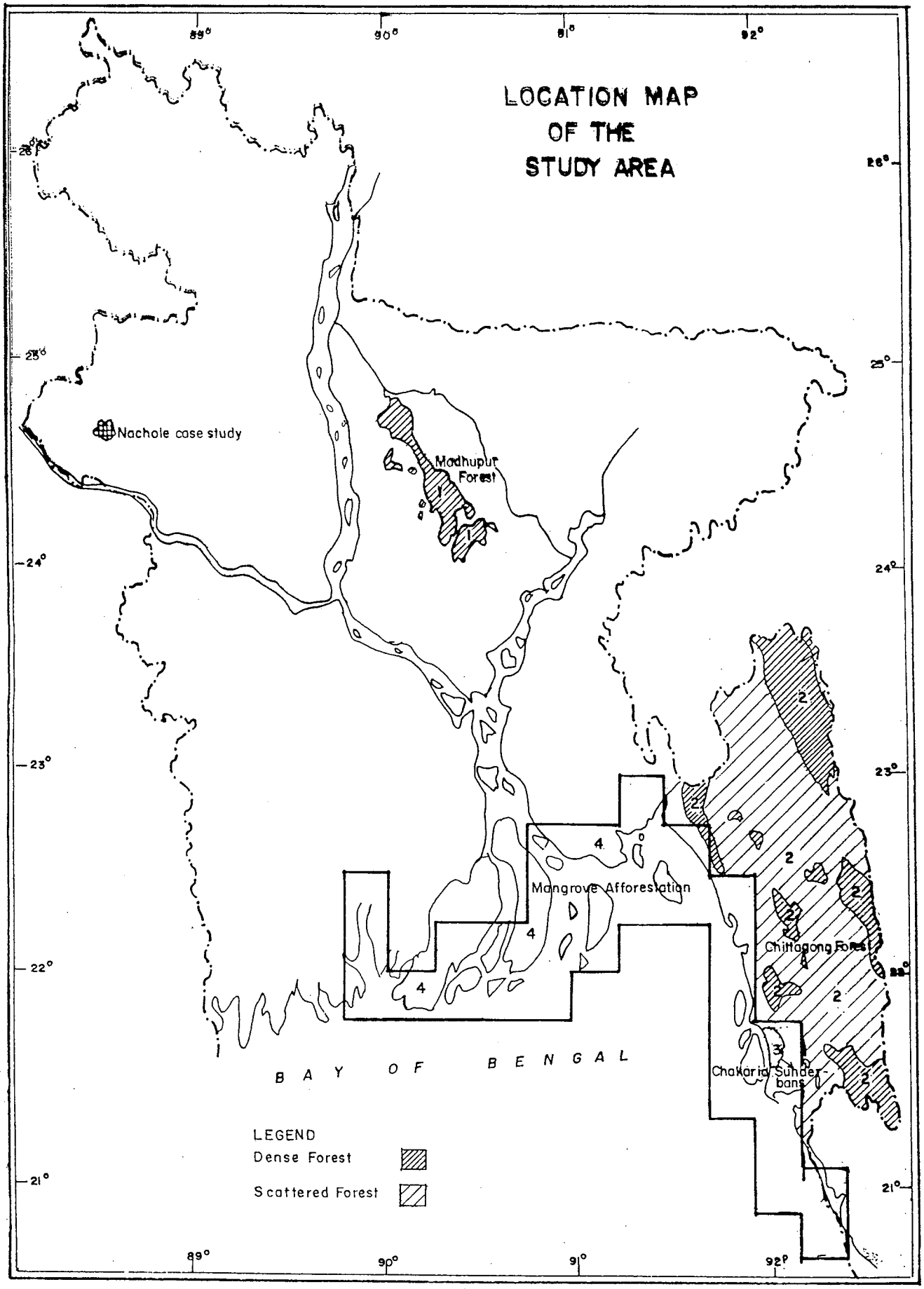
LOCATION MAP
OF THE
STUDY AREA
89°
90°
91°
92°
28°
25°
24°
23°
22°
21°
Nachole case study
Madhupur
Forest
Mangrove Afforestation
Chittagong Forest
Chakaria Sundar-
bans
B A Y O F B E N G A L
LEGEND
Dense Forest
Scattered Forest

Fig. 1

A Comparative Study of Urbanisation and Impact on the Natural Environment in Colombo City in Sri Lanka and Nagoya City in Japan Using Remote Sensing Data

Makoto Kawamura(*) Sanath Jayamanna(**) Yuji Tsujiko(***)

* Associate Professor
Department of Regional Planning
Toyohashi University of Technology
Tempaku-Cho, Toyohashi, Aichi 441, Japan.

** Graduate Student
Department of Regional Planning
Toyohashi University of Technology

*** Research Associate
Department of Civil Engineering
Fukui National College of Technology
Geshi Sabae Fukui 916 Japan.

Abstract

In this study we investigate a method to evaluate urbanisation and its impact on the natural environment of two cities which have different developing situations. Urban Index defined by the authors and the Normalised Difference Vegetation Index both derived from Landsat TM data have been used in the study to investigate the relationship between a city and its natural environment. As a case study, this method was applied to Colombo City in Sri Lanka and Nagoya City and it was found that the indices mentioned reflected the socio-economic position of the cities precisely.

1. Introduction

Many Urban areas around the world have been responsible for severe damage to the natural environment. To examine the influence of a large urban area on the natural environment of the surrounding suburban areas a comparison was made between Nagoya City from a large urban region in a developed country with Colombo City from a developing country. The different urbanisation situations of the two cities is recognized in the following description.

Nagoya is one of the three great urban regions of Tokyo, Osaka and Nagoya comprising an extended metropolis known as the Pacific Coastal Belt. Japan's economic, administrative, cultural and social functions are to a considerable degree concentrated in these great urban regions. Nagoya City has a population of a little over 2 million with a land area of 326 sq. km. Its population doubled during a period of rapid expansion between 1950 and 1970 accompanied by rapid industrial growth in the major urban regions. Nagoya City has a population density of 6085 per square km within a radius of 10 km from the city center. (These figures are based on 1975 statistics).

Colombo City in Sri Lanka is the commercial, financial and administrative center of the Island. The urban population in the region is largely concentrated in and around the City of Colombo resulting in a high concentration of population and activities in this area. The City experienced growth and expansion after the mid nineteenth century when the Colombo Port was developed to facilitate the rapidly growing plantation based export trade. The administrative limits of the city extends over an area of 37.3 sq.km with a population of 594,182 (figures are based on 1981 statistics) resulting in a population density of 15917 per sq. km within the cities municipal limits.

2. Remote sensing data applied to estimate urbanisation and the quality of the natural environment.

In this study digital data from the following Landsat TM scenes have been used.

(a) A scene covering Nagoya City and surroundings acquired in June 1994.
(b) A scene covering Nagoya City and surroundings acquired in Nov 1987.
(c) A scene covering Colombo City and environs acquired in February 1993.

2.1 Remote sensing data applied to estimate urbanisation

In a previous study by the same authors (Kawamura et al, 1994) it was established that there exists a strong correlation between the Landsat TM band ratio UI shown below and the density of building cover.

$$UI = \left(\frac{BAND\ 7\ -\ BAND\ 4}{BAND\ 7\ +\ BAND\ 4} + 1.0\right) X\ 100 \qquad (1)$$

In this study UI has been used to estimate the density of the built-up-area.

2.2 Remote sensing data applied to estimate the quality of the natural environment

The Normalised Difference Vegetation Index (NDVI) is used in this study to estimate the quality of the natural environment . In this study it is defined as follows.

$$NDVI = \left(\frac{BAND\ 4\ -\ BAND\ 3}{BAND\ 4\ +\ BAND\ 3} + 1.0\right) X\ 100 \qquad (2)$$

3. Comparison of the relation between UI and NDVI for Colombo City and Nagoya City.

As explained above the relation between UI and NDVI for an urban area represents the relation between urbanisation and the natural environment. This relation for the two cities have been examined by separating the pixels into those of central and suburban areas and also by separating them into those of different categories of land cover.

3.1 Based on central and suburban areas

Average UI and NDVI values for pixels of 20x20 image pixels were computed eliminating pixels from water areas by overlaying with a classified image. These pixels were picked up from an area of 1024x800 image pixels. The central areas of the cities were separated by selecting an area of 400x640 image pixels covering the central part of the cities. The remaining pixels in the 1024x800 pixels image were considered to be the suburban areas. The Landsat TM scene used for this computation for Nagoya City was from June 1994 (Summer Season)and for Colombo City was from February 1993. The scatter diagram of UI and NDVI for the two cities is seen in Fig: 1.

The basic difference between the two cities could be identified by this figure. The large concentration of high UI and low NDVI pixels in the case of Nagoya City shows that the density of the built up area is high and also that its spread over a large area. The low NDVI values of the suburban areas show that they are affected by the dense development over a large central area and its expansion into the suburbs. The central area of the Colombo City is not so densely developed over a large area and its green level is higher. Its suburban areas are hardly influenced by the central part indicated by the high NDVI value of the suburban area.

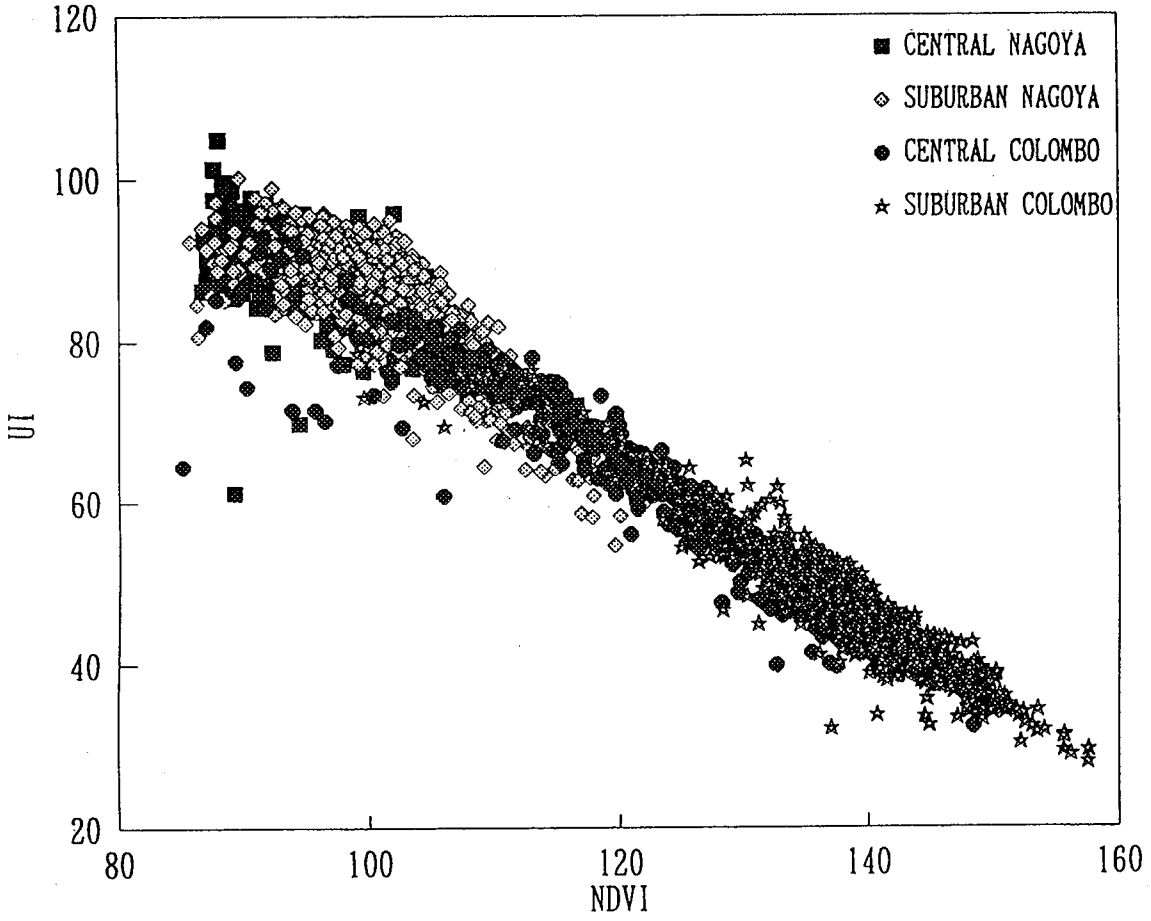

Fig. 1 UI-NDVI Relation for Nagoya City and Colombo City

3.2 Based on land cover type

Land cover information of Nagoya City has been obtained from digital land cover data available for Nagoya City. Digital land cover data of Colombo City has been obtained by scanning a 1:50000 land use map of 1981. The UI and NDVI images were registered with images of digital land cover data by removing geometrical distortions using ground control points and Affine Transformation technique. Resampling was done using nearest neighbour method. Each pixel was assigned to a category if more than 60% of the original 20x20 image pixels within the considered pixel belonged to that category.

The UI - NDVI relation for the two cities based on land cover category is shown in Fig 2 and 3. It is seen that with increased human activity on the land the UI value increases and the NDVI value decreases. The lesser number of relatively pure pixels in the case of Nagoya City shows a higher density of land use. It also shows that the green areas are affected by the development in the central area of Nagoya City. In the case of the Colombo City the large plantation areas away from the city are unaffected by the development in the central areas.

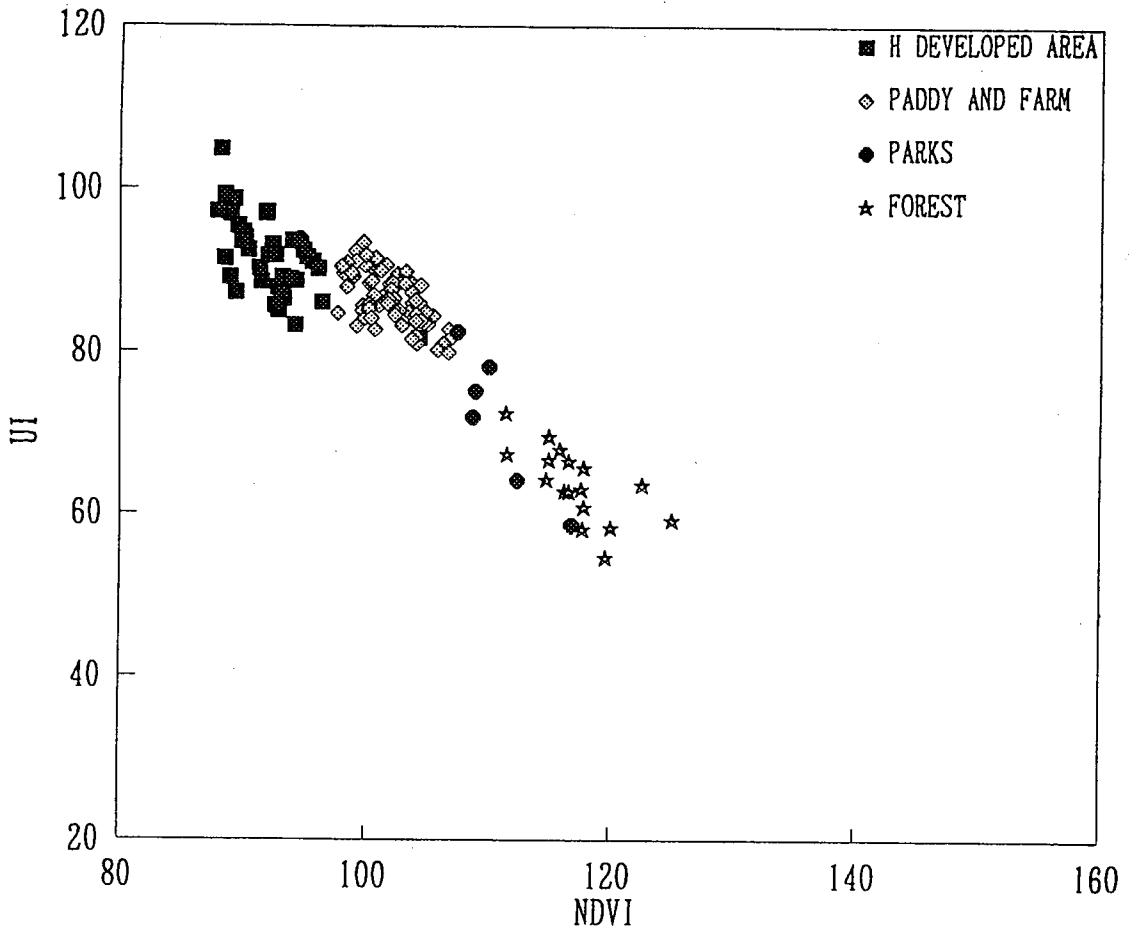

Fig.2 UI-NDVI Relation with land cover for Nagoya City

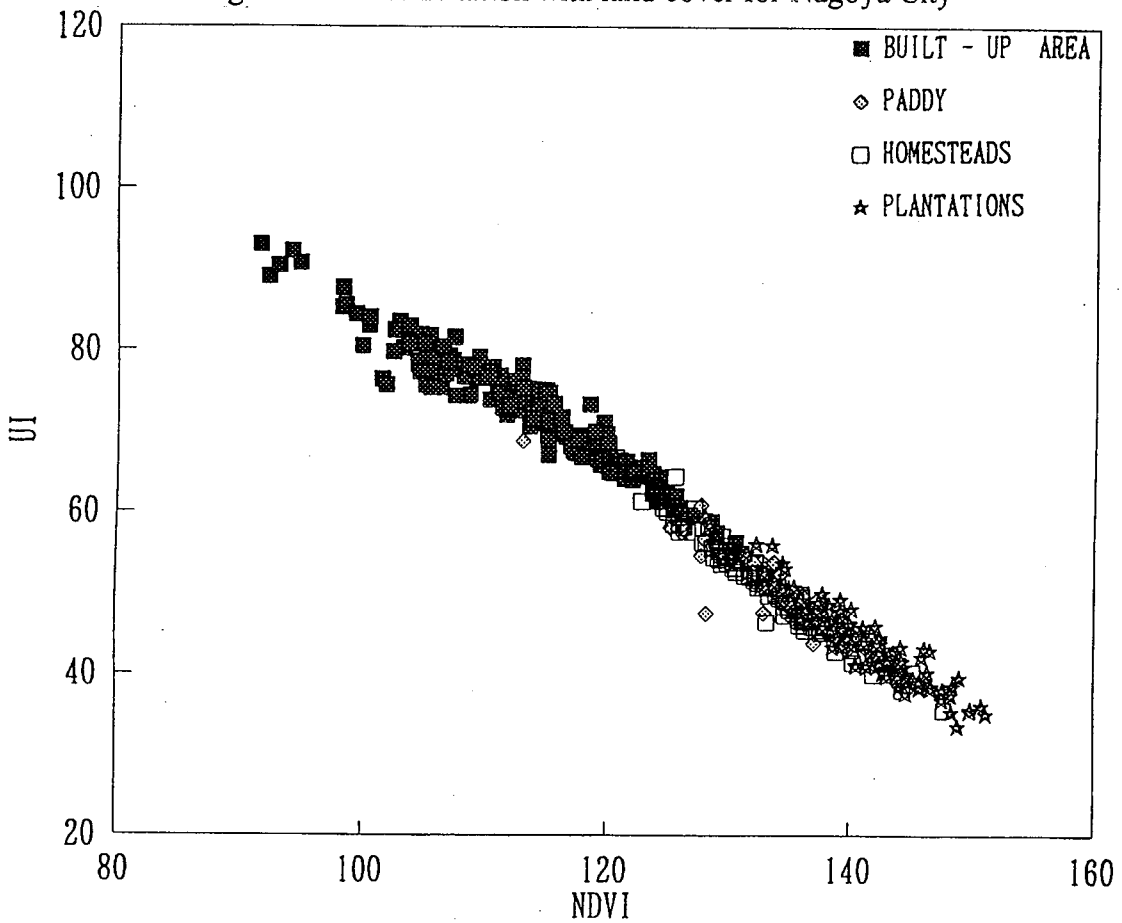

Fig 3. UI-NDVI Relation with land cover for Colombo City

4. Change in urbanisation and the natural environment in central parts of Nagoya City and Colombo City.

4.1 Central Nagoya

A Landsat TM image of Nov 1987 and an image of June 1994 was used to estimate changes in Urbanisation and the change in the natural environment in Nagoya City. The selected image was 512 x 400 pixels. In order to reduce the variations due to the difference in season of the two images histogram matching was done using ground truth from the high density area in the city center and a linear scale conversion was done for each TM band used of 1987.

The computed change in urbanisation from 1987 to 1994 represented by the change in UI for the two dates is seen in Fig: 4 . The change in the central part of Nagoya is small as could be seen which is expected for recent times due to the already saturated development in the inner city areas.

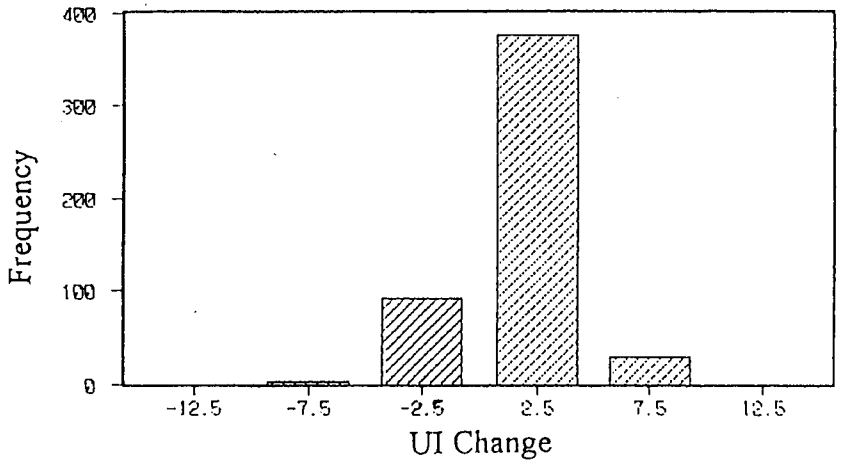

Fig 4 Change in UI - Nagoya City

The corresponding change in the natural environment in the central parts of Nagoya City is represented by the change in NDVI of the two dates. The vectors in Fig 5 show the change in the natural environment due to urbanisation for some of the areas.

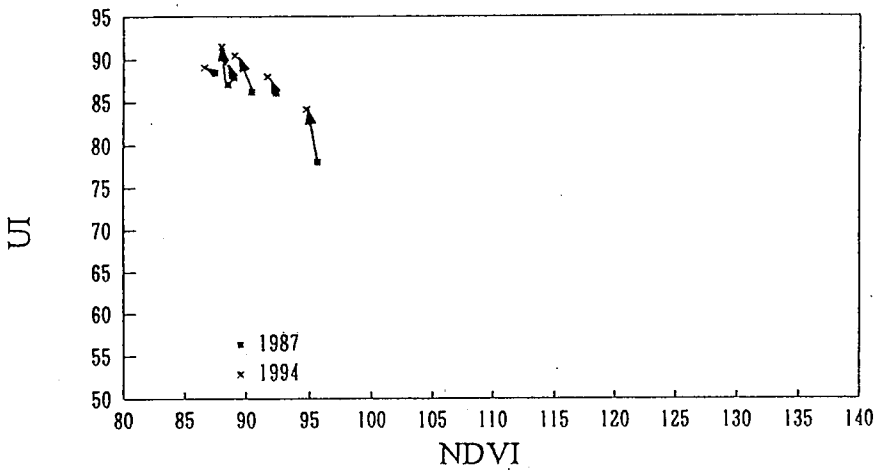

Fig 5 UI-NDVI - Nagoya City

4.2 Central Colombo

A Landsat TM image of February 1994 and digitised building cover data of 1970 obtained by scanning a 1:12673 (16 chains to one inch) map of the building cover in Colombo City and Environs was used to estimate changes in urbanisation and the natural environment during the past two decades.

The map of Colombo City covers the area within the municipal limits of the city and its immediate surroundings. The percentage of building cover (UD) was estimated by using digitised data of this map. The relation between UI and UD and also the relation between UI and NDVI for Colombo City were estimated in a previous study by the same authors(Kawamura et.al, 1994) and is as appears below.

$$UI = (0.47 \text{ X } UD) + 49.2$$
$$UI = (-0.94 \text{ X } NDVI) + 178.3 \qquad (3)$$

Using these equations the UI and NDVI values for 1970 were estimated from building cover data of 1970. The UI and NDVI values for 1994 were estimated from TM data.

The computed change in urbanisation represented by the change in UI of the two dates is as shown in Fig:6.

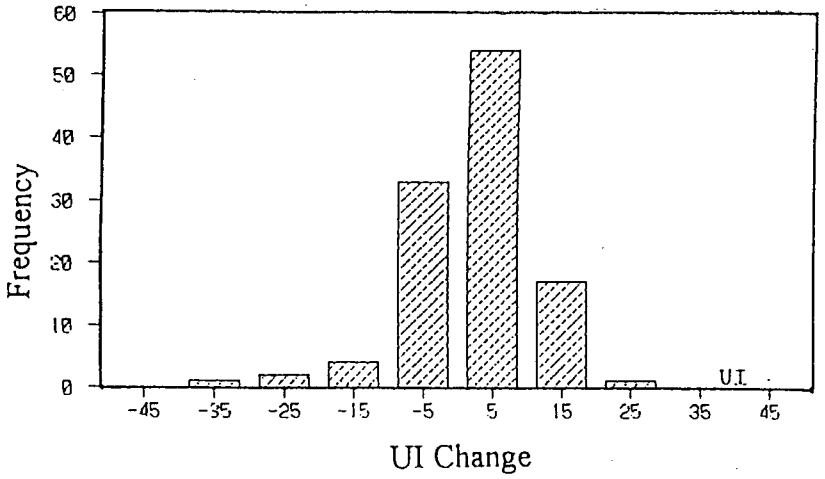

Fig. 6 Change in UI - Colombo City

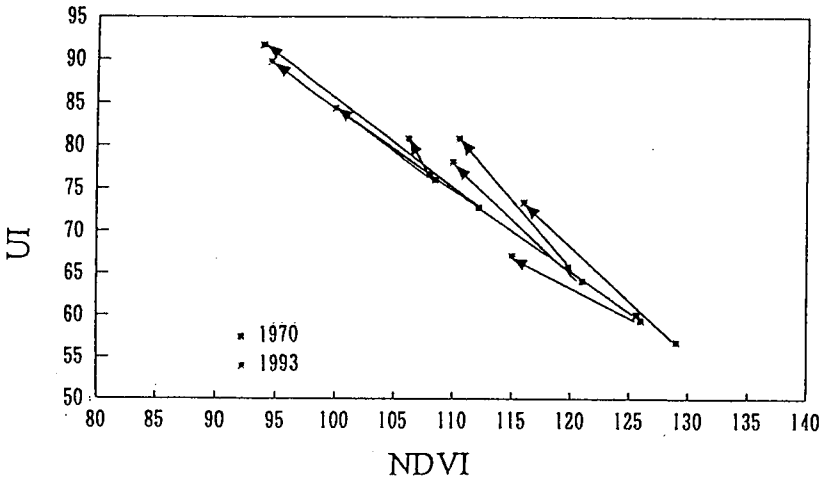

Fig. 7 UI-NDVI - Colombo City

More than half the UI increase is from 5 to 15 corresponding to an increase in urban density from 10% to 30% for a period of two decades for more than half the area considered.

The change in the natural environment is represented by the change in NDVI of the two dates. The vectors in Fig 7 show the change in the natural environment due to urbanisation for some of the areas.

5. Conclusion

Using remote sensing data it was possible to see how the high density urban area spread over a large extent in Nagoya City affected the natural environment in the surrounding suburbs. In comparison Colombo City's high density urban area is limited to a very much smaller area and its suburban areas are hardly affected by the urbanisation. The analysis of remote sensing data of the central areas of Nagoya City and Colombo City showed the position of urbanisation in the two cities precisely. Hence the method adopted could be used to study the relationship between urbanisation and the natural environment of cities in different developing situations.

References

Jensen John R ,"Urban change detection mapping using Landsat digital data", The American Cartographer, Vol. 8, No 2, pp.127-147, 1981.

Kawamura,M.,S.Jayamanna,Y,Tsujiko,"An analysis of urbanisation and environment change in Colombo, Sri Lanka ,using remote sensing data, Proc.of Environmental Information Science Center,Japan,No8, pp 177-122,April 1995.

Marga Institute Sri Lanka.,"Housing Development in Sri Lanka 1971 to 1981".

Ministry of Local Government Housing and Construction ,"City of Colombo Development Plan",1985.

Ormsby,J.P.,"Evaluation of natural and man-made features using Landsat TM Data",Int.J.Remote Sensing, Vol 13, No 2, pp 303-318,1992.

Monitoring Global Vegetation Degradation using GVI data

Shiro Ochi(*) and Shunji Murai(**)

* Department of Forestry, Utsunomiya University
350, Mine, Utsunomiya, Japan, 321
TEL:+81-286-49-5537, FAX:+81-286-49-5545
Email:ochi@cc.utsunomiya-u.ac.jp
**Asian Institute of Technology(AIT)
TEL/FAX:+66-2-524-5705
Email:smu@cs.ait.ac.th

Abstract

Monthly GVI data show unique fluctuations based on vegetation types and climatic and topographic conditions on the spots. By using GVI data for years in combination with digital maps of ecosystem, meteorological data, elevation, etc., relationships between GVI fluctuation pattern and geographic information is clarified. A index estimating vegetation degradation in global scale is proposed using GVI data. The index can be applied to assess the global land degradation which is difficult to be monitored directly with remotely sensed data.

Introduction

For the assessment of desertification and land degradation with climatic change in global/continental scale, long-term observation with several decades is necessary(Justice, et. al, 1985, Tucker, et al, 1986). On the other hand, desertification and land degradation has been defined as the phenomena which makes land desert or degraded induced by human activities(UNEP, 1992). As vegetation degradation is mainly caused by deforestation, vegetation destruction as well as land degradation, monitoring vegetation degradation with meteorological data can indicate the land degradation.

Data

Following data used in this study were extracted from GLOBAL VIEW DATASET published by NOAA National Environmental Satellite Data and Information Service:

1. Monthly GVI data

(from April 1985 to December 1988(45 months), 10 minutes pixel resolution)

2. Leemans and Cramer IIASA Climate data

2.1 Average Monthly Air Temperature

2.2 Average Monthly Precipitation

(30 minutes pixel resolution)

3. Baily Ecoregions of Continents

(10 minutes pixel resolution)

4. Willson, et al: Soil Type data

(1 degree pixel resolution)

Analysis

Data analysis consists of 4 components as follows;

(A) Calculate statistics of GVI data : To understand characteristics of GVI fluctuation of each point, mean of GVI in 45 months, standard deviation of GVI in 45 months, and trend of fluctuation of GVI in 45 months are computed. (B) Calculate statistics of meteorological data. (C) Define the formula forecasting vegetation fluctuation based on meteorological data, elevation and soil data. (D) Calculate vegetation degradation index which is the sum of deference of GVIs and calculated values for 12 months(or 45 months). (E) Evaluate the vegetation index comparing the existing land degradation map such as GLASOD database.

Discussions

The index developed in this study is showing the trend of vegetation degradation in global scale which is 10 minutes resolution(about 18km at equator). However land degradation is considered to happen with area of several hectares to several square kilometers depending the types of degradation. So the accuracy of resolution is expected to be improved. Whereas a similar analysis using 8km AVHRR NDVI data is now undertaken, it is difficult to get high-resolution meteorological information.

References

Justice, C.O., Townshend, J.R.D., Holden, B.N. and Tucker, C.J., INT.J Remote Sensing, 1985, vol.6, NO8,1271-1318

Tucker, C.J., Maximum normalized difference vegetation Index images for sub-Sahara Africa for 1983-1985, INT.J. Remote Sensing, 1986, vol.7, NO11, 1383-1384

UNEP, World Atlas of Desertification, 1992

Monthly Vegetation Changes in the Arabian Peninsula: Observations from AVHRR Global Vegetation Index Composite Data

Andy Yaw Kwarteng and Dhari Al-Ajmi

Kuwait Institute for Scientific Research
Division of Environmental and Earth Sciences
P.O. Box 24885
13109 Safat, Kuwait
Fax: +965-481-5202
Email: andyk@sunpci.kisr.edu.kw

Abstract

Satellite remote sensing offers an unparalleled technique to map land cover types at local, regional and global scales. Methods to map seasonal and yearly vegetational changes are critical to studying desert dynamics and providing the best techniques to combat desertification in arid environments. Such techniques facilitate the mapping of arable lands, areas threatened by desertification, as well as areas susceptible to erosion and subsequent generation of sand and dust storms. Selective principal component analysis applied to the AVHRR data of the Arabian Peninsula acquired in 1992 depicted the monthly vegetation dynamics of the Arabian Peninsula. For the majority of the areas that showed changes, the amount of vegetation increased substantially from November through April, a period coinciding with cooler temperatures and higher rainfall. On the contrary, vegetation either decreased or remained unchanged from June to August. Exceptions to the observed trends were found in the southwestern part of the Peninsula, along the east coast of the Mediterranean Sea, and in the Mesopotamian Basin.

1. Introduction

Mapping of land cover from space offer an unparalleled technique to monitor vegetation changes at both local, regional and global scales. The principal image sensor for global or broadscale land cover analysis has been the Advanced Very High Resolution Radiometer (AVHRR) onboard National Oceanic and Atmospheric Administration (NOAA) series of polar orbiting meteorological satellites. Several studies using NOAA AVHRR data to monitor vegetation cover in diverse environments have been reported in the literature (Townshend and Justice, 1986; Choudhury and Tucker, 1987; Goward et al., 1991; Justice et al., 1991; Tucker et al., 1991). The most commonly used technique for vegetation analysis is the normalized difference vegetation index (NDVI), a parameter derived from the red and near-infrared bands. The ratio is computed as follows:

$$NDVI = (Ch2-Ch1)/(Ch2 + Ch1) \quad (1)$$

where Ch1 and Ch2 are digital number (DN) values in AVHRR's visible (0.58-0.68 μm) and near-infrared (0.72-1.1 μm) bands, respectively. The ratio is a measure of the deviations between a vegetation spectrum's chlorophyll absorption minimum and the infrared plateau, and therefore, a direct indication of the amount of photosynthetically active green biomass (Tucker and Sellers, 1986). NDVI is suitable for global vegetation monitoring as it partially compensates for slope, viewing aspect and changing illumination conditions (Kidwell, 1994).

Methods to map seasonal and yearly vegetational changes are critical to studying desert dynamics and providing the best techniques to combat desertification in arid environments. Such techniques facilitate the mapping of arable lands, areas threatened by desertification, as well as areas susceptible to erosion and subsequent generation of sand and dust storms. Vegetation, undoubtedly, is the single most effective and environment friendly way to stabilize soils and reduce wind erosion. In arid environments NDVI must be used with caution as the ratio may not show any sensitivity in areas with less than 20% vegetation (Choudhury and Tucker, 1987). Additionally, Chavez and MacKinnon (1994) observed that in arid and semi-arid environments, a calibrated visible band was better than NDVI in mapping vegetation changes.

This study provides some preliminary results on the analysis of the vegetation dynamics of the Arabian Peninsula. We applied selective principal component analysis (PCA) to the scaled calibrated vegetation index (SCVI) in Global Vegetation Index (GVI) product acquired in 1992 to map monthly vegetation changes in the Arabian Peninsula. SCVI is computed in the same manner as NDVI, but the digital numbers of AVHRR's channels 1 and 2 are first converted to albedos (Kidwell, 1994).

2. General Description of the Arabian Peninsula

The Arabian Peninsula encompasses a large sub-continental land mass with a dimension of 2000 by 2700 km, and an area of approximate 3 x 10^6 km^2 (Fig. 1). An important and distinctive feature of the Arabian Peninsula is the desert type of environment that transcends between inter-tropical and sub-tropical arid belts. Dry, hot summers, mild, rainy winters, low humidity, dry strong wind conditions, and absence of standing water are common phenomena. Mean monthly temperatures range from approximately 10° C in the highlands of the southwest to 36° C along the Arabian Gulf coast (Anton, 1985).

The periphery of the Peninsula is characterized by highlands, whereas the central part is homogeneous and consists of dune fields, a succession of flat pediplains and alluvial fans. The area is home to different deserts or sand seas, supporting more than twenty individual sand fields greater that 1000 km^2 (Anton, 1985). Eoalian deposits and landforms, with many instances of an abrupt transition from one type to another are widespread. Majority of the dunes in the north-central and northwestern part (e.g., An Nafud and Northern Ad Dahna) have some grass cover and therefore have been kept stable. On the contrary, dunes in the south (Southern Ad Dahna, Jafurah and Rub al Khali) experience strong eolian activity due to the absence of protective covers (Fig. 1). There is a transition zone between the two areas where sand fields are either partially stabilized or have experienced increased degradation of previously stabilized dunes.

Rainfall is scanty and erratic and ranges between 400-500 mm per year in the south-western highlands in Yemen to nearly 0 mm in some areas of Rub al Khali desert, Saudi Arabia. The eastern and western margins average less than 100 mm of rainfall annually with decreasing precipitation in other parts. The annual evapotranspiration values are between 1100 and 1700 mm. October to May brackets the rainfall season in most of the Peninsula, but nearly all the rainfall occurs between December to February. During the rainy season the area is hit by extra-tropical cyclones with considerable amounts of moisture. Due to the southwest monsoon, the rainfall season in the highlands of Yemen is from July to September. It is not uncommon for most of the year's rain to occur within a short period leaving the rest of the season with little or no rainfall. Lack of rainfall intensifies aridity and causes degradation of natural vegetation.

The Arabian Peninsula can be classified as either arid, semiarid, or hyperarid. Whereas most of the Peninsula is free of perennial vegetation, the arid regions can support numerous ephemeral and

perennial vegetation. For most areas shifting sand dunes are incapable of sustaining plant life. The Peninsula abounds in flora communities that can contain a notable variety of species. The geomorphology, vegetation, human and animal life are strongly affected by the harsh environment.

3. Methods

3.1 Change Detection Techniques

Several change detection techniques applied to satellite digital data have been reported in the literature. Some of these include image difference, ratioing, principal component analysis, and selective principal component analysis (Chavez et al., 1977; Singh, 1989; Chavez and Kwarteng, 1989; Chavez and MacKinnon, 1994). To apply change detection, radiometric calibration of data is critical. The required calibration can either be absolute or relative depending upon the intended use. In absolute calibration the satellite digital number (DN) is converted to ground reflectance, while in relative the sense the same DN in two images represent the same reflectance. A third type of calibration is a hybrid between the absolute and the relative methods. Application of relative calibration is only meaningful if the DN changes between two images is statistically small and does not alter the overall dynamic range of the images. Such conditions are usually observed in arid and semi-arid environments (Chavez and MacKinnon, 1994).

Principal component analysis (PCA) is a statistical technique that rotates the axes of a multi-dimensional image space in the direction of maximum variance. The generated components or axes, which are simple linear combinations of the original image data, are orthogonal to each other and, thus, have no further mathematical relations. Eigenvectors are used as multiplication coefficients or loadings in the PCA for each pair of input bands.

3.2 Data Analysis

In this study we applied selective principal component in the same manner as used by Chavez and Kwarteng (1989), where only two bands are used as input in the PCA. Information that is common to the two images/bands, typically topographic, albedo or reflectance, is mapped to the first component (PC1), whereas information that is unique to either of the input images is mapped to the second component (PC2). Consequently, PC2 maps the spectral contrast if the two images were collected at the same time, or the temporal contrast if the images were takes at different times. In transforming the data into a new coordinate system, the selective principal component technique performs a first-order relative image to image calibration, and therefore, automatically eliminates most low-frequency noise between the two images. Such noise reduction capabilities enhance the quality of images generated. A major advantage of selective principal components over the traditional PCA analysis (with several bands as input in the PCA) is the relatively ease and straight-forward interpretation of the resulting images.

Image processing was performed on a UNIX-based SUN workstation with PCI's EASI/PACE image processing software at Kuwait Institute for Scientific Research's (KISR) Remote Sensing Lab. The resolution of the GVI data is 16 km at the equator. A histogram matching procedure from PCI software was used to create a lookup table matching an input image to a master image. Consequently, the same DN values in the images represent the same reflectance. The October-January PC2 image with the largest DN spread was used as the master.

4. Discussion of results

Table 1 shows the percent information mapped to principal components 1 and 2 (PC1 and PC2), and the eigenvectors vectors that are used as multiplication coefficients or loadings in the PCA for the input images. The larger the percentage of information for PC2 the less the correlation between the input images and, therefore the larger the amount of vegetation variation. For example, vegetation changes in the June-July are less than those computed for the November-December PC2 image. The loadings for PC1 is approximately equal to the average of the input images, whereas the loadings for PC2 is equal to their difference. The loadings for PC2 is either negatively or positively biased in favor of one of the images and that must be taken into consideration in their interpretation. The PC2 variance ranges from 2.57-6.63% (Table 1), indicating that monthly vegetation changes are quite significant even at the scale of the AVHRR NDVI composite data.

The PC2 images (Fig. 2), map the NDVI spectral contrast information between the input pairs of consecutive monthly data. Lighter or darker tones than gray represent either increase or decrease in vegetation depending upon the sign of the PC2 loadings (Table 1). Images with positive loadings refer to all areas brighter than gray while negative loadings refer to all areas darker than gray. The Arabian Gulf, Red Sea, Arabian Sea and Mediterranean Sea which do not manifest any NDVI changes are all shown as gray on the images. The degree of light or dark tones gives an indication of the extent of vegetation variation.

Vegetation changes between the composite AVHRR NDVI data for January-February account for 3.49% of the total information between the data for the two months. Areas that had more vegetation in January than February (white areas) are the eastern Rub al Khali, southern Western Highlands and eastern coast of the Mediterranean Sea [Fig. 2(a)]. Vegetation increased from January-February (black areas) primarily in the Northern Dahna, southern part of An Nafud, and in the Mesopotamian Basin in Iraq and Iran. The rest of the Peninsula did not show any significant vegetation changes. The trend for monthly vegetation increase (white area) in the An Nafud, Northern Ad Dahna and Mesopotamian Basin is further observed in the PC2 image of February-March [Fig. 2(b)]. Other areas with more vegetation in March than February include the northwestern area along the Mediterranean Sea, and parts of the Western Highlands. The few locations that had more vegetation in February than March (dark areas) are in the Southern Ad Dahna and in the southern part of the Peninsula. The trends observed in Figure 2(c) are similar to Figure 2(b), i.e., the Mediterranean coast, the Mesopotamian Basin and sections of the An Nafud continued their monthly vegetation increase (white areas). The southwestern part of the Peninsula show slight increase in vegetation from March to April. Vegetation cover also increased in the Northern and Southern Dahna.

The PC2 image of April-May has one of the largest percent variance, evidence of the end of spring and the onset of summer. The lighter areas in Figure 2(d) had more vegetation in April than May. The monthly vegetation increase in the An Nafud , Ad Dahna, Mesopotamian Basin and the Mediterranean coast is reversed due to the dawn of the hot dry summer weather. The southeastern and southwestern sections of the Peninsula show slight increase in vegetation from April to May. Figure 2(e) depicts vegetation differences between May and June. Areas in the Western Highlands, Rub al Khali, Mesopotamian Basin and scattered locations throughout the Peninsula display increase in vegetation, indicating the continuation of rainfall in these areas in May-June. Figure 2(f), representing the PC2 image of June-July shows relatively minor vegetation changes in the Peninsula and that is reflected in the small percent variance mapped to PC2 (Table 1). Areas to the southwest, southeast, parts of the Mesopotamian Basin and the east coast of the Mediterranean Sea display more vegetation in June as compared to July. The rest of the Peninsula either shows only slight or no vegetation changes in June-July. Some of the trends observed in Figure 2(f) continue in Figure 2(g). Along the Western Highlands, the east coast of the Mediterranean Sea and Mesopotamian Basin there was more vegetation in July than in August (white areas). The co-existence of areas showing decrease and increase in vegetation in the Mesopotamian Basin is attributed to irrigated

lands. The only areas with slight vegetation increase from July to August are southwestern corner of the Peninsula in Yemen, and the eastern parts in Oman and the United Arab Emirates. The majority of the Peninsula portrays either a decrease or no change in vegetation. The similarity in the patterns of the summer months, i.e., constant decrease in vegetation due to the hot dry conditions is reflected in the relatively low percent variance mapped to their respective PC2 images.

The percent variance mapped to the August-September image show an increase over the previous values in Table 1. The southern part of the Western Highlands depicts an increase in vegetation (white areas) from August to September as observed in Figure 2(h). This is due to the moist laden southwest monsoons hitting the area between July to September. The rest of the Peninsula displays either no or slight vegetation decreases from August to September. Locations in the Mesopotamian Basin showing an increase in vegetation may be due to cultivated lands. The PC2 image of the September-October image [Fig. 2(i)] has the least percent variance mapped to PC2. Only a few areas show significant vegetation changes. Small sections in the western and southern part of the Peninsula display slight vegetation increases (white areas) from September to October.

Figure 2(j) displays more vegetation in October compared to November in the southern Western Highlands, along the eastern Mediterranean Coast and in the Mesopotamian Basin. Vegetation decrease in the Western Highlands is an indication of the end of the rainfall season. The rest of the Peninsula shows either a slight increase or no vegetation changes in November compared to October. The significant increase in the percent variance of PC2 signaled the onset of the rainfall season for most the Peninsula. The PC2 image of November-December has the highest percent variance mapped to PC2. The lighter tones in Figure 2(k) are the locations with increased vegetation from November to December. The significant areas are along the Western Highlands, and in general, in the northern part of the Peninsula. Figure 2(l) shows continued monthly increase in vegetation (white areas) in most parts of the Arabian Peninsula with the exception of the southwestern sections that portray more vegetation in December than in January.

The maps shown provide spatial as well as temporal variation in vegetation across the Arabian Peninsula. The dynamics of vegetation is reflected in the percent variance mapped to the PC2 images. The percentages would certainly be higher if the total area analyzed excluded the marine environment. The principal causes for local monthly variation in vegetation was primarily due to the climate, and more importantly rainfall. For the majority of the areas that showed changes, the amount of vegetation increased substantially from November through April, a period coinciding with cooler temperatures and higher rainfall. On the contrary, vegetation either decreased or remained unchanged from June to August. Exceptions to the observed trends were found in the southwestern part of the Peninsula, along the east coast of the Mediterranean Sea, and in the Mesopotamian Basin. In the southern Western Highlands and southern parts of the Peninsula vegetation increased from July through October. The coincidence of increase and decrease of vegetation in the Mesopotamian Basin is ascribed to rainfall and cultivation of lands.

Areas that showed fluctuations in NDVI are most like to support plant life in the presence of abundant water. From the analysis of the 1992 AVHRR NDVI data, such areas were predominantly found in the Mesopotamian Basin, the east coast of the Mediterranean Sea, the Western Highlands and parts of the An Nafud and Ad Dahna deserts. Locations that consistently showed no monthly vegetation changes were dried and would support little plant and animal life. The desert area in the central part of the Peninsula, namely, Rub al Khali, Jafurah, and parts of the Ad Dahna and An Nafud displayed such qualities. These areas are most likely to be vulnerable to severe wind erosion and generation of sand and dust storms. More vegetation variations were observed in the An Nafud and Northern and Southern Ad Dahna as compared to the Rub al Khali

and Jafurah deserts. The latter are therefore more likely to be active and subjected to stronger wind erosion. Such observations have been reported by Anton (1985).

5. Conclusion

Application of selective principal component analysis technique to NOAA AVHRR data proved very valuable in mapping areas subjected to fluctuations in natural vegetation in the Arabian Peninsula. Such locations are most suitable for supporting plant and animal life, especially in the presence of abundant water. On the contrary, the areas that did not display significant changes in NDVI are barren and vulnerable to severe wind erosion and generation of sand and dust storms. NOAA AVHRR database with a much better resolution would furnish more detail local potential arable lands and areas prone to desertification.

6. Acknowledgments

We thank the management of KISR for the support of this research.

7. References

Anton, D., "Environmental changes and aeolian dynamics during the Quaternary in the Arabian Peninsula", in Proceedings on the International Workshop on Sand transport and desertification in arid lands, 17-26 November 1985, Khartoum, Sudan, 1985.

Chavez, P.S., Jr., G.L., Berlin, and W.B. Mitchell, "Computer enhancement techniques of Landsat MSS digital images for land use/cover assessment", in Proceedings of the Sixth Remote Sensing of Earth Resources Symposium, Tullahoma, Tenn. p. 259-275, 1977.

Chavez, P.S., Jr., and A.Y. Kwarteng, "Extracting spectral contrast in Landsat Thematic Mapper image data using selective principal component analysis", Photogrammetric Eng. and Remote Sensing, Vol. 55, no. 3, pp. 339-348, 1989.

Chavez, P.S., Jr., and D. MacKinnon, "Automatic detection of vegetation changes in the southwestern United States using remotely sensed images", Photogrammetric Eng. and Remote Sensing, Vol. 60, No. 5, pp. 571-583, 1994.

Choudhury, B.J., and C.J. Tucker, "Satellite observed seasonal and inter-annual variation of vegetation over the Kalahari, the Great Victoria Desert, and the Great Sandy Desert: 1979-1984", Remote Sensing of Environment, Vol. 23, pp. 233-241, 1987.

Goward, S.N., B. Markham, D.G. Dye, W. Dulaney, and J. Yang, "Normalized difference vegetation index measurements from the Advanced Very High Resolution Radiometer", Remote Sensing of Environment, Vol. 35, pp. 257-277, 1991.

Justice, C.O., J.R.G. Townshend, and V.L. Kalb, "Representation of vegetation of continental data sets derived from NOAA-AVHRR data", Int. J. Remote Sensing, Vol. 12, pp. 999-1021, 1991.

Kidwell, K.B., "Global vegetation index users guide", U.S. Department of Commerce, NOAA/NESDIS/NCDC/SDSD, Washington, DC, 1994.

Singh, A., "Review article: Digital change detection techniques using remotely-sensed data", Int. J. Remote Sensing, Vol. 10(6), pp. 989-1003, 1989.

Townshend, J.R.G., and C.O. Justice, "Analysis of the dynamics of African vegetation using the normalized difference vegetation index", Int. J. Remote Sensing, Vol. 7 (11), pp. 1435-1445, 1986.

Tucker, C.J., and P.J. Sellers, "Satellite remote sensing of primary production", Int. J. Remote Sensing, Vol. 7, pp. 1395-1416, 1986.

Tucker, C.J., W.W. Newcomb, S.O. Los, and S.D. Prince, "Mean and inter-year variation of growing-season normalized difference vegetation index for the Sahel 1981-1989", Int. J. Remote Sensing, Vol. 12 (6), pp. 1133-1135, 1991.

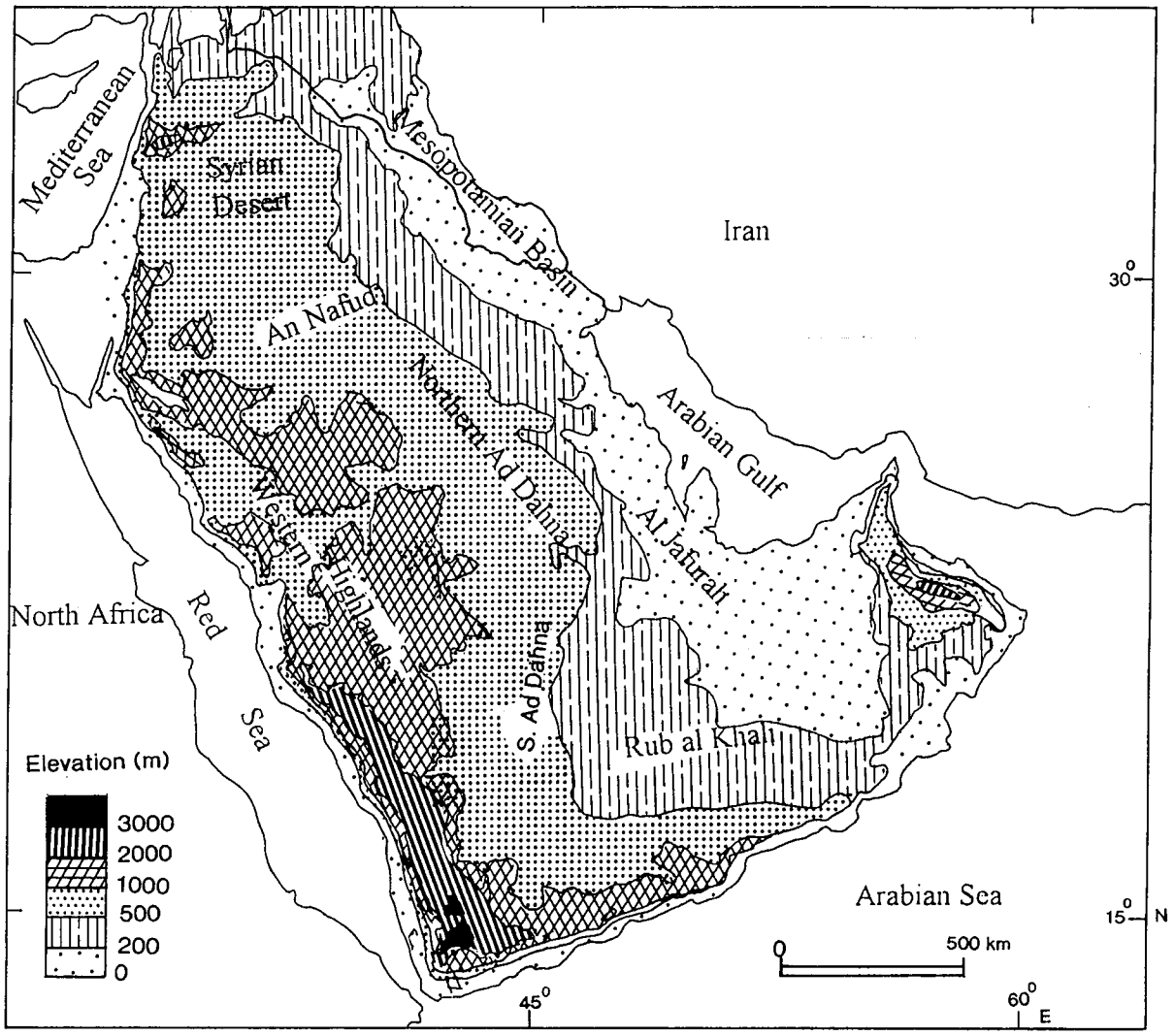

Figure 1. Map of the Arabian Peninsula showing topography and the location of the major deserts.

Table 1. Percent of Variance Mapped to PC1 and PC2, and the Loadings Used in PCA for Each Monthly Pair of AVHRR NDVI for the Arabian Peninsula.

Input Pair	% Variance PC1	% Variance PC2	Loadings PC1	Loadings PC2
Jan-Feb	96.51	3.49	(-0.74,-0.68)	(0.68,-0.74)
Feb-Mar	96.82	3.18	(-0.67,-0.74)	(-0.74,0.67)
Mar-Apr	96.33	3.67	(-0.66,-0.75)	(-0.75,0.66)
Apr-May	95.73	4.27	(-0.77,-0.63)	(0.67,-0.77)
May-Jun	97.10	2.90	(-0.70,-0.71)	(-0.71,-0.70)
Jun-Jul	97.43	2.57	(-0.72,-0.69)	(0.69,-.0.72)
Jul-Aug	97.34	2.66	(-0.73,-0.68)	(0.68,-0.73)
Aug-Sep	96.23	3.77	(-0.67,-0.74)	(-0.74,0.67)
Sep-Oct	97.41	2.59	(-0.71,-0.71)	(-0.71,0.71)
Oct-Nov	95.86	4.14	(-0.77,-0.63)	(0.63,-0.77)
Nov-Dec	94.71	5.29	(-0.68,-0.74)	(-0.73,0.68)
Dec-Jan	95.72	4.28	(-0.64,-0.77)	(-0.77,0.64)

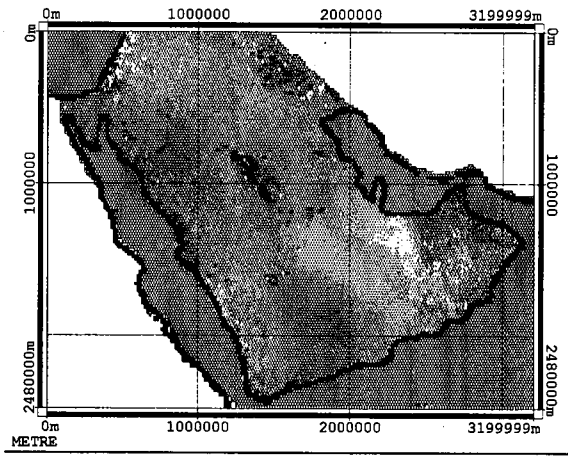

Figure 2(a). PC2 Jan-Feb

1:50 000 000 Scale

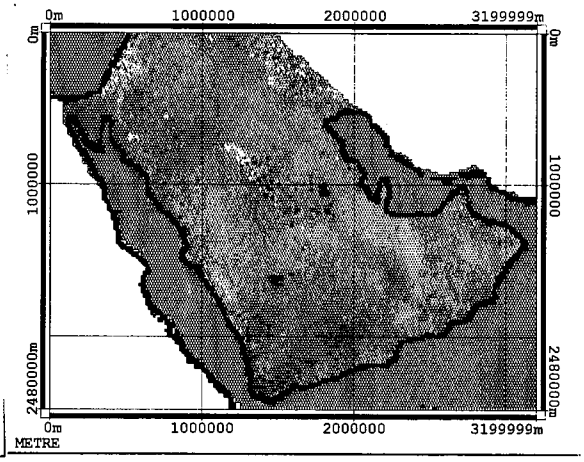

Figure 2(b). PC2 Feb-Mar

1:50 000 000 Scale

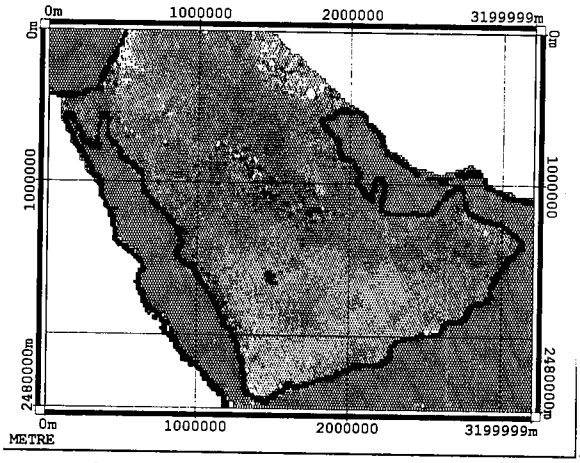

Figure 2(c). PC2 Mar-Apr

1:50 000 000 Scale

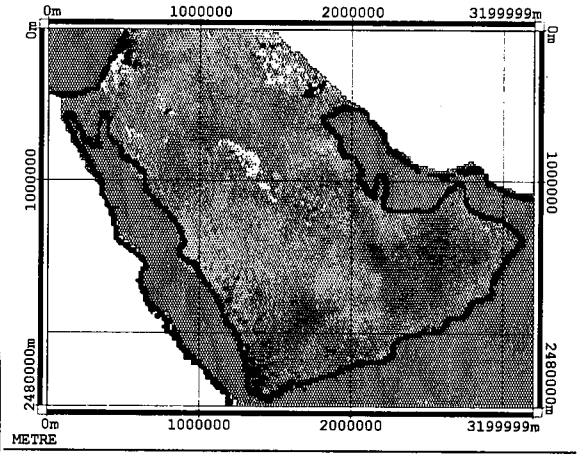

Figure 2(d). PC2 Apr-May

1:50 000 000 Scale

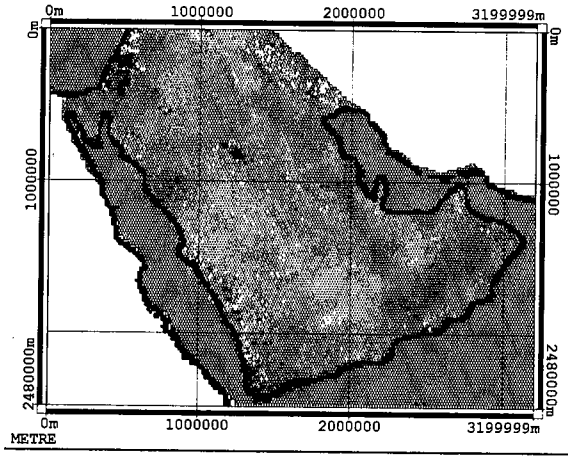

Figure 2(e). PC2 May-Jun

1:50 000 000 Scale

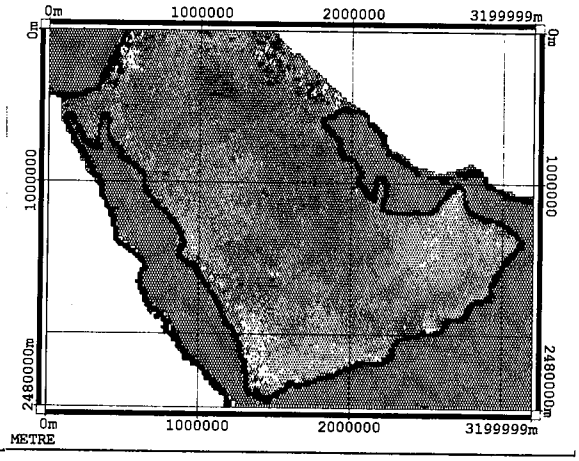

Figure 2(f). PC2 Jun-Jul

1:50 000 000 Scale

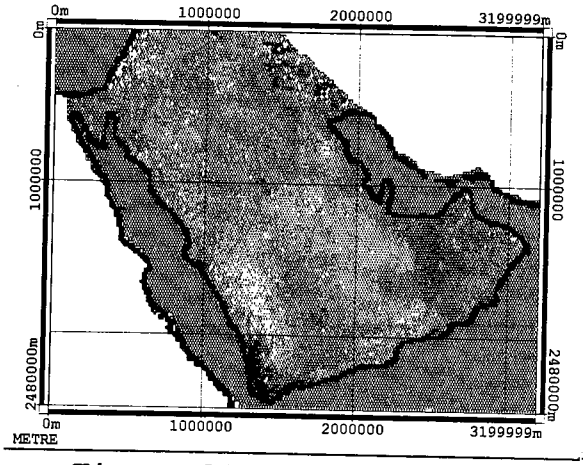

Figure 2(g). PC2 Jul-Aug

1:50 000 000 Scale

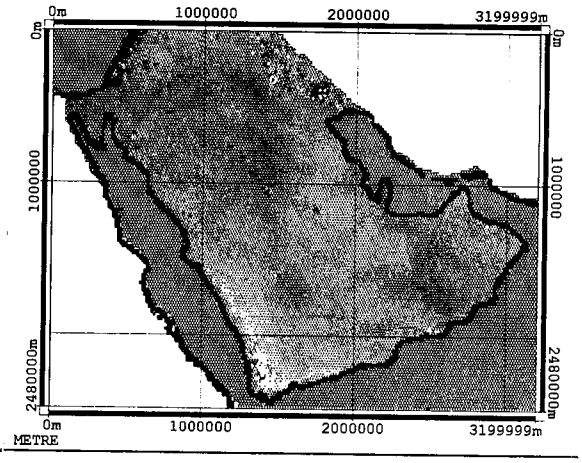

Figure 2(h). PC2 Aug-Sep

1:50 000 000 Scale

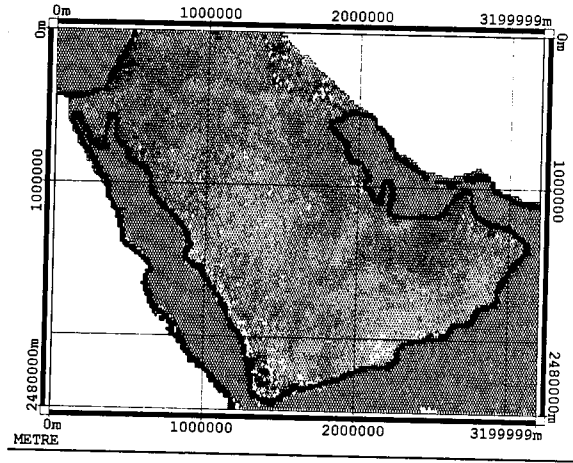

Figure 2(i). PC2 Sep-Oct

1:50 000 000 Scale

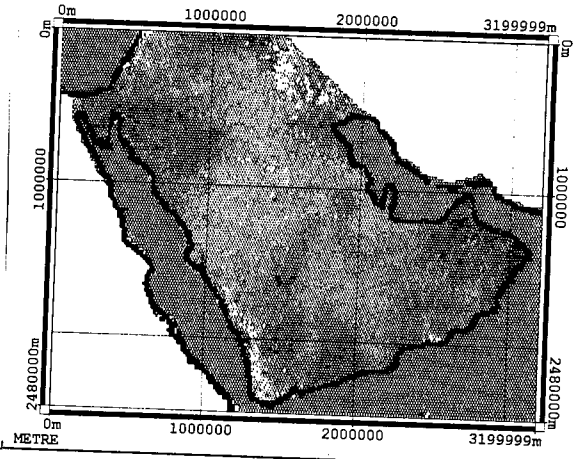

Figure 2(j). PC2 Oct-Nov

1:50 000 000 Scale

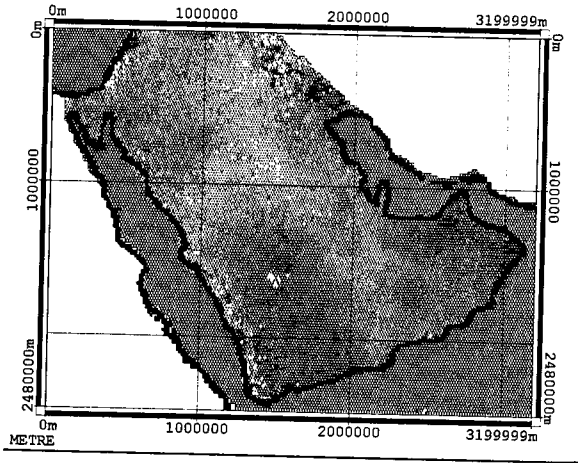

Figure 2(k). PC2 Nov-Dec

1:50 000 000 Scale

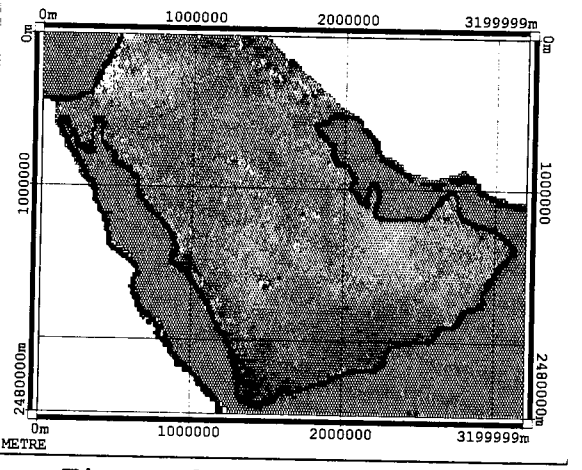

Figure 2(l). PC2 Dec-Jan

1:50 000 000 Scale

Figure 2. Principal component number two monthly pair images of AVHRR NDVI composite data of the Arabian Peninsula acquired in 1992. The gray areas do not show any changes, whereas the darker or lighter tones represent increase or decrease in vegetation.

Monitoring of Climax Forest Area for Global Environment Study

Haruo Sawada, Hideki Saito
Forestry and Forest Products Research Institute
P.O.Box 16, Tsukuba-Norin, Ibaraki, 305 Japan
Fax:+81-298-73-1541
Email: sawady@ffpri.affrc.go.jp
rslsaito@ffpri.affrc.go.jp

abstract

We have been trying to establish an international network system of a long term monitoring for the purpose of understanding global environment change from a forestry point of view.

The climax forests in Japan, especially those protected in Forest Biosphere Reserves are very precious, because they have been formed as the result of the balance which have lasted quite a long time between the forests and the surroundings.

These forests not only hold various kinds of creatures but also show ecological activities which will directly reflect the changes of natural condition such as temperature and precipitation.

Therefore, it will be possible to comprehensively estimate those changes by observing the phenological aspect of climax forests for a long period of time.

In order to do so, however, the following procedures may be essential: Collecting the forest condition data through aerial photographs and field surveys; Making database for collected data; Long term observation using satellite; and International collaborations.

It is expected to make it possible to estimate the effects on the land ecosystem, such as of global warming which is predicted to be unevenly distributed on the earth.

1. Introduction

With the collaboration of more than one hundred forestry researchers in the world, IUFRO (International Union of Forestry Organization) summed up the international guideline for forest monitoring on the minimum requirement for global monitoring in order to contribute international activities in forestry community (IUFRO, 1994).

Based on this guideline, we, the World Forest Environment Monitoring Research Team of FFPRI, have started a new research project "Monitoring of Climax Forests for Global Environment Study" in 1995. The objective of the study is to obtain the information of global environment changes through climax forest monitoring for estimating the effects on the land ecosystem such as of global warming which are predicted to be unevenly distributed on the earth.

The climax forests, especially those protected in Forest Biosphere Reserves are very precious, because they have been formed as the result of the balance which have lasted quite a long time between the forests and the surroundings. These forests not only hold various kinds of creatures but also show ecological activities which will directly reflect the changes of natural condition such as temperature and precipitation.

Therefore, it will be possible to comprehensively estimate those changes by observing the phenological aspect of climax forests for a long period of time. In order to do so, however the following procedures may be essential:

Collecting the forest condition data through aerial photography and field surveys;
Making database for collected data;
Long term observation using satellite remote sensing; and
International collaborations.

As the first study area, we selected Azumayama Biosphere Reserve in Japan.

2. Methodology

2.1 NDVI

Channel 3 (red : 630 - 690 nm) and channel 4 (near-infrared : 760 - 900 nm) of TM are considered the most useful for creating the index NDVI for monitoring vegetation. The NDVI is the difference of near-infrared and visible red reflectance values normalized over total reflectance of the two channels as follows.

$$NDVI = (Near\_IR\ (TM\_4) - Red\ (TM\_3)) / (Near\_IR\ (TM\_4) + Red\ (TM\_3))$$

This equation produces NDVI values in the ranges of -1.0 to 1.0, where negative values generally represent clouds, water and other non-vegetated surfaces, and positive values represent vegetated surfaces. The NDVI relates to photosynthetic activity of living plants. The higher the NDVI value, the more "green" the cover type (Deering et al.). It means that the NDVI increases as the quantity of green biomass increases in an area (Burgan and Hartford, 1993). To interpret the NDVI values for field use, we have devised methods to convert the NDVI data into more easily understandable representations of vegetation greenness as is used for AVHRR (Burgan and Hartford, 1993). These are called "Visual greenness" and "Relative greenness".

2.2 Visual Greenness (VG) and Relative Greenness (VG)

VG indicates how green each pixel is in relation to a standard reference such as a highly green and densely vegetated evergreen forest. It is calculated as:

$$VG = NDVI / V\_dens$$

where NDVI = observed NDVI value
V_dens = NDVI value of densely vegetated evergreen forest

An image can be produced that portrays vegetation greenness as we would expect to see it if we were flying over the landscape. In this context, normally deforiaged, sparsely vegetated area will look cured compared to fully vegetated area such as the evergreen forest. Because

the visual greenness image may indicate rather limited changes over time, a second measure of vegetation greenness is considered useful.

Relative greenness (RG) is also a percentage value. It expresses "how green each pixel currently is" in relation to the range of greenness calculated for that pixel from the collected and overlaid remote sensing data set. It is calculated as:

RG = (NDV - ND_min) / (ND_max - ND_min)
where NDV: observed NDVI value
ND_min: minimum NDVI value observed historically for that Pixel
ND_max: maximum NDVI value observed historically for that Pixel

Historical maximum and minimum NDVI maps for the study area are necessary to be produced by searching all the TM NDVI values of collected data and saving the largest and smallest values observed for each pixel. Pixels affected by clouds and snows are excluded. These NDVI values are then composed into maximum and minimum maps and used with current NDVI maps to perform the visual and the relative greenness calculations.

3. Study Area

3.1 Forest Biosphere Reserves in Japan

Under the circumstances that the public has recently shown growing interest in forests, demand for preservation of primeval natural forest has been rising. Thus, in order to harmonize forestry and nature preservation in National Forest, in 1989, Forestry Agency completely revised its protected forest system established in 1915. The protected forests were classified into 7 types including Forest Biosphere Reserves, etc. As of the end of 1993, 779 areas with total area of 358 thousand hectors are designated as protected forests.

Forest Biosphere Reserves, which aim to preserve natural environment and to protect important flora and fauna, have already been designated in 17 areas covering about 207,401 hectors at the end of 1993. Yakushima region and Shirakami mountainous region among them have recently been registered as natural heritage sites under the World Heritage Convention.

3.2 Outline of the Azumayama Forest Biosphere Region

Azumayama (Azuma mountain range) designated as a subject sight for the research is on the Nasu volcanic zone. It is constituted of mountains over 1,900 m above the sea level, which makes Azumayama the biggest group of isolated mountains among the Nasu volcanic mountain range. It is made up of East Azumayama mountain range and West Azumayama mountain range. And the highest among them is West Azumayama, 2,035 meters above the sea level. East Azumayama mountain range is composed of five main mountains. One of the mountains, Mt. Issaikyou (1,949m) is an active volcano since 1950. West Azumayama mountain range is also composed of five main mountains. All of them stopped their volcanic activities quite a long time ago. That is why each mountain has long mountain ridge with small ups and downs , and holds forest nearly up to the mountain top.

The local climate pattern around Azumayama applies to a shifting zone between the Japan Sea side climate zone and the Pacific Ocean side one. It is estimated according to the data from the

nearest meteorological observatory that the annual average temperature is 2.0 C , annual precipitation is 2000 mm , and the deepest snowfall is over 4 m. Azumayama topographically features a volcanic land with considerable ups and downs. And the ravines along Ookura River and Nakatsu River show an obviously eroded bluff. Its geological features are andesite type lava and agglomerate rock resulted from eruptions during the fourth diluvian epoch.

In terms of vegetation, beech trees can be seen up to 1,400 m to 1,600 m, above which semi alpine coniferous forests such as Tsuga diversifolia Mast. and Abies Mariesii Mast. develop almost to the mountain top, particularly in West Azumayama mountain range. This phenomenon cannot be seen in any other volcanic mountain, which makes Azumayama unique. Azumayama is the northern limit of Abies Veitchii Lindl. which usually don't grow well in the area on the Japan Sea side. It is also a shifting point of semi-alpine coniferous forests. This makes Azumayama a precious area from a scientific point of view.

There are a number of dump plains developed in Azumayama owing to the topographical factors which is characteristic to a shield volcano (an aspite). A lot of spring-fed ponds can be seen in the grassy plains surrounded by shrubs like : Tsuga diversifolia Mast. and Abies Mariesii Mast..

Alpine plants such as Sieversia pentapetala Greene, Veratrum stamineum Maxim, Phyllodoce aleutica A. Heller, etc. also grow in banks here.

The entire Azumayama is designated to Bandai-Asahi National Park especially because of its beautiful mountainous view. So quite a few tourists visit Azumakofuji and Johdodaira. Many people come to the mountain from Yamagata Prefecture side , from which it is relatively easier to climb.

The northern side of Azumayama is national forests administered by Akita regional forestry office. They have been examining the upper reaches of Ootaru River , Matsu River. Shibu River, which are headwaters of Monami River. They intend to establish these regions as protected areas focusing on the forestry ecology around Azumayama

4. Result

The data set for the monitoring system has been developed. Four Landsat TM data in 1990's and derived vegetation index images were used for obtaining the information on phenological changes of climax forests of Mt. Azumayama. This data set is considered showing the phenological aspects of Mt. Azumayama area in early 1990's.

Eight aerial photograph sets since 1955 were collected for the area and stereo pairs of the typical forest types were digitized. These numerical photo images were linked to the Digital Forestry Map (figure 1, original map scale is 1:20,000) on a GIS system (TNTmips). These aerial photographs shows the effect of historical human activities and natural disasters.

Forest survey records of the forestry agency were collected every five years in Japan and were also collected and liked to the forest compartments of the Forestry Map in the database of TNTmips.

Vegetation map (original scale is 1 : 50,000, 1981) of the Environment Agency was also digitized and overlaid for analyzing vegetation types on the satellite images.

Climate data of three climate stations around the study area were also collected.

These data set are made available on the Internet: /ffpri.affrc.go.jp/

5. References

Burgan, R.E. and R.A. Hartford, Monitoring Vegetation Greenness with Satellite Data, USDA Forest Service 14p, 1993

Deering D.W., J.W.Rouse, R.H.Haas, J.A.Schall, Measuring foriage production of grazing units from Landsat MSS, Proceedings of 10th International Symposium on Remote Sensing of Environment, ERIM, pp.1169-1174,1975

IUFRO, International Guideline for Forest Monitoring, 1994

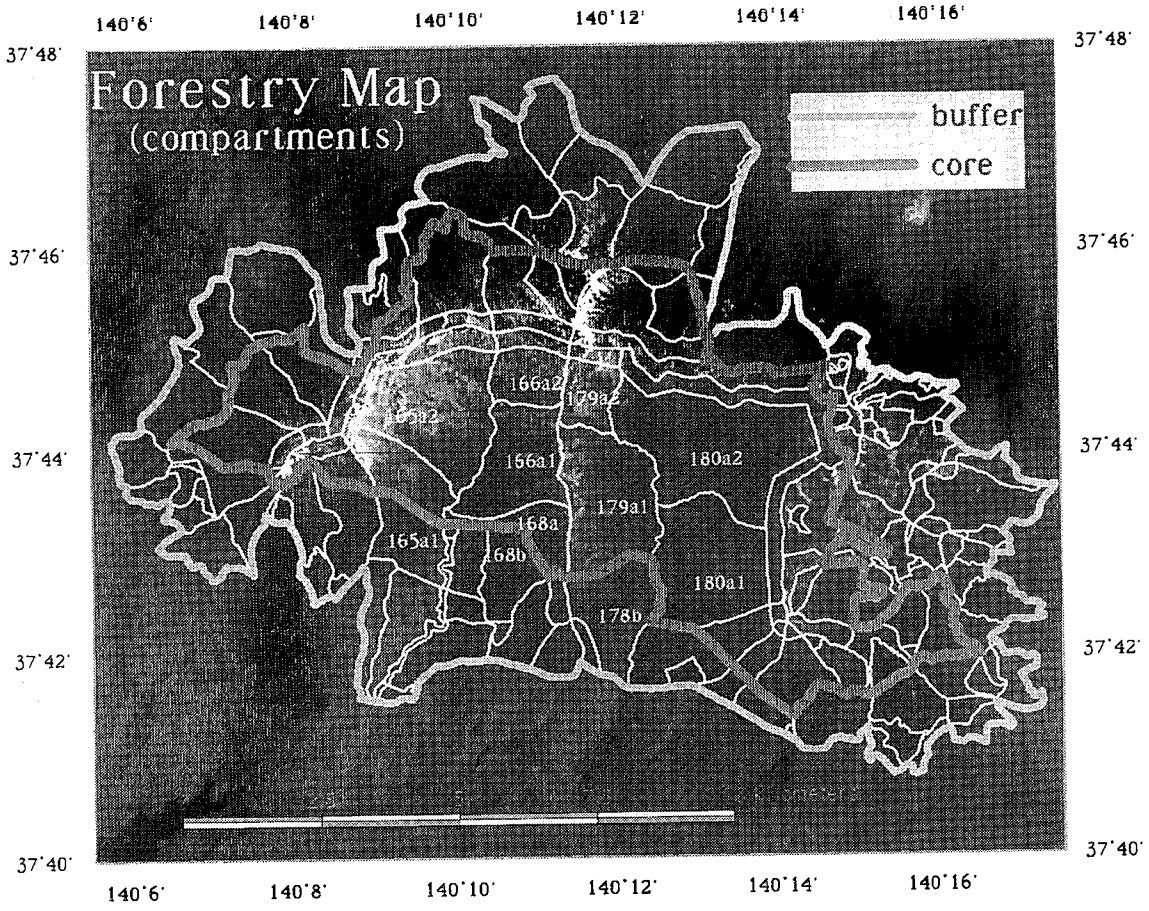

Figure 1. Forestry map of Azumayama Biosphere Reserve over Landsat TM Image

Forest Restoration Monitoring and Erosion Control Work Planning

Kiyoshi Honda(*), Shunji Murai(**), Ryousuke Shibasaki(**)

* Mie University, Faculty of Bio-resources
1515 Kamihama-cho, Tsu-shi, Mie 514, Japan
Email:honda@bio.mie-u.ac.jp

** University of Tokyo, Institute of Industrial Science
7-22-1 Roppongi, Minato-ku, Tokyo 106, Japan

Abstract

This paper describes the qualitative evaluation of forest destruction and erosion control work at Asio copper mine.

The vegetation restoration process is grasped using remote sensing and GIS. This data is used to develop the vegetation restoration model.. The vegetation restoration process is expressed by a growth curve that is applied to the vegetation index. The sediment and flood discharge models are also developed which can use the result of the vegetation restoration model.

Under some scenarios about executing erosion control work, vegetation restoration process, sediment and flood discharge are simulated for 200 years. As a result, the serious influence of forest destruction and the remarkable effect of erosion control work can be seen.

1. Introduction

Forest destruction causes sediment and flood disasters. On the other hand, Erosion control work plants trees on bare land, helps the forest to be restored quickly, and prevents flood and sediment disasters. This is evident when we see many past examples of forest destruction and erosion control work. But it is a qualitative evaluation.

Quantitative evaluation of forest destruction and erosion control work is needed, such as how much faster erosion control work can restore the vegetation compared with natural restoration, or how much it deters floods and sediment yield. In order to make more suitable and reliable plans, or to get the agreement of people about executing erosion control work, quantitative simulation models are needed. To make quantitative evaluation, the forest restoration model, sediment dischage model, and flood discharge model have to be developed.

We selected Asio copper mine as a study area. Asio copper mine is very famous for severe forest destruction (Fig.1,2). A vast area of forest was severely damaged mainly by sulfurous acid gas that

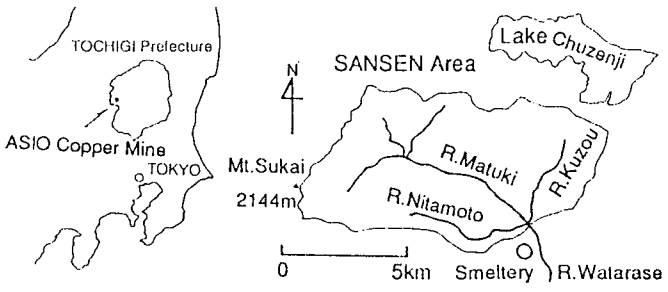

FIG.1 Map of Asio Copper Mine

FIG.2 Photo of Study Area

had been exhausted from the smeltery. It continued for more than 60 years until 1956. The damaged forest area extended to 149km^2. Especially within 32km^2, all of the trees were lost and the soil was entirely washed away. Within another 38km^2, only plants that were resistant to sulfurous acid gas such as bamboo grass remained[Maebashi Forestry bureau 1990]. With the loss of forest, flood and sediment disasters happened very frequently. Since 1957 when just after the dischage of sulfurous acid gas stopped, full-scale erosion control work has been executed continuously at a huge expense. At the work area, the forest is now restoring and disasters happen less frequently than before. At Asio, the vegetation restoration model has been developed[K.Honda 1993].

2. Vegetation restoration model

2.1 Growth curve

To describe the vegetation restoration process, Mitscherlich's growth curve that is very popular in growth prediction of tree height or diameter [Minowa 1990] is applied to the vegetation index.

$$V.I. = V.I.min + M(1 - Le^{-kt}) \quad (1)$$

Where V.I.min denotes the minimum of the V.I. (134.5), M denotes the range of V.I. fluctuation(102.5), t denotes time, L is the fall ratio of V.I. when t is zero. k is a constant. k is directly related to time t; k is called as a restoration speed.

2.2 Grasping restoration process

Overlaying the vegetation index image and the erosion control map, the restoration process was grasped.

Fig.3 shows the vegetation restoration process in the work area. The vegetation Index is NDVI, which is scaled from its range of -1.0, 1.0 to 0, 256. Elapsed time after erosion control work is obtained from the map of erosion control work. It is clear that vegetation has been restored steadily, and that the Mitscherlich's growth curve is applicable to the vegetation restoration process.

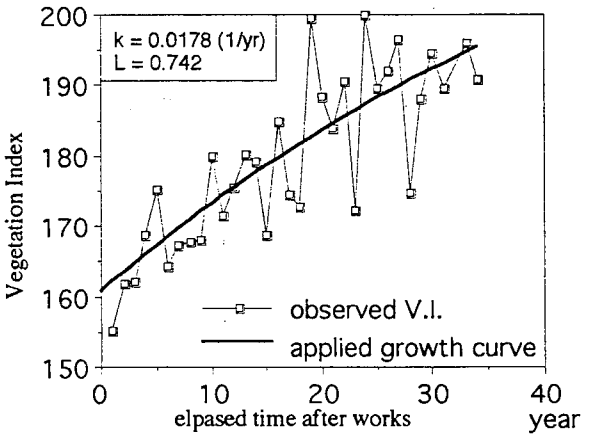

FIG.3 Vegetation Restoration Process in Work Area

Fig.4 shows the vegetation restoration process in

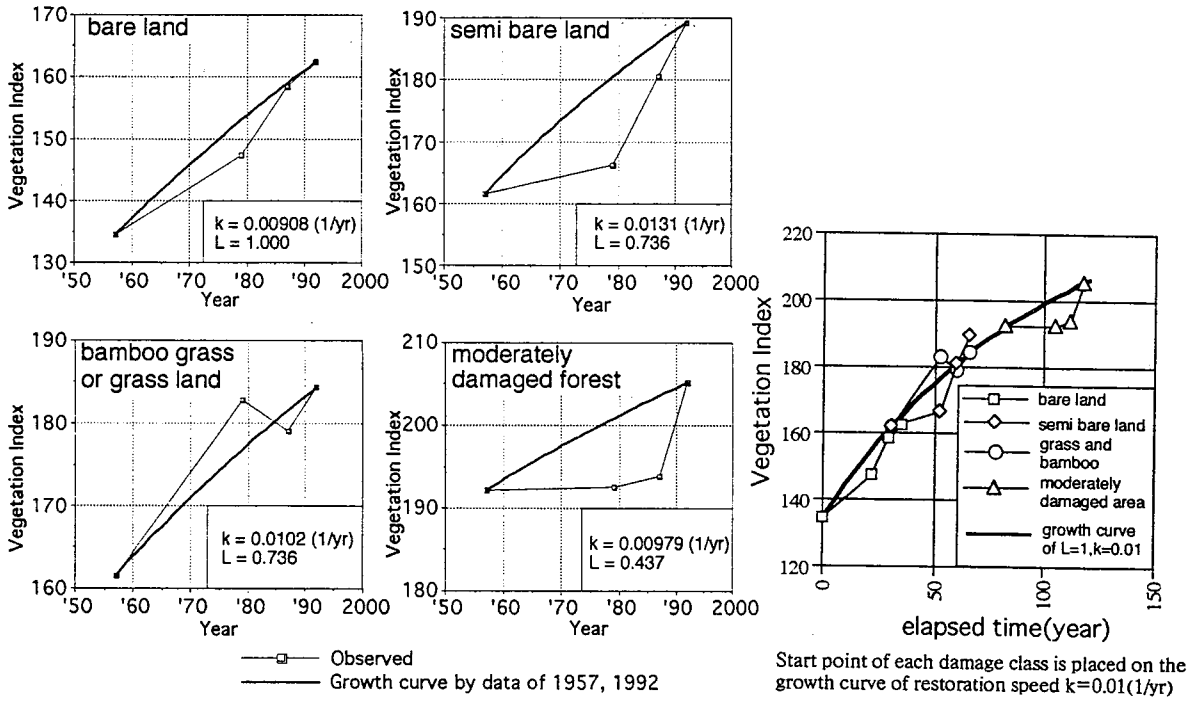

FIG.4 Vegetation Restoration Process in Non Work Area

a non work area. The vegetation index of 1957 when the vegetation restoring started was calculated from the 1957 photo interpretation image using the relationship between interpreted damage class and vegetation index. The vegetation index change is not smooth or natural, so, the growth curves are decided using 1957's and 1992's data. Restoration speeds are all nearly 0.01(1/yr). When each starting point is located on the growth curve of k=0.01(1/yr), it shows good fitness as a whole. It indicates that the restoration process at non work area also can be expressed by the growth curve and the restoration speed is nearly 0.01(1/yr) in whole process.

In the work area, V.I. at elapsed year=1 and the value of the growth curve at t=0 are both higher than the V.I. range of bare land. The restoration speed k in the work area is twice as much as that of the bare land. Therefore, in the work area, right after the execution of erosion control work, vegetation is introduced firmly. After that, vegetation restores twice as fast as in non work area.

2.3 Vegetation restoration prediction model

To make it possible to predict vegetation restoration considering various conditions of each mesh, restoration speed k is decided as a function of conditions using multi regression analysis at each class and at each slope direction.

k = f(altitude, slope inclination, area of watershed,
point of geology[National Land Agency 1986], PRV)

2.4 PRV index

PRV is an index of Proximity to Remaining Vegetation.

$$PRV = \sum \frac{1}{R^2} \qquad (2)$$

Where R is distance from an object mesh to the remaining vegetation. The remaining vegetation means the forest in 1957. The relationship between PRV value and remaining vegetation is shown in Fig.5.

PRV has a highly positive correlation with vegetation restoration speed of non work bare land. It is concluded that vegetation restoration is more difficult in a large block of forest loss than spatially dispersed blocks even if the extent of forest loss area may be the same.

3. Developing water and sediment discharge model

3.1 Water discharge model

Fig.6 shows the element of water movement in the model.

Parameters of crown interception, evaporation, evapo-transpiration are estimated using V.I. (Fig.7).

Soil layer depth is estimated from land cover at 1957 (Fig.8) . Parameter D_{30} is decided from adapting calculation to the observed discharge. Soil layer is assumed to grow at 2.5mm/year, after V.I. becomes greater than the range of grass land.

Motion equation of under ground flow is as following.

$$Q1 = Ks\ S^{\beta} \sin\omega\ D\ L \qquad \text{[Kubota 1987]} \qquad (3)$$

Q1 : flow in soil layer
Ks : saturation transmission coefficient 0.2cm/sec
S : mean of saturation ratio
ω : parameter that indicates fall of transmission coefficient in non saturated area
β : gradient
D : soil layer depth
L : mesh interval 50m

Motion equation of surface flow is as following.

$$Q2 = V2\ A$$
$$V2 = \frac{1}{n} R^{2/3} I^{1/2} \qquad (4)$$

Q2 : flow of surface water
V2 : velocity
A : cross-sectional area
H2 : water depth
n : roughness of manning
R : hydraulic mean depth

$A = H2\,L$ I : gradient of slope

where

$$R = 0.255 F^{-0.171} A^{2/3} \quad \text{[Ishihara 1977]} \tag{5}$$

R : hydraulic mean depth (m)
F : watershed area (km^2)
A : cross-sectional area (m^2)

3.2 Sediment discharge model

Sediment discharge is calculated as average annual sediment yield at slope surface.

$$E = E_{30}\left(\frac{S}{S_{30}}\right)^{0.9} \tag{6}$$

E : surface erosion of a year
E_{30} : surface erosion of a year when gradient is 30(deg)

land cover	vegetation index	E_{30}(mm/yr)
bare land	- 145	20
grass land	146 - 175	1
forest	176-	0.1

S : gradient of object mesh(%)
S_{30} : tan 30(deg) = 0.57735

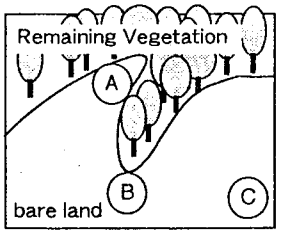

FIG.5 PRV Proximity to Remaining Vegetation INDEX

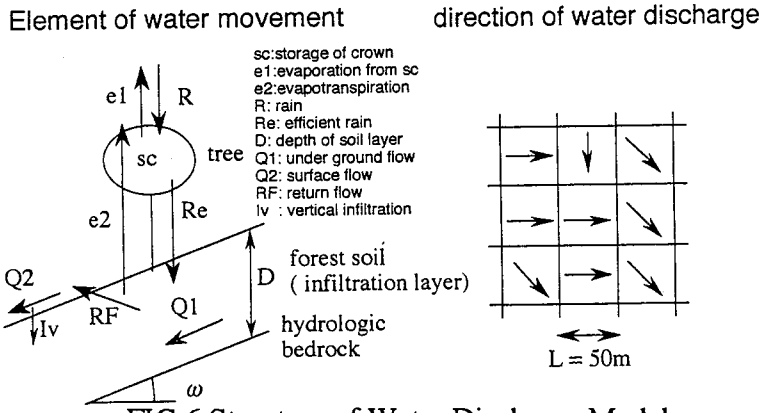

FIG.6 Structure of Water Discharge Model

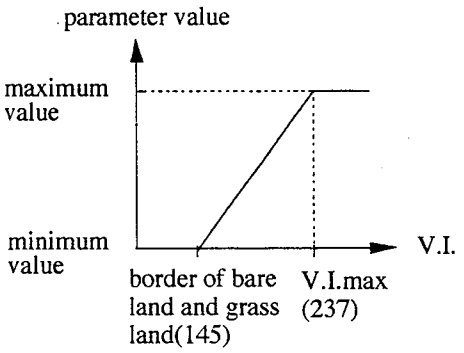

parameter			mini.	max.
storage of crown	sc	(mm)	0	2.5
evaporation	e1	(mm/hr)	0	0.4
evapo-transpiration	e2	(mm/day)	1.7	5.0

FIG.7 Estimation of Crown Interception, Crown evaporation, Evapo-transpiration from Vegetation Index

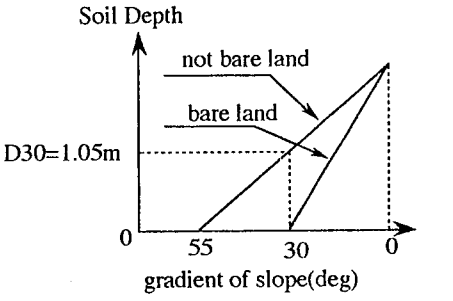

FIG.8 Estimation of Soil Depth

4. Simulation and evaluation

4.1 Scenarios

To evaluate the effect of erosion control work, the following cases were assumed.

Case I Do nothing from the starting point of vegetation restoration (1957)

Case II Stop erosion control work in 1992

Case III Continue erosion control work until the bare land has disappeared (until 2007)

In addition, calculation at natural state was done assuming that there was not a copper mine and the watershed was covered by a good forest.

4.2 Vegetation restoration

Fig.9 shows the result of vegetation restoration simulation for 200 years.

Comparing Case I and II at the west area, where erosion control work has been executed at high priority, the effect of erosion control works is remarkable in all the predicted period.

Comparing Case II and III at the center area, where terrain is very steep and erosion control works is not executed yet, if erosion control works were stopped now, there would remain bare land. But by continuing erosion control works, vegetation restoration is expected.

4.3 Sediment yield

Fig.10 shows the simulated sediment yield from the result of vegetation restoration simulation .

At 1957, sediment yield was very large compared to the natural state.

Past erosion control work and future erosion control work have a remarkable effect to lower sediment yield. Past erosion control work prevent will 4.2 million m^3 in 200 years. Future erosion control work will prevent adding 4.7 million m^3.

4.4 Flood discharge

Fig.11 shows the peak flow of simulated flood hydrograph at 100 years probable rain. At 1957, the peak flow increased 46%. Even if erosion control work has a significant effect on sediment discharge, there is a not big effect to lower the peak flow. It is clear that erosion control work helps forest restoration and the restoration of soil layer, but the speed of soil creation is very slow, so the effect of erosion control work on peak flow is small. It indicates that forest destruction that causes soil loss increases the flood peak flow for a long term.

5. Conclusions

A method to make quantitative evaluation of forest destruction and erosion control work was totally developed. Forest restoration process, sediment yield, and flood peak in each scenario is calculated and evaluated. Followings are the result of evaluation.

(1) Erosion control work has make forest restoration twice as faster as natural restoration. If we continue work, fully forest restoration is expected.

(2) Erosion control has a remarkable effect on preventing sediment yield. Past and Future erosion control work would prevent 8.9 million m^3 sediment yield in 200 years.

(3) Forest destruction that causes soil loss, increases peak flow seriously for a long term. We have to avoid such a forest destruction.

References

K.Honda, S.Murai, R.Shibaski," Prediction of vegetation restoration by erosion control works in Asio copper mine, Japan", IGARSS'93, 106-108,1993

Y.Ishihara, S.Kobatake, "On the Propagation speed of a flood wave", Annual transaction of Kyoto Univ. disaster prevention institute, No.20B-2,149-167

J.Kubota,Y.Fukushima,M.Suzuki, "Observation and modeling of the runoff process on a hillslope", Journal of Japan Forestry Society, Vol.69,No.7,258-269,1987

Maebashi Forestry Bureau, Ministry of Forest, Japan, "Walking of forty years", 75-98,1990

M.Minowa, "Forest Measurement", Tokyo: Tikyusha corp. , 163, 1990

National Land Agency Japan, "Land and water investigation database study report", 104, 1986

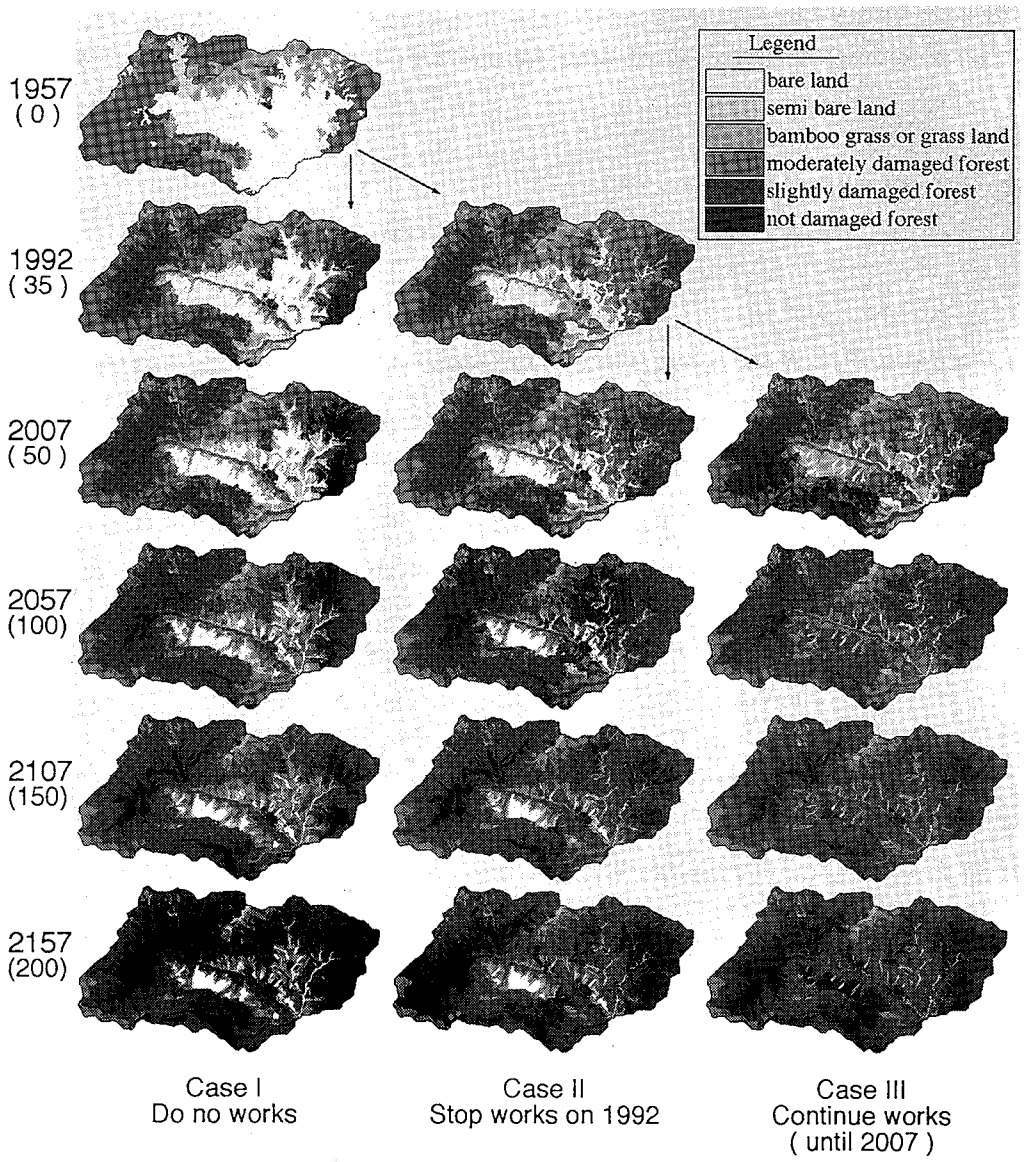

FIG.9 Vegetation Restoration Simulation

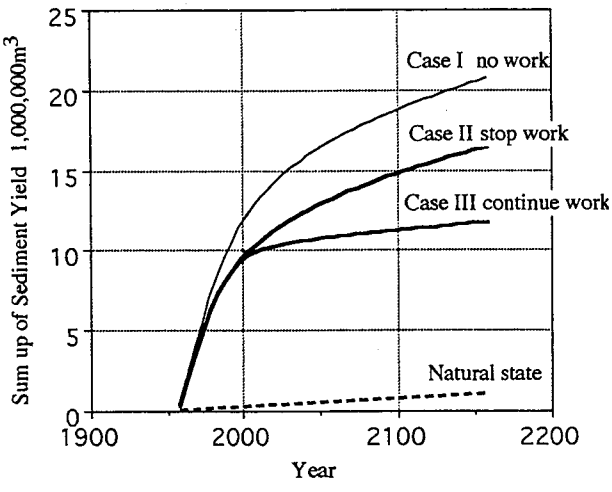

FIG.10 Change of Sediment Yield

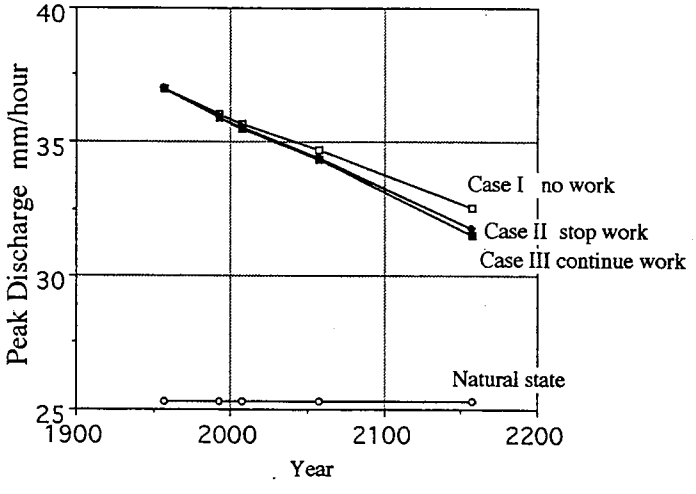

FIG.11 Change of Peak Flow at 100 Year Probable Rain

Monitoring Changes of Lake Water and Vegetation Area in Central Asia

Y. NAKAYAMA(*), S. TANAKA(*), K. ENDO(**) and Y. SUGA(***)

*Remote Sensing Technology Center of Japan
1-9-9 Roppongi, Minato-ku, Tokyo, 106 Japan
Fax:+81-3-5561-9542
Email:NAKAYAMA@naseoc.eoc.nasda.go.jp

**Department of Earth Science, Nihon University
3-25-40 Sakurajosui, Setagaya-ku, Tokyo, 156 Japan

***Hiroshima Institute of Technology
2-1-1 Miyake, Saeki-ku, Hiroshima, 731-51 Japan

Abstract

Recent changes of Aral Sea, Lake Balkhash, Bosten Lake and other lakes in Central Asia were analyzed with the multi-temporal LANDSAT/MSS and NOAA/AVHRR data. The relationship between changes of water area and vegetation was investigated based on the analyzed results of satellite data and GIS data. It was presumed that the water area decrease was caused by water consumption in vegetation area.

1. Introduction

This study aims to monitor the recent changes of Aral Sea, Lake Balkhash, Bosten Lake and other lakes in central Asia. The features were examined by analyzing the multi-temporal LANDSAT/MSS and NOAA/AVHRR data. The changes of water and vegetation area around the lake and its vicinity for the 1970 to 1990 year were measured by comparing the land cover classification images based on satellite data with the geographical information data. Referring to the meteorological data, the analyzed results indicated the characteristics of changes on individual lakes. It was presumed that the method using satellite image was most effective to investigate the rapid changes of lakes and its neighboring vegetation area in arid and semi-arid land.

2. Geographical features of object areas

The object areas of lakes are drawn by broken lines in Figure 1. The geographical features of object lakes are as follows:

(1) Aral Sea

Aral Sea is a salt lake laying on the boundary between Kazakhstan and Uzbekistan in Central Asia. Syr Dar'ya and Amu Dar'ya

flow into Aral Sea. Large deltas used for agricultural land are formed in each river mouth. According to statistical sources, Aral Sea has about 66,500km^2, 53m in lake surface elevation, 15m in average depth, and 68m in deepest water. A NOAA AVHRR image of the object area is shown in Figure 2.

(2) Lake Balkhash

Lake Balkhash is elongated from east to west in east Kazakhstan. Several rivers including Ili, Karatal and Aksu flow into southern part of Lake Balkhash. Vegetation areas used for agricultural land spread along these rivers. According to statistical sources, Lake Balkhash has about 18,430km^2, 6m in average depth, and 26m in deepest water. A NOAA AVHRR image of the object area is shown in Figure 3.

(3) Bosten Lake

Bosten Lake is located in north-east Tarim Basin of China. Kaidu river flow into north-west of Bosten Lake. There is a outflow river from south-west. According to statistical sources, Bosten Lake has about 990km^2, 8m in average depth, and 16.5m in deepest water. A NOAA AVHRR image of the object area is shown in Figure 4.

3. Analysis of satellite data

LANDSAT MSS and NOAA AVHRR data in summer season from the 1970's to the 1990's were analyzed. The analysis procedure is as shown in Figure 5.

The mosaicked images were generated by using several scenes of LANDSAT MSS after radiometric and geometric correction. Ground control point(GCP)s were selected on the satellite images with referring to maps and geographical information data for the orientation to the coordinates of a map projection. The resampling operation was performed for each satellite image by nearest neighborhood method.

Normalized difference vegetation index (NDVI) image was generated for each data using visible and near-infrared bands. Landcover types of water, bare soil and vegetation were discriminated with NDVI images by a threshold method. Water and vegetation area, and these changes around the lake and its vicinity for the 1970 to 1990 year were analyzed by comparing with the multitemporal landcover classified images and geographical information data. Finally, a comparative analysis of features among the lakes was carried out referring to the meteorological data.

4. Changes of water and vegetation area

Each lake's water and vegetation area, and these changes obtained from the analysis of LANDSAT MSS and NOAA AVHRR were observed as follows:

2.1 Aral Sea

By 1992, the water area of Aral Sea was shrunk to about 55% of the area shown in the statistical table and geographical information data of 1960's. The shoreline indicated remarkable changes in the east and south lake side. However, the changes could not be clearly seen along the west shoreline because the west side touches the steep cliff of the plateau. The movement of east shoreline for the past about 30 years has attained approximately 70km in maximum by comparing with those of map and geographical information data. On the other hand, the vegetation areas along the inflow rivers indicated clearly increase. It was presumed that the rapid shrinkage of water area was caused by the inflow decrease due to the irrigation expansion in vegetation area.

2.2 Lake Balkhash

By 1992, about 9% shrinkage of Lake Balkhash to the water area of 1975 was indicated in the area along the south shoreline. The rapid change of water area was observed for the period from the second half of the 1970's to the 1980's. The remarkable changes of shoreline could be clearly seen around spit in the central part of Balkhash and its vicinity. The vegetation areas along the inflow rivers indicated clear increase. However, the change of water area was smaller than that of Aral Sea because the expansion of vegetation area was not so rapid as in the Aral Sea.

2.3 Bosten Lake

The relationship between slight changes of water area and vegetation area in Bosten Lake was indicated. In contrast with the changes of Aral Sea and Lake Balkhash, the variation of Bosten Lake was a little because of the balance between inflow and outflow volume of river water. Multi-temporal satellite observed High spatial resolution data more than that of NOAA AVHRR data is necessary to analyze the detail changes in Bosten Lake.

5. Result of data analysis

As the analysis results of satellite data, the shrinkage of water areas corresponding to the expansion of vegetation areas in the region of Aral Sea and Lake Balkhash were clearly shown as Figure 6. According to the meteorological observation data in recent years based on the World Monthly Surface Station Climatology, the precipitation and the vapor pressure were indicating a slight increase tendency or almost unchanged level, the temperature was slightly rising in and around these object areas.

Due to the above results, the changes in these areas could not be explained only from climate changes in the vicinity. It was presumed that the main reason of these lakes was caused by the inflow water decrease due to the irrigation expansion along

the inflow rivers. The remarkable changes caused by the influence of human activities shown in this paper were observed in other lakes of central Asia. In contrast with the above lakes, the slight variation of Bosten Lake was indicated by reason of the balance between inflow and outflow volume of river water.

On the other hand, Caspian Sea, the world's largest lake in area, showed the rising of sea level in the recent years based on the analysis result of satellite data.

6. Summary

The changes of lake water and vegetation area in Central Asia were summarized based on the time series satellite data.

1) The remarkable shrinkage of water area in the region of Aral Sea and Lake Balkhash was recognized. This results corresponds to the inflow water decrease due to the irrigation expansion, because the vegetation area was growing along the inflow rivers.

2) The variation of Bosten Lake was a little because of the balance between inflow and outflow volume of river water.

3) By 1992, about 45% shrinkage of water area in Aral Sea, about 9% shrinkage of water area in Lake Balkhash were indicated.

4) It is presumed that satellite image is most effective to investigate the rapid changes of lakes in arid and semi-arid land.

References

Y.Nakayama, S.Tanaka, K.Endo and Y.Suga,"Monitoring water and vegetation area changes in arid lands studied with satellite data", Journal of Arid Land Studies, Vol.4, pp.21-38, 1994

Y.Nakayama, S.Tanaka, K.Endo and Y.Suga,"Monitoring changes of Aral Sea and its vicinity with satellite data", Journal of The Remote Sensing Society of Japan, Vol.15, pp.54-69, 1995

Y.Nakayama, S.Tanaka, K.Endo and Y.Suga,"A changes of Aral Sea's water area by satellite data", Proceeding of IGARSS'93, Vol.1, pp.194-196, 1993

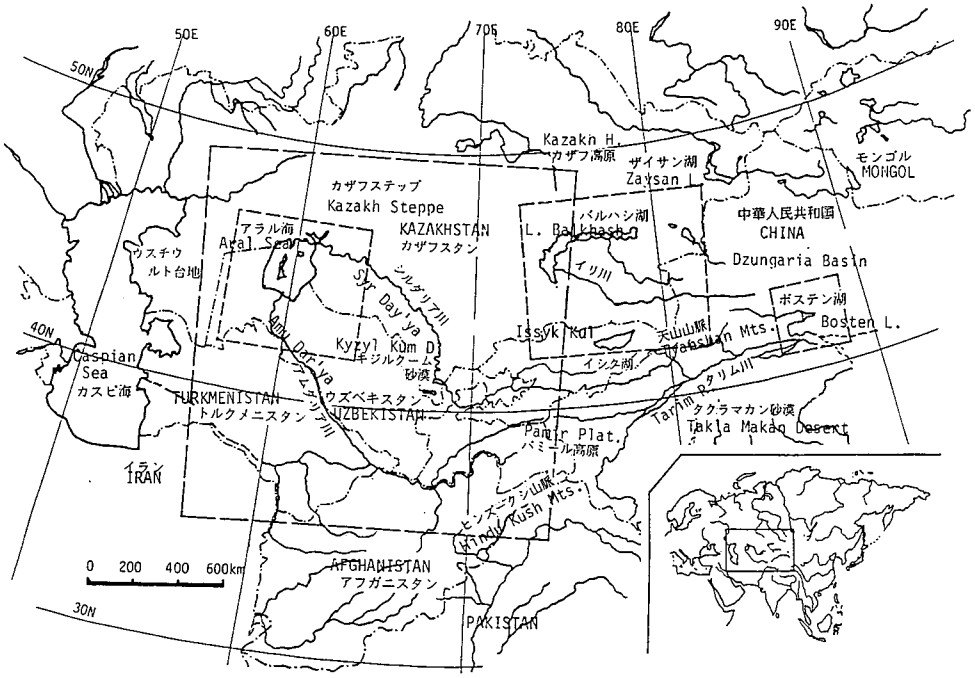

Fig.1 Location map of lakes in Central Asia

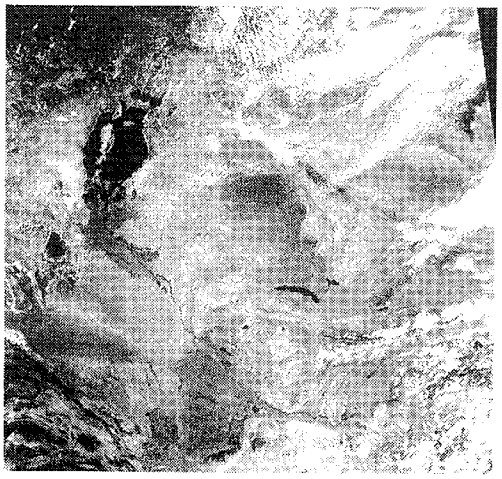

Fig.2 False color composite of Aral Sea area by NOAA AVHRR data (August 14, 1992)

Fig.3 False color composite of Lake Balkhash area by NOAA AVHRR data(August 1, 1990)

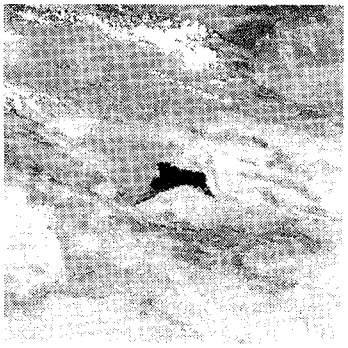

Fig.4 False color composite of Bosten Lake area by NOAA AVHRR data (August 1, 1990)

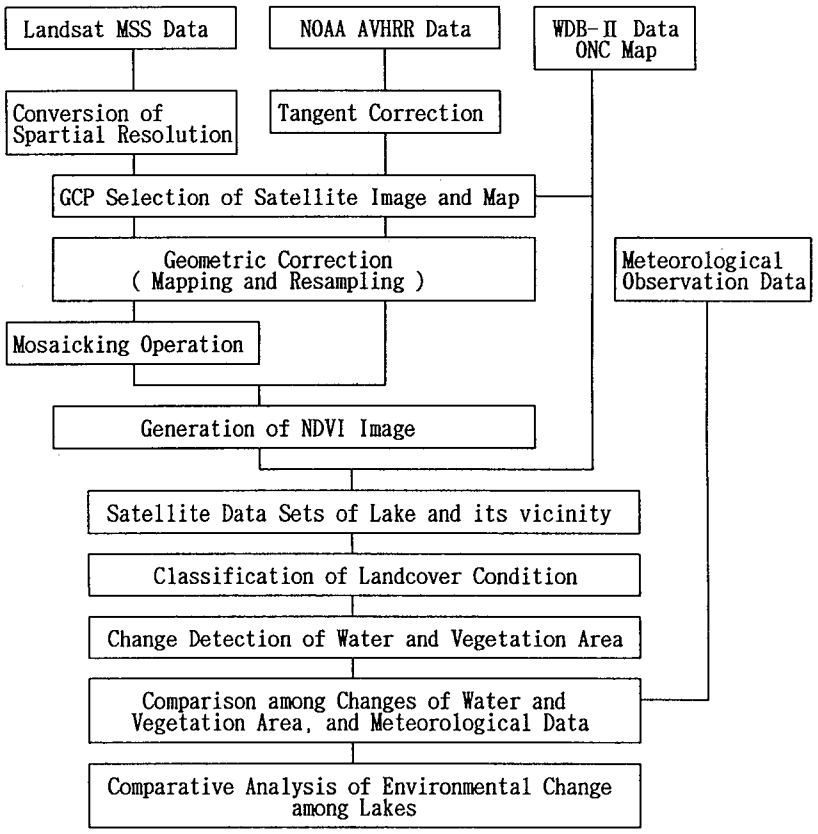

Fig.5 Flow of satellite data analysis

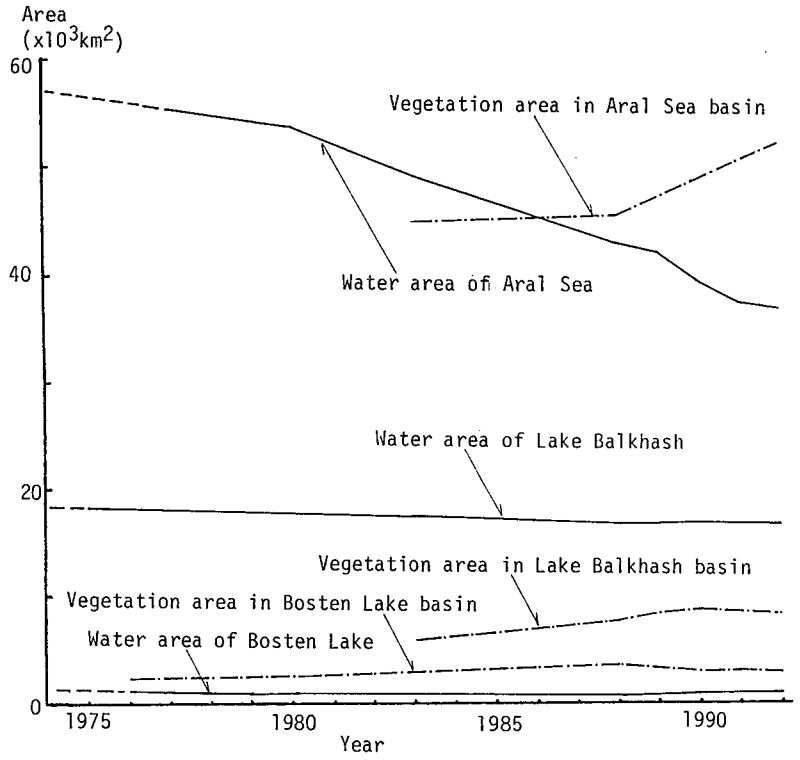

Fig.6 Changes of water and vegetation area

MONITORING DEFORESTATION IN LUZON, THE PHILIPPINES USING REMOTE SENSING DATA

Akira HIRANO, Genya SAITO and Nobuyuki MINO

National Institute of Agro-environmental Sciences (NIAES)
3-1-1 Kannondai, Tsukuba, Ibaraki 305, JAPAN
Tel : +81-298-38-8225, Fax : +81-298-38-8199

ABSTRACT

A comparison was made between a land use map derived from remote sensing data and an existing land use map. A GIS (Geographic Information System) was implemented to evaluate the land use change of the Camiling district, Luzon island, the Philippines. Deforestation in the study area was monitored. Soil/Vegetation matrix method was used to create land use map from MOS-1/MESSR data. Satellite data taken during the dry season and the rainy season, respectively, in the study area were used to make the classification more accurate.

Following procedures were taken for both satellite images taken during the dry season and during the rainy season in 1990. Pixels of the image were classified according to their VCR (Vegetation Coverage Ratio) and SDI (Soil Dryness Index) using a matrix. Classified images derived from two different seasons were then logically related to each other to generate the satellite-derived land use map. Land use information was extracted from an existing topographic map published in 1977. The information was then input to a GIS (Geographic Information System).

Land use maps of two different times were logically overlaid onto each other to evaluated the land use change happened during the period. Clear decrease in forest area, namely deforestation was monitored. Forest area in the Camiling district was about 457 km^2 in 1977, whereas it was about 246 km^2 in 1990. It had shrunk by about 48 percent. Spatial analysis of this area showed that 45 percent of the ex-forest area turned into paddy field.

1. INTRODUCTION

Recent deforestation of tropical forest in Asia has come to be one of the most pressing environmental problems. The major causes of deforestation in Asia are commercial logging, shifting cultivation, transmigration, acquiring of fuel woods, forest fire, agricultural development, resort development, mining and urbanization.

Deforestation leads such deterioration of natural conditions as follows (Murai, 1991):

1) Run off ratio increases resulting in flash flood.
2) Water level and volume of ground water decline.
3) Wild animals and species become extinct.
4) Soil is eroded or degraded.
5) The climate may change to dry weather condition; characterized by less rainfall, higher temperature and more evaporation.

Land use map is one of the most important thematic maps because it provides the present status of land use and pattern of its change. Land use change is very fast in Asia. Up-to-date land use map is required for monitoring the urban and rural environment. This is why satellite remote sensing is widely used for land use/land cover mapping.

However, current digital classification technique, for example, maximum likelihood method has not sufficient accuracy for operational utilization. Using two independent parameters derived from the information on vegetation coverage and soil dryness can result in the higher accuracy in classification of land use patterns. Cross-examination of two data sets from different seasons can raise the classification accuracy.

2. STUDY AREA

To monitor the typical deforestation in the Philippines, Camiling district was selected as the study area. Camiling district is located at western-central part of Luzon island. It is about 150 km northwest of Manila City. The study area covers about 25 km east to west, 27 km north to south and encompasses approximately 675 km^2. The area is located at the eastern foot of Zambales mountains, land use is mainly paddy field and tropical forest. Terrain consists of relatively flat alluvial plain and steep mountain slope with elevations ranging from 20 to 1180 meters (Figure 1).

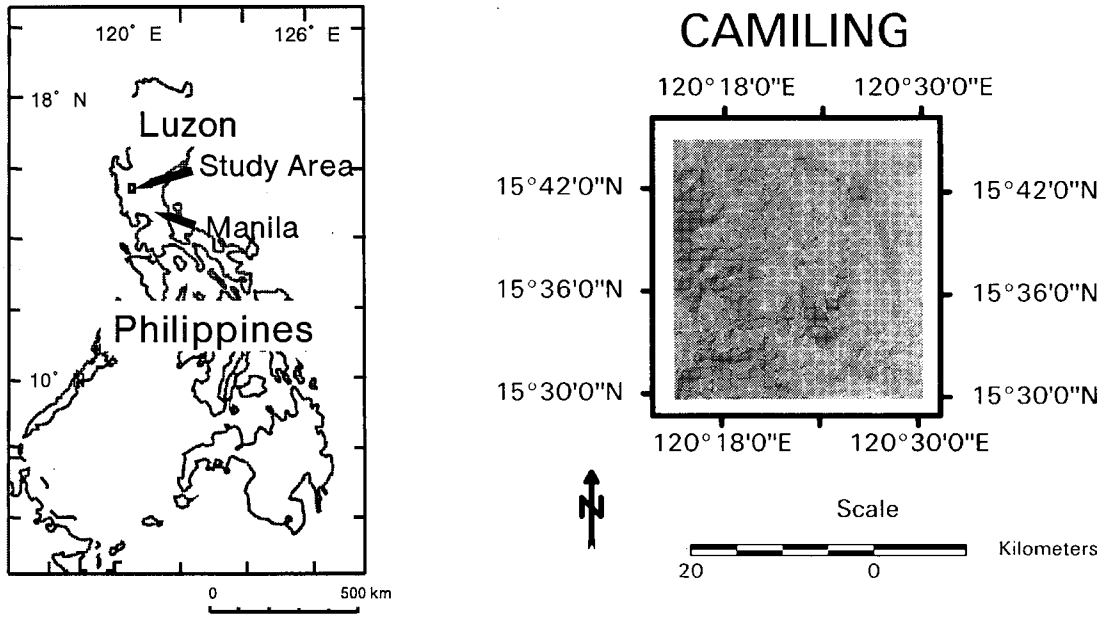

Figure 1. The study area (Camiling district, Luzon island, the Philippines).

3. DATA

3.1 Satellite data

Two MOS-1/MESSR data (Path-Row : 29-98W) that cover the western-central part of Luzon island taken during the dry season (February 1, 1990) and the rainy season (October 31, 1990) were utilized to create the land use map. These satellite images include the study area.

In order to minimize the effects of sun elevation when comparing the data obtained in different seasons, radiometric correction was applied to these multi-temporal images. Each CCT value in the image was divided by $\sin\theta$, where θ is the sun elevation at the date when the satellite data were

acquired. The images were then geo-coded to UTM coordinate system. Geo-coding was performed using 1:50,000 scale topographic maps published by NAMRIA (National Mapping & Resource Information Authority) (Figure 2).

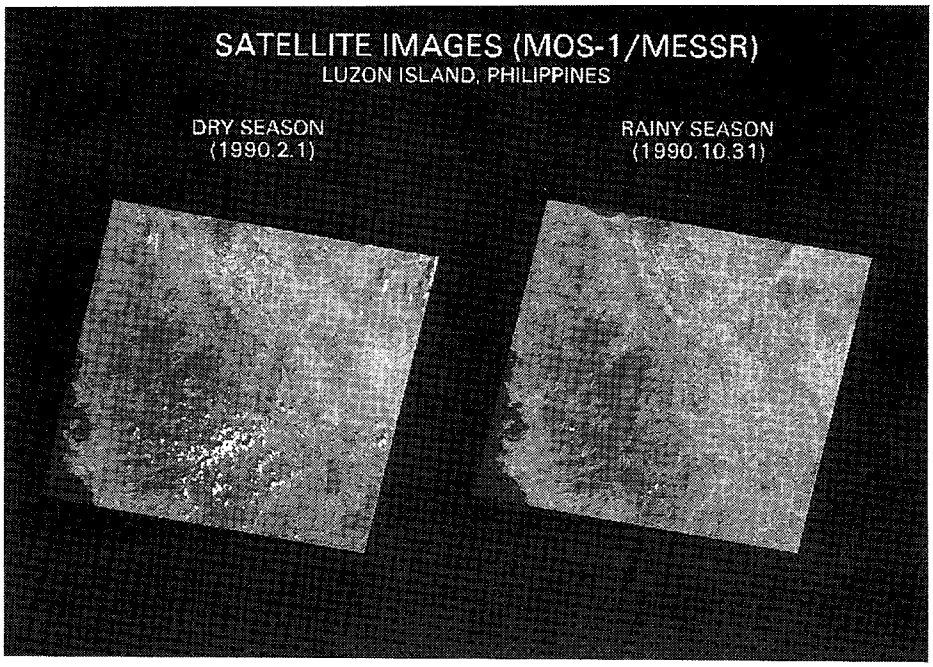

Figure 2. Satellite images after sun-elevation correction and geo-coding.

3.2 Existing map

As for the existing map, topographic map at a scale of 1:50,000 compiled and published by NAMRIA in 1977 was utilized.

4. ANALYSIS AND DISCUSSION

4.1 Land use classification procedures using soil/vegetation matrix method

Using soil/vegetation matrix method, pixels on the satellite image were classified according to their vegetation coverage and to their soil dryness. Soil/vegetation matrix method procedures are described as follows.

4.1.1 Vegetation Index

To evaluate the vegetation coverage information, K-Vegetation Index (KVI) was utilized. KVI is a vegetation index based on reflectance of vegetation in near IR wavelength as shown schematically in Figure 3 (Yoshida et al. 1993). KVI is given by

$$KVI = Band3 - (a \times Band2 + b) \quad (1)$$

where a and b are constants. Here a is obtained from the slope, and b is the y-segment of the least square line fit through the data points that constitute the description of bare soil on the scatter plot of band 2 versus band 4. This regression line is conventionally called the Soil Line. Band2 and Band3 are the CCT (computer compatible tape) values of the pixel concerned at MOS-1/MESSR band 2 (Red: 610-690 nm) and band 3 (IR: 800-1100 nm), respectively. Using KVI, Vegetation Cover Ratio (VCR) was then calculated for each pixel to estimate the proportion of vegetation coverage to the area of the pixel concerned. VCR is given by

$$VCR = KVI / KVI_{max} \tag{2}$$

where KVI_{max} is the maximum value of KVI recorded in the image of the study area. VCR of any pixel on the Soil Line is equal to 0 for there is no vegetation on these pixels. Pixels in the image were classified into 5 levels according to their VCR values from high to low.

4.1.2 Vegetation Cover Ratio

To evaluate the soil dryness information, Soil Dryness Index (SDI) was utilized. SDI, referred to as Soil Index (SI) by Fukuhara et al.(1979), is sensitive to the soil brightness, which depends on soil moisture and soil organic matter conditions. SDI is given by

$$SDI = \arctan \frac{P4 - Band4}{Band2 - P2} \tag{3}$$

where P2 and P4 are the x-coordinate (Red) and the y-coordinate (IR) of the pixel that has the maximum vegetation coverage, respectively. The higher the SDI value of a pixel, the drier the soil of the pixel is. Pixels in the image were then again classified into 5 levels according to their SDI values from high to low.

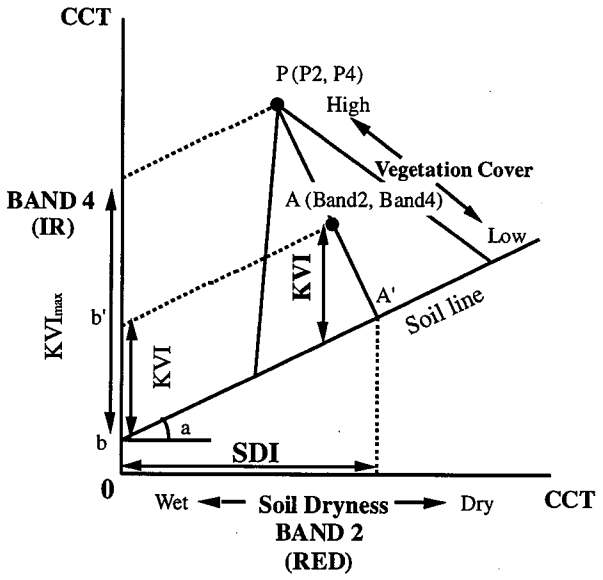

Figure 3. Conceptual figure of KVI, VCR, and SDI.

4.1.3 Soil/vegetation matrix method

Each pixel was distributed over 5×5 matrix of VCR and SDI, and they were classified into 8 classes as shown in Table 1 according to their land cover conditions (Figure 4).

Table 1. Land use/land cover classification classes using VCR and SDI.

Class number	Class
1	Ground water
2	Dr bare soil
3	Wet bare soil
4	Dry small vegetation
5	Wet small vegetation
6	Dry high vegetation
7	Wet high vegetation
8	Forest

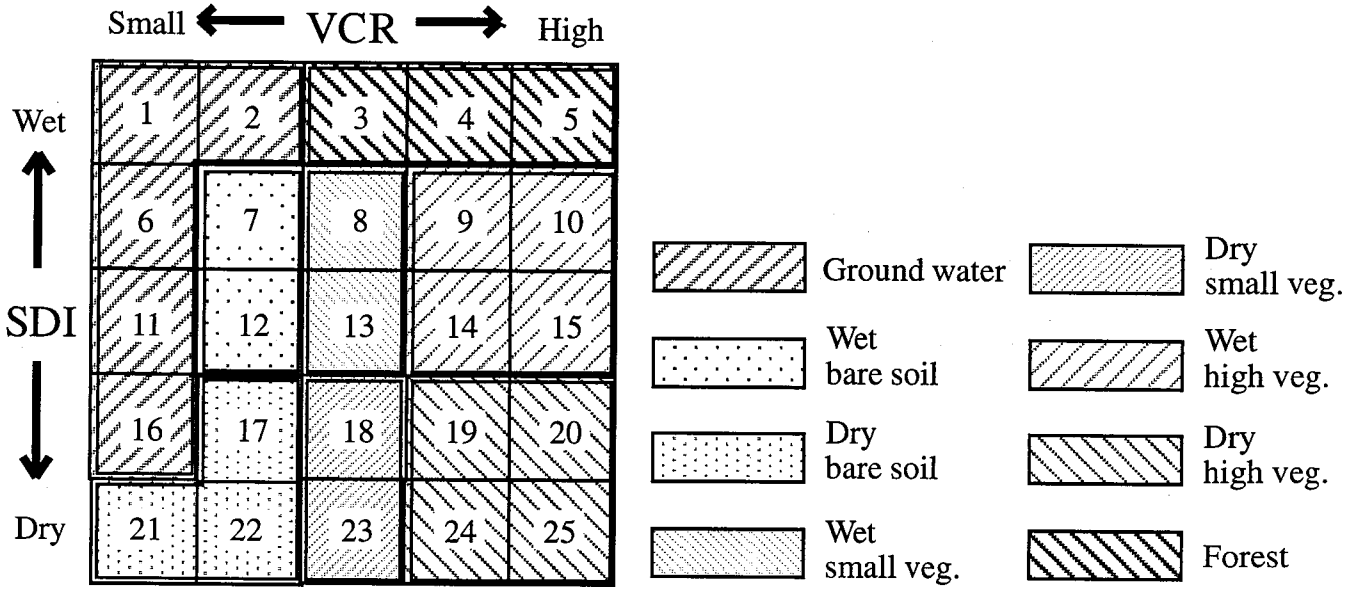

Figure 4. Soil/vegetation matrix according to VCR and SDI.

4.1.4 Re-classification

Soil/vegetation matrix method was carried out to both images taken during the dry season and the rainy season that resulted in two sets of land use/land cover classified images. Using GIS overlay function, these two images were cross-examined to generate a re-classified land use map in order to make the land use classification more accurate. Classification classes were determined in order to keep the consistency with the classes derived from the existing map (Table 2).

Table 2. Land use classification classes.

Class number	Class
1	Water
2	Fish pond
3	Bare soil
4	Upland farming field
5	Paddy
6	Forest

4.2 Extracting land use information from the existing map

Land use information was extracted from an existing topographic map compiled and published by NAMRIA in 1977. In order to maintain the consistency with the satellite-derived land use map, land use information was digitized with the aid of GIS software so that overlay analysis can be carried out. At the same time, major roads and rivers in this area were also digitized to make the geographical registration easier.

4.3 Land use change analysis

Satellite-derived land use map and the land use map derived from the existing map were input into a GIS to perform an overlay analysis in order to detect the land use change happened between 1977 and 1990 (Figure 5). With the help of GIS, spatial distribution of land use change was also detected. Distinct deforestation was monitored during the period. Considerable amount of forest area decreased by nearly half (Figure 6). Of 4.6×10^2 km^2 of forest area in 1977, 2.1×10^2 km^2 turned into paddy in 1990. This explains 93.9 percent of the total loss of forest area (Figure 7).

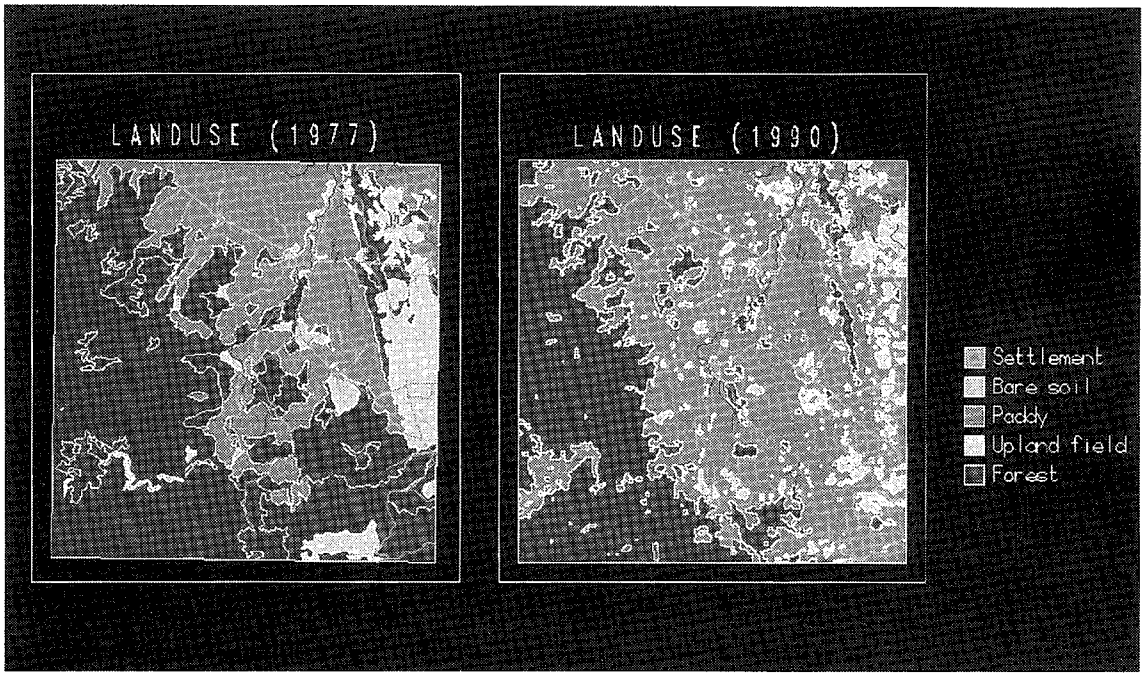

Figure 5. Land use maps : Topographic map origin (1977) and satellite-derived (1990).

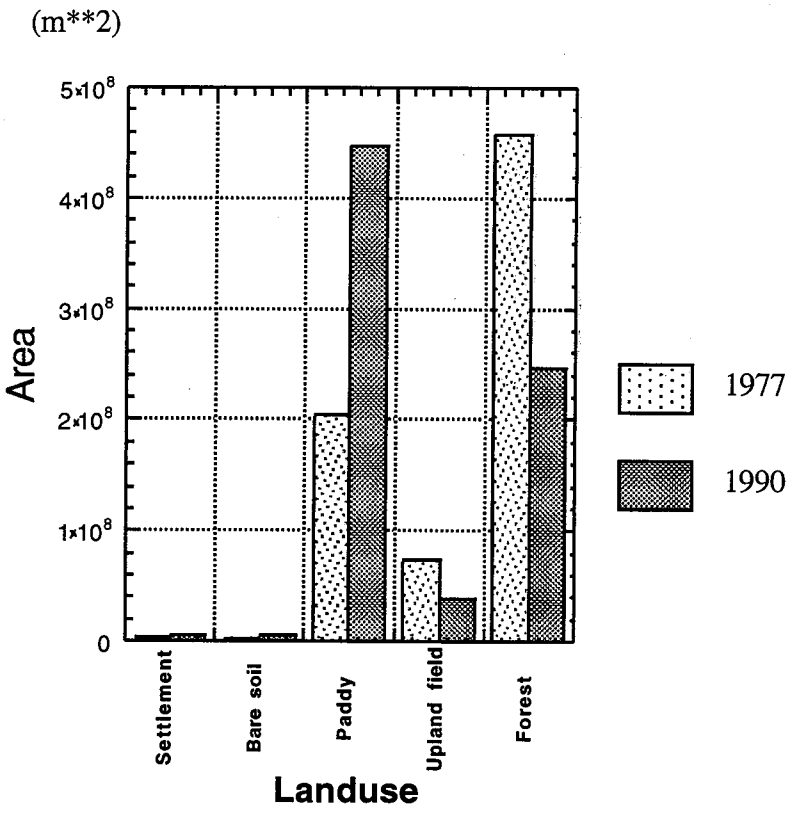

Figure 6. Land use change for settlement, bare soil, paddy, upland field, and forest : 1977 to 1990.

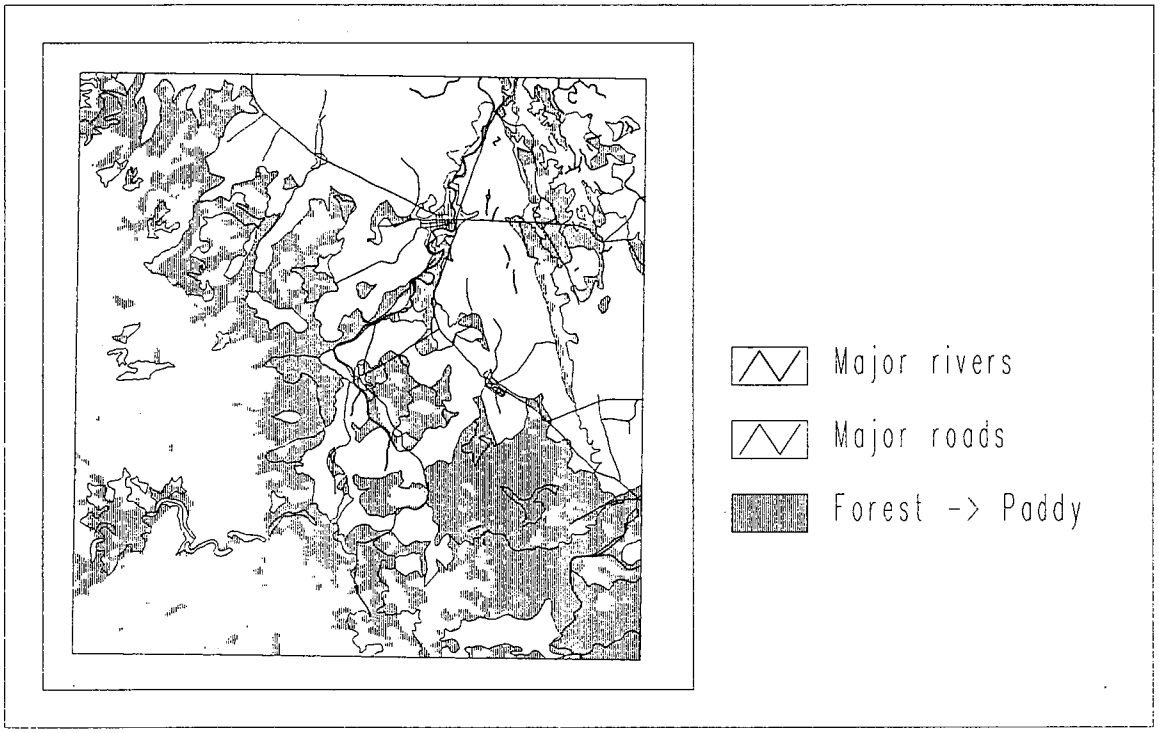

Figure 7. Spatial distribution of land use change (Forest (1977) -> Paddy (1990)).

5. CONCLUSION

Deforestation in Luzon island, the Philippines was monitored and evaluated both numerically and spatially with the help of soil/vegetation matrix method and GIS technique. From 1977 to 1990, a considerable amount of forest area turned into paddy in the study area. Soil/vegetation matrix method, a land use classification method using the information on vegetation coverage and on soil dryness is effective to generate a land use map from satellite data. Using two sets of satellite data acquired during the dry season and the rainy season, respectively, makes the classification accuracy higher.

ACKNOWLEDGMENTS

Part of this study was made as the cooperative work with National Space Development Agency (NASDA) of Japan. The authors are grateful to NASDA for providing the MOS-1/MESSR data.

REFERENCES

1. Fukuhara, M., Hayashi, H., Yasuda, Y., Asanuma, I., Emori, Y., and Iisaka, J., "Extraction of soil information from vegetated area.", Machine Processing of Remotely Sensed Data Symposium, pp.242-252., 1979.
2. Murai, S., "Application of remote sensing in Asia and Oceania. - Environmental change monitoring -", (Asian Association on Remote Sensing: Murai, S.), 1991.
3. Yoshida, M., Rondal, D.J., Evangelista, M.A.M., and Saito, G., "Land-use/Land-cover analysis by the matrix method using remote sensing", *Asian-Pac. Remote Sensing J.*, Vol.5, pp.79-84, 1993.

Use of Vegetation Index of Satellite Data for Updating Land Use Data in Japan

Kohei CHO, Haruhisa SHIMODA, Toshibumi SAKATA (*)
Mitsunori YOSHIMURA (**)

*Tokai University Research & Information Center
2-28-4, Tomigaya, Shibuya-ku, Tokyo 151 Japan
Fax: +813-3481-0611, Tel:+813-3481-0610
Email:kcho@keyaki.cc.u-tokai.ac.jp

*Remote Sensing Technology Center of Japan
1-9-9, Roppongi, Minato-ku, Tokyo 106 Japan

Abstruct

Since 1991, the National Land Agency of Japan has been updating the digital land use data of Japan using Landsat TM and SPOT satellite images. It is well known that point wise classification method such as maxmum likelihood classification are not so efficient in updating conventional land use data with satellite data. In this project, instead of using the point wise classification method, the image interpretation method is used for updating the data. This paper describes how the vegetation index derived from satellite data is used for effectively updating the land use data in Japan.

1. Introduction

1.1 Digital National Land Information

Since 1974, the National Land Agency of Japan has been collecting and updating various land information of Japan in digital form called the Digital National Land Information. This information include but not limited to topographic data, geological data, climate data, land use data, administrative division data. Most of the data are produced and updated by in situ investigations, air photo interpretation, topographical map interpretation etc. In order to reduce the time and expence for the data renewal, in 1991, the National Land Agency had installed satellite remote sensing technology for updating the land use data. Table 1 shows the items of the land use data.

1.2 Limitation of Point Wise Classification

Landsat TM and SPOT images suggested us possibilities of extracting detailed land cover information from satellite data. However, at the same time, limitation of applying

traditional point-wise classification method, such as the maximum likelihood classification, to the high spatial resolution data have become clear. There are two main reasons for this limitation.

One is that the conventional land use items can not always be represented by particular spectral characteristics of satellite data. A symbolic example is the item "Golf courses" . A golf course consists of Grass, woods, ponds and others. This means that the golf course can't be classified with only spectral information. Moreover, the spectral characteristics of some items are likely to be overlapped with others, which reduces the classification accuracy.

The other is the mixel problem. One pixel is not always occupied by single land use/cover item. In not a few cases, one pixel is consists of two or more land use/cover items. In this case, the spectral characteristics of each items are mixed up and the spectral characteristic of the mixel becomes completely different from each land use/cover item which are composing the pixel. Texture analysis is expected to be one of the solution. But, it is still on the way. These situation suggest us the necessity of introducing human image interpretation approach to the procedure of land use data renewal with satellite data.

2. Strategies for satellite data utilization

2.1 Concept

In order to break the limitation of conventional classification methods, a kind of hybrid approach was adopted in this project. Basically, image interpretation technique is used for land use data updating procedure. However, various digital image processing techniques are also used to reduce the labor. The basic concept of the system development are summarized as follows.

(1)Utilize human image interpretation technique.
(2)Only update the changed areas of the old land use data.
(Do not perform new classification to all data.)
(3)Utilize various digital image processing technique.
(4)Use additional information such as maps

2.2 Modification of Land Use Items

Considering the spectral and spacial characteristics of satellite data, the 15 land use items were modified to 10 items and "golf courses" was added as a new item. This kind of modificaiton is an important compromise for the practical used of satellite data for land use data renewal. table 1 shows the relationship between the new and the old land use items.

Table 1. Land use data items

No.	New land-use item	No.	Old land-use item
1.	Rice fields	1.	Rice fields
2.	Gardens or fields other than rice fields	2.	Fields other than rice fields
3.	Forests	3.	Fruit gardens
4.	Wastelands	4.	Tree gardens other than fruit gardens
5.	Construction areas	5.	Forests
6.	Arterial roads or railroads	6.	Wastelands
7.	Golf courses	7.	Construction areas A (high density)
8.	Other areas	8.	Construction areas B (low density)
9.	River areas, lakes or marshes	9.	Arterial roads or railroads
10.	Seashore	10.	Other areas
11.	Seawater	11.	Lakes or marshes
		12.	River areas A: non-artificial areas
		13.	River areas B: artificial areas
		14.	Seashore
		15.	Seawater

2.2 Satellite Data Use

For high dense urbanized area, Landsat TM data and SPOT panchromatic(PA) data are composed and used for information extraction. For the other area, only TM data are used. This is to reduce the data cost without reducing the accuracy of land use data renewal.

3. Methodology

3.1 Pre Processing

(1) Geometric Correction

Firstly, SPOT PA data and TM data are geometrically corrected to overlay on grid type old land use data.

(2) SPOT/TM Data Composite Using HSI Transformation

In order to integrate SPOT PA data with TM data, HSI transformation is performed to the both data. Fig.1 shows the concept of SPOT/TM data composite using HSI transformation.

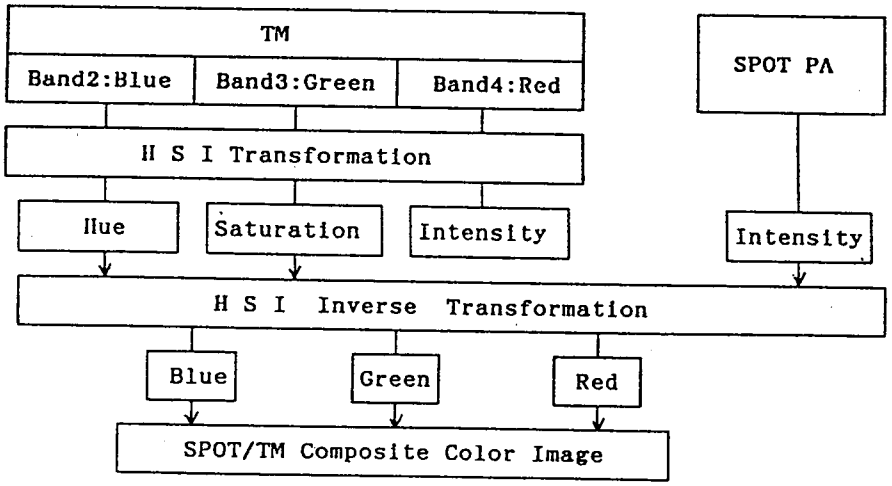

Figure 1. The concept of SPOT PA/TM compositing using HSI transformation.

(3) NVI Data Production

To support land use data updating procedure, the Normalized vegetation Index(NVI) was computed from TM data using the following formula.

$$NVI = \frac{\text{Band 4 - Band 3}}{\text{Band 4 + Band 3}} \times 100 + 128$$

3.2 Land Use Data Updating Procedure

The preprocessed data will be provided to the personal computer based interactive processing sub-system and the old land use data are updated. Fig.2 shows the main flow of the concept of the updating procedure.

3.2.1 Water/Vegetation/Non-Vegetation Discrimination

(1)Firstly, SPOT/TM false color image is displayed on the CRT(see Fig.3(a)).

(2)The NVI level sliced image is overlaid on the false color image and the threshold level for discriminating water areas from land areas is selected.

(3)similarly, the threshold level for dividing land areas into vegetation areas and non-vegetation areas is selected.

3.2.2 Vegetation to Non-Vegetation Renewal

(1)The NVI non-vegetation areas which items were vegetation in the old land use data are extracted. These areas will be the candidate for land use change. Fig.3(b) to (d) shows a example of this procedure.

(2)The candidate areas are colored in yellow and overlaid on the SPOT/TM false color image(see Fig.3(d)).

(3)The land use changed areas are selected by image interpretation and are enclosed with mouse(see Fig.3(e)).

(4)The new non-vegetation items are assigned to the enclosed areas.

3.2.3 Vegetation to Water Renewal

(1)The NVI water areas which items were vegetation in the old land use data are extracted. These areas will be the candidate for land use change.

(2)The candidate areas are colored in yellow and overlaid on the SPOT/TM false color image.

(3)The land use changed areas are selected by image interpretation and are enclosed with mouse.

(4)The new water items are assigned to the enclosed areas.

3.2.4 Vegetation to Vegetation Renewal

(1)The NVI vegetation areas which items were vegetation in the old land use data are

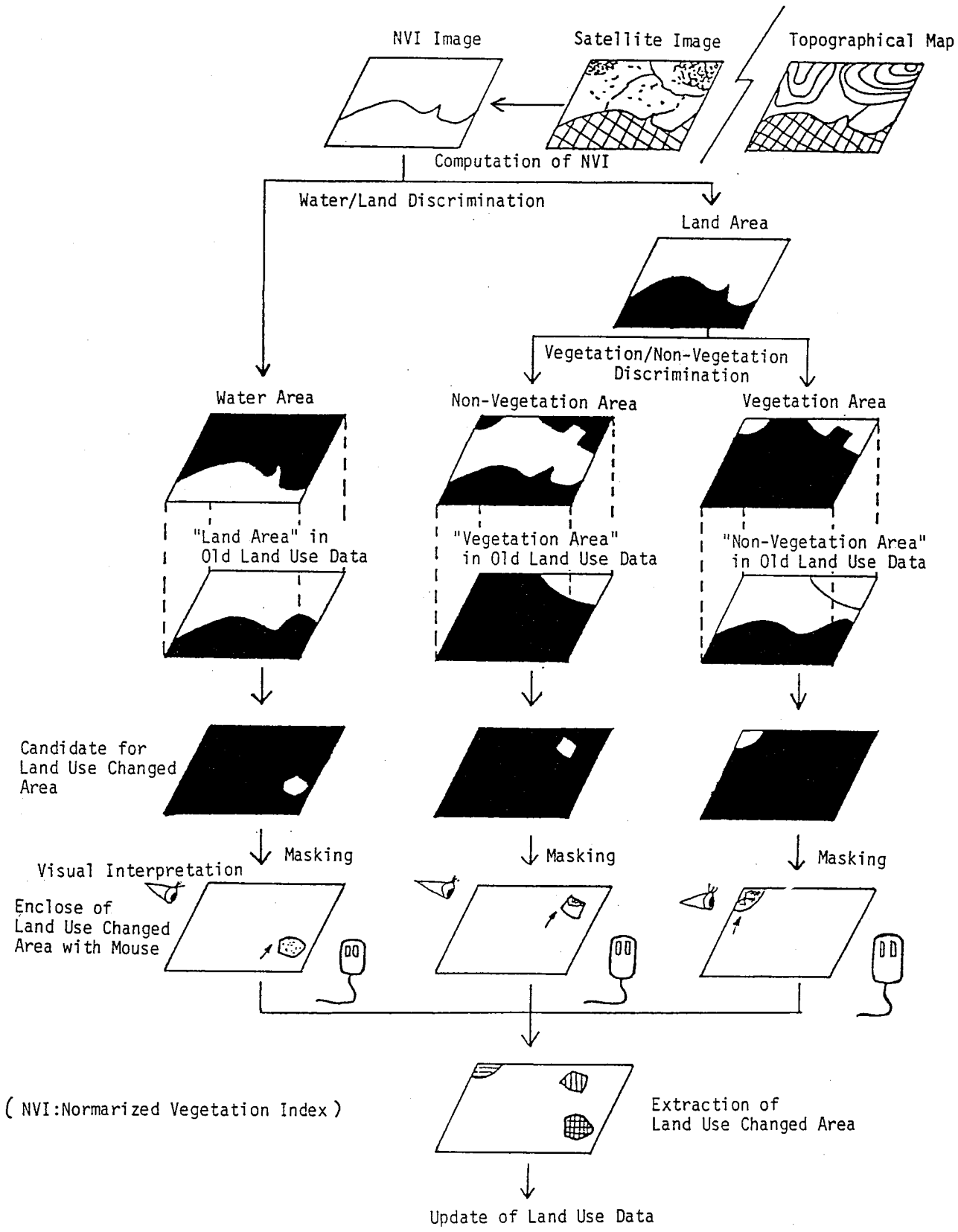

Figure 2. The concept of the land use data updating procedure.

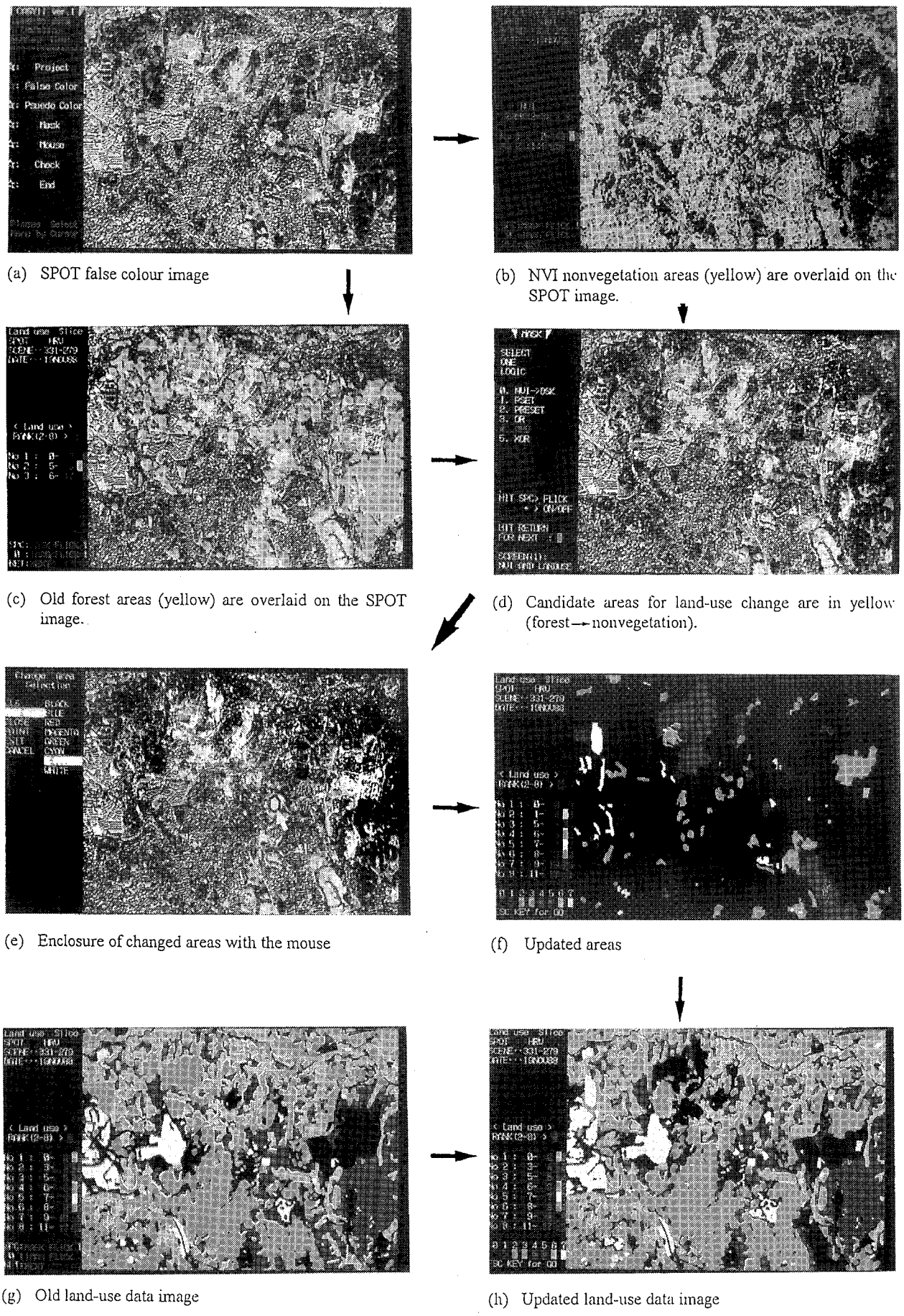

(a) SPOT false colour image

(b) NVI nonvegetation areas (yellow) are overlaid on the SPOT image.

(c) Old forest areas (yellow) are overlaid on the SPOT image.

(d) Candidate areas for land-use change are in yellow (forest→nonvegetation).

(e) Enclosure of changed areas with the mouse

(f) Updated areas

(g) Old land-use data image

(h) Updated land-use data image

Figure 3. The land use data updating procedure.

extracted. These areas will be the candidate for n o change or land use item change within vegetation area.

(2)The candidate areas are colored in yellow and overlaid on the SPOT/TM false color image.

(3)The land use change areas are selected by image interpretation and are enclosed with mouse.

(4)The new vegetation items are assigned to the enclosed areas.

3.2.5 Non-Vegetation/Water Renewal

Similarly, old non-vegetation item areas and old water item areas are updated.

4. Evaluation

In 1990, the pirot project was performed at Kanagawa Prefecture by the National Land Agency under the cooperation with other institutions. In order to evaluate the updated result, 30 areas were selected for evaluation and a field survey was performed. Fig. 4 shows an example of the evaluation sheet. Among the 30 areas, 27 areas were updated correctly, and 3 areas were changed areas but the updated items were wrong. This proved the effectiveness of the new approach using satellite data.

5. Conclusion

The image interpretation approach seems to be retrogressive to the computer technology advancement. However, so far, the image interpretation approach is one of the most practical way to smoothly transfer the air photo based renewal system to the satellite data based renewal system. Moreover, the various digital image processing functions allow users to update land use data more effectively and efficiently than only using photo interpretation technique.

Reference

a) Asianont S., 1988, "Base Map Updating in Thailand Using SPOT Imagery", Proc. of the 9th Asian Conference on Remote Sensing, d-7.

b) Cushine L. Janis, 1987, "The interactive effect of spatial resolution and degree of internal variability within land-cover types on classification accuracies", Int. J. Remote Sensing, vol.8, no.1, pp.15-29.

c) Hosomura, T. et al, 1989, "Performance of MESSR data for land cover classification Proc. of the Third Symposium on MOS-1 Verification Program, vol.1, pp.199-213.

d) Cho, K., et al, 1990, "Personal Computer Based Image Interpretation Using SPOT Image and Conventional Land Use Information", Proc. of ISPRS Comm. IV, vol.22, no.4, pp.467-474.

(a) SPOT/TM image

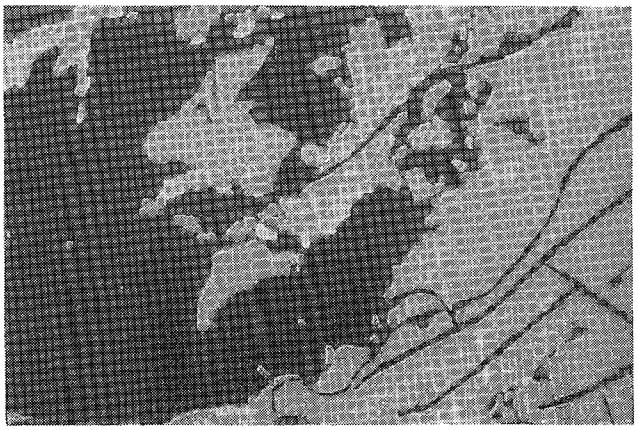

(b) Old land-use data image

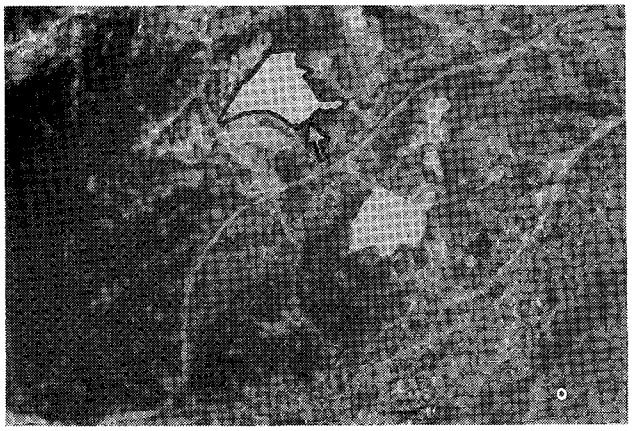

(c) Extracted change areas in the SPOT/TM image

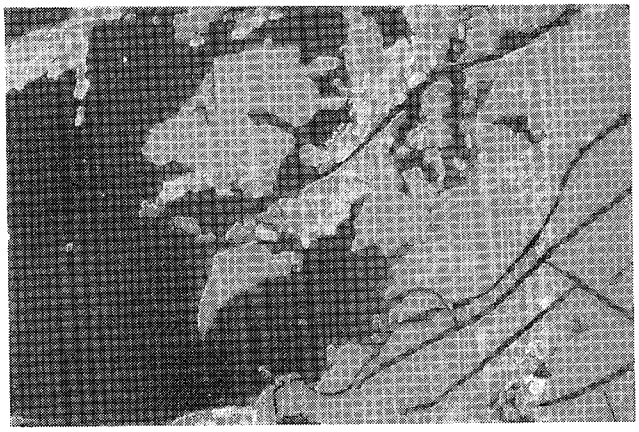

(d) Updated land-use data image

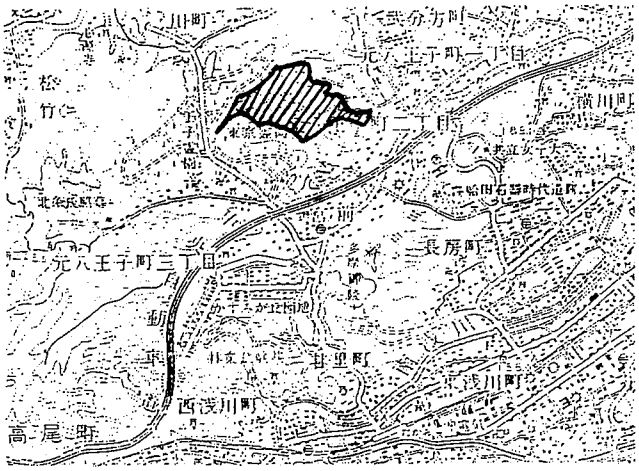

(e) Map

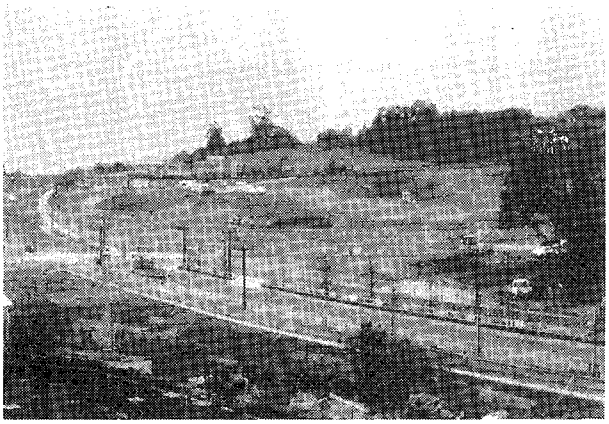

(f) Field site

[Area No. 1] [Change Item: 3. Forest -> 8. Other uses] [Evaluation: A. Correctly updated]

Figure 4. An example of the updated area evaluation sheet.

Crop Maps and Yield Maps of Sugar Beets in the Tokachi Plains,Japan,Developed from Multitemporal Landsat TM Data

Chiharu Okano*, Katsuo Okamoto**, Michikazu Fukuhara** and Akira Nishimune***

*Center for Environmental Remote Sensing, Chiba University
1-33 Yayoi-cho Inage-ku Chiba 263 Japan

**National Institute of Agro-Environmental Sciences
3-1-1 Kannondai Tsukuba-shi Ibaraki 305 Japan

***Hokkaido National Agricultural Experiment Station
1 Hitsujigaoka Toyohira-ku Sapporo-shi Hokkaido 062 Japan

Abstract

Crop maps were made using Landsat TM data of the Tokachi plains, Hokkaido, Japan, to investigate the relationship between soil organic matter content and planting ratio. Sugar content and root weight of sugar beets were also estimated using Landsat TM data obtained around harvesting time in 1986.

The study site was classified into 5-subclasses. Sugar beets, potatoes and wheat were distinguished with 95 per cent accuracy. Sugar content and root yield also could be estimated with accuracy using this method. Planting ratio and yield of sugar beets varied according to soil organic matter content. These results suggest that Landsat TM data are useful for constructing crop maps and for estimating sugar content and root weight for sugar beets. Application of this approach may increase productivity of sugar beets by improving fertilization.

1.Introduction

The main crop of upland field agriculture in Hokkaido, Japan is sugar beet. The purchase system of sugar beet changed in 1986, the producer price of sugar beets has been determined on a quality basis. However, prior to 1986 the price was determined by weight. Heavy fertilization resulted in excessively high nitrogen levels, which decreased the sugar content and the root weight. The farmers have become concerned about the current crop management plan and application of fertilizer because of the present soil environment.

It is necessary to collect data regarding sugar content and root weight per unit or grid to apply the fertilizer properly. Unfortunately, data for planted area and yield of each producer are combined in Japan. Neither data for individual fields nor grid data is available. Therefore, Landsat TM data was used to estimate root weight and sugar content of agriculturally grown sugar beets.

A TM sensor has been installed in the fourth Landsat satellite, which was launched in 1984. The number of bands and resolution have been improved. The TM data are available and have been put to practical use in the fields of agriculture, in addition to other fields in Japan.

As the first step in applying TM data, random selection of agricultural fields is necessary to estimate the yield and quality of the object crops. A crop map is required as foundation information. If root weight and sugar content of sugar beets can be estimated, cultivation management can be adjusted to nonuniform conditions.

In this study, a crop map was made using multitemporal Landsat TM data of the Tokachi area, Hokkaido, Japan, to estimate sugar content and root weight of sugar beets at the time of harvest. In addition, relationships between the yield of sugar beets and soil environment were surveyed.

2.Constructing a crop map using TM data

2.1 Study site and data

The study was conducted in the Tokachi plain, in the western portion of Hokkaido. This is an important agricultural region in Japan. The Landsat TM data of the Tokachi plain were acquired from 1985(May 24,July 27,August 12 and October 15) and 1986(July 30,September 16 and October 18). These data are computer compatible tape data.

Hand made crop maps of Nishisikari,Sinsei and Hokoku in the Tokachi plains were produced from the ground truth data. Maps of soil organic matter content for the Tokachi plain were used as soil environmental data. Soil data were reorganized for three levels of organic matter content; high, middle and low.

2.2 Procedure

The image analysis followed the flow chart shown in Figure 1. Mask files were created to remove pixels of the nonagricultural field such as the urban,forest and grass land. The fields of sugar beets, potatoes,wheat,corn and legumes were selected by the supervised classification method using the maximum likelihood decision rule. The logical operation then was applied to the selected fields. Because the boundary pixels of each selected crop contain some information such as adjoining crops and farming roads, the classified area of crops may be underestimated. In the next step, the neighboring pixel process was executed. For example, if at least one targeted crop's pixel in eight pixels were included, a center pixel was judged to be an object crop.

Finally, the files of each crop were overlaid to form the crop map. When one pixel contained two or more kinds of crops following the overlay process, then that pixel was unclassified.

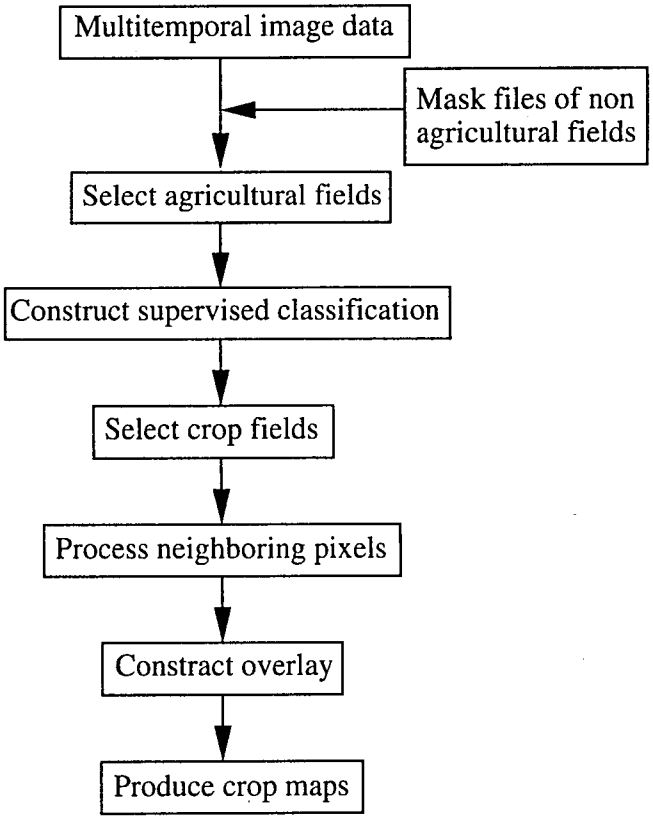

Figure 1 The procedure for constructing crop map.

2.3 Results and discussion

2.3.1 Evaluation of a crop map made from the TM data

The classification was evaluated at the Kamifushiko test field. In addition, the crop maps and the map of soil organic matter content were overlaid and the relationship of the planting ration according to the soil organic matter content were surveyed.

An example of a crop map made using 1985 multitemporal TM data is shown in Figure 2. The area of crop fields were estimated to be 29,353ha in 1985. This value was 34.5% of the total study site area. That area contained sugar beets, potatoes,wheat, corn and legumes at planting ratios of

24.3%, 29.7%, 17.2%, 15.3% and 13.5% respectively.

The black portion in Figure 2 contained urban areas, forests, grass land, river basins and unclassified areas. Unclassified areas included boundary regions of each crop field, another kind of vegetation fields, the self defense forces station and, established grounds for housing.

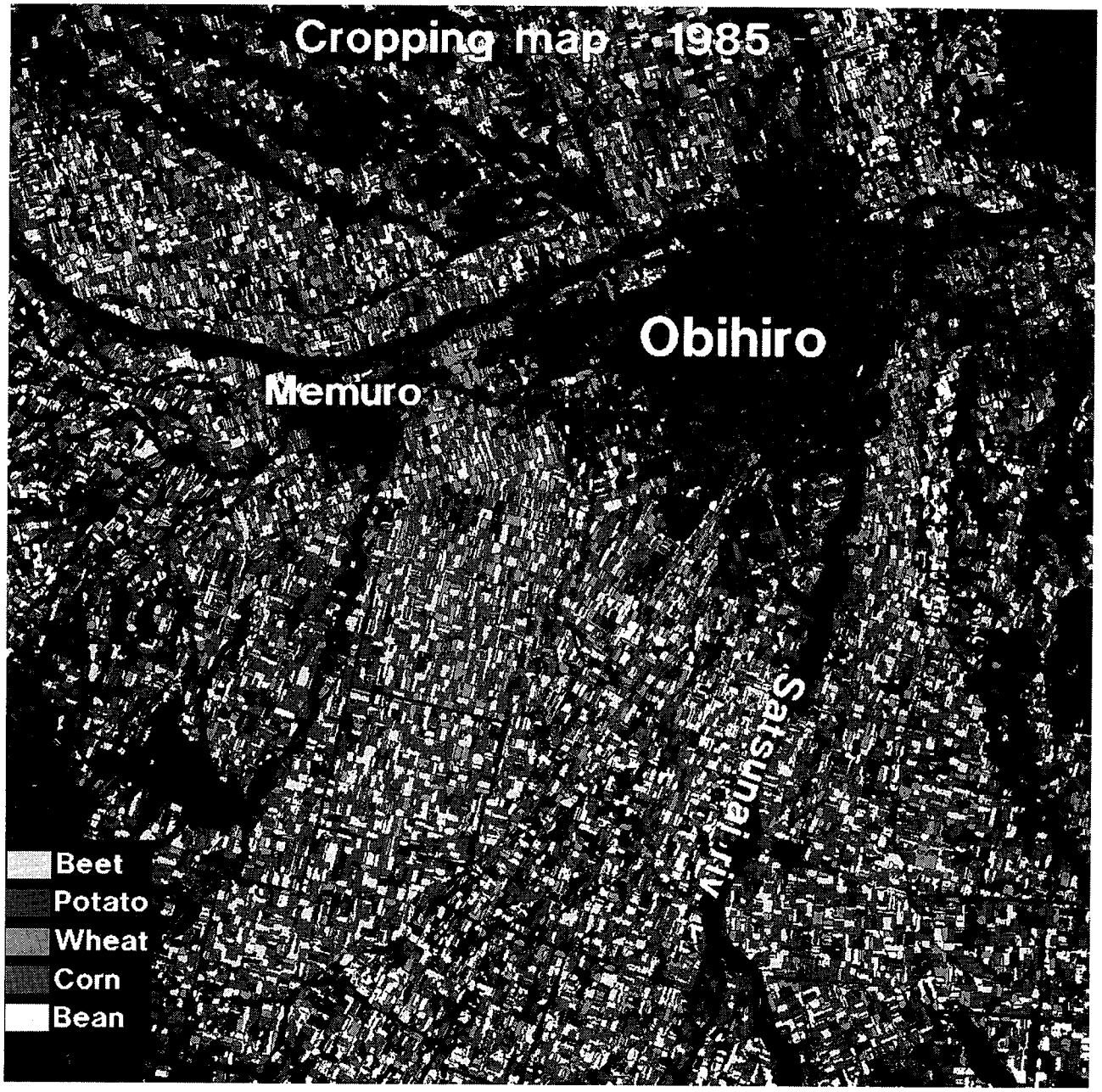

Figure 2 A crop map in Tokachi plains,Hokkaido,Japan, developed from 1985 multitemporal LANDSAT TM data.

Sugar beets, potatoes and wheat were distinguished with 95% accuracy in both 1985 and 1986 TM images (Table1). These results show that Landsat TM band ratios reflecting differences in the period of vegetation are effective in constructing crop maps in Japan.

The described method of constructing a map from Landsat TM data can be used in the Tokachi plain, Japan, where agricultural fields are wider than any other place in Japan. If the information of boundary pixels can be selected with precision the maps created will have high degree of accuracy.

Table 1. The classification accuracy of test fields (%).

1985

	Sugar beets	Potatoes	Wheat	Corn	legumes	unclassified
Sugar beets	100.0	0.0	0.0	0.0	0.0	0.0
Potatoes	0.0	95.6	0.0	0.0	0.0	4.9
Wheat	0.0	0.0	96.9	0.0	0.0	3.1
Corn	0.0	0.0	0.0	81.3	0.0	18.7
legumes	0.0	0.0	0.0	0.0	80.4	19.6

1986

	Sugar beets	Potatoes	Wheat	Corn	legumes	unclassified
Sugar beets	96.7	0.0	0.0	0.0	0.0	3.3
Potatoes	0.0	98.6	0.0	0.0	0.0	1.4
Wheat	0.0	0.0	98.6	0.0	0.0	1.4
Corn	0.0	0.0	0.0	88.4	0.0	11.6
legumes	0.0	0.0	0.0	0.0	88.1	11.9

2.3.2 Characteristics of planting ratio according to soil organic matter content

The planting ratio was calculated from the crop map and the map of soil organic matter content (Table2). The planting ratio achieves 100% with the levels of soil organic matter content. The planting ratio was higher for potatoes and sugar beets in soils with low and middle organic matter content in 1985. However, in 1986, the area planted in sugar beets increased in areas with high organic matter content.

These results were consistent with the findings of an actual investigation of the cultivation system executed near Memuro in the Tokachi plain. Cultivation of sugar beets has continued in areas of high soil organic matter content, to avoid water damage and the decrease of sugar content due to excessive absorption of nitrogen. Recently the planting ratio of root crops has increased due to improved drainage. However, cultivation of crops is not suited to the soil organic matter content. The farmers still believe their experiences. This satellite data can be used for large areas and agricultural fields which can be judged objectivity.

3.Estimation of sugar content and root weight of sugar beet

3.1 Study site and data

The study site for this analysis is the same area described in Section 2.1.

The TM data was collected on September 16 and October 18 in 1986 for the analysis.

Measured values of sugar content and root weight determined at the time of harvest represent an

average increase each production association. Each association is composed of eight farms. The regression analysis was based on 22 data points and verification of estimated values was based on 15 data points.

Table 2. Planting ratio according to soil organic matter content (%).

1985

	Soil organic matter content (%)		
Crops	< 5	5~8	> 8
Sugar beets	26	27	22
Potatoes	37	34	24
Wheat	8	12	24
Corn	19	16	14
legumes	10	11	17
Total	100	100	100

1986

	Soil organic matter content (%)		
Crops	< 5	5~8	> 8
Sugar beets	21	22	28
Potatoes	28	30	25
Wheat	26	21	16
Corn	19	19	19
legumes	6	8	12
Total	100	100	100

3.2 Procedure

The image analysis is described in Figure 3. The fields of sugar beets were selected from a crop map which was made using multitemporal Landsat TM data.

The CCT average for sugar beet fields were calculated based on increased production for each association. The analytical data of CCT value, sugar content and root weight were used for multiple linear regression. The sugar content and root weight maps were based on estimation equations. The relationships between sugar content, root weight and soil environment were evaluated.

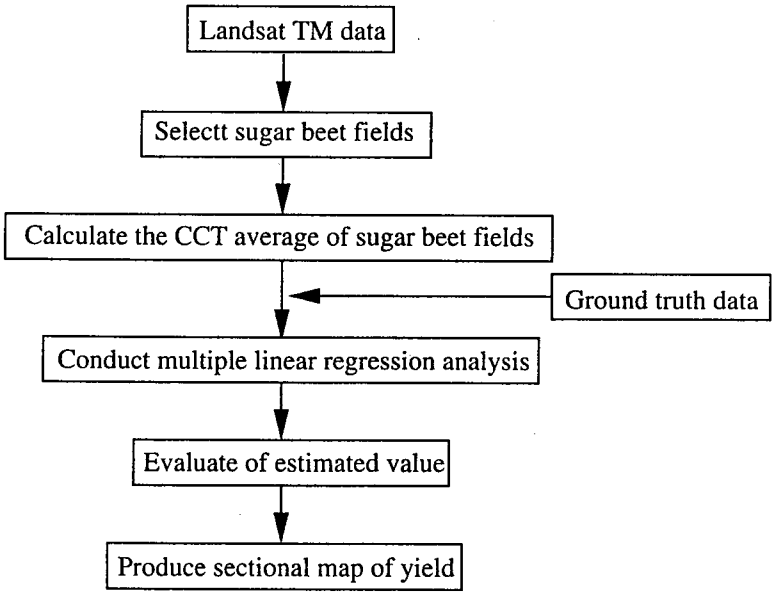

Figure 3 The procudure for constructing sectinal map of yield.

3.3 Results and discussion

Correlation coefficients between sugar content and CCT values of each band were higher in October than in September (Table 3). Conversely, correlation coefficients between root weight and CCT values of each band were higher in September than in October (Table 3).

Table 3. Correlation coefficients between sugar content (SC), root weight (RW) and CCT values of each band on September 16 and October 18 in 1986.

Band	9.16		10.18	
	SC	RW	SC	RW
TM1	-0.01	0.69**	0.65**	-0.12
TM2	-0.07	0.44**	0.60**	-0.28
TM3	-0.09	0.58**	0.72**	-0.26
TM4	-0.52	-0.06	-0.26	-0.25
TM5	-0.45	0.11	-0.10	-0.36
TM7	-0.36	0.20	-0.44	-0.10

** Indicates P<0.01

The following equations were derived to estimate the sugar content and root weight successfully:

sugar content=0.172TM1o+0.342TM3o-3.013 (r=0.83**)

root weight=2.664TM1s+0.849TM4s-1.395TM5s-198.839 (r=0.91**)

Where TM1o and TM3o are Band1 and Band3, respectively, derived from TM data on October 18. TM1s, TM4s and TM5s are Band1, Band4 and Band5, respectively, derived from TM data on September 16.

The fields producing sugar beets with low sugar content and low root weight were detected frequently on the soil rich in organic matter, while the fields with soil low in organic matter tended to produce sugar beets with high sugar content and high root weight (Figure 4,5).

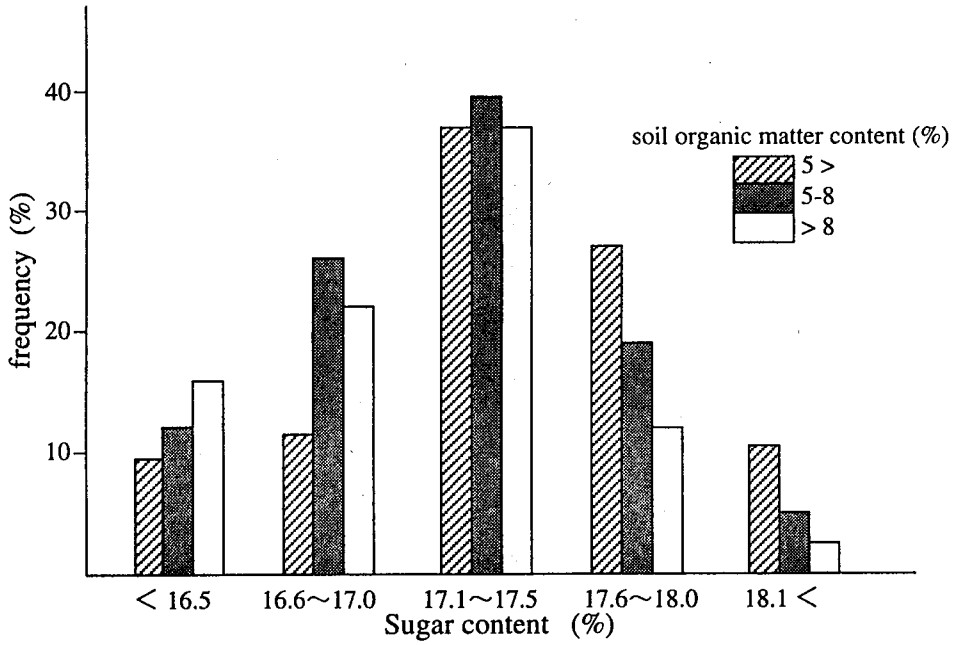

Figure 4 The frequency of sugar content of sugar beet caltivated with three levels of soil organic matter content.

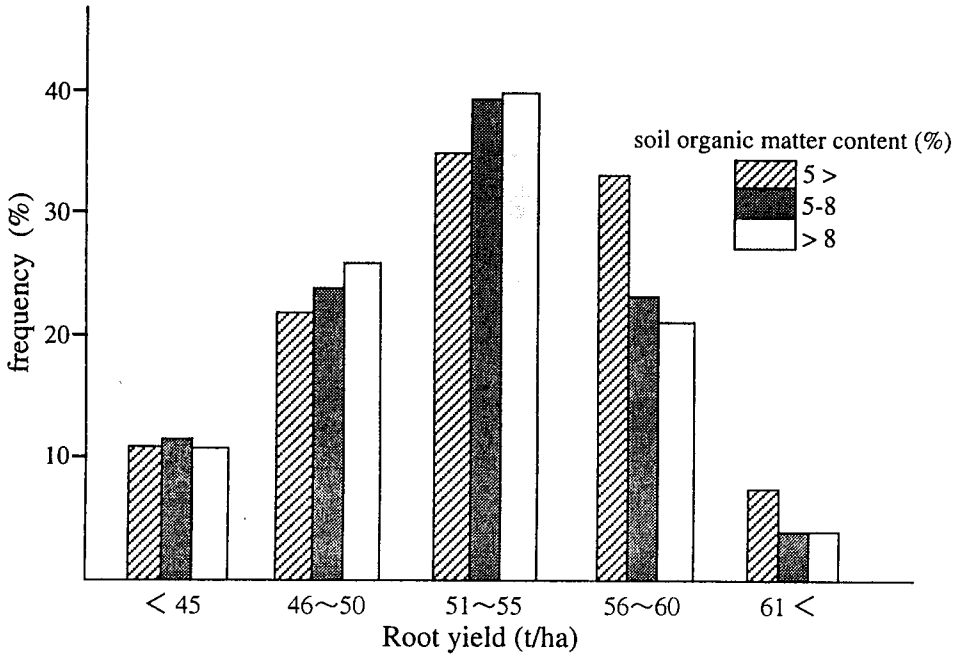

Figure 5 The frequency of root yield of sugar beet caltivated with three levels of soil organic matter content.

It was possible to estimate the sugar content and root weight of sugar beet for large areas using Landsat information. This facilitated an understanding of the relationship between soil environment and yield. However, yield of sugar beets is affected not only by the amount of nitrogen supplied from soil but also by the amount of chemical fertilizer and compost added to the soil.

In the future, it will necessary to consider weather conditions, nutrient uptake availability, planting history and topography during the analysis process.

Agriculture Monitoring in Japan Using NOAA/AVHRR Data

Genya SAITO*, Nobuyuki MINO** and Yoshizumi YASUDA***

*National Institute of Agro-Environmental Sciences
3-1-1 Kannondai, Tsukuba, Ibaraki Japan
Tel:+81-298-38-8225, fax:+81-298-8199
Email:genya@niaes.affrc.go.jp

**National Institute of Agro-Environmental Sciences
3-1-1 Kannondai, Tsukuba, Ibaraki Japan
tel+81-298-38-8225, fax+81-298-8199
Email:minonobu@niaes.affrc.go.jp

***Chiba University
1-33 Yayoicho, Inage-ku, Chiba, Japan
tel:+81-43-290-3258, fax:+43-290-3270
Email:yasuda@ics.tj.chiba-u.ac.jp

Abstract

Using NOAA/AVHRR Local Area Coverage(LAC) data received in Japan, we made NDVI Maximum Value Composites(MVCs) and got the monthly data set of 12 Japan Vegetation Index (JVI) for one year. Cropping-pattern was analyzed in agricultural areas in Japan using JVI.

1. Introduction

Many studies have shown that satellite remote sensing technique is a powerful tool for agriculture monitoring. However LANDSAT data can only be acquired once in 16 days and are highly restricted by clouds. This makes LANDSAT data not very reliable source for temporal variation analyses in countries like Japan. NOAA/AVHRR data on the other hand, can be acquired daily and comparatively free from cloud restriction.

National Oceanic and Atmospheric Administration(NOAA) has prepared weekly Global Vegetation Index(GVI) images using NOAA/AVHRR data since April 1982. A Very high correlation is reported between vegetation Index and the biomass production (Justice et al., 1985).

Spatial resolutions of GVI images are more than 10km. It is excessive large value to apply to monitoring agricultural crop-pattern in Japan. So we prepared monthly Japanese Vegetation Index(JVI) images that have spatial resolution of 1km using NOAA/AVHRR data.

2. Methods

2.1. Sensor and data

We used NOAA-11/AVHRR data to prepare JVI images. Scanning width of NOAA/AVHRR is 2800km. Spatial resolution is 1.1km at nadir observation. The JVI images were created using AVHRR CH1(visible red: 580 - 680nm) and CH2(near-infrared: 725 - 1100nm) measurements.

2.2. NDVI

Some remote sensing data are related to the activity of the vegetation. Often visible and near-infrared reflectances are combined to compute vegetation indices in order to bring out the difference of radiometric response between the active green canopy and bare soils. Normalized Differential Vegetation Index (NDVI) (Yates et al., 1984) is most commonly used to estimate the amount of vegetation. NDVI is defined as follows:

$$NDVI=(CH2-CH1)/(CH2+CH1) \quad \ldots\ldots\ldots\ldots \quad (1)$$

where CH1, CH2 are observation data of CH1 and CH2

The value of the NDVI takes theoretically between -1 and 1. The higher the vegetation activity is the closer the NDVI gets to 0.5. Where there is no vegetation cover(bare soil), the NDVI is nearly 0. The values of the NDVI become negative in cloud, snow and water areas.

2.3. Japan Vegetation Index (JVI)

Using NOAA/AVHRR Local Area Coverage(LAC) data received in Japan, daily LAC datasets were created. We then compiled monthly NDVI images using NDVI Maximum Value Composites(MVCs) and got 12 JVI for one year.

Cropping-pattern was analyzed in agricultural areas in Japan using JVI. These areas were shown figure 1.

3. Results

3.1. Temporal variations of NDVI in agricultural area

JVI images from April 1991 to March 1992 were compiled. In April, the most values of the NDVI to the north of Kanto-district are less than 0.2 while those to the south of Kanto-district are higher than 0.2. In June, the values of the NDVI throughout Japan become higher than 0.2 except in the agricultural areas(paddy fields and upland farming fields) where the values of NDVI are about 0.1. This is because crops in those areas are at the beginning stage of their growth. In August, the values of the NDVI higher than 0.25 are found everywhere except urban areas like Tokyo and Osaka. At this time of the year, the agricultural areas are widely covered with grown crops. In October, after the harvest time, the values of the NDVI fall steeply in the agricultural areas.

3.1.1. Paddy fields

As for paddy fields, we selected the following 10 sites; Ishikari Plain, Hachiro-gata, Sendai Plain, Niigata Plain, Aizu Basin, Kanto Plain(near Utsunomiya), Nobi Plain, Okayama Plain, Tokushima Plain and Saga Plain. Shown in figure 2 are monthly NDVI variations from April 1991 to March 1992. Figure 2(a) represents northern part of Japan, (b) central part and (c) south-western part respectively. NDVI variations of Niigata Plain are shown both in (a) and (b) as a standard used for purposes of comparison.

In northern part of Japan shown in figure 2(a), the NDVIs reach their maximum values either in July or in August and keep values less than 0.05 from December to March everywhere. Only in May, a clear difference in the value of the NDVI can be found. The kind of crop planted in paddy fields not used for rice and the area of these fields make this difference. There are few paddy fields for winter wheat in Niigata while there are 20% of all paddy field in Sendai, 40% in Ishikari and Hachiro-gata. In Hachiro-gata, winter wheat grows fast resulting in an apparent peak in May while there is no such peak in Ishikari. Less snowfall in Sendai makes wheat and vegetable grow in wintertime resulting in the NDVIs about 0.05.

In central part of Japan, as shown in figure 2(b), the general shape of the two curves of Niigata and Aizu is the same. The NDVIs of both Utsunomiya and Nobi reach their maximum value in August and maintain a certain amount of value even in wintertime. This is partly because their winter wheat and vegetables grow in winter and also because their rice yield late in comparison with other areas. Average NDVIs are low in Nobi because of the urbanization.

In south-western part of Japan, two-crop system is possible which results in an apparent double-peak shape of NDVI time profiles in figure 2(c). These peaks represent the harvest time of rice and winter crops' mainly winter wheat.

3.1.2. Upland farming fields

As for upland farming fields, we selected the following 6 sites; Tokachi Plain, Abashiri Plain, Hokuso Plateau in Chiba prefecture, Tsumakoi Plateau in Gumma prefecture, Nansatsu district in Kagoshima prefecture and Miyakonojyo Basin in Miyazaki prefecture. Monthly NDVI variations are shown in figure 3.

Shown in figure 3(a) are Tokachi, Abashiri and Hokuso that are located in potato and sugar-beet zone. The NDVI time profiles show an apparent peak in summertime. Snowfall in Tokachi and Abashiri keeps NDVIs almost zero from December to March.

Shown in figure 3(b) are Tsumakoi, Miyakonojyo and Nansatsu that are located in vegetable zone. The NDVI curves in these areas have multiple peaks according to the dominant vegetables in each area. Miyakonojyo and Nansatsu located in south-western part of Japan maintain a certain value of NDVI even in wintertime.

3.1.3. Grassland

As for grassland, we selected Konsen Plain in Hokkaido and Aso district in Kyusyu. In both areas the NDVIs in figure 4 increase as pasture plant grows from Spring to Summer. In Summer, the NDVIs drop because of grazing.

3.1.4. Urban areas

As for urban areas, we selected Tokyo and Osaka. Figure 4 shows the NDVI time profiles of the two cities. The NDVIs in Tokyo show a kind of seasonal variation while the NDVIs in Osaka keep low values throughout the year.

Acknowledgments

This work was performed as cooperative project JVI. We wish to thank this project members, Dr. Sei-ichi SAITOH Hokkaido University, and Ms. Azumi GOTOH Japan Weather Association, etc.

References

C. O.Justice, J. R. G. Townshend, B. N. Holben and C. J. Tucker (1985) : Analysis of the phenology of global vegetation using meteorological satellite data, Int. J. Remote Sensing 6, 1271-1318

H. W. Yates, J. D. Tarpley, S. R. Schneider, D. F. Mcginnis and R. A. Scofield (1984) : The role of meteorological satellite in agricultural remote sensing, Remote Sensing of Environ., 14, 219-233

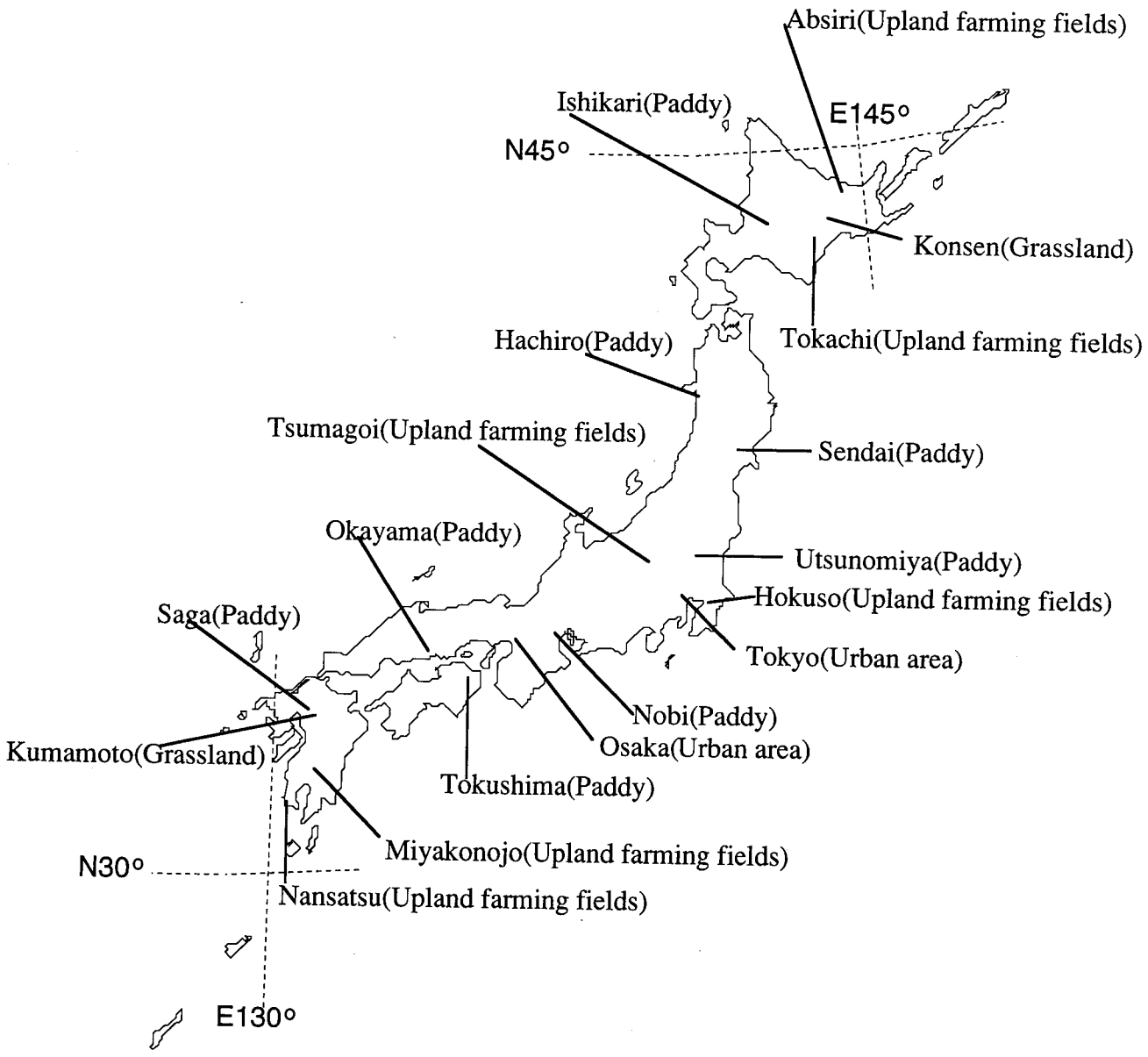

Fig. 1 The Areas of Cropping-Pattern Analysis

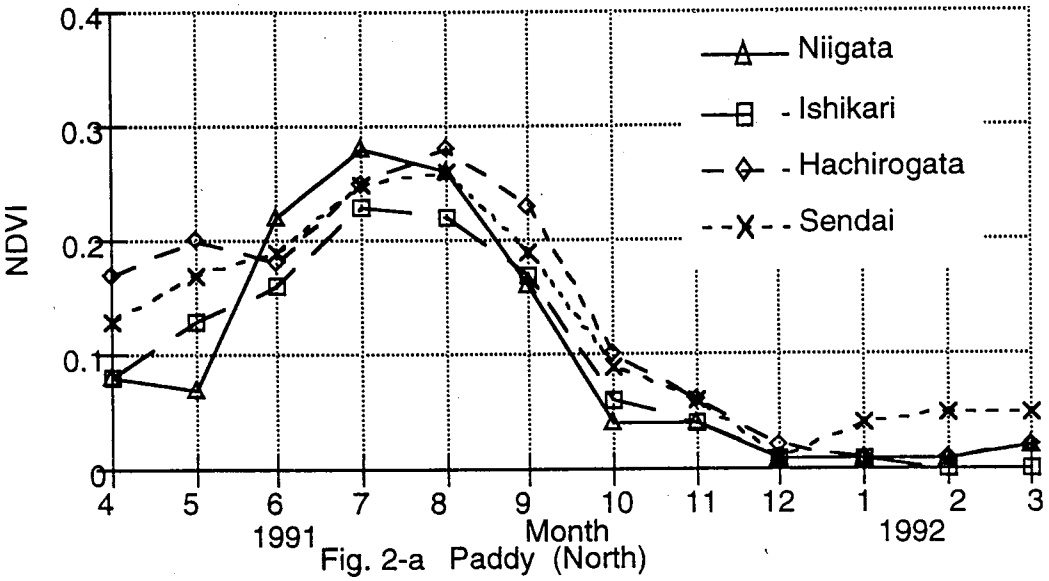

Fig. 2-a Paddy (North)

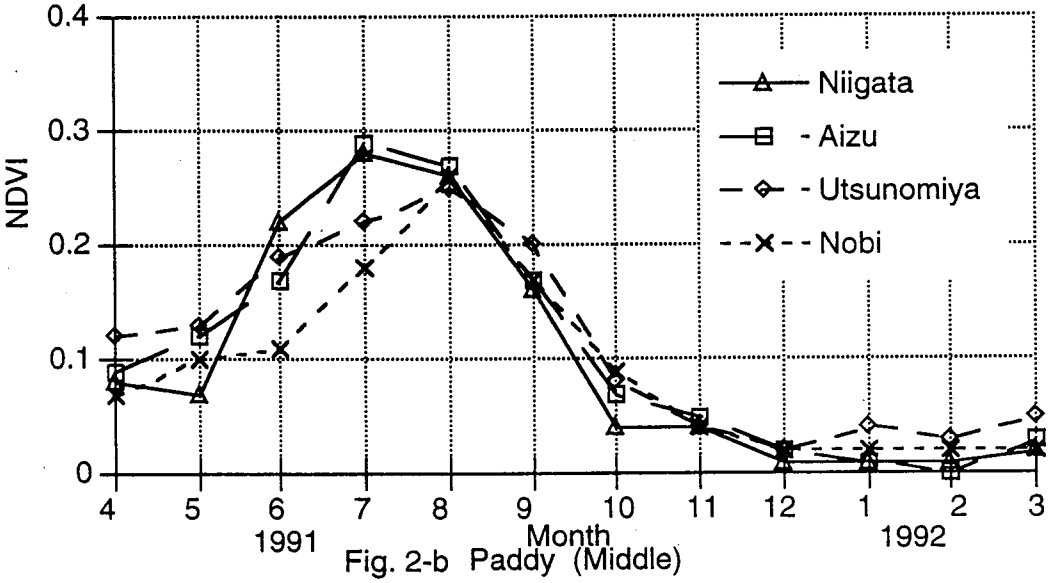

Fig. 2-b Paddy (Middle)

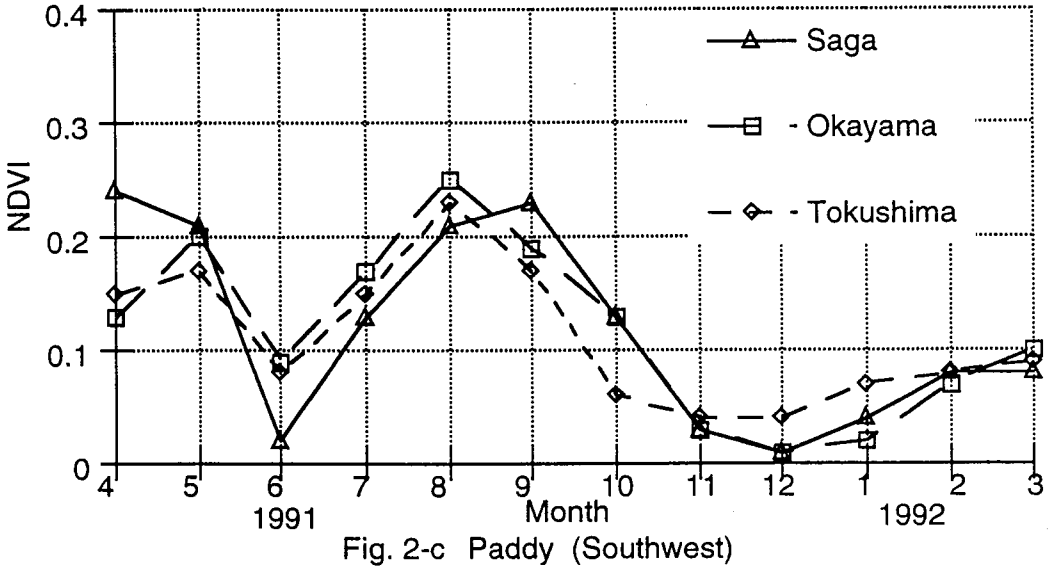

Fig. 2-c Paddy (Southwest)

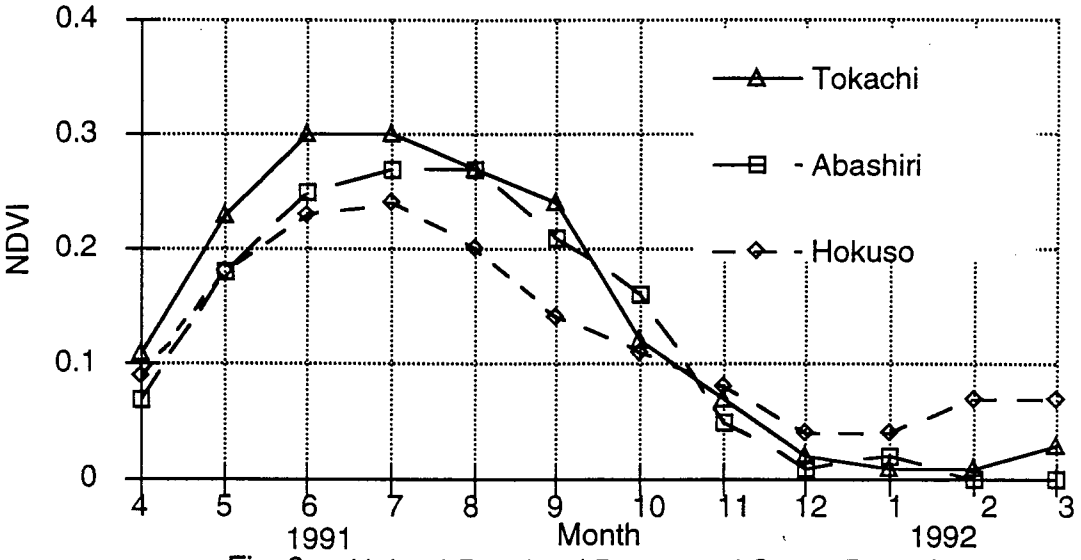

Fig. 3-a Upland Farming (Potato and Sweet Potato)

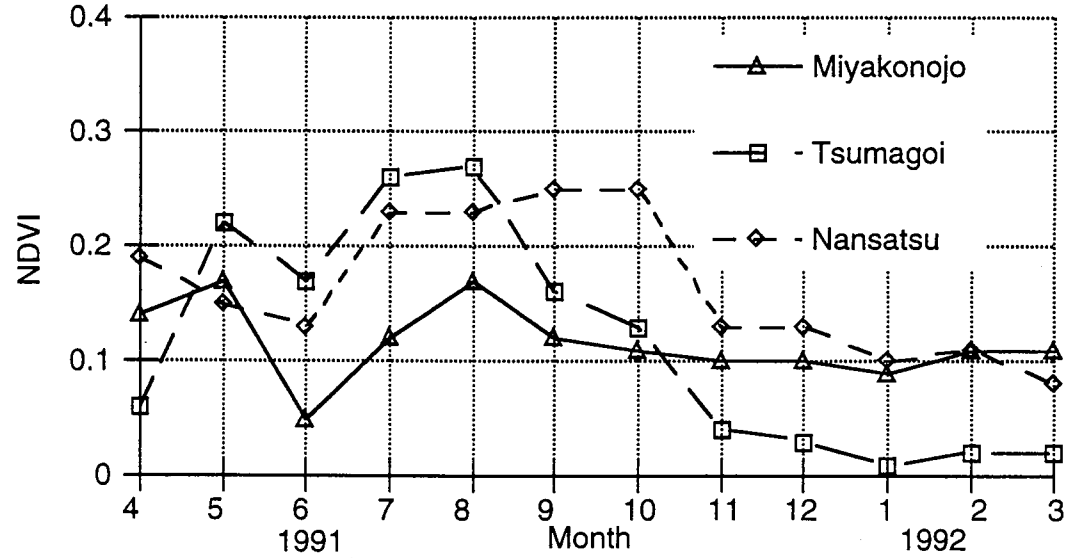

Fig. 3-b Upland Farming (Vegetable etc.)

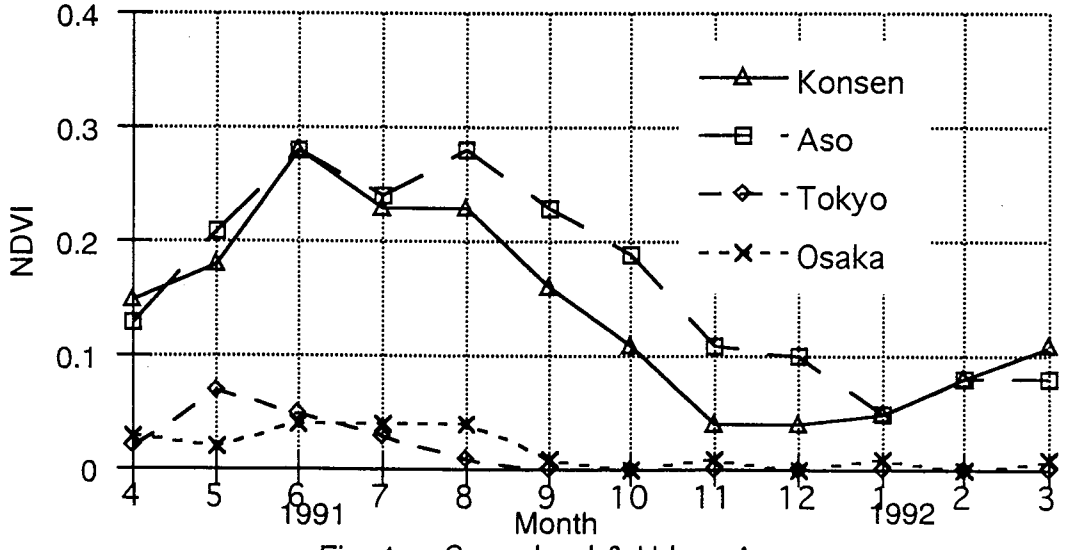

Fig. 4 Grass-land & Urban Area

THE STATE OF LAND COVER AND PASTURE CONDITION ON TERRITORY OF MONGOLIA

G. Tsolmon
Land Policy Institute of Ministry for Nature & Environment.
Ulaanbaatar-35, Chenguunjav str.2, Mongolia.

The territory of Mongolia is divided into such natural zones as forestry steppe, steppe, desert steppe and the gobi-desert. In general the territory has mountainous surface and 60% of the whole territory is covered with mountain range and 40% is valleys and steppes.

The mountainous feature of the surfaces are being created by the Altai, Khangai, and Khentei mountains and by their branch ranges and in between them lay the vast valleys and steppes of the Lowland of the Depression of Great lakes (Ikh Nuuruudyn Khotgor), plain steppe of the Middle Khalkha (Dundat Khalkha), Dornot (Eastern plain steppe) and the Gobi lowlands of the Transaltai Gobi.

The Mongolian land fund reserve is for its surface is classified in general into:
1. prime nature 2. originated nature as by their appearances.

1. The prime nature is divided into:

- Permanent snows
- Areas covered with forest
- Grassland
- Shrub and bushes
- Rivers and lakes
- Swampy
- Sands
- Dry beg
- Rocks and cliffs

2. The originated nature is divided into:

- Towns and settlements
- Cultivated land
- Roads
- Communication networks
- Planted of woodland
- Water basins
- Areas and places polluted by household and industrial wastes.

Due to the natural influences on and the unfavorable impacts of human activities the above-mentioned areas have changed much by the present time having been exposed to sudden natural disasters as floods which create land erosion and gorges shifting and moving of the sand, destruction of the grain growing fields, the pastures become filled with harmful pesticides. The fields for having faced with human constant dangerous

treatment and the gap of change remain useless for exploitation and the pastures are being destroyed by great numbers of bypassing rods. These kinds of negative changes are being reflected in the registration and monitoring books being usually kept for the given year.

THE PRESENT CONDITION OF THE PASTURE

The foundation for the basis of or for the cattle-breeding fodder's of the agriculture of Mongolia, which represents the main branch of the country's economy's the given pasture land.

The pasture land is the most significant and the biggest usage area which gains 76% of the land reserves of Mongolia.

Due to the fact that the territorial surface of Mongolia mountainous, starting from the mountain-cap till the mountain bed the supply of warm atmospheric air temperature and the accumulation level of sediments are varying much. On the basis of this the vegetation zone is being originated.

According to the studies and investigations results the spreading out of the features of our country's pasture is involved by the 6 vegetation zones.(Fig.1).

5.3% of the whole pasture of the country is filled with the high mountain, 29.2% mountain steppe and mountain meadow, 22.8% plain steppe, 23.3% desert steppes and 19.4% gobi desert with vegetation cover. Among them 2.1% of the mountain forest steppe and the mountain meadows pastures have river valley plants and the 3.8% of the desert steppe pastures have the plants of interzonal and low meadows herbs.

The pastures of the high mountain are spread through the mountain gorges and slopes in various ways and levels of altitudes and in the Mongolian Altai and the Gobi Altai mountain ranges they are being found at the altitude of 2900-3100 meters and the height of plants here are low and you can across with the features of plants belonging to the two big groups of high mountain steppe and the high mountain meadows.

Among the prevailing plants are: *Cobresia sibirica, C. Bellardi, C.filifolia sedges and forbs*. In summer and autumn period it is possible to get eatable for cattle dry herbs, amounting to 2.4 cwt per hectare.

The mountain steppe pastures will be met usually at the height of 1500-2300 meters in the micro mountains systems . Here you will easily find *Festuca ovina, F.Lenensis, F.rubra, Poa botryoides, Koeleria gracilis, K.altaica* prevailing groups of plants. In the southern slopes of the mountains there will be found petro-variations of the plants and in the back sides of the mountains the meadows type grassland.

The pasture lands of the mountains during the winter and spring periods are being used as the main and principle areas of reserves for animal fodder's. In summer and autumn period there can be harvested 4.6 cwt fodder per hectare for the dry eatable use of cattle's.

The mountain meadow pastures are being spread out and lays between the zones of forest steppe and steppe at the heads of narrow valleys an here the prevailing plants are those that like the moisture and sediments more characteristic for meadow areas plants and in addition, the harvest volume is more constant, reliable and during the and

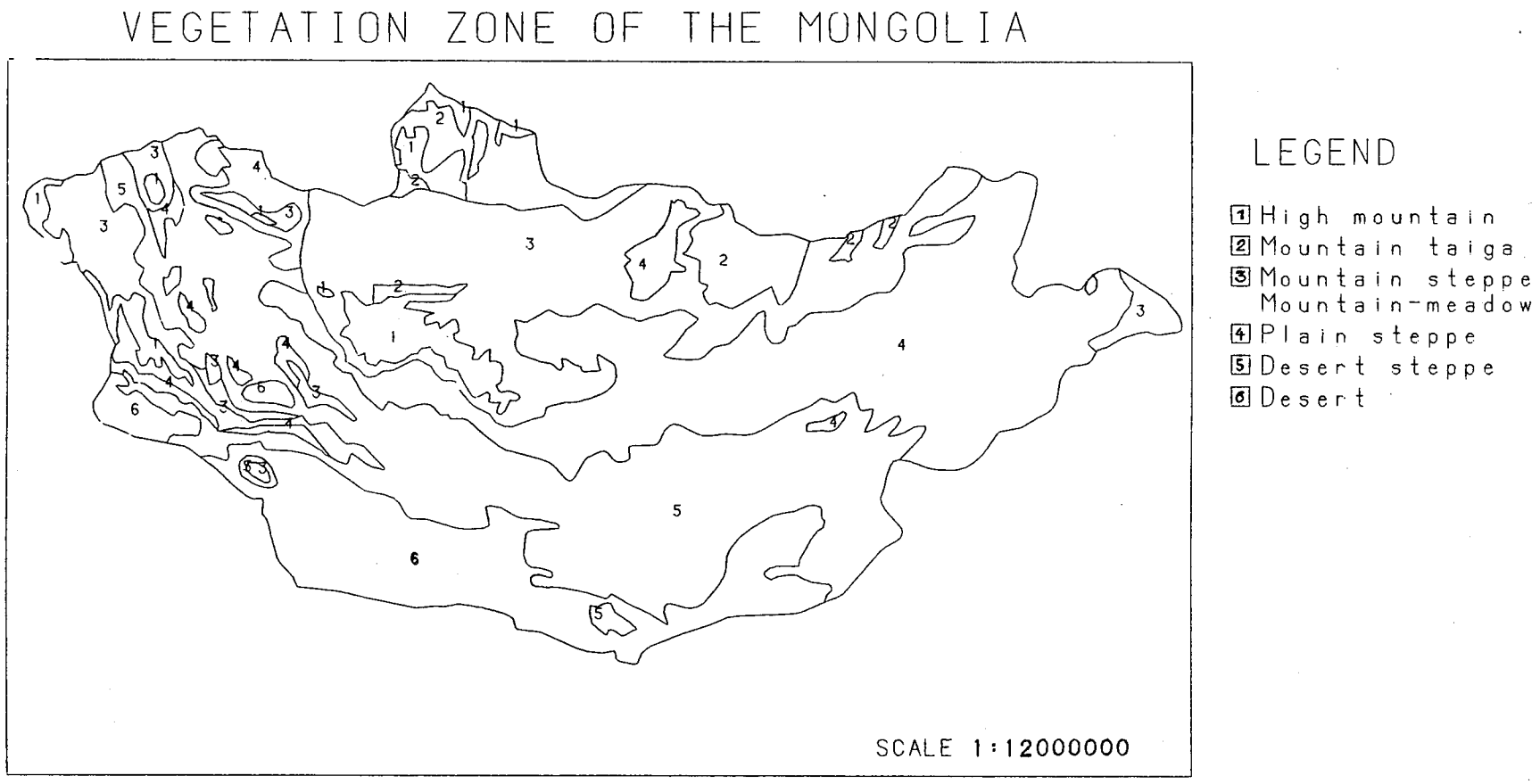
VEGETATION ZONE OF THE MONGOLIA
LEGEND
1 High mountain
2 Mountain taiga
3 Mountain steppe
Mountain-meadow
4 Plain steppe
5 Desert steppe
6 Desert
SCALE 1:12000000

Fig. 1

autumn periods it is possible to harvest 8.4 cwt dry fodder plants for cattle from 1 hectare.

The plain steppe pasture is being widely spread out in between the mountains valleys and during the whole year they become the main area for the cattle fodder and nutrition in the country. The prevailing herbs and plants here are: *Stipa.capillata, S.decipiens, S.grandis, Cleistogenes sguarrosa* and the medium prevailing are *Artemisia frigida,* in the Dornod tal steppe together with or alongside with the *Stipa capillata* there grow the *Leymus chinensis* mainly. During summer and autumn period there are the possibilities of harvesting from one hectare of square 5.7 cwt animal fodder plants.

In between the desert steppe and the gobi desert zones there prostrates the middle zone which is very often met. The prevailing plants here are the *Stipa gobica, S.glareosa,* and the medium prevailing are the *Kochio prostrata, Allium polyrrhizum, A. mongolicum*. In summer and autumn period there is the possibility of harvesting 1.6 cwt cattle fodder from 1 hectare.

The gobi desert pasture is widely spread out in the southern edges parts of the country. The main features of the desert area of Mongolia is being defined by the gravel desert characters. Here the plant cover is very rare and not tense. The prevailing plants here are: *Anabasis brevifolia, Salsola passerina, Zygophyllum xanthoxylon, Tanacetum achillaeoides, Reaumuria soongorica*. During the summer and autumn seasons about 0.9 cwt harvest for cattle fodder can be get from 1 hectare at this zone.

The pasture lands of the river valleys have very rich sediments and moisture supplies, constant fodder as will reliable too and these fodder's and herbs are usually being used and spent for cattle nutrition in summer and autumn periods. The dry fodder to be utilized by the cattle here in summer and autumn season is average 8.7 cwt. per hectare.

For the lower meadows pastures, which are situated by around side of small and big lakes, stream and springs, it is characteristic the wide growing and prevailing of *Achnatherum splendens, Hordium brevisubelatum, Agrostes clavata, Elymus dahuricus* groups. In the summer and autumn seasons over 6.7 cwt from 1 hectare would be fodder in a dry form.

Due to the fact that the pasture usable lands are situated at different and various natural and geographical zones, the economic exploitation and usage features are also varying. 26.8% of the total pasture is stony, 18.8% shrub and bushes, 4.1% knoll, and the 1.8% swampy.

In general the pasture lands are divided into the winter-spring, summer-autumn exploitation for the time-being, but under the conditions of shifting into the market economy relations, the wells and water usage is overloaded, the population density near the settled areas and towns is growing and the concentration of human beings and cattle's is increasing carrying capacity for these reasons the pasture load is extreme and the composition of the plants and herbs is changed greatly and 6% of the whole pasture lands has been degraded out already.

According to the investigations conducted by us, the average summer and autumn dry harvest for cattle from 1 hectare constitutes 3.8 cwt, the winter and spring harvest 2.2 cwt and their annual average is 2.9 cwt witness that the harvesting level established by the Water Economics Expedition in 1965 decreased from 19.5% to 24.2% by now.

Monitoring of grassland annual change using multi-temporal satellite data

Nobuyuki MINO, Genya SAITO and Akira HIRANO

National Institute of Agro-Environmental Sciences
3-1-1 Kannondai Tsukuba Ibaraki 305 JAPAN

1. Introduction

In Hokkaido which is northern part of Japan, many dairy farming regions lie, grassland of those is managed intensively for mowing or grazing. Such artificial grassland is expected to have a large amount of yield or support grazing many animals for a long period. Grassland just after seeding has high productivity, but, to maintain it for many years is very difficult. To maintain high productivity of grassland, proper management should be conducted according to various conditions of grassland. Therefore, monitoring grassland condition is very important. Especially, annual change of grassland affects grass-yield seriously, so that it is a key item to be monitored.

Since, grassland cover wide area, field survey costs much labor and time to collect spatial information of annual grassland change. Satellite observation can collect a wide range of spatially distributed information. If satellite data can be used for grassland monitoring, it will be an effective tool for various managements. Most researches on remote sensing of grassland have aimed to discriminate grassland from non-grassland and to estimate the production of grass (AKIYAMA, 1992 (a) (b)). There are only a few studies that attempt to monitor grassland change in spectral reflectance using satellite remote sensing. The objective of this study is to make clear characteristics of grassland annual change in reflectance.

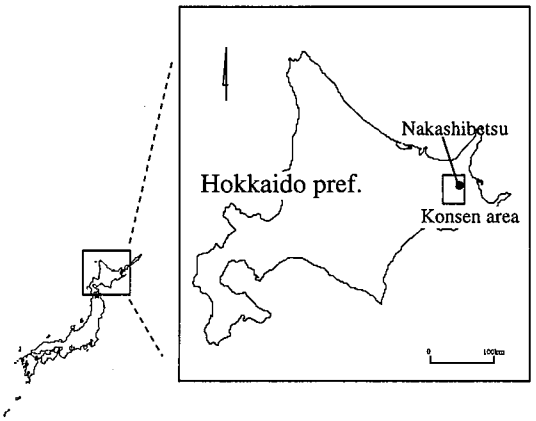

Fig. 1. Study site (Konsen area in Hokkaido pref.)

2. Study site

The study site is Konsen area in Hokkaido prefecture (Fig. 1). Konsen area is a major dairy farming region in Hokkaido. Due to the low temperature and insufficient sunlight in summer, agricultural land in this area is not suitable for crop except for grass. Therefore, more than 97% of agricultural lands in this area is grassland. Usually, grasslands in study site are mowed in June and August, or are grazed from May to September.

3. Method

For the study of grassland annual change in reflectance, there is a method to compare multi-temporal satellite data directly. However, both observation dates and annual difference of grass growth may affect grassland reflectance. Therefore, direct comparison among multi-temporal satellite data can not supply the information about annual change of grassland reflectance. In this work, using the characteristics of grassland just after renovation, we study annual change of grassland reflectance.

Once productivity of the grassland decreases, grass-renovation which is accompanied with plowing and seeding needs to be conducted to improve its productivity. On grassland just after renovation, bare soil appears in growing season, such grassland can be distinguished easily from the other grassland coverage using satellite data. Using multi-temporal satellite data, we can compile a map which contains spatially distributed information of grass-renovation year. By overlaying this map and individual satellite image, we can compare the grassland of different age with each other on one satellite image. Such comparison can be seen as observing the annual change of grassland reflectance (Fig. 2).

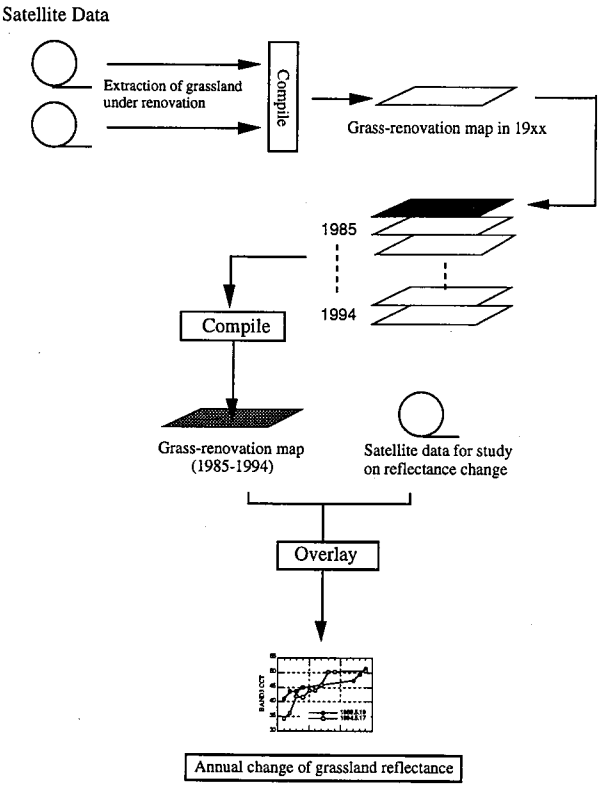

Fig. 2. Outline of the study

Suppose we have satellite data acquired from 1985 to 1994, we are analyzing the satellite data of 1994. For grassland coverage which renovated in 1993, we can extract 1-year old grassland reflectance. In the same way, for grassland coverage which

renovated in 1992, we can extract 2-years old grassland reflectance. Further, using 1991, 1990, 1989, 1988, 1987, 1986, 1985 satellite data, we can extract reflectance of 3-years to 9-years old grassland. Using this method, we study annual change of grassland reflectance in satellite data acquired in May and June respectively. The grassland age of annual change which was made clear in this study are listed in Table 1.

Table 1. The grassland age detectable in each satellite data

Satellite data	1993.6.8.	1992.6.28.	1991.6.26	1990.6.7.	1989.6.13.	1994.5.17	1989.5.19
Grassland age	1 year 2 year 3 year 4 year 5 year 6 year 7 year 8 year 1 year before renovation	1 year 2 year 3 year 4 year 5 year 6 year 7 year 1 year before renovation 2 year before renovation	1 year 2 year 3 year 4 year 5 year 6 year 1 year before renovation 2 year before renovation 3 year before renovation	1 year 2 year 3 year 4 year 5 year 1 year before renovation 2 year before renovation 3 year before renovation	1 year 2 year 3 year 4 year 1 year before renovation 2 year before renovation 3 year before renovation	1 year 2 year 3 year 4 year 5 year 6 year 7 year 8 year 9 year	1 year 2 year 3 year 4 year 1 year before renovation 2 year before renovation 3 year before renovation

4. Satellite data

As for satellite data, we used LANDSAT/TM, MOS-1/MESSR acquired during 1985-1994. We collected 2 satellite data in growing season of each year as possible. Before the analysis, geometric correction was applied to the original images and a pixel size of 25m by 25m was used.

5. Results and Discussions

(1) Annual change in data acquired in May

For satellite data acquired in May, an increase in visible, near-infrared, middle-infrared reflectance with aging was observed. (Fig. 3) In May, grass-field is covered with only a little vegetation. For satellite data acquired in May, reflectance of grassland is dependent on that of its background. On the ground, that is the background of grassland, an increase of dead leaves

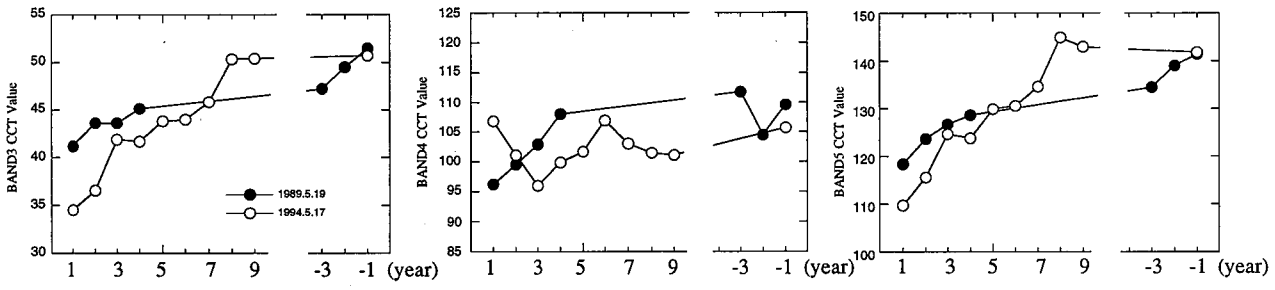

Fig. 3 Annual change of grassland reflectance in Landsat TM data acquired in May

accumulation with aging was observed (MIKI, 1993). Accumulation of dead leaves on the ground is a very little on the grassland just after renovation, or young grassland. Whereas, old grassland, accumulation of dead leaves on the ground has a lot of amount. Dead leaves present bright color. Therefore, ground surface on which the accumulation of dead leaves exists appear to be brighter than ordinary bare soil. We considered that an increase in visible, near-infrared, middle-infrared reflectance with aging is due to the accumulation of dead leaves on ground surface (Fig. 5).

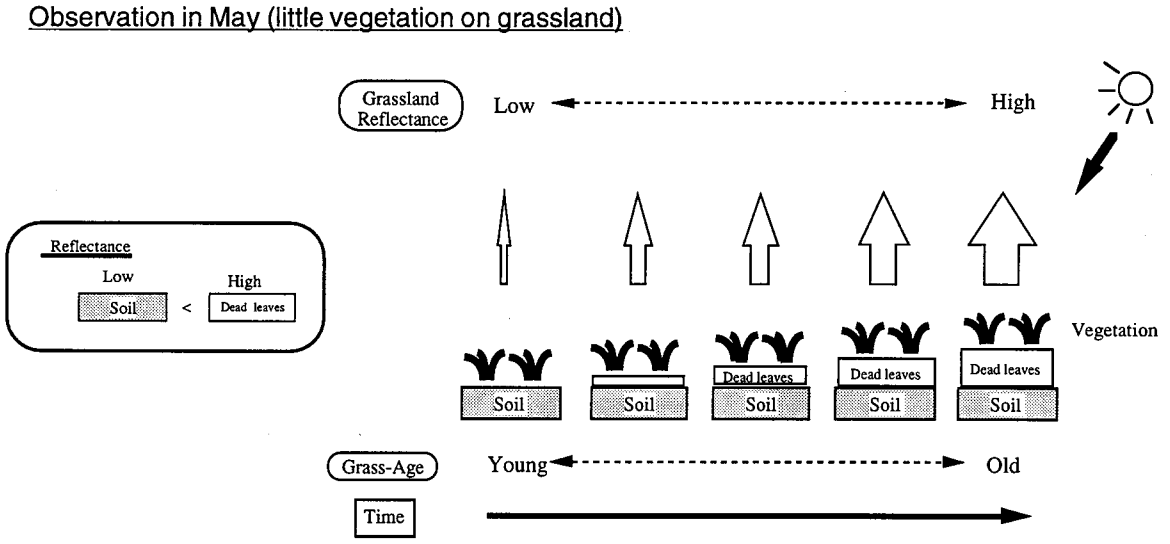

Fig. 4. Conceptual figure about annual change of grassland reflectance in data acquired in May

(2) Annual change in data acquired in June

For satellite data acquired in June, a sudden decrease in near-infrared, middle-infrared reflectance was observed approximately in 4 years period after grass-renovation, while, visible reflectance maintain its constant value (Fig. 4).

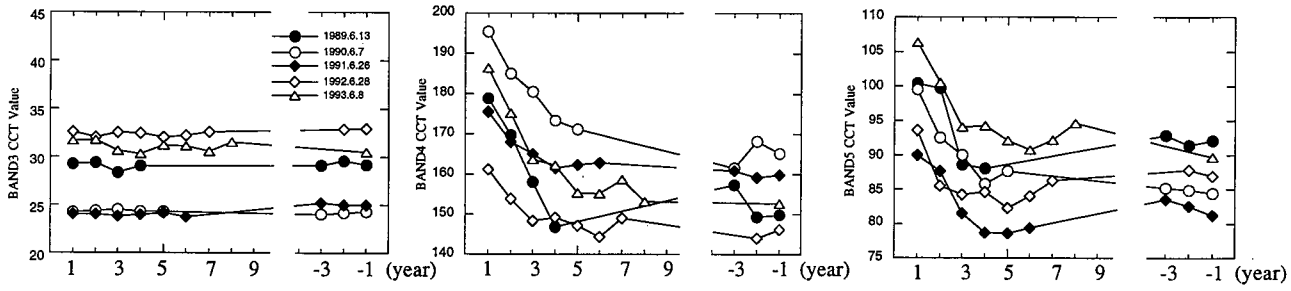

Fig 5. Annual change of grassland reflectance in Landsat TM data acquired in June

June is just before harvest season. Grass-field is covered with much vegetation. In June, contribution of the ground surface to the grassland reflectance is considered to be very little. In some previous field survey studies about annual change of grassland in Konsen area, the change of grass-species composition with aging had been reported. As a major change, it is reported that clover crown cover suddenly decreases and ordinary grass occupied mainly in approximately 4 years period after grass-renovation. (MATSUNAKA, 1983, 1984)

The decrease trend of near-infrared and middle-infrared reflectance and the decreasing trend of clover crown cover are similar. There is a structural difference between clover and ordinary grass, clover has a horizontal leaf angle distribution whereas ordinary grass has vertical. This means that for a given area and biomass clover leaves may have higher reflectance than ordinary grass. Therefore, it is considered that young-age grassland with much clover crown cover has higher reflectance than old-age grassland with ordinary grass. From those, we considered that the major factor of the sudden decrease of reflectance is due to the change of grass-species composition with aging (Fig. 6).

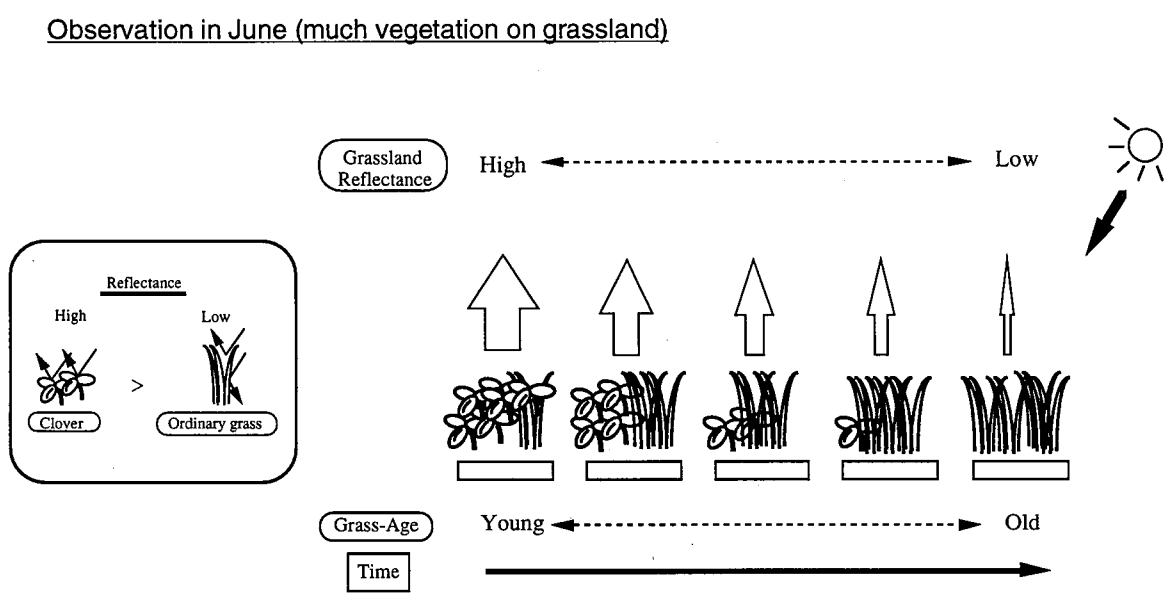

Fig 6. Conceptual figure about annual change of grassland reflectance in data acquired in June

Those results represent that satellite data can be distinguish the grassland of different grass-age, and also indicate ability of satellite data to evaluate grassland quality. It can be concluded that satellite remote sensing is very valuable for extensive grassland field.

Reference

1) Akiyama, T., "Grasslands and Remote Sensing 1 - Global monitoring of rangeland vegetation using space-borne sensors - ", J. Japan. Grassl. Sci., Vol.37, pp.475-481, 1992 (a)

2) Akiyama, T., "Grasslands and Remote Sensing 2 - Grassland management with satellite remote sensing - ", J. Japan. Grassl. Sci., Vol.38, pp.343-349, 1992 (b)

3) Matsunaka, T., J. Koseki, H. Matsushiro, T. Sekijyo, and K. Nishikage, "Change of yield with the years in cutting swards on different soils characterized by chemical properties", J. Japan. Grassl. Sci., Vol.29, pp.212-218, 1983

4) Matsunaka, T., J. Koseki, H. Matsushiro, T. Sekijyo, and K. Nishikage, "Botanical composition in the sward as a limiting factor of the yield", J. Japan. Grassl. Sci., Vol.30, pp.59-64, 1984

5) Miki, N., "Study on the effective application of nitrogen fertilizer to cutting sward based on evaluation of soil nitrogen release in Tenpoku district", Hokkaido Pref. Agric. Exper. Sta. Report, Vol 79, pp.1-98, 1993

Similarities between Mandah, Sumatera and Iriomote, Okinawa on the Distribution of TM Data of Landsat 5 in the Multidimensional Space for Mangrove and the Surroundings

Dwi Setyono* and Kazuhiro Sato*

*** Laboratory for Forest Product and Environment,**
College of Agriculture, University of the Ryukyus,
1 Senbaru, Nishihara, Okinawa 903-01, Japan
Tel. 098-895-2221 (Ex.2912), Fax. 098-895-2864

Abstract

It was synthetically reexamined for two mangrove area between the tropics and subtropics that individual categories on mangrove and surroundings occupied each distinctive position in the three dimensional space with three bands of TM data of Landsat 5. From the reexamination of the results investigated separatively, similarities on the space occupation for similar categories were pointed out. Furthermore it was explained from the view point of forestry that the difference of tendency for arrangement of points was dependent on the different state of mangrove forest.

1. Introduction

The mangrove is one of the most important and fragile ecosystem in the tropical and subtropical coastal regions. Dwellers in such area are usually dependent on the mangrove in various degrees for their needs. It has been a reliable subject of local and traditional uses for them. But recently it has been made a target unrestrained, unconsidered and harsh utilization because of the high productivity and geographical features to enter and develop easily. It is an urgent necessity for restrained, sustainable and effective utilization of multilateral potential of mangrove area to establish management and control methods on this ecosystem. Remote sensing is expected as an effective technique for that.

Although separation of mangrove as a category from other vegetation and land-use types through several remote sensing procedures of satellite data has been described in many papers, reports on the way to classify mangrove into some categories are few. It becomes to be recognized that the classification of mangrove into several categories is important for considerable management and control of it.

We have investigated the structure of satellite data to collect fundamental information for effective classification, reasonable interpretation of classified results and better understanding the mechanism and background of classification on mangrove and surroundings. Distribution of TM data of Landsat 5 in the three dimensional space with three bands had been investigated

for mangrove and surroundings in Iriomote Island, Okinawa and Mandah area, Sumatera (Sato *et al*., 1993 and Dwi *et al*., 1994).

In this paper, investigated results mentioned above were comparatively discussed to extract similarities for mangrove area between the tropics and subtropics.

2. Data and study area

The data used in this paper never been newly collected. The results examined in two papers presented until now (Sato *et al.*, 1993 and Dwi *et al.*, 1994), were synthetically investigated here. Used TM data of Landsat 5 in the papers had been acquired on 25 April 1990 for Mandah and on 24 August 1984 for Iriomote Is..

One of study area was Mandah area in the estuary of the Inderagiri River, Sumatera and the other was Iriomote Is.,Okinawa as shown Fig.- 1. Mandah area lay south 30 km of the equator and Iriomote Is. was located north 90 km of the Tropic of Cancer.

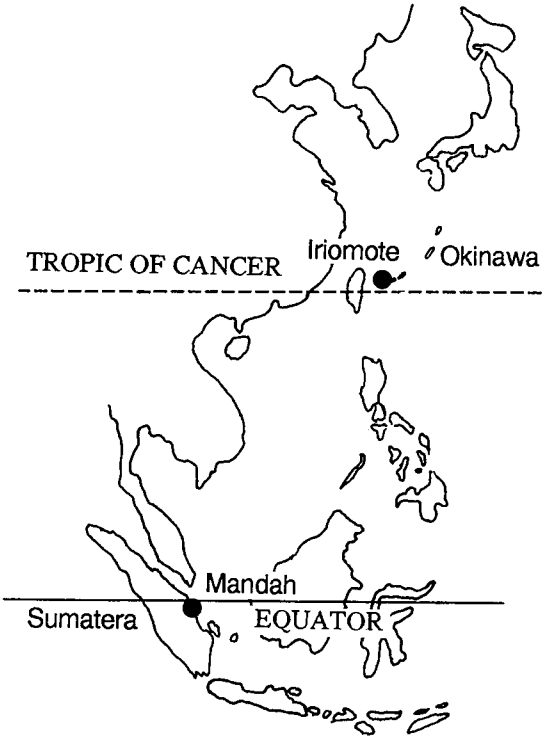

Fig.-1 Location map of two study area

In Mandah, a mangrove concession area was established and had been managed as a production forest of chip wood for pulp. *Rhizophora apiculata* predominated in this area. Artificial stands were almost covered with this species, but natural regenerated stands almost contained mixes of *R. apiculata* with *R. mucronata, Bruguiera* spp., *Ceriops* spp., *Xylocarpus* spp., *Nypa fruticans* and so on. Tree height in a typical mature stand was approximately 30 m. Nipa (*Nypa fruticans*) had a tendency to make large community by itself.

Iriomote Is. held 77 % (446 ha) of total mangrove area in Japan. It was considered that there was no remarkable change and disturbance in mangrove area because this island was almost inside of a national park. *R. stylosa* and *B. gymnorrhiza* predominated in this island and minor mangrove species of *Avicennia marina, Sonneratia alba, Lumnitzera racemosa, Kandelia candel, Excoecaria agallocha* were distributed. These minor species did not occupied significant area for remote sensing.

3. Method

An method to compare some figures in two papers mentioned above was taken for extraction of similarities of mangrove area between two study area. In the figures, CCT counts of sample pixels picked up from each categorized area were plotted at the three dimensional coordinates corresponding with combined three bands. Although the way of thinking for the

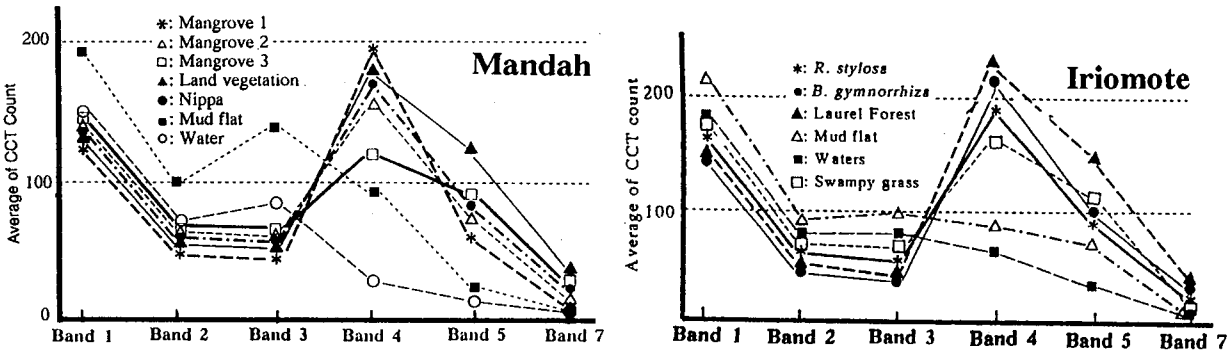

Fig.-2 Average of CCT count on six bands for each categories

figures was slightly like the multi level slice classifier, the former took interest in the degree of gathering or scattering plotted dots and the direction or tendency for arrangement of them, the latter did interest in threshold value of classification.

For Mandah categories were set as seven of mangrove 1, mangrove 2, mangrove 3 , nipa, land vegetation, mud flat and waters because the separation with stand state was thought applicable than with species for mangrove. Mangrove 1 corresponded to an old rich stand, mangrove 2 did to a reforested intermediate stand and mangrove 3 did to reforested young and poor stand. For Iriomote they were set as six of dominant stands of *R. stylosa* and *B. gymnorrhiza*, laurel forest, swampy grass, mud flat and waters because the zonation of two species was clear for mangrove.

4. Results and Discussion

The average values of CCT count in six bands for each categories were shown in parallel for two study area as Fig.-2. For Mandah the values were generally smaller because of the different for latitude, season, time and a level of reflectance in the whole scene between two study area. Although the tendency for vegetational categories was almost similar, it was slightly different for mud flat and waters. It was considered that the reason was dependent on the amount of suspended load, water color and the degree of relation between mud flat and the tide.

Four examples of diagram for data distribution in the three dimensional space with three bands were shown as Fig.-3 in parallel. It was clearly shown in the upper row that the distribution range of points for mud flat was remarkable separated with the other categories for Mandah. It was assumed the probable samples to distributed in the space had not been collected in this case. As such intermediate samples were collected in Iriomote, a direction was recognized for arrangement of points on mud flat and waters. There were replacement of distributed range of points on mud flat and waters, and remarkable different in CCT count level of band 3 on mud flat for two study area what was probably depended on the different conditions mentioned above paragraph.

In the second row, vegetational categories occupied clearly higher distributed range for band 4 on both area and all categories were commonly arranged in one direction for band 2 and 3. As it could be estimated that the range of mud flat in Mandah also was located on the extension of the line, the existence of high correlation between band 2 and 3 was suggested.

There was a clear different direction of point arrangement between waters or mud flat and

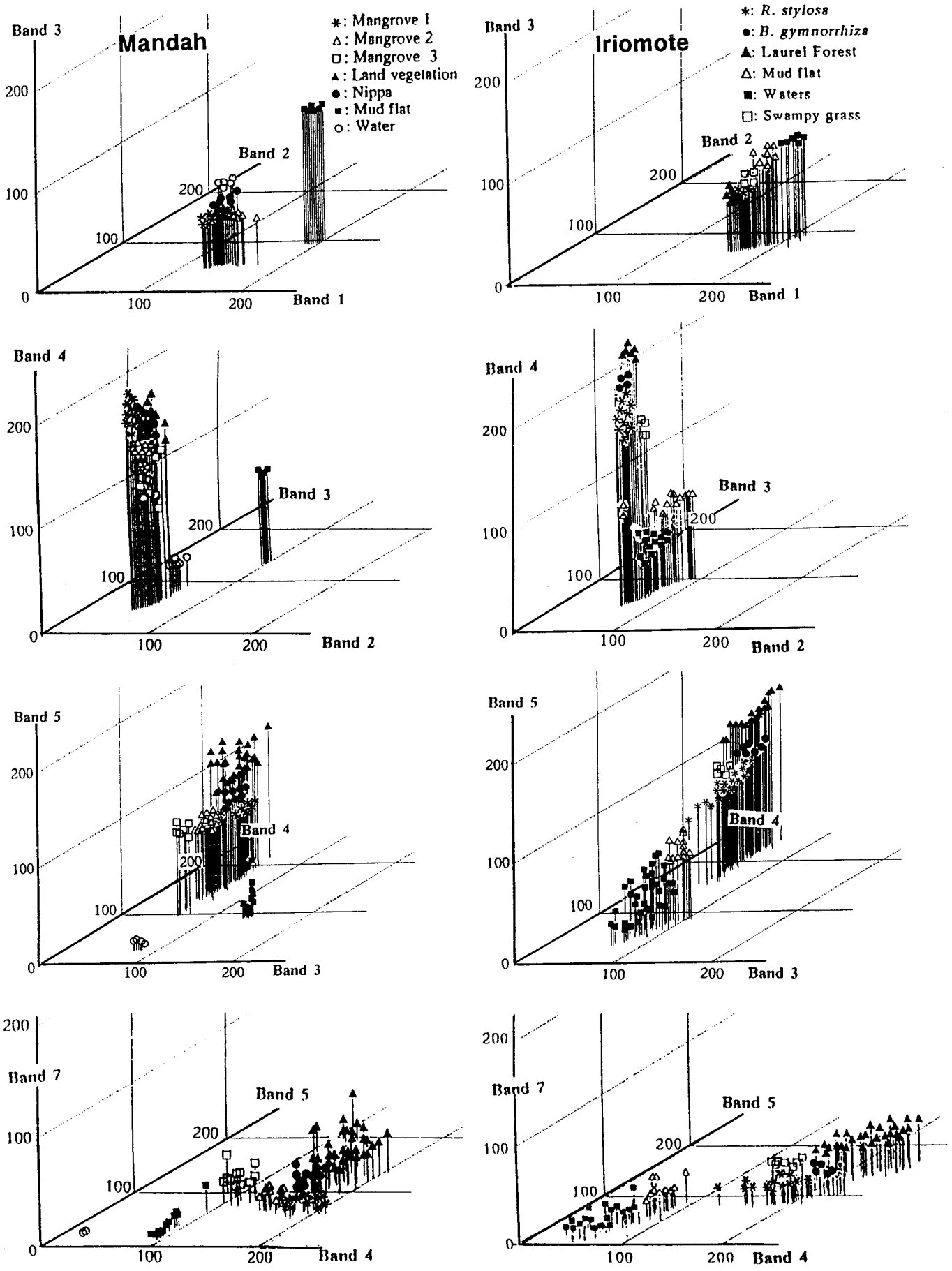

Fig.-3 Data distribution in the three dimensional space with three bands

vegetational categories for band 3 and 4 in the third row. This matter was common to both area. Furthermore the remarkable gap of point arrangement was recognized between mangrove and land vegetation including laurel forest for band 5. The distributed ranges of nipa and swampy grass were located between two layers formed with the both arrangements. It was considered that the difference among them for band 5 was dependent on the degree of their relation with the tide.

In the bottom row the arrangements were easily observed for band 4 and 5. The direction of

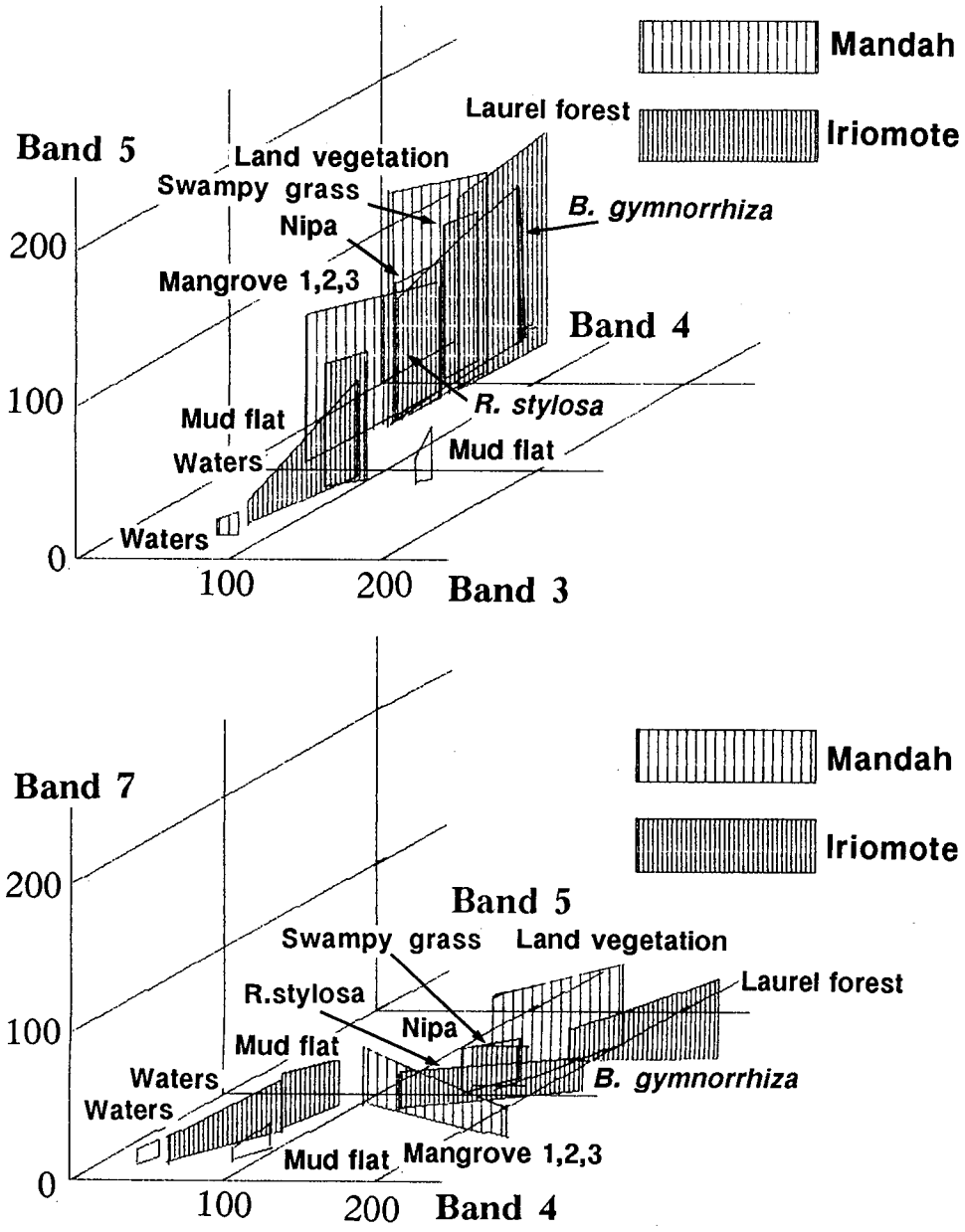

Fig.-4 Models of arrangement, gathering and direction on each categories in three dimensional space for two study areas

point arrangements on waters or mud flat was slightly different between two area. From this matter, it could be assumed that the general data on them were almost distributed in the defined range with arrangements indicated in the both diagrams depending on the tide and condition of water quality. Although the indicated level of CCT count on land vegetation in Mandah and laurel forest in Iriomote for band 4 was slightly different, the tendency of point arrangements was almost similar. It was very interest that two categories of nipa and swampy grass occupied close position. Although mangrove in the both area too occupied near position, the direction of point arrangements was opposite.

In the investigation as described above, we have referred to several similarities and some different for mangrove and surroundings between Mandah area and Iriomote Is,. To make these more clear, two diagrams on the lower two rows in Fig.-3 were overlapped for two area and the point arrangements were drawn as some models. The diagrams were shown as Fig.-4.

We could easily find the similarities on the data distribution in the three dimensional space from Fig.-4. Each categories could be divided into four groups of water and mud flat, nipa and swampy grass, land vegetation and laurel forest, and mangrove. It was suggested that the similar categories between the tropics and subtropics occupied near position even if the contents such as species and structure were different.

Finally the important different on mangrove between Mandah and Iriomote must be described here. The significant information has been extracted from it. For band 4 and 5, the point arrangement on mangrove in Iriomote showed a plus correlation and it in Mandah did a minus correlation.

Generally in Iriomote Is., *R. stylosa* as pioneer species predominated in the seaward stand and *B. gymnorrhiza* did in the land ward stand, and the leaf-biomas was more rich in the latter than the former. Although under natural conditions it was considered such state was similar in Mandah, the actual situation was opposite because of that the rich forest belt was remained in the seaward side and forestry operation were done in the land ward side from the view point of forest conservation. So opposite state with Iriomote was assumed in Mandah.

5. Conclusion

From this investigation several similarities and some difference between the tropics and subtropics on TM data of Landsat 5 for mangrove area were extracted. It was clearly pointed out that there were significant information to relate with the stand state or forestry circumstances. This matter suggested high possibility of remote sensing to find detailed effective information for mangrove area in the future.

References

1) D. Setyono & K. Sato: Structure of Thematic Mapper Data of LANDSAT 5 for Mangrove Area in the River Mouth of Inderagiri, Riau, Sumatera, Proc.15th ACRS, G-5-1~6,(1994)

2) K. Sato, D. Setyono & S.E. Dah: Structure of Satellite data for Mangrove Area in Okinawa (I)-Structure of TM Data of Landsat 5 for Mangrove Area in Iriomote-, Proc.14th ACRS, E-3-2~6,(1993)

Identification and Mapping of Mangrove Forests along the Coast of Pakistan

Jawed Ali, Amina Rangoonwala

Remote Sensing Applications Division
Pakistan Space & Upper Atmosphere Research Commission (SUPARCO)
P.O. Box 8402, Karachi-75270, Pakistan

Abstract

The environmental and socio-economic significance of mangroves has widely been recognized over the past few decades. The objective of this study is to identify and describe mangrove forests occurring along the coast of Pakistan for the preparation of a reliable and updated data base to contribute to the efforts being made for sustenance of the coastal ecosystem and resources. SPOT FCC images were analysed to identify the spatial distribution and relative density of the mangrove forests along the estuaries of major rivers. Mangroves and the major landforms were identified and mapped at several locations on various scales in order to meet the requirements of national user agencies. The study revealed mega changes in the distribution of mangroves and associated landforms on comparison with the existing information bases.

1. Introduction

The coastline of Pakistan is approximately 850 kms long. It extends from Sir Creek in west (India) to the Pak-Iran border in east. The mangrove forests occur at the estuaries of major rivers under different environmental regimes. The spatial distribution and relative density of the mangroves is basically dependent upon the quantity of river discharge into the sea in addition to other environmental attributes. Most extensive mangrove forests occur in the Indus delta in the west of Karachi where the river Indus debouches huge quantities of fresh water throughout the year. The other important locations where mangroves exist include the coast of Karachi, Miani lagoon, Kalmat lagoon and the Gwatar Bay (Fig.1).

Availability of a reliable and updated coastal data base is an essential requirement for undertaking resource and environmental surveys. Satellite images present an updated picture of a very dynamic coastal situation. In order to serve the national planning resource and environmental agencies in Pakistan, satellite image analysis was undertaken to analyze and map the mangrove forests along the coast. The image analysis was also supplemented by field/aerial surveys to facilitate and enhance the interpretation accuracy.

2. Description of Mangrove Forests

Following is a brief description of the several location along the coast of Pakistan where mangroves have been identified and mapped;

2.1 The Indus Delta

The 100 Km wide delta "The Indus Delta" at the mouth of river Indus is a result of hundreds of centuries of silt deposition by the river. The seaward margins of the delta are bounded by sand spits, beaches and mangrove swamps extend from 10-28 km to the interior. Above the mangrove swamp are mixed alluvial deposits, which are in part, cultivated through seasonal irrigation from the Indus river. Most of the Indus delta consists large tidal channels, many of which are remnant courses of the Indus river with extensive mudflats in between. The sandy areas are completely barren. Behind the sand spits are extensive mudflats covered with varying densities of mangrove forest. Avicennia alba and Rhizophora conjugata L, are the common mangrove species. These occur as thin ribbons along tidal channels and streams or as scattered shrubs no more than a few meter high. Most dense varieties have been found between Karachi (Port Qasim) and the Keti Bander area. The entire delta was mapped at 1:250,000 scale and a selected section was mapped at 1:50,000 scale to serve as base map for undertaking detailed socio-economic surveys of the region.

The mangroves are rapidly deteriorating in the Indus delta. One of the major threats to the mangrove ecosystem is the reduction in fresh water flows, silts and nutrients delivered by the river Indus reduce as a results of upstream barriers. Overgrazing by animals, use of plant wood as fuel by local inhabitants and marine pollution are some other factors putting the ecosystem into crisis.

2.2 Coast of Karachi

A large segment of Karachi coast is fringed by a sand spit, behind which lies a lagoon, 8 Kms long and 4 Kms wide. Lyari and some other small tidal streams discharge into this lagoon. Clumps of mangrove shrubs dominate here. Some scattered plant assemblages may also be seen at the mouth of Malir river in Ghizri creek in the east of Karachi. The mangrove forests around Karachi were mapped at 1:100,000 scale.

2.3 Miani Lagoon

The Porali river and its distributories drain Lasbela valley into the Miani lagoon located in the NW of Karachi. The tidal lagoon is about 50 kms long and 20 kms wide. The lagoon charges greatly between high and low tides. Typically the area comprises narrow twisting channels, with steep mud banks visible at low tide surrounded by numerous flat islets of mud covered with mangrove trees. Extensive mud flats are exposed on the west side of the lagoon indicates that the lagoon is filling with sediments. Aviciennia alba and Rhizophora Conjugata are the common varieties of mangroves in the Miani lagoon. Dense mangroves have grown at the estuary of Porali river where fresh water supply is in abundance. The lagoon is fringed by tens of kilometers long beach ridges. This area was mapped at 1:100,000 scale.

2.4 Kalmat Lagoon

The lagoon is one of the largest tidal lagoons located along the western coast of Pakistan. The region is extremely dry and barren therefore the lagoon occassionly receives fresh water from the hill torrents from the north. On the seaward side it is

fringed by long beach ridges and show extensive mud flats inside. Limited fresh water supply has permitted a few scattered mangrove shrubs to grow at the central estuaries in the lagoon. The area was mapped at 1:100,000 scale).

2.5 Gwatar Bay

The Gwatar bay lies between the headlands at Pak-Iran border. The region enjoys extreme arid climatic conditions. The back zone is an extensive alluvial plain. The town of Jiwani is located near the rocky platform at the coast. The bay is fringed by buried beach ridges. Dasht is the largest river draining into the bay alongwith numerous other small rivers and tidal streams. Bare mud flats and swamps extends for tens of kilometers behind the beach ridges. The mangroves grow here in a ribbon like pattern along the streams and tidal distributories. These were also mapped at 1:100,000 scale.

3. Conclusion

The maps derived from satellite images have proven enormously useful tool for obtaining updated information on spatial distribution of mangroves in areas subject to dynamic coastal process.

4. References

Meynell, P.J., "Use of Remote Sensing for Mangrove Ecosystem Management in the Indus Delta", Proc. of ESCAP Seminar on Environment, PP.114-117, Karachi, 1991

Saifullah, S.M., "Future Prospects of Mangroves in Development of Makran Coast", Proc. of Seminar on Makran Coast, Quetta, 1992

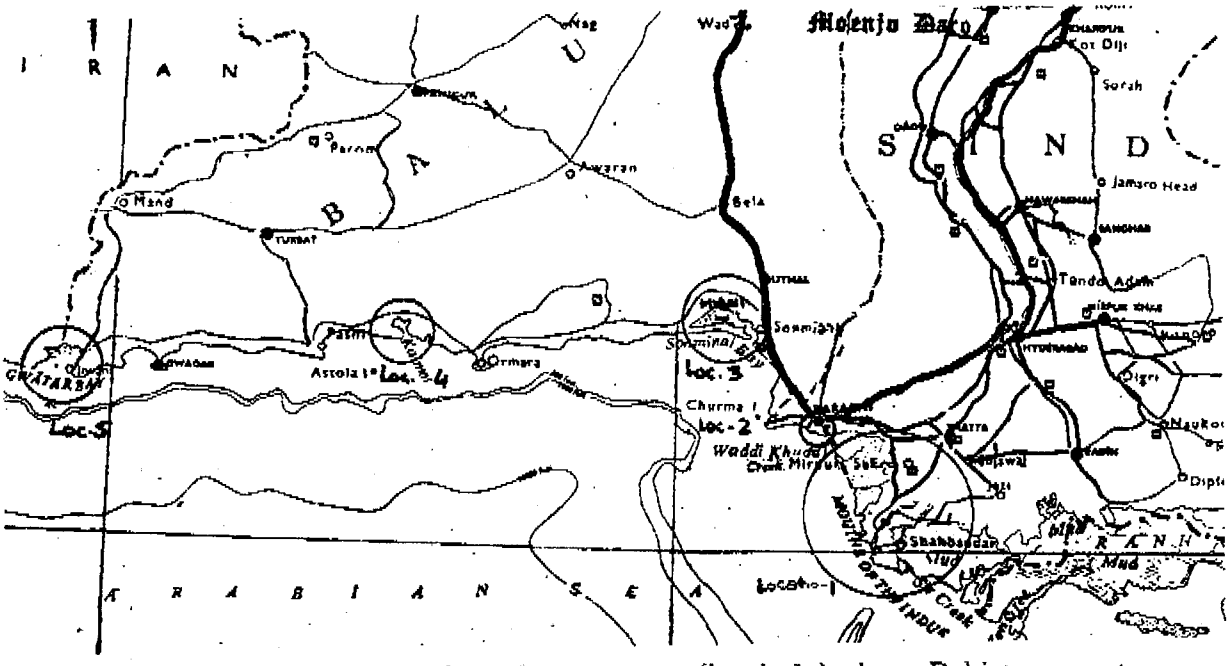

Fig. 1 Map showing location of mangroves (in circle) along Pakistan coast

Ground Surface Features of Taklimakan Desert

---Features of Spectral Reflectance of Soils, Vegetation etc.---

Takashi Ishiyama(*), Shigehiko Sugihara(**),and Kiyoshi Tsuchiya(***)

*Center for Environmental Remote Sensing(CEReS), Chiba University, 1-33, Yayoi-cho, Inage, Chiba, 263 Japan
**National University of Fisheries, Nagata-Honmachi 2-7-1, Shimonoseki, Yamaguchi, 759-65 Japan
***School of Science and Engineering, Teikyo University, Utsunomiya, 320 Japan

Abstract

In an attempt to utilize satellite data to obtain land surface features of Taklimakan Desert in China, in situ measurements of spectral reflectance of the land surface is made with the portable spectro radiometer in the spectral range of 400 ~ 2500 nm. The analyses of the data show following features. (1) The difference in spectral reflectance of different soils is comparatively small. (2) There is a tendency that spectral reflectance of soils increases with increases of wavelength, for example, the average reflectance of the sands in the periphery areas of Taklimakan Desert is 21 and 38 % in visible and near infrared spectra respectively. (3) It is found that reflectance of the soils decreases with increase of moisture content. The large decrease is recognized in 1450 and 1950 nm spectra, water absorption bands. This fact suggests that the monitoring of soil moisture is possible by measuring the radiance at these spectra, thus Landsat TM Bands 5 and 7 will be effective for monitoring soil moisture content.

Introduction

The spatial distribution and temporal variation of various materials in wide arid and semi-arid zones are significant parameters for studies of a desert itself and desertification mechanism. To obtain these parameters for a wide area such as Taklimakan Desert is not so easy due to its large size and severe natural environments. With a capability of observing a wide area nearly simultaneously and repetitive manner with a same sensor, a satellite observation offers a powerful tool for this purpose. In order to obtain the land surface features accurately from the satellite data, information on spectral reflectance of materials on the desert surface is necessary. There are not a few papers on the spectral reflectance of land surface(Leu, 1977, Becker, 1985, Cierniewski, 1987, Jackson et. al., 1990, Hick and Russell, 1990), however there are only a few reports on the in situ observation on spectral reflectance over Taklimakan Desert(Tsuchiya et. al., 1991, Ishiyama et. al., 1992, 1993, 1994) .The moisture content in the sand is a very important parameter, particularly in arid and semi arid lands. If it is retrieved over the wide areas from the satellite data, the result can surely contribute to the studies of desert itself and desertification mechanism as well. Estimation of moisture content in the sands and soils may be possible, if the relation between the reflectance and the soil moisture content is determined experimentally. However, a simultaneous measurements of spectral reflectance and water content of sands and soils are not easy due to the difficulty in measuring the water content in situ.

In addition to the in situ measurements of spectral reflectance of various materials on the land

surface of Taklimakan Desert, the various kinds of sands and soils were sampled in the southern and northern parts of the desert in the neighborhood of Hotan and Aksu respectively to obtain reliable background data on the relationship between soil moisture content and reflectance. Then spectral reflectance of sampled sands and soils was measured in the range between 400 nm and 2500 nm in the laboratory under different soil moisture content. In this paper, soil moisture content(SMC) is defined by the following equation,

$$SMC(\%\text{ in weight}) = 100(a - b) / a \quad (1)$$

where a and b are weight of a sample and weight of a dried sample respectively.

Results

In Situ Measurements of Spectral Reflectance

The spectral reflectance of typical vegetations observed in Taklimakan desert are shown together with spectral solar irradiance in Fig 1. In the visible spectrum no significant difference in the spectral reflectance among the samples is recognized. However there is a large difference in near-infrared spectrum among the species. The spectral reflectance of Salsola collina and Halostashys caspica, distributed sparsely in a gobi desert (stony desert). Gates(1965), Allen(1968), Sinclair(1971) pointed out that the reflectance of plants in near-infrared is influenced by the leaf area, water content and cell structure of the leaves. Since the leaf area of the vegetations in the dry area is small compared with those of non-dry area, the reflectance of the vegetation in Taklimakan Desert will be smaller than that in non-dry area vegetation in near-infrared spectra. In case of Tamarix however leaf density is generally larger than that of the former two vegetation, thus spectral reflectance of Tamarix is larger than that of the two, especially in near-infrared spectra.

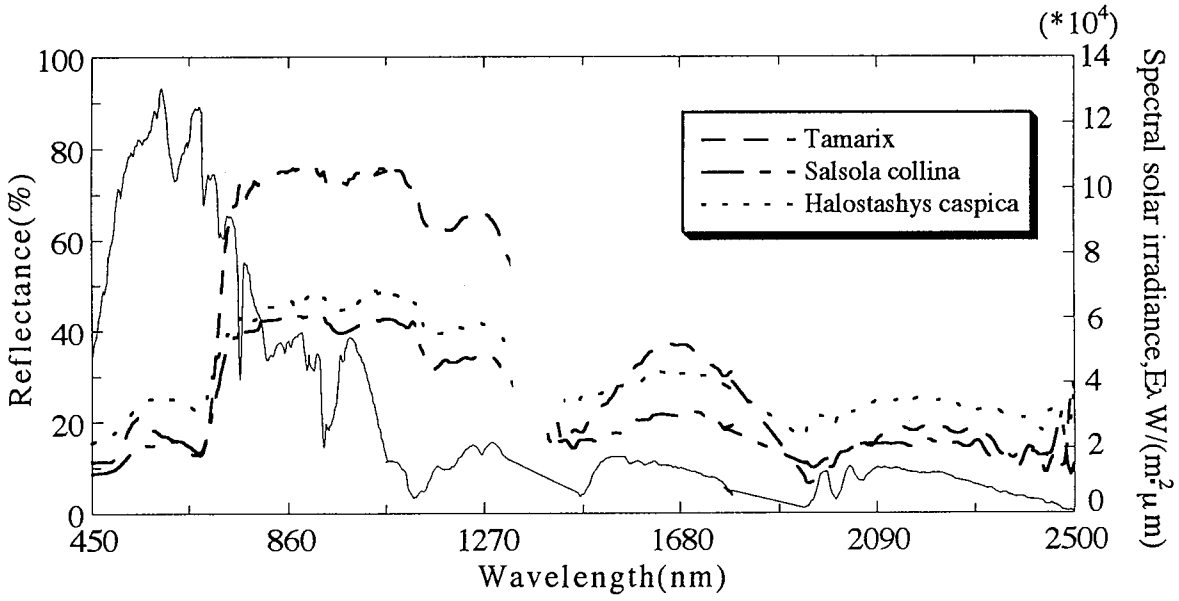

Fig. 1 Canopy reflectance of Sasola collina, Halastays caspica and Tamarix hispida together with incoming spectral solar irradiance.

Fig. 2 shows the spectral reflectance of sands at the surface and 4 different depth in the sand dune area located 30 km to the east of Kashgar (39:32N/ 76:10E). With increasing depth, the reflectance decreases showing the increase of moisture content toward deeper layer. Variation of reflectance with moisture contents is described later in detail. Fig. 3 indicates the spectral reflectance of rich and poor salined soils. The reflectance of salined soils is higher than that of slightly salined soils in whole spectral region. Salined sand is often observed in the river beds and agricultural land. In Hotan and Aksu areas, the suffering from damage of salt were frequently observed.

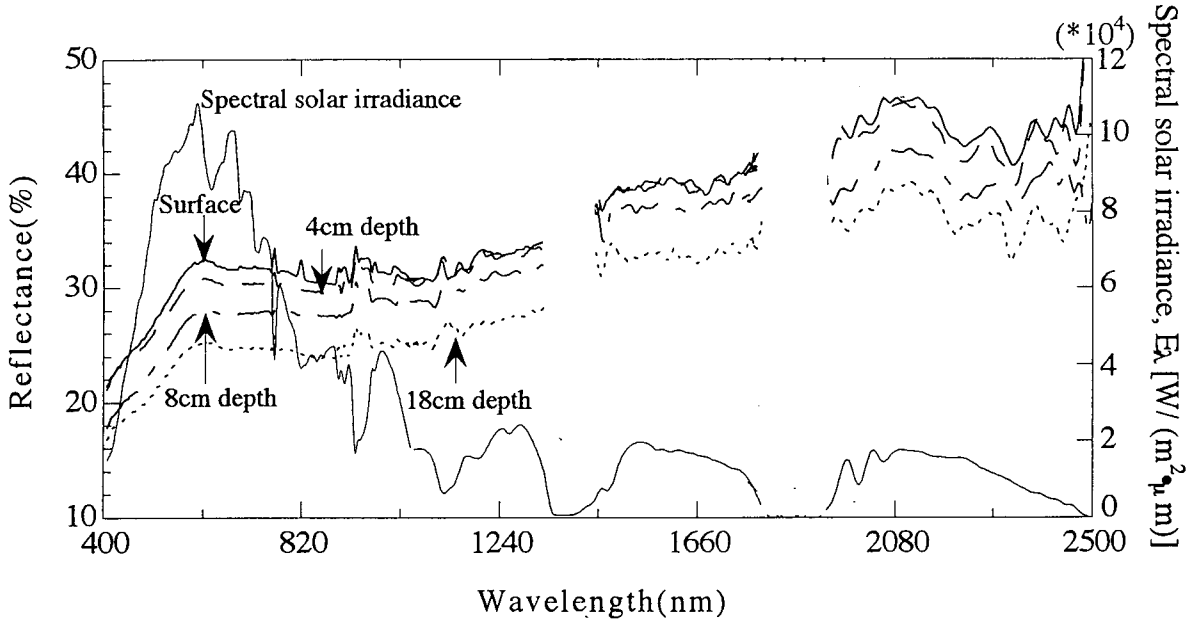

Fig. 2 Spectral reflectance of four different depth of sand dune and solar irradiance of located 30 km to the east of Kashgar(39:32N/ 76:10E) in situ survey.

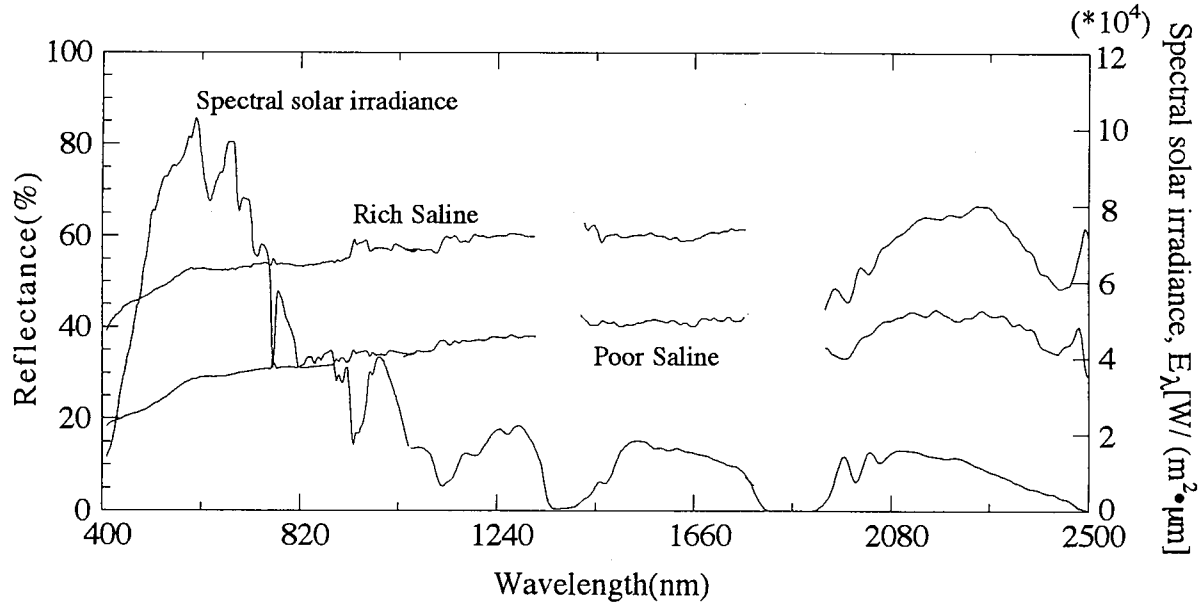

Fig. 3 Spectral reflectance of saline soil at two levels of salinization and spectral solar irradiance at a sample point.

Laboratory measurements of spectral reflectance of sampled sands and soils

The samples of sands were dried up in an air oven at constant temperature of 100°C for 10 hours. After cooling them in a desiccator, the spectral reflectance of the samples was measured with a spectro-radiometer, GER Mark IV in the spectral range from 400 to 2500 nm under different soil moisture content. As a light source 500W tungsten lamp was used. The reference reflectance was a standard white paint manufactured by Kodak. Soil moisture content was controlled through spraying distilled water on the samples in a vinyl pouch and mixed well by shaking. Thus measurements were made first under a completely dry condition then under the condition of gradual increment of soil moisture content. Fig. 4 shows the spectral reflectance of dry sands sampled in the periphery of Taklimakan Desert. The reflectance of red sand sampled in Kashgar is smaller than that of other sands. On the other hand reflectance of salined sand sampled in Hotan is comparatively high due to the fact that the sand surface is covered with a thin whitish crust of salt.

The results of the measurements of spectral reflectance in visible and near-infrared spectra for the dry sands sampled in southern and northern edges of Taklimakan Desert are given in Table 1. The sand reflectance in Bachu and Turfan is smaller than that of other samples. These samples may consist of a similar type of the reddish brown soils which are found frequently in the areas from Kashgar as shown in Fig. 4 to Bachu and Turfan in northern part of Taklimakan Desert. The average reflectance of the soil in southern and northern edge of Taklimakan Desert is 21.2 and 28.8% in visible and near-infrared spectra respectively showing that the reflectance in near-infrared part is fairly larger than that in visible part (for dry soil). Table 2 indicates reflectance within the spectral bands of Landsat MSS and TM, SPOT HRV for various dry sands sampled in southern and northern west edge of Taklimakan Desert. They were calculated from the spectral reflectance measured in the laboratory. Since the observed spectral reflectance data of the soil in the visible to IR part in Taklimakan Desert is few, these results will be useful for interpretation of satellite image data of Taklimakan Desert.

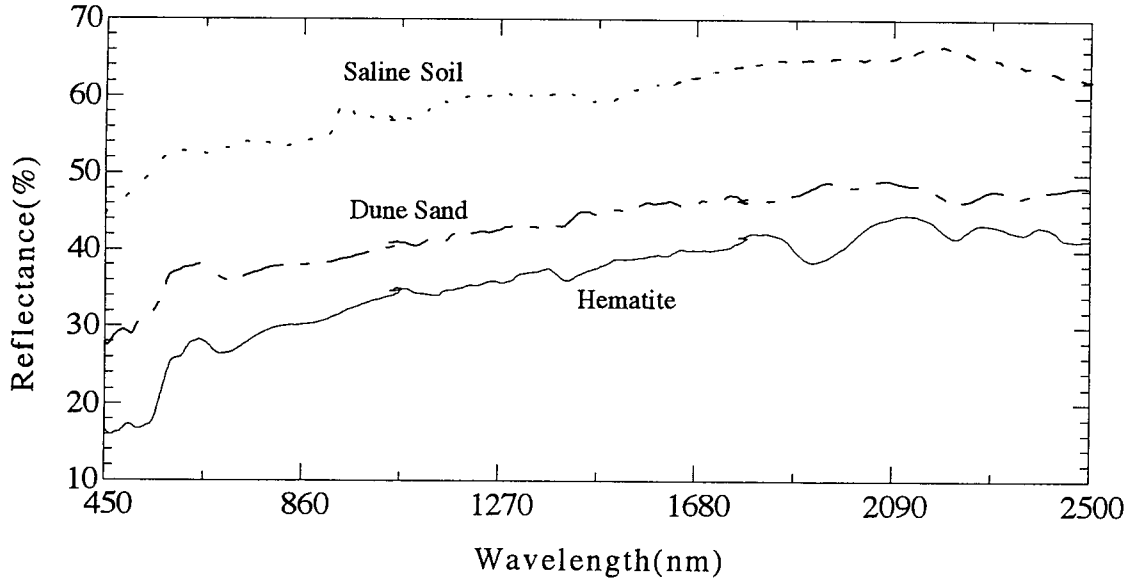

Fig. 4 Spectral reflectance of Hematite, Dune sand and saline soils collected at Kashgar(39:48N/77:26E), Sache, Hotan(37:10N/ 80:02E) respectively.

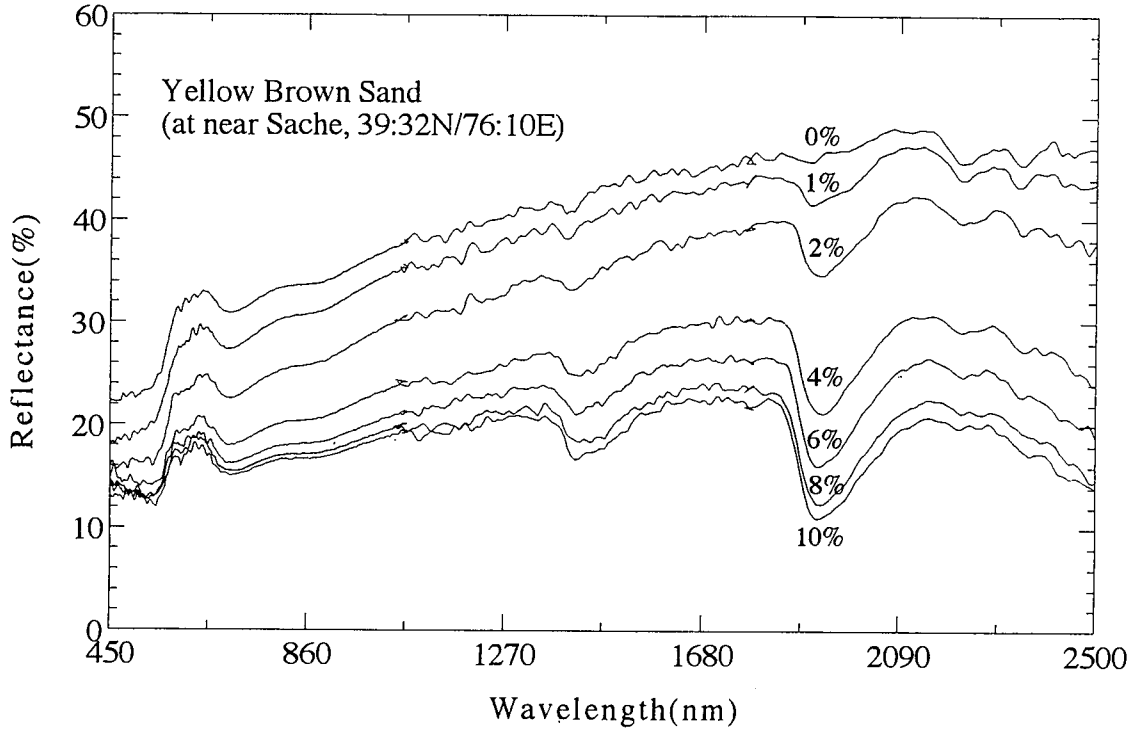

Fig. 5 Moisture content vs spectral reflectance relationship for yellow brown sand sampled near Sache in southern part of Taklimakan Desert.

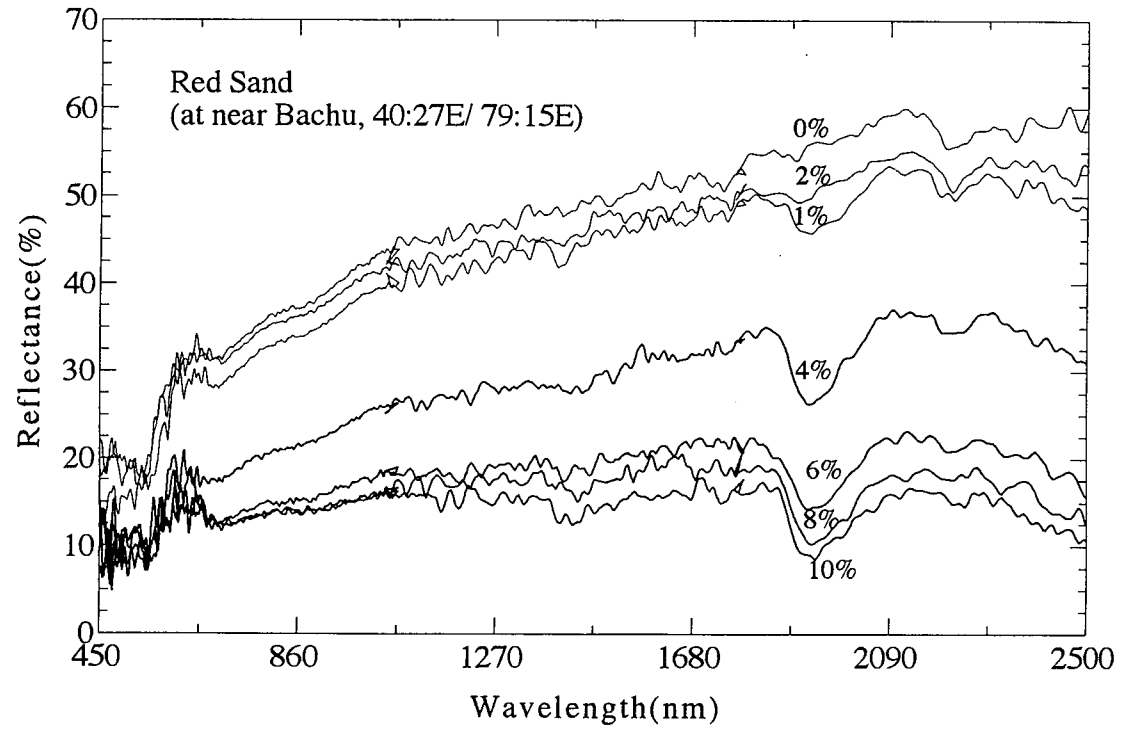

Fig. 6 Moisture content vs spectral reflectance relationship for reddish silt sampled near Bachu in northwestern part of Taklimakan Desert.

Laboratory experiments of spectral reflectance vs moisture contents

Fig. 5 shows moisture content vs spectral reflectance relationship for a yellow soil sampled near Sache of southern part of Taklimakan Desert. At 0.5% moisture content, an effect of moisture contents on spectral reflectance is small. At 1.0 % moisture content, however it is reduced by 5.6%. Above 3.0% of water content, the variation becomes smaller in visible region.
At 1452 and 1941 nm H_2O absorption bands, a rate of decrease of reflectance is larger than that in visible spectra. This is ascribed to the strong absorption of water. Ishiyama et. al.(Ishiyama et. a., 1992) reported that the decreases in the reflectance with the water contents can be explained by the relative decrease of the refractive index. This explains the decrease in the reflectance in the visible light when the water content below is 3.0 %. On the other hand, the large rate of reflectance decrease in near-infrared region is ascribed to the strong absorption of water itself along with the effect of relative decrease of refractive index of sand with water.

Fig. 6 shows spectral reflectance of the soil(reddish tan color silt) sampled near Bachu of north western part of Taklimakan Desert. In the visible spectrum, reflectance is small at 1 % moisture content. The color of the soil changes from red tan to dark red in response to increase of soil moisture content up to 2 %. Beyond 4 % the color change becomes negligibly small. In near-infrared spectrum, however, a large change in the reflectance is observed in similar way as shown in Fig. 6.

Table 1 Average reflectance(%) of soils sampled in the periphery of Taklimakan Desert in visible, near and middle infrared spectra

Stations	Reflectance(%)		
	Visible Spectrum (400-700nm)	Near, middle Infrared Spectra (750-1050nm)	(700-2500nm)
Hotan(37:10N/ 80:02E)	25.2	33.8	
Sache(38:20N/ 77:03E)	24.0	35.0	
Kashgar (39:13N/ 76:10E)	24.9	30.2	
Kashgar (39:13N/ 76:10E)	22.9	29.3	
Kashgar (39:13N/ 76:10E)	23.9	32.1	
Bachu(39:48N/ 77:26E)	15.2	20.5	39.7
Bachu(38:30N/ 76:46E)	24.4	36.8	33.7
Bachu(40:27N/ 79:15E)	19.4	36.1	39.1
Bachu(40:03N/ 78:41E)	15.4	31.2	41.4
Turfan(42:54N/ 89:29E)	14.1	21.7	
Turfan(42:54N/ 89:29E)	14.5	18.6	
Average Reflectance(%)	21.2	29.3	38.4
Average Reflectance for 400-2500nm			30.0
Standard Deviation(σ)	4.19	6.21	2.89

Table 2 Estimated spectral reflectance(%) in the spectral bands of Landsat MSS, TM and SPOT HRV for various dry soils sampled in southern and northern edges of Taklimakan Desert

Target	Spectral Reflectance(%) of the Soils												
	Landsat MSS Bands				Landsat TM Bands						SPOT HRV Bands		
	4	5	6	7	1	2	3	4	5	7	1	2	3
Hotan (1)	29.5	33.7	32.4	35.1	27.2	31.4	33.7	33.4	45.9	46.7	30.5	34.0	33.5
Sache (2)	25.5	31.5	31.1	33.7	22.1	26.3	31.6	32.1	45.2	48.2	24.9	31.8	32.2
Sache (3)	32.6	37.3	36.9	39.1	28.9	33.4	37.4	37.8	46.2	47.6	32.2	37.6	37.9
Kashgar (4)	20.0	27.2	28.1	32.1	16.6	20.8	27.5	29.9	27.2	43.3	19.4	27.5	30.1
Kashgar (5)	22.1	30.8	32.4	38.3	19.9	22.6	31.2	34.9	47.3	53.2	21.4	31.2	35.2
Bachu (6)	21.1	30.4	31.5	37.2	18.4	22.0	30.5	33.7	47.2	50.4	20.4	30.6	33.9
Standard Deviation	5.0	3.4	2.8	2.7	4.9	5.3	3.3	2.7	2.8	3.4	5.4	3.4	2.7

Concluding Remark

The foregoing analysis leads to the following conclusion. The average reflectance of the soil in the periphery area of Taklimakan Desert is 21.2 and 28.8% in visible and near-infrared spectra respectively. In the longer part of near infrared spectrum the reflectance increases to 38.4%. The effect of soil moisture content is larger in 1450 and 1950 nm water absorption bands and decreases in accordance with increase of soil moisture content. Although the use of radiance at Landsat TM bands 5 and 7 are theoretically effective for monitoring soil moisture content, the relationship between reflectance and moisture content is too weak to predict accurate water moisture content. In order to overcome this situation, the absolute values of radiance should be utilized. In this case, however, the removal of atmospheric effect is required since its effect is same order of magnitude as that of water content.

The spectral reflectance of vegetations and soils of Taklimakan Desert obtained in this research will be useful for interpretation of satellite image data of Taklimakan Desert.

References

1. D. J. Leu, Visible and near-infrared reflectance of beach sands: a study on the spectral reflectance/ Grain size relationship, *Remote Sensing of Environment*, 6, 169-182 (1977).
2. F. Becker, P. Ramanantsizehena and M. P. Stoll, Angular variation of the bidirectional reflectance of bare soils in the thermal infrared band, *Applied Optics*, 24, 365-375 (1985).
3. J. Cierniewski, A model for soil surface roughness influence on the spectral response of bare soils in the visible and near-infrared range, *Remote Sensing of Environment*, 23,97-115 (1987).
4. R. D. Jackson et. al., Bidirectional measurements of surface reflectance for view angle corrections of oblique imagery, *Remote Sensing of Environment*, 32, 189-202 (1990).
5. P. T. Hick and W. G. R. Russell, Some spectral considerations for remote sensing of soil salinity. *Aust. J. Soil Res.*, 28, 417-431 (1990).
6. K. Tsuchiya, T. Ishiyama and S. Sugihara, Investigation of surface condition in Taklimakan Desert, Pre ISY(International Space Year) -Present and Features Earth Environment Data Set-.

2nd International Conference on Japanese Earth Observation Program, Proceedings of Pre ISY International Symposium, 209-226 (1991).
7. T. Ishiyama, S. Sugihara, K. Tsuchiya, P. J. Liu and G. F. Lu: Reflectance variation of Taklimakan Desert sands in relative to soil moisture content, Proceedings of Japan-China Intl. Symposium on the study of the mechanism of desertification, 135-153 (1993).
8. T. Ishiyama and S. Sugihara, Studies on the desertification/ Studies on the changes of the surface condition in the desert, -Distribution and physical properties of surface materials- (in Japanese) Annual Report, Japan-China Joint Study on Desertification, Science and Technology Agency of Japan, 63-84 (1992).
9. T. Ishiyama, K. Tsuchiya, S. Sugihara and P. J. Liu, Investigation of the surface condition in Taklimakan Desert (in Japanese), *Journal of Geography*, 103, 4, 334-351 (1994).
10. D. M. Gates, H. J. Keegan, J. C. Schleter and V. C. Weidner, Spectral properties of plants, *Appl. Opt.*, 4: 11-20 (1965).
11. W. A. Allen and A. J. Richardson, Interaction of light with a plant canopy: *J. Optical Soc. America*, 58, 8, 1023-1028 (1968).
12. T. R. Sinclair, R. M. Hoffer and M. M. Schreiber, Reflectance and internal structure of leaves from several crops during a growing season, *Agronomy Journal*, 63, 864-868 (1971).
13. T. Ishiyama, S. Sugihara, K. Tsuchiya, P. J. Liu, and G. G. Lu, Variation of Sand Reflectance with Moisture Content. *J. Arid Land Studies*, 2, 39-43 (1992).

MONITORING OF ANTHROPOGENIC CHANGES IN DESERT VEGETATION

By N. Kharin, Desert Research Institute, Ashgabat Turkmenistan

Turkmenistan is a country of deserts. More then 90% of its terrotiry belongs to the Karakum desert. Adverse human activity (tree and shrub cutting, overgrazing, overirrigation etc.) is the main cause of land degradation (desertification) in Turkmenistan. Severely degraded lands occupy some 6% of its territory, moderately degraded lands I6%. (N.G. Kharin, G. S. Kalenov, V.A.Kurochkin, I993). Economic losses from desertification are given in Table I. Economic losses total 34 875.8 thou american dollar, that makes about 3% of the national income.

Desertification is a problem of global extent. As known more than I00 countries of the world have signed the International Convention to Combat Desertification (ICCD). National Action Programme to Combat Desertification (NAPCD) has been elaborated in Turkmenistan (A.G.Babaev, N.G.Kharin, I995). Now national institutions of many countries are developing an instrument of observance of the ICCD at national level.

NACCD in Turkmenistan includes the proposal on desertification monitoring. National Monitoring Centre (NMC) is to be established. NMC will summerize and process all information collected by monitoring stations located in many points of the country. According to the recommendations of the International Negotiating Committee for a Convention to Combat Desertification (INCD) monitoring must include the following data sets :

Minimum data sets

Climate variables : albedo, rainfall, air temperature, air humidity, wind velocity, dust storms,

Soil and water variables : ground water, major surfase waters, wind erosion, water erosion, soil salinization, waterlogging,

Vegetation variables : plant species composition, woody biomass, fod-

Table I

Annual economic losses from desertification in Turkmenistan

Name of losses	Sum thou american dollar
Direct losses (income foregone)	
A. Losses in animal production	I60.6
B. Losses in agricultural production	II27I3.7
Total A + B	II2874.3
Indirect losses	
C. Expences on rehabilitation od desert rangelands	I56780.0
D. Expences on rehabilitation of irrigated farm lands	64727.9
E. Expences on regeneration of forests	768.9
F. Expences on stabilization of moving sands	II724.7
Total C + D + E + F	23400I.5
TOTAL A + B + C + D + E + F	346875.8

der biomass, disappeared plant and animal species,
Land use variables: land use system, land tenure system, change in land use, structure of sown areas, yield of major staple crops, composition and number of live - stock, animal pressure,
Socio - economic variables: human population, population changes, infant and adult mortality rates, length of life, human disease status, per capita income, income distribution, sources of income, market prices of key food stuffs, energy availability and prices.

Vegetation monitoring is based on ground observations and interpretation of space (or aerial) photos. Combination of ground observations and remote sensing could give the best results in study of anthropogenic changes in desert vegetation.

NMC will prepare small scale (I :2500000) desertification maps covering the whole territory of Turkmenistan. This map will register annual changes in desert ecosystems occured by the human impact. Above that maps of larger scales (I : I00000 - I : 500000) will cover the country where desertification process is especially intensive. Criteria for assessment of the vegetative cover degradation are given in Table 2.

The quality and quantity of information extracted from aerial and space photos depends on proper selection of spectral bands and seasons of photography. Our recommendations on this topic are given in Table 3. These recommendations are based on spectral reflectance study in the field.

Desert landscapes are characterized by low optical contrasts during the whole year. Spring is the best season of space photography in the desert. Phenological indicators of the optimal season are as follows :

I). The beginning of photography is marked by growth of Haloxylon persicum,

2). The end of growth of Carex physodes indicates the end of this period.

The second period of space (aerial) photography is confined to

Table 2

Criteria for assessment of the vegetative cover degradation

Assessment factors	Class limits		
	Slight	Moderate	Severe
I. Characteristics of plant communities	Climax or slightly changed communities	Long-existing secondary communities	Ephemeral secondary communities
2. Reduction in productivity, %	<30	30 - 70	>70
3. Reduction in composition of climax species,%	<25	25 - 50	>50
4. Reduction in plant cover,%	<25	25-50	>50

Table 3

Optimal seasons and spectral bands of aerial and space photography for vegetation monitoring in Turkmenistan

Regions	Seasons	Spectral bands, nm
Karakum desert	20.03 - 20.04	400 - 525 600 - 675
	20.09 - 30.I0	600 - 675
Foothill country	05.04 - 25.04	400 - 500 625 - 675
Agricultural oases	I5.05 - 30.05	600 - 650 700 - 800
	0I.I0 - 30,I0	500 - 550 700 - 800

autumn. The indicators are as follows :

I). Ripening of seeds of Haloxylon persicum indicates the beginning of the optimal period,

2). Fall of seeds of the same species indicates the end of this period.

Vegetation of foothill country is richer in plant composition and abandance, to be comperes with desert. The most contrast period of space photography in spring is marked by the following indicators:

I). The beginning-by flowering of Roemeria refracta,

2). The end-by drying up of Carex pachystylis.

Agricultural oases have cultural vegetation with dense cover because the land is irrigated. Under these conditions near infrared spectral band is more useful for interpretation of vegetation. Two optimal seasons of space photography have been selected - spring and autumn. The optimal spring period is marked by the following indicators :

I). The beginning - by milk stage of ripening of barley,

2). The end - by full ripening of wheat.

The autumn period is marked by the following indicators :

I). The beginning - by opening of cotton bolls,

2). The end - by leaf fall of Armeniaca vulgaris.

NMC will built up a database on desertification. Database on desertification has been developed by N. G. Kharin et al.(I990). It includes the following blocks :

Desertification causes (climatic criteria and anthropogenic factors including all aspects of human impact on desert environment).

Desertificarion status (Data on areas and intensity of land degradation, including soil degradation, water use, change of biodiversity etc).

Social and economic response (sanitary conditions, diseases, migration, length of life, birth rate, income, use of water, market prices on main food - stuff etc.).

Measures to combat desertification (land improvement, efficiency of realization of NAPCD, forecast of desertification).

All countries signed the ICCD will coordinate their activities on desertification monitoring. This coordination will include several levels : subregional (e.g. countries of Central Asia), regional (all countries of Asia), and global (all countries of the world affected by desertification). So our proposals giving in the paper could be used for development of a standard methodology of desertification monitoring.

Referencies.

A.G. Babaev, N.G. Kharin. National Action Programme to Combat Desertification in Turkmenistan. Desert Research Institute, Ashgabat, I995. 7I p.

N.G. Kharin et al.Methodology of Application of Space Photos for Compilation of Thematic Maps in the Desert Zone. Desert Reserch Institute, Ashgabat,I978.73 p.(In Russian).

N.G. Kharin, et al. Arid Centre for Collection and Processing of Remote Sensing Information. Noosfera, Ashgabat,I990. II2 p. (In Russian).

N.G. Kharin, G.S. Kalenov and V.A. Kurochkin. Map of Human - Induced Land Degradation in the Aral Sea Basin. Desertification Control Bulletin, I993, No 23, p. 24 - 28.

Monitoring of Desertification and Possibility for Agro-Farming-Forestry Development

Nishida Ken
Japan Agricultural Land Development Agency(JALDA)
4-1, 2-Chome, Shiba-Kouen, Minato-ku
Tokyo, JAPAN, 105
TEL 03-3433-0171
FAX 03-3436-1929

Shibata Ken-ichi, Makita Fumiko
KOKUSAI KOGYO CO., LTD
2-6-Bancho, Chiyoda-ku
Tokyo, JAPAN, 102
TEL 03-3237-3677
FAX 03-3237-3786

Abstract

The development of desertification is intense in Sahel region at the rim of Sahara Desert, giving various influence on the agriculture, cattle grazing and forestry as well as the regional society. This study has been carried out by Japan Agricultural Land Development Agency (JALDA) as a part of its Desertification Control Measures Verification Survey, in which we (1)implemented the monitoring of desertification at the typical urban area and rural area in the Sahel region where the desertification is advancing and (2) discussed the possibility agricultural/ grazing/forestry development at the village area at the vicinity of Niamey in Niger.

In monitoring of desertification, we used the multitemporal data of artificial satellite LANDSAT and timeserially identified the development of desertification from the changes of vegetation and land form observed at urban area and village area.

On the other hand, we discussed the possibillty for agro/grazing/forestry develoment by assuming the productivity and supporting soil fertility from the soil classfication based on the LANDSAT TM data.

1. Outline of the Study.

1.1 Outline of the study area.

The study area were the urban area around Niamey, the capital of Niger, and rural area around

Magou village located 50 km south-west from Niamey (Fig. 1). These areas are located under the severe climatic condition where annual precipitation is 600 - 700mm, while evapotranspiration is 1,900 - 2,000mm, and rain-fed agriculture and cattle grazing are carried out actively in these areas. The topography here is flat in general, and composed of three kinds of land form of plateau, gentle slope and wadis. The Niger River is running from north-west to south-east and Gorubi River which is a wadis running from west to east is flowing into the Niger River. The fertile soil is built up at the flood plain of wadis such as Gorubi river,and vegetables and fruit tress are grown at a part of them. In addition, gravels of weathered graite and unweathered rocks are exposed at the plateaus and gentle slope around them.

1.2 Study method

The study was implemented by the method shown below.

(1) Artifical satellite data:

The artificial satellite data used for the study is LANDSAT data of 6 different times from 1972 to 1992, which are respectively covered by one scene of PATH 195 -ROW 51 and SPOT of 1992.

(2) Monitoring of desertification

1) Vegetation change based on vegetaion index: Vegetation index is used when the plant activities are compared using the multi-temporal data of LANDSAT. The plant with higher activity has higher water content, and exhibits higher reflection property at near-infrared region, and withered plant has lower reflection property. Taking advantage of this principle, we calculated normalized vegetation index (NVI) and observed the changes of vegetation by constructing vegetation distribution map for each observatoin time.

2) Change of land use identified by image classification and image interpretation: In this stage, we made land cover classification using maximum likelihood method, added correction thereto by image interpretation, and identified the changes by constructing land use map of each observation time.

3) Clarification of development of desertification: We clarified the development of desertification basing on the changes in vegetation and land use identified by the above processes. As a result, we could clarify the decrease of vegetation at plateaus and wadis, soil erosion at plateaus and gentle slope, expansion of under area and appearance of green belt resulting for afforestation.

(3) Discussion on the possibillty for agro/grazing/forestry development

1) Basin area classification and selection of model areas: We classified the basin area bassed on the geographic maps of village area for agro/grazing/forestry development according to the mode of development.

2) Soil classification: The soil classification was made by interpreting the false color image compiled from the most recent LANDSAT TM data and taking into account the results of site survey.

3) Assumption of land productivity: We established the unit of land productivity for each soil classification from the statistic data and results of experimental farm, and assumed the

productivity of total area.

4) Trial calculation of supporting soil fertility: Basing on the above results and statistic data of Niger, we calculated the soil fertilty to support human and animal (cattle) population.

2. Monitoring of Desertification

As for the monitoring of desertification, we calculated the vegetation index from the LANDSAT data of 1972 - 1992. Clarified the change of vegetation area and erosion of land in detail through the classification and interpretation of images .

2.1 Desertification in the total study area

(1) Changes of vegetation

1) The density of vegetation varies largely from north to south in the study area. The vegetation is dense in general in the south, while the vegetation is sparse in the north excepting river side of wadis and green belt around the city of Niamey where dense vegetations are observed. Partially, the paddy fields along the Niger River are expressed as dense vegetation area.

2) The comparison of vegetation indices of different observation times shows clear declining tendency of vegetation as a whole during the period from 1972 to 1992. The vegetation which occupied about 60% of total study area decreased to 50% in 1984 and to approximately 20% in 1990.

3) The decline of vegetation started at the vicinity of Niamey and expanded to suburbs along with the lapse of time. This is due to the lumbering of firewood.

4) The decline of vegetation is more intense in the rims of plateau rather than in the plateau itself.

5) In the LANDSAT data of dry season, the representative vegetation millet is not identified as plant because all of them have been eaten by livestock and only the bases are left.

6) True grasses are dominant among the herbaceous plants and die away in dry season just like crops such as millet. The herbaceous plants are decresing due to the grazing of cattle.

(2) Erosion of soil

We verified the situation of soil erosion using the LANDSAT TM images of 1984 and 1989, The following tendency was observed at the plateaus located at the south-west of Niamey.

1) In the false color image of 1992, the surface of plateau is expressed in whitish color as a whole at the upper layer of plateau, and sandy soil of plateau is exposed to the surface. As a result, run-off of sandy soil is occourring at the banks of wadi rivers.

2) Sand and soil existing in wadi river are those which have run out from plateaus and gentle slope, which in some part have caused the closure of river-mouth.

2.2 Desertification at urban area (Fig.2)

(1) Decline of vegetation

1) As for the vegetation at the vicinity of Niamey, the tress have been lumbered as firewood, and shrubs have also decreased extremely at the plateaus and rim of plateaus located at the suburb of the city. According to the vegetation index, the vegetation which occupied 12% of total urban area in 1972 decreased to 9% in 1975, and to 6% in 1989 - 1990.

2) The demands for fuel wood in Niamey City amounts to 130,000 tons of firewood and 100,000 tons of charcoal every year, and about 500,000 stales (until of fuelwood equivalent to m^3) of fuelwood are lumbered and transported to the city.

(2) Expansion of city area

Intensive inflow of population is taking place from village area to city area in the study area, and the population of Niamey has more than doubled during 15 years from appoximately 240,000 in 1977 to appoximately 500,000 in 1992. According to the LANDSAT TM data, as a result, the city area expanded 3.6 times during 18 years from 14 km^2 in 1972 to 45km^2 in 1990.

(3) Greenbelt

Incerase of vegetation is observed at the green belt around Niamey, which is useful as wind brealing and sand arrestation of the city. The green belt was started from 1965 by continuously planting Niem and Eucalyotus, and it has expanded to 1,600 ha. around the city
area.

2.3 Desertification at village area (Fig.3)

Magou is a typical farming village located at about 50 km south-west of Niamey. JALDA established experimental farm along the Gorubi river which runs across Magou Village, and is implementing each kind of verification tests for the purpose of agriculture/village development which willbe beneficial for desertification control.

(1) Increase of bare land at gentle slope

Vegetation has rapidly decreased around the plateau due to lumbering of firewood and cattle grazing, and bed rock is exposing at many place because the surface soil was eroded by strong
precipitation of rain. Rain-fed agriculture of millet, etc. is carried out at the gentle slope with some fallow period, and there are some seasons when the gentle slope are covered with green. But the area of farm land tends to decrease along with the expansion of bare land.

(2) Flood plain along wadis

Fruit trees, etc. are planted at the flood plain along wadis, and Kabey (Mitragyna Inermis; botanical name = Rubialeae) distributes most widely. Here too, deciline of vegetation is observed partly due to lumbering.

(3) Decline of vegetation

According to vegetation index, vegetation occupied about 38% of Magou Village area in 1972 and 34% in 1975, which acutely decreased to 8% in 1984 and 7% in 1989. This decline is

considered to be due to lumbering of firewood. As Magou village is near to Niamey the shrubs around the plateau are widely used as firewood.

3. Discussion on the Possibility for Agro-Farming-Forsetry Development

3.1 Present state of agriculture/grazing/forestry at village area.

As is clear from the monitoring of desertification, the advance of desertification at village area is mainly attributable to (1) increse of bare land due to overgrazing and over-cultivation and (2) decrease of vegetation due to lumbering of firewood. As a result, land productivity declined and farm lands were abandoned more widely, resulting in impoverishment of agriculture/grazing/forestry development at wadis, and the develoment is comparatively difficult in most cases because not only water resources but also personnel and physical resources are limited. The agriculture/village development at the rural area can be summarized as follows.

1) Chronical food shortage due reduction of water resources resulting from drought and aridity as well as to the deterioration of land fertility resulting from over-cultivation.

2) Shortage of forage and energy and develoment of soil erosion cause by the decrease of vegetation resulting from over-grazing and lumbering of firewood

3) Collapse of production base and living base of local residents (most of them are farmers) resulting from the shortage of food, forage and energy

4) Increase of refugees of farmers who lost the basis of production and livelihood

5) Staggering of national economy and increase of social anxiety

3.2 Measures for agriculture/grazing/forestry

The following measures can be considered for the agricluture/grazing/forestry which take into account the deseritification control at the village areas.

(1) Farm land conservation measures

1) Since the precipitation force of rain is very strong, run-off of soil is plenty and soil layer is thin. As a result, the cultivate farm lands easily become bare land if land management is neglected. In order to cope with these situation, it is necessary to implement contour line farrowing agriculture to prevent the outflow of soil.

2) Since exposed laterite rock is conspicuous at plateau rim, it is exposed laterite rock is construction and weathering of these rocks by constructing water channels at the rim of plateau. This will be useful for preventing rapid outflow of plateau. This will be useful for preventing rapid outflow of water to gentle slope and also for preserving the water resources at the upper part of gentle slope . Furthermore, afforestation must be done at lower parts of plateau rim to reserve the water resources and secure the firewood.

(2) Measure for restoration of lost land

1) Production of sand and soil is restrained by piling up stones along the contour line at acute slope land at the lower part of plateau.

2) As for the outflow of sand and soil, on the other hands, acute production of sand and soil must be restrained by placing sand breaker such as sandbags at gullies and wadis.

(3) Measure for land use

1) Afforestation must be implemented on the plateau and at the acute slope land to reserve the water resource and secure the supply of firewood.

2) Effective land use must be implemented by establishing the system of rotation of millet, grassland and grazing land at the gentle slope and flood plain.

Here, we took the vicinity of representative village Magou as an example, and calculated the productivity and supporting soil fertility of land when the conservation measures mentioned above are actually implemented.

4. Diagnosis of desertification at Magou village area and planning of agriculture/grazing/forestry development

In this stage, we made diagnosis of desertification and drafted the agriculture/grazing/forestry development plan in an aim to control the desertification for Magou Village area where the " experimental farm " is located. In diagnosing the deseritification, we constructed (1) geomorphological classification map, (2)devastation state map and (3) land use map, and at the same time, implemented the land resource investigation for the total area of Magou Village, and finally, drafted (4) agriculture/grazing/forestry davelopment plan basing on these results.

4.1 Diagnosis of desertification

The main purpose of diagnosis of desertification is to grasp the present state and identify the cause of desertification at the study area for which the agrculture/grazing/forestry development plan is drafted. In case of present state diagnosis model and cause diagnosis model , it was necessary to investigate various factors such as present state of land use, geomorphological classification and devastation state using the artification satellite data.

(1) Geomorphological classification

We implemented geomorphological classification using the data of artificial satellite LANDSAT TM and SPOT in order to diagnose the desertification at Magou village. In greneral, the most idealistic way to classify the topography is to use the aerial photographs which have the highest resolution. However, the use of artificial satellite data is effective and more realistic in the areas such as surrent study area where it is difficult to make site survey and take new aerial photographs.

The geomorphology in Magou village and its vicinity is roughly classified into plateaus, acute cliffs, gentle slope, wadis and flood plain. Wadis and plateaus can be identification in more detail if the respective data.

2) Devastation state

As for the devastation state of Magou Village, the sandy/soil production and accumulation is conspicuous at wadi river. This is the interpretation results based on the vegetation index. As a result, the areas of soil erosion and sand accumulation have became clear at plateau rims around the wadis river which runs across the center of village.

(3) State of land use

As for the land use map of Magou Village, we decided to use the data which would make it possible to identify the millet fields, grassland, plateau and floodplain. We attempted to construct land use map using the data of LANDSAT TM and SPOT, but as a result, the vegetation index data of LANDSAT TM were most correctly coincident with actual state of the site. Generally,the vegetation index isued to identify the extent of vegetation vitality at the time(Fig.4).

It has become clear that 35% of total area of millet field and 23% is fallow land, and in total, virtually 58% is used as millet fields. The lands used for grazing are heabaceous plant/shrub area offallow land which amounts to 17% of the total area. in addition, a part of other fallow lands are used for grazing.

In the analysis in relation to geomorphological classification, gentle slope land occupies nearly 70% of the total area, and plateau/small hill and low land share about 15% respectivcly. Most of the gentle slope is millet field, fallow land and sparse forest.

4.2 Drafting of agriculture/grazing/forestry development plan

The agricultural/grazing/forestry develoment plan was compiled by calculating the balance of demand and supply at present land use and considering the measures for desertification control.

5. Conclusion

This study was carried out as a part of " Desertification Contorol Measures Verification Survey " at the vicinty of Niamey, and adjacent village area among Sahel region in order to (1) implement monitoring of desertification at under area and rural area and (2) to study the possibility of agriculture/grazing/forestry development at village area. As a result, we obtained the following conclusions.

(1) The city area is expanding at Niamey, the capital of Niger, due to the inflow of population from village area resulting from the develoment of deseritification.

(2) It was verified that a) conversion of farm land into bare land, b) deveopment of soil erosion and c) reduction of trees due to lumbering of firewood are conspicuous at the village area.

(3) In this study, we place the main focus on the agricultural/grazing/foresty development based on food and water measures. It is necessary in future to study the measures against damages.

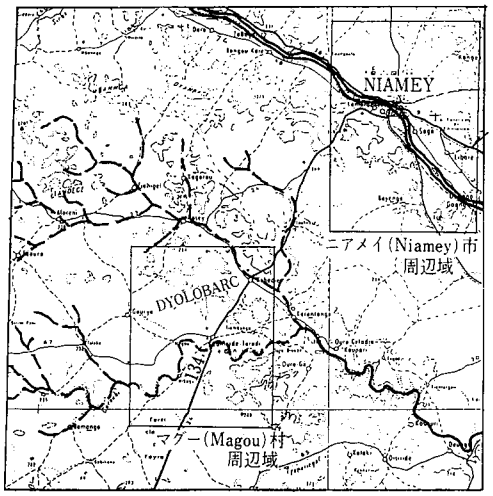

Fig.1. Study Area

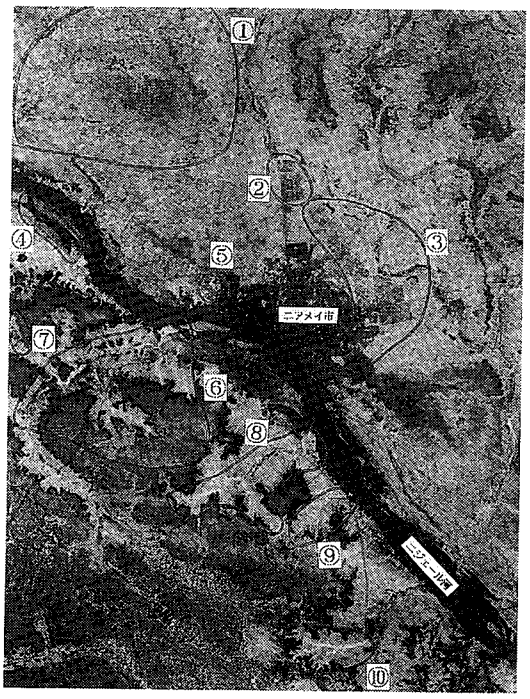

Fig.2. Niamey City

Fig.3. Magou Village

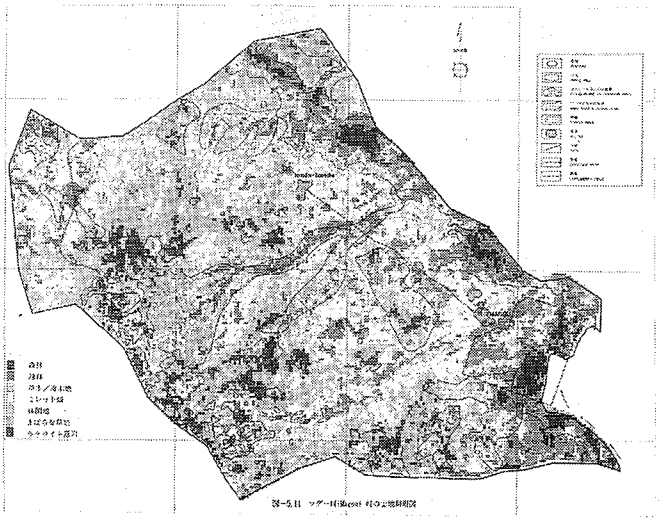

Fig.4. Land Use (Magou)